

Organic-Inorganic Hybrids and Charge Transfer Salts with N-Methylpyridoneazine and its Derivatives

Dissertation
zur
Erlangung des Doktorgrades (Dr. rer. nat.)
der
Mathematisch-Naturwissenschaftlichen Fakultät
der
Rheinischen Friedrich-Wilhelms-Universität Bonn

vorgelegt von
Rebecca Atima Isenberg
aus
Bonn

Bonn 2023

Angefertigt mit Genehmigung der Mathematisch-Naturwissenschaftlichen Fakultät der Rheinischen Friedrich-Wilhelms-Universität Bonn

1. Gutachter: Prof. Dr. Johannes Beck
2. Gutachter: Prof. Dr. Arne Lützen

Tag der Promotion: 25.08.2023
Erscheinungsjahr: 2023

*"Geduld ist das Schwerste und Einzige, was zu lernen sich lohnt.
Alle Natur, alles Wachstum, aller Friede, alles Gedeihen und Schöne
in der Welt beruht auf Geduld, braucht Zeit, braucht Stille, braucht
Vertrauen."*

– Hermann Hesse

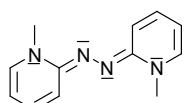
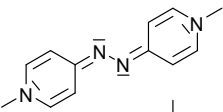
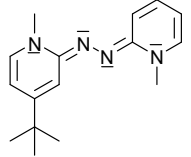
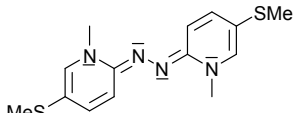
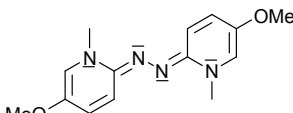
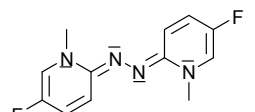
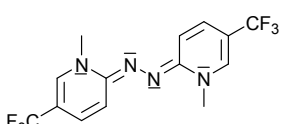
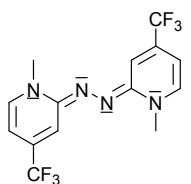
Contents

1	Introduction	1
1.1	Organic Metals	1
1.1.1	Charge Transfer Compounds	2
1.1.2	Organic-Inorganic Hybrids	9
1.1.3	Polymorphism in Organic Solids	12
1.2	Organic Donor Molecules	13
2	Analytical Methods	17
2.1	X-Ray Single Crystal Diffraction	17
2.2	X-Ray Powder Diffraction	17
2.3	Energy Dispersive X-Ray Spectroscopy (EDX)	18
2.4	Cyclic Voltammetry	18
2.5	Conductivity Measurement	18
2.6	Magnetic Susceptibility Measurement	19
2.7	Differential Scanning Calorimetry	19
2.8	Computational Details	20
2.9	Synthesis	21
3	Heterocyclic Azines	27
4	Radical Cation Salts with Halogenocuprates	31
4.1	Crystal Structures	32
4.1.1	(1)[CuCl ₂]	32
4.1.2	(1)[CuBr ₂]	34
4.1.3	(8)[CuBr ₂]	36
4.2	Magnetism	38
4.3	Conductivity	40
5	Dicationic Salts with Halogenocuprates	41
5.1	Crystal Structures	42
5.1.1	(1)[Cu ₂ Br ₄]	42
5.1.2	α -(2)[Cu ₂ Br ₄]	44
5.1.3	β -(2)[Cu ₂ Br ₄] · CH ₃ CN	46
5.1.4	(2)[CuBr ₃]	49
5.1.5	(2)[CuBr ₄]	51
5.1.6	(8)[CuBr ₄]	53
5.2	Magnetism	55
5.3	Conductivity	57

6 Charge Transfer Compounds with TCNQ	61
6.1 Crystal Structures	63
6.1.1 α -(1)(TCNQ)	63
6.1.2 α -(2)(TCNQ)	66
6.1.3 β -(2)(TCNQ)	68
6.1.4 (3)(TCNQ)	70
6.1.5 (4)(TCNQ)	72
6.1.6 (7)(TCNQ)	74
6.1.7 (7)(TCNQ) ₂	77
6.1.8 (8)(TCNQ)	79
6.2 Magnetism	82
6.3 Band Structure and PDOS	85
6.4 Conductivity	92
7 Charge Transfer Compounds with TCNP	97
7.1 Crystal Structures	99
7.1.1 (5)(OTCNP) ₂	99
7.1.2 (7)(TCNP)	101
7.2 Magnetism	103
7.3 Conductivity	104
8 Charge Transfer Salt with DTeF	105
8.1 Crystal Structure of (1)(DTeF)	107
8.2 Theoretical calculations on (1)(DTeF)	111
8.2.1 Band Structure and PDOS	111
8.2.2 Conductivity	113
9 Conclusion	115
A Useful Information	119
A.1 Used Computer Programs	119
A.2 Radical Cation Salts with Halogenocuprates	120
A.3 Dication Salts with Halogenocuprates	130
A.4 Charge Transfer Salts with TCNQ	143
A.5 Charge Transfer Salts with TCNP	182
A.6 Charge Transfer Salt with DTeF	187
Bibliography	227
Danksagung	235

Molecule Glossar

No. Molecular Formula Name

1		Bis(<i>N</i> -methylpyridone)azine
2		Bis(<i>N</i> -methyl-4,4'-pyridone)azine
3		Bis(<i>N</i> -methyl-5-tertbutyl-pyridone)azine
4		Bis(<i>N</i> -methyl-4-thiomethyl-pyridone)azine
5		Bis(<i>N</i> -methyl-4-methoxy-pyridone)azine
6		Bis(<i>N</i> -methyl-4-fluoro-pyridone)azine
7		Bis(<i>N</i> -methyl-4-trifluoromethyl-pyridone)azine
8		Bis(<i>N</i> -methyl-5-trifluoromethyl-pyridone)azine

Abstract

The pyridone azine *N*-methylpyridoneazine (MPA, **1**) is electron-rich and a planar organic donor molecule. As two-stage redox system, it can undergo two one-electron oxidation steps forming a radical cation species and an azo-bis(*N*-methyl-2,2'-pyridinium) dication. Its structural and electronic features make it highly attractive candidate for the generation of organic-inorganic hybrid solids and organic charge transfer (CT) salts with exotic magnetic and conducting characteristics.

Modifications of the basic scaffold MPA provide the pyridone azines **3–8**. The +M substituents OMe and SMe, the steric demanding *t*Bu group and the –I substituents F and CF₃ in meta- or para-position of the pyridinium N atoms and a constitutional isomer with 4,4'-substitution were investigated regarding their redox behaviour. Cyclic voltammetry shows that the two one-electron oxidation processes proceed fully reversible. Especially, for the CF₃ derivatives, the reductive power of the molecules decreases significantly. The differentiation of the oxidation states 0, +1 and +2 of the azines is possible by the bond lengths in the central CNNC azine moiety.

Reactions with copper(II) halides afford the one-electron transfer as well as the two-electron transfer. A series of new organic-inorganic hybrids were obtained in reactions with CuCl₂ and CuBr₂. Pyridone azines **1** and **8** in reactions with copper(II) halides yielded the radical cation salts (**1**)[CuCl₂], (**1**)[CuBr₂] and (**8**)[CuBr₂]. Six new dication salts were obtained containing the azo-bis(*N*-methyl-4,4'-pyridinium) dication or the azo-bis(*N*-methyl-2,2'-pyridinium) dication. (**1**)[Cu₂Br₄], α -(**2**)[Cu₂Br₄], β -(**2**)[Cu₂Br₄]·CH₃CN, (**2**)[CuBr₃], (**2**)[CuBr₄] and (**8**)[CuBr₄] are synthesised successfully. Especially, the twofold oxidation of **2** afforded a multi-phase system. In the crystals, the common structural feature is stacks made up by the corresponding azine cation species. The corresponding bromido cuprate anions differ regarding the oxidation state of copper, the number of bromine ligands as well as their structural coordination. The magnetic properties are predominantly determined by the oxidation state of copper. However, in case of (**8**)[CuBr₂] the magnetism is dominated by the **8**⁺ radical cation. For the conducting properties of the organic-inorganic hybrids even the respective cation as the anion are responsible. Overall, they represent small band gap semiconductors or typical insulators.

Ten new charge transfer salts were obtained in reactions of the azines **1–8** with the organic acceptor molecules TCNQ, TCNP and DTeF: α -(**1**)(TCNQ), α -(**2**)(TCNQ), β -(**2**)(TCNQ), (**3**)(TCNQ), (**4**)(TCNQ), (**7**)(TCNQ), (**7**)(TCNQ)₂, (**8**)(TCNQ), (**5**)(OTCNP)₂, (**7**)(TCNP) and (**1**)(DTeF).

Their structural arrangement consisting of mixed or segregated stacks yield various magnetic and conducting properties. Experimental results have a broad consensus with predicted electronic properties by band structure and PDOS calculations. Especially, the polymorphism observed for α -(**2**)(TCNQ) and β -(**2**)(TCNQ) expresses clearly the structure-property relationship. Thus, hybrid density functional theory with dispersion correction and triple-zeta basis sets represents a suitable method for the prediction of the electronic properties of CT salts.

Zusammenfassung

Das Pyridonazin *N*-Methylpyridonazin (MPA, **1**) ist ein elektronenreiches und planares organisches Donor Molekül. Als zweistufiges Redoxsystem kann es zwei Ein-Elektronen-Oxidationsschritte durchlaufen, wobei ein Radikalkation und ein Azo-bis(*N*-methyl-2,2'-pyridinium)-dikation entstehen. Die strukturellen und elektronischen Eigenschaften machen es zu einem äußerst attraktiven Kandidaten für die Synthese von organisch-anorganischen Hybriden und organischen Charge-Transfer (CT) Verbindungen mit interessanten magnetischen und leitenden Eigenschaften.

Modifikationen des Grundgerüsts MPA liefern die Pyridonazine **3–8**. Die +M-Substituenten OMe und SMe, die sterisch anspruchsvolle *t*Bu-Gruppe und die –I-Substituenten F und CF₃ in meta- oder para-Position der Pyridinium N Atome und ein Konstitutionsisomer mit 4,4'-Substitution wurden auf ihr Redoxverhalten hin untersucht. Zyklische Voltammetrie zeigt, dass die Ein-Elektronen-Oxidationsprozesse der Azine reversibel verlaufen. Insbesondere bei den CF₃ Derivate verringert sich das Reduktionsvermögen der Moleküle deutlich. Die Unterscheidung der Oxidationsstufen 0, +1 und +2 der Azine ist durch die Bindungslängen im zentralen CNNC-Teil möglich.

Reaktionen mit Kupfer(II)halogeniden ermöglichen sowohl die Ein-Elektronen- als auch die Zwei-Elektronenübertragung. Eine Reihe neuer organisch-anorganischer Hybride wurde in Reaktionen mit CuCl₂ und CuBr₂ erhalten. Die Pyridonazine **1** und **8** ergaben in Reaktionen mit Kupfer(II)halogeniden, die Radikalkationensalze (**1**)[CuCl₂], (**1**)[CuBr₂] und (**8**)[CuBr₂]. Es wurden sechs neue Dikationensalze, die das Azo-bis(*N*-methyl-4,4'-pyridinium)-dikation oder das Azo-bis(*N*-methyl-2,2'-pyridinium)-dikation enthalten, erfolgreich synthetisiert: (**1**)[Cu₂Br₄], α -(**2**)[Cu₂Br₄], β -(**2**)[Cu₂Br₄]·CH₃CN, (**2**)[CuBr₃], (**2**)[CuBr₄] und (**8**)[CuBr₄]. Insbesondere die zweifache Oxidation von Azine **2** führte zu einem mehrphasigen System. Die Kristalle bestehen aus Stapeln des jeweiligen Dikations. Die entsprechenden Bromidocupratanionen unterscheiden sich hinsichtlich der Oxidationsstufe von Kupfer, der Anzahl der Bromliganden sowie ihrer strukturellen Koordination. Die magnetischen Eigenschaften werden in erster Linie durch die Oxidationsstufe des Kupfers bestimmt. Im Fall von (**8**)[CuBr₂] ist der Magnetismus durch das **8**⁺ Radikalkation dominiert. Für die leitenden Eigenschaften der organisch-anorganischen Hybriden sind Kation oder Anion verantwortlich. Insgesamt stellen sie schmalbandige Halbleiter oder typische Isolatoren dar.

Zehn neue Charge-Transfer Salze wurden in Reaktionen der Azine **1–8** mit den organischen Akzeptormolekülen TCNQ, TCNP und DTeF synthetisiert: α -(**1**)(TCNQ), α -(**2**)(TCNQ), β -(**2**)(TCNQ), (**3**)(TCNQ), (**4**)(TCNQ), (**7**)(TCNQ), (**7**)(TCNQ)₂, (**8**)(TCNQ), (**5**)(OTCNP)₂, (**7**)(TCNP) und (**1**)(DTeF). Ihre strukturelle Anordnung, die aus gemischten oder getrennten Stapeln besteht, führt zu unterschiedlichen magnetischen und leitenden Eigenschaften. Die experimentellen Ergebnisse stimmen weitgehend mit den vorhergesagten elektronischen Eigenschaften durch Bandstruktur- und PDOS-Berechnungen. Insbesondere der für α -(**2**)(TCNQ) und β -(**2**)(TCNQ) beobachtete Polymorphismus bringt die Struktur-Eigenschaft Beziehung deutlich zum Ausdruck. Daher stellt die hybride Dichtefunktionaltheorie mit Dispersionskorrektur und Triple-Zeta Basissätzen eine geeignete Methode für die Vorhersage elektronischer Eigenschaften von Charge-Transfer Salzen dar.

CHAPTER 1

Introduction

1.1 Organic Metals

The specific electrical conductivity σ (Scm^{-1}) is the physical unit that describes the property of a material to conduct. For a long time, high conducting characteristics were associated with inorganic materials exclusively. Consequently, organic polymers are used broadly in insulation techniques. However, in the 1950s, black solids obtained in reactions of perylene or phenothiazine (Fig. 1.2) with bromine and iodine were found to show semiconductivity ranging from 10^{-3} to 50 Scm^{-1} [1, 2].

Since then, the generation of organic materials with electrical properties attracted considerable attention. Especially, the concept of W.A. Little, that implies superconductivity in macro-molecules and polymers, generated a great deal of interest[3]. Despite, the theory could not be confirmed experimentally, the research field of organic metals as well as semiconductors became rapidly extraordinary fruitful. Nowadays, the area of the broadest practical application is the organic semiconductors. Selected examples are photovoltaic devices, electronic and optoelectronics, capacitors and rechargeable batteries and solar cells[4–7].

It was revealed that planar molecules with an delocalised π system are particular suitable starting materials. Organic compounds are commonly inexpensive and the possibility of manufacturing them on large scales makes them highly attractive compared to traditional inorganic materials as silicon (Si) or gallium arsenide (GaAs).

In Fig. 1.1 the room temperature (RT) specific electrical conductivities, σ_{RT} , of selected inorganic

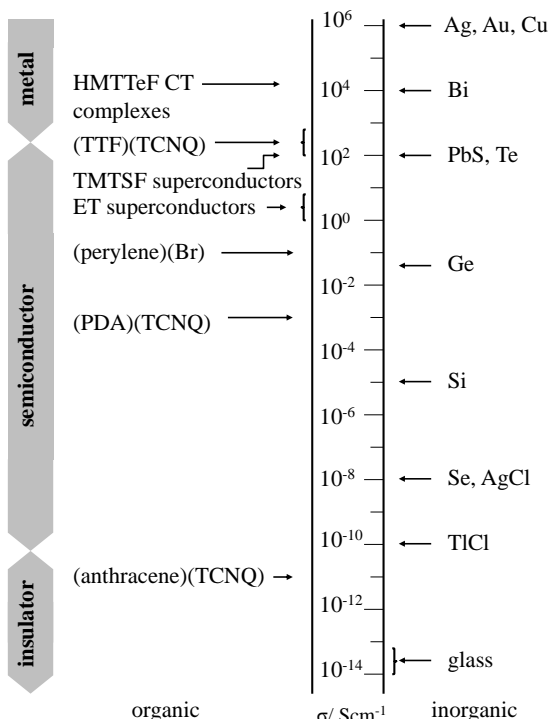


Figure 1.1: The room temperature conductivities σ_{RT} (Scm^{-1}) of inorganic solids (right) and organic charge transfer solids (left). TTF: tetrathiafulvalene, TMTSF: tetramethyltetraselenafulvalene, HMTTeF: hexamethylenetetratellurafulvalene, ET: bis(ethylenedithio)-TTF, PDA: *p*-phenylenediamine and TCNQ: tetracyanoquinodimethane.

(right) and organic (left) materials are presented. The corresponding chemical structures of the organic fragments are depicted in Fig. 1.2. In general, the classification into metals ($\sigma \geq 10^2$), semiconductors ($10^2 \geq \sigma \geq 10^{-10}$) and insulators ($\sigma \leq 10^{-10}$) is used. Among the transition metals, silver (Ag) represents the best conductor with a conductivity in the order of 10^6 Scm^{-1} closely followed by copper (Cu) and gold (Au). Typical inorganic semiconductors are germanium (Ge) or silicon (Si). On the organic side, charge transfer (CT) salts and organic-inorganic hybrids cover the whole conductivity range. From insulating CT compounds made of anthracene and tetracyanoquinodimethane (TCNQ), (anthracene)(TCNQ)[8], to superconductors made by bis(ethylenedithio)tetrathiafulvalene (ET)[9, 10]. The impact on the physical properties of these organic CT compounds and organic-inorganic hybrids is discussed in the following.

1.1.1 Charge Transfer Compounds

CT compounds were first described by F.A. Wöhler in 1844[11].

In general, these low-dimensional, strongly correlated electron systems result from co-crystallisation of an electron donor (*D*) and an electron acceptor (*A*) molecule. The crystal structures are highly dominated by the remarkably increased Coulomb and dipolar interactions that promote an enhanced charge carrier mobility. In contrast to almost all inorganic metals, most organic conductors have anisotropic characteristics, meaning that in one crystallographic axis the electrical conductivity can be up to factor 10^5 larger compared to the other directions. Thus, organic CT salts are labelled as anisotropic or 1D solids[12].

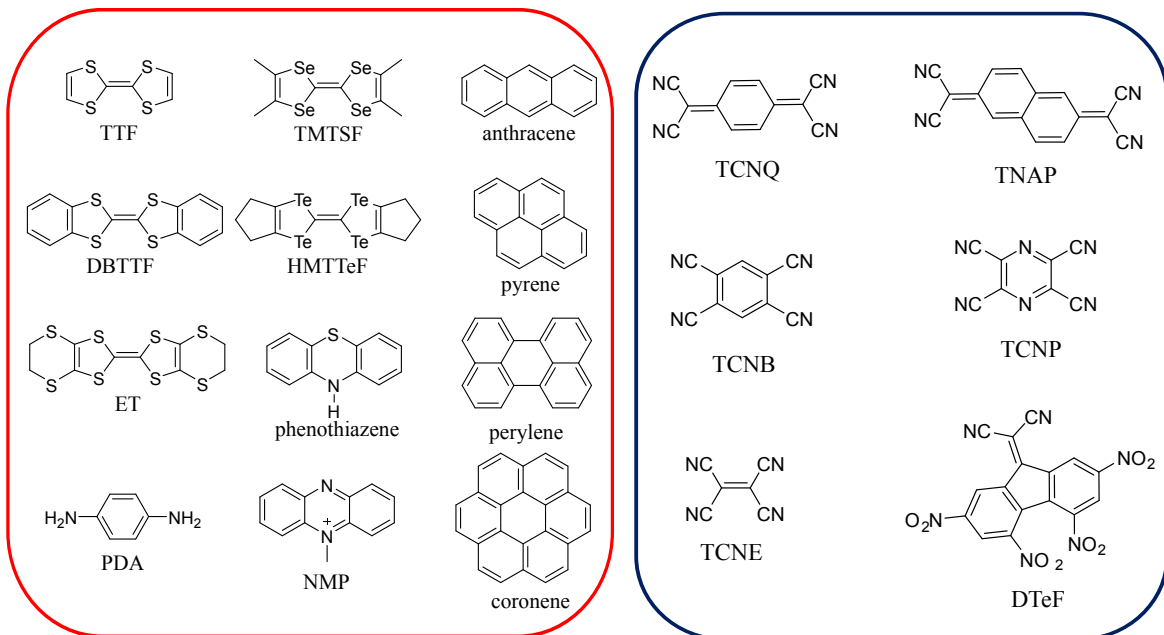


Figure 1.2: Chemical structures of selected organic donor and acceptor molecules. Donors (left): TTF: tetrathiafulvalene, DBTTF: dibenzotetrathiafulvalene, ET: bis(ethylenedithio)tetrathiafulvalene, PDA: *p*-phenylenediamine, TMTSF: tetramethyltetraselenafulvalene. HMTTeF: hexamethylenetetratellurafulvalene, NMP: *N*-methylphenazinium. Acceptors (right): TCNQ: tetracyanoquinodimethane, TNAP: tetracyanonaphtho-2,6-quinodimethane, TCNB: tetracyanobenzene, TCNP: tetracyanopyrazine, TCNE: tetracyanoethylene, DTeF: 2,4,5,7-tetranitro-9-dicyanomethylenefluorene.

In the design of CT solids, the two main key factors that strongly determine the transport properties are the crystal structure (molecular stacking) and the charge transfer (ionicity).

In these 1D solids, two principal stacking motifs are possible: mixed or segregated stacks (Fig. 1.3).

In the first case, donor and acceptor are stacked in alternating fashion with a stacking sequence: ...DADA.... For the second case, donor and acceptor are stacked separately as ...DDDD... and ...AAAA.... A necessity for metallic conductivity at room temperature is the presence of segregated stacks, however, it is not a reliable indicator.

Experimentally, the ionicity was first investigated in 1964 by Matsunaga[13–15]. Methods as IR, UV-vis-NIR and Raman spectra, and electrical conductivity, magnetic properties, structural properties and/or stoichiometry of the compounds have been allowing the estimation of charge transfer.

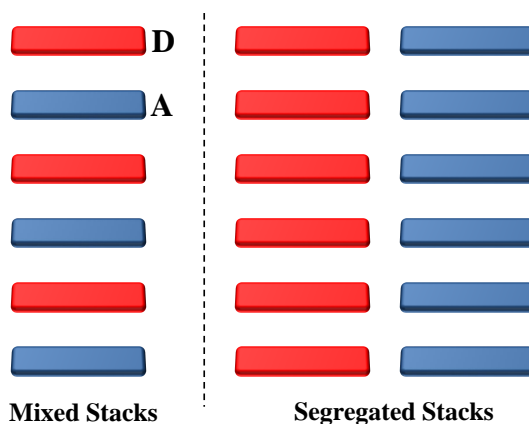


Figure 1.3: The general types of crystal packing: mixed stack motif (left) and segregated stack (right). Red bars presents the donor (*D*) and blue the acceptor (*A*) molecules.

According to the theory of McConnell *et al.*[16], the ionicity boundary in solids is described by the following formula:

$$I_P - E_A \sim M \quad (1.1)$$

where I_P is the ionisation potential of the donor, E_A the electron affinity of the acceptor molecule and M the Madelung energy of the crystal. As stated by the Koopman's theorem, I_P and E_A correspond to the highest occupied molecular orbital (HOMO), or respectively, the energy level of the lowest unoccupied molecular orbital (LUMO)[17]. In real systems additional effects as ionicity dependence of M [18], transfer interactions[19, 20] and size and shape effects on M [21, 22] are present. As one of the most essential requirements for organic metals, partial CT state appears in a narrow region. In compounds where the Madelung energy, M , exceeds the energy cost ($I_P - E_A < M$) full ionicity is reached by formation of radical ion salts. For $I_P - E_A > M$ region, molecules with neutral ground state co-crystallise.

neutral	
<u>mixed</u>	<u>segregated</u>
band insulators	band insulators
• non-linear optics	

mixed valent	
<u>mixed</u>	<u>segregated</u>
metals	metals
insulators	superconductors
• ferroelectrics	insulators
	• Peierls systems
	• Mott systems
	• spin-density waves
	• anion-ordered
	• charge-ordered

ionic	
<u>mixed</u>	<u>segregated</u>
band insulators	metals
• (anti) ferromagnetic	insulators
• ferroelectric	• Mott systems
• spin-Peierls	• spin-Peierls
	• spin-ladder

Figure 1.4: Classification of CT solids divided by ionicity: neutral, mixed valent and ionic. ($0 \leq \delta \leq \delta_c$), II: partially ionic conductors for $I_P - E_A \approx M$ ($\delta_c \leq \delta < 1$) and III: fully ionic insulators ($\delta = 1$) (Fig. 1.4). δ_c as threshold value depends on the electronic dimensionality of a

specific *DA* system. With increasing dimensionality of the system δ_c decreases. In compounds where $\delta < \delta_c$, the tendency to form alternating stacks is rather higher than segregated.

The achievement of mixed valency is mainly influenced by the choice of the *DA* system. Hence, $I_P - E_A$, or the solution redox potentials, $\Delta E(DA)$ with $E_D - E_A$ have to be in an appropriate range. In Fig. 1.5 ionicity phase diagram of compounds derived from the system TTF·TCNQ (*D*: TTF - tetrathiafulvalene; *A*: TCNQ - tetracyanoquinodimethane) is presented. Based on conductivity data, G. Saito and J. Ferraris separate the CT solids in the three regions using the modified Eq. 1.1, $E_A = I_P - M(\delta_c)$. For this specific system, the regime of mixed valency is between the black lines **a** and **b** and described by the following expression by an estimated $\delta(\delta_c)$ of 0.5:

$$-0.02 \text{ V} \leq \Delta E(DA) \leq +0.34 \text{ V}. \quad (1.2)$$

(Potential range vs. SCE corresponds to $-0.07 \leq \Delta E(DA) \leq +0.30 \text{ V}$ vs. Ag/AgCl). For $\Delta E(DA) < -0.02 \text{ V}$ vs. SCE the materials are fully ionic Mott insulators or antiferromagnets. For $\Delta E(DA) > +0.34 \text{ V}$ vs. SCE neutral CT solids are expected behaving as insulator.[23]

Simple band theory predicted metallic behaviour for 1D solids at zero temperature. However, it often turns out in semiconductivity or insulation. This can be explained by their electronic structures that are able to undergo spontaneous break in symmetry by charge density waves (CDW) or spin density waves (SDW). The former case is ensued by a static structural distortion, usually dimerisation. This structural change is described by the Peierls theorem[24]. It states that the total energy at zero temperature is always lowered by a finite distortion. Thus, the effect of pair formation is observed frequently. As a consequence, a band gap opening between valence band (VB) and conduction band (CB) occurs and additional band splitting leading to semiconducting or insulating materials (Fig. 1.6). With temperature increase, a Peierls transition from insulating to a gapless state can happen directly. Then the structural distortion has been cancelled.[25]

The most important contribution to the binding energy in molecular solids provides Van der Waals (VdW) interactions. As a result, the intermolecular transfer and overlap integral are quite small that lead to narrow HOMO and LUMO bands. These bands possess widths of 0.1 to 0.3 eV, while the energy gaps can take up to several eV. In Fig 1.6 the schematic energy dispersion of the bands is illustrated, presenting these aspects in a qualitative fashion.

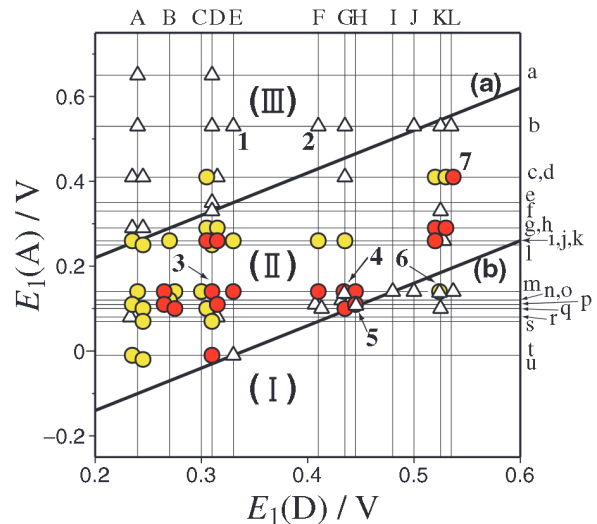


Figure 1.5: Ionicity phase diagram for compounds derived from the system TTF·TCNQ. The first oxidation potential of the donor $E_1(D)$ is plotted against the first reduction potential of the acceptor $E_1(A)$ vs. SCE. Triangles: insulators or semiconductors; yellow circles: highly conducting in compaction studies; red circles: organic metals. Several donors are B: TMTTF, D: TTF, E:HMTTF, G: TMTSF, K: ET and L: DBTTF. Some TCNQ derivatives are a: 2,5-(CN)₂, b:F₄, e: 2,5-I₂ and m: TCNQ. Numbers 1-7 depict selected CT compounds, e.g., 1: (HMTTF)(F₄TCNQ), 3: (TTF)(TCNQ) and 4: (TMTSF)(TCNQ). Region I: neutral, II: partial CT, III: fully ionic. Line **a**: $\Delta E = -0.02 \text{ V}$ and line **b**: $\Delta E = +0.34 \text{ V}$ vs. SCE. The diagram is taken from ref [23].

The discovery of the first organic metal, consisting of the electron donor 1,4,5,8-tetrathiafulvalene (TTF) and the electron acceptor 7,7,8,8-tetracyanoquinodimethane (TCNQ), the (TTF)(TCNQ)[26], was a milestone in this research field. An incredible variety of organic as well as radical ion materials was found that have characteristics moving from semiconducting over conducting to even though superconducting properties[27–29].

The exotic and interesting attributes of (TTF)(TCNQ) have been studied intensively by experimental as well as theoretical approaches[26, 30–35]. In the crystals, the specific structural feature is segregated stacks that consist of partially charged TTF ^{$\delta+$} or TCNQ ^{$\delta-$} molecules (Fig. 1.7).

The conductivity has a broad maximum of 10^4 Scm^{-1} at 60 K[36] that is comparable to those of copper at room temperature[37]. However, compared to Cu, the carriers per unit cell of (TTF)(TCNQ) are decreased by a factor of 100.

Below 54 K, the metallic character of (TTF)(TCNQ) decreases progressively due to a cascade of phase transitions associated to charge density waves (CDWs)[30]. The electronic band structure and band parameter, based on tight-binding approximation, have been estimated through molecular-orbital calculations[38, 39]. For several sets of the band parameters, Shitzkovsky *et al.* evaluated the Fermi surface shape and the density of states near the Fermi energy[40]. Ishibashi and Kohyama performed *ab initio* band dispersion calculations using the local density approximation (LDA) and the generalised gradient approximation (GGA) as level of theory[32]. Band dispersions mirror the anisotropic and metallic character of this compound (Fig. 1.8).

In molecular solids VdW interactions play a significant role. Neither Hartree-Fock (HF) nor the local density approximation (LDA) and the generalised gradient approximation (GGA) in the density functional theory (DFT) are able to describe VdW interactions sufficiently. Therefore, more advanced schemes have to be the method of choice to describe the electronic exchange–correlation interaction and the dispersion correction more accurately. To the best of our knowledge, no studies of the electronic properties of (TTF)(TCNQ) with hybrid methods have been published so far. Since the description of the electronic properties of CT solids are a powerful tool, calculations with hybrid density functional theory as level of theory with dispersion correction were performed for (TTF)(TCNQ) as benchmark study. The method is described in Chapter 2.8 and the corresponding results are presented in Chapter 6.

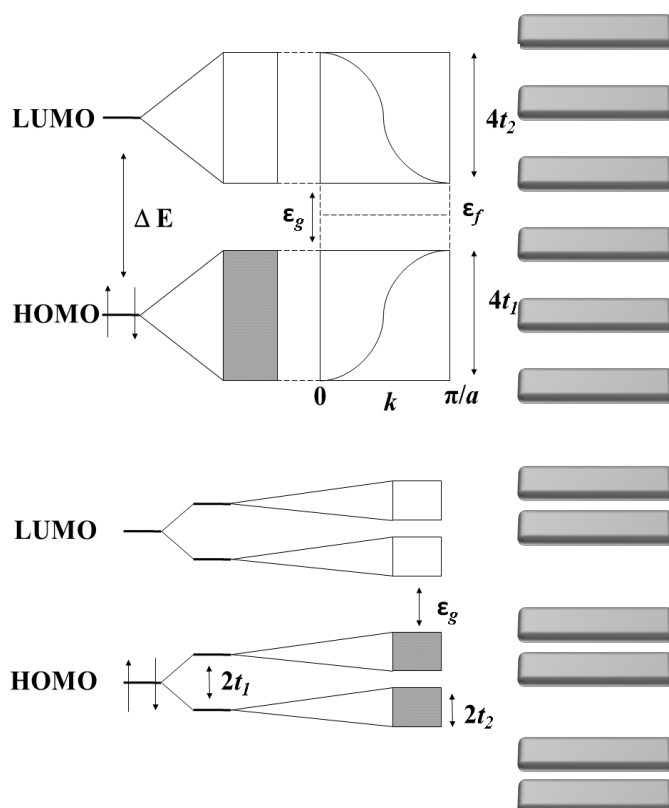


Figure 1.6: Schematic energy dispersion of the bands showing the HOMO and LUMO splitting of a molecular crystal (on top). Band structure for a molecular crystal with Peierls distortion (dimerisation) showing additional band splittings (on bottom).

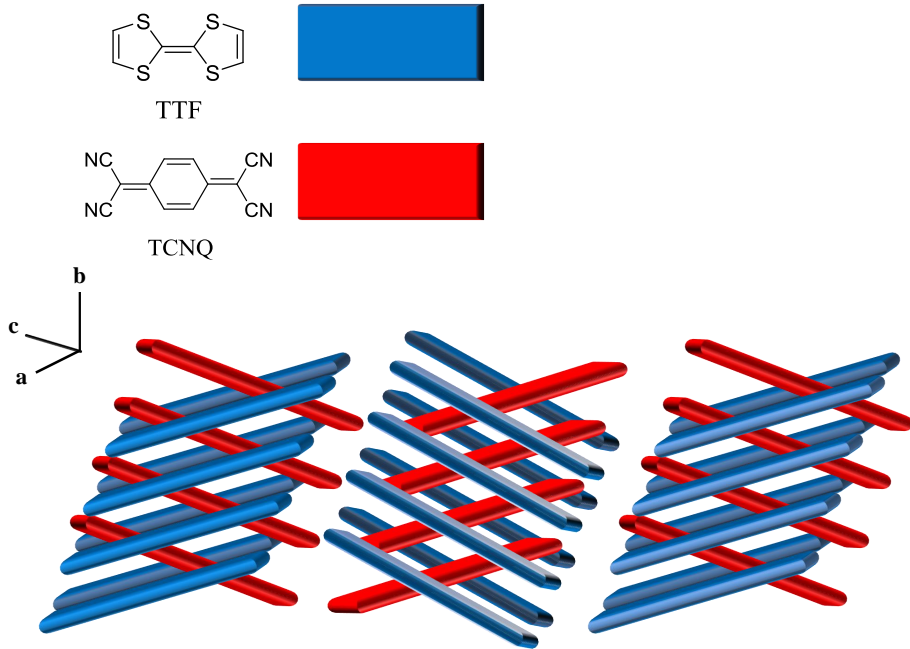


Figure 1.7: The structural formula of 1,4,5,8-tetrathiafulvalene (TTF) and 7,7,8,8-tetracyanoquinodimethane (TCNQ) (on top). A systematic view on the crystal structure with its herring bone pattern of segregated stacks (on bottom).

Since the discovery of (TTF)(TCNQ), a row of new CT compounds and therein new electron donor and electron acceptor molecules have been synthesised. The wealth of literature reflects the strong interest and the innovative capabilities that become possible in the generation of conducting organic solids. Simple modifications of the organic building blocks enable many variations, influencing not merely the crystal structures but also the transport properties, essentially.

Tetracyanoquinodimethane (TCNQ) as one of the most potent π electron acceptors has generated a great deal of interest in organometallic compounds, ion-pair complexes and coordination polymers[41–44]. Hence, polycyano hydrocarbons as tetracyanopyrazine (TCNP) or the polycyano/polynitro substituted aromatic hydrocarbon 2,4,5,7-tetranitro-9-dicyanomethylenefluorene (DTef) display potential electron acceptor functionality (Fig. 1.2).

Tab. 1.1 contains a limited selection of CT solids having one of the three electron acceptors TCNQ, TCNP and DTef, as a constituent. The ratio of donor to acceptor ($D:A$), the crystal packing and electronic properties are included.

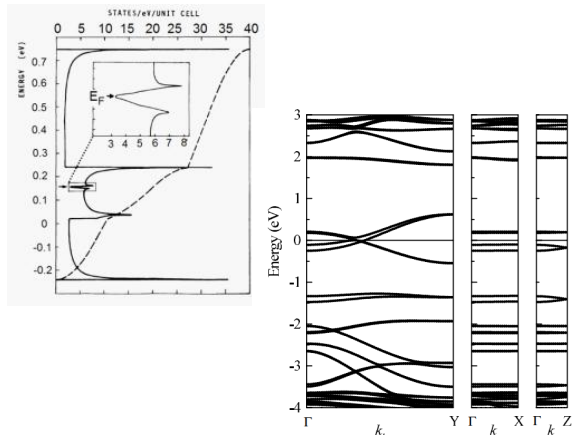


Figure 1.8: (TTF)(TCNQ): The density of states from ref [40] (top left) and electronic band structure at 100 K with GGA(PBE) from ref [32] (bottom right).

Table 1.1: Limited selection of charge transfer salts obtained by organic donor (*D*) and the acceptor (*A*) molecules TCNQ, TCNP and DTeF, as a constituent. Their *D:A* ratios, the main structural features as the electrical properties are presented. ^a : σ_{RT} in Scm^{-1} .

donor (<i>D</i>)	acceptor (<i>A</i>)	<i>D:A</i>	crystal packing	electrical properties ^a	ref
TTF	TCNQ	1:1	equidistant segregated stacks; herringbone motif	200–600	[26]
HMTTF	TCNQ	1:1	equidistant segregated stacks; herringbone motif	300–400	[45, 46]
TMTSeF	TCNQ	1:1	equidistant segregated stacks; herringbone motif	800–1000	[47]
TMTTF	TCNQ	1.3:2	equidistant segregated stacks; herringbone motif	10^3	[46, 48]
ET	TCNQ	1:1 (α)	mixed stacks; herringbone motif	10^{-6} – 10^{-4}	[49]
ET	TCNQ	1:1 (β')	equidistant segregated stacks; herringbone motif	1–100	[50]
ET	TCNQ	1:1 (β'')	segregated stacks; separate layers of <i>D</i> or <i>A</i>	$\geq 10^3$ (20 K)	[51, 52]
pyrene	TCNQ	1:1	mixed stacks; herringbone motif	10^{-12}	[53, 54]
perylene	TCNQ	1:1	mixed stacks; separate layers of <i>D</i> or <i>A</i>	10^{-10} – 10^{-8}	[55–57]
perylene	TCNQ	2:1	mixed stack arrays; inserted <i>D</i> molecules between the stacks	10^{-11} – 10^{-9}	[55–57]
perylene	TCNQ	3:1	mixed stacks with repetitive unit ... <i>ADD...</i> ; additional <i>D</i> molecules located between the stacks	10^{-11} – 10^{-9}	[55–57]
coronene	TCNQ	1:1	mixed stacks; adjacent stacks form a pseudo-hexagonal arrangement	10^{-12} – 10^{-10}	[58]
NMP	TCNQ	2:3	stacks of TCNQ triads; holes are filled with pairs of NMP molecules	0.7	[59]
perylene	TCNP	1:1	mixed stacks; parallel stacks form infinite ribbons alternating of perylene and TCNP	$5.04 \cdot 10^{-9}$	[60]
TTSC	TCNP	1:1	mixed stacks; TTSC form infinite ribbons perpendicular to stacking direction	–	[61]
TTF	DTeF	1:1	mixed stacks; sheets formed by adjacent stacks	–	[62]
HMTTeF	DTeF	3:2	no structure	$2.4 \cdot 10^{-3}$	[63]
BEDOTTF	DTeF	2:1	no structure	18	[64]

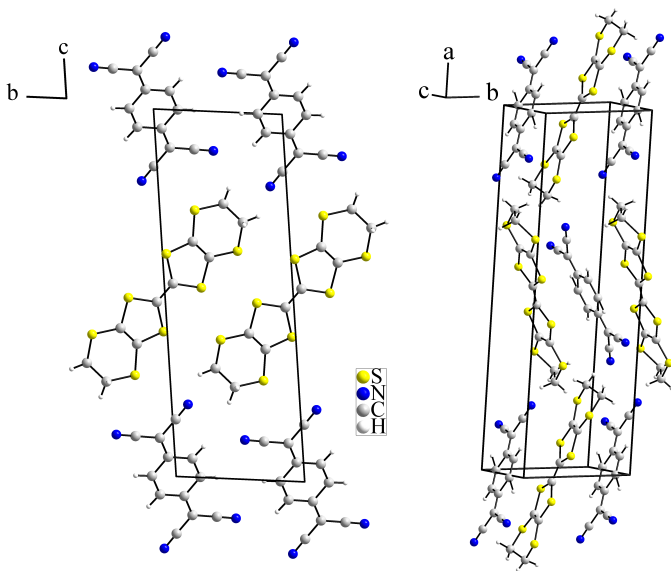


Figure 1.9: Crystal structures of two morphs from the donor ET and the acceptor TCNQ: monoclinic (ET)(TCNQ) (α)[49] in a perspective view (right) and triclinic (ET)(TCNQ) (β'')[51] depicted along the crystallographic a axis (left). The main structural feature of the α form is mixed stacks, whereas the β'' form is dominated by segregated stacks.

not clear[52].

Typical examples for π electron systems, that are able to donate electrons, are polycyclic aromatic hydrocarbons. The reaction of pyrene with TCNQ affords the 1:1 CT salt (pyrene)(TCNQ). Donor and acceptor molecules are slightly tilted against each other and arranged in alternating fashion. The resulting stacks form a herringbone motif in the crystals[53]. The low room temperature specific conductivity σ_{RT} of $10^{-12} \text{ Scm}^{-1}$ indicates predominantly insulating behaviour[54].

By stoichiometric variation between donor and acceptor the charge transfer is tunable. Combining TCNQ with perylene, as donor molecule, affords CT salts in the ratio 1:1, 1:2 and 1:3. The degree of charge transfer in these materials increases from 0.03 to 0.2 parallel to the raising number of perylene molecules in the crystals. (perylene)(TCNQ) is a n -type semiconductor that becomes ambipolar in $(\text{perylene})_2(\text{TCNQ})$ and changes into a p -type semiconductor for $(\text{perylene})_3(\text{TCNQ})$.[55–57]

In the reaction of perylene and the polycyano hydrocarbon tetracyanopyrazine (TCNP) the 1:1 CT salt (perylene)(TCNP) could be obtained that consists of neutral co-crystallised components. The mixed stacked arrays in the crystals lead to nearly insulating

Early investigations of reactions between bis(ethylenedithio)tetrathiafulvalene (ET) with TCNQ discovered different phases of 1:1 CT salts (ET)(TCNQ), a monoclinic form that consists of mixed stacks[49] (Fig. 1.9) and a triclinic form build up by segregated stacks[50]. Below room temperature, the conducting properties of the materials are basically semiconductive.

In 2003 Yamamoto *et al.* found a third morph using tetraiodoethylene (TIE) as catalyst. Apparently, this polymorph has its origin in the nucleation process controlled by TIE and consists of separate layers parallel to the ac plane (Fig. 1.9)[51]. In contrast to the other two polymorphs, this third form exhibits metallic character down to the lowest temperature. Anomalies in the resistivity occur at 175 K, 80 K and 20 K, however, the intrinsic cause is

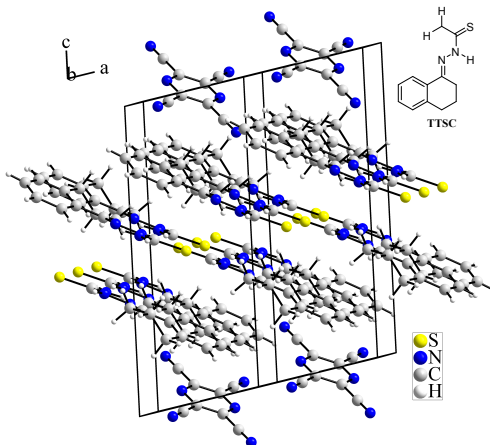


Figure 1.10: The structure formula of 2-(1,2,3,4-tetrahydro-naphthalen-1-ylidene)-hydrazinecarbothioamide (TTSC) (top right) and the unit cell of (TTSC)(TCNP)[61] in a perspective view. Donor and acceptor form mixed stacks. By hydrogen bonding the TTSC molecules create infinite ribbons.

transport properties in the magnitude of 10^{-9} Scm^{-1} .[60]

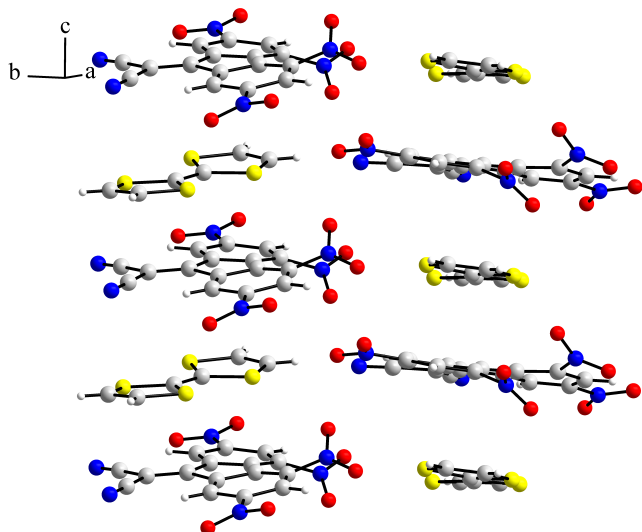


Figure 1.11: The stacks in the crystals of (TTF)(DTeF) in which donor and acceptor molecules are stacked in alternating fashion.

the semiconducting range of $2.4 \cdot 10^{-3} \text{ Scm}^{-1}$ at room temperature[63].

Combination of bis(ethylenedioxy)tetrathiafulvalene (BEDOTTF) and DTeF results in the metallic conductor $(\text{BEDOTTF})_2(\text{DTeF})$ with σ_{RT} of 18 Scm^{-1} [64].

1.1.2 Organic-Inorganic Hybrids

Molecular crystals with dual-functionality as magnetism, such as antiferromagnetism or ferromagnetism in long range order, and conductivity, in the range of semiconductivity to superconducting properties, present an attractive topic for potential application e.g. in spintronics[65–67].

In that context, radical ion salts containing metal complexes as counter part are of particular interest. These organic-inorganic hybrid materials enable bi-functionality by coexistence of extraordinary magnetism and conductivity by π -*d* interactions. Therefore, the design of new dual-function compounds is a key factor in understanding the interplay between spins and electrons. Usually, magnetic phenomena are induced by the *d* electrons of the transition metal in the counter part, whereas the π electron systems of the organic units provide conducting properties[68].

Divalent Cu²⁺ provides an appropriate oxidation potential for converting electron rich molecules with low oxidation potential to the respective radical cation, parallel it is reduced to its monovalent ion, Cu⁺.

In their halides, Cu²⁺/Cu⁺ (d^9/d^{10} electron configuration) have remarkably diverse coordination chemistry and multiple bridging capabilities[69]. A spread variety of discrete, oligomeric and polymeric species have been observed, based on primarily corner or edge sharing planar CuX₃ or tetrahedral CuX₄ (regular or distorted) species[70–74].

The structural and physical properties of several organic-inorganic hybrid compounds, that contain cuprate counter ions, are summarised and shown in Tab. 1.2.

J. Beck *et al.* synthesised a TCNP containing charge transfer compound with 2-(1,2,3,4-tetrahydro-naphthalen-1-ylidene)-hydrazinecarbothioamide (TTSC). The structural parameters indicate co-crystallisation of neutral species, as for (perylene)(TCNP). In the crystal, stacks in alternated fashion are present. By hydrogen bonding, the TTSC molecules generate infinite ribbons perpendicular to the stacking direction (Fig. 1.10).[61]

Tetrathiafulvalene reacts with DTeF to the 1:1 CT salt, (TTF)(DTeF). The structure is made up by stacks alternating of donor and acceptor. Adjacent stacks form sheets linked by different types of weak interactions (Fig. 1.11)[62].

Hexamethylenetetratellurafulvalene (HM-TTeF) and DTeF form a 3:2 CT solid. The black powder shows transport properties in

Table 1.2: Structural and physical properties of organic-inorganic hybrids with cuprate counter anions. ^a: σ_{RT} in Scm^{-1} ; ^b: PM = paramagnetic, AFM = antiferromagnetic, TIP: temperature independent paramagnetism; ^c: anisotropic electrical conductivity.

compound	packing	electrical properties ^a	magnetic properties ^b	ref
(TTF) ₂ [CuCl ₂]	uniform columns of donor	metal-semiconductor transition at 160 K; 50 ^c	TIP	[75, 76]
(TTF) _{7/3} [CuCl ₂]	no structure	10	TIP	[75]
(TTF) _{5/3} [CuBr ₂]	no structure	1.5, $E_a = 0.05$ eV	TIP	[75]
(TTF) _{4/3} [CuCl ₂]	no structure	0.3, $E_a = 0.08$ eV	TIP	[75]
(TTF) ₆ [CuBr ₄]	uniform columns of donor	900 ^c	TIP	[75]
(TMTSF) _{3/2} [CuBr ₂]	no structure	9·10 ⁻² , $E_a = 0.07$ eV	TIP	[75]
(TMTSF) ₂ [CuCl ₂]	no structure	7·10 ⁻⁴ , $E_a = 0.18$ eV	TIP	[75]
(ET) ₂ [CuCl ₂]	stacks of donor pairs; 2D network	3·10 ⁻³ , $E_a = 0.25$ eV	AFM $J = 55 \pm 5$ K	[75, 77]
(ET)[CuCl ₂]	uniform columns; 2D network	–	–	[75, 78]
(ET) _{7/5} [CuBr ₂]	no structure	1.7, $E_a = 0.04$ eV	TIP	[75]
(ET) ₃ [CuBr ₄]	α -stacked layers; planar CuBr ₄ ²⁻	0.25, $E_a = 0.07$ eV	AFM; $C = 2.77 \text{ emuKmol}^{-1}$; $\theta = -140$ K	[79]
(ET) ₃ [CuCl ₄]·H ₂ O	layers of donor trimers; layers of anions	metal	PM	[80]
(ET) ₆ [Cu ₂ Br ₆]	2D network of donor; linear CuBr ₂ ⁻ and square planar CuBr ₄ ²⁻	1.7, $E_a = 0.17$ eV	AFM; $T_N = 7.5$ K, $J = -11.8 \text{ cm}^{-1}$	[81, 82]
(TTMTTF)[CuBr ₄]	nonplanar TTMTTF ²⁺	10 ⁻¹⁰	PM; $\theta = -0.5$ K	[82]

Copper(II) halides react with TTF and its derivatives to highly electron conducting (TTF)_n[CuX₂]⁻ type materials. Several compounds with TTF and its derivatives could be synthesised in reactions with Cu²⁺ salts (X= Br, Cl). It is assumed, that the main structural feature is stacks generated by the donor molecule, however, X-ray crystal structure determination was hardly experimentally possible. Reactions of Cu(II)X₂ with TTF analogues as tetramethyltetraselenafulvalene (TMTSF) and bis(ethylenedithio)tetrathiafulvalene (ET) yielded various new organic-inorganic hybrids. Of particular interest was the (TTF)₂[CuCl₂] exhibiting a quasi-metallic state above 200 K. Electron spin resonance, infrared and X-ray photoelectron studies show partial electron transfer from Cu²⁺ to TTF⁰. The uniform columns of the fractional charged TTF molecules explain the high electron conducting properties of the material. Ambient reaction conditions with copper(II) bromide as oxidant, led to (TTF)_{5/3}[CuBr₂]. The dihalogenido cuprate counter anions are isolated between the donor stacks in the structure as [CuX₂]⁻ (X = Br, Cl) units.[75, 76]

By diffusion, ET reacts with CuCl_2 to a 1:1 salt, $(\text{ET})[\text{CuCl}_2]$. Reflection spectra of the crystals show metallic characteristics in the lower energy region. Thus, the ET molecules have fractional charge resulting in mixed valency of the cuprate anion as Cu(I)Cl_2^- and Cu(II)Cl_2^0 . The donor molecules are arranged in uniform stacks wherein the isolated linear cuprate anion units are located (Fig. 1.12).[78]

By electrocrystallisation, the 1:2 hybrid salt $(\text{ET})_2[\text{CuCl}_2]$ was obtained. The donor molecules are stacked in pairs along the crystallographic c axis. The short $\text{S}\cdots\text{S}$ contacts in the ab plane generate a two-dimensional network. Within the stacks, the shortest $\text{S}\cdots\text{S}$ contacts are much longer. The linear dichlorido cuprate anions are packed in the cavities between the ethylenic hydrogen atoms of the ET molecules.[77]

In the organic conductor $(\text{ET})_6[\text{Cu}_2\text{Br}_6]$, the donor molecules form a two-dimensional network in which charge separation is present. The charge distribution shows neutral ET^0 as well as fractional charged $\text{ET}^{+0.75}$. The anion layers of CuBr_4^{2-} and CuBr_2^- show mixed valency with $\text{Cu}^{2+}/\text{Cu}^+$ [81]. Magnetic susceptibility measurement indicates antiferromagnetic coupling between the Cu^{2+} localised spins and the π electrons of the donor with Néel temperature T_N of 7.5 K and a coupling constant J of -11.8 cm^{-1} . Hence, the cooperation of the transport system and the magnetic system via $\pi-d$ interactions is recognisable[82].

Copper(II) bromide affords a direct twofold oxidation in the reaction with tetra(methylthio)tetraphiafulvalene (TTMTTF). The structure of the TTMTTF^{2+} cation deviates strongly from planarity. The resulting ionic structure explains the low transport properties around $10^{-12} \text{ Scm}^{-1}$. Magnetic susceptibility follows the Curie-Weiss law with a small negative Weiss constant θ of -0.5 K .[82]

N-methylquinoxalinium (MQ) forms with Cu(I)Br the hybrid compound $(\text{MQ})[\text{CuBr}_2]_\infty$. In the structure, the planar donor molecules are antiparallel and equidistantly arranged and the $[\text{CuBr}_2^-]_\infty$ anions build one-dimensional chains of edge-sharing CuBr_4 tetrahedra running parallel to the donor stacks (Fig. 1.13). Magnetic susceptibility demonstrates the mainly diamagnetic nature of the compound, however, a low temperature paramagnetic effect suggests low amounts of divalent Cu^{2+} . The presence of a substantial charge transfer is still controversial and under discussion. Anisotropic single crystal conductivity measurements show low transport properties in the range of 10^{-9} Scm^{-1} at room temperature and a band gap of 1.3 eV.[83]

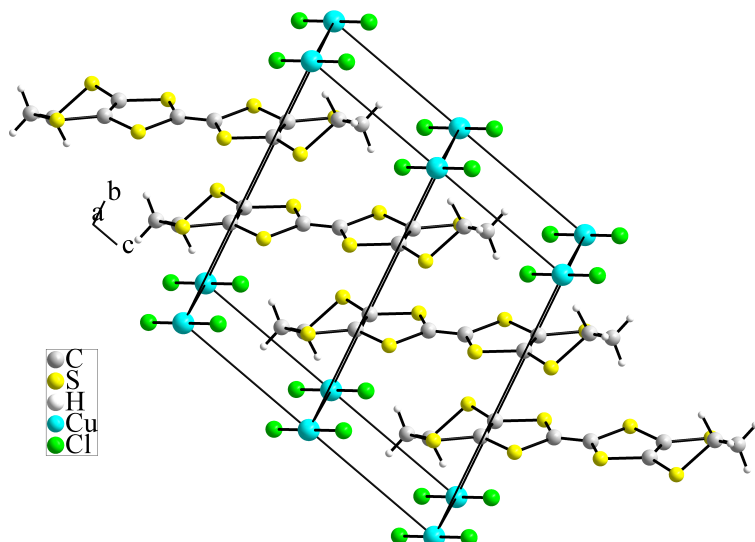


Figure 1.12: Crystal structure of the 1:1 organic-inorganic hybrid $(\text{ET})[\text{CuCl}_2]$ [78]. Fractionally charged ET molecules are arranged in uniform stacks. The dichlorido cuprate anions lie isolated between the cation stacks.

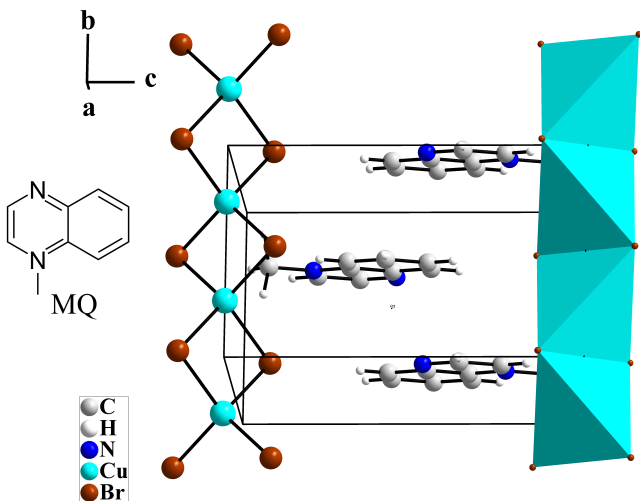


Figure 1.13: The molecular structure of *N*-methylquinoxalinium (MQ) and the unit cell of $(\text{MQ})[\text{CuBr}_2]_\infty$ [83] in a perspective view. The one-dimensional chains of edge-sharing CuBr_4 and the oblique stacks generated by the MQ molecules.

Even though, the electrical current is carried by the organic donor molecules, the cuprate counter ions display an important role in the production of current carriers into the donor lattice. Therefore, the application of copper(II) halogenides as oxidants initiated the design of various types of conducting salts, especially, in combination with organic donor molecules derived from TTF.

Summarising, a huge number of charge transfer salts and organic-inorganic hybrid solids with exotic and interesting electrical properties have been found. Notwithstanding, prediction of conducting properties of these compounds is challenging and therefore the choice of a promising class of organic donor molecules.

1.1.3 Polymorphism in Organic Solids

The design of materials with specific properties represents one of the most challenging goal of chemists. The understanding of the structure-property relationship display therein an important key factor. Especially, for organic molecules systematic variation is possible by mode and type of substitution. Oftentimes, types of substituents influence the spatial arrangement and therefore the crystal packing.

The occurrence of different modifications of a solid with the same chemical composition is termed polymorphism. In polymorphs the only deviating parameter is the structure. Hence, they are prone for investigations of the structure-property relationship since property differences are caused by structure variation[84].

Initially, the phenomenon of polymorphism was discovered by Mitscherlich[85]. A widely quoted statement by McCrone[86] is reported as follows: "Virtually all compounds dare polymorphic and the number of polymorphs of a material depends on the amount of time and money spent in research on that compound". Prediction of crystal structure of organic materials with any level of confidence is still unfeasible. Systematic research of polymorphs in solid states should involve a broad variety of techniques and conditions for growing crystals. Unfortunately, crystal growth conditions can be combined and ranged infinitely.

Usually, properties of organic materials are considered in terms of molecular structure, since most of chemistry was carried out in solution. Thus, molecules interact or react in pairwise fashion. In contrast, solid state properties in organic materials, caused by three-body interactions, enabled a wealth of opportunities in designing and application. Therefore the role of the solid state interactions can be investigated excellently regarding polymorphic forms. Moreover, energetic relationships between the modifications can be investigated and provide insights in the required conditions for crystal growth.

The discovery of polymorphic 1:1 compounds consisting of tetramethyltetraselenfulvalene (TMTSF) and tetracyanoquinodimethane (TCNQ) gives a proof of the relative stability of mixed and segregated stacks. Since the red, transparent crystals, made up of mixed stacks show semiconducting behaviour, the black and opaque crystals, build up by segregated stacks, are conductors. The red semiconducting morph is the thermodynamically stable form and can be obtained by slow evaporation of a mixture of equimolar solutions of donor and acceptor. Mixing of hot equimolar solutions of donor and acceptor in acetonitrile and subsequent rapid cool-down enable formation of the black crystals that present the kinetically stable form. This explicit example shows well the strong structure-property relationship as the highly conducting morph exhibits the necessity of segregated stacks, whereas the mixed stacks in the other morph reaches only semiconducting transport properties.[87, 88]

1.2 Organic Donor Molecules

A prominent example for an electron donor molecule represents the above-mentioned TTF which undergoes oxidation to a stable radical at a potential of +0.35 V vs. Ag/AgCl[89]. The radical cation shows remarkably high stability due to its aromatic character[90]. This discovery led to an explosion of generation of TTF-derived materials that subsequently got components of organic metals and even though organic superconductors. Modifications of TTF as substitutions of the peripheral hydrogen atoms and exchange of the sulfur atoms by selenium[91, 92] or tellurium[93, 94] enabled the synthesis of numerous appropriate electron donor compounds.

Already in the 1960s S. Hünig *et. al* investigated organic molecular two-stage redox systems among them the symmetric heterocyclic azines[95–97]. Bis(*N*-methylpyridone)azine (MPA, **1**) as the basic scaffold of this class of compounds is formed in a reaction of *N*-methyl-2-halogeno-pyridinium salt with hydrazine. By sublimation, red prismatic crystals of MPA are accessible. X-ray single crystal analysis shows an unusual molecular arrangement. Three nearly equal, but symmetrically independent MPA molecules form a pseudo-trigonal structure in the crystals (Fig. 1.15).[98]

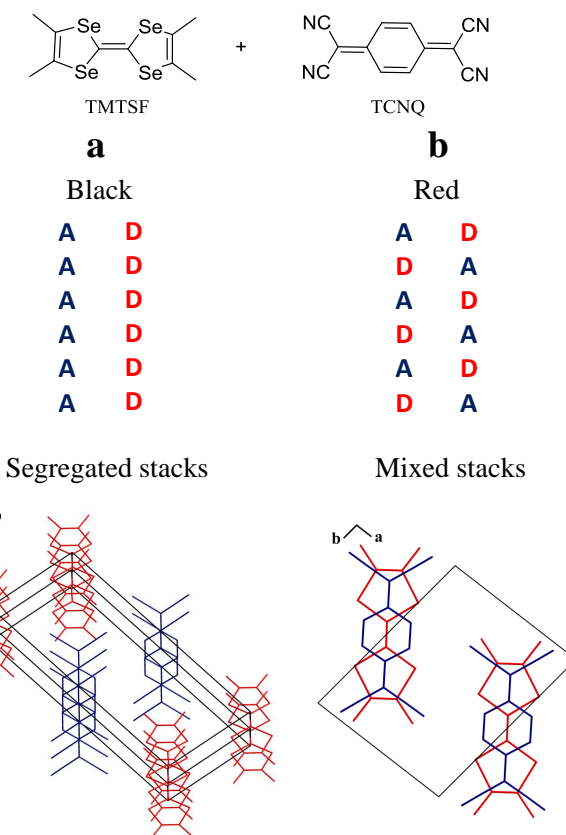


Figure 1.14: The polymorphic 1:1 compounds consisting of TMTSF and TCNQ[87, 88]. The black crystals made up by segregated stacks, (**a**) and the red crystals build up by mixed stacks, (**b**). The molecules are presented as wires, the donor in red and the acceptor in blue.

MPA is highly electron rich and easily oxidisable in two reversible consecutive oxidation processes. In the first one-electron oxidation step the radical cation MPA^+ and in the second one-electron oxidation step the dication MPA^{2+} , an azo-bis(*N*-methyl-2,2'-pyridinium) cation, are obtained. The two processes are well separated with a large potential difference of $\Delta E = 0.5 \text{ V}$ (Fig. 1.16). The electronic doublet state of the radical cations has found to be persistent in solid as well as in solution[99].

An explicit criteria for determining the predominant oxidation state 0, +1 or +2 of this pyridone azine constitutes the bond lengths relations in the central CNNC moiety. In the neutral state the N–N bond length amounts to 1.41 Å and the C–N bonds to 1.31 Å in average matching to $-\text{C}=\text{N}=\text{N}=\text{C}-$ bond characters.

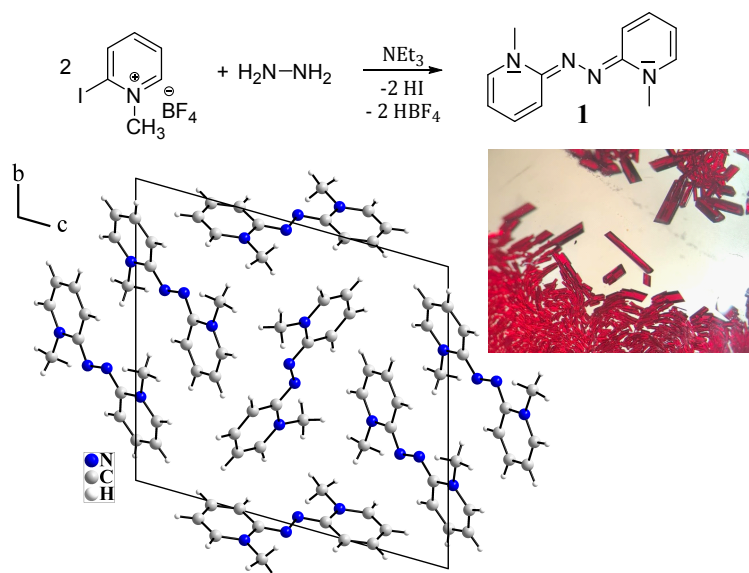


Figure 1.15: Synthesis route to bis(*N*-methylpyridone)azine (MPA) **1**, the red prismatic crystals and the peculiar crystal structure containing three symmetrically independent MPA molecules[98].

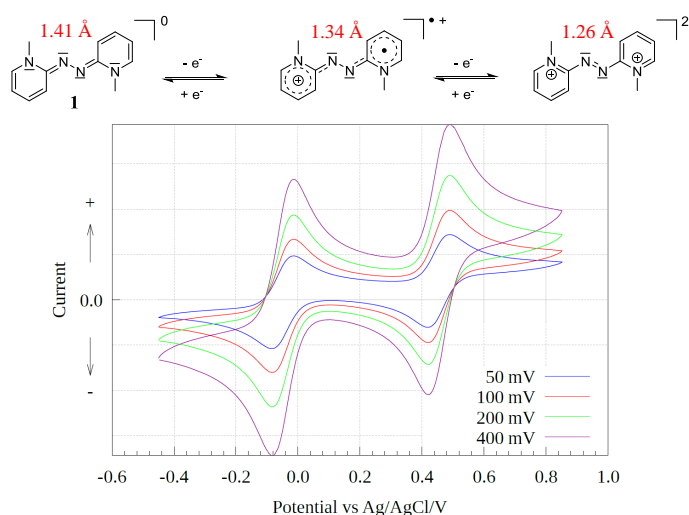


Figure 1.16: The two-stage redox system of MPA. The two oxidation steps of **1** to the radical cation MPA^+ and the azo-bis(*N*-methyl-2,2'-pyridinium) dication MPA^{2+} . Cyclic voltammogram of the compound showing the full reversibility of the two one-electron oxidation processes at potentials $E_1 = -0.05 \text{ V}$ and $E_2 = +0.45 \text{ V}$ vs. Ag/AgCl.

general, MPA in oxidation state zero is red, in the radical state dark violet and the dication state light red. However, colourfulness is an inadequate indicator due to fact that additional charge transfer

In respect to that in the radical cation species the N–N bond is substantially shortened to around 1.34 Å and ranges in between a N–N single and a N=N double bond[37]. Coincidentally, the C–N bonds are elongated to around 1.35 Å. The equality of the bonds in the central CNNC moiety mirrors the electron delocalisation over the whole molecule in the radical state. In the oxidation state +2, a distinct bond length alteration is observed compared to the neutral species. The central N–N bond is shortened to 1.26 Å, whereas the C–N bonds are elongated to 1.41 Å. Thus, an inverted order of single and double bond ($-\text{C}=\text{N}=\text{N}=\text{C}-$) in the azo-bis(*N*-methyl-2,2'-pyridinium) $^{2+}$ is present.[98]

Since electronic charge transfer reactions lead to intense colours, consideration might be a sufficient criteria to differ between the three states. In

processes can occur and the anion could influence the light absorption.

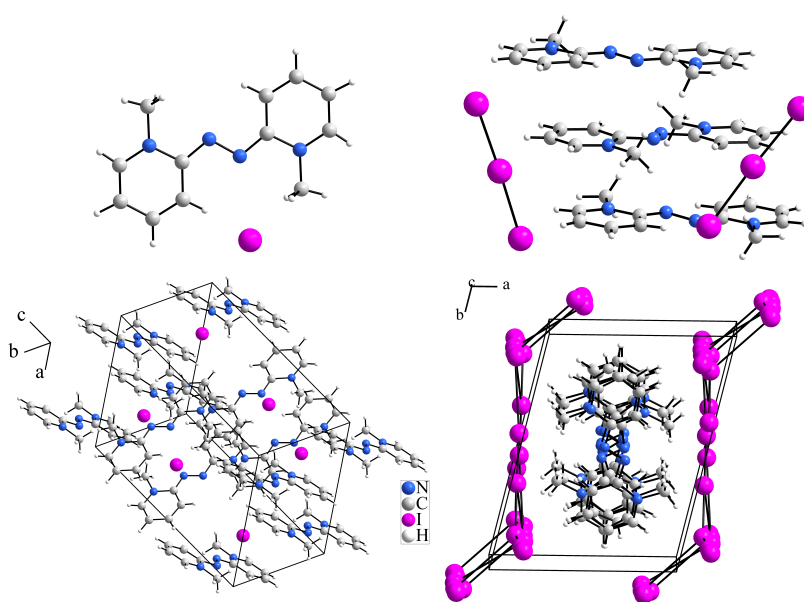


Figure 1.17: The building units and the crystals structures of the two radical cation salts obtained in the reaction of MPA with iodine, (MPA)I (left) and (MPA)[I₃] (right).

fragments overlap hardly. In (MPA)[I₃], linear triiodide [I₃]⁻ molecules are present. However, a distinct Peierls distortion leads to dimeric aggregates in the stacks.[101]

By electrocrystallisation experiments of MPA and the conducting salt NBu₄[Mo₆Cl₁₄], the 2:1 salt (MPA)₂[Mo₆Cl₁₄] is obtained. The large chlorido molybdenum cluster, [Mo₆Cl₁₄]²⁻, functions as weakly coordinating as well as weakly basic ligand, supporting the formation of radical cation stacks in the crystal. Due to the two negative charges of the cluster, MPA is present in their radical cation state, even underlined by the bond lengths of the central CNNC moiety. The MPA⁺ molecules form step-like stacks that are separated by the sterically demanding [Mo₆Cl₁₄]²⁻ clusters.[102]

As shown in the chapters before, the amount of already published CT and organic-inorganic hybrid solids is highly large. Especially, materials with TTF based donor molecules have been paid much attention. However, the pyridone azines possess similar electronic and structural properties, the number of publications is relatively limited. Therefore, the generation of new charge transfer and organic-inorganic hybrid solids with MPA and its derivatives as organic donor molecules were the motivation for this work. This thesis deals with the experimental results of reactions between the pyridone azines with copper(II) halogenides and organic acceptor molecules such as TCNQ. Determination of the crystal structures by X-ray diffraction and investigations of the physical properties will allow for insights concerning the magnetic and the transport properties and therefore enable to set up structure-property relationships.

Since their discovery, pyridone azines and their derivatives found little attraction for further studies. Only, the conversions to oligomeric azines and the respective oligoradical ion were reported[100].

J. Beck synthesised compounds containing MPA with sterically less demanding counter parts[101]. In reactions with iodine, the radical cation salts (MPA)I and (MPA)[I₃] are obtained. In the former case, isolated iodine atoms and a brick wall pattern of the MPA⁺ radicals are present. Minor intermolecular interactions are assumed since the aromatic and radical cation stacks are

CHAPTER 2

Analytical Methods

2.1 X-Ray Single Crystal Diffraction

Suitable crystals of the samples were selected and glued to a glass fibre via perfluorinated immersion oil (NVH). The crystals were fixed on a goniometer head for insertion into a cold nitrogen gas flow. The diffractometer used was a “Bruker” Nonius κ -CCD four circle diffractometer featured with a molybdenum X-ray source. The monochromator was a graphite single crystal supplying monochromatised Mo-K α radiation with a wavelength of $\lambda = 0.71031 \text{ \AA}$. The detector was a CCD area detector with a diameter of 95 mm. Data collection was performed with the program COLLECT[103]. The unit cells were determined by HKL scale-package and data integration and reduction were made using the program HKL-Denzo[104]. Semi-empirical absorption corrections were performed by multi-scan. For the structure solutions and refinements the SHELX program suite[105] was used. The program DIAMOND 4.6.5[106] was used for the visualisation of the crystal structures. The displacement ellipsoids of the crystal structures presented in this work are generally scaled to a probability of 50 %, except the hydrogen atoms, which are drawn as spheres of arbitrarily chosen radii.

2.2 X-Ray Powder Diffraction

Samples for X-ray powder diffraction were prepared in two different ways depending on the crystal form. Compounds crystallising in very fine needles or hairs were filled into glass capillaries (wall thickness: 1.0 mm). Therefore the thin needles or hairs were carefully stuffed into the capillaries that were sealed by a hot filament. For compounds crystallising in isometric crystals, the crystals were placed between two thin Mylar foils. The crystals were placed into the corresponding sample holders without any further processing to minimise texture effects. Therefore, some orientations of the crystals are over-presented or respectively others under-presented leading to systematic errors in the recorded intensities. Nonetheless, identification of the samples was possible by comparison using the crystal data obtained by X-ray single crystal diffraction. The powder diffractometer used was a STADI P from company STOE (Darmstadt) equipped with a cobalt X-ray source (PANalytical, Almelo, NL) and a germanium (111)monochromator (Co-K α 1 wavelength of $\lambda = 1.78896 \text{ \AA}$). The diffractometer was equipped with two different position sensitive detectors (PSD), one with a smaller (opening angle of $2\theta = 4^\circ$) and a larger (opening angle of $2\theta = 35^\circ$) position sensitive detector (PSD, STOE, Darmstadt). The software suite *Win XPow*[107] was used to control the diffractometer and to examine and process the collected data. Data analyses were performed with MATCH[108].

2.3 Energy Dispersive X-Ray Spectroscopy (EDX)

For several organic-inorganic solids the Cu:Br ratio was examined by energy dispersive X-ray spectroscopy. The setup consisted a scanning electron microscope (Hitachi SU3800) that was equipped with an electron detector (EDAX EDS System *Octane Elect Super EDS*) for quantitative analysis. Measurement samples were prepared onto an aluminium sample holder that was laminated with a conducting graphite foil to keep the sample from statically charging itself. The accelerating voltage for all quantitative measurements was 10 kV. Quantitative analysis was done with the software EDAX APEX Advanced (EDAX).

2.4 Cyclic Voltammetry

The redox behaviour of the pyridone azines was investigated by cyclic voltammetry. A three-electrode setup was used. Distilled acetonitrile was used as solvent and tetrabutylammonium hexafluorophosphate, NBu_4PF_6 , as conducting salt to enhance the electrical conductivity of the solution. As working and counter electrode (WE and CE), platinum electrodes were used. The applied voltage between WE and CE was varied at four different scan rates (50, 100, 200 and 400 mV/s). As reference a Pt wire electrode in addition with the internal standard Fc/Fc^+ [109] was used. In the following, the potentials were referenced to the potential of an Ag/AgCl electrode. Control of the measurements were performed via a potentiostat/galvanostat (μ Autolab Type III, Metrohm Corp.). All measurements were performed under inert gas atmosphere to avoid the formation of undesired intermediates during process.

Information accessible from the signals in the cyclic voltammogram are: the position of oxidation or reduction and the reversibility of the redox process. Determination of the redox potentials was carried out by regarding the half-wave potentials $E_{1/2}$. The redox process proceeds reversibly if the half-wave potential is constant and independent from the used scan rate, the peak current of forward and back reaction are evenly large and the differences in the peak voltages (maxima) are approximately 57 mV[110]. Referred to the last, for inhibited charge transfer the condition is not fulfilled. For that case, the measurement performed by the smallest scan rate was taken into account.

2.5 Conductivity Measurement

In a two-point measurement setup the electrical conductivities of the samples were measured using a Keithley 2400 SourceMeter. The substances, in form of powder, were compressed in a quartz tube of 2 mm inner diameter between two gold plated steel pistons. By applying constant voltage of 0.8 V or alternatively constant current, the electrical resistances in dependence of temperature of the samples were detected. Temperature control was ensured by a PT100 thermo couple. The specific conductivities could be determined by taking the thickness of the respective samples into account. In case of semiconductors and insulators, application of the Arrhenius equation 2.1 allows estimation of the band gap.

$$-\ln(R^{-1}) \propto \frac{\Delta E}{2k_B} \cdot T^{-1} \quad (2.1)$$

with R: resistance, ΔE : activation energy, k_B : Boltzmann constant.

The slope of the linear plot corresponds to the activation energy needed to overcome the band gap. The band gap itself can be expected to be close to this activation energy.

$$\Delta E = 2k_B \cdot m \quad (2.2)$$

with m: slope.

2.6 Magnetic Susceptibility Measurement

In general, the magnetic moment of atoms or ions is determined by the angular momentum of the electron spins. Strong magnetic behaviour is expected for unpaired electrons. A magnetic field might lead to a specific orientation of the spins. The change in the magnetic field indicates the present magnetic properties of a sample in the field. In case of an enhanced magnetic field, the corresponding material is paramagnetic. Paramagnetic compounds contain unpaired electrons. The distribution and interactions of the electron spins lead to different magnetic effects. Diamagnetism is an intrinsic property of any substance and is associated with fully occupied orbitals of atoms or ions. Therefore, experimental obtained magnetic susceptibilities consist of diamagnetic and paramagnetic contribution (Eq. 2.3).

$$\chi_{exp} = \chi_{dia} + \chi_{para} \quad (2.3)$$

with χ_{exp} : experimental magnetic susceptibility, χ_{dia} : diamagnetic susceptibility, χ_{para} : paramagnetic susceptibility. Application of the reciprocal paramagnetic susceptibility vs. temperature allows the determination of the magnetic moment:

$$\frac{1}{\chi_{para}} = \frac{1}{C} \cdot T \quad (2.4)$$

with T: temperature, C: Curie constant.

The magnetic moment μ of an ion or molecule bearing unpaired electrons can approximately be estimated by the spin-only equation:

$$C = \sqrt{2.828} \cdot \mu_B \quad (2.5)$$

The spin-only equation is applicable for main group radicals and first row transition metal ions, where orbit moments and spin-orbit couplings are suppressed by the ligand field.

The magnetic susceptibilities of the samples were measured with a Quantum design *PPMS* vibrating sample magnetometer (VSM). The samples quantity ranged between 1.5 mg to 10 mg. Usually, the experiments were performed in the temperature range of 1.9 K to 300 K by an applied magnetic field of 1 Tesla. The raw data were corrected by a capsule correction as well as an incremental diamagnetic correction. To estimate these increments, either Eq. 2.6 or the Pascal's rule were used[111].

$$\chi_{dia} = \frac{MW}{2} \times 10^{-6} \text{cm}^3 \text{mol}^{-1} \quad (2.6)$$

with MW: molecular weight.

2.7 Differential Scanning Calorimetry

Thermal processes of solids, e.g. phase transitions, were investigated by differential scanning calorimetry (DSC). The samples were filled into aluminium (Al) pans and were tightly closed. An

empty Al pan was used as reference. The pans were examined in a specific temperature range and the temperature difference of sample and reference was detected. The DSC 204 F1 thermal analyser of Netzsch was used as setup.

Broad differences between sample and reference indicate thermal processes proceeding by exothermic or endothermic conditions. Position of the signal shows the temperature at which the effect occurs. By integration of the signal area, the amount of transferred energy can be calculated.

2.8 Computational Details

All of the *ab initio* calculations in this work were performed using the CRYSTAL17[112, 113] program package (version 1.0.2). Hybrid density functional theory (DFT) with dispersion correction and basis sets based on linear combination of atomic orbitals were used. For both geometry optimisation and electronic properties, the global hybrid functional PW1PW[114, 115] was used in combination with the Grimme D3 dispersion correction with Becke-Johnson damping[116, 117]. All-electron Gaussian type basis sets, rev2-pob-TVZP[118, 119], of triple-zeta quality including polarisation were employed.

For the geometry optimisation, only the positions of the H atoms were optimised employing the FRAGMENT keyword. In the SCF procedure, 75% of the previous Kohn-Sham-Matrix were considered by setting FMIXING to 75. The respective Monkhorst-Pack grids for the partial geometry optimisations are summarised in Tab. A.83 in the appendix. The truncation criteria for bi-electronic integrals were set to 10^{-7} for the overlap and penetration threshold for Coulomb integrals and for the overlap threshold for HF exchange integrals. For the pseudo overlap in the HF exchange series, the truncation criteria were set to 10^{-7} and 10^{-14} (TOLINTEG 7 7 7 7 14).

Different open- and closed shell spin states were investigated by setting the total magnetic moment via SPINLOCK as well as setting individual up- and downspins through ATOMSPIN. All compounds were calculated with restricted Kohn-Sham for non-magnetic (NM) and unrestricted Kohn-Sham for ferromagnetic (FM) and different antiferromagnetic (AFM1, AFM2) spin states. The respective spin distributions are presented in the corresponding chapters.

Before setting the spin in the periodic bulk calculations, each substrate was calculated as an individual molecule. The molecular structures were generated by molden[120] and optimised in CRYSTAL with the previously described settings. Each molecule was calculated in a neutral state or as a radical cation/anion. For atoms that have spin densities about 0.2 up- and downspins were set individually.

AFM spin states were achieved by setting anti-parallel spins (ATOMSPIN) and locking the total magnetic momentum to zero (SPINLOCK). Differing spins on symmetry equivalent atoms were achieved by applying MODISYMM beforehand. Spin states with an energy difference of less than 10 kJ/mol per formula unit were considered degenerate. For degenerate spin states, the simplest spin distribution, NM or FM was chosen for subsequent analyses.

For calculations of the electronic properties, the Monkhorst-Pack grid was increased to an uniform grid of $16 \times 16 \times 16$. In order to cover all special points in the band structure calculations, the κ -path was chosen according to the recommendations by Hinuma *et al.*[121]. The directional electrical conductivity ($3 \times 3 \times 3$ tensor) was estimated using the Boltzmann transport equation as implemented by BOLZTRA[113] in CRYSTAL17.

The relaxation parameter was set to $\tau = 1$. The temperature was set to 298 K, room temperature, for all compounds and, for those that were experimentally accessible at low temperature, to 123 K. Due to the anisotropy of the electrical conductivity, the contribution of the respective corresponding stacking direction should be the highest. The small off-diagonal elements are neglected.

Charge transfer was approximated by the total atomic charges obtained via Mulliken population analysis.

2.9 Synthesis

(1)[CuCl₂]

12.3 mg (0.057 mmol) of **1** and 9.7 mg (0.057 mmol) of CuCl₂·2H₂O were dissolved in about 4 mL acetonitrile under slight heating. The yellow color of the copper chloride solution reveals replacement of water ligands from copper ion by nitrile ligands. Slow addition of the copper chloride solution to the orange solution of **1** led to a color change into dark violet and a dark solid precipitated immediately. After one day, dark violet crystals of unspecific shape were formed. These were filtered and washed with about 50 mL acetone. Recrystallisation in dichloromethane led to dark violet crystal needles. Yield approx. 60 %. Melting point: 180–181 °C. Analysis for C₁₂H₁₄N₄CuCl₂: calc. C 41.29, H 4.01, N 16.06, found C 41.63, H 3.73, N 16.05.

(1)[CuBr₂]

9.8 mg (0.046 mmol) of **1** and 10.2 mg (0.046 mmol) CuBr₂ were solved in about 4 mL acetonitrile while slightly heated. The CuBr₂ solution achieved an intensive green colour. Drop-wisely the copper bromide solution was added to the azine solution of **1**. A colour change into dark violet and an immediate precipitation of dark crystals were observed. The crystals were filtered and washed three times with about 10 mL ethanol. Recrystallisation in dichloromethane led to dark violet needles, finally. Yield approx. 75 %. Melting point: 182–183 °C. Analysis for C₁₂H₁₄N₄CuBr₂: calc. C 32.91, H 3.20, N 12.80, found C 33.50, H 3.35, N 13.08.

(8)[CuBr₂]

10 mg (0.029 mmol) of **8** and 6.38 mg (0.029 mmol) of CuBr₂ were solved in about 4 mL acetonitrile, separately. To the red solution of **8**, the copper bromide solution was added drop-wisely. An immediate colour change into dark violet could be observed as well as a precipitation of a solid. The dark needle-shaped crystal were filtered and washed with about two portions of 10 mL hot water and then five portions of 10 mL ethanol. Yield approx. 50 %. Melting point: 205 °C. Analysis for C₁₄H₁₂N₄F₆CuBr₂: calc. C 29.29, H 2.09, N 9.76, found C 29.02, H 2.39, N 8.83.

(1)[Cu₂Br₄]

25 mg (0.057 mmol) of the radical cation salt **(1)**[CuBr₂] was solved in 5 mL acetonitrile resulting in dark violet solution. A dark green concentrated solution of 12.8 mg CuBr₂ (1 equiv., 0.057 mmol) in acetonitrile was added to the radical cation solution. The mixture was heated to reflux for 15 min and subsequent was cooled down slowly to ambient temperature. Fine violet to black crystalline precipitation of **(1)**[Cu₂Br₄] was obtained and further filtered and washed with two portions of 5 mL acetonitrile. Yield approx. 80 %. Melting point: 250 °C. Analysis for C₁₂H₁₄N₄Cu₂Br₄: calc. C 21.81, H 2.13, N 8.48, found C 22.21, H 2.21, N 8.39.

α-(2)[Cu₂Br₄]

40 mg (0.187 mmol) of **2** were solved in hot 5 mL acetonitrile. 41.7 mg (0.187 mmol) CuBr₂ were solved in a few mL acetonitrile providing a dark green solution. To that solution 1.8 mL (1 equiv., 0.187 mmol) of Br₂ were added. A colour change from dark green to yellow happened. Under cooling, the CuBr₂/Br₂ solution was added to the azine solution drop-wisely. The precipitation of a black solid could be observed. The precipitate was washed with two portions of about 5 mL acetonitrile. After removal of solvent from the filtrate the dark needle-shaped crystals of *α*-(2)[Cu₂Br₄] were obtained. Yield approx. 40 %. Melting point: 220–221 °C. Analysis for C₁₂H₁₄N₄Cu₂Br₄: calc. C 21.81, H 2.13, N 8.48, found C 22.18, H 2.91, N 9.46.

β-(2)[Cu₂Br₄]·CH₃CN and (2)[CuBr₃]

Equimolar amounts of **2** and CuBr₂ were solved in about 5 mL acetonitrile, separately. The dark green CuBr₂ solution was added drop-wisely leading to an immediate colour change into dark violet. By quick removal of solvent, the formation of crystals in form of dark violet plates, rods and needles could be observed. The reaction led to a multi-phase system. X-ray single crystal determination identified the plates as β-(2)[Cu₂Br₄]·CH₃CN, the rods as (2)[CuBr₃] and the needles as (2)[CuBr₄]. By EDX the different Cu:Br ratios in the crystals could be validated.

(2)[CuBr₄]

40.0 mg (0.187 mmol) of **2** were solved in about 3 mL of acetonitrile. An equimolar amount of Br₂ (29.8 mg, 0.187 mmol) was added to a CuBr₂ (1 equiv, 0.187 mmol) solution that was prepared from 41.7 mg CuBr₂ dissolved in about 5 mL acetonitrile. Addition of the CuBr₂/Br₂ mixture to the azine solution led to colour change from red to violet to nearly black and the precipitation of a solid. Subsequently, the mixture was treated slightly with heat. Removal of solvent led to the precipitation of dark red-shining needles, (2)[CuBr₄]. Yield approx. 50 %. Melting point: 225–226 °C. Analysis for C₁₂H₁₄N₄CuBr₄: calc. C 24.31, H 2.36, N 9.38, found C 23.51, H 2.50, N 8.53.

(8)[CuBr₄]

48.0 mg (0.137 mmol) of **8** were dissolved in 5 mL acetonitrile. As in the reaction of *α*-(2)[Cu₂Br₄], equimolar amounts of Br₂ (22 mg, 0.137 mmol) were added to the CuBr₂ (1 equiv, 0.137 mmol) solution that was prepared from 30.06 mg CuBr₂ solved in 5 mL acetonitrile. Addition of the CuBr₂/Br₂ mixture to the azine solution led to colour change from red to violet to nearly black, however, precipitation of a solid could not be observed. Subsequently, the mixture was treated slightly with heat. Partial removal of solvent led to the precipitation of black, needle-shaped crystals.

(8)[CuBr₄] was obtained after filtration of the remaining solvent. Yield approx. 60 %. Melting point: 218–219 °C. Analysis for C₁₄H₁₂N₄F₆CuBr₄: calc. C 22.93, H 1.65, N 7.64, found C 23.26, H 1.94, N 7.60.

***α*-(1)(TCNQ)**

20.0 mg (0.093 mmol) of **1** and 19.1 mg (0.093 mmol) of TCNQ were solved in about 5 mL acetone, separately. Subsequently, the TCNQ solution was added drop-wisely to the azine solution. After filtration, dark rod-shaped crystals were received. Yield approx. 60 %. Melting point: 210–212 °C. Analysis for C₂₄H₁₈N₈: calc. C 68.90, H 4.34, N 26.78, found C 68.30, H 4.52, N 26.27.

***α*-(2)(TCNQ)**

20.0 mg (0.093 mmol) of **2** and 19.1 mg (0.093 mmol) of TCNQ were solved in about 5 mL acetonitrile separately. Both solutions were combined leading to an immediate colour change. Subsequently the mixture was heated to about 35 °C. Fast removal of solvent led to tiny plate-shaped greenish shining crystals were obtained. Yield approx. 50 %. Melting point: < 300 °C. Analysis for C₂₄H₁₈N₈: calc. C 68.90, H 4.34, N 26.78, found C 69.87, H 3.92, N 25.58.

***β*-(2)(TCNQ)**

20.0 mg (0.093 mmol) of **2** and 19.1 mg (0.093 mmol) of TCNQ were solved in about 5 mL acetonitrile separately. Both solutions are cooled down to about –20 °C, subsequently, the slight green TCNQ solution was added drop-wisely to the azine solution. A colour change into dark green blueish could be observed, immediately, and further the precipitation of a solid. After filtration, dark rod-shaped crystals were received. Yield approx. 70 %. Melting point: 188 °C. Analysis for C₂₄H₁₈N₈: calc. C 68.90, H 4.34, N 26.78, found C 68.23, H 4.42, N 26.44.

(3)(TCNQ)

20.0 mg (0.061 mmol) of **3**, and 12.5 mg (0.061 mmol) of TCNQ were dissolved in about 3 mL acetonitrile. To the orange azine solution, the TCNQ solution was added slowly. An immediate colour change into dark violet could be observed and the precipitation of a solid. The suspension was stored for two days. By slow removal of the solvent, needle-shaped metallic shining crystals were obtained. These were washed with about 50 mL ethanol. Yield approx. 50 %. Melting point: 199 °C. Analysis for C₃₂H₃₄N₈: calc. C 72.37, H 6.41, N 21.11, found C 70.78, H 6.56, N 19.84.

(4)(TCNQ)

20.0 mg (0.065 mmol) of **4** and 13.3 mg (0.065 mmol) TCNQ were dissolved in about 3 mL acetonitrile. Under cooling, the TCNQ solution was added slowly to the dark orange solution of **4**. An immediate colour change into dark blue greenish could be observed in combination with the precipitation of a solid. Filtration and subsequent washing with three portions of 5 mL ethanol led to thin dark blue greenish shining needles. Yield approx. 50 %. Melting point: 224 °C. Analysis for C₂₆H₂₂N₈S₂: calc. C 61.11, H 4.31, N 21.94, S 12.56, found C 60.75, H 4.37, N 21.80, S 12.52.

(7)(TCNQ)

In the reaction of **7** with TCNQ in acetonitrile, two different kinds of crystals in form of cuboids and needles could be observed. X-ray single crystal determination showed the formation of a 1:1 CT salt, **(7)(TCNQ)**, and a 1:2 CT salt, **(7)(TCNQ)₂**. CHNS analyses of several charges underlined that the 1:2 CT salt is the main product in that reaction, whereas the 1:1 CT salt the side phase. X-ray powder diffraction of hand selected needle-shaped crystal could validate the presence of **(7)(TCNQ)**. Pure **(7)(TCNQ)** was not experimentally accessible.

(7)(TCNQ)₂

40.0 mg (0.114 mmol) of **7** and 46.7 mg (0.228 mmol) of TCNQ were each dissolved in about 5 mL dimethylformamide. Slowly, the light green TCNQ solution was added to the orange azine solution. By contact of both solutions, an immediate colour change was observed. After a few minutes, precipitation of a solid took place. Slow removal of solvent and washing with three portions of 5 mL ethanol led to the cuboid crystals of **(7)(TCNQ)₂**. Yield approx. 80 %. Melting point: 252–253 °C. Analysis for C₃₈H₂₀N₁₂F₆: calc. C 60.18, H 2.66, N 22.16, found C 60.10, H 2.86, N 21.85.

(8)(TCNQ)

20.0 mg (0.057 mmol) of **8** and 11.7 mg (0.057 mmol) of TCNQ were solved in about 3 mL acetonitrile, separately. By addition of the TCNQ solution to the dark orange solution of **8**, an immediate colour change into dark green and the precipitation of a dark solid could be observed. The solid was filtered and washed with three times with 10 mL toluene. Dark violet metallic shining needles of **(8)(TCNQ)** were obtained. Yield approx. 80 %. Melting point: 186 °C. Analysis for C₂₆H₁₆N₈F₆: calc. C 56.29, H 2.89, N 20.20, found C 56.00, H 3.23, N 19.97.

(5)(OTCNP)₂

Equimolar amounts of **5** and TCNP were solved in ethyl acetate. The solution were mixed slowly. After removal of solvent, orange transparent needles were observed. X-ray single crystal determination showed the formation of a 1:2 CT salt, **(5)(OTCNP)₂**. Herein, the ambient conditions led to a hydrolysis of the TCNP molecules in the presence of water. Pure **(5)(OTCNP)₂** was not experimentally accessible.

(7)(TCNP)

20 mg (0.057 mmol) of **7** and 10.3 mg (0.057 mmol) of TCNP were each solved in ethyl acetate. Drop-wisely, the TCNP solution was added to the solution of **7**. The mixture was stored for several days under slow removal of solvent. After few hours the solutions turned into light green. Complete removal of solvent, the formation of greenish shining needles was observed. These crystals were washed with about three portions of 10 mL of ethanol. Yield approx. 30 %. Melting point: 175 °C. Analysis for C₂₂H₁₂N₁₀F₆: calc. C 49.83, H 2.28, N 26.41, found C 49.36, H 2.29, N 25.64.

(1)(DTeF)

20 mg (0.093 mmol) of **1** and 38.1 mg (0.093 mmol) of DTeF were solved in acetonitrile, separately. To the red azine solution, the yellow DTeF solution was added slowly. An immediate colour change into dark violet and the precipitation of very thin, dark needles were observed. After removal of solvent, the thin needles and dark rod-shaped crystals were received. By washing with three portions of 20 mL dimethylformamide, the rod-shaped crystals were obtained. X-ray single crystal determination led to 1:1 CT salt, **(1)(DTeF)**. X-ray powder diffraction of the rod-shaped crystals indicates the presence of an additional crystalline phase. Even CHNS analyses of several charges provided nearly similar results of 1:1 CT compounds. Nonetheless, only the crystal structure of one phase could be examined.

CHAPTER 3

Heterocyclic Azines

Symmetric heterocyclic pyridone azines present a promising class of organic donor molecules. Their electron richness as well as their planarity make them fruitful candidates in the formation of highly conducting materials. In the course of this work, the basic scaffold MPA (**1**) has been modified by different types of organic substituents to investigate the impact on the redox behaviour and the crystal packing (Fig. 3.1).

The synthesis of these pyridone azines follows the straightforward known protocols by S. Hünig[95]. It starts from the respectively substituted 2-halogeno-pyridines that is *N*-methylated with methyl iodide (MeI), initially. For **7** and **8**, the basicity of pyridinium N atoms is lowered due to the negative inductive effect of the trifluoromethyl (CF_3) groups and thus show less reactivity in the alkylation reaction. In that case, trifluoromethanesulfonic acid (MeOTF) is used as alkylation resource. Subsequently, the resulting *N*-methyl-2-halogeno-pyridine iodides and triflates react with a half equivalent of hydrazine under basic conditions.[98, 101]

This class of compounds can undergo two one-electron oxidation processes from the neutral oxidation state ± 0 to the radical cation with the oxidation state +1 proceeding further to the dicationic stage with the charge +2 (Fig. 3.1). Materials containing pyridone azines in an oxidation state between 1 and zero dedicate the greatest attention.

2 displays a constitutional isomer of **1**, wherein instead of a 2,2'-substitution of the pyridinium rings a 4,4'-substitution is present. The introduction of *tert*-butyl (^tBu) groups in para-position to the pyridinium N atoms, in **3**, allows to investigate the small positive inductive effect on the redox behaviour. Furthermore the steric demand of the large side group might affect the crystal packing. The positive mesomeric effect (+M) of the thiomethyl (SMe) and the methoxy (OMe) groups in **4** or **5** should shift the redox potential to smaller values corresponding to an increase of their reductive power. Whereas, the negative inductive effect (-I) of the F and CF_3 groups in **6**, **7** and **8** should have the opposite effect by lowering of reductive strength. The CF_3 substitution was performed in two different ways, in meta- or in para-position with respect to the pyridinium N atoms, leading to **7** or, respectively, **8**.

To investigate the influence on the redox behaviour, cyclic voltammetry was used. Fig. 3.2 presents the cyclic voltammograms of the pyridone azines **1–8**. Independent from substitution, two reversible one-electron oxidation processes reveal the common characteristic feature. Derivative **5** shows additional redox processes. In Tab. 3.1 the potentials for the first oxidation step to the respective radical cations E_1 and for the second oxidation step to the corresponding dications E_2 as well as the potential differences ΔE are listed.

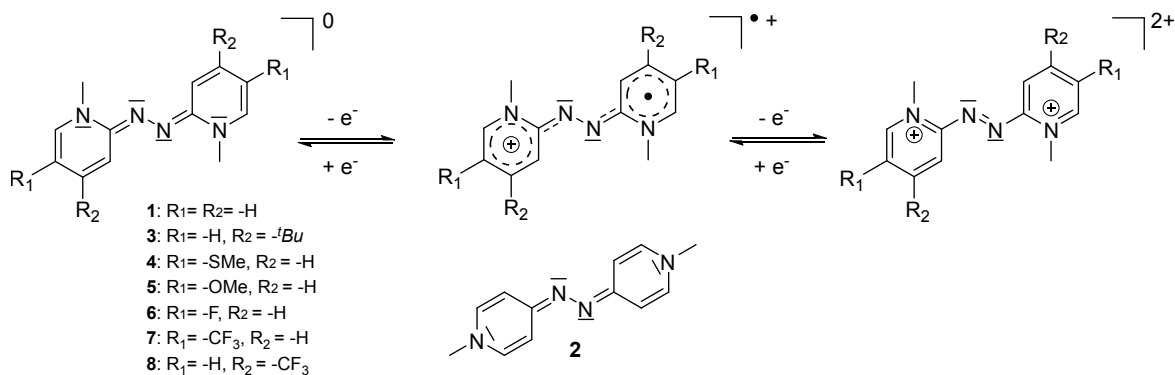


Figure 3.1: The two reversible one-electron oxidation steps of MPA (**1**) and its derivatives to the radical cations and the respective azo-bis(*N*-methyl-pyridinium)²⁺ dications. The labeling of the corresponding azines is marked as number **3-8**. **2** displays a constitutional isomer of **1** with almost similar redox behaviour.

The basic scaffold **1** is very easily oxidised since the potentials are at -0.05 V and +0.45 V vs. Ag/AgCl and well-separated with a potential difference ΔE of 0.5 V. For **2**, the potentials are less separated with ΔE of 0.3 V at -0.10 V and +0.20 V vs. Ag/AgCl. Thus, obtaining the radical cation stage might be more challenging compared to **1**.

The introduction of the steric demanding *t*Bu groups in **3** shows no remarkable change in the redox activity. The potentials are very close to that of **1** with -0.10 V and +0.40 V vs. Ag/AgCl possessing the same well-separated potential difference ΔE of 0.5 V.

The positive mesomeric effect of the SMe and OMe groups should increase the reductive power of the compounds. Contrary to expectation, in case of **4**, there is only a minor effect observed with ± 0.00 V and +0.40 V vs. Ag/AgCl with ΔE of 0.4 V. As expected, for **5**, a significant shift to lower potentials can be observed lying at -0.20 V and +0.25 V vs. Ag/AgCl. Thus, the reductive power of **5** is comparably higher than that of the basic scaffold **1**. Beyond the two reversible one-electron redox processes, further redox activity is observed, especially, around the conversion of the radical cation species to the dicationic stage. Interactions of the radical with the methoxy groups might explain that[122].

The introduction of fluorine does not influence the redox behaviour. Therefore potentials of **6** are quite similar to that of **1**. The respective potentials for **7** and **8** are at +0.40 V and +0.80 V or +0.30 V and +0.75 V vs. Ag/AgCl. The electron-withdrawal effect by the CF₃ substituents has a strong impact on the oxidation potential, apparently. Shifts of about 0.4 V or 0.3 V to higher values show that the reductive powers of **7** and **8** are substantially lowered.

The bond lengths in the central CNNC moiety correlates to the predominant oxidation state. The neutral species has -C=N-N=C- bond characteristics, the radical state shows nearly -C-N-N-C- bond equality, whereas the dication has inverted order of single and double bond -C-N=N-C- compared to the neutral state (see Chapter 1.2).

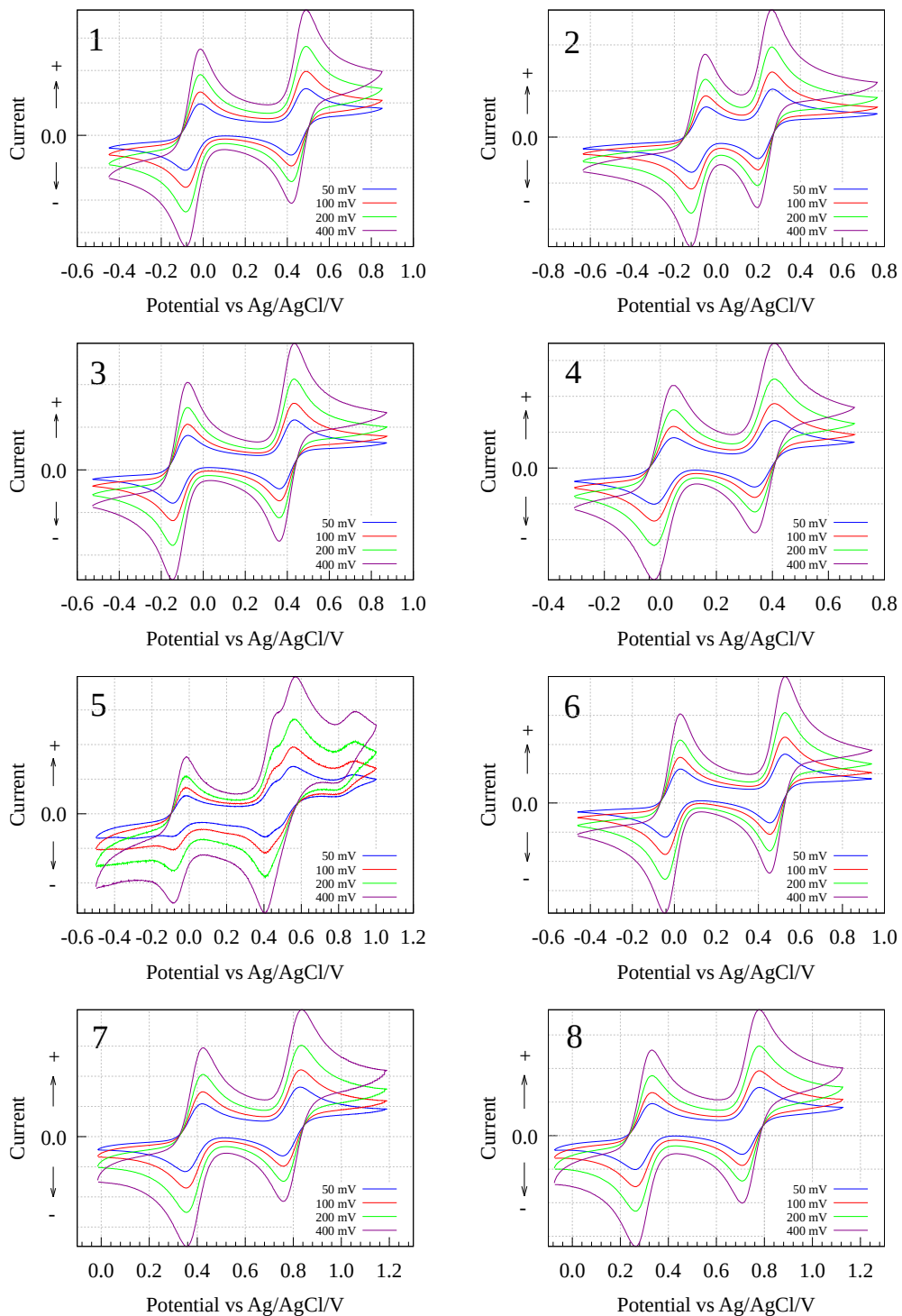


Figure 3.2: Cyclic voltammograms of the pyridone azines **1-8**. Two well-separated reversible one-electron oxidation processes are observed. For **5** additional redox processes around the conversion of the radical cation to the dication stage proceed.

Table 3.1: The potentials of the pyridone azines **1-8** for the two one-electron oxidation processes. The first oxidation step to the respective radical cations (E_1) and the second oxidation step to the corresponding dications (E_2) as well as the potential difference ΔE .

Azine	E_1	E_2	ΔE
1	-0.05	+0.45	0.50
2	-0.10	+0.20	0.30
3	-0.10	+0.40	0.50
4	± 0.00	+0.40	0.40
5	-0.20	+0.25	0.45
6	-0.05	+0.45	0.50
7	+0.40	+0.80	0.40
8	+0.30	+0.75	0.45

Investigations of the redox activity demonstrate clearly the influence of the different substituents. The constitutional isomer **2** has the smallest potential difference with ΔE of 0.3 V and is slightly easier to oxidise as its 2,2'-derivative **1**. Specific substitution of electron-donating or -withdrawing groups have significant impact on the reductive power. In case of **5** with a +M substituent (OMe) the tendency for oxidation is increased, whereas for **7** and **8** with its -I substituent (CF₃) the reductive strength is lowered significantly. For the latter two the potentials E_1 and E_2 are very close to that of TTF[89, 90]. The redox activity of **3**, **4** and **6** is not affected appreciably compared the basic scaffold **1**.

In the 60 years since their discovery, the compounds of this class found only little attraction and the promising redox properties have not been used for materials design. Only the conversion to oligomeric azines and their corresponding radical ions was reported[100]. Still, known to form stable radical cations, the pyridone azines present a highly promising group of organic building blocks for molecular conductors and charge transfer compounds. Reactions of the azines **1-8** with Cu(II) halides, CuCl₂ and CuBr₂, provided a series of new organic-inorganic hybrids in form of radical cation salts and dicationic salts with halogenido cuprates(I)/(II) as counter ions. For the generation of charge transfer compounds the organic acceptor molecules TCNQ, TCNP and DTeF have been combined with the azines **1-8**. Especially, the reactions with TCNQ have been highly fruitful.

CHAPTER 4

Radical Cation Salts with Halogenocuprates

Radical cation salts examined in this work consist of organic donor molecules with metallate anions. The organic-inorganic hybrid compounds are highly interesting due to the combination of physical properties as electrical conductivity with magnetism.

The heterocyclic azines act as electron donor molecules with an appropriate oxidant and are able to form solids that contain both, a radical cation and a metal-containing counter anion.

Since the reduction potential of divalent Cu(II) to monovalent Cu(I) is at -0.02 V vs. Ag/AgCl, copper(II) halides constitute appropriate oxidants for the azines **1-8**.

Nonetheless, the redox potentials of the first oxidation of **1** and **8** differ by 0.5 V, reactions of **1** and **8** with copper(II) halides afford via an one-electron transfer process the three radical cation salts (**1**)[CuCl₂], (**1**)[CuBr₂] and (**8**)[CuBr₂]. All compounds crystallise as air-stable and dark crystals. Thereby, Cu²⁺ is reduced to the appropriate cuprate(I) counter anion [CuX₂]⁻ (X = Cl, Br).

Crystal structures, magnetic as well as electrical conducting properties were investigated for the three compounds.

4.1 Crystal Structures

4.1.1 (1)[CuCl₂]

The reaction of **1** with CuCl₂ in acetonitrile yields in dark violet crystals, the radical cation salt **(1)[CuCl₂]** (Fig. 4.1). The compound crystallises in the monoclinic space group *C*2₁/c (No. 14).



Figure 4.1: Dark violet rod-shaped crystals of **(1)[CuCl₂]**.

over the whole molecule in the radical state. In the counter anion, [CuCl₂]⁻, Cu(I) is coordinated approximately linear by two chloride atoms.

The Cl–Cu–Cl angle is around 176°. The Cu–Cl distances are in a typical range for chlorido cuprates(I) with about 2.08 Å[123].

The crystals are made up by **1**⁺ radical cations and [CuCl₂]⁻ anions (Fig. 4.2). The center of gravity of the cation, the mid of the N2–N2^{*i*} bond, is positioned at an inversion center. The Cu atom of the anion is located at the special position 4*e* (0, *y*, 1/4) which corresponds to a twofold symmetry axis, 2 ≡ *C*₂.

The radical cation is substantially planar. The N2–N2^{*i*} bond length ranges with 1.34 Å in between the length of N–N single and a N=N double bond that is shortened with respect to neutral state. Simultaneously, the N2–C1 bond is stretched to 1.35 Å. The equality of bond lengths is a measure to estimate the electron delocalisation

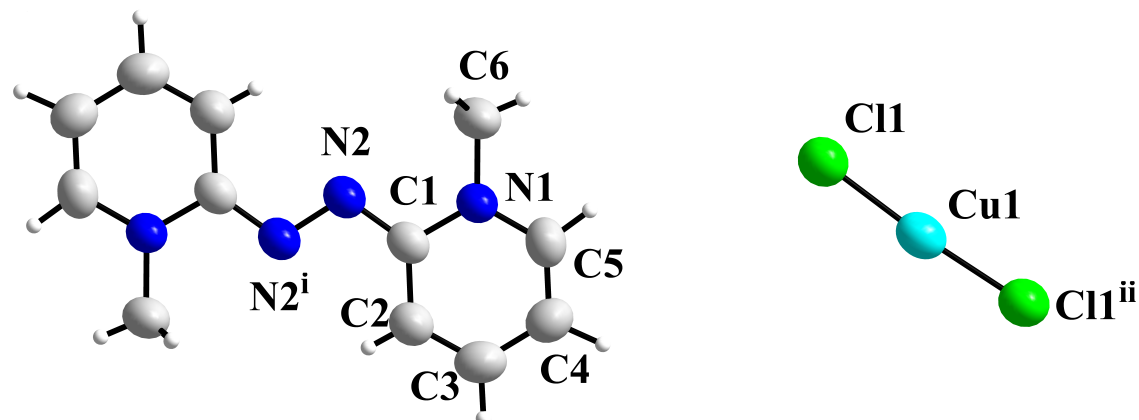


Figure 4.2: The building units of **(1)[CuCl₂]**, the planar **1**⁺ radical cation and the almost linear dichlorido cuprate(I) anion, [CuCl₂]⁻. The superscripts denote the symmetry operations: *i* = -*x*, 1-*y*, 1-*z*; *ii* = 1-*x*, *y*, 0.5-*z*. Bond lengths/Å: N2–N2^{*i*} 1.3374(6), N2–C1 1.349(5), Cu1–Cl1 2.0772(11).

In the crystals, the planar $\mathbf{1}^+$ radical cations form stacks in c direction. The molecules are not strictly parallel stacked. Hence, between adjacent $\mathbf{1}^+$ radicals, the interplane angle amounts to 5.2° . The $\mathbf{1}^+$ radical cations are arranged equidistantly by a center-of-gravity distance of 3.95 \AA . The stacks are highly oblique with an offset of 2.26 \AA in average. With reference to the molecular planes, an average plane-to-plane distance of 3.36 \AA can be determined. The axes of the linear dichlorido cuprate(I) anions are orientated in the direction of the cation stacks (Fig. 4.3).

By recording X-ray single crystal data at 123 K , a pronounced anisotropic lattice parameter contraction is observed. The c axis, representing the propagation direction, diminishes by about 2.06% from 7.904 \AA to 7.741 \AA . As a result, the average plane-to-plane distance between the $\mathbf{1}^+$ radical cations shrinks from 3.36 \AA to 3.30 \AA . For the lengths of the a and b axis, only minor impact is observed with decrease of just 0.30% and 0.36% .

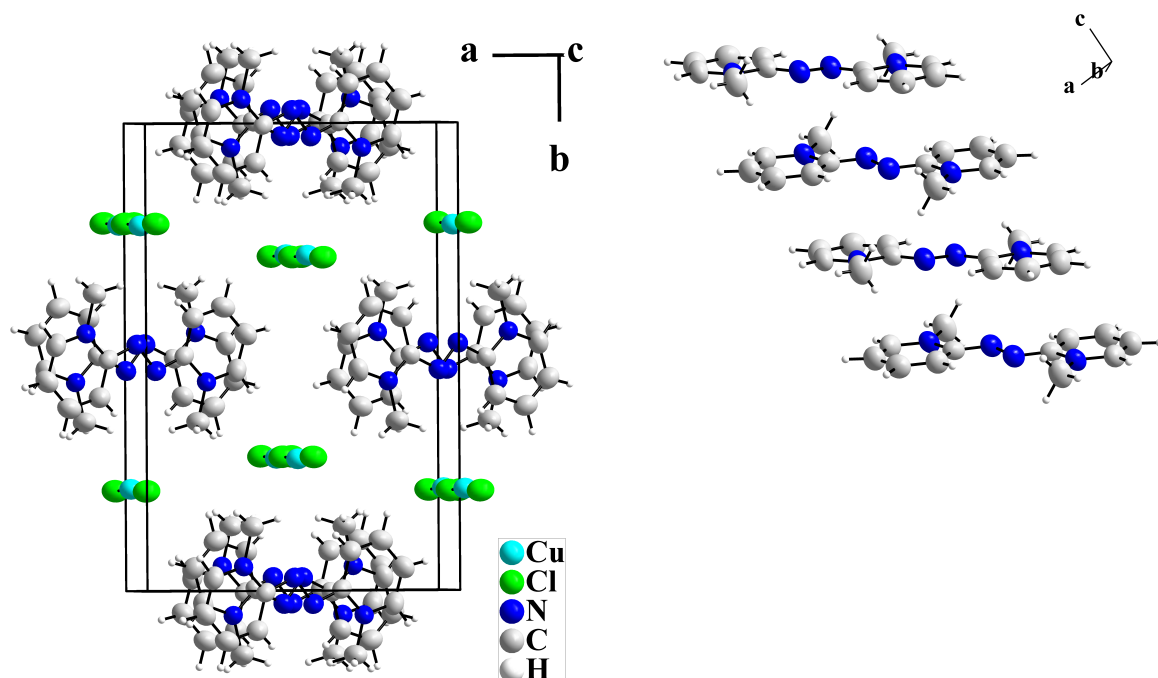


Figure 4.3: The crystal structure of $(\mathbf{1})[\text{CuCl}_2]$. The planar $\mathbf{1}^+$ radical cations are equidistantly arranged in oblique stacks running in c direction. The arrangement of the linear dichlorido cuprate(I) anions, $[\text{CuCl}_2]^-$, is demonstrated by perspective view (right). The cation stacks are separated by the counter anions (left).

4.1.2 (1)[CuBr₂]

The reaction of **1** and CuBr₂ leads to dark violet needles of the radical cation salt **(1)[CuBr₂]** (Fig. 4.4). It crystallises in the tetragonal space group *P4₂/mcm* (No. 132).

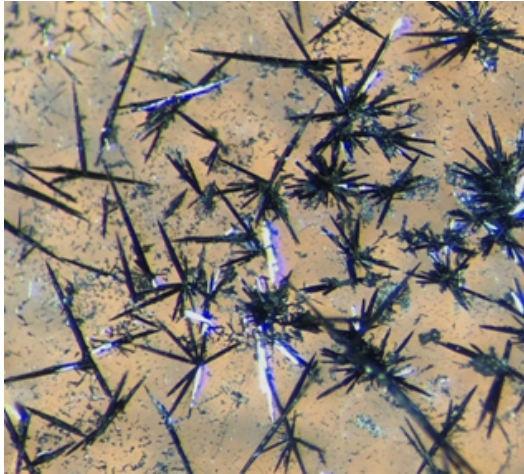


Figure 4.4: The crystals of **(1)[CuBr₂]** in shape of dark violet needles.

exactly coincident. This disorder phenomenon was observed for all inspected crystals. Neither single crystal diffraction images nor the powder diffraction pattern give hints for lower symmetry or an enlarged cell. The disorder is not effected by temperature variation. Nonetheless, this disorder model implies physically impossible overlap of the hydrogen atoms of molecules in adjacent unit cells in the *ab* plane (Fig. 4.6). Since ordered domains in the crystal exist, the model is kept valid. In fact, the diffraction images give no hint of superstructure reflections or lattice distortions leading to the assumption that ordered domains must be irregularly distributed over the crystals.

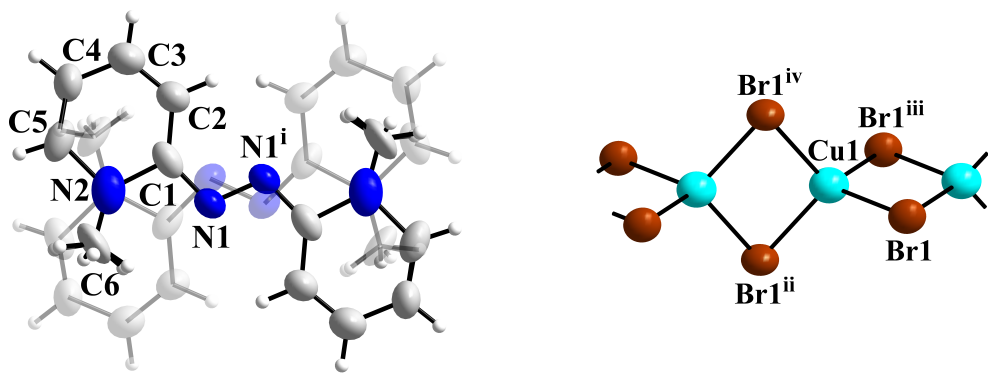


Figure 4.5: The two building units in the structure of **(1)[CuBr₂]**. The **1⁺** radical cations occur as superposition of two different orientated molecules (left). For the sake of clarity, one molecule is drawn in transparent mode. A section of the $[\text{CuBr}_{4/2}]_n$ bromido cuprate(I) anion chain (right). The superscripts denote the symmetry operations: $i = 1-x, 1-y, z$; $ii = -1+y, 1-x, 0.5+z$; $iii = -x, 2-y, z$; $iv = 1-y, 1+x, 0.5+z$. Bond lengths/ \AA : N1–N1^{*i*} 1.32(2), N1–C1 1.33(2), Cu1–Br1 2.5042(7).

(1)[CuBr₂] is made up by planar **1⁺** radical cations and bromido cuprate(I) anions, $[\text{CuBr}_2]_n$, which form one-dimensional infinite chains of edge-sharing CuBr₄ tetrahedra (Fig. 4.5).

The radical cation has the point symmetry $2/m$ (C_{2h}). However, in the crystals, the molecules are located at the special position $2c$ ($\frac{1}{2}, \frac{1}{2}, 0$) with a site symmetry of $m.m\bar{m}$ (D_{2h}). Thus, the parent symmetry of the molecule is exceeded by two conjugate diagonal mirror planes along the *c* axis, forcing the disorder over two positions. For all atoms in the cation, the site occupancy factor *s_{of}* had to be set to 0.5, except the atom N2 with *s_{of}* = 1.

Relatively large displacement ellipsoid are gained, since the position of these atoms of the two superimposed molecules are not

With respect to the neutral state, the CNNC moiety bonds change in a way consistent with the radical cation $\mathbf{1}^+$ in $(\mathbf{1})[\text{CuCl}_2]$. The bond lengths N1–C1 and N1–N1ⁱ of about 1.33 Å, within standard deviations, validate an electronic state with high delocalisation and the charge $\mathbf{1}^+$. In the structure, the $\mathbf{1}^+$ radical cations are arranged in a face-to-face stacking running in *c* direction. The centers of gravity overlap directly. The molecules are stacked parallel and equidistantly to each other. The plane-to-plane distance between adjacent radical cations amounts to 3.23 Å related to half the length of the crystallographic *c* axis. Compared to $(\mathbf{1})[\text{CuCl}_2]$ with 3.36 Å, the plane-to-plane distance is significantly shorter.

In contrast to the structure of $(\mathbf{1})[\text{CuCl}_2]$, the bromido cuprate(I) anion, $[\text{CuBr}_2]^-$, forms one-dimensional chains of edge-sharing CuBr_4 tetrahedra running parallel to the cation stacks. The Cu–Br distances are in a typical range around 2.50 Å. In the CuBr_4 tetrahedra, the Br–Cu–Br angles of 114° and 99° show slight distortion from ideal tetrahedra symmetry. In the crystals, the anion chains are arranged separately between the $\mathbf{1}^+$ radical cation stacks and generate a tetragonal rod packing.

Related to $(\mathbf{1})[\text{CuCl}_2]$, low temperature data show an anisotropic lattice shrinking. The *c* axis is much stronger affected than the other lattice parameters. From ambient temperature to 123 K, the *c* axis contracts about 1.84 % from 6.459 Å to 6.340 Å. The contraction of the crystallographic *a* axis ranges in the significance level with 0.18 %. This anisotropic contraction affects the plane-to-plane distance between the radical cations which is reduced from 3.23 Å to 3.17 Å. Furthermore, in the polymeric bromido cuprate(I) anions, the Cu···Cu distances decrease from 3.23 Å to 3.17 Å and the Cu–Br–Cu angles are reduced from 80.3° to 78.8°, while the Cu–Br bonds do not alter significantly.

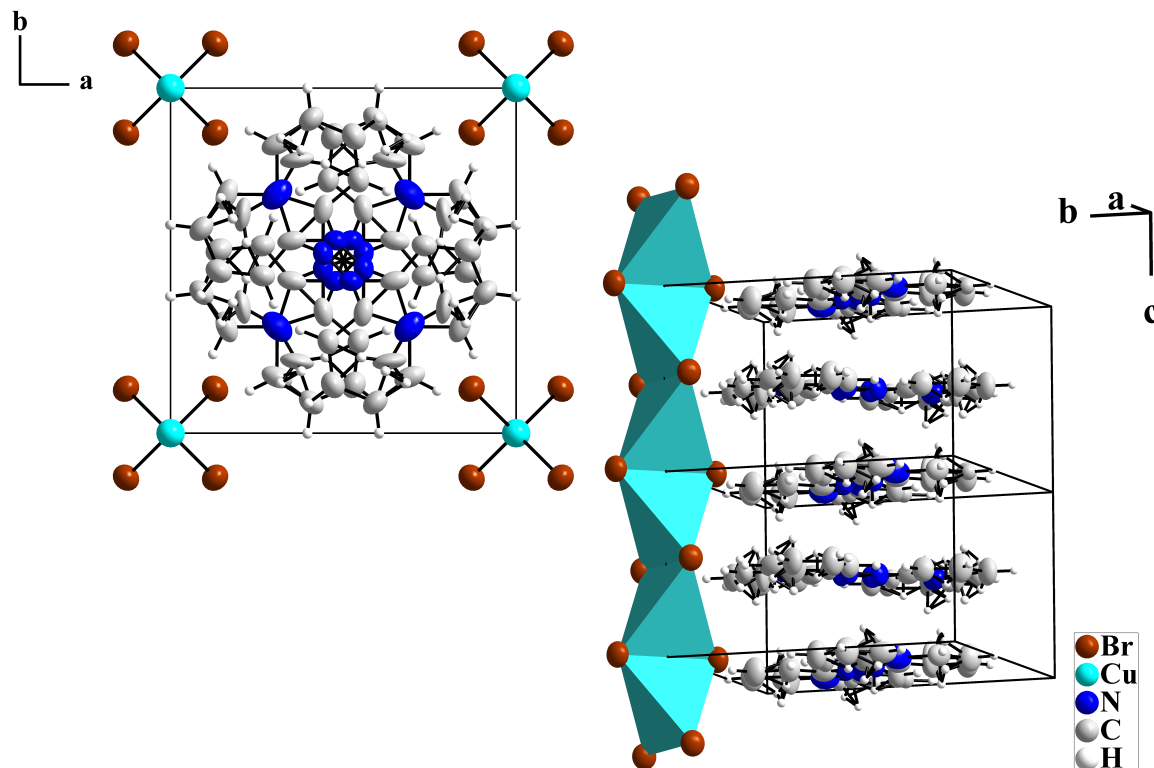


Figure 4.6: The unit cell of $(\mathbf{1})[\text{CuBr}_2]$ depicted in *c* direction (top left) and perpendicular to that axis (bottom right, 1×1×2 cells are drawn), demonstrating the stacking as well as the overlap of the $\mathbf{1}^+$ radical cations.

4.1.3 (8)[CuBr₂]

Again, the reaction of **8** with copper(II) bromide, performed under the same conditions as for **(1)[CuCl₂]** and **(1)[CuBr₂]**, leads to the formation of the radical cation salt **(8)[CuBr₂]**. It crystallises in shape of thin dark metallic-shining needles (Fig. 4.7).



Figure 4.7: The dark metallic-shining needles of **(8)[CuBr₂]**.

The molecules in the crystals of **(8)[CuBr₂]** are equidistantly arranged forming loose stacks parallel to the crystallographic *c* axis. As for the **8⁺** stacks, the anion chains are orientated along *c* direction, imparting the crystal an anisotropic character. The intermolecular plane-to-plane distance between adjacent molecules amounts to 3.87 Å. In the loose stacks the molecules are highly oblique. The angle between the molecular plane of **8⁺** and the stacking direction amounts to 50.1°. Hence, no essential overlap of the radical cations is observed and only minor electronic interactions are expected due to the large separation. In the unit cell, a herring bone pattern is generated by four symmetry related but translationally different stacks.

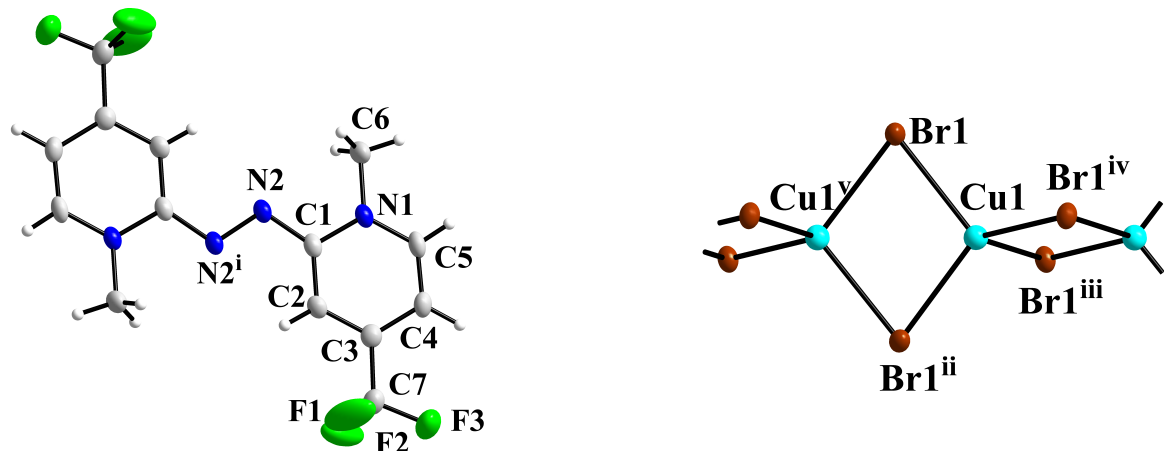


Figure 4.8: The molecules in the crystals of **(8)[CuBr₂]**, the **8⁺** radical cation and a section of the bromido cuprate(I) anion chains, **[CuBr_{4/2}]⁻**. Thermal ellipsoids based on the diffraction data collected at 123 K. The superscripts denote the symmetry operations: *i* = 1-x, 1-y, z; *ii* = -1+y, 1-x, 0.5+z; *iii* = -x, 2-y, z; *iv* = 1-y, 1+x, 0.5+z. Bond lengths/Å: N1-N1^{*i*} 1.32(2), N1-C1 1.33(2), Cu1-Br1 2.5042(7).

(8)[CuBr₂] consists of **8⁺** radical cations and bromido cuprate(I) anions, **[CuBr₂]⁻**, in form of one dimensional infinite chains, **[CuBr_{4/2}]_n** (Fig. 4.8) and crystallises in the tetragonal space group **P4₂/n** (No. 86).

The cation is entirely planar and the almost equal bond lengths in the CNNC moiety amount to 1.34 Å for N2–N2^{*i*} and 1.36 Å for N2–C1, underlying the presence of the radical cation, **8⁺**. The CF₃ groups perform an almost free rotation at ambient temperature. This rotational disorder turns into an ordered state on cooling to 123 K.

The **8⁺** radical cations are

equidistantly arranged forming loose stacks parallel to the crystallographic *c* axis.

As for the **8⁺** stacks, the anion chains are orientated along *c* direction, imparting the crystal an anisotropic

character. The intermolecular plane-to-plane distance between adjacent molecules amounts to 3.87

Å. In the loose stacks the molecules are highly oblique. The angle between the molecular plane of

8⁺ and the stacking direction amounts to 50.1°. Hence, no essential overlap of the radical cations is

observed and only minor electronic interactions are expected due to the large separation. In the unit cell,

a herring bone pattern is generated by four symmetry related but translationally different stacks.

In the bromido cuprate(I) anion, the Cu(I) is coordinated by four bromine atoms. The Cu–Br distances around 2.47–2.49 Å are in a typical range and the Br–Cu–Br angles are with 105–111° slightly deviating from ideal tetrahedral symmetry. As in (1)[CuBr₂], infinite one-dimensional chains parallel to the *c* axis made up of edge-sharing CuBr₄ tetrahedra are present. However, with respect to (8)[CuBr₂], the bromido cuprate(I) chain in (1)[CuBr₂] is elongated along the propagation direction. Thus, the Cu···Cu distances amount to 2.99 Å in (8)[CuBr₂] and 3.17 Å in (1)[CuBr₂]. Correspondingly, the Cu–Br–Cu angles are 74.1° and 78.8° in (8)[CuBr₂] or respectively in (1)[CuBr₂].

Though, in the structure of (1)[CuBr₂], the stacking of the **1**⁺ radical cations has a high impact on the bromido cuprate(I) chains. The translational period of the chains relates directly to the intermolecular distance between adjacent radical cations.

As for (1)[CuCl₂] and (1)[CuBr₂], low temperature data of (8)[CuBr₂], demonstrate a lattice parameter contraction. Opposing to the radical cation salts of **1**, the shrinking of the axes is rather isotropic and affects the *a* axis by 1.02 % and *c* axis by 0.8 %. In contrast to (1)[CuCl₂] and (1)[CuBr₂], no distinct anisotropic shrinking in the cation stacking direction is observed.

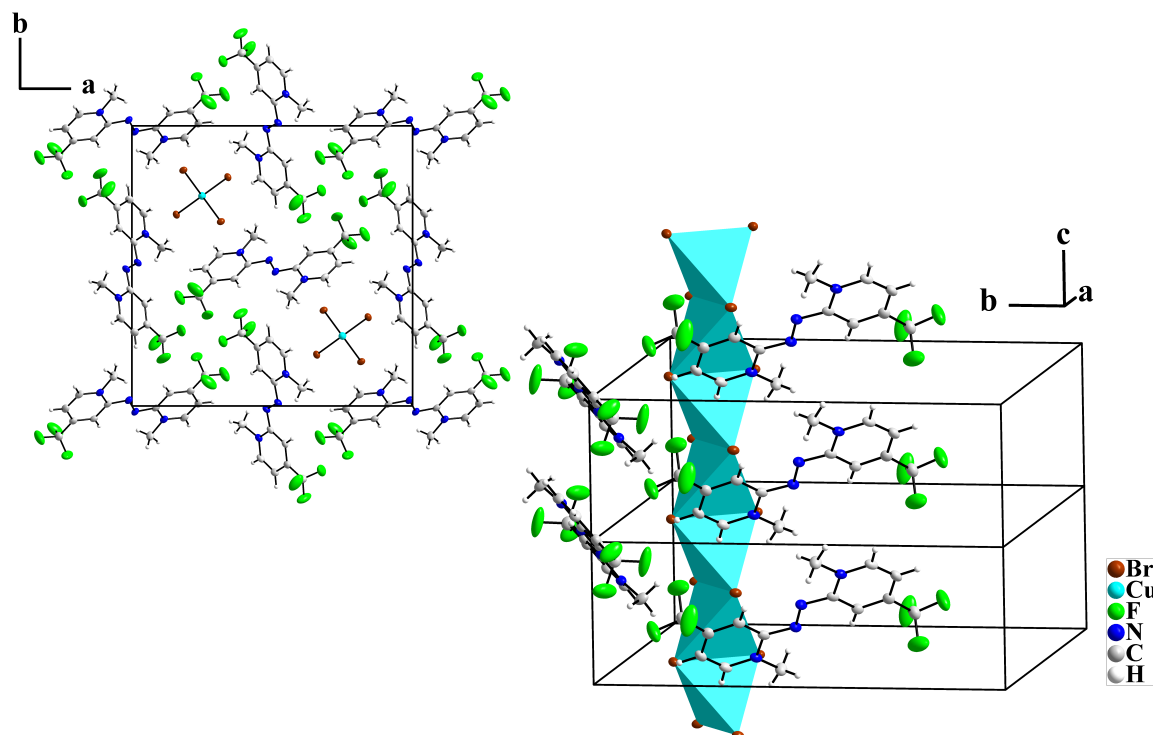


Figure 4.9: The unit cell of (8)[CuBr₂] depicted in *c* direction (top). The extended unit cell (bottom, 1×1×2 cells are drawn) showing the loose stacks arranged in a herring bone pattern and the linear chains of edge-sharing [CuBr_{4/2}]_n tetrahedra.

4.2 Magnetism

The compounds **(1)**[CuCl₂], **(1)**[CuBr₂] and **(8)**[CuBr₂] are made up from radical cations and halogenido cuprate(I) counter anions. The d^{10} electron configuration of Cu(I) is associated with diamagnetic behaviour. Nonetheless, the doublet state of the organic radicals, **1**⁺ and **8**⁺, suggests magnetic phenomena.

Fig. 4.10 shows the magnetic susceptibilities of **(1)**[CuCl₂], **(1)**[CuBr₂] and **(8)**[CuBr₂] in the temperature range from 1.9 K to 300 K.

(1)[CuCl₂] and **(1)**[CuBr₂] exhibit very similar magnetic behaviour. Over the whole measured temperature range, the magnetic susceptibilities are small and positive.

For $T > 50$ K, the molar susceptibilities are nearly temperature-independent in the order of $10^{-4} \text{ cm}^3 \text{ mol}^{-1}$. At lower temperatures, an almost gradual decrease in the function $\chi_{mol}^{-1} = f(T)$ is observed. Application of the Curie law up to 50 K provides small magnetic momenta of $0.59 \mu_B$ with θ of -2.28 K for **(1)**[CuCl₂] and $0.61 \mu_B$ with θ of -4.31 K for **(1)**[CuBr₂]. Thus, the magnetic properties suggest strong coupling between the spin centers on the radical ion stacks.

The small paramagnetic momenta may be attributed to d^9 -configured Cu²⁺ in the compounds. To estimate the amount of Cu²⁺ in a substance, the experimental Curie constant of a pure Cu²⁺ paramagnet ($C = 0.446 \text{ cm}^3 \text{ Kmol}^{-1}$ for $S = \frac{1}{2}$ and $g_{eff} = 2.18$ [125]) can be taken into account. The experimental Curie constants for **(1)**[CuCl₂] and **(1)**[CuBr₂] are $0.043 \text{ cm}^3 \text{ Kmol}^{-1}$ or, respectively, $0.061 \text{ cm}^3 \text{ Kmol}^{-1}$ corresponding to 9.6 % or 13.7 % amount of Cu(II) in the respective compound. The relatively high Cu(II) content can be comprehended as a charge transfer process from monovalent Cu(I) to the **1**⁺ radical cation resulting in **(1)**⁰[Cu(II)X₂]⁰.

However, since Cu(II) readily oxidises **1**, this inverse formation reaction seems to be rather unlikely.

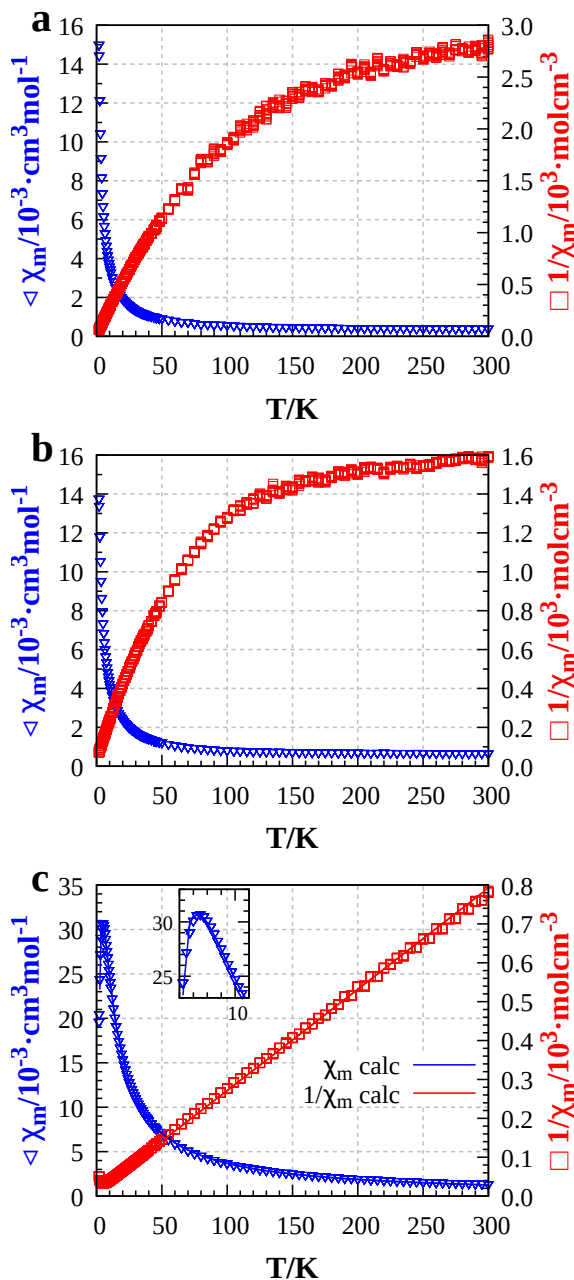


Figure 4.10: Magnetic properties of **(1)**[CuCl₂] **a**, **(1)**[CuBr₂] **b** and **(8)**[CuBr₂] **c**. The plots $\chi_{mol} = f(T)$ (open, blue triangles) and $\chi_{mol}^{-1} = f(T)$ (open, red squares) are presented. For **(8)**[CuBr₂], the simulated functions obtained by the 1D Heisenberg chain model[124] are given as solid lines.

Possibly, defects in form of missing $\mathbf{1}^{\cdot+}$ radical cations might be charge balanced by paramagnetic Cu(II). But no evidence for such extensive defects could be found.

In contrast to **(1)**[CuCl₂] and **(1)**[CuBr₂], in the measurement of the magnetic susceptibility for **(8)**[CuBr₂] antiferromagnetism is observed. The maximum of the molar susceptibility is at a Neél temperature T_N of 6 K. Thus, a weak coupling phenomenon of mainly free paramagnetic momenta is suggested. The simulation of the magnetic data was performed with the 1D Heisenberg chain model following the expression[124]:

$$\chi_{mol} = \frac{N\beta^2 g^2}{4k_B T} \times \left[\frac{1 + Ax + Bx^2 + Cx^3 + Dx^4 + Ex^5}{1 + Fx + Gx^2 + Hx^3 + Ix^4} \right]^{2/3} \quad (4.1)$$

with the parameters x = |J|/k_BT, A = 5.7979916, B = 16.902653, C = 29.376885, D = 29.832959, E = 14.036918, F = 2.7979916, G = 7.0086780, H = 8.6538644 and I = 4.5743114. The best fit to data leads to a Landé factor of 2.023, fulfilling the expectation of 2.00 for organic radicals, and a coupling constant J of -2.1 cm⁻¹. Above 20 K, data evaluation shows an almost linear $\chi_{mol}^{-1} = f(T)$ function and enables the application of the Curie law. It provides a characteristic Curie temperature θ of -1 K and a magnetic moment of 1.76 μ_B corresponding well to the moment expected for one unpaired electron per formula unit. The magnetic coupling of the **8**^{·+} radical cations at low temperature is apparently weak. The differences in magnetic behaviour compared to **(1)**[CuCl₂] and **(1)**[CuBr₂] is in line with the structural arrangement of the **8**^{·+} radicals in **(8)**[CuBr₂]. The large intermolecular distance and the loose stacking inhibit an effective magnetic interaction of the radical cations.

The magnetic properties of the three radical ion containing halogenido cuprates offer a clear differentiation.

On the one hand, the temperature dependence of the susceptibilities of **(1)**[CuCl₂] and **(1)**[CuBr₂] with their radical cation stacks is nearly identical. Spin momenta are largely suppressed and therefore substantial coupling between the cations has to be assumed. At above 50 K, the strong reduced magnetic momenta lead to almost temperature-independent paramagnetism with susceptibilities in the order of 10⁻⁴ cm³ mol⁻¹. The small paramagnetic moments correspond to 9.6 % Cu²⁺ for **(1)**[CuCl₂] and 13.7 % for **(1)**[CuBr₂]. A still controversial discussion is the proof of the presence of a substantial charge transfer in halogeno cuprates with organic cations, as for example discussed for N-methylquinoxalinium bromido cuprate(I), (MQ)⁺[CuBr₂]_n⁻[83].

On the other hand, **(8)**[CuBr₂] is mainly paramagnetic with one unpaired electron per formula unit. The doublet state of the **8**^{·+} radical cation leads to magnetic phenomena. A weak antiferromagnetism with a coupling constant J of -2.1 cm⁻¹ and a Neél temperature T_N of 6 K is present.

4.3 Conductivity

Measurements of the electrical conductivity of the compounds **(1)**[CuCl₂], **(1)**[CuBr₂] and **(8)**[CuBr₂] were performed from room temperature up to 400 K. Semiconducting properties for all three halogenido cuprate(I) radical cation salts are observed. The electrical resistance decreases with increasing temperature (Fig. 4.11).

The specific electrical conductivities are quite small with 7.3×10^{-10} Scm⁻¹ at 310 K and 1.8×10^{-7} Scm⁻¹ at 400 K for **(1)**[CuCl₂], 1.4×10^{-9} Scm⁻¹ at 310 K and 7.4×10^{-8} Scm⁻¹ at 400 K for **(1)**[CuBr₂], and 2.0×10^{-10} Scm⁻¹ at 310 K and 2.5×10^{-8} Scm⁻¹ at 400 K for **(8)**[CuBr₂]. The activation energy for the thermally activated electron transfer into the conduction band is available using the Arrhenius plot of the functions $-\ln(R^{-1}) = f(T^{-1})$. The activation energies amount to 1.34 eV for **(1)**[CuCl₂], 0.95 eV for **(1)**[CuBr₂] and 1.18 eV for **(8)**[CuBr₂].

Summarising, the electrical conductivities of the three compounds are found to be very similar in the region of 10^{-10} and 10^{-9} Scm⁻¹ at 310 K. However, from structural point of view, the conductivities follow only partially the structural parameters. Since **(1)**[CuBr₂] has the smallest intermolecular distance between adjacent radical cations with 3.23 Å, it exhibits the smallest activation energy. Thus, stronger interactions in the radical cation stacks is assumed especially in comparison to **(1)**[CuCl₂] with an intermolecular distance of 3.36 Å. Compared to **(1)**[CuBr₂], the specific conductivity of **(1)**[CuCl₂] is slightly higher by a factor of 3. Although there is no pronounced stacking in **(8)**[CuBr₂], the conductivity is in the same region as found for **(1)**[CuCl₂] and **(1)**[CuBr₂].

As a conclusion, there is no straightforward relation between the structural features of the compounds and their conductive properties. For **(1)**[CuCl₂] with isolated [CuCl₂]⁻ units, it is assumed that the conductivity arises from the radical cation stacks solely. In contrast to that, the polymeric [CuBr₂]⁻ anions in **(1)**[CuBr₂] and **(8)**[CuBr₂] might contribute to the conduction. This point is discussed in the next chapter, more detailed.

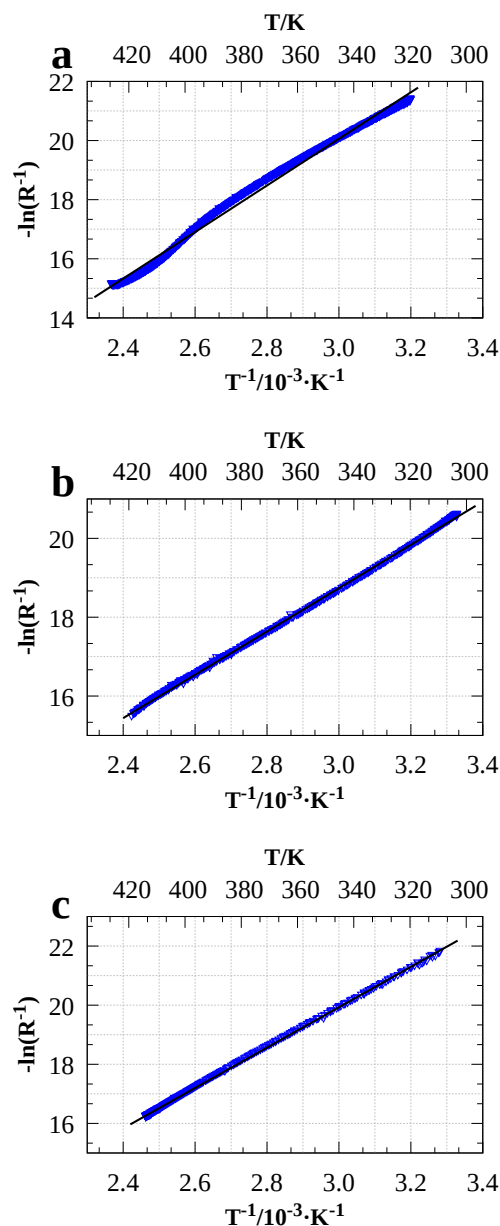


Figure 4.11: The Arrhenius plot $-\ln(R^{-1}) = f(T)$ for the electrical resistivities of **(1)**[CuCl₂] **a**, **(1)**[CuBr₂] **b** and **(8)**[CuBr₂] **c**. The blue circles are the measured resistances and the black lines present the best linear fit. All three compounds show typical semiconducting properties with small band gaps.

CHAPTER 5

Dicationic Salts with Halogenocuprates

As seen in Chapter 4, the copper(II) halides enable the one-electron oxidation of the pyridone azines to the corresponding radical cation. Beyond that, the two-electron oxidation process to the azo-bis(*N*-methyl-2,2'-pyridinium) dication is observed.

Oxidation of the radical cation salt (**1**)[CuBr₂] with one additional equivalent of CuBr₂ lead to (**1**)[Cu₂Br₄] consisting of the azo-bis(*N*-methyl-2,2'-pyridinium) dication, **1**²⁺.

Interestingly, the pyridone azine **2** reacts with copper(II) bromide to a variety of new dication salts containing the azo-bis(*N*-methyl-4,4'-pyridinium) dication, **2**²⁺. The four different compounds α -(**2**)[Cu₂Br₄], β -(**2**)[Cu₂Br₄]·CH₃CN, (**2**)[CuBr₃] and (**2**)[CuBr₄] are obtained as multi-phase system. Targeted synthesis of (**2**)[CuBr₄] and α -(**2**)[Cu₂Br₄] is feasible by use of stoichiometric amounts of bromine acting as oxidant. In the compounds, the bromido cuprate anions differ regarding the oxidation state of copper, the number of bromine ligands as well as their structural coordination.

8 reacts with CuBr₂ and Br₂ to the dication salt (**8**)[CuBr₄] including the azo-bis(*N*-methyl-2,2'-pyridinium) dication **8**²⁺.

The compounds crystallise as air-stable and dark-shining crystals. In the following, crystal structures as well as the magnetic and conducting properties are presented.

5.1 Crystal Structures

5.1.1 (1)[Cu₂Br₄]

Using an excess of CuBr₂ enables the two-electron oxidation of **1**. X-ray powder diffraction pattern of the radical cation salt **(1)[CuBr₂]** shows additional reflections that could be identified as the dication salt **(1)[Cu₂Br₄]**. Reaction of one equivalent of the radical cation salt **(1)[CuBr₂]** with one additional equivalent CuBr₂ provides pure **(1)[Cu₂Br₄]**.

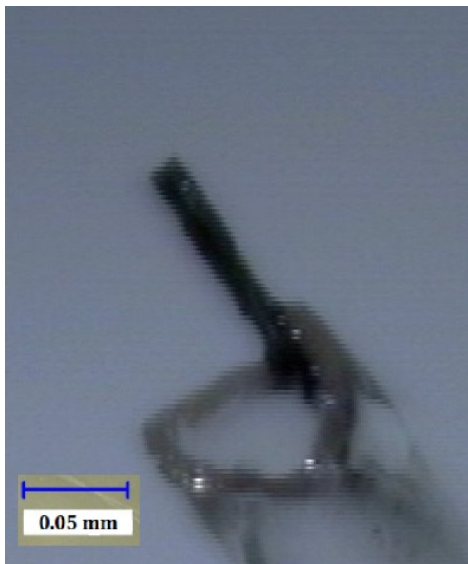


Figure 5.1: Dark needle of **(1)[Cu₂Br₄]** used for the X-ray data collection.

It crystallises in the triclinic space group $P\bar{1}$ (No. 2). The crystals consist of **1²⁺** dications and polymeric [CuBr_{4/2}]_n anions in form of edge-sharing CuBr₄ tetrahedra (Fig. 5.2). The center of gravity of the **1²⁺** dication is located at the special position $1c$ ($0, \frac{1}{2}, 0$) corresponding to inversion symmetry $\bar{1} \equiv C_i$. The bond lengths in the central CNNC moiety amount to 1.26 Å for N2–N2ⁱ and 1.41 Å for N2–C1 corresponding to –C=N=N–C– bond character.

In the cuprate anion, the one symmetry independent Cu atom is located at an inversion center $\bar{1} \equiv C_i$. The Cu–Br distances are in average 2.50 Å and the Br–Cu–Br angles range between 100–114°. The Cu···Cu distance amounts to 3.18 Å.

In the crystals, stacks of cation molecules are present, running parallel to the [CuBr_{4/2}]_n anion chains in *a* direction (Fig. 5.3). In the **1²⁺** dication stacks, the molecules are equidistantly arranged with a center-of-gravity distance of 6.39 Å by an high offset of 5.48 Å.

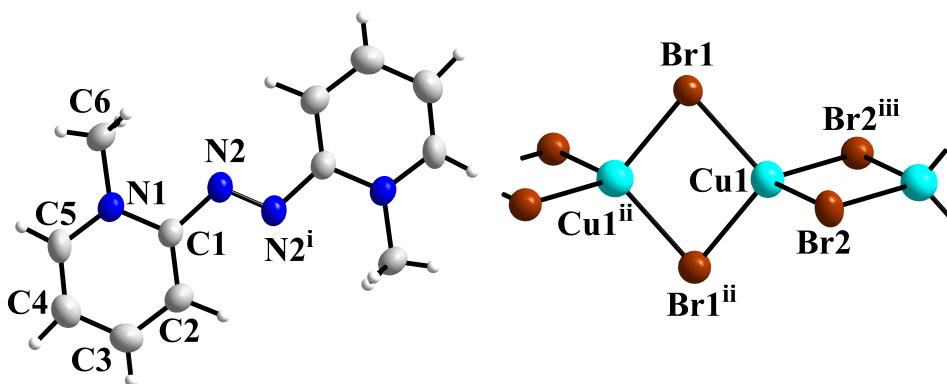


Figure 5.2: The molecules in the structure of **(1)[Cu₂Br₄]**, the planar azo-bis(*N*-methyl-2,2'-pyridinium) dication **1²⁺** and a section of the one-dimensional chains of the edge-sharing [CuBr_{4/2}]_n tetrahedra. The superscripts denote the symmetry operations: $i = -x+2, -y+1, -z+2$; $ii = -x+1, -y+1, -z+1$; $iii = -x, -y+1, -z+1$. Bond lengths/Å: N2–N2ⁱ 1.260(7), N2–C1 1.408(5), Cu1–Br1 2.4925(8), Cu1–Br2 2.5001(7) and Cu1–Cu1ⁱⁱ 3.1799(1).

The plane-to-plane distance amounts to 3.29 Å and is therefore significantly shorter. Nonetheless, the inclination angle of the cations with respect to the stacking direction as well as the large horizontal slippage between adjacent dications provide no indication of an effective molecule overlap.

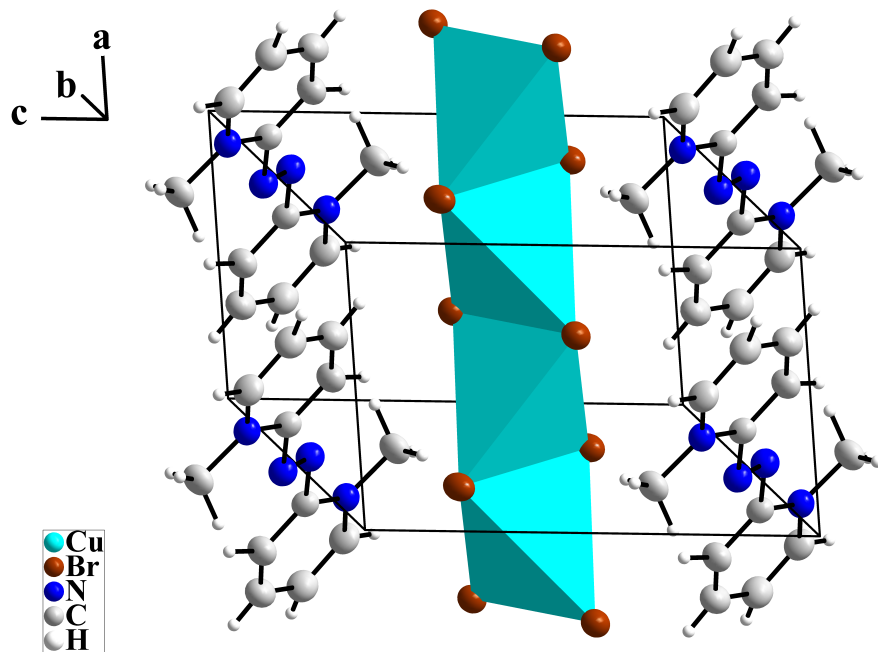


Figure 5.3: The unit cell of $(\mathbf{1})[\text{Cu}_2\text{Br}_4]$ in a perspective view illustrating the loose stacks of the molecular $\mathbf{1}^{2+}$ ions running parallel to the one-dimensional chains of the edge-sharing $[\text{CuBr}_{4/2}]_n$ tetrahedra.

In the reactions of **2** and copper(II) bromide in acetonitrile a multi-phase system was evolved. Four new dication salts α -(**2**) $[\text{Cu}_2\text{Br}_4]$, β -(**2**) $[\text{Cu}_2\text{Br}_4]\cdot\text{CH}_3\text{CN}$, (**2**) $[\text{CuBr}_3]$ and (**2**) $[\text{CuBr}_4]$ were found and the structures were elucidated by X-ray single crystal determination.

5.1.2 α -(**2**) $[\text{Cu}_2\text{Br}_4]$

In the reaction of **2** with one equivalent CuBr_2 and Br_2 in acetonitrile, α -(**2**) $[\text{Cu}_2\text{Br}_4]$ could be obtained from the filtrate in form of thin needles (Fig. 5.4). It crystallises in the tetragonal space group $P4_2/mbc$ (No. 135). By energy dispersive X-ray spectroscopy measurement, the Cu:Br ratio of 1:2 in α -(**2**) $[\text{Cu}_2\text{Br}_4]$ was confirmed.

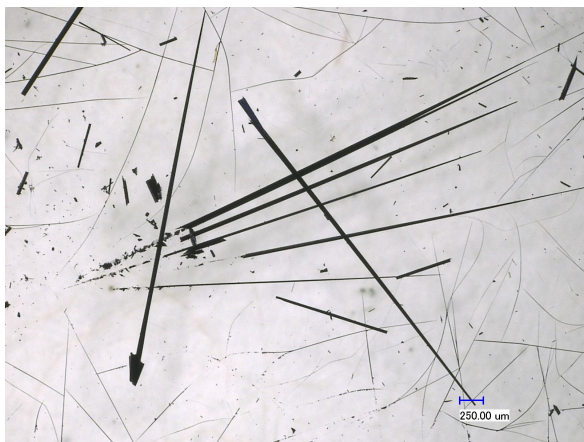


Figure 5.4: Dark, thin needles of α -(**2**) $[\text{Cu}_2\text{Br}_4]$.

cuprate(I) anion, the one symmetry independent Cu atom is located at the Wyckoff position $8g \equiv C_2$. As the atoms of the $\mathbf{2}^{2+}$ dications, the bromine atoms are positioned at the Wyckoff position $8h \equiv C_s$.

The crystals of α -(**2**) $[\text{Cu}_2\text{Br}_4]$ are made up by $\mathbf{2}^{2+}$ dications and bromido cuprate(I) anions forming one-dimensional chains of edge-sharing CuBr_4 tetrahedra, $[\text{CuBr}_{4/2}]_n$ (Fig. 5.5). The presence of the dicationic species is shown by the bond lengths in the central CNNC moiety with 1.23 Å for $\text{N}2-\text{N}2^i$ and 1.45 Å for $\text{N}2-\text{C}3$. Therein, the center of gravity is located at the Wyckoff position $4a \equiv C_{2h}$. Besides the hydrogen atoms of the methyl groups at general positions, all atoms of $\mathbf{2}^{2+}$ are located at the mirror plane perpendicular to the crystallographic c axis (Wyckoff position: $8h \equiv C_s$).

In the one-dimensional bromido cuprate(I) anion, the one symmetry independent Cu atom is located at the Wyckoff position $8g \equiv C_2$. As the atoms of the $\mathbf{2}^{2+}$ dications, the bromine atoms are positioned at the Wyckoff position $8h \equiv C_s$.

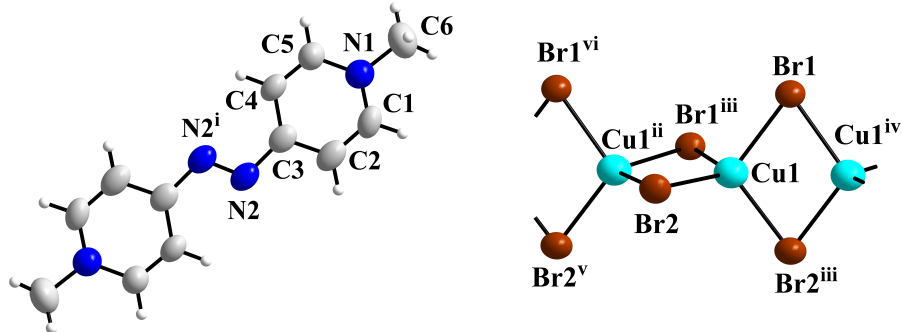


Figure 5.5: The molecules in the crystals of α -(**2**) $[\text{Cu}_2\text{Br}_4]$, the planar $\mathbf{2}^{2+}$ dication and a section of the bromido cuprate(I) anion, $[\text{CuBr}_{4/2}]_n$, forming one-dimensional chains of edge-sharing CuBr_4 tetrahedra. The superscripts denote the symmetry operations: $i = 1-x, 1-y, z$; $ii = x, y, 1-z$; $iii = \frac{1}{2}+y, -\frac{1}{2}+x, \frac{3}{2}-z$; $iv = x, y, 2-z$; $v = \frac{1}{2}+y, -\frac{1}{2}+x, \frac{1}{2}-z$; $vi = x, y, -1+z$. Bond lengths/Å: $\text{N}2-\text{N}2^i$ 1.228(14), $\text{N}2-\text{C}3$ 1.446(14), $\text{Cu}1-\text{Br}1$ 2.5326(11), $\text{Cu}1-\text{Br}2$ 2.4857(12) and $\text{Cu}1-\text{Cu}1^{ii}$ 3.0393(1).

The Cu–Br distances are in average 2.50 Å. The Br–Cu–Br angles range between 101–118°, close to the ideal tetrahedral angle. The Cu···Cu distance amounts to 3.04 Å.

In the crystals, the 2^{2+} dication form stacks running in *c* direction. The molecules are arranged parallel in a face-to-face stacking with a center-of-gravity distance of 3.04 Å. However, the distance between adjacent 2^{2+} dications is relative small, they are twisted by 90° to each other providing slight overlap. Therefore minor interactions between the positively charged pyridinium fragments are assumed.

The cation stacks form a tunnel structure along the *c* axis. These tunnels are filled with the $[\text{CuBr}_{4/2}]_n$ anion chains (Fig. 5.6).

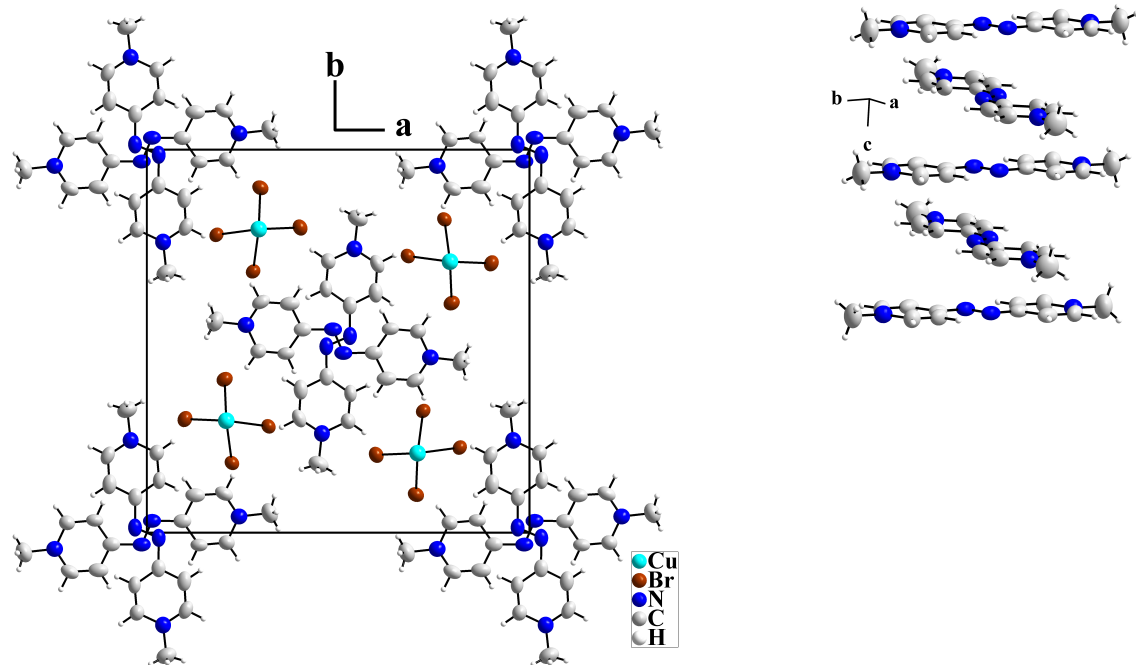


Figure 5.6: The unit cell of α -(2) $[\text{Cu}_2\text{Br}_4]$ depicted in *c* direction (right). The planar 2^{2+} dication molecules form equidistant stacks along the *c* axis creating a tunnel structure (left). These tunnels are filled with the one-dimensional bromido cuprate(I) chains $[\text{CuBr}_{4/2}]_n$.

5.1.3 β -(2)[Cu₂Br₄] · CH₃CN

β -(2)[Cu₂Br₄] · CH₃CN forms dark platelets (Fig. 5.7). It crystallises in the monoclinic space group P2₁/n (No. 14). By energy dispersive X-ray spectroscopy the Cu:Br ratio of 1:2 in the compound was confirmed.

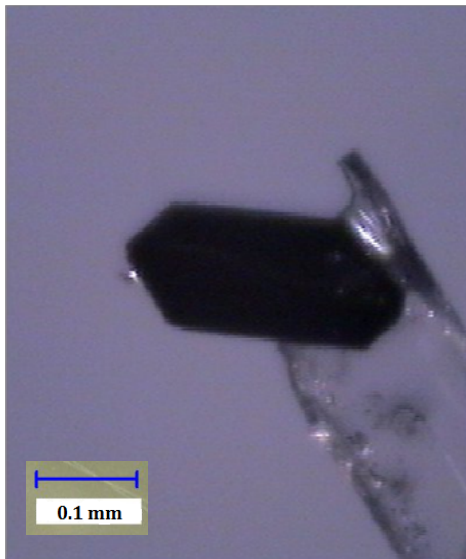


Figure 5.7: Dark platelet of β -(2)[Cu₂Br₄] · CH₃CN used for the X-ray data collection.

pyridinium fragments in a distance of 0.32 Å. In the central CNNC moiety the bonds are 1.15 Å for N8–N8ⁱⁱ and 1.47 Å for N8–C21. For all 2^{2+} molecules, the bond lengths in the CNNC moiety correspond to the azo-bis(*N*-methyl-4,4'-pyridinium) dication.

In the crystal, the dications form a stacking structure along the *b* direction. The stacks contain molecules of 2_t^{2+} and 2_p^{2+} forming trimeric aggregates. Hence, one molecule of 2_p^{2+} is encircled by two molecules of 2_t^{2+} . Therein, the molecules of 2_p^{2+} are obliquely arranged with an offset of 1.15 Å. The centers of gravity of 2_t^{2+} are orientated oppositely to 2_p^{2+} . In the trimers, the center-of-gravity distance amounts to 3.25 Å. The positive charges on the N atoms in the pyridinium fragments hinder an effective overlap of the aromatic systems. Thus, only interactions between the central CNNC moiety are assumed, solely. Between the aggregates, the intermolecular distance is highly enlarged by 5.99 Å. Consequently, the loose stacking leads to no signs of appreciable interactions. The 2_s^{2+} dications are isolated in the crystals. The molecules are strongly inclined to the stacking direction. The CH₃CN solvent molecules are located in between the 2_s^{2+} dications. As in the crystals of α -(2)[Cu₂Br₄], the 2^{2+} dications and, here additionally the solvent molecules, generate a tunnel structure running in *b* direction (Fig. 5.9). The stacks of 2^{2+} dications and the one-dimensional edge-sharing CuBr₄ tetrahedra are the common structural features. The lattice parameter gives hint to pseudo-tetragonal symmetry. However, the unit cell contains one 2^{2+} and one CH₃CN, additionally, and the angle β deviates substantially from rectangularity with 93.17°.

The structure of β -(2)[Cu₂Br₄] · CH₃CN contains three symmetrically independent 2^{2+} dications, two dibromido cuprate(I) anions [CuBr₂⁻]_n in form of infinite one-dimensional chains of edge-sharing CuBr₄ tetrahedra and a CH₃CN solvent molecule (Fig. 5.8).

Extraordinarily, the three 2^{2+} dications differ in their shape. For further discussion, the differences are connoted with: 2_p^{2+} (*p*: planar), 2_s^{2+} (*s*: step) and 2_t^{2+} (*t*: tilted). The atoms as the center of gravity in the 2_t^{2+} dication are located at general positions. The centers of gravity of 2_p^{2+} and 2_s^{2+} are positioned at inversion centers (Wyckoff position: 2*b*/2*c* ≡ $\bar{1}$). In 2_t^{2+} , the bond lengths in the central CNNC moiety amount to 1.22 Å for N2–N3, 1.44 Å for N2–C3 and 1.45 Å for N3–C9. The two 4'-(py)-N units are slightly tilted by an angle of about 8°. The 2_p^{2+} dication is essentially planar with bonds lengths of 1.21 Å for N6–N6^{*i*} and 1.47 Å for N6–C15. The 2_s^{2+} dication shows a twist along the N=N bond, resulting in two parallel planes created by the

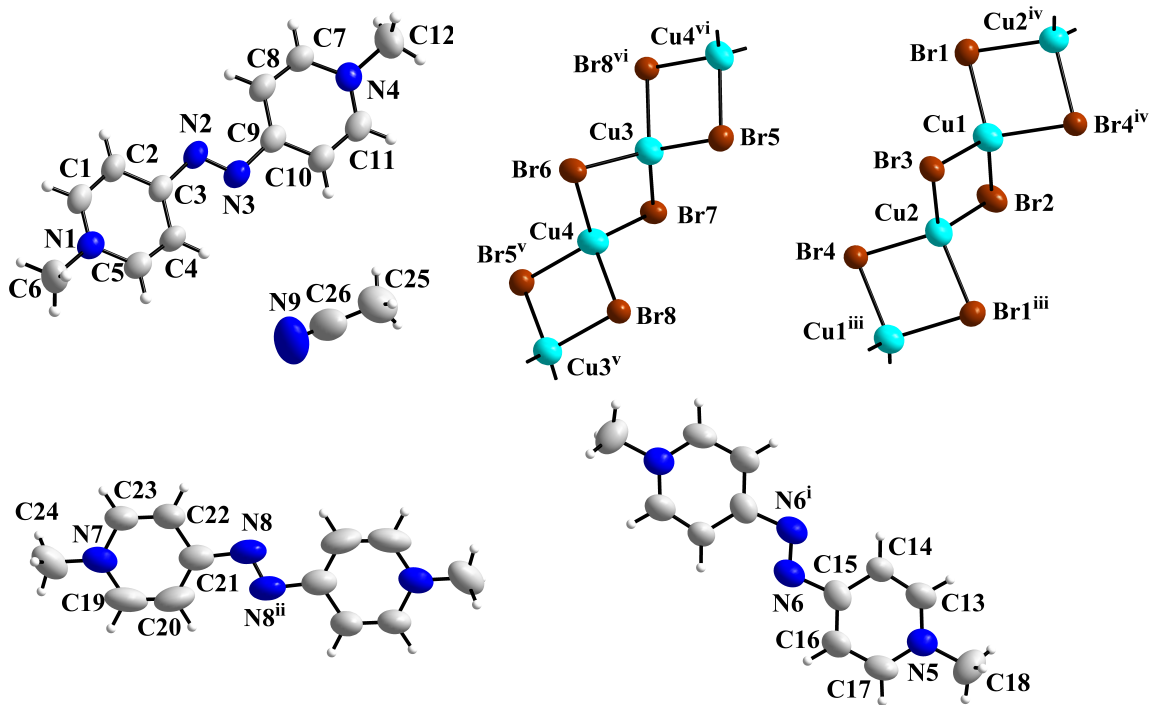


Figure 5.8: The structure of β -(2) $[\text{Cu}_2\text{Br}_4]\cdot\text{CH}_3\text{CN}$ is built up by three symmetry independent 2^{2+} dications, the two infinite one-dimensional chains of edge-sharing CuBr_4 tetrahedra, $[\text{CuBr}_{4/2}^-]_n$, and a CH_3CN solvent molecule. The superscripts denote the symmetry operations: $i = 1-x, -y, 1-z$; $ii = -x, -y, 1-z$; $iii = \frac{1}{2}-x, -\frac{1}{2}+y, \frac{1}{2}-z$; $iv = \frac{1}{2}-x, \frac{1}{2}+y, \frac{1}{2}-z$; $v = \frac{3}{2}-x, -\frac{1}{2}+y, \frac{1}{2}-z$; $vi = \frac{3}{2}-x, -\frac{1}{2}+y, \frac{1}{2}-z$. Bond lengths/ \AA : N2–N3 1.221(10), N2–C3 1.440(11), N3–C9 1.446(12), N6–N6ⁱ 1.206(16), N6–C15 1.474(13), N8–N8ⁱⁱ 1.156(17), N8–C21 1.474(16), Cu1–Br1 2.4872(17), Cu1–Br2 2.4648(16), Cu1–Br3 2.4920(15), Cu1–Br4^{iv} 2.5813(17), Cu2–Br2 2.4728(16), Cu2–Br3 2.5025(15), Cu2–Br4 2.4765(15), Cu2–Br1ⁱⁱⁱ 2.5691(17), Cu1–Cu2 2.9704(19), Cu1ⁱⁱⁱ–Cu2 3.2929(1), Cu3–Br5 2.4940(17), Cu3–Br6 2.4925(16), Cu3–Br7 2.4960(15), Cu3–Br8^{vi} 2.5692(16), Cu4–Br5^v 2.5623(18), Cu4–Br6 2.4585(15), Cu4–Br7 2.4989(15), Cu4–Br8 2.5362(17), Cu3–Cu4 2.973(2) and Cu3–Cu4^{vi} 3.3117(1).

In between these tunnels, the bromido cuprate(I) anions are located. The one-dimensional chains of the $[\text{CuBr}_{4/2}^-]_n$ anions form a rod packing. The Cu–Br distances vary from 2.46 \AA to 2.56 \AA , corresponding closely to monovalent Cu(I). The tetrahedra are strongly distorted with Br–Cu–Br angles between 98–120°. The Cu \cdots Cu distances in the chains alternate by about 0.3 \AA by 2.97 \AA and 3.30 \AA .

In reactions of the pyridone azines with CuBr_2 , the anion structure motif of one-dimensional chains of edge-sharing CuBr_4 tetrahedra is observed in (1) $[\text{CuBr}_2]$, (8) $[\text{CuBr}_2]$, (1) $[\text{Cu}_2\text{Br}_4]$, α -(2) $[\text{Cu}_2\text{Br}_4]$ and β -(2) $[\text{Cu}_2\text{Br}_4]\cdot\text{CH}_3\text{CN}$. The common structural feature contains monovalent Cu(I), predominantly, whereas the oxidation state of the corresponding azine is +1 or +2.

In **(1)**[CuBr₂], **(8)**[CuBr₂] (see Chapter 4), **(1)**[Cu₂Br₄] and α -**(2)**[Cu₂Br₄] only one crystallographic independent Cu atom is present. The Cu \cdots Cu distances amount to 2.99 Å in **(1)**[CuBr₂], 3.17 Å in **(8)**[CuBr₂], in average 3.19 Å in **(1)**[Cu₂Br₄] and 3.04 Å in α -**(2)**[Cu₂Br₄]. The symmetries of the chains differ with $\bar{4}2m \equiv D_{2h}$ for the Cu atom in **(1)**[CuBr₂], $\bar{4} \equiv S_4$ for the chains in **(8)**[CuBr₂], $2 \equiv C_2$ for α -**(2)**[Cu₂Br₄] and only inversion symmetry $\bar{1} \equiv C_i$ in **(1)**[Cu₂Br₄]. In contrast, the structure of β -**(2)**[Cu₂Br₄]·CH₃CN contains four symmetrically independent Cu atoms with significantly alternating Cu \cdots Cu distances of about 0.3 Å by 2.99 Å and 3.30 Å. Nonetheless, the structural parameters in all these [CuBr_{4/2}]_n chains are almost identical. The Cu–Br bond lengths are around 2.50 Å, the Br–Cu–Br angles are between 100–120°, and the Cu–Br–Cu angles are 73–82°. The parameters are in accordance with the presence of monovalent copper in all five compounds, analogous to the bromido cuprates of protonated bases [126–128]. In case of divalent Cu, the Cu–Br bond lengths are shortened by 0.1 Å. Localised valence states of Cu(I) and Cu(II) are observed if mixed-valency is present in the bromido cuprate chains[129].

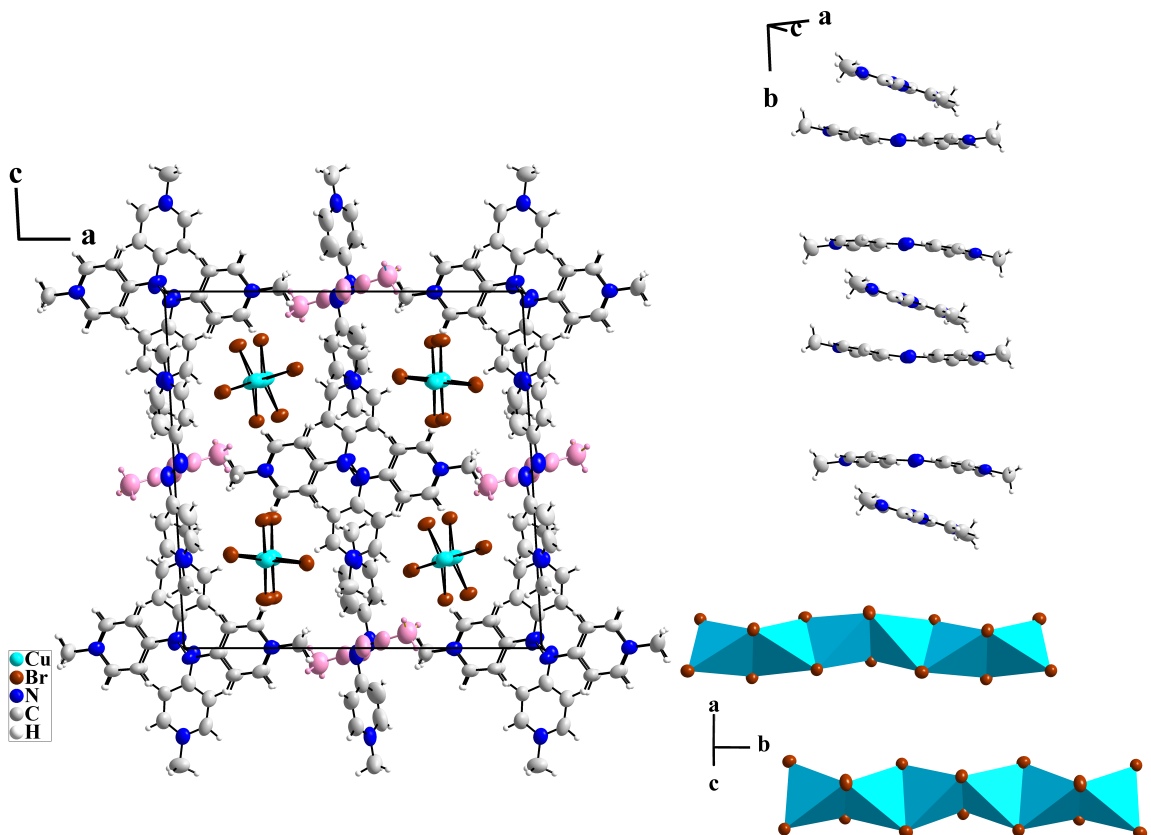


Figure 5.9: The unit cell of β -**(2)**[Cu₂Br₄]·CH₃CN depicted in *b* direction (left). The CH₃CN solvent molecules are highlighted in pink. The stacks of the dications 2_t^{2+} and 2_p^{2+} along the crystallographic *b* axis consisting of trimeric units (top right) and the two symmetrically independent one-dimensional chains of [CuBr_{4/2}]_n anions (bottom right).

5.1.4 (2)[CuBr₃]

(2)[CuBr₃] forms cuboid, dark shining crystals that crystallise in the monoclinic space group $P2_1/n$ (Fig. 5.10).

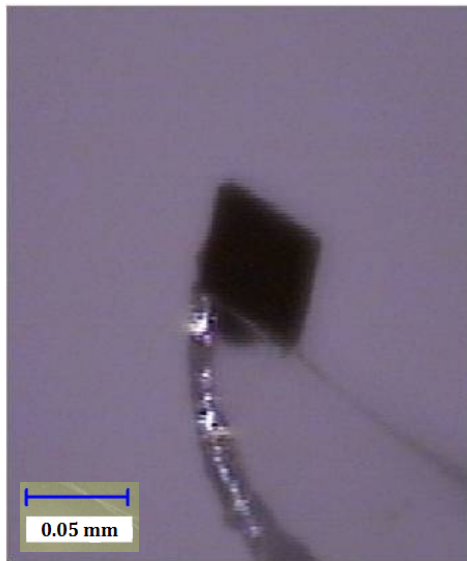


Figure 5.10: Cuboid-shaped, dark crystal of (2)[CuBr₃] used for the X-ray data collection.

for Cu1–Br1, 2.37 Å for Cu1–Br2 and 2.36 Å for Cu1–Br3. The Br–Cu–Br angles are between 117–123°.

The structure is built up by two symmetry independent $\mathbf{2}^{2+}$ dication and discrete triangular-shaped tribromido cuprate(I) anions, [CuBr₃]²⁻ (Fig. 5.11). One of the dications is planar, $\mathbf{2}_p^{2+}$ (*p*: planar), whereas the other one shows a step along the N=N bond, $\mathbf{2}_s^{2+}$ (*s*: step).

The centers of gravity of the dications are located at special positions that correspond to inversion symmetry (Wyckoff positions: $2a/2d \equiv \bar{1}$).

In the molecules of $\mathbf{2}_p^{2+}$, the bond lengths in the central CNNC moiety are 1.27 Å for N2–N2^{*i*} and 1.42 Å for N2–C3. In $\mathbf{2}_s^{2+}$, the bond lengths amount to 1.24 Å for N4–N4^{*ii*} and 1.45 Å for N4–C9. These fit to –C–N=N–C– bond order that is inverted to neutral **2**. Hence, azo-bis(*N*-methyl-4,4'-pyridinium) dications are present. Compared to $\mathbf{2}_p^{2+}$, the central N=N bond in $\mathbf{2}_s^{2+}$ is twisted resulting in two almost parallel layers made by the (py)-*N* units and shifted by 0.59 Å.

In the tribromido cuprate(I) anion, the Cu atom is trigonal planar coordinated by three bromine atoms. The Cu–Br distances amount to 2.38 Å

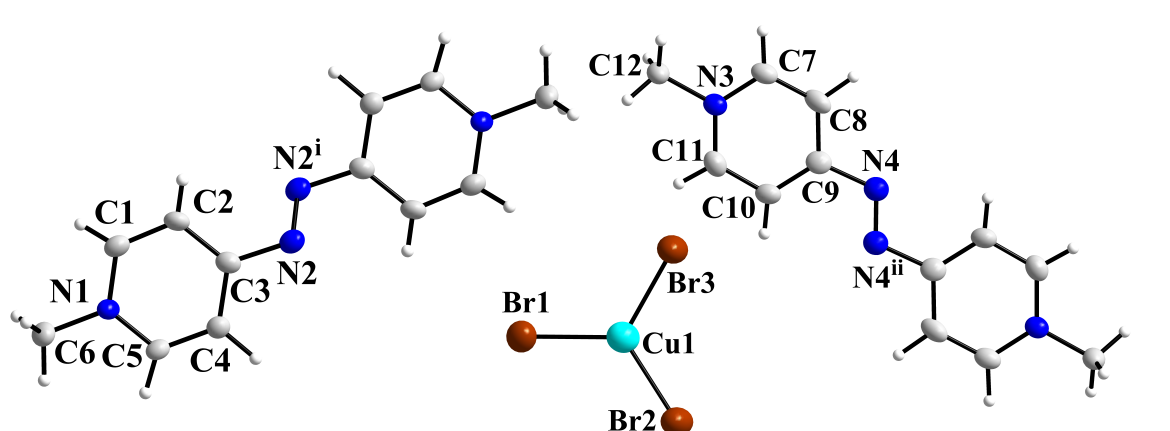


Figure 5.11: The three constitutional units in the crystals of (2)[CuBr₃]: the step-shaped and the planar $\mathbf{2}^{2+}$ dications, $\mathbf{2}_p^{2+}$ and $\mathbf{2}_s^{2+}$, and the tribromido cuprate(I) anion, [CuBr₃]²⁻. The superscripts denote the symmetry operations: *i* = 2–*x*, 1–*y*, 1–*z*; *ii* = 1–*x*, 1–*y*, 1–*z*. Bond lengths/Å: N2–N2^{*i*} 1.270(8), N2–C3 1.422(7), N4–N4^{*ii*} 1.240(9), N4–C9 1.450(7), Cu1–Br1 2.3816(9), Cu1–Br2 2.3676(8) and Cu1–Br3 2.3559(8).

In the structure, the dicationic form oblique stacks running along the crystallographic a axis that are made up alternating of $\mathbf{2}_p^{2+}$ and $\mathbf{2}_s^{2+}$ molecules. In the stacks, the molecules are nearly parallel to each other. Therein, the centers of gravity are aligned equidistantly by 3.74 Å. However, the step along the N=N bridge in the molecules of the $\mathbf{2}_s^{2+}$ leads to intermolecular plane-to-plane distances of 3.15 Å and 3.39 Å. The offset between adjacent molecules amounts to 1.82 Å. Due to the electrostatic repulsion by the two positive charges per molecule, the pyridinium fragments are sterically shielded from each other which is emphasised by the large distances of 3.93 and 5.23 Å between the centroids of the aromatic fragments. The $[\text{CuBr}_3]^{2-}$ anions are isolated in between the dication stacks connected via weak hydrogen bonds (Fig. 5.12).

First, the discrete, trigonal planar tribromido cuprate(I) anion was structurally characterised in $\text{Cu}_4\text{Br}_7\text{L}_3 \cdot 3\text{H}_2\text{O}$ ($\text{L} = \text{Tris}(1\text{-pyrazolylethyl})\text{amine}$) [130]. S. Andersson and S. Jagner investigated the Cu(I) coordination in dependence of the ligand concentration and synthesised the tetraphenylphosphonium salt $[\text{P}(\text{CH}_3)_4]_2[\text{CuBr}_3]$ [71]. Herein, the $[\text{CuBr}_3]^{2-}$ anion has perfect D_{3h} symmetry. Reactions of bis(methyltriphenylphosphonium) (PPh_3Me) and CuBr_2 lead to two different crystalline forms. One contains the trigonal planar $[\text{CuBr}_3]^{2-}$ while the other form is made up by separate $[\text{CuBr}_2]^-$ and Br^- anions. The organic-inorganic hybrid bis(2,3-dimethoxyquinoxalinium) tribromido cuprate(I) is built up by mono-protonated cations and trigonal planar $[\text{CuBr}_3]^{2-}$ [131]. The studies underline that the transition of two- to three-co-ordination in copper(I) complexes depends on the bromide concentration [132].

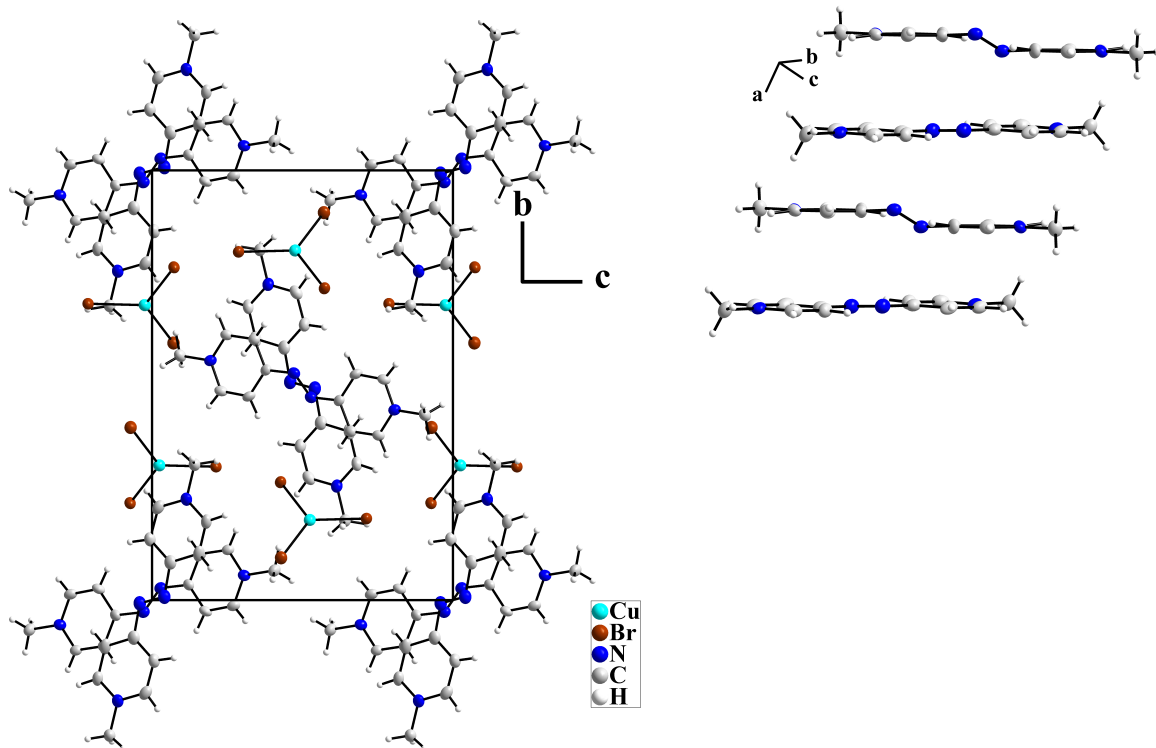


Figure 5.12: The unit cell of (2)[CuBr₃] in view along the a axis (left). Both $\mathbf{2}^{2+}$ dication molecules form oblique equidistant stacks running along the crystallographic a axis. The planar $\mathbf{2}_p^{2+}$ and the step-shaped $\mathbf{2}_s^{2+}$ dications are stacked alternately with intermolecular plane-to-plane distances of 3.15 Å and 3.39 Å (right). The $[\text{CuBr}_3]^{2-}$ triangles are isolated in between the cation stacks.

5.1.5 (2)[CuBr₄]

Stoichiometric amounts of CuBr₂ and Br₂ reacted with **2** to the dication salt **(2)[CuBr₄]** in form of dark needles (Fig. 5.13). It crystallise in the monoclinic space group *P2₁/n*. Energy dispersive X-ray spectroscopy confirmed the Cu:Br ratio of 1:4 in the compound.



Figure 5.13: Dark needle-shaped crystal of **(2)[CuBr₄]** used for the X-ray data collection.

The structure of **(2)[CuBr₄]** is closely related to that of **(2)[CuBr₃]** (see 5.1.4). As in the crystals of **(2)[CuBr₃]**, there are two symmetry independent 2^{2+} dications. However, in contrast to the [CuBr₃]²⁻ anion in **(2)[CuBr₃]** with monovalent Cu(I), the bromido cuprate anion presents a distorted tetrahedra containing divalent Cu(II), [CuBr₄]²⁻ (Fig. 5.14). The centers of gravity of the dications are positioned at inversion centers (Wyckoff positions: $2a/2d \equiv \bar{1}$). The structural features of the dications are similar to those in **(2)[CuBr₃]**; one dication is planar, 2_p^{2+} , and one is step-shaped along the N=N bridge, 2_s^{2+} . The large displacement ellipsoids indicates low diffraction data quality leading to problems in the determination of precise atom positions.

The bond lengths in the central CNNC moiety of 2_p^{2+} amount to 1.19 Å for N2–N2^{*i*} and 1.47 Å for N2–C3. In 2_s^{2+} , the central N=N bond amounts to 1.08 Å for N4–N4^{*ii*} and 1.56 Å for N4–C9. Uncertainties result from low data quality. Nonetheless, charge balance emphasises the presence of azo-bis(*N*-methyl-4,4'-pyridinium) dications.

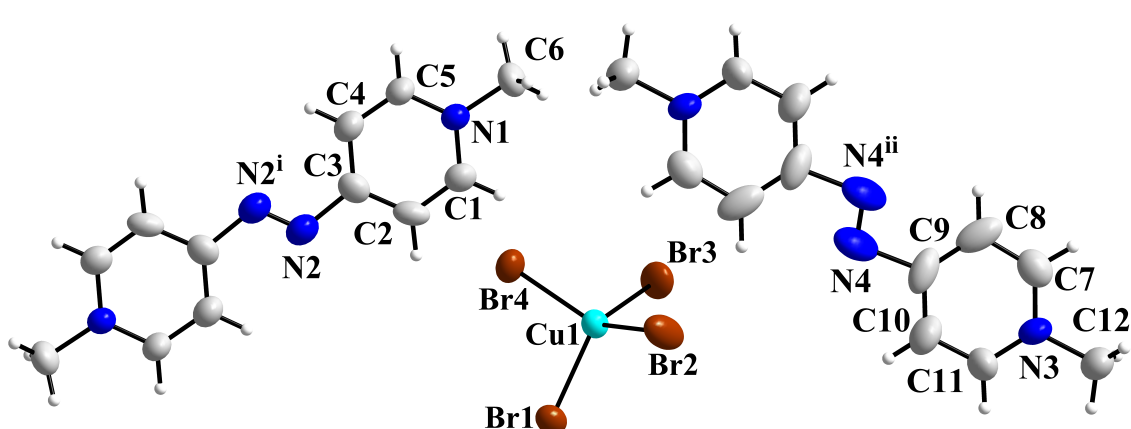


Figure 5.14: The building units in the crystals of **(2)[CuBr₄]**. As in the structure of **(2)[CuBr₃]**, the structure includes step-shaped and planar 2^{2+} dications, 2_p^{2+} and 2_s^{2+} . The tetrabromido cuprate(II) counter anions, [CuBr₄]²⁻, form distorted tetrahedra. The superscripts denote the symmetry operations: *i* = -x, 1-y, 1-z; *ii* = 1-x, 1-y, 1-z. Bond lengths/Å: N2–N2^{*i*} 1.186(15), N2–C3 1.470(13), N4–N4^{*ii*} 1.084(16), N4–C9 1.560(15), Cu1–Br1 2.4061(14), Cu1–Br2 2.3728(17), Cu1–Br3 2.3634(16) and Cu1–Br4 2.3932(15).

In $\mathbf{2}_s^{2+}$, the central N=N bond is twisted slightly. The planar 4'-(py)-N units are parallel and shifted by 0.19 Å which is significantly shorter to 0.59 Å in the $\mathbf{2}_s^{2+}$ dications in $(\mathbf{2})[\text{CuBr}_3]$.

In the tetrabromido cuprate(II) counter anion, $[\text{CuBr}_4]^{2-}$, the Cu atom is coordinated by four bromine atoms in distorted tetrahedral fashion. The Cu–Br distances are between 2.36–2.40 Å.

If the t_2 orbitals in a tetrahedra or octahedra are occupied inconsistently, Jahn-Teller distortion is observed. In general, the Jahn-Teller theorem implies that certain electronic configurations leads to a break in symmetry. In an octahedra, Jahn-Teller distortion effects bond length deformation. Ideal O_h symmetry is reduced to D_{4h} via stretching or flattening of the axial bonds. In a tetrahedra, the ligands are rejected unequally leading to angle deformation resulting in a flattening or stretched tetrahedra. The ideal T_d symmetry is lowered to $C_{2v}[133]$. The phenomenon is quite well known for compounds containing d^9 -configured Cu(II). In $(\mathbf{2})[\text{CuBr}_4]$, Jahn-Teller distortion is apparent since the Br–Cu–Br angles in the CuBr_4 tetrahedra vary between 95–138°.

Comparably to $(\mathbf{2})[\text{CuBr}_3]$, the two $\mathbf{2}^{2+}$ dications, $\mathbf{2}_p^{2+}$ and $\mathbf{2}_s^{2+}$, are alternately stacked along the crystallographic a axis. Adjacent molecules are stacked nearly parallel by a center-of-gravity distance of 3.69 Å. The intermolecular plane-to-plane distances amount to 2.94 Å and 3.43 Å due to the step-shaped $\mathbf{2}_s^{2+}$. The stacks are slightly oblique with an horizontal slippage of 1.86 Å. The electrostatic repulsion between the two positive charges on the N atoms results in steric divergence of the pyridinium rings. The $[\text{CuBr}_4]^{2-}$ tetrahedra are isolated between the cation stacks connected by weak hydrogen bonds (Fig. 5.15).

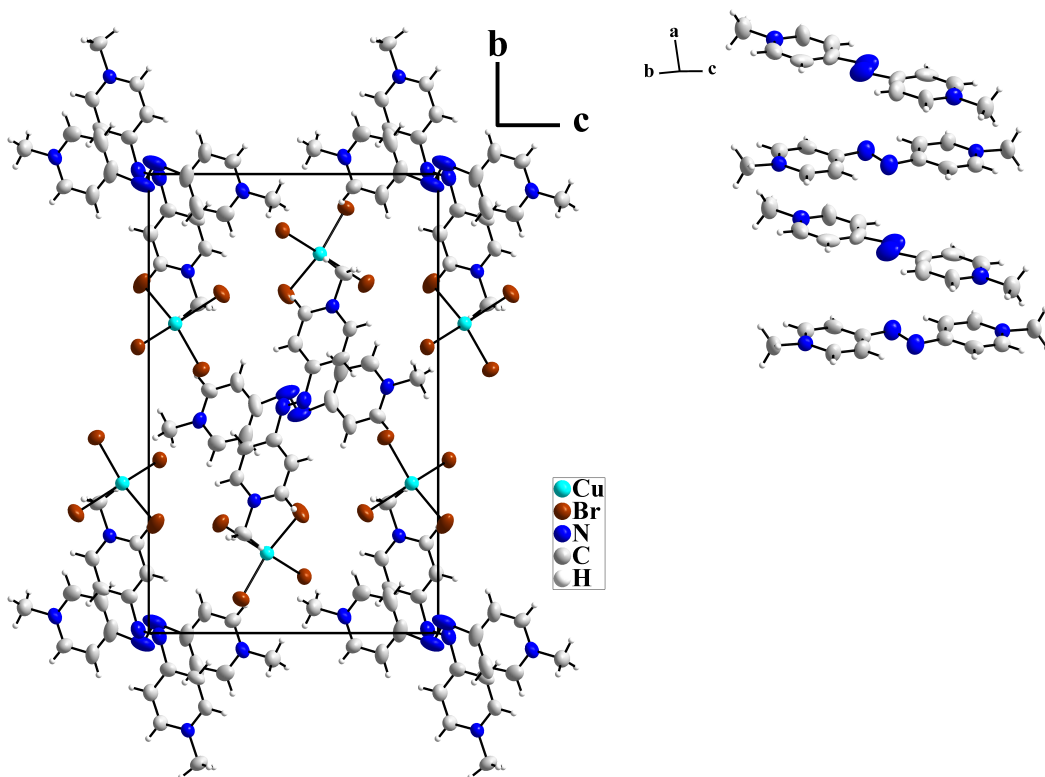


Figure 5.15: The crystal structure of $(\mathbf{2})[\text{CuBr}_4]$ in a view along the a axis (left). The $\mathbf{2}^{2+}$ dications form oblique equidistant stacks running in a direction (right). The distorted $[\text{CuBr}_4]^{2-}$ tetrahedra are isolated in between the cation stacks linked by weak hydrogen bonds.

5.1.6 (8)[CuBr₄]

Reaction of **8** with stoichiometric amounts of CuBr₂ and Br₂ in acetonitrile led to fine dark needles (Fig. 5.16). (8)[CuBr₄] crystallises in the monoclinic space group *C2/c* (No. 14).

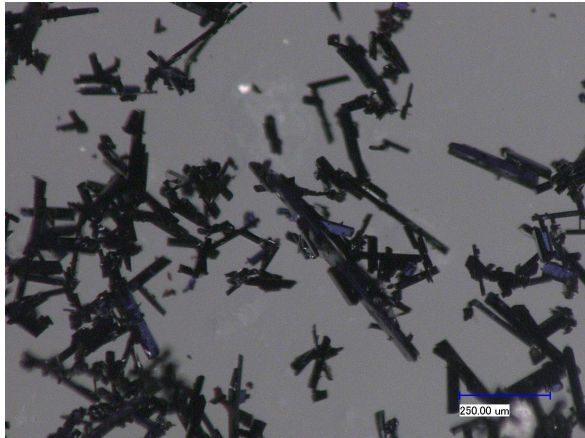


Figure 5.16: Fine needle-shaped crystals of (8)[CuBr₄].

methyl-2,2'-pyridinium) dication, **8**²⁺. The dications form along the crystallographic *c* axis. The molecules are arranged in a zig-zag pattern. The intermolecular plane-to-plane angle of adjacent molecules is about 50°. The shortest intermolecular distance amounts to 4.35 Å between the atoms C6···C6^{*ii*}. No effective overlap of the molecules is expected due to individual inclination and the large intermolecular distance.

The crystals are made up by **8**²⁺ dications and discrete tetrabromido cuprate(II) anions, [CuBr₄]²⁻ (Fig. 5.17). The CF₃ groups of the cation perform an almost free rotation, indicated by the large displacement ellipsoids of the fluorine atoms. The dication is planar with its center of gravity, in the mid of the N2–N2^{*i*} bond, located at an inversion center (Wyckoff position: 4*a* ≡ $\bar{1}$).

Compared to neutral **8**, the central CNNC moiety shows bond length alteration. The central N2–N2^{*i*} bond is shortened to 1.27 Å while the C1–N2 bond is elongated to 1.40 Å. Bond length order of –C–N=N–C– emphasises the presence of the azo-bis(*N*-methyl-2,2'-pyridinium) dication, **8**²⁺.

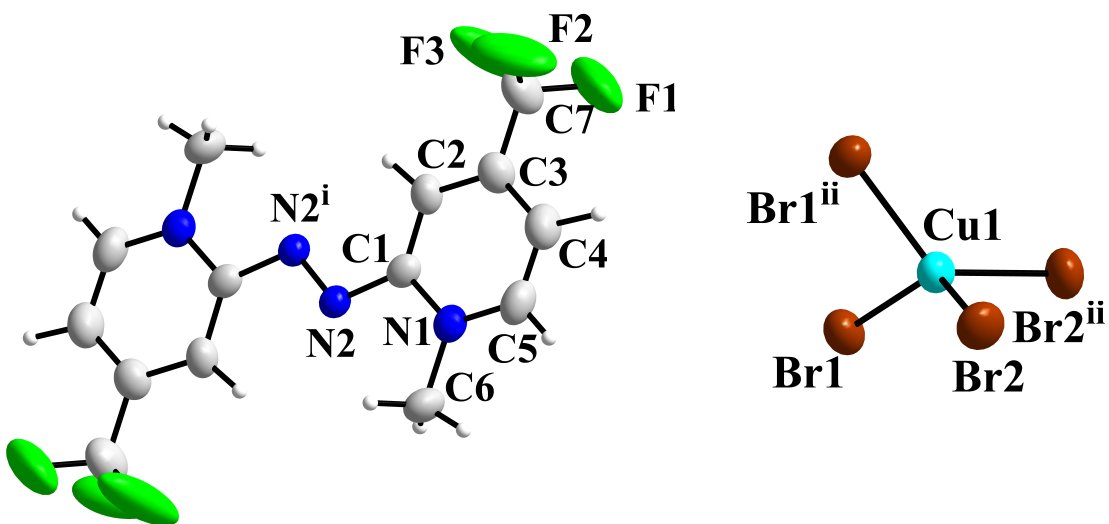


Figure 5.17: The planar **8**²⁺ dication and the tetrabromido cuprate(II) anion, [CuBr₄]²⁻, in the crystals of (8)[CuBr₄]. The superscripts denote the symmetry operations: *i* = 1–*x*, 1–*y*, 1–*z*; *ii* = 1–*x*, *y*, $\frac{3}{2}$ –*z*. Bond lengths/Å: N2–N2^{*i*} 1.270(8), N2–C1 1.401(7), Cu1–Br1 2.3939(9), Cu1–Br2 2.3828(9).

The discrete $[\text{CuBr}_4]^{2-}$ tetrahedra are located between the loose dication stacks. Due to the high positive charge of $\mathbf{8}^{2+}$, the bromine atoms interact strongly via hydrogen bonding. The bromido cuprate units contain divalent Cu(II), which is distorted tetrahedrally coordinated by four bromine atoms. Cu^{2+} is located at the special position $4e$ corresponding to a twofold symmetry axis $2 \equiv C_2$. The Cu–Br bond lengths are 2.38–2.39 Å and the Br–Cu–Br angles range between 97–131°. As for Cu^{2+} in (2)[CuBr_4], Jahn-Teller distortion is indicated by the large Br–Cu–Br angle range in the tetrabromido cuprate(II) anion. In comparison, the bromido cuprates of monovalent Cu show Cu–Br bond lengths longer by about 0.1 Å.

Since the one-electron as the two-electron oxidation process of the pyridone azines are possible by reactions with copper(II) halogenides, investigations of the magnetic susceptibility as well as measurements of the conducting properties are highly interesting. The magnetism and the electrical conductivity give insights in the electronic structure of these organic-inorganic hybrids.

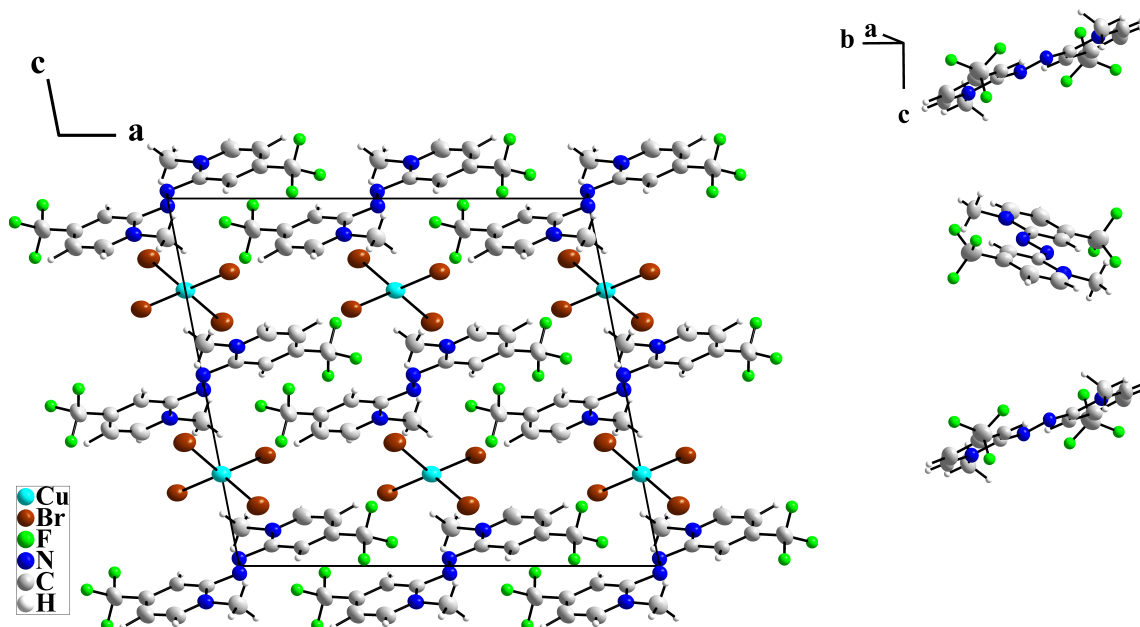


Figure 5.18: The unit cell of (8)[CuBr_4] depicted in *b* direction (left). The planar $\mathbf{8}^{2+}$ dications form loose stacks along the *c* axis wherein the molecules form a zig-zag pattern (right).

5.2 Magnetism

The magnetic susceptibility of (**1**)[Cu₂Br₄], α -(**2**)[Cu₂Br₄], (**2**)[CuBr₄] and (**8**)[CuBr₄] were measured in the temperature range from 1.9 K and 300 K (Fig. 5.19).

All four compounds are made up by azo-bis(*N*-methyl-2,2'-pyridinium) or, respectively, azo-bis(*N*-methyl-4,4'-pyridinium) dications, that are associated with singlet state and therefore diamagnetic behaviour. (**1**)[Cu₂Br₄] and α -(**2**)[Cu₂Br₄] contain [Cu(I)₂Br₄]²⁻ anions with closed-shell Cu(I) (*d*¹⁰-configuration). Thus, both substances consist of diamagnetic molecules exclusively. In contrast, (**2**)[CuBr₄] and (**8**)[CuBr₄] contain divalent Cu²⁺ in form of [CuBr₄]²⁻ tetrahedra. *d*⁹-Configurated Cu²⁺ is connected to paramagnetic phenomena.

In (**1**)[Cu₂Br₄] and in α -(**2**)[Cu₂Br₄] diamagnetism is observed predominantly. For (**1**)[Cu₂Br₄], above T > 50 K, the sensitivity limit of the instrument is reached since very weak momenta are monitored. At temperatures T < 50 K, a small paramagnetic moment is detected. Applying the Curie law to the linear $\chi_{mol}^{-1} = f(T)$ function results in a magnetic moment of 0.28 μ_B with θ of -4.8 K. For α -(**2**)[Cu₂Br₄], at T > 40 K, the molar susceptibility is nearly temperature independent in order of about 10⁻⁴ cm³ mol⁻¹. Below 40 K, the application of the Curie law leads to 0.42 μ_B with θ of 0.1 K. For both compounds, the small paramagnetic momenta may be attributed to inherent Cu(II) with *d*⁹ electron configuration. As for the radical cation salts (**1**)[CuCl₂] and (**1**)[CuBr₂] (see 4.2), the amount of Cu²⁺ is estimated by comparison of the Curie constants of (**1**)[Cu₂Br₄] and α -(**2**)[Cu₂Br₄] with the experimental Curie constant of the pure Cu(II) paramagnet ($C = 0.446 \text{ cm}^3 \text{Kmol}^{-1}$ for S = $\frac{1}{2}$ and $g_{eff} = 2.18$ [125]). The experimental Curie constants for (**1**)[Cu₂Br₄] and α -(**2**)[Cu₂Br₄] are 0.009 cm³ Kmol⁻¹ and 0.02 cm³ Kmol⁻¹ corresponding to 2.2 % or 4.5 % amount of Cu(II) in the respective compound. Similar amounts of divalent Cu²⁺ have been found in the (paraquat)²⁺[Cu₂Br₄]²⁻ salt[123].

(**2**)[CuBr₄] and (**8**)[CuBr₄] show paramagnetic phenomena. For (**2**)[CuBr₄], at T < 10 K, the linear $\chi_{mol}^{-1} = f(T)$ function shows nearly ideal Curie behaviour with Curie constant of 0.24 cm³ Kmol⁻¹, θ of -4.32 K and 1.38 μ_B corresponding to $\frac{3}{4}$ electrons. For T > 10 K, the paramagnetism passes into Curie-Weiss behaviour. The Curie constant amounts to 0.51 cm³ Kmol⁻¹ and the Curie temperature θ to -22.84 K. The magnetic moment of 2.02 μ_B is slightly larger than the moment expected for one unpaired electron per formula unit. However, the large Weiss constant is an indication of magnetic coupling, which reduces the overall magnetic moment.

In (**8**)[CuBr₄], the linear $\chi_{mol}^{-1} = f(T)$ function results in a Curie temperature θ of -2.26 K and magnetic momentum of 1.87 μ_B . The Curie constant of 0.44 cm³ Kmol⁻¹ is close to that of a pure Cu(II) paramagnet. Experimentally, the presence of *d*⁹ configurated Cu(II) in both compounds could be confirmed.

To conclude, measurements of the magnetic susceptibility of the four dication salts enable differentiation between monovalent and divalent copper Cu(I/II), explicitly. In agreement with experiment, the magnetic state of the compounds is dominated by the *d* electrons of copper in the specific bromido cuprate(I/II) counter anions.

As evident from experiment, the magnetic susceptibilities of the dication salts with monovalent Cu(I) are consistent with the magnetic behaviour of the radical cation salts (**1**)[CuCl₂] and (**1**)[CuBr₂]. As for (**1**)[CuCl₂] and (**1**)[CuBr₂], for (**1**)[Cu₂Br₄] and α -(**2**)[Cu₂Br₄] the occurrence of small magnetic momenta at low temperature that run into nearly temperature independent paramagnetism is observed. The magnetic momenta are connected to a certain amount of Cu²⁺ in the corresponding compounds. The singlet state of the dications, **1**²⁺ or **2**²⁺, does not influence the magnetic phenomena. The spin momenta of the radical cations **1**⁺ in (**1**)[CuCl₂] and (**1**)[CuBr₂] are largely suppressed. Consequently, the magnetic behaviour in the compounds is predominantly determined by the respective bromido cuprate(I) anion.

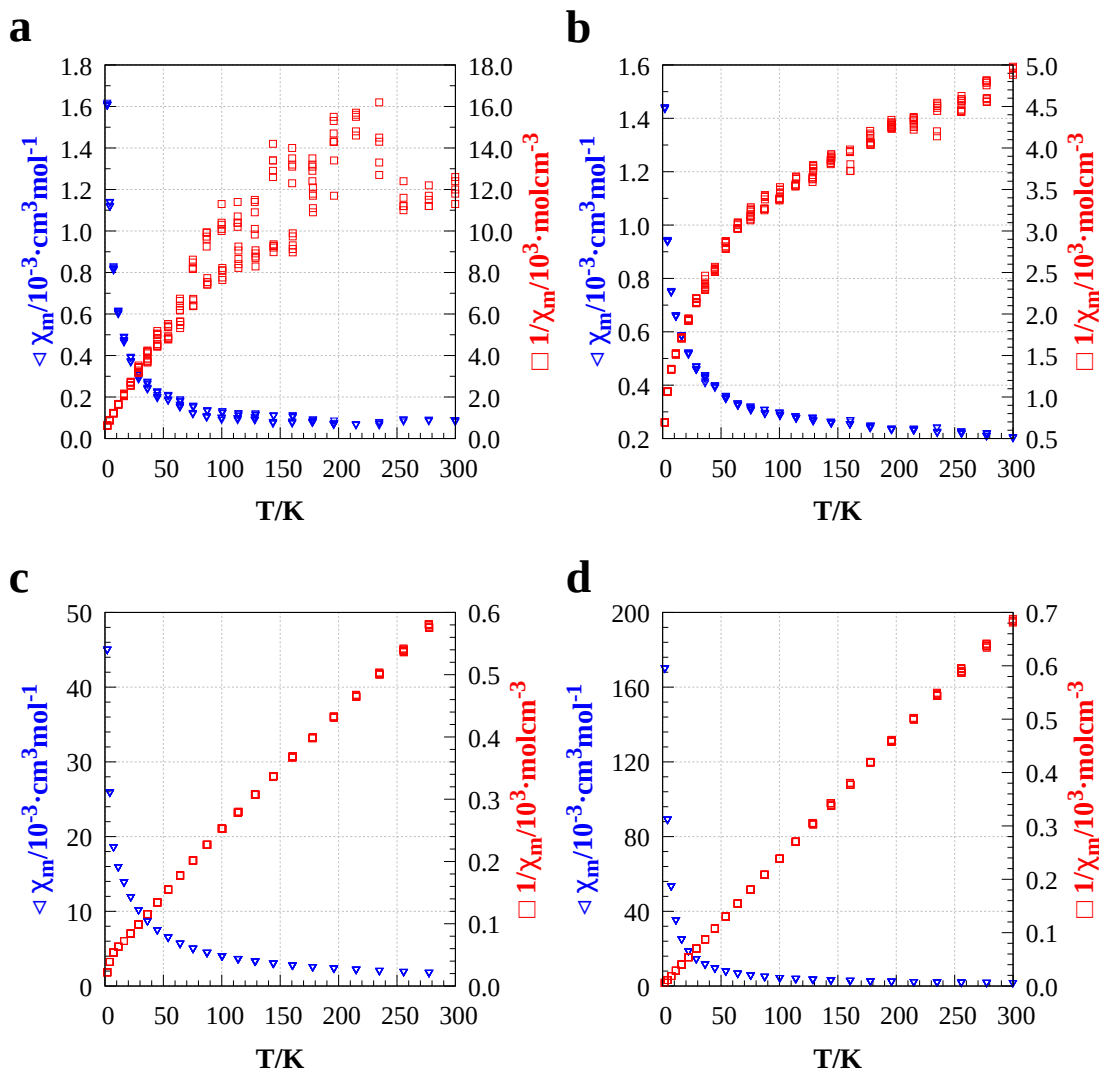


Figure 5.19: Magnetic properties of (**1**)[Cu₂Br₄] **a**, α -(**2**)[Cu₂Br₄] **b**, (**2**)[CuBr₄] **c** and (**8**)[CuBr₄] **d**. The plots $\chi_{mol} = f(T)$ (open, blue triangles) and $\chi_{mol}^{-1} = f(T)$ (open, red squares) are presented.

5.3 Conductivity

For the dication salts (**1**) $[\text{Cu}_2\text{Br}_4]$, α -(**2**) $[\text{Cu}_2\text{Br}_4]$, (**2**) $[\text{CuBr}_4]$ and (**8**) $[\text{CuBr}_4]$ conductivity measurements on powders were carried out. For all four compounds the electrical resistance decreases with increasing temperature.

(**1**) $[\text{Cu}_2\text{Br}_4]$ shows typical semiconducting behaviour. The conductivity measurements of α -(**2**) $[\text{Cu}_2\text{Br}_4]$ show an uncommon gradient with two local maxima of the resistance. At room temperature, the resistances of (**2**) $[\text{CuBr}_4]$ and (**8**) $[\text{CuBr}_4]$ do widely spread, that is associated with insulation. By increase of temperature both compounds are transferred into semiconductors (Fig. 5.23).

Phase transitions describe a process in which any property of a compound, as for example the electrical conductivity, changes discontinuously. In general, these transitions are connected to structural changes. Irreversible phase transformations are termed monotropic, reversible as enantiotropic. For solids with the same composition the phenomenon of polymorphism or, respectively, the occurrence of different modifications are present[134].

The electrical conductivity measurements of α -(**2**) $[\text{Cu}_2\text{Br}_4]$ show significant deviations from typical semiconducting behaviour. The resistance decreases with increasing temperature, however, two local maxima are observed amounting to $2.14 \times 10^8 \Omega$ at 330 K and $1.76 \times 10^8 \Omega$ at 360 K. The effect occurs at the first heating run, solely. Subsequently, typical semiconductivity is observed (Fig. 5.20). X-ray powder diffraction of the treated sample shows structural changes after heating (Fig. 5.21). Hence, differential scanning calorimetry (DSC) measurement of the compound was performed in the temperature range from 273 K to 430 K. The first heating run shows an endothermic process at an onset temperature of about 377 K and a heating exchange of 27.02 kJ/mol. The cooling run shows an exothermic process with end temperature of 382 K and a heat exchange of -12.74 kJ/mol (Fig. 5.22). The hysteresis of about 5 K indicate a first-order phase transition according to Ehrenfest[135]. Nonetheless, the process is highly irreversible, since the effect vanishes after the first heating cycle. The second local maxima fits well to the endothermic process detected via DSC. Nonetheless, the first observed maxima seems to belong not to a structural change. Thus, α -(**2**) $[\text{Cu}_2\text{Br}_4]$ might undergo an irreversible or monotropic phase transition. Unfortunately, crystal structure determination using single crystals of the second modification were not experimentally accessible. Partially decomposition of the compound can not be excluded. Probably, it refers to a displacive transformation[136] in which intermolecular interactions were broken and differently reconnected.

In general, the specific conductivities are extremely small with $1.1 \times 10^{-9} \text{ Scm}^{-1}$ at 310 K and $9.7 \times 10^{-8} \text{ Scm}^{-1}$ at 400 K for (**1**) $[\text{Cu}_2\text{Br}_4]$, $4.3 \times 10^{-9} \text{ Scm}^{-1}$ at 400 K for (**2**) $[\text{CuBr}_4]$ and $1.7 \times 10^{-9} \text{ Scm}^{-1}$ at 400 K for (**8**) $[\text{CuBr}_4]$. For α -(**2**) $[\text{Cu}_2\text{Br}_4]$ determination of the specific conductivity is rather possible for room temperature and is around $1.0 \times 10^{-9} \text{ Scm}^{-1}$. However, specific conductivity of the second modification was examined and amount to $1.2 \times 10^{-9} \text{ Scm}^{-1}$ at 310 K and $1.1 \times 10^{-6} \text{ Scm}^{-1}$ at 400 K. The Arrhenius plot of the functions $-\ln(R^{-1}) = f(T^{-1})$ enables the determination of the activation energy for the thermally activated electron transfer into the conduction band. The activation energy of (**1**) $[\text{Cu}_2\text{Br}_4]$ amounts to 1.08 eV. For the case of α -(**2**) $[\text{Cu}_2\text{Br}_4]$, only the activation energy of the second phase can be determined and amounts to 1.78 eV. Since (**2**) $[\text{CuBr}_4]$ and (**8**) $[\text{CuBr}_4]$ represent insulators at room temperatures, the activation energies E_a at temperatures above 380 K are determined to 2.05 eV for (**2**) $[\text{CuBr}_4]$ and 2.06 eV for (**8**) $[\text{CuBr}_4]$.

Remarkably, the room temperature specific conductivities of the dicationic salts (**1**) $[\text{Cu}_2\text{Br}_4]$ as well as for α -(**2**) $[\text{Cu}_2\text{Br}_4]$ found to be in the same region as in the group of the radical-containing compounds (**1**) $[\text{CuCl}_2]$, (**1**) $[\text{CuBr}_2]$ and (**8**) $[\text{CuBr}_2]$. At 310 K, the specific electrical conductivities of the compounds are in the order of 10^{-9} Scm^{-1} . Whereas the conductivity of (**1**) $[\text{CuCl}_2]$ might arise from the radical cation stacks, solely, it is assumed that the conductivity of the other four salts is

influenced by the polymeric $[\text{CuBr}_{4/2}]_n$ anion.

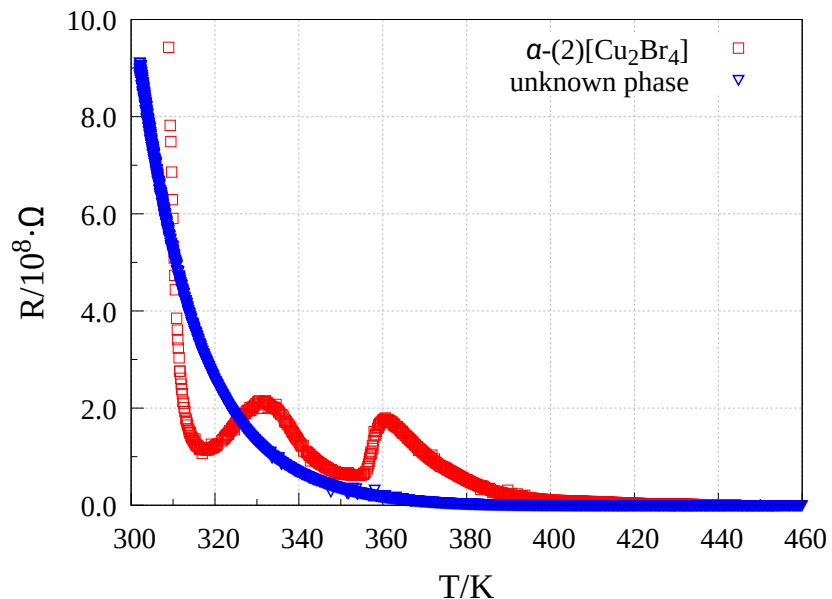


Figure 5.20: Measurement of the electrical resistance vs. temperature of α -(2) $[\text{Cu}_2\text{Br}_4]$ on first heating cycle (red) and last heating cycle (blue). The resistivity behaviour described by the progression in blue belongs to an unknown crystalline phase.

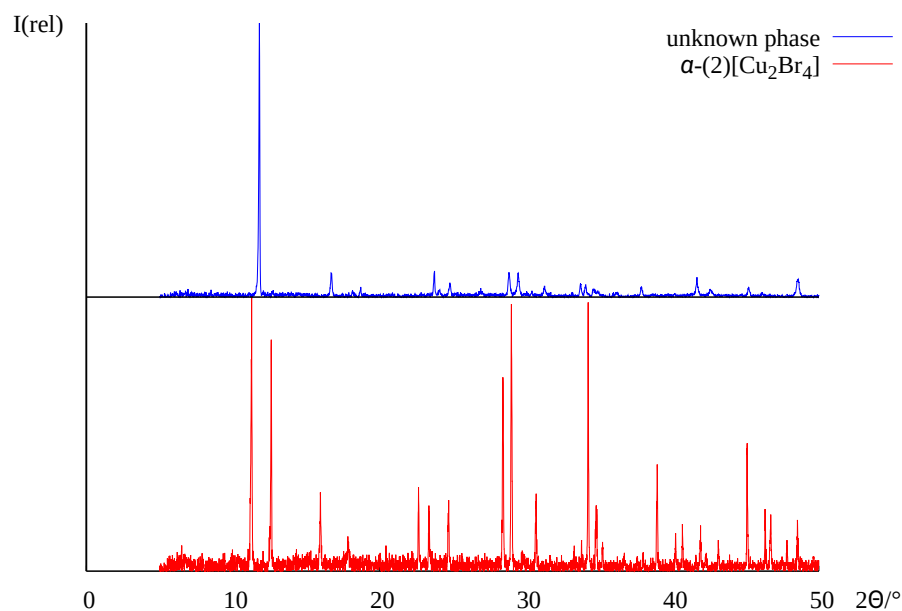


Figure 5.21: Powder diffractogram of α -(2) $[\text{Cu}_2\text{Br}_4]$ (on bottom, red) and after thermal treatment during conductivity measurement (on top, blue). The different powder diffractograms indicate a phase transformation of α -(2) $[\text{Cu}_2\text{Br}_4]$ under heating. Used radiation: Co-K α_1 .

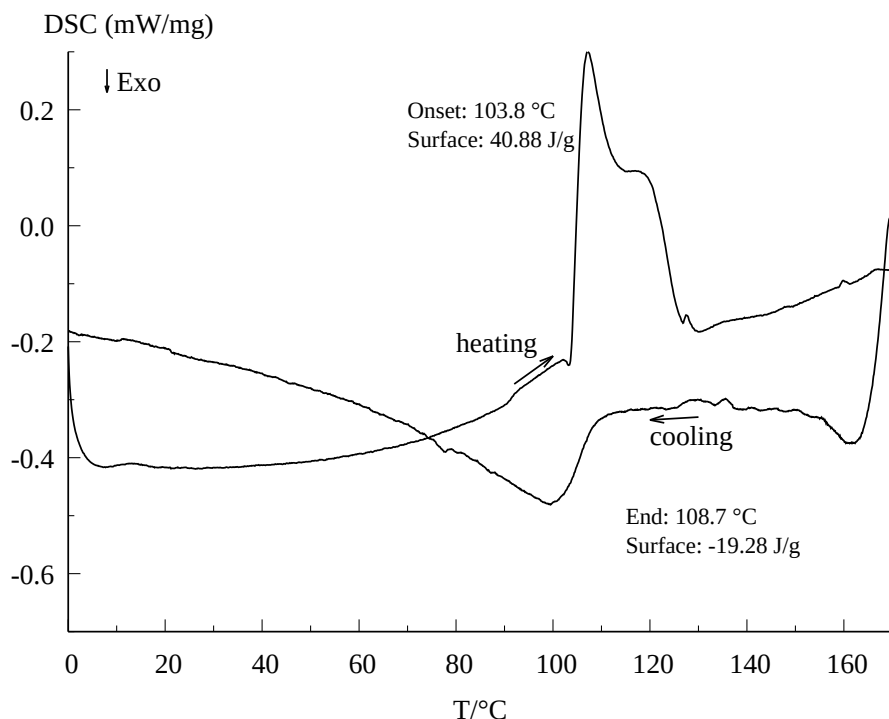


Figure 5.22: Differential scanning calorimetry plot of α -(2)[Cu₂Br₄]. The heating run shows an endothermic process at an onset temperature of about 377 K and a heating exchange of 27.02 kJ/mol. The cooling run shows an exothermic process with end temperature of 382 K and a heating exchange of -12.74 kJ/mol.

In general, the radicals **1**^{·+} or **8**^{·+} have an electronic doublet state and the azo-bis(*N*-methyl-pyridinium) dication, **1**²⁺ or **2**²⁺, an electronic singlet state. Especially, the measurement of (1)[Cu₂Br₄], with the closed-shell **1**²⁺ dication, emphasises that the [CuBr_{4/2}]_n chains are mainly responsible for conduction whereas the cation-cation interactions are negligible.

The activation energies, or respectively band gaps, for the thermally activated electron transfer into the conduction band ranges are around 1 eV. For (1)[Cu₂Br₄] and α -(2)[Cu₂Br₄] the conductivity is predominantly determined by the anion.

Concerning the radical cation as well as the dication salts, the structures and physical properties of these organic-inorganic hybrid materials indicate interesting structure-property relations.

The radical salts (1)[CuCl₂], (1)[CuBr₂] and (8)[CuBr₂] and the dication salts (1)[Cu₂Br₄] and α -(2)[Cu₂Br₄] containing cuprate(I) counter anions show small magnetic momenta at low temperatures that turns into nearly temperature independent paramagnetism. The dication salts (2)[CuBr₄] and (2)[CuBr₄] with integrated Cu²⁺ exhibit paramagnetic phenomena. Thus, magnetic phenomena are induced by the *d* electrons of respective cuprate anions.

Usually, in compounds containing organic stacks, the π electron systems of the organic units are responsible for conduction. In case of (1)[CuCl₂] with a molecular [CuCl₂]⁻ anion, the conductivity arises from the cation-cation interaction along the stacks. However, in the radical cation salts as the dication salts containing the polymeric [CuBr_{4/2}]_n chains, the conductivity is found to be in the same order of magnitude. Hence, the different electronic states of the dications (singlet) and the radical (doublet) emphasise that conduction is caused predominantly from the polymeric anion. Compounds containing the molecular distorted tetrahedral [CuBr₄]²⁻ unit, (2)[CuBr₄] and (8)[CuBr₄], present insulators.

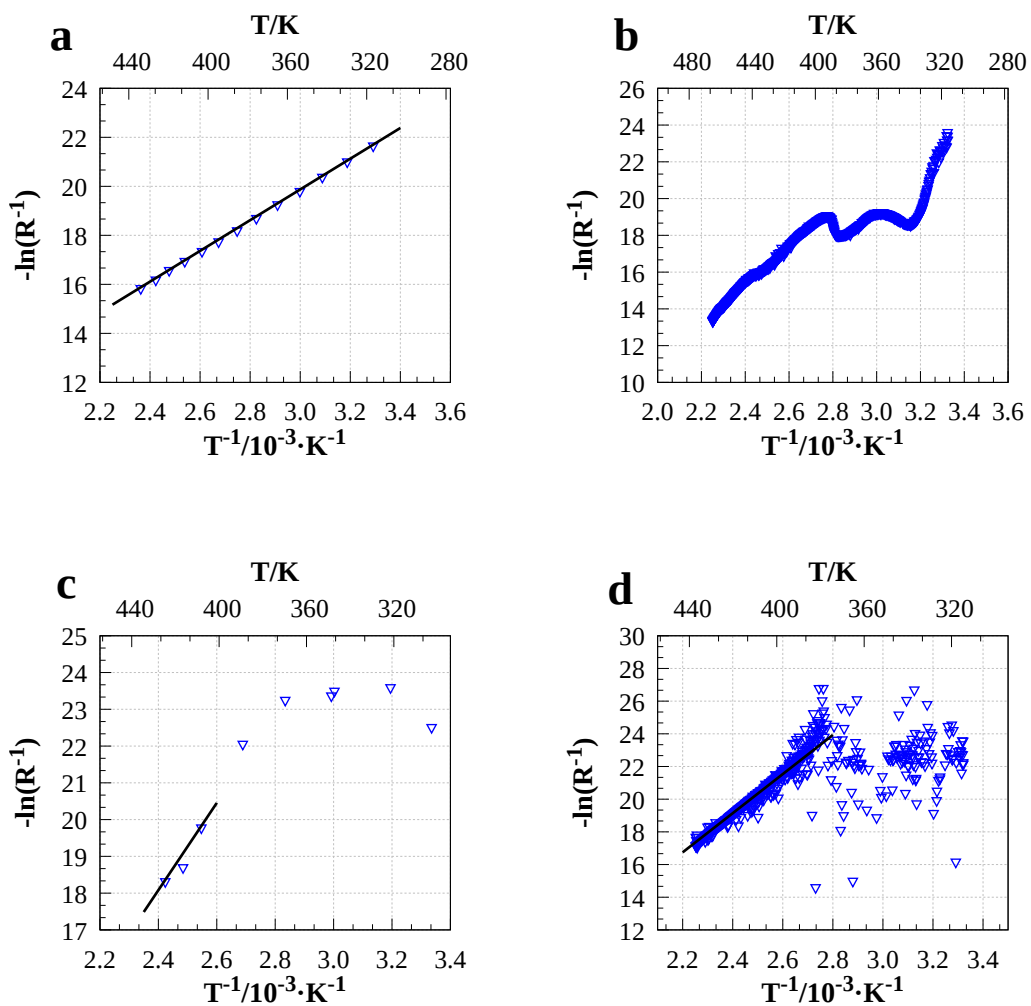


Figure 5.23: The Arrhenius plot $-\ln(R^{-1}) = f(T^{-1})$ for the electrical resistivities of (1) $[\text{Cu}_2\text{Br}_4]$ **a**, α -**(2) $[\text{Cu}_2\text{Br}_4]$** **b**, **(2) $[\text{CuBr}_4]$** **c** and (8) $[\text{CuBr}_4]$ **d**. The blue circles are the measured resistance and the black lines present the best linear fit.

CHAPTER 6

Charge Transfer Compounds with TCNQ

In the 1960s, 7,7,8,8-tetracyanoquinodimethane (TCNQ) was synthesised by condensation of malononitrile and 1,4-cyclohexanedione[137]. It has an electron affinity of 2.88 eV (277.9 kJ/mol)[30]. Due to its electron deficiency, TCNQ represents an appropriate candidate as electron acceptor for the generation of attractive CT salts.

Cyclic voltammetric measurement of TCNQ shows two well-separated one-electron reduction processes. Both reduction steps are fully reversible with the potentials $E_1 = 0.25$ V and $E_2 = -0.31$ V vs. Ag/AgCl (Fig. 6.1).

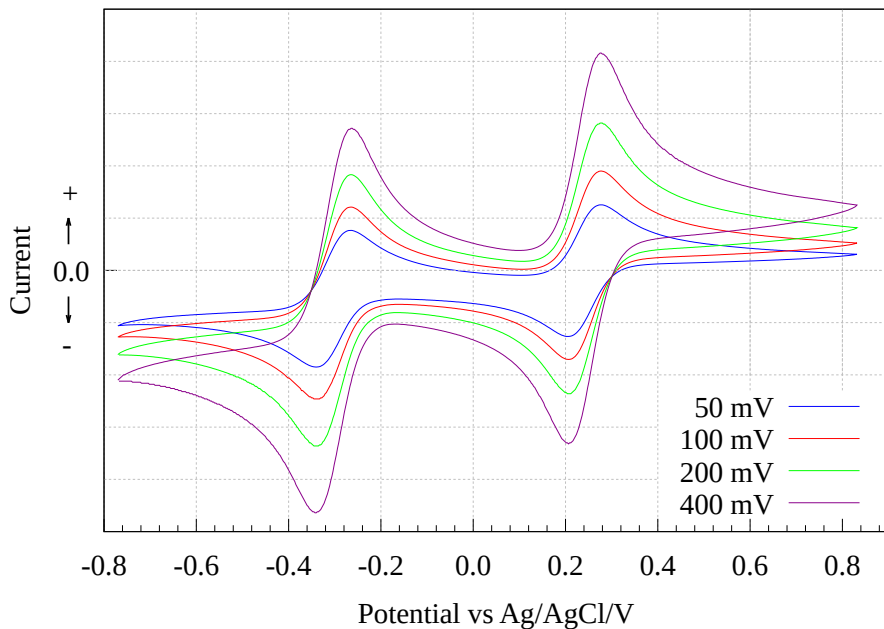
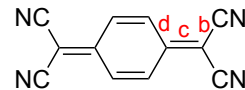


Figure 6.1: Cyclic voltammogram of TCNQ shows two reversible one-electron reduction processes at $E_1 = 0.25$ V and $E_2 = -0.31$ V vs. Ag/AgCl.

To estimate the charge on the TCNQ molecule within CT compounds, the Kistenmacher relationship[138] can be taken into account. It describes an empirical correlation of the bond length character with the corresponding oxidation state in the TCNQ molecule and is defined as follows:

$$q = A[c/(b + d)] + B \quad (6.1)$$



where q is the estimated charge, A and B are coefficients derived from neutral, anionic and dianionic TCNQ and b , c and d are specific bond lengths in TCNQ. Beside the widespread Kistenmacher formula, further empirical relations have been developed by Flandrois and Chasseau[139], and Coppens and Guru[140] with quite similar character.

In general, for all approaches, the simple idea stands behind, that the conversion from quinoid to benzenoid character increases with negative charge on TCNQ. Thus, the oxidation state of TCNQ is reflected by the C–C bond lengths.

Direct ionisation of TCNQ was investigated in the reaction with tetraethylammonium iodide (TEAI). In dependence of the TEAI concentration, the degree of charge transfer could be determined by powder IR absorption spectra[141].

Table 6.1: The potentials E_D for the first oxidation of the azines **1–8** to the corresponding radical cation, the potential E_A for the reduction of TCNQ to its mono-radical anion, $\text{TCNQ}^{\cdot-}$, and the potential difference $\Delta E_{DA} = E_D - E_A$.

Azine	E_D	E_A	ΔE_{DA}
1	-0.05	+0.25	-0.30
2	-0.10	+0.25	-0.35
3	-0.10	+0.25	-0.35
4	± 0.00	+0.25	-0.25
5	-0.20	+0.25	-0.45
6	-0.05	+0.25	-0.30
7	+0.40	+0.25	+0.15
8	+0.30	+0.25	+0.05

To predict the ionicity or, respectively, the degree of charge transfer in reactions of the azines **1–8** with TCNQ, the potential difference between the first oxidation of the azine to its corresponding radical cation and the reduction potential of TCNQ to its radical anion can be regarded (Tab. 6.1). By definition from Eq. 1.2, mixed-valency might be achievable for (TTF)(TCNQ) derived systems showing a potential difference ΔE_{DA} between -0.07 V and +0.30 V vs. Ag/AgCl.

Therefore, reactions of TCNQ with the azines **1–6** are expected to yield fully ionic CT salts, whereas in reaction with **7** and **8**, mixed-valent CT are expected.

In the following, eight new pyridone azine-containing CT salts with TCNQ are presented. Their crystal structures, and, if experimentally accessible, the magnetic and conducting properties were investigated. Furthermore, theoretical calculations of the band structures, PDOS, electrical conductivities and Mulliken population analyses were performed.

6.1 Crystal Structures

6.1.1 α -(1)(TCNQ)

In the reaction of **1** with TCNQ in acetone, the phenomenon of dimorphism is observed. Dark rods (α -(1)(TCNQ)) and fibrous thin dark-shining crystals (β -(1)(TCNQ)) were formed under ambient conditions (Fig. 6.2).



Figure 6.2: The dimorphic phases obtained in the reaction of **1** and TCNQ in acetone. Dark rods and fibrous thin dark-shining crystals of α -(1)(TCNQ) and β -(1)(TCNQ).

sured, however, the purity and the presence of texture effects disallowed an appropriate structure determination.

The crystals of α -(1)(TCNQ) are made up by planar molecules of **1** and TCNQ (Fig. 6.3). All atoms are located at general positions.

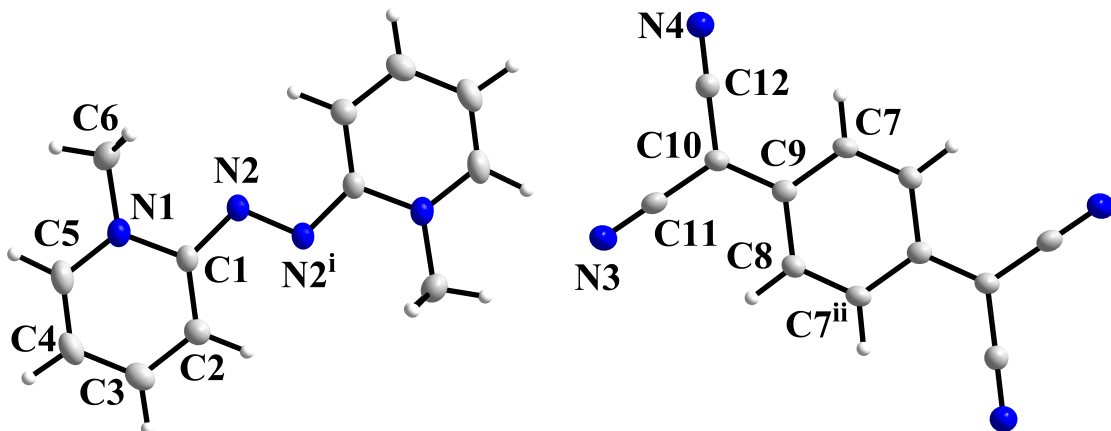


Figure 6.3: The planar molecules of **1** and TCNQ in the structure of α -(1)(TCNQ). The superscripts denote the symmetry operations: $i = 2-x, 1-y, 1-z$; $ii = 1-x, 1-y, 1-z$. Bond lengths/Å: $N2-N2^i$ 1.335(3), $C1-N2$ 1.357(2), $C7-C9$ 1.418(2), $C9-C8$ 1.419(2), $C8-C7^{ii}$ 1.364(2), $C9-C10$ 1.419(2), $C10-C11$ 1.418(3), $C10-C12$ 1.412(2).

The separation of both phases is possible by the kinetics of the crystallisation. The formation of β -(1)(TCNQ) is much faster than that of α -(1)(TCNQ). Thus, the combination of solutions of both components, cooled to -25 °C, leads to the precipitation of the β form, whereas from the filtrate at ambient temperature the α -form crystallises. X-ray single crystal determination of α -(1)(TCNQ) was performed successfully. In Fig. 6.4, the X-ray powder diffraction pattern detected from mixture of α - and β -(1)(TCNQ) is presented. The simulated powder pattern from X-ray single crystal data of α -(1)(TCNQ) do not cover all recorded reflections. Thus, the crystalline character of fibrous β -(1)(TCNQ) is as-

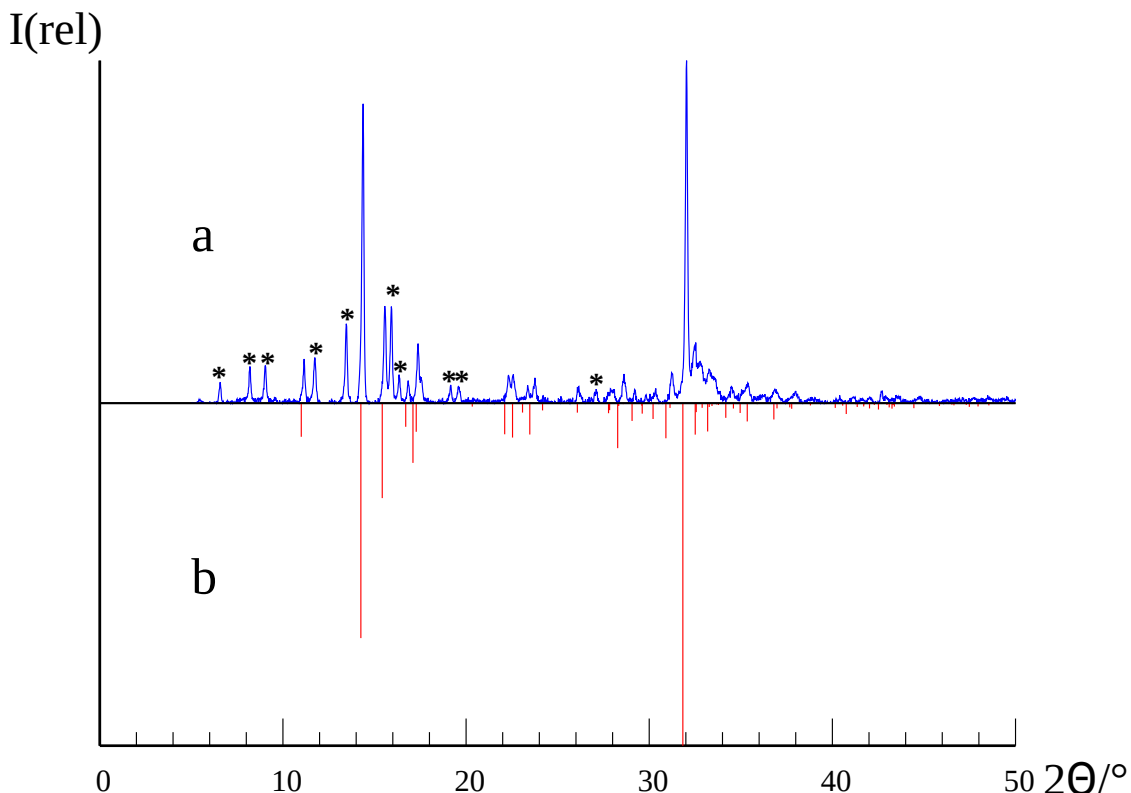


Figure 6.4: Powder diffractogram of a mixture of the dark rod-shaped crystals of α -(**1**)(TCNQ) and the fibrous thin needles of β -(**1**)(TCNQ) obtained in the reaction of **1** with TCNQ in acetone. It is assumed that the reflections marked with black asterisks belong to β -(**1**)(TCNQ). Used radiation: Co-K α_1 , a = measured diffractogram, b = simulated diffractogram on basis of single crystal data of α -(**1**)(TCNQ).

The molecule of **1** is essentially planar. The center of gravity is allocated at an inversion center (Wykoff position: $1b \equiv \bar{1} \equiv C_i$). The bond lengths of the central CNNC moiety amount to 1.34 Å for N2–N2 $'$ and 1.36 Å for C1–N2. These structural parameters indicate the presence of the radical cation species **1** $^{+}$, since the delocalisation of the electron over the whole systems generates bond lengths equality, ideally.

As the donor, the TCNQ molecule is planar. The center of gravity is positioned at an inversion center (Wykoff position: $1f \equiv \bar{1} \equiv C_i$). The application of the Kistenmacher equation provides a charge of -1.05 , approximately -1 , on TCNQ. The following bonds/Å are taken into account: C7–C9 1.418(2), C9–C8 1.419(2), C8–C7 ii 1.364(2), C9–C10 1.419(2), C10–C11 1.418(3) and C10–C12 1.412(2). Therefore, a complete charge transfer of one electron from **1** to TCNQ is assumed, resulting in the ionic CT salt α -(**1**) $^{+}$ (TCNQ) $^{-}$, fitting well to the predicted ionicity by Eq. 1.2.

In the crystals, donor and acceptor molecules form mixed stacks running along the crystallographic *a* axis. The stacking sequence is $\dots DA \dots$. The molecules are stacked nearly parallel and equidistantly. The intermolecular plane-to-plane distance amounts to 3.25 Å, whereby the centers of gravity of the molecules are shifted by 1.97 Å. The mixed stacks form a layered structure perpendicular to the stacking direction (Fig. 6.5).

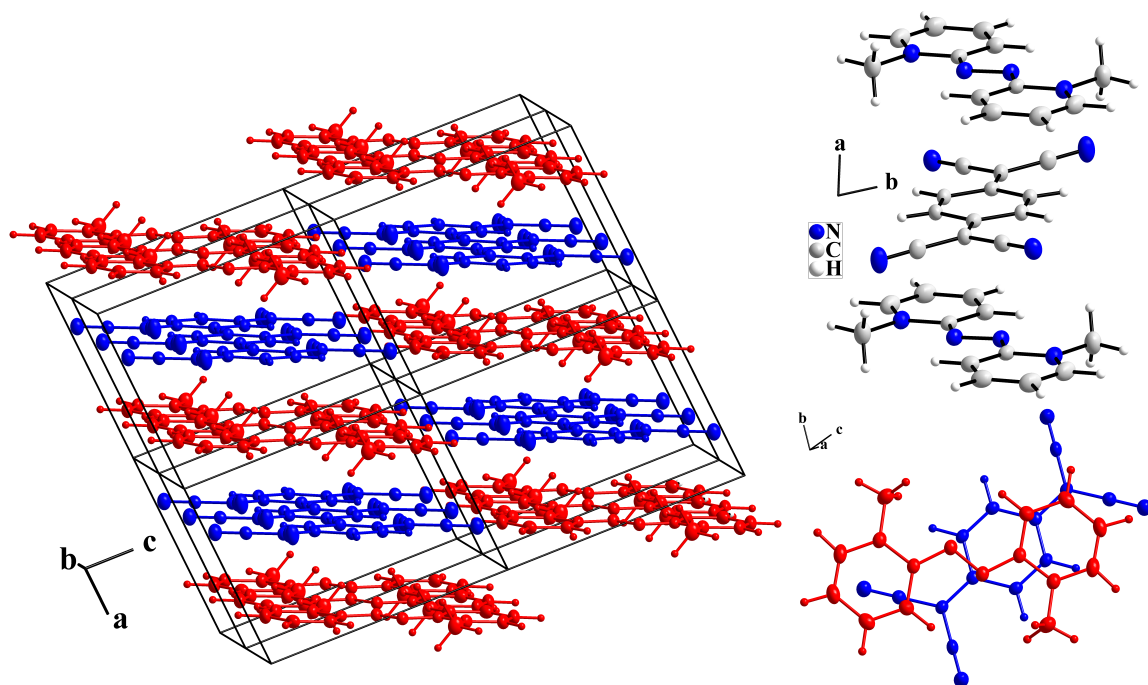


Figure 6.5: The extended unit cell of α -(1)(TCNQ) in a perspective view (left), the equidistant stacks made up from donor and acceptor molecules (top right) and the shifted overlap in the repetitive DA unit, the donor molecules are drawn in red and the acceptor molecules in blue.

6.1.2 α -(2)(TCNQ)

As for **1**, the reaction of pyridone azine **2** with TCNQ in acetonitrile led to dimorphic phases, α -(2)(TCNQ) and β -(2)(TCNQ). X-ray single crystal structure determination of both compounds could be performed, successfully. α -(2)(TCNQ) could be synthesised by mixing both substrates at ambient temperature with subsequent heating to 35 °C. The combination of solutions of both substrates at -20 °C, enabled the synthesis of β -(2)(TCNQ) in pure form.

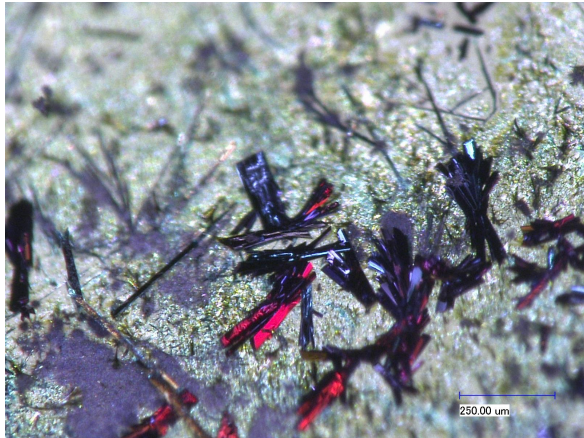


Figure 6.6: Dark needle-shaped crystals of α -(2)(TCNQ).

1.44 Å for C1–N1, 1.32 Å for N1–N2 and 1.48 Å for N2–C7. Since the bond length of the N–N bridge indicates a delocalised character of the system and, thus, the presence of the radical cation species, the C–N bonds are in agreement with the neutral form **2**⁰.

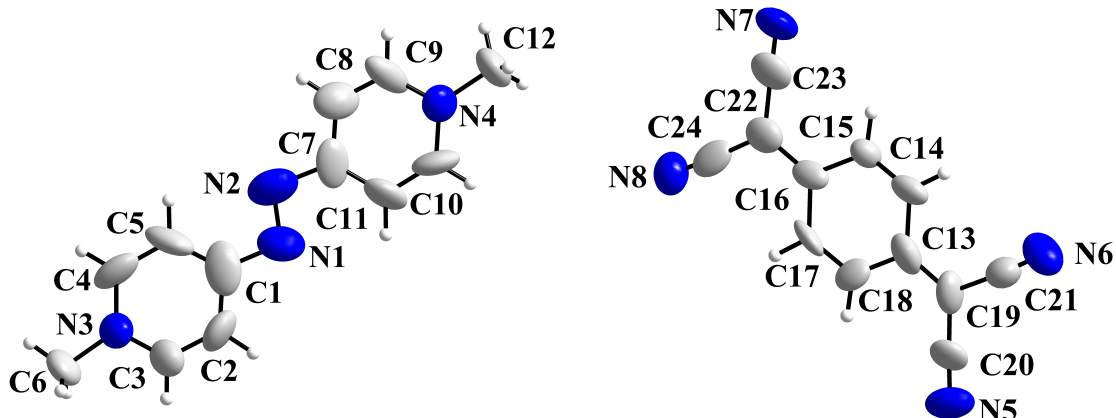


Figure 6.7: The constitutional units in the crystals of α -(2)(TCNQ), the bent molecules of **2** and TCNQ. Bond lengths/Å: N1–N2 1.320(14), C1–N1 1.442(18), C7–N2 1.479(17), C13–C14 1.439(19), C13–C18 1.389(19), C13–C19 1.38(2), C15–C16 1.441(18), C16–C17 1.422(17), C16–C22 1.42(2), C19–C20 1.45(2), C19–C21 1.42(2), C22–C23 1.44(2), C22–C24 1.46(2).

α -(2)(TCNQ) crystallises in the monoclinic space group $P2_1/n$ (No. 14) forming dark needle-shaped crystals which are violet in reflected light (Fig. 6.6). The R_{int} value with 31.91 % indicates low data quality. Therefore, the structural parameter such as the displacement ellipsoids and the bond lengths have to be regarded with caution.

The crystals contain slightly bent molecules of **2** as well as of TCNQ (Fig. 6.7). All atoms are located at general positions.

The molecules of **2** are slightly bent with an angle of 13.12° between the 4'-(py)-N units. The bond lengths of the central CNNC moiety amount to

The TCNQ acceptor molecules are slightly bent with an angle of 9.38° between the terminal $\text{C}(\text{CN})_2$ groups. For the Kistenmacher relationship the following bond lengths/ \AA are taken into account: C13–C14 1.439(19), C13–C18 1.389(19), C13–C19 1.38(2), C15–C16 1.441(18), C16–C17 1.422(17), C16–C22 1.42(2), C19–C20 1.45(2), C19–C21 1.42(2), C22–C23 1.44(2) and C22–C24 1.46(2). The TCNQ charge obtained by this relationship is determined to -0.54 . As the data quality is low, any statement of the charge transfer derived from bond lengths is not assured. Still, by reasons of comparability, the compound is denoted as mixed-valent CT salt $\alpha\text{-}(\mathbf{2})^{+0.54}(\text{TCNQ})^{-0.54}$. From ionicity prediction (Eq. 1.2), the reaction of **2** and TCNQ should result in a fully ionic compound.

In the crystals, the structure is built up by segregated stacks consisting of donor or respectively acceptor molecules. The stacks run along the crystallographic *c* axis. In the donor stacks, the molecules are arranged equidistantly and highly oblique with an offset of 5.85 \AA between the centers of gravity of neighboring molecules. Due to that, the center-of-gravity distance is strongly elongated with 6.72 \AA . However, the intermolecular plane-to-plane distance, generated through the central CNNC moiety of neighboring molecules, is about 3.31 \AA and therefore significantly shorter.

By contrast, the acceptor molecules form stacks with alternating center-of-gravity distances of 3.28 \AA and 3.87 \AA . Hence, the acceptor molecules form stacks that are made up by TCNQ dimers arranged in a zig-zag pattern. In the TCNQ dimer, the intermolecular plane-to-plane distance amounts to 3.20 \AA with horizontal slippage of 0.72 \AA and between the dimers to 3.39 \AA with offset of 1.87 \AA .

Donor and acceptor stacks form in the structure a herring bone pattern (Fig. 6.8).

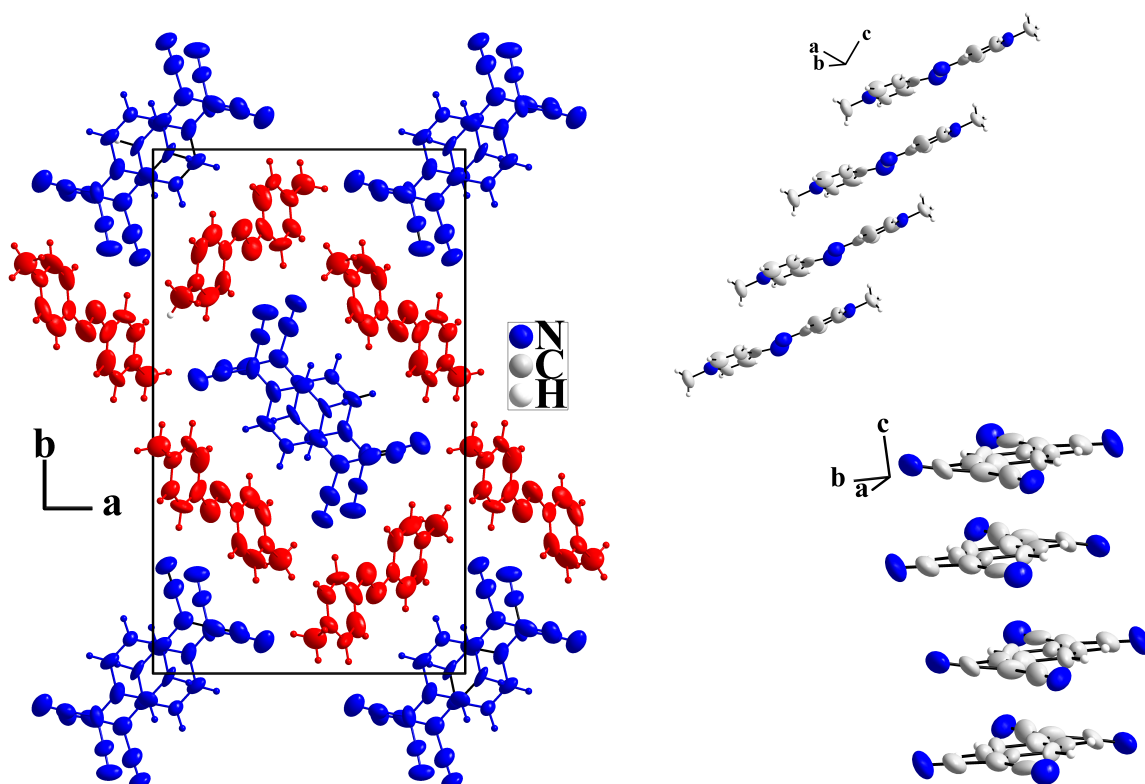


Figure 6.8: The unit cell of $\alpha\text{-}(\mathbf{2})(\text{TCNQ})$ depicted along the crystallographic *c* axis. The donor molecules are drawn in red and the acceptor molecules in blue (left). The equidistant stacks made up from donor molecules (top right) and the stacks of acceptor molecules consisting of TCNQ dimers (bottom right).

6.1.3 β -(2)(TCNQ)

If the reaction of **2** with TCNQ in acetonitrile was performed at low temperatures, black rod-shaped crystals were formed, the β -(2)(TCNQ) (Fig. 6.9). β -(2)(TCNQ) crystallises in the orthorhombic space group *Ccce* (No. 68).



Figure 6.9: Black rod-shaped crystals of β -(2)(TCNQ).

(Wykoff position: $8e \equiv 2 \equiv C_2$). The angle between the terminal $C(CN)_2$ groups amounts to 9.8° . The aromatic bonds amount to $1.426(2)$ Å, $1.408(3)$ Å and $1.358(2)$ Å for $C7-C8$, $C7-C9^i$ and $C8-C9$, and the terminal bond to $1.420(2)$ Å for $C10-C7$. Application of the Kistenmacher relationship leads to a charge of -1.0 on TCNQ. Since the bond lengths in both molecules indicate a complete transfer of one electron, the compound is termed as a fully ionic CT salt β -(2) $^{+}$ (TCNQ) $^{-}$, still, in agreement with ionicity prediction by Eq. 1.2.

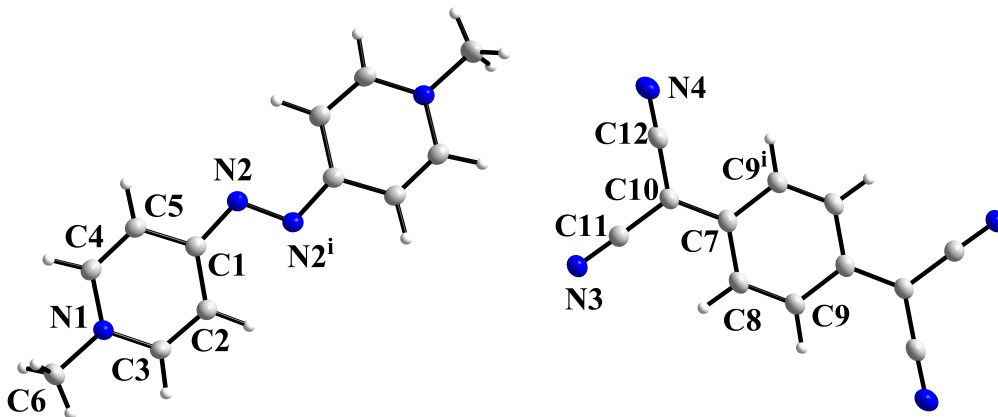


Figure 6.10: The two building units of β -(2)(TCNQ): the slightly bent molecules of 2^{+} and $TCNQ^{-}$. The superscript denotes the symmetry operation: $i = x, 0.5-y, 1.5-z$. Bond lengths/Å: $N2-N2^i$ 1.323(3), $C1-N2$ 1.3692(19), $C7-C8$ 1.426(2), $C7-C10$ 1.420(2), $C7-C9^i$ 1.408(3), $C8-C9$ 1.358(2), $C10-C11$ 1.406(3), $C10-C12$ 1.419(2).

The structure consists of nearly planar molecules of **2** and TCNQ (Fig. 6.10).

The arrangement of the donor **2** deviates slightly from planarity, since the angle between the two planes generated by the symmetric equivalent $4'-(py)-N$ units amounts to 13.1° . The center of gravity, in the mid of the N–N bridge, is located at a twofold rotation axis (Wykoff position: $8e \equiv 2 \equiv C_2$). The equality of the bond lengths in the central CNNC moiety with 1.37 Å for $C1-N2$ bond and 1.32 Å for $N2-N2^i$ bond indicates the presence of the radical cation species 2^{+} .

The center of gravity of TCNQ is positioned at a twofold symmetry axis

The structural feature of the crystals is mixed stacks containing both types of molecules with the stacking sequence: ...DAA'D'... ("': marks another orientation). The stacks run along the crystallographic *a* axis. In these stacks the molecules overlap face-to-face forming DA or A'D' units. The center-of-gravity distance between adjacent TCNQ molecules amounts to 3.57 Å. The distance between the centers of gravity in DA units is significantly shorter with 2.98 Å. Since an inclination of the both molecules to the opposite charged molecules is clearly present, the distance alternation is caused by mutual electrostatic attraction.

In the crystal, four symmetry related but translational different stacks are present forming a layered structure wherein each donor or acceptor is surrounded by four counter ions (Fig. 6.11).

On cooling down to 123 K, a pronounced anisotropic lattice parameter contraction is present. The crystallographic *a* axis shrinks by about 1.88 % from 13.03 Å to 12.78 Å. In comparison, the *b* and *c* axes are less effected with contractions of 0.27 % and respectively 0.76 %. Parallel to the lattice shrinking, the distances between the centers of gravity are shortened from 2.98 Å to 2.92 Å in the DA units and from 3.57 Å to 3.51 Å among the DA and A'D' units corresponding to a decrease of about 2.02 % and 1.12 %. Since the bonds in the CNNC moiety and in TCNQ do not change significantly on thermal treatment, the amount of charge transfer is apparently not affected. This assumption is underlined by the Kistenmacher formula that provides a minor charge difference on TCNQ of -1.0 at 123 K comparing to -1.1 at ambient temperature.

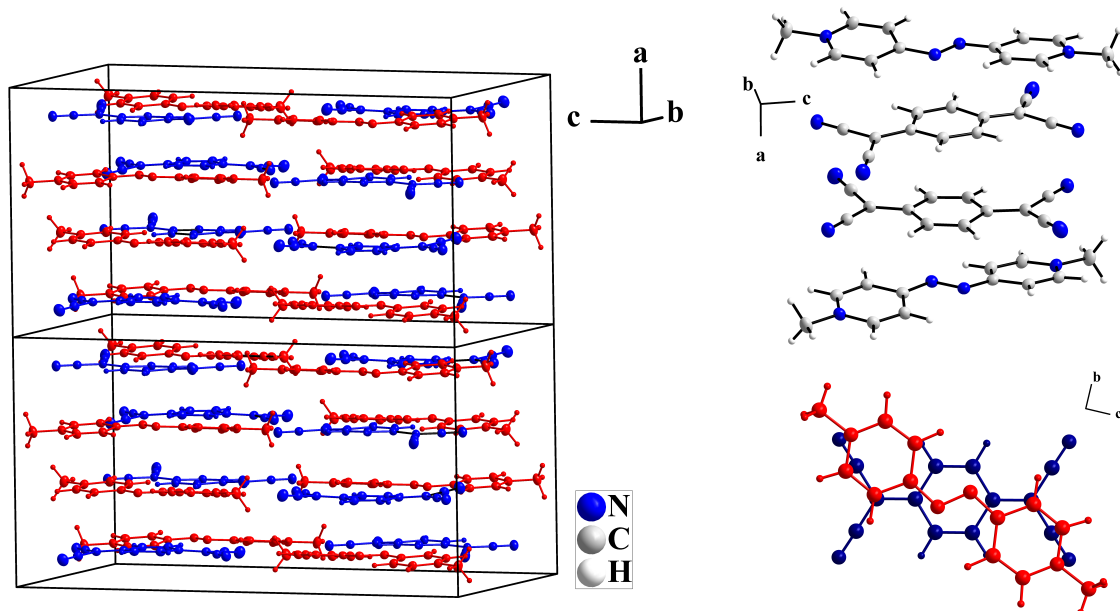


Figure 6.11: The extended unit cell of β -(2)(TCNQ) in a perspective view along the crystallographic *c* axis (left), the stacking of the DAA'D' unit (top right) and the face-to-face overlap of donor and acceptor molecules (bottom right). The donor molecules are drawn in red and the acceptor molecules in blue.

6.1.4 (3)(TCNQ)

In the reaction of **3** with TCNQ in acetonitrile, **(3)(TCNQ)** was obtained in form of dark violet needles (Fig. 6.12). It crystallises in the monoclinic space group $P2_1/c$ (No. 14) and is made up by molecules of **3** and TCNQ (Fig. 6.13). All atoms are located at general positions.



Figure 6.12: Dark violet needles of **(3)(TCNQ)**.

C27–C29 1.408(3), **C30–C31** 1.408(3), **C30–C32** 1.412(3). The charge on the TCNQ molecule could be estimated to -1.1 , close to -1.0 . Since the bonds in the donor molecule indicate a complete charge transfer of one electron, the compound is designated as ionic CT salt $(\mathbf{3})^{+}(\text{TCNQ})^{-}$ in accordance with ionicity prediction by Eq. 1.2.

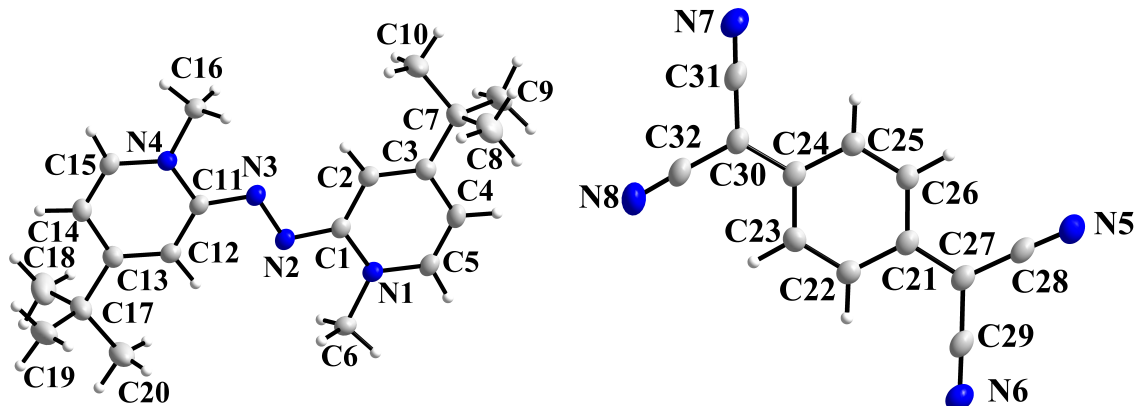


Figure 6.13: The two building units in the structure of **(3)(TCNQ)**, the bent molecules of $\mathbf{3}^{+}$ and TCNQ^{-} . Bond lengths/ \AA : N_2-N_3 1.334(2), C_1-N_2 1.357(2), N_3-C_11 1.360(2), C_21-C_27 1.421(3), C_24-C_30 1.415(3), C_21-C_26 1.411(3), C_21-C_22 1.403(3), C_23-C_24 1.414(3), C_24-C_25 1.403(3), C_27-C_28 1.404(3), C_27-C_29 1.408(3), C_30-C_31 1.408(3), C_30-C_32 1.412(3).

The arrangement of the molecules of **3** is not strictly planar. The angle between the $2'$ -(py)-*N* units amounts to 7.7° . The equality of bond lengths in the central CNNC moiety with 1.36 \AA for C_1-N_2 , 1.33 \AA for N_2-N_3 and 1.36 \AA for N_3-C_11 suggests the presence of the radical cation species $\mathbf{3}^{+}$.

Such as the alignment of the donor molecule, the acceptor molecule TCNQ is also slightly bent. The angle between the $\text{C}(\text{CN})_2$ groups amounts to 8.2° . In the Kistenmacher relationship the following bonds/ \AA are taken into account: C_21-C_27 1.421(3), C_24-C_30 1.415(3), C_21-C_26 1.411(3), C_21-C_22 1.403(3), C_23-C_24 1.414(3), C_24-C_25 1.403(3), C_27-C_28 1.404(3),

The crystals consist of oblique, mixed stacks made up from donor and acceptor molecules running along the crystallographic *b* axis. Predominantly, *DA* aggregates are present with the stacking sequence ...*DA*... In the *DA* aggregates, donor and acceptor molecules have a center-of-gravity distance of 3.12 Å and show face-to-face overlap. Between adjacent *DA* aggregates, the molecules have a center-of-gravity distance of 4.23 Å with an horizontal slippage of 2.29 Å.

Since the orientation of the oppositely charged molecules in the *DA* units is mutual to each other, electrostatic attraction is observed. Due to that, both molecules show structural deviations from planarity. In the unit cell, two symmetry related but translationally different stacks are present forming a herring bone pattern (Fig. 6.14).

On cooling to 123 K, a pronounced anisotropic lattice parameter contraction could be observed. Compared to room temperature, the *b* axis is shortened by 1.81 % from 7.061 Å to 6.933 Å. The effect on the lattice parameter *a* with 0.45 % and *c* with 0.43 % are significantly smaller. The change of the β angle is in the range of standard variance. Consequently, the center-of-gravity distances are shortened to 3.01 Å (-3.53%) and 4.20 Å (-0.71 %). Therefore, the impact on the distances in the *DA* aggregates is highly larger than between the aggregates. The offset is slightly larger with 2.32 Å (2.29 Å at RT). Thus, at ambient temperature, stronger electrostatic attraction is present between donor and acceptor in the *DA* aggregates. The charge transfer is not influenced on cooling. The bond lengths in the central CNNC moiety in **3**⁺ and in TCNQ⁻ do not change significantly.

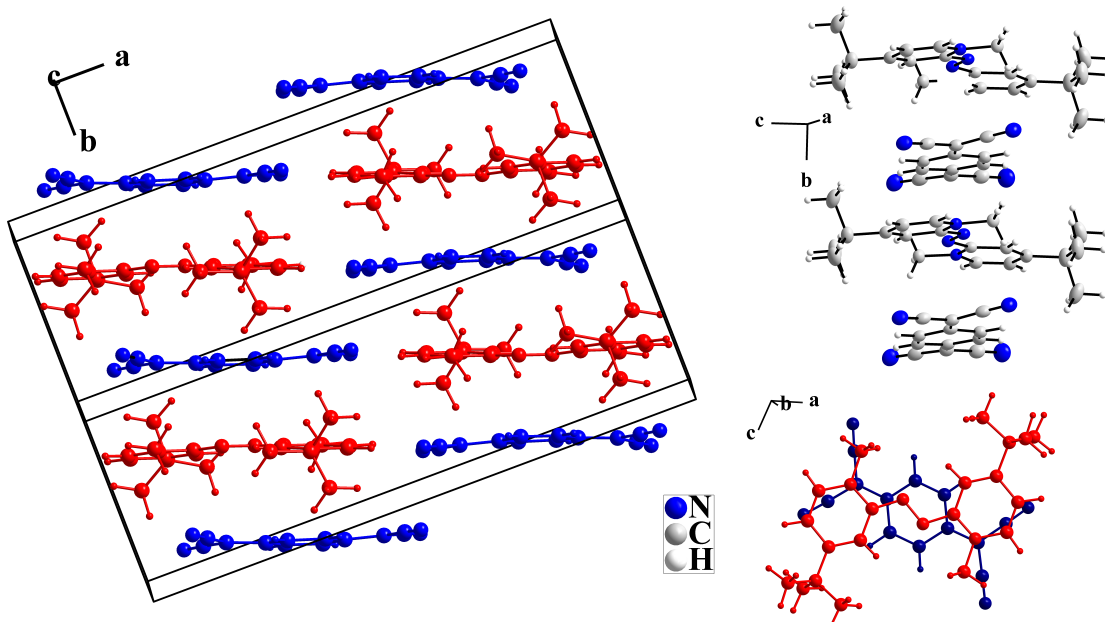


Figure 6.14: The extended unit cell of **(3)**(TCNQ) in a perspective view (left), the mixed stacks (top right) and the face-to-face overlap in the *DA* aggregates (bottom right). The donor molecules are drawn in red and the acceptor molecules in blue.

6.1.5 (4)(TCNQ)

(4)(TCNQ) could be obtained in reaction of **4** and TCNQ in acetonitrile as thin dark green-blue needles (Fig. 6.15). It crystallises in the monoclinic space group $P2_1/c$ (No. 14). The crystals are built up from molecules of **4** and TCNQ (Fig. 6.16). All atoms are located at general positions.

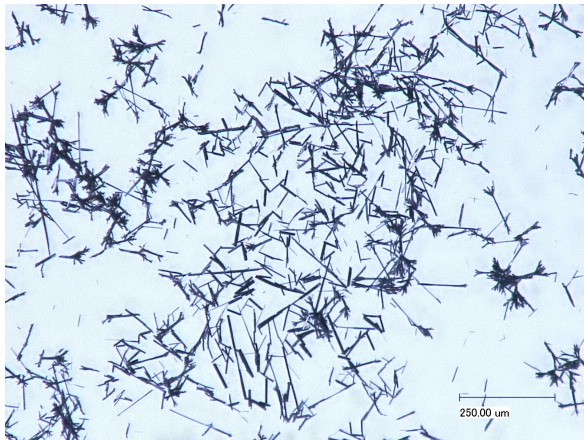


Figure 6.15: The thin needle-shaped crystals of (4)(TCNQ).

into account. Thus, it can be labelled as mixed-valent CT salt $(\mathbf{4})^{+0.8}(\text{TCNQ})^{-0.8}$. Ionicity prediction emphasises a complete electron transfer (Eq. 1.2).

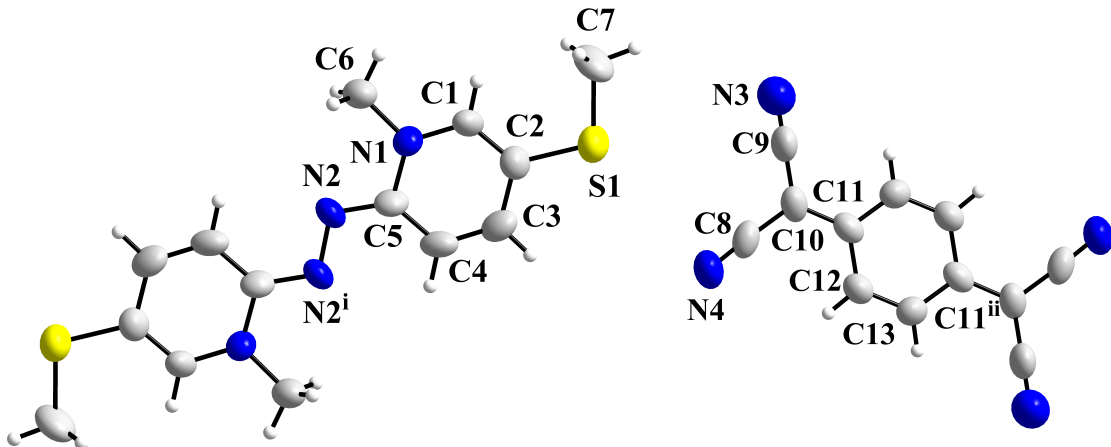


Figure 6.16: The building units in the crystals of (4)(TCNQ), the planar molecules of **4** and TCNQ. The superscripts denote the symmetry operations: $i = 1-x, 2-y, 1-z$; $ii = 1-x, 1-y, 1-z$. Bond lengths/ \AA : $\text{N}2-\text{N}2^i$ 1.363(11), $\text{C}5-\text{N}2$ 1.339(8), $\text{C}8-\text{C}10$ 1.420(11), $\text{C}9-\text{C}10$ 1.416(12), $\text{C}10-\text{C}11$ 1.403(10), $\text{C}11-\text{C}12$ 1.429(10), $\text{C}11-\text{C}13^{ii}$ 1.399(10).

The molecules of **4** are essentially planar. The centers of gravity, in the mid of the N–N bridge, are located at inversion centers (Wykoff position: $2d \equiv \bar{1} \equiv C_i$). The bond lengths in the central CNNC moiety with 1.34 \AA and 1.36 \AA for $\text{N}2-\text{N}2^i$ and $\text{C}5-\text{N}2$, indicate the presence of the radical cation species $\mathbf{4}^+$.

The TCNQ molecules are still planar. The centers of gravity are positioned at inversion centers (Wykoff position: $2b \equiv \bar{1} \equiv C_i$). The Kistenmacher formula allows a charge estimation of -0.8. The bond lengths/ \AA : $\text{C}8-\text{C}10$ 1.420(11), $\text{C}9-\text{C}10$ 1.416(12), $\text{C}10-\text{C}11$ 1.403(10), $\text{C}11-\text{C}12$ 1.429(10) and $\text{C}11-\text{C}13^{ii}$ 1.399(10) are taken

In the crystals, stacks, made up of donor and acceptor molecules, are present running along the crystallographic *b* axis. The stacking sequence is . . . DA The center-of-gravity distance amounts to 3.67 Å with an horizontal slippage of 1.50 Å between adjacent molecules. Donor and acceptor molecules are not strictly parallel arranged. Slight dumping of 4.6° between the molecular planes of both components make it substantially difficult to measure unequivocally the averaged plane-to-plane distance. It is roughly estimated to 3.4 Å. In the unit cell, two symmetry related but translationally different stacks form a herring bone pattern (Fig. 6.17).

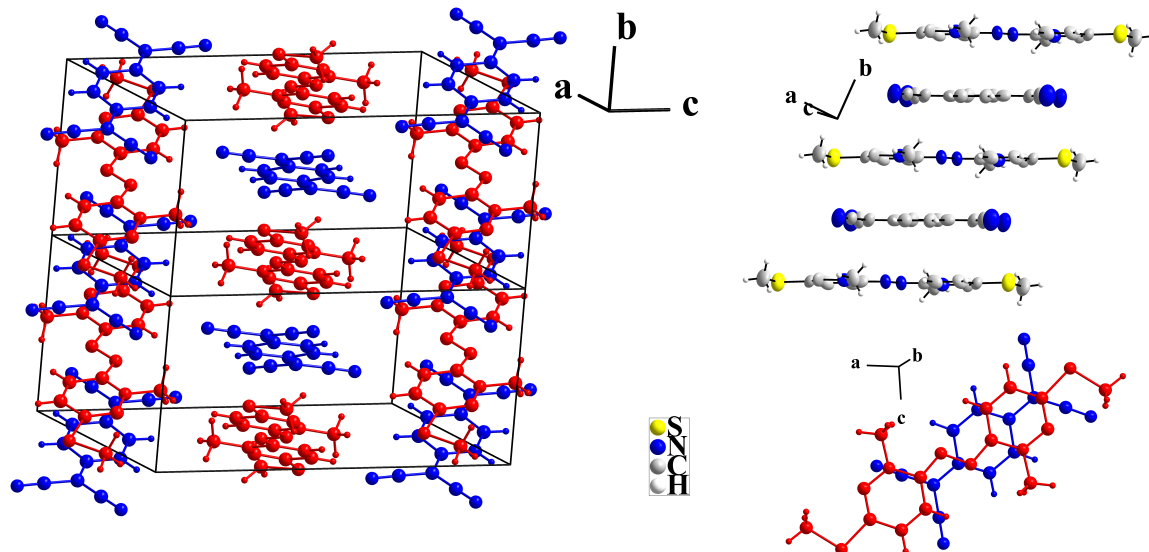


Figure 6.17: The extended unit cell of (4)(TCNQ) in a perspective view (left), the mixed stacks (top right) and the overlap in the *DA* unit (bottom right). The donor molecules are drawn in red and the acceptor molecules in blue.

6.1.6 (7)(TCNQ)

In the reaction of **7** with TCNQ in acetonitrile under ambient conditions, two different crystalline phases were observed: dark red needle-shaped and cuboid-shaped crystals. The X-ray single crystal determination reveals the needles as the 1:1 CT salt $(\text{7})(\text{TCNQ})$, while the cuboid-shaped crystals as the 1:2 CT salt $(\text{7})(\text{TCNQ})_2$. X-ray powder diffraction and CHNS analysis show that the 1:2 CT salt represents the main phase.

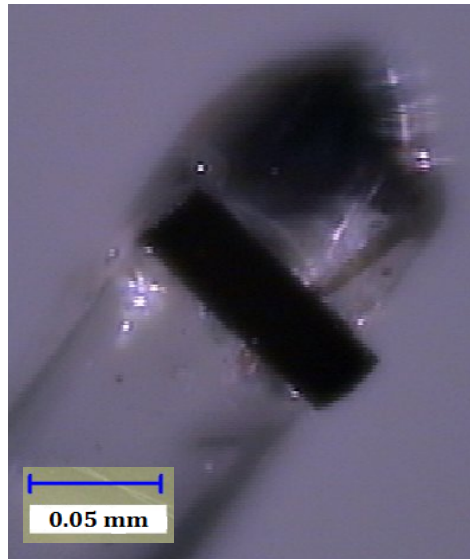


Figure 6.18: Dark red needle-shaped crystal of $(\text{7})(\text{TCNQ})$.

According to the shape of the donor molecule, the TCNQ molecule is planar and its center of gravity is positioned at an inversion center (Wykoff position: $1e \equiv \bar{1} \equiv C_i$). To estimate the charge by the Kistenmacher equation, the following bond lengths/ \AA are considered: C8–C11 1.384(10), C8–C9 1.414(10), C8–C10^{*i*} 1.443(10), C11–C12 1.436(11), C11–C13 1.453(12). The empirical formula results in a slight negative charge of -0.3 on TCNQ. Therefore, the compound is interpreted as mixed valent CT salt $(\text{7})^{+0.3}(\text{TCNQ})^{-0.3}$ implying a low degree of charge transfer.

In the crystals, oblique, mixed stacks consisting of donor and acceptor molecules are present. These stacks run along the crystallographic *a* axis with the stacking sequence $\dots DA \dots$. The molecules are almost parallel arranged. The centers of gravity are stacked equidistantly by 3.63 \AA with a horizontal slippage of 1.47 \AA . The average plane-to-plane distance is slightly shorter with 3.30 \AA . In the structure, the two symmetrical related but translational different stacks form layers (Fig 6.21).

Mechanical separation of the needle-shaped crystals allowed the identification of $(\text{7})(\text{TCNQ})$ by X-ray powder diffraction. However, the pure phase was experimentally not accessible. The reflections marked with a black asterisk belong to $(\text{7})(\text{TCNQ})_2$.

The needles of $(\text{7})(\text{TCNQ})$ (Fig. 6.18) crystallise in the triclinic space group $P\bar{1}$ (No. 2). The crystals consist of planar molecules of **7** and TCNQ (Fig. 6.20).

The donor molecule **7** is essentially planar with its center of gravity located at an inversion center (Wykoff position: $1c \equiv \bar{1} \equiv C_i$). In the CNNC moiety, the C1–N2 bond amounts to 1.32 \AA and the N2–N2^{*i*} to 1.40 \AA . Due to the absence of electron delocalisation in **7**, the bond order of neutral 7^0 is present.

According to the shape of the donor

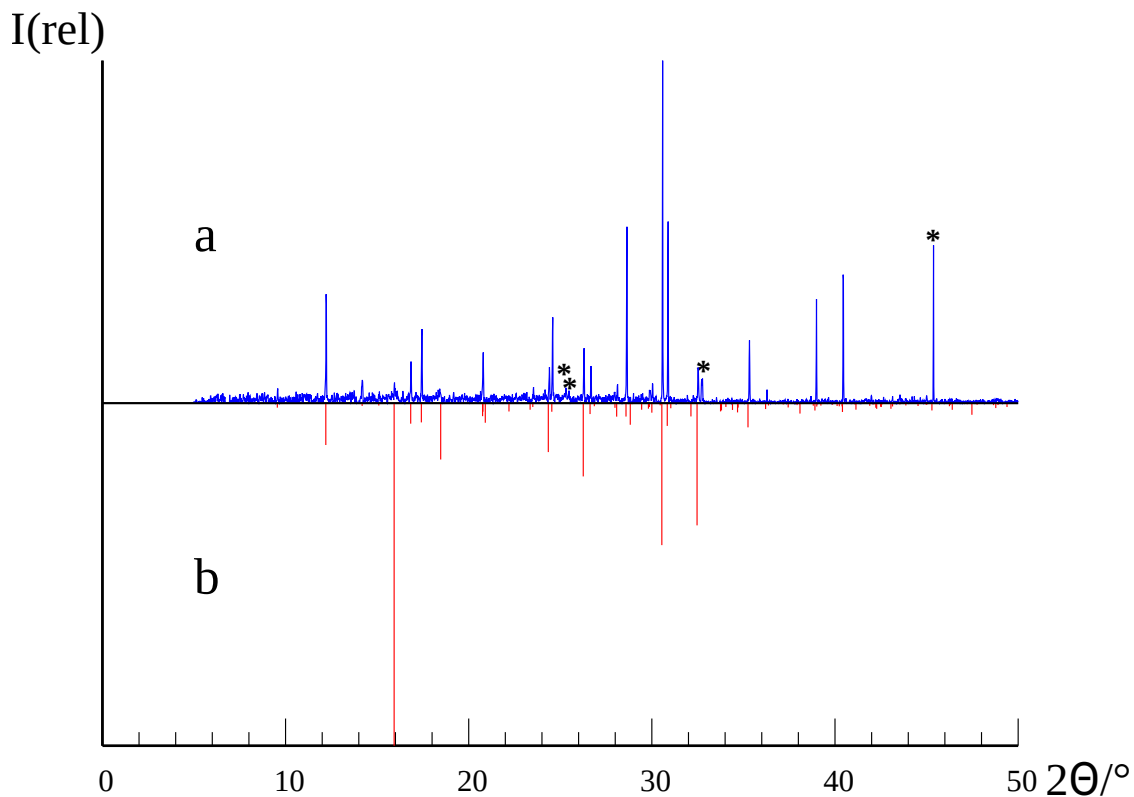


Figure 6.19: Powder diffractogram of mechanically separated crystals of (7)(TCNQ). The reflections marked with black asterisks belong to the 1:2 CT salt (7)(TCNQ)₂. Used radiation: Co-K_{α1}, a = measured diffractogram, b = simulated diffractogram on basis of single crystal data of (7)(TCNQ).

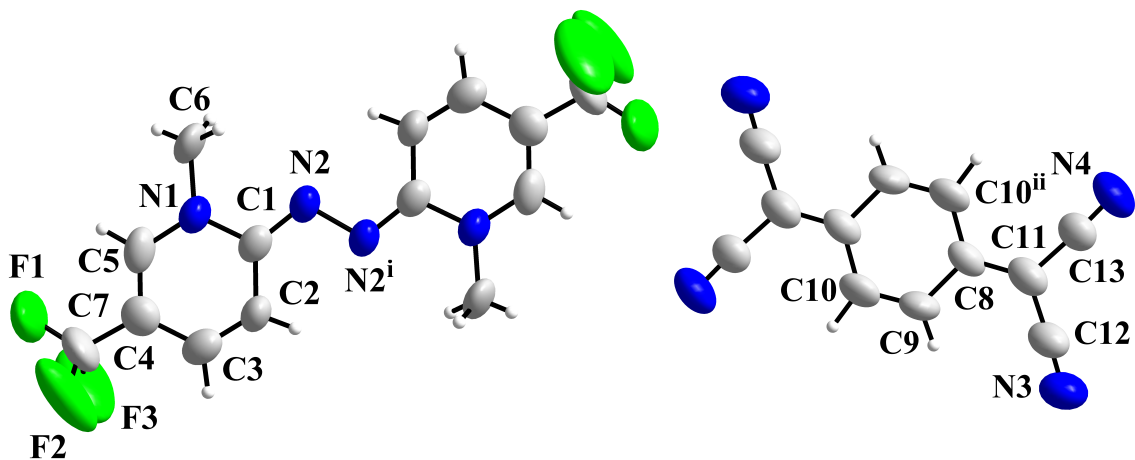


Figure 6.20: The two building units of (7)(TCNQ), the planar molecules of **7** and TCNQ. The superscripts denote the symmetry operations: $i = -x, 1-y, 2-z$, $ii = 1-x, 1-y, 2-z$. Bond lengths/Å: N2–N2^{*i*} 1.40(1), C1–N2 1.317(8), C8–C11 1.384(10), C8–C9 1.414(10), C8–C10^{*ii*} 1.443(10), C11–C12 1.436(11), C11–C13 1.453(12).

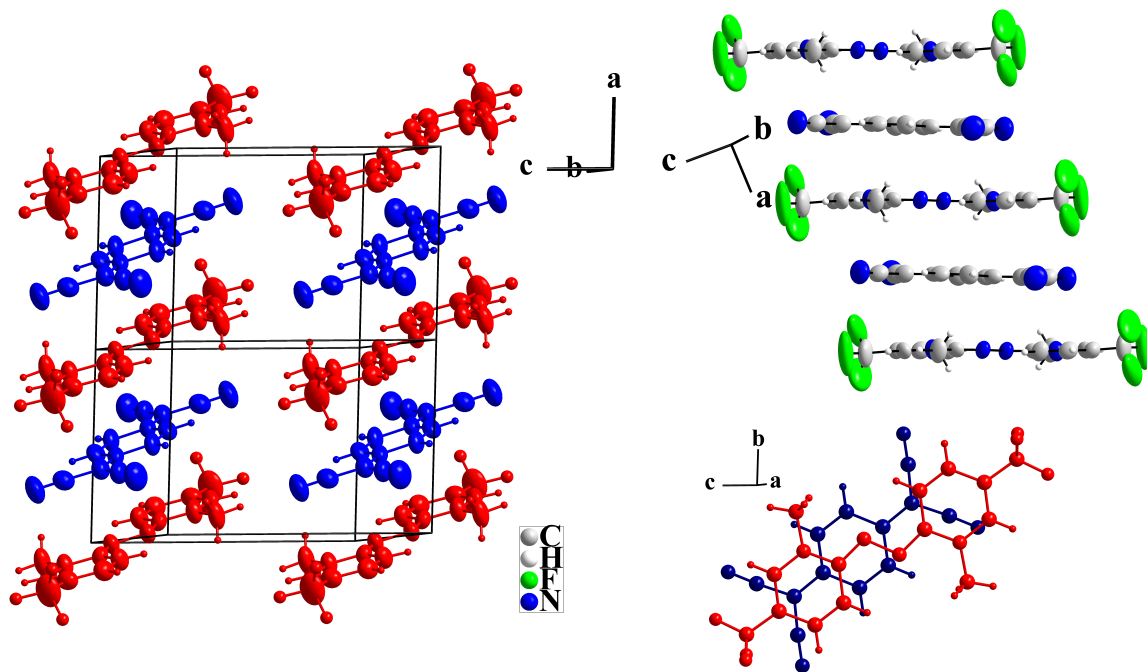


Figure 6.21: The extended unit cell of (7)(TCNQ) depicted in a perspective view (left), the mixed stacks (top right) and the overlap in the *DA* unit (bottom right). The donor molecules are drawn in red and the acceptor molecules in blue.

6.1.7 (7)(TCNQ)₂

In the reaction of **7** and TCNQ in dimethylformamide, (7)(TCNQ)₂ was obtained in form of cuboid-shaped, dark red crystals (Fig 6.22). It crystallises in the triclinic space group $P\bar{1}$ (No. 2) and consists of planar molecules of **7** and slightly bent TCNQ molecules (Fig. 6.23). All atoms are located at general positions.

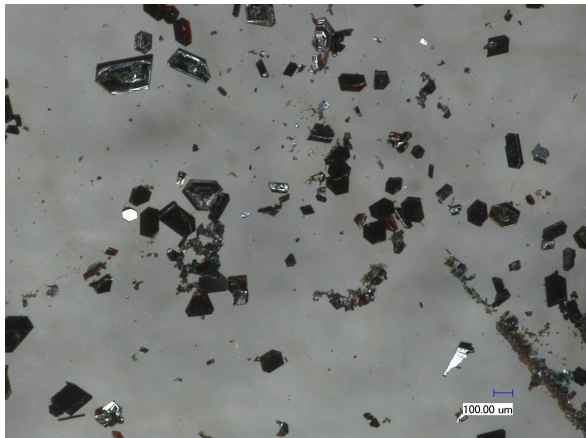


Figure 6.22: Dark red crystals of (7)(TCNQ)₂.

The molecule of **7** is essentially planar. The center of gravity, in the mid of the N–N bridge, is located at an inversion center (Wykoff position: $1h \equiv \bar{1} \equiv C_i$). The bonds of the central CNNC moiety amount to 1.40 Å for N2–Nⁱ2 and to 1.30 Å for C1–N2. Since the absence of bond delocalisation, it is assumed that neutral **7**⁰ is integrated. At ambient temperature, the CF₃ groups perform an almost free rotation in the crystal. Low temperature data confirm the dynamical character of this phenomenon.

In the TCNQ molecule, the angle between the opposing C(CN)₂ groups amounts to 4.8° resulting in a slight bend. For the application of Kistemaker's formula the following bonds/Å are taken into account: C8–C14 1.373(4), C11–C17 1.373(4), C8–C9 1.451(3), C8–C13 1.440(3), C10–C11 1.449(3), C11–C12 1.445(3), C14–C15 1.431(3), C14–C16 1.432(3), C17–C18 1.431(3), C17–C19 1.432(4). The estimated charge on TCNQ is close to 0. As for the 1:1 CT salt (7)(TCNQ), a minor charge transfer is observed. Therefore, (7)(TCNQ)₂ is interpreted as neutral CT salt. From Eq. 1.2 mixed-valency has been predicted.

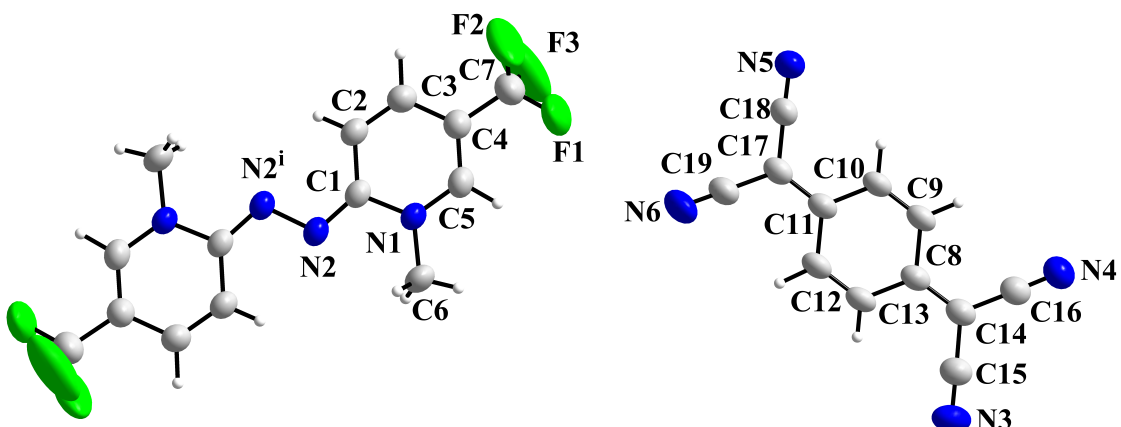


Figure 6.23: The two building units of (7)(TCNQ)₂, the planar molecule of **7** and the slightly bent TCNQ molecule. The superscript denotes the symmetry operation: $i = 1-x, 1-y, 1-z$. Bond lengths/Å: N2–Nⁱ2 1.396(3), C1–N2 1.305(3), C8–C14 1.373(4), C11–C17 1.373(4), C8–C9 1.451(3), C8–C13 1.440(3), C10–C11 1.449(3), C11–C12 1.445(3), C14–C15 1.431(3), C14–C16 1.432(3), C17–C18 1.431(3), C17–C19 1.432(4).

The crystals are built up from mixed oblique stacks running in *c* direction that consist of donor and acceptor molecules. The stacking sequence is ...ADA'.... Thus, one molecule of **7** is enclosed with two TCNQ molecules forming a sandwich or ADA' trimer. In the ADA' aggregate, the inter-plane angle between the planar molecule of **7** and the adjacent planar benzene fragments of the TCNQ molecules amounts to 6.3° . The center-of-gravity distance of the two neighbouring TCNQ molecules to the **7** molecule is 4.15 Å. However, the intermolecular plane-to-plane distance between the donor and acceptor molecules could be roughly appreciated to 3.2 Å. Between the ADA' aggregates, the center-of-gravity distance between TCNQ molecules of adjacent ADA' sandwiches is determined to 4.03 Å with an horizontal slippage of 2.04 Å. The mean intermolecular plane-to-plane distance is estimated to 3.5 Å. Thus, the structural feature is zig-zag stacked ADA trimers along the crystallographic *c* axis forming layers perpendicular to the stacking direction (Fig. 6.24).

Low temperature data show a pronounced anisotropic lattice parameter contraction. On cooling to 123 K, the *c* axis contracts by 2.51 % from 11.30 Å to 11.01 Å. The *a* and *b* axes as well as the angles β and γ are less effected by a shrinking of 0.28 % and 0.83 % or 0.45 % and 0.27 %. The angle α enlarges slightly from 73.72° to 74.17° by about 0.60 %. As a consequence, the center-of-gravity distances between the ADA trimers shrink from 4.03 Å to 3.98 Å (-1.34%), in the trimer from 4.15 Å to 4.05 Å (-2.43%). The packing of the molecules is denser with inter-plane distances of about 3.1 Å (-3.13%) in the aggregates and 3.4 Å (-2.86%) between them. The charge transfer is not influenced by cooling.

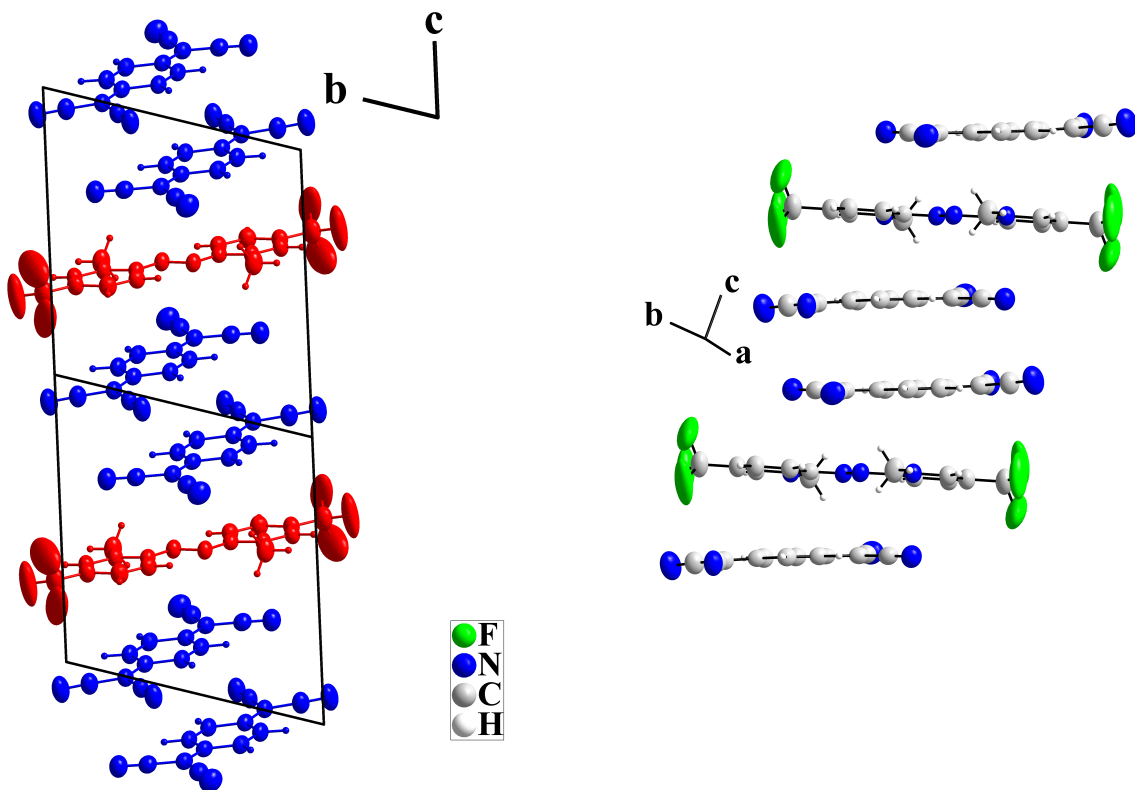


Figure 6.24: The extended unit cell of $(7)(\text{TCNQ})_2$ depicted along the crystallographic *a* axis (left) and the stacking of the ADA' units (right). The donor molecules are drawn in red and the acceptor molecules in blue.

6.1.8 (8)(TCNQ)

The dark needle-shaped crystals of (8)(TCNQ) were obtained in the reaction from **8** and TCNQ in acetonitrile and crystallises in the triclinic space group $P\bar{1}$ (No. 2) (Fig. 6.25). The crystals consist of molecules of **8** and TCNQ (Fig. 6.26). All atoms are located at general positions.



Figure 6.25: Dark shining needle-shaped crystals of (8)(TCNQ).

1.3922(2) Å and 1.3865(2) Å, and the aromatic bonds to 1.4389(2) Å, 1.3339(2) Å, 1.4412(1) Å, 1.4391(2) Å, 1.3375(2) Å and 1.4269(1) Å for C15–C16, C16–C17, C17–C18, C18–C19, C19–C20 and C15–C20 respectively. Charge estimation by the Kistenmacher equation results in a charge of -0.41 on TCNQ, which can be compared with the literature-known fractionally charged TCNQ $^{-0.5}$ anion[142, 143]. Since both molecules in (8)(TCNQ) indicate partially charged state, an appropriate label for the mixed-valent CT salt is $(8)^{+0.41}(\text{TCNQ})^{-0.41}$. Predicted ionicity by Eq. 1.2 is in accordance with structural parameters.

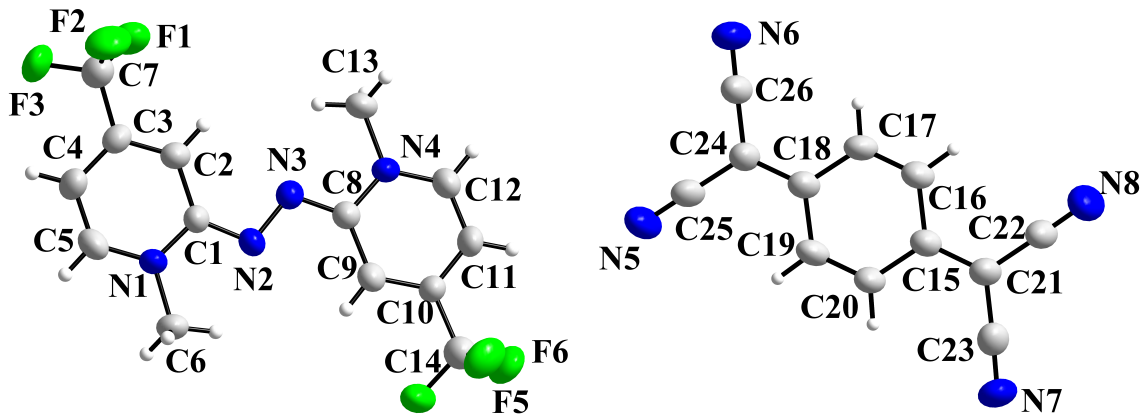


Figure 6.26: The two building units of (8)(TCNQ), the planar molecules of **8** and TCNQ. Bond lengths/Å: N2–N3 1.3843(8), C1–N2 1.3210(1), C8–N3 1.3234(1), C15–C21 1.3922(2), C18–C24 1.3865(2), C15–C16 1.4389(2), C16–C17 1.3339(2), C17–C18 1.4412(1), C18–C19 1.4391(2), C19–C20 1.3375(2), C15–C20 1.4269(1).

The molecule of **8** is essentially planar. In the CNNC moiety, the bond lengths do not show a complete delocalisation. The N2–N3 bond amounts to 1.38 Å which is slightly shortened to the neutral state, parallel, the C1–N2 and the C8–N3 bonds are slightly elongated to 1.32 Å. As reference, the radical cation **8** $^{+}$ in (8)[CuBr₂] (see Chapter 4.1.3) shows almost ideal bond delocalisation. Thus, the bonding situation indicates the presence of a non-integer charged **8** $^{n+}$ species with $0 < n < 1$.

According to the shape of the donor molecule, the TCNQ molecule is essentially planar. The terminal bonds C15–C21 and C18–C24 amount to

In the crystals, segregated stacks of donor or acceptor molecules are present, respectively. These stacks run along the crystallographic *a* axis forming the typical herring bone pattern. The molecules of **8** are stacked highly oblique and parallel to each other with alternating center-of-gravity distances of 4.38 Å with an offset of 2.72 Å and 3.99 Å with an offset of 2.01 Å. However, the intermolecular plane-to-plane distances of neighbouring **8** molecules are close to equidistance and amount in average 3.43 Å.

Pursuant to the structural arrangement of the donor molecules, the TCNQ molecules form oblique stacks. The center-of-gravity distances alternate with 4.37 Å and 3.98 Å with the corresponding horizontal displacements of 2.59 Å and 2.17 Å. Unlike the donor stacks, the plane-to-plane distances of adjacent TCNQ molecules alternate by 3.33 Å to 3.51 Å. As a consequence, stacks of Peierls distorted TCNQ dimers are present (Fig. 6.27).

X-ray single crystal data recorded at 123 K, 150 K, 200 K and 250 K show a pronounced anisotropic lattice parameter contraction on cooling. Tab. 6.2 contains the experimental lattice parameters. The stacking direction (*a* axis) is compressed by about 2.94 % from 8.326 Å to 8.080 Å. The γ angle is shortened by 1.09 % from 100.67° to 99.57°. The *b* axis length is reduced by about 0.76 %. The other lattice parameters are less affected by temperature variation. The crystallographic *c* axis, the α and β angles are shortened by only 0.16 %, 0.13 % and 0.35 %, ranging in the area of standard deviation.

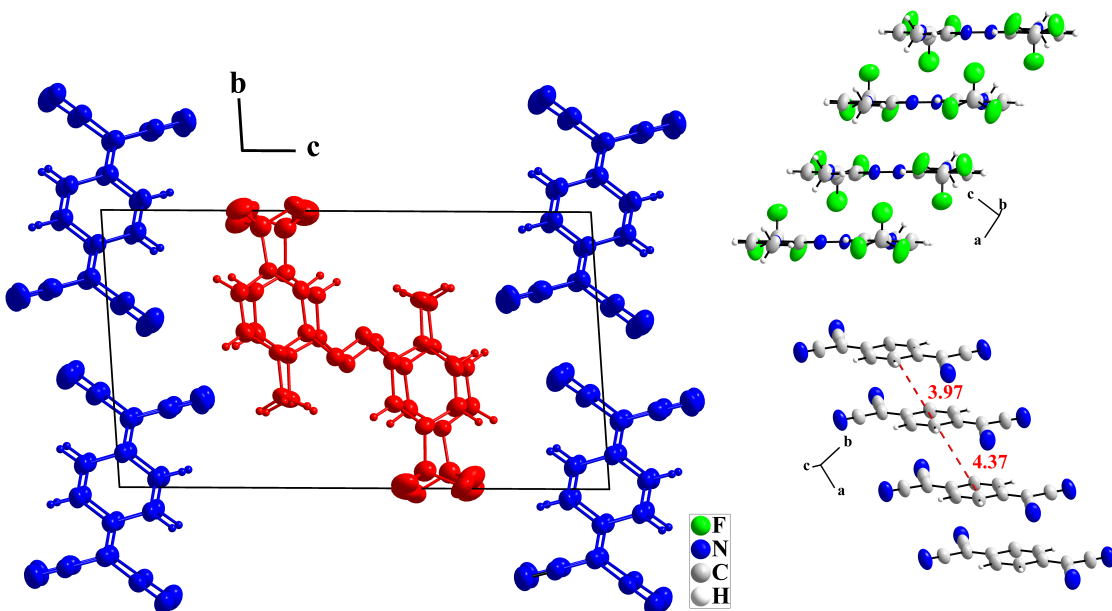


Figure 6.27: The unit cell of **(8)(TCNQ)** depicted in *a* direction (left) and the oblique stacks of **8** (top right) and TCNQ (bottom left). For the TCNQ stacks the alternating center-of-gravity distances are given in Å. The donor molecules are drawn in red and the acceptor molecules in blue.

Table 6.2: Lattice parameters of **(8)(TCNQ)** recorded at 123 K, 150 K, 200 K, 250 K and 295 K. It crystallises in the triclinic space group $P\bar{1}$ (No. 2). The relative contraction refers to RT data related to data recorded at 123 K and is expressed in percent.

T/K	$a/\text{\AA}$	$b/\text{\AA}$	$c/\text{\AA}$	$\alpha /{}^\circ$	$\beta /{}^\circ$	$\gamma /{}^\circ$
295	8.3256(12)	9.285(8)	16.144(2)	93.025(7)	95.149(4)	100.671(8)
250	8.2505(5)	9.2619(5)	16.1416(6)	92.984(3)	95.040(3)	100.399(2)
200	8.1771(4)	9.2431(5)	16.1273(7)	92.914(3)	94.948(4)	100.062(2)
150	8.1147(4)	9.2265(5)	16.1205(7)	92.935(3)	94.818(3)	99.753(2)
123	8.0800(4)	9.2147(4)	16.1186(9)	92.908(3)	94.818(2)	99.570(3)
Rel. Contr./%	-2.94	-0.76	-0.16	-0.13	-0.35	-1.09

Since the symmetry of the lattice is not altered on cooling, the structure feature remains and only minor changes are apparent. Through the shrinking of the crystallographic a axis the averaged plane-to-plane distances between the stacked molecules decrease, consequently. The distance between the molecules of **8** (d_D) decreases about 1.89% from 3.43 Å to 3.37 Å. In the TCNQ dimers, the distance (d_{A1}) is shortened by 2.1 % from 3.33 Å to 3.26 Å and between them (d_{A2}) about 2.9 % from 3.51 Å to 3.41 Å. The charge on the TCNQ molecule, determined by the Kistenmacher equation, shows a tendency that with decreasing temperature the negative charge on TCNQ increases (Tab. 6.3).

Table 6.3: Average plane-to-plane distances in the structure of **(8)(TCNQ)** in the segregated equidistant stacks of **8** (d_D) and the alternating distances in the TCNQ stacks in the TCNQ dimers, (d_{A1}), and between them (d_{A2}) at 123 K, 150 K, 200 K, 250 K and 295 K, and the estimated charge transfer by the Kistenmacher equation.

T/K	$d_D/\text{\AA}$	$d_{A1}/\text{\AA}$	$d_{A2}/\text{\AA}$	Kistenmacher
295	3.43	3.51	3.33	-0.41
250	3.42	3.48	3.31	-0.51
200	3.40	3.45	3.29	-0.54
150	3.38	3.43	3.27	-0.55
123	3.37	3.41	3.26	-0.64

Summarising, in reactions of the azines **1-8** with TCNQ, the three ionic CT salts $\alpha\text{-}(\mathbf{1})^{+}\text{(TCNQ)}^{-}$, $\beta\text{-}(\mathbf{2})^{+}\text{(TCNQ)}^{-}$ and $(\mathbf{3})^{+}\text{(TCNQ)}^{-}$, the new four mixed valent CT salts $\alpha\text{-}(\mathbf{2})^{+0.54}\text{(TCNQ)}^{-0.54}$, $(\mathbf{2})^{+0.82}\text{(TCNQ)}^{-0.82}$, $(\mathbf{7})^{+0.30}\text{(TCNQ)}^{-0.30}$ and $(\mathbf{8})^{+0.41}\text{(TCNQ)}^{-0.41}$ and the neutral CT salt $(\mathbf{7})(\text{TCNQ})_2$ were obtained.

Investigations of the magnetic susceptibility as well as measurements of the conducting properties were performed. To get an appropriate description of the electronic structures, band structures, projected densities of states, anisotropic conductivities and Mulliken population analyses calculations were made.

6.2 Magnetism

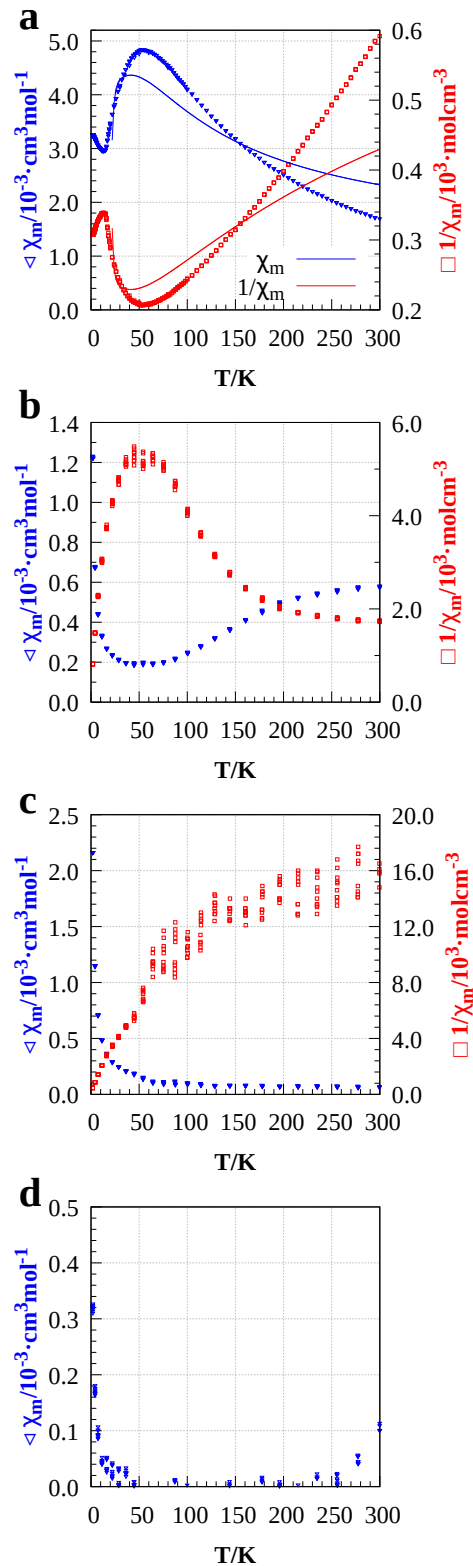
The CT salts are built up from electron transfer reactions in which the degree of charge transfer vary. The magnetic susceptibilities of α -(1)(TCNQ), α -(2)(TCNQ), β -(2)(TCNQ), (3)(TCNQ), (4)(TCNQ), (7)(TCNQ)₂ and (8)(TCNQ) were measured in the temperature between 1.9 K and 300 K (Fig. 6.28).

For α -(1)(TCNQ), β -(2)(TCNQ) and (3)(TCNQ) magnetic phenomena are expected since the organic radical ions 1^+ , 2^+ or 3^+ and TCNQ⁻ are present in these compounds. The mixed-valent CT salts α -(2)(TCNQ), (4)(TCNQ) and (8)(TCNQ) are also associated with magnetic phenomena, whereas, for the neutral CT salt (7)(TCNQ)₂ diamagnetism is expected.

The measurement of the magnetic susceptibility of α -(1)(TCNQ) shows antiferromagnetic behaviour. The Néel temperature T_N is observed at about 50 K with a maximum of the molar susceptibility. At low temperature a paramagnetic impurity ρ was observed. It is assumed that the magnetic behaviour of the paramagnetic impurity follows the Curie law. To simulate the magnetic data the 1D Heisenberg chain model[124] was used (Eq. 4.1).

The best fit to data for the model leads to a coupling constant of J of -19 cm^{-1} and Curie temperature θ of -20 K and ρ of 0.03. The Landé factor is taken from EPR measurements of the radical cation 1^+ and is determined to 2.0039, which fulfill the expectation of 2.00 for organic radicals[99]. However, the fit does not give an appropriate description of the antiferromagnetic behaviour. From structural point of view, the 1D Heisenberg chain model might be more accurate due to the absence of dimerisation. For $T > 100 \text{ K}$, the evaluation by the Curie Weiss law is possible. The data results in a Curie constant of $C = 0.560 \text{ cm}^3 \text{Kmol}^{-1}$ with θ of -28.48 K and a magnetic momentum of $2.12 \mu_B$ belonging to about $\frac{3}{2}$ unpaired electrons, however, the Weiss constant reduces the magnetic momentum. Since two unpaired electrons are expected, one from each radical ion, a part of the spin momenta are largely suppressed and substantially coupled in the crystal.

For α -(2)(TCNQ), β -(2)(TCNQ), (4)(TCNQ) and (7)(TCNQ)₂ the respective magnetic behaviour is similar. The molar susceptibilities are small and positive over the measured temperature range. At low



temperature, a nearly linear decay in the function $\chi_{mol}^{-1} = f(T)$ is present passing into an almost temperature independent small paramagnetism (TIP). The application of the Curie-Weiss law results in Curie constants, magnetic momenta and Weiss constants of $C = 0.007 \text{ cm}^3 \text{Kmol}^{-1}$, $0.24 \mu_B$ with θ of -7.85 K for $\alpha\text{-}(2)(\text{TCNQ})$ (up to $T < 40 \text{ K}$), $C = 0.009 \text{ cm}^3 \text{Kmol}^{-1}$, $0.26 \mu_B$ with θ of -4.8 K for $\beta\text{-}(2)(\text{TCNQ})$ (up to $T < 45 \text{ K}$), $C = 0.068 \text{ cm}^3 \text{Kmol}^{-1}$, $0.74 \mu_B$ with θ of -0.08 K for $(4)(\text{TCNQ})$ (up to $T < 25 \text{ K}$) and, $C = 0.007 \text{ cm}^3 \text{Kmol}^{-1}$, $0.23 \mu_B$ with θ of 0.17 K for $(7)(\text{TCNQ})_2$ (up to $T < 60 \text{ K}$). At higher temperatures the molar susceptibilities are nearly temperature independent in the order of $10^{-4} \text{ cm}^3 \text{mol}^{-1}$ for $\alpha\text{-}(2)(\text{TCNQ})$, $10^{-5} \text{ cm}^3 \text{mol}^{-1}$ for $\beta\text{-}(2)(\text{TCNQ})$, $10^{-3} \text{ cm}^3 \text{mol}^{-1}$ for $(4)(\text{TCNQ})$ and for $(7)(\text{TCNQ})_2$. For $\alpha\text{-}(2)(\text{TCNQ})$ and $(4)(\text{TCNQ})$, a minor change into slightly larger molar susceptibilities is observed at around 150 K or respectively 170 K . However, the order of magnitude of the molar susceptibilities remains at $10^{-4} \text{ cm}^3 \text{mol}^{-1}$ for $\alpha\text{-}(2)(\text{TCNQ})$ or $10^{-3} \text{ cm}^3 \text{mol}^{-1}$ for $(4)(\text{TCNQ})$. This behaviour might indicate changes in the lattice, however, thermal analyses by differential scanning calorimetry show no signs of any phase transition phenomena. Beside $\alpha\text{-}(2)(\text{TCNQ})$, the structural feature of the other three compounds is mixed stacks. Structural parameters of $\alpha\text{-}(2)(\text{TCNQ})$ indicate partial electron transfer, whereas, for $\beta\text{-}(2)(\text{TCNQ})$ and $(4)(\text{TCNQ})$ a high degree charge transfer is assumed. Due to the magnetic behaviour, strong coupling of the spin centers along the stacks is anticipated. The neutral CT salt $(7)(\text{TCNQ})_2$ is associated with diamagnetic behaviour, however, experimentally the molar susceptibilities are in the same region as for the ionic $(4)(\text{TCNQ})$. Missing donor or acceptor molecules, as defects in the crystals, might lead to magnetic interactions. But no evidence for such imperfections could be found.

(3)(TCNQ) is mainly diamagnetic. At lower temperature, the magnetic susceptibility is slightly positive, but changes into negative values at $T > 20 \text{ K}$. In the crystals, 3^{+} and TCNQ^{-} form mixed stacks wherein the oppositely charged molecules show electrostatic attraction to each other. This structural feature clarify the strong coupling of the adjacent spin centers resulting in largely suppressed spin momenta of 3^{+} and TCNQ^{-} .

For **(8)(TCNQ)**, the plot of χ_{mol}^{-1} versus T reveals that the material obeys paramagnetic behaviour in the high-temperature region ($T > 100 \text{ K}$) with $C = 0.378 \text{ cm}^3 \text{Kmol}^{-1}$ and θ of -79 K corresponding to

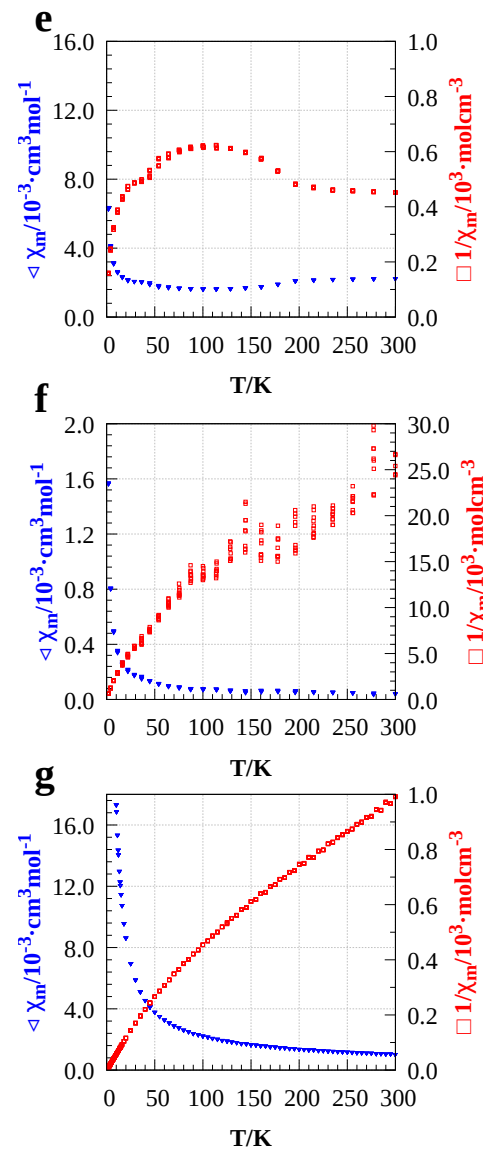


Figure 6.28: Magnetic properties of $\alpha\text{-}(1)(\text{TCNQ})$ **a**, $\alpha\text{-}(2)(\text{TCNQ})$ **b**, $\beta\text{-}(2)(\text{TCNQ})$ **c**, $(3)(\text{TCNQ})$ **d**, $(4)(\text{TCNQ})$ **e**, $(7)(\text{TCNQ})_2$ **f** and $(8)(\text{TCNQ})$ **g**. The plots $\chi_{mol} = f(T)$ (blue triangles) and $\chi_{mol}^{-1} = f(T)$ (red squares) are presented. For $\alpha\text{-}(1)(\text{TCNQ})$, the simulated functions obtained by the 1D Heisenberg chain model[124] are given as solid lines.

$1.74 \mu_B$. This quantity fits well to $S = \frac{1}{2}$ one free electron per formula unit, however, the large Weiss Constant reduces the magnetic momentum. In the low-temperature region ($T < 100$ K), almost ideal Curie behaviour is observed with $C = 0.183 \text{ cm}^3 \text{Kmol}^{-1}$ and θ of -0.4 K. The magnetic momentum amounts to $1.21 \mu_B$ corresponding to $\frac{2}{3}$ unpaired electrons.

Summarising, the magnetic susceptibilities of the pyridone azine CT salts with TCNQ do not reflect the empirically estimated charge transfer or respectively the ionicity. α -(2)(TCNQ), β -(2)(TCNQ), (4)(TCNQ) and (7)(TCNQ)₂ show nearly similar magnetic behaviour. At low temperatures, small magnetic moment is observed that runs into a nearly temperature independent paramagnetism. Diamagnetic behaviour is detected in (3)(TCNQ). Substantial coupling of the electron in the stacking framework might lead to largely suppressed spin momenta. Paramagnetic phenomena are observed in α -(1)(TCNQ) and (8)(TCNQ). Antiferromagnetic effect with a Néel temperature T_N of 50 K for α -(1)(TCNQ) is examined. (8)(TCNQ) show paramagnetism with a magnetic moment that corresponds to almost a have unpaired electron.

6.3 Band Structure and PDOS

In order to investigate the electronic properties of CT salts, band structure and projected density of states (PDOS) calculations were performed. The PDOS were calculated for individual atoms as well as the donor and acceptor molecules. Investigated CT salts are α -(2)(TCNQ), β -(2)(TCNQ), (3)(TCNQ), (4)(TCNQ), (7)(TCNQ), (7)(TCNQ)₂ and (8)(TCNQ). Hybrid density functional theory with dispersion correction and triple-zeta basis sets (PW1PW+D3/pob-TZVP-rev2[114–119]) were employed. All of the *ab initio* calculations in this work were performed using the CRYSTAL17[112, 113] program package (version 1.0.2). The method is described in Chapter 2.8 in detail.

For each donor and acceptor pair, four different spin states were investigated. Closed shell states with paired electrons are referred as non-magnetic, NM. For a ferromagnetic, FM, state the unpaired electrons of all atoms have parallel spin per definition in the majority channel. Two different antiferromagnetic (AFM) states were investigated. In the AFM1 state, both, the donor and the acceptor molecule exhibit a net magnetic moment of zero with antiparallel spins on neighbouring atoms. For AFM2 the donor and acceptor molecules are FM individually but antiparallel with respect to the each other. Fig. 6.29 shows a schematic representation of the spin ordering.

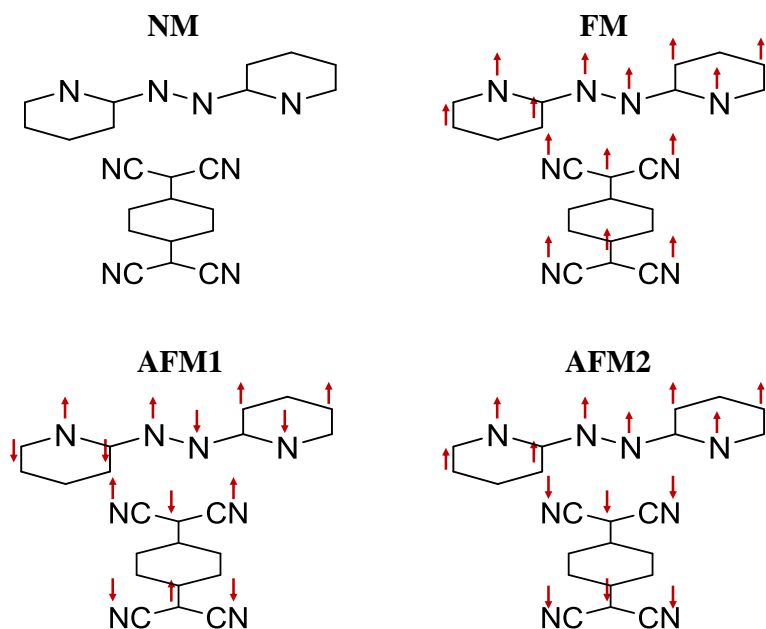


Figure 6.29: Investigated spin states for the pyridone azine CT salts: non-magnetic (NM), ferromagnetic (FM), antiferromagnetic (AFM1 and AFM2), with schematic molecules. Up- and downside spins are drawn in red.

As a benchmark, PW1PW+D3/pob-TZVP-rev2 calculations on (TTF)(TCNQ) were performed. In Chapter 1.1.1 the structural and electronic properties are described accurately. It is one of the best investigated organic metals in experimental as well as in theoretical studies[32–35].

Spin states with an energy difference smaller than 10 kJ/mol were considered as degenerate. Accordingly, the spin states with the fewest variables, NM or, if the degenerate states are open shell, FM was chosen. Fig. 6.30 shows the calculated band structures and PDOS for experimental structures at RT, 100 K and 60 K.

The band dispersions calculated for all temperatures suggest both the metallic and the anisotropic character of (TTF)(TCNQ), accurately. From Γ to Z, corresponding to the crystallographic *b* axis, a band crossing of the Fermi level is observed. Smaller dispersions are observed along B to Γ (*c* axis) and Y₂ to Γ (*a* axis). Thus, the selected method implies metallic conductivity along the crystallographic *b* axis in agreement with experimentally found properties. Even calculations for low temperature structures obtained at 60 K and 100 K validate the one-dimensional metallic character of (TTF)(TCNQ). Below 54 K, (TTF)(TCNQ) undergoes a metal-insulator transition[30].

The calculated PDOS imply that the energy densities around the top of the valence band come from all types of atoms (except hydrogen). For all temperatures, contributions of S, N and C atoms to the VBM are observed. The C atoms have the largest impact. At the Fermi level, $\varepsilon_f = 0$ eV, a PDOS minimum occurs. Summarising, band structure calculations from PW1PW+D3/pob-TZVP-rev2 on (TTF)(TCNQ) are in accordance with experiments. The anisotropic metallic character of (TTF)(TCNQ) is well mirrored by the use of a hybrid functional in combination with the dispersion correction. Therefore, the electronic structure of CT salts can be described accurately by this method.

For the investigated CT salts, band structures and PDOS for structures at RT data are shown in Fig. 6.31. Here PDOS are calculated for donor (*D*) and acceptor (*A*) molecules. Only the immediate vicinity of the band gap (± 1.0 eV) is considered. Further calculations of electronic properties for low temperature structures are shown in the appendix A.4. Complementary, Tab. 6.4 summarises the energetically favoured state, conducting behaviour derived from band structures, calculated band gaps and charge transfer calculated from the empirical Kistenmacher relationship as well as calculated charge transfer by Mulliken population analysis of the CT salts for RT.

Table 6.4: Spin states, conducting behaviour, band gaps and charge transfers via Mulliken population analyses on PW1PW+D3/pob-TZVP-rev2 and charge transfers from empirical Kistenmacher relationship of the CT salts for RT; *c*: conducting, *sc*: semiconducting.

compound	Spin State	Conductivity	Band Gap/eV	Kistenmacher	Mulliken
$\alpha\text{-}(\mathbf{2})(\text{TCNQ})$	NM	<i>c</i>	-	0.54	0.89
$\beta\text{-}(\mathbf{2})(\text{TCNQ})$	NM	<i>sc</i>	0.79	1.00	0.98
(3)(TCNQ)	AFM2	<i>sc</i>	1.20/1.65	1.00	0.91
(4)(TCNQ)	AFM1	<i>sc</i>	1.02	0.82	0.87
(7)(TCNQ)	NM	<i>sc</i>	0.61	0.30	0.31
(7)(TCNQ) ₂	NM	<i>sc</i>	0.37	0.00	0.10
(8)(TCNQ)	AFM2	<i>c</i>	-	0.42	0.49

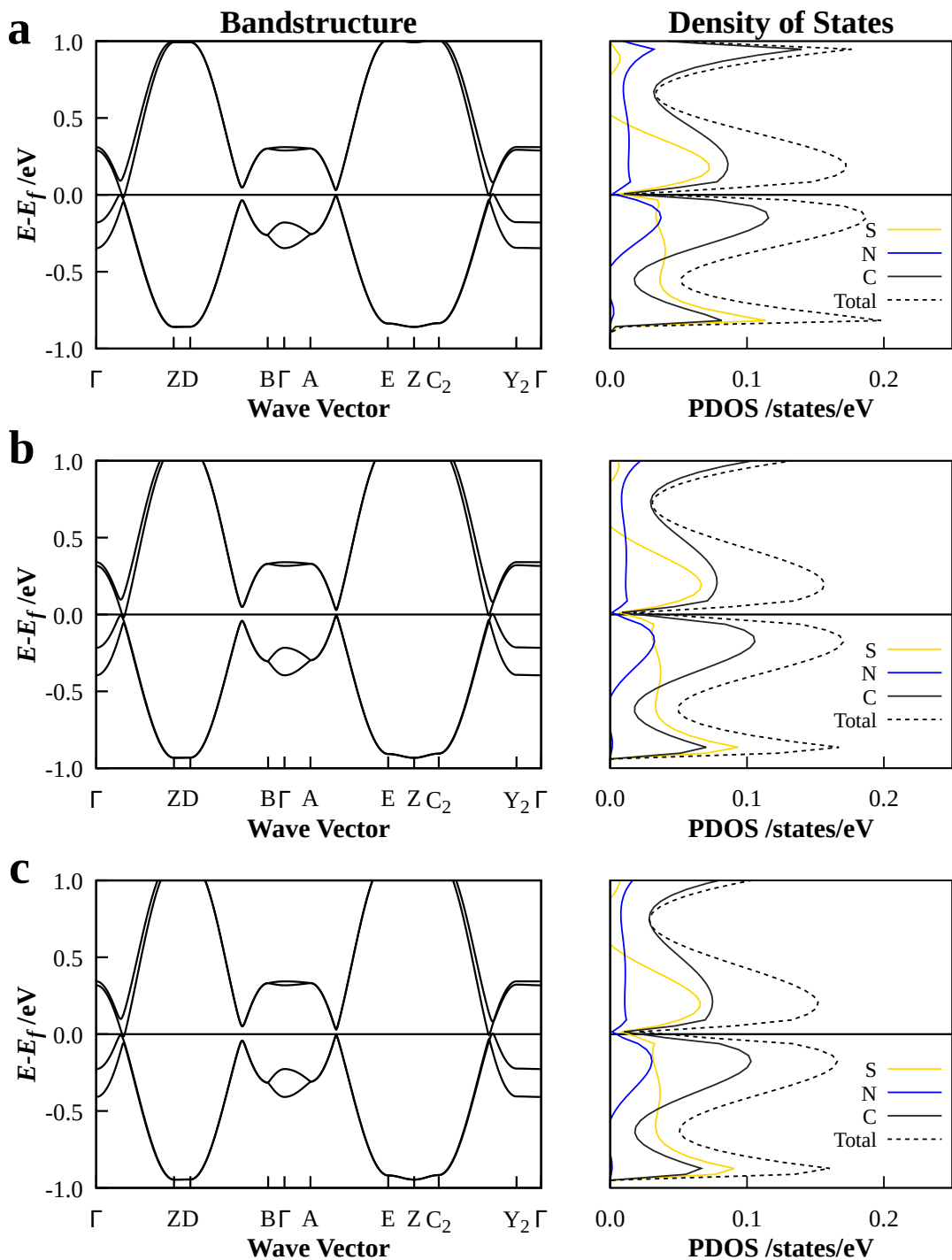


Figure 6.30: Band structures and projected densities of states (PDOS) in states/eV of (TTF)(TCNQ) for experimental structures at RT **a**, 100 K **b** and 60 K **c** calculated with CRYSTAL17, PW1PW+D3/pob-TZVP-rev2.

For α -(2)(TCNQ), the energetically favoured state is NM. Band dispersions in c direction (B to Γ) are recognised, while along a (Y_2 to Γ) and b axis (Γ to Z) minor dispersions are observed. The band structure implies anisotropic metallic conductivity along the stacking direction. As evident from the calculated PDOS for the donor and acceptor molecule, the electron densities close to the E_F are purely from the donor molecule. In contrast, the acceptor molecules contribute to both VBM and CBM. The Kistenmacher relationship predicts a partial charge transfer of 0.54 electron per molecule, whereas the Mulliken population analysis results in a larger electron transfer of 0.89 electron per molecule. Since the structure-data quality is quite low, the CT estimated according to Kistenmacher's formula has to be considered with lower reliability.

In contrast, β -(2)(TCNQ) implies semiconducting behaviour with a NM ground state and a direct band gap of 0.76 eV. The κ -point pathways in the irreducible Brillouin zone (IBZ) run from Γ to S (a axis), from Γ to Y (b axis) and Γ to Z (c axis). Both, donor and acceptor molecules contribute electron densities in the VBM and CBM as shown in the PDOS. The charge transfer estimated by Kistenmacher's relation is with about one electron per molecule in agreement with the Mulliken population analysis of 0.98 electrons per molecule. For the low temperature structure the calculated electronic properties of the substance remain the same, albeit with a slightly larger calculated band gap of 0.79 eV.

For (3)(TCNQ), AFM2 is the calculated, energetically favoured state. The κ -point pathways in the IBZ run from Y_2 to Γ (a axis), from Γ to Z (b axis) and B to Γ (c axis). Small band dispersions are observed, thus, the compound suggests semiconducting properties with indirect band gaps of 1.20 eV and 1.65 eV. Both, orbitals of donor and acceptor molecule, contribute electron densities in the VBM and CBM. Resultingly, the PDOS implies a complete electron transfer which is consistent with the Kistenmacher relationship and the Mulliken population analysis resulting 1.0 or respective 0.91 electrons per molecule. For low temperature structure, band structure and PDOS are expected to exhibit minor changes with indirect band gaps of 1.21 eV and 1.57 eV.

The energetically favoured state of (4)(TCNQ) is AFM1. The κ -point pathways in the IBZ run from Y_2 to Γ (a axis), from Γ to Z (b axis) and B to Γ (c axis). The calculated direct band gap amounts to 1.02 eV. Since the PDOS implies that orbitals of donor and acceptor contribute to VBM and CBM, a large degree of charge transfer is expected. The Kistenmacher relationship yields in a charge transfer of 0.82 electrons per molecule in accordance with 0.87 e⁻/molecule via Mulliken population analysis.

For (7)(TCNQ), NM is the energetically favoured state. The κ -point pathways in the IBZ run from Γ to X (a axis), from Γ to Y (b axis) and Γ to Z (c axis). Semiconducting behaviour with a band gap of 0.61 eV is predicted from the band structure. Here, the VBM is dominated by donor molecule orbitals and the CBM by acceptor molecule orbitals. Additionally, the density of states suggests small charge transfer. Estimated charge transfer by the Kistenmacher relationship of 0.3 e⁻/molecule is in agreement with 0.31 e⁻/molecule via Mulliken population analysis.

(7)(TCNQ)₂ is NM. The κ -point pathways in the IBZ run along from Γ to X (a axis), from Γ to Y (b axis) and Γ to Z (c axis). In the band structure, only little band dispersions without Fermi level crossing are observed with a small calculated band gap of 0.37 eV. As evident from the PDOS, the VBM comprises of donor and acceptor orbitals while the CBM primarily consists of acceptor orbitals. Both, the Kistenmacher relationship and the Mulliken population analysis imply an oxidation state close to 0, underlying the VBM and CBM differentiation in the PDOS. For low temperature structure, the calculated band gap is slightly larger with 0.39 eV.

The AFM2 and FM states for **(8)**(TCNQ) are energetically favoured and regarded as degenerate. Calculations with both spin states led to similar results. In the following the calculations based on the AFM2 spin state are presented. The κ -point pathways in the irreducible Brillouin zone (IBZ) run from Γ to X (a axis), from Γ to Y (b axis) and Γ to Z (c axis). At ambient temperature, the band structure shows band dispersions along the a axis. The band crossing around the Fermi level indicates anisotropic metallic character of the material. In the PDOS, the donor molecules contribute the majority of the electron densities close to the Fermi level E_F . However, the acceptor molecules contribute to the states close to the Fermi level. The VBM is dominated by the donor molecules and the CBM by the acceptor molecules. Not only the PDOS, but also the Kistenmacher equation (0.42 e⁻/molecule) and Mulliken population analysis (0.49 e⁻/molecule) suggest a partial electron transfer. Calculations of low temperature structure-data (123 K, 150 K, 200 K and 250 K, see appendix A.4) of **(8)**(TCNQ) predict a retention of the anisotropic metallic behaviour on cooling.

All calculated PDOS show overall contributions from every element except hydrogen. As expected, the largest contribution to the electron density originates from carbon. Hetero atoms, such as S or F included by SMe or CF₃ groups do not contribute to the states close to the Fermi level E_F .

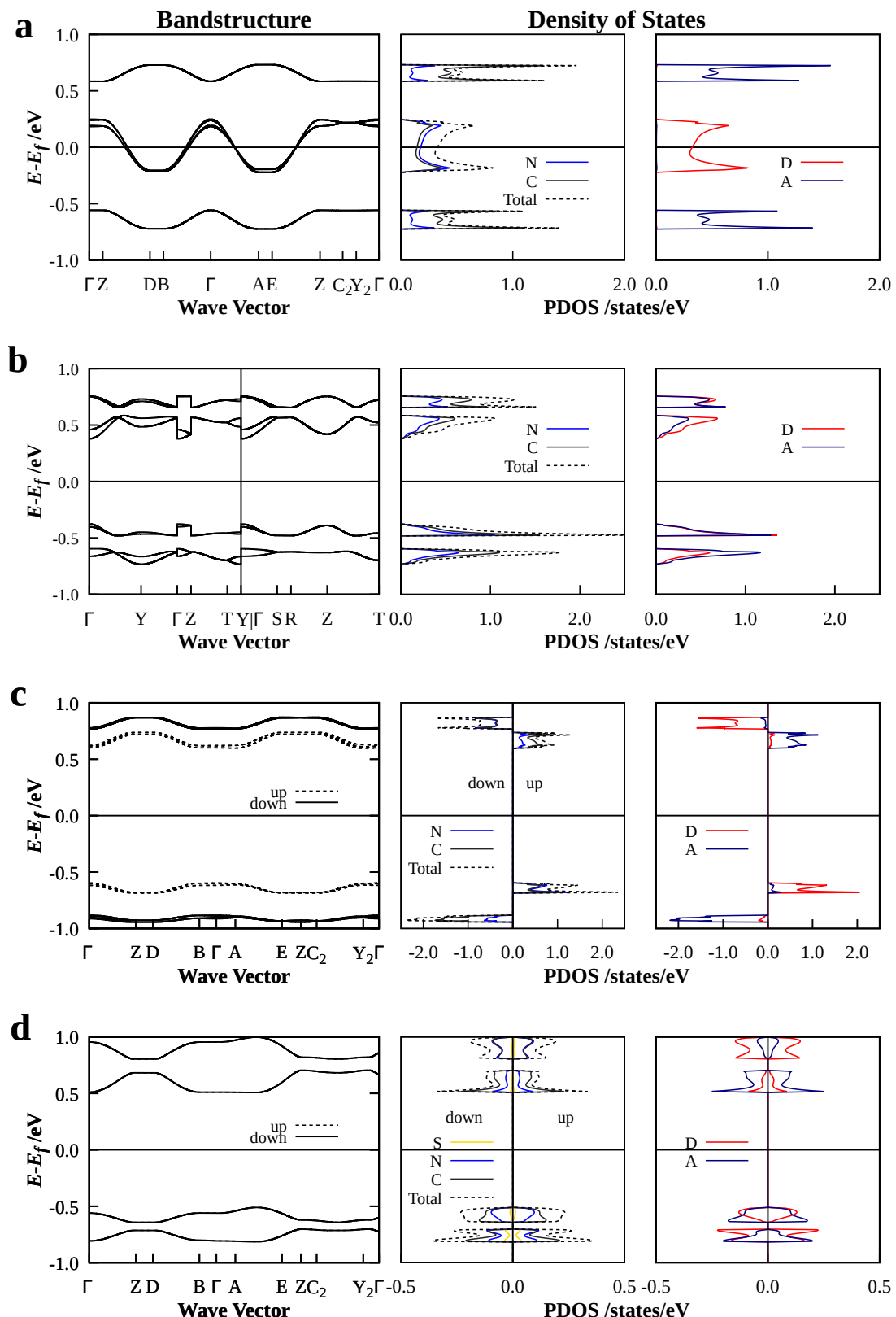
The magnitude of charge transfer estimated via Kistenmacher relationship and Mulliken population analysis correlates directly with the PDOS. If a complete electron transfer is anticipated, the PDOS of VBM and CBM shows contributions from orbitals of both molecules. When the magnitude of the charge transfer is expected to be small, the VBM is suggested to be largely dominated by the donor molecule orbitals and the CBM by the acceptor molecule orbitals. Separation of the DOS into donor and acceptor molecules gives an indication which molecule is responsible for electrical conductivity.

The predictions based on the calculated band structures and the PDOS correlate directly with the crystal structures as well as the empirical determined charge transfers. α -(**2**)(TCNQ) and **(8)**(TCNQ) crystallise in segregated stacks and imply crossing of the bands at the Fermi level with intrinsic anisotropic character. Band dispersions occur along the corresponding stacking direction facilitating electron migration.

In the PDOS of α -(**2**)(TCNQ), the electron densities around E_F comprise predominantly of states from the donor molecules. The structure is made up by equidistant stacks of the donor molecules, whereas stacks of dimeric aggregates are present in the acceptor stacks. The calculations suggest that conductivity of α -(**2**)(TCNQ) derives only from electron migration along the donor stacks in the crystal.

In **(8)**(TCNQ), the structural features are similar to that of α -(**2**)(TCNQ). Nonetheless, the molecules of **8** form nearly equidistant stacks. The steric demand of the additional CF₃ groups is significantly larger compared to that of hydrogen in α -(**2**)(TCNQ). However, the computational results are quite similar. From a crystallographic point of view, the results from calculation are reasonable.

Calculations of the other 1:1 CT compounds (**3**)(TCNQ), (**4**)(TCNQ), β -(**2**)(TCNQ) and (**7**)(TCNQ) result in semiconducting behaviour with band gaps of 1.21 eV and 1.57 eV, 1.02 eV, 0.76 eV and 0.61 eV, respectively. Their structures consist of mixed stacks wherein migration of electrons is hindered due to the formation of Coulomb sinks. For the 1:2 CT salt (**7**)(TCNQ)₂ semiconducting properties are observed as well. However, the calculated band gap of 0.37 eV, is smaller compared to that of 1:1 CT salt (**7**)(TCNQ). In the PDOS, the contributions of the donor and acceptor orbitals to the VBM, or respectively to the CBM, suggest a direct relation to the amount of charge transfer.



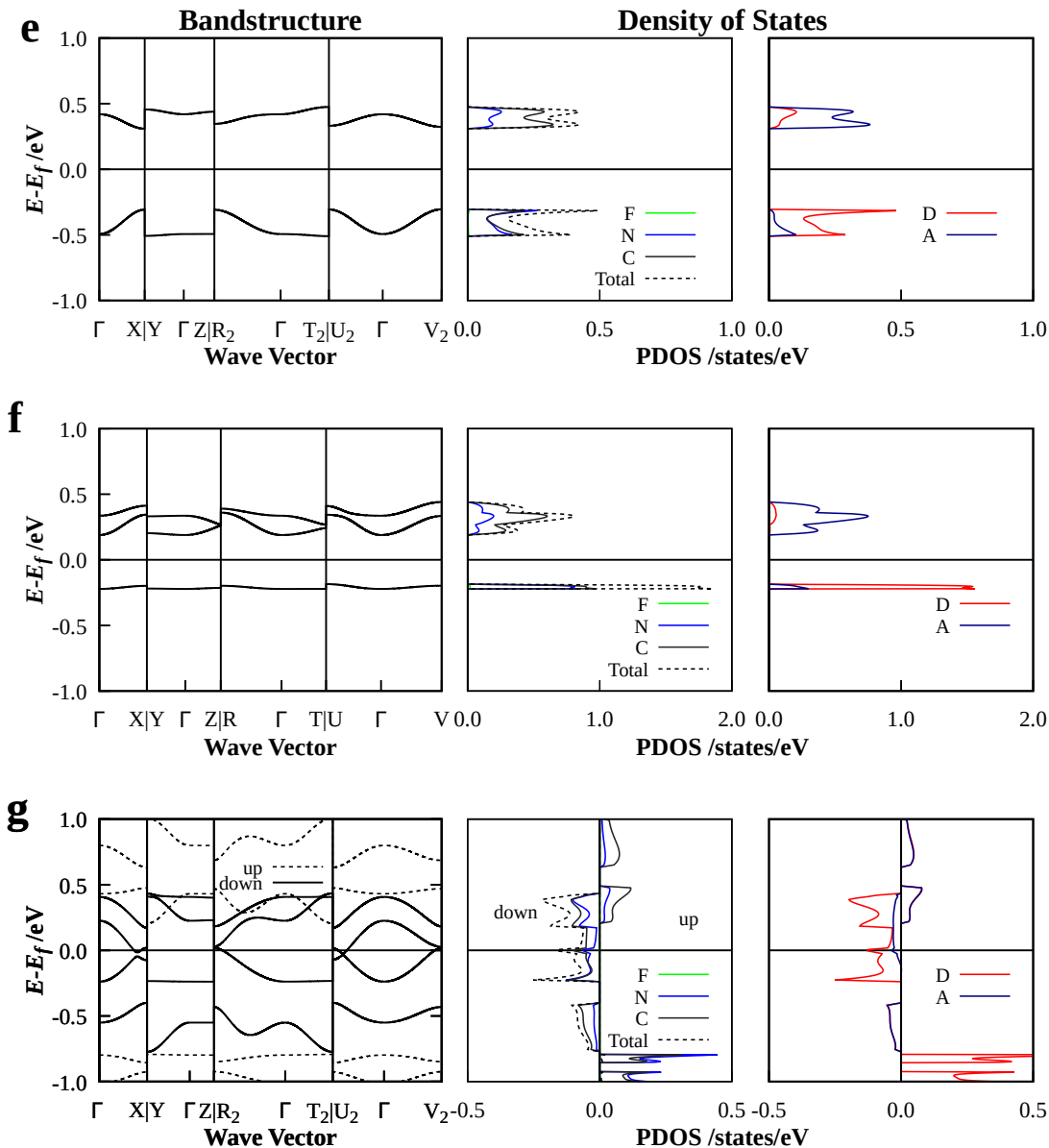


Figure 6.31: Band structures, PDOS for atom orbitals and PDOS for orbitals belonging to donor or acceptor for RT of α -(2)(TCNQ) **a**, β -(2)(TCNQ) **b**, (3)(TCNQ) **c**, (4)(TCNQ) **d**, (7)(TCNQ) **e**, (7)(TCNQ)₂ **f** and (8)(TCNQ) **g** calculated with CRYSTAL17, PW1PW+D3/pob-TZVP-rev2.

In the case that both molecules contribute evenly to CBM and VBM, a significant charge transfer is expected. Yet if the donor orbitals are predicted to dominate the VBM and the acceptor orbitals the CBM only small amount of charge transfer is anticipated.

The empirically estimated charge transfers via Kistenmacher relationship agree well with the calculated PDOS as well as the calculated charge transfers from Mulliken population analysis.

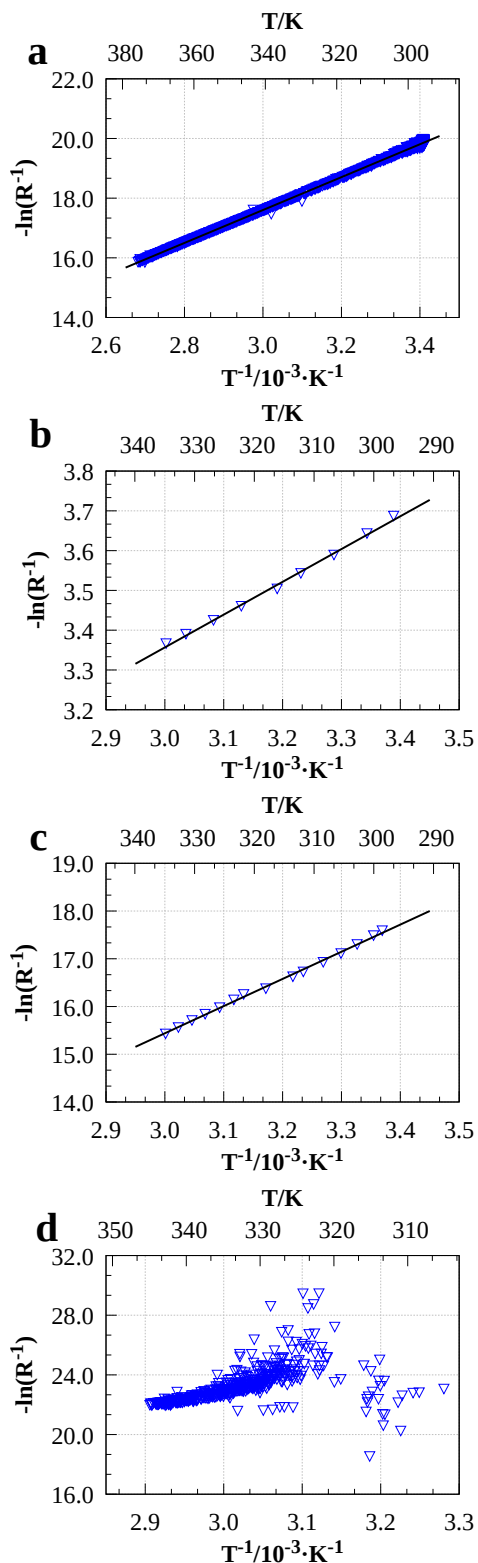
6.4 Conductivity

Conductivity measurements were carried out on powders for the CT salts α -(1)(TCNQ), α -(2)(TCNQ), β -(2)(TCNQ), (3)(TCNQ), (4)(TCNQ), (7)(TCNQ)₂ and (8)(TCNQ). For (8)(TCNQ), the anisotropic electrical conductivity along the stacking direction (*a* axis) was experimentally accessible.

Additionally, the electrical conductivities were calculated by the Boltzmann transport equation implemented as BOLTZTRA[113] in CRYSTAL17. By definition, the conductivity σ is calculated as a 3×3 tensor for a three-dimensional system. The anisotropy is expected to correlate with the order of magnitude of σ_a , σ_b and σ_c , small off-diagonal elements are neglected.

The CT salts α -(1)(TCNQ), α -(2)(TCNQ), β -(2)(TCNQ), (4)(TCNQ), (7)(TCNQ)₂ and (8)(TCNQ) show semiconducting properties in the corresponding measured temperature range. Therefore, the electrical resistance decreases with increasing temperature. (3)(TCNQ) shows typical insulating behaviour at room temperature. In Fig. 6.32, the corresponding Arrhenius plots are presented and in Tab. 6.5 the measured specific conductivities are listed.

The experimental specific conductivities vary from insulating to weakly conducting behaviour. The conductivity of α -(1)(TCNQ) increases from $8.2 \times 10^{-9} \text{ Scm}^{-1}$ at 310 K to $6.0 \times 10^{-8} \text{ Scm}^{-1}$ at 350 K. For α -(2)(TCNQ), the conductivities range in the upper semiconducting area with 0.06 Scm^{-1} at 310 K and 0.07 Scm^{-1} at 330 K. β -(2)(TCNQ) presents a semiconductor with $1.5 \times 10^{-8} \text{ Scm}^{-1}$ at 310 K and $4.2 \times 10^{-8} \text{ Scm}^{-1}$ at 330 K. In contrast, (3)(TCNQ) show typical insulating behaviour with $\approx 10^{-10} \text{ Scm}^{-1}$ around 310 K. For (4)(TCNQ) the specific conductivity increases from $1.5 \times 10^{-6} \text{ Scm}^{-1}$ (310 K) to $5.6 \times 10^{-6} \text{ Scm}^{-1}$ (350 K). (7)(TCNQ)₂ shows a similarly specific conductivity of $2.9 \times 10^{-7} \text{ Scm}^{-1}$ at 310 K and $1.9 \times 10^{-6} \text{ Scm}^{-1}$ at 350 K. When measuring (8)(TCNQ) as a powder its conductivity is 8.5×10^{-4} at 310 K and $1.8 \times 10^{-3} \text{ Scm}^{-1}$ at 350 K. Anisotropic conductivity measurement along the *a* axis yields in higher specific conductivity of $8.3 \times 10^{-3} \text{ Scm}^{-1}$ at 310 K and $1.6 \times 10^{-2} \text{ Scm}^{-1}$ at 350 K. As expected, in stacking direction the electron migration is by a factor of 10 larger.



The activation energy of the thermally activated electron transfer into the CB is obtained from the plots of the Arrhenius function, $-\ln(R^{-1}) = f(T^{-1})$ shown in Fig. 6.32. This energy, E_a , correlates to the band gap (Tab. 6.7).

For α -(1)(TCNQ) E_a is determined to 1.0 eV, for α -(2)(TCNQ) to 0.1 eV, for β -(2)(TCNQ) to 1.0 eV, for (4)(TCNQ) 0.6 eV, for (7)(TCNQ)₂ to 0.9 eV and for (8)(TCNQ) to 0.3 eV (powder and anisotropic along the a axis). For (3)(TCNQ), the large band gap of 2.9 eV is obtained about 330 K.

Before calculating electronic properties for the aforementioned compounds, (TTF)(TCNQ) was used as benchmark for the prediction of the specific electrical conductivity via CRYSTAL17, PW1PW+D3/pob-TVZB-rev2. As shown in Tab. 6.6 experimental and calculated specific electrical conductivities at 60 K and room temperature are in good agreement. Concluding, the transport properties of (TTF)(TCNQ) are described accurately by this method. Relative order of magnitude in the crystallographic directions, $\sigma_b > \sigma_c > \sigma_a$, suggests anisotropic conduction. Moreover, the absolute order of magnitude is in close proximity to experiment. Therefore, the dispersion corrected hybrid DFT-functional (PW1PW) presents an appropriate method for describing the transport properties of CT salts.

In addition to the estimated band gaps, Tab. 6.7 lists calculated band gaps, experimentally determined specific conductivities as calculated anisotropic conductivities of the CT salt structures for room temperature. However, experimental results gained from powders are not directly comparable to calculations based on single crystal data. Calculations allow to distinguish anisotropic conductivities along the different crystal axes.

α -(2)(TCNQ) is expected to exhibit conductivities in the metallic range. The relative order of magnitude is calculated to: $\sigma_c > \sigma_a > \sigma_b$. Along the crystallographic c axis the largest electrical conductivity $3.94 \times 10^3 \text{ Scm}^{-1}$ is obtained. The conductivity in the other two directions is calculated to be 10 times smaller in a direction with $2.03 \times 10^2 \text{ Scm}^{-1}$ and 1000 times smaller in b direction with $1.84 \times 10^0 \text{ Scm}^{-1}$. Band structure, PDOS and conductivity calculations are in sufficient agreement with experiments. Crystal structure indicates metallic properties and the order of the specific conductivities of the powder is in close proximity to conducting range.

Calculations of β -(2)(TCNQ) reveal semiconducting behaviour. The calculated order of anisotropic

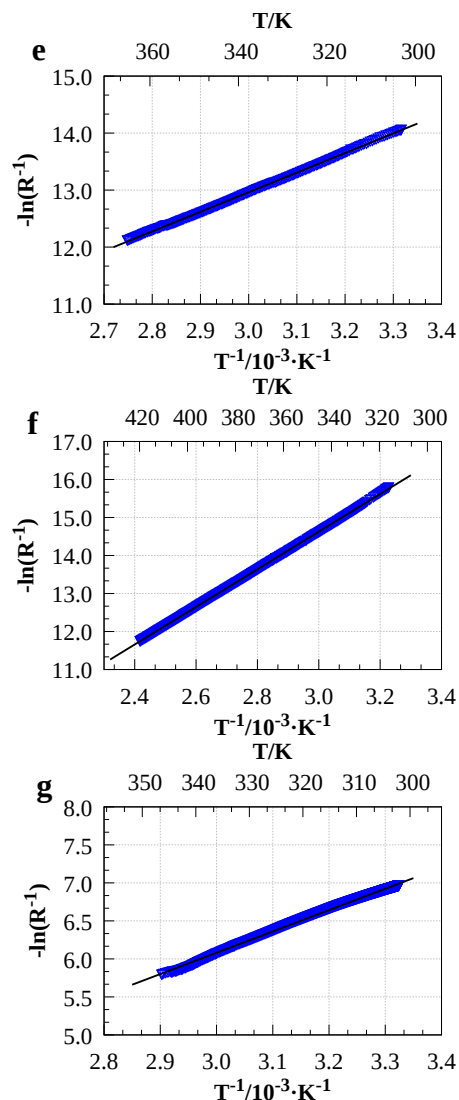


Figure 6.32: Arrhenius plots $-\ln(R^{-1}) = f(T^{-1})$ of the electrical resistivities of α -(1)(TCNQ) **a**, α -(2)(TCNQ) **b**, β -(2)(TCNQ) **c**, (3)(TCNQ) **d**, (4)(TCNQ) **e**, (7)(TCNQ)₂ **f** and (8)(TCNQ) **g**. Blue circles are the measured resistances and black lines present the best linear fit. All compounds, except insulating (3)(TCNQ), show typical semiconducting properties with small band gaps.

conductivities in relative scale is: $\sigma_a > \sigma_b > \sigma_c$. Therein, the absolute computed conductivity along the a direction amounts to $2.55 \times 10^{-4} \text{ Scm}^{-1}$, along the b direction to $5.48 \times 10^{-5} \text{ Scm}^{-1}$ and in c direction to $4.98 \times 10^{-5} \text{ Scm}^{-1}$ (Tab. 6.6). In accordance to the crystal structure of β -(2)(TCNQ), consisting of mixed stacks running along the crystallographic a axis, the magnitude of the electrical conductivity in stacking direction is the largest. By experiment, the specific conductivity is determined to $7.4 \times 10^{-9} \text{ Scm}^{-1}$. The band gap obtained from the Arrhenius equation, 0.98 eV, is slightly larger than the calculated band gap of 0.79 eV.

Table 6.5: Specific conductivities, σ , and activation energies, E_a , of α -(1)(TCNQ), α -(2)(TCNQ), β -(2)(TCNQ), (3)(TCNQ), (4)(TCNQ), (7)(TCNQ)₂ and (8)(TCNQ) at 310 K and 350 K in Scm^{-1} . a : anisotropic conductivity; b : determined at 330 K.

Compound	$\sigma_{310 \text{ K}}/\text{Scm}^{-1}$	$\sigma_{350 \text{ K}}/\text{Scm}^{-1}$	E_a/eV
α -(1)(TCNQ)	8.2×10^{-9}	6.0×10^{-8}	0.95
α -(2)(TCNQ)	0.06	^b 0.07	0.14
β -(2)(TCNQ)	1.5×10^{-8}	^b 4.2×10^{-8}	0.98
(3)(TCNQ)	$\approx 10^{-10}$		2.9
(4)(TCNQ)	1.5×10^{-6}	5.6×10^{-6}	0.59
(7)(TCNQ) ₂	2.9×10^{-7}	1.9×10^{-6}	0.85
(8)(TCNQ)	8.5×10^{-4}	1.8×10^{-3}	0.27
(8)(TCNQ) ^a	8.3×10^{-3}	1.6×10^{-2}	0.33

For (3)(TCNQ) the calculated conductivities are in agreement with experiment. The order of magnitude follows: σ_b ($5.07 \times 10^{-10} \text{ Scm}^{-1}$) $>$ σ_a ($1.26 \times 10^{-11} \text{ Scm}^{-1}$) $>$ σ_c ($7.64 \times 10^{-12} \text{ Scm}^{-1}$) (Tab. 6.6). Along the stacking direction b the specific conductivity is suggested to be larger by a factor of 10 compared to the a direction and by a factor of 1000 compared to the c direction. The calculated results are in agreement with experimental obtained specific conductivity of $\approx 10^{-10} \text{ Scm}^{-1}$. Again the calculations mirror the anisotropy, here, mixed stacks along the b direction. Due to the insulating ground state, experimental E_a is determined over 330 K and amounts to 2.9 eV. However, calculations predict smaller band gaps of 1.20 eV and 1.59 eV.

Table 6.6: Specific electrical conductivities of (TTF)(TCNQ) from experiment and calculated with CRYSTAL17, PW1PW+D3/pob-TZVP-rev2 in Scm^{-1} at 60 K and RT.

T/K	$\sigma_{b,exp}$	σ_a	σ_b	σ_c
60	$0.3\text{--}1.8 \times 10^4$ [26, 36]	1.46×10^2	1.40×10^4	4.01×10^2
RT	$2.0\text{--}9.2 \times 10^2$ [144]	2.74×10^1	4.43×10^3	1.29×10^2

The calculated specific conductivities of (4)(TCNQ) confirm the experimentally found semiconducting behaviour. In *a* direction it amounts to 5.58×10^{-7} Scm⁻¹, in *b* direction to 2.48×10^{-6} Scm⁻¹ and in *c* direction to 2.05×10^{-9} Scm⁻¹, resulting in the order: $\sigma_b > \sigma_a > \sigma_c$ (Tab. 6.6). The crystallographic motif of mixed stacks, which occurs along the *b* direction, correlates with the calculated specific conductivities. In *a* (*c*) direction the conductivity is 10 (1000) times smaller. The experimental band gap E_a of 0.6 eV is accompanied by a calculated one of 1.02 eV.

Table 6.7: Experimental electrical conductivities ($\sigma_{RT,exp}$) and calculated anisotropic electrical conductivities ($\sigma_{RT,calc}$: σ_a , σ_b and σ_c) in Scm⁻¹, activation energies of the electron excitement from valence into conduction band via experiment ($E_{a,exp}$) and calculations ($E_{a,calc}$) in eV at RT for α -(2)(TCNQ), β -(2)(TCNQ), (3)(TCNQ), (4)(TCNQ), (7)(TCNQ)₂, (7)(TCNQ) and (8)(TCNQ) with CRYSTAL17, PW1PW+D3/pob-TZVP-rev2. *ins*: insulator; *cs*: conducting state; *n*: no experimental data.

compound	$\sigma_{RT,exp}$ /Scm ⁻¹	$\sigma_{RT,calc}$ /Scm ⁻¹	σ_a	σ_b	σ_c	$E_{a,exp}$ /eV	$E_{a,calc}$ /eV
α -(2)(TCNQ)	0.06	2.03×10^2		1.84×10^0	3.94×10^3	0.14	<i>cs</i>
β -(2)(TCNQ)	7.4×10^{-9}	2.55×10^{-4}		5.48×10^{-5}	4.98×10^{-5}	0.98	0.79
(3)(TCNQ)	$\approx 10^{-10}$	1.26×10^{-11}		5.07×10^{-10}	7.64×10^{-12}	2.90	1.20/1.65
(4)(TCNQ)	1.5×10^{-6}	5.58×10^{-7}		2.48×10^{-6}	2.05×10^{-9}	0.6	1.02
(7)(TCNQ)	<i>n</i>	2.46×10^{-2}		3.84×10^{-4}	7.69×10^{-4}	<i>n</i>	0.61
(7)(TCNQ) ₂	2.9×10^{-7}	5.02×10^{-1}		2.61×10^{-2}	1.67×10^{-1}	0.9	0.37
(8)(TCNQ)	8.5×10^{-4}	2.82×10^2		1.07×10^2	6.05×10^{-3}	0.33	<i>cs</i>
(8)(TCNQ) ^a	8.3×10^{-3}	2.82×10^2	-	-	-	0.27	<i>cs</i>

No experimental data for the E_a or σ of (7)(TCNQ) is available, however, the calculated properties predict semiconducting behaviour. Along the *a* axis the largest specific conductivity of 2.46×10^{-2} Scm⁻¹ is obtained. Contributions from *b* and *c* axis, respectively, 3.84×10^{-4} Scm⁻¹ and 7.69×10^{-4} Scm⁻¹, are expected to be nearly similar (Tab. 6.6). Compared to the stacking direction *a*, the electron migration is predicted to be 100 times slower. Thus, band structure, PDOS and conductivity calculations correlate to the crystal structure dominated by mixed stacks along the *a* axis.

For (7)(TCNQ)₂, the calculated anisotropic conductivities are in the semiconducting range. The order of magnitude in relative scale is: $\sigma_a > \sigma_c > \sigma_b$. The largest contribution, 5.02×10^{-1} Scm⁻¹, is predicted in *a* direction followed by *c*, 1.67×10^{-1} Scm⁻¹, and *b*, 2.61×10^{-2} Scm⁻¹ (Tab. 6.6). The specific conductivities along the crystallographic *a* and *c* axes are quite close, while in *b* direction it is by a factor of 10 smaller.

Experimentally, the specific conductivity at room temperature is found to be 2.9×10^{-7} Scm⁻¹ strengthening the semiconducting properties. By examining the crystal structure, the largest contribution to the calculated conductivity is expected to arise along the stacking direction, here, the *c* axis. In contrast to the other CT salts, the stacking direction *c* is not predicted to exhibit the largest specific conductivity. However, since the magnitude of σ_a and σ_c is nearly the same, it still agrees reasonably well with experiment. The calculated band gap of 0.9 eV is considerably larger than E_a determined by Arrhenius to 0.37 eV.

For (8)(TCNQ) anisotropic metallic conduction is calculated. The specific conductivity in a direction is calculated to $2.82 \times 10^2 \text{ Scm}^{-1}$, in b direction to $1.07 \times 10^2 \text{ Scm}^{-1}$ and in c direction to $6.05 \times 10^{-3} \text{ Scm}^{-1}$. The relative order of magnitude is: $\sigma_a > \sigma_b > \sigma_c$. The specific conductivities in a and b direction range in the conducting area, while semiconductivity in c direction is calculated. From experiment, the RT specific conductivity, measured from powder, shows semiconducting character with $8.5 \times 10^{-4} \text{ Scm}^{-1}$. As expected, measurements of the electrical conductivity in the stacking direction $8.3 \times 10^{-3} \text{ Scm}^{-1}$ is by a factor of 10 larger. Nonetheless, the calculated metallic character of (8)(TCNQ) could not be verified experimentally. The Arrhenius plot delivers a small band gap of 0.3 eV. The calculations, however, predict a conducting state without a band gap.

Summarising, results obtained from calculated electronic properties by hybrid density functional theory with dispersion correction and triple-zeta basis sets confirm the expectations derived from crystallographic point of view. Experimental findings are in agreement with calculations, except for (8)(TCNQ) where experimental and calculated results disagree. Reasons for disagreements could be experimental as well as theoretical, since defects in the crystals lower electrical conductivity as the multi-determinant system is not accurately described by the chosen method. However, calculations and reported experimental properties of (TTF)(TCNQ), with the same structural feature (segregated stacks), are in very good agreement.

α -(2)(TCNQ) and (8)(TCNQ), crystallising in segregated stacks, are expected to exhibit metallic character and band dispersion in the corresponding stacking direction. In the PDOS, electron densities close to E_F are calculated. In the case of α -(2)(TCNQ), the electron densities close to E_F arise purely from donor molecules, since the acceptor molecules do not contribute to the conductivity due to dimerisation. Referring to experiment, these findings are in quite good agreement. The metallic character of (8)(TCNQ) predicted by theory could not be confirmed experimentally. The isotropic as well as the anisotropic measurements display typical semiconducting behaviour. In the crystal, additional intra- or intermolecular interactions may influence the electron movement.

For the compounds crystallising in mixed stacks, semiconductivity is observed by experiment and predicted by calculation. β -(2)(TCNQ), (4)(TCNQ), (7)(TCNQ) and (7)(TCNQ)₂ can be classified as semiconductors. Considering the conductivities along the crystallographic axes, the largest contribution arises from the electron mobility along the corresponding stacking direction. (7)(TCNQ)₂ presents an exception, here, σ_c is calculated to be four times larger than σ_a , the stacking direction.

The calculated anisotropic conductivities of (3)(TCNQ) anticipate insulation. The anisotropy of the specific conductivities follows the expectation. Despite the overall small absolute values, the specific conductivity along the stacking direction is 10 (1000) times larger in comparison with the non-stacking directions. Experimentally, the material is an insulator.

To conclude, calculations of the electronic properties of CT salts by hybrid density functional theory with dispersion correction and triple-zeta basis sets yield reasonable results.

CHAPTER 7

Charge Transfer Compounds with TCNP

The $-M$ effect of the cyano groups makes tetracyanopyrazine (TCNP) highly electron deficient and therefore to another appropriate electron acceptor candidate. Cyclic voltammetry shows a mainly reversible single electron reduction process at -0.2 V vs. Ag/AgCl (Fig. 7.1). Compared to the polycyano-substituted TCNQ, TCNP is less harder to reduce[145].

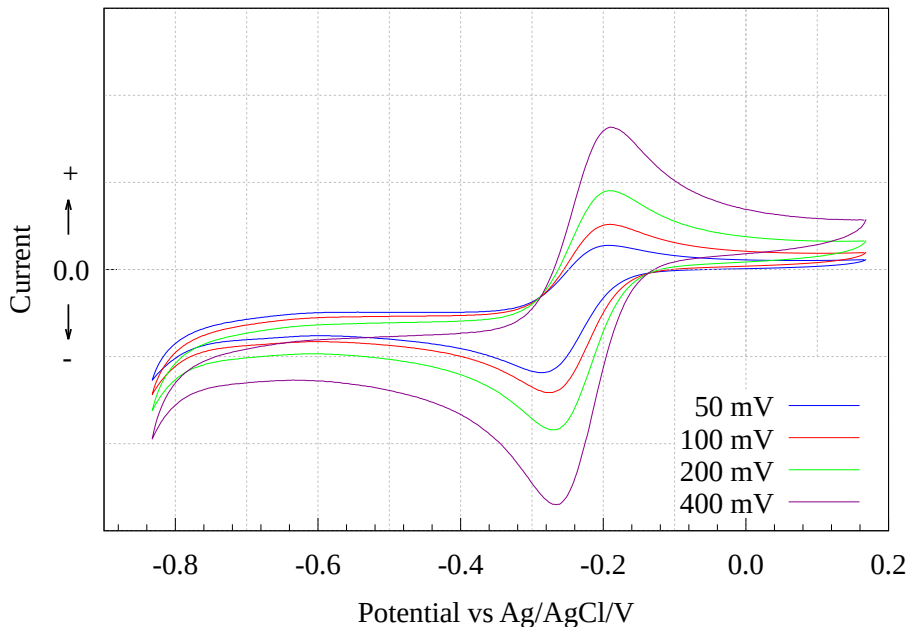


Figure 7.1: Cyclic voltammogram of tetracyanopyrazine (TCNP) showing a mainly reversible one-electron reduction process at -0.2 V vs. Ag/AgCl.

In Tab. 7.1 the bond lengths in TCNP depending on the oxidation state 0 and -1 and, additionally, in the CT salts with the donors tetrathiafulvalene, (TTF)(TCNP), or pyrene, (PYR)(TCNP), are summarised. Compared to neutral TCNP^0 , addition of one electron reveals an increase of the $\text{C}_{Ar}-\text{N}_{Ar}$ bond length (α) of circa 0.03 Å in the radical anion TCNP^{-} . The $\text{C}_{Ar}-\text{C}_{Ar}$ (γ) and the $\text{C}_{Ar}-\text{C}_{CN}$ (β) bonds are slightly shortened and hence less effected by the reduction process. The $\text{C}\equiv\text{N}$ bonds do not change by electron transfer. Therefore, the length of the $\text{C}_{Ar}-\text{N}_{Ar}$ bond is a sufficient indicator for estimation of the charge on the TCNP molecule within a CT compound[146].

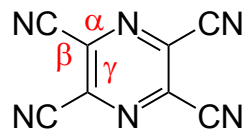


Table 7.1: Bond lengths of TCNP in the oxidation state 0 and -1 and in the CT salts (TTF)(TCNP) and (PYR)(TCNP).

Compound	α	β	γ
TCNP ⁰ [146]	1.331 ± 0.002	1.447 ± 0.003	1.405 ± 0.002
TCNP ⁻ [146]	1.359 ± 0.004	1.433 ± 0.004	1.388 ± 0.002
(TTF)(TCNP)[146]	1.337 ± 0.002	1.446 ± 0.004	1.407 ± 0.002
(PYR)(TCNP)[146]	1.332 ± 0.002	1.447 ± 0.004	1.405 ± 0.002

In the following, two new azine-containing CT salts with TCNP, (**5**)(OTCNP)₂ and (**7**)(TCNP) are presented. Their crystal structures are discussed in the following. For (**7**)(TCNP), the electronic properties were investigated by measurements of the magnetic susceptibility and the electrical conductivity.

7.1 Crystal Structures

7.1.1 (5)(OTCNP)₂

In the reaction of **5** with TCNP in acetonitrile, orange needle-shaped crystals were obtained (Fig. 7.2).



Figure 7.2: The orange shining needle-shaped crystals of $(\mathbf{5})(\text{OTCNP})_2$.

to 1.40 Å for C1–N2 and 1.26 Å for N2–N2^{*i*}. With respect to the neutral state of **5**, inverted bond order is present. Accordingly, the crystals contain the azo-bis(*N*-methyl-2,2'-pyridinium)²⁺ cation, **5**²⁺, with the central functional group –C=N=N–C–.

By charge balance, the OTCNP molecule is a mono-anion, OTCNP[–]. As the shape of the donor, it is planar arranged. Ambient conditions during reaction enabled the carbonylation of TCNP. Under basic environment and the presence of H₂O hydrolysis of TCNP to the mono-anion OTCNP[–] occurred by evolution of hydrogen cyanide (HCN) (Fig. 7.3). The bond lengths/Å in the molecule amount to: N3–C8 1.373(4), N3–C11 1.333(4), C8–C9 1.457(4), C10–C11 1.387(4), N4–C9 1.313(4), N4–C10 1.347(4), C9–C12 1.443(5), C10–C13 1.424(5), C11–C14 1.449(5) and C8–O2 1.239(4). The length of the carbon–oxygen bond is in a typical range with 1.24 Å.

In the crystals, the two constitutional units form a salt-like structure. The packing can be derived from the cubic body-centered tungsten structure type[147] in which the pseudo-tetrahedral holes are partially filled. Therein, the packing is generated by the **5**²⁺ cations and one half of the holes are filled by the OTCNP[–] molecules (Fig. 7.5).

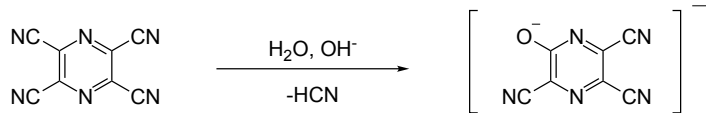


Figure 7.3: Hydrolysis of TCNP to OTCNP[–] under basic conditions and the presence of H₂O.

X-ray single crystal structure determination results in the 1:2 CT salt $(\mathbf{5})(\text{OTCNP})_2$. TCNP undergoes hydrolysis in which course one CN group is substituted by oxygen, forming the anionic tricyanopyrazine oxide OTCNP[–]. All atoms are located at general positions.

$(\mathbf{5})(\text{OTCNP})_2$ crystallises in the monoclinic space group *P*2₁/*n* and is made up by molecules of **5** and OTCNP (Fig. 7.4). The molecules of **5** are essentially planar. The center of gravity, in the mid of the bridging nitrogen atoms N2–N2^{*i*}, is located at the special position 2*a* corresponding to inversion symmetry (Wykoff position: 2*a* ≡ 1 ≡ *C*_{*i*}). The bond lengths in the central CNNC moiety amount

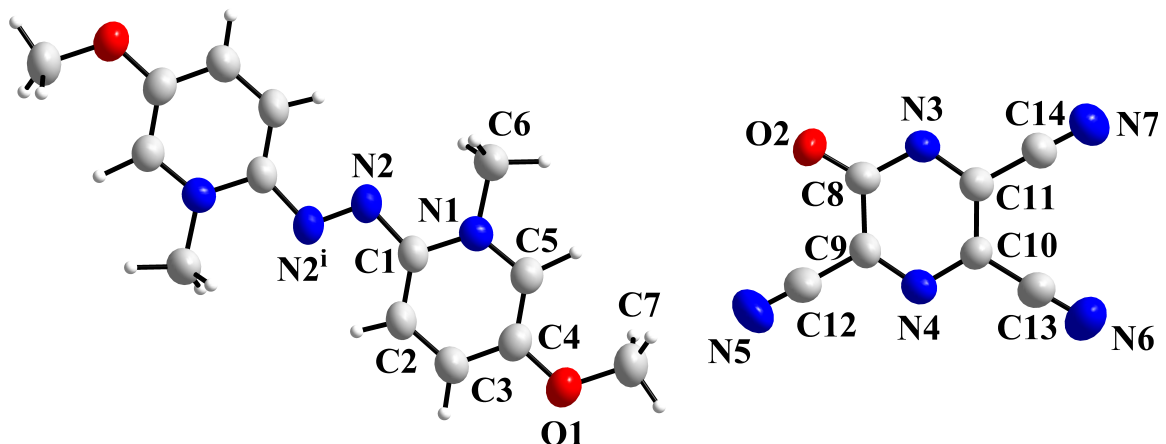


Figure 7.4: The two building units in the structure of $(\mathbf{5})(\text{OTCNP})_2$, the planar molecules of the azo-bis(*N*-methyl-2,2'-pyridinium) $^{2+}$ dication, $\mathbf{5}^{2+}$, and the carbonylated TCNP anion, OTCNP $^-$. The superscript denotes the symmetry operation: $i = 1-x, 1-y, 1-z$. Bond lengths/ \AA : C1–N2 1.398(4), N2–N2^{*i*} 1.263(5), N3–C8 1.373(4), N3–C11 1.333(4), C8–C9 1.457(4), C10–C11 1.387(4), N4–C9 1.313(4), N4–C10 1.347(4), C9–C12 1.443(5), C10–C13 1.424(5), C11–C14 1.449(5) and C8–O2 1.239(4).

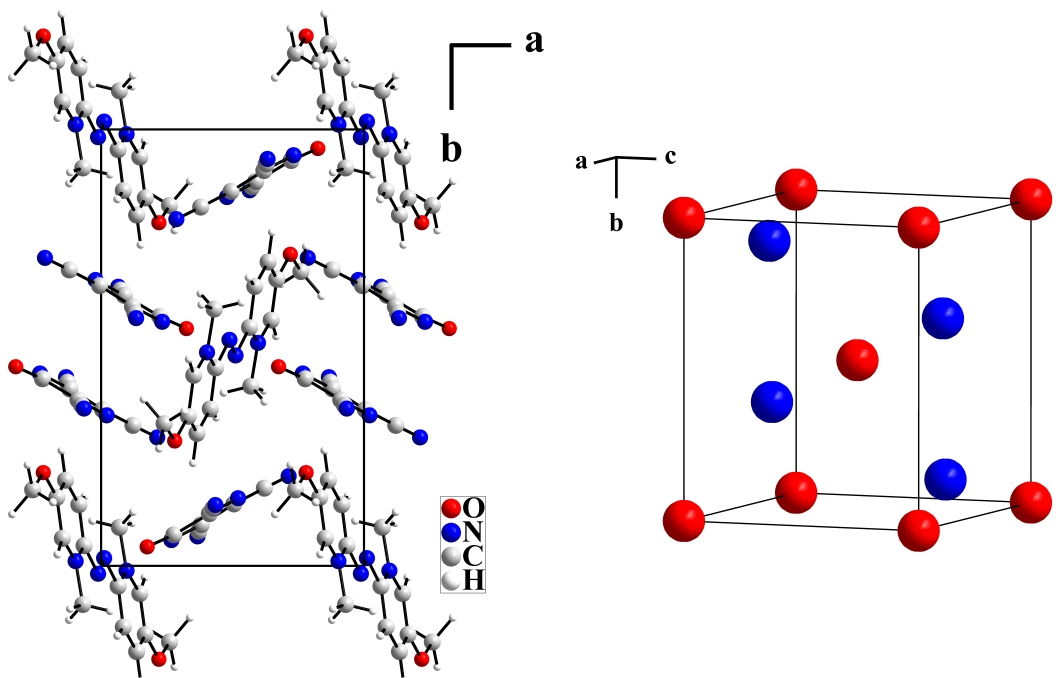


Figure 7.5: The unit cell of $(\mathbf{5})(\text{OTCNP})_2$ depicted in c direction (left). The schematic presentation of the structure packing generated by the two building units (right). The $\mathbf{5}^{2+}$ molecules form a cubic body-centered packing (red balls) and the OTCNP $^-$ molecules (blue balls) fill one half of the pseudo-tetrahedral holes. Atoms and balls (donor = red; acceptor = blue) are drawn in arbitrary radii.

7.1.2 (7)(TCNP)

The reaction of **7** with TCNP in ethyl acetate yielded in green needle-shaped crystals (Fig. 7.6). Since combining **7** with TCNQ led to an immediate intense colour change, in the reaction with TCNP only a minor colour change was observed. (**7**)(TCNP) crystallises in the monoclinic space group $P2_1/c$. The crystals consist of molecules of **7** and TCNP (Fig. 7.7).

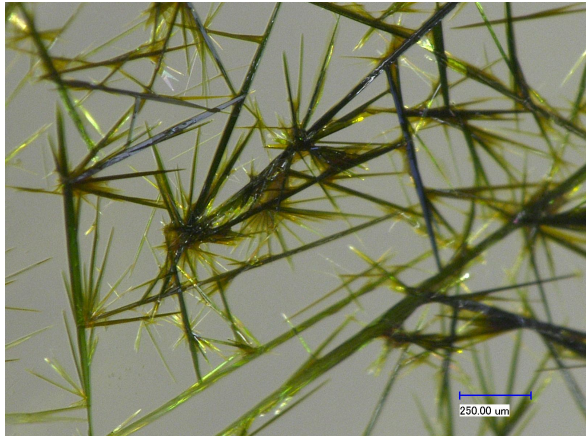


Figure 7.6: Green tin needles of the compound (**7**)(TCNP).

the molecule amount to: N5–C8 1.335(4), N5–C9 1.334(5), C9–C11 1.452(6), N3–C9 1.138(5) and N4–C10 1.135(5). The structural parameters anticipate the presence of TCNP in the oxidation state 0. Resultingly, (**7**)(TCNP) can be interpreted as neutral CT salt since the bond lengths in both molecules imply low degree of charge transfer.

The molecules of **7** are essentially planar. The center of gravity, in the mid of the N–N bridge, is located at the special position $2a$ corresponding to inversion symmetry (Wyckoff position: $2a \equiv \bar{1} \equiv C_i$). In the central CNNC moiety, the N1–N1^{*i*} bond amounts to 1.42 Å and the C1–N1 bond to 1.31 Å. The bond lengths indicate the bond order $-C=N-N=C-$ that is associated with neutral **7**. The high rotational freedom of the CF₃ groups explains the relatively large displacement ellipsoids of the fluorine atoms.

The TCNP molecules are also planar. The centers of gravity are positioned at inversion centers (Wyckoff position: $2c \equiv \bar{1} \equiv C_i$). The bond lengths/Å in

$C8-C9^{ii}$ 1.391(5), C8–C10 1.449(6),

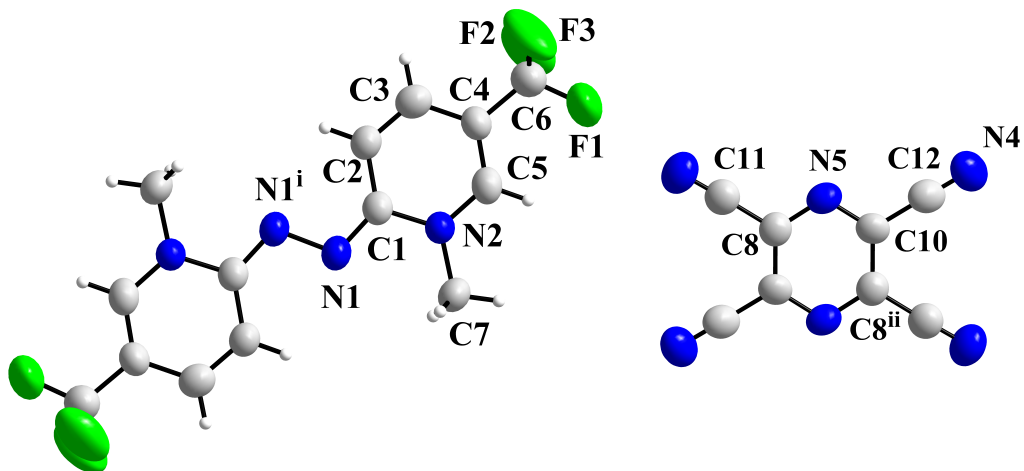


Figure 7.7: The two building units in the crystals of (**7**)(TCNP), the planar molecules of **7** and TCNP. The superscripts denote the symmetry operations: $i = -x, 1-y, 1-z$, $ii = 2-x, 1-y, 2-z$. Bond lengths/Å: C1–N1 1.313(4), N1–N1^{*i*} 1.416(5), N5–C8 1.335(4), N5–C9 1.334(5), C8–C9^{*ii*} 1.391(5), C8–C10 1.449(6), C9–C11 1.452(6), N3–C9 1.138(5), N4–C10 1.135(5).

The crystals consist of oblique mixed stacks made up from donor and acceptor molecules running along the crystallographic c axis. The stacking sequence is $\dots DA\dots$, wherein the molecules are not strictly parallel with an intermolecular plane-to-plane angle of 9° . The centers of gravity are equidistantly arranged by 3.50 \AA and a rather small offset of 1.08 \AA . In the unit cell, two symmetry related but translationally independent stacks are present forming the typical herring bone pattern (Fig. 7.8).

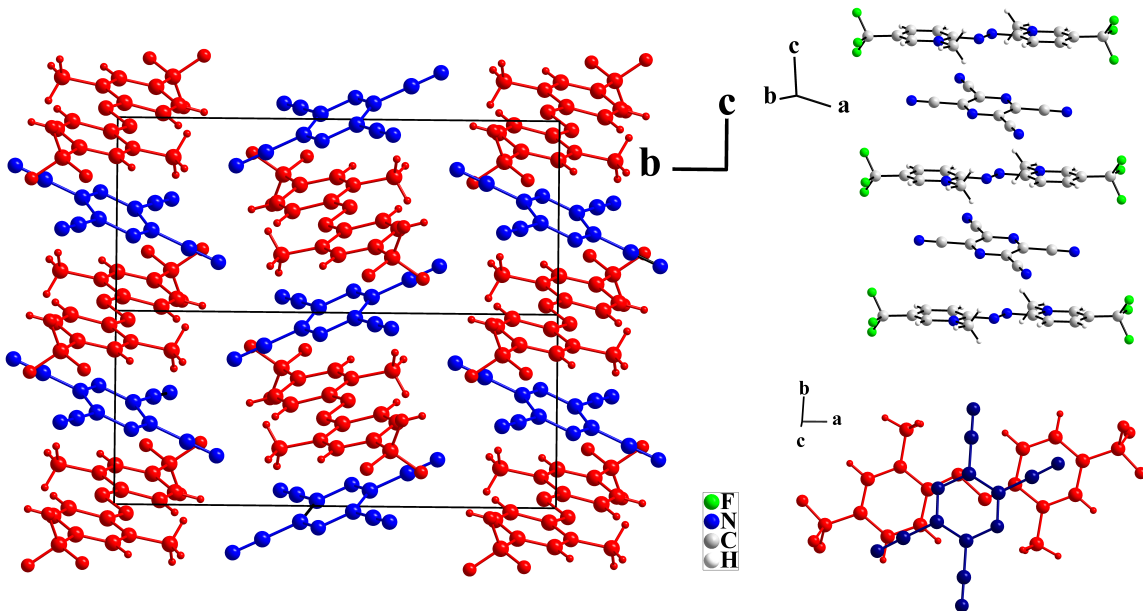


Figure 7.8: The extended unit cell of (7)(TCNQ) depicted in a direction (left), the equidistant stacks made up from donor and acceptor molecules (top right) and the overlap in the repetitive $\dots DA\dots$ stacking sequence (bottom right). The donor molecules are drawn in red and the acceptor molecules in blue. All atoms are drawn as balls in arbitrary radii.

Investigation of the magnetic susceptibility as well as measurement of the conducting properties on (7)(TCNP) were performed.

7.2 Magnetism

(7)(TCNP) is built up from neutral **7** and neutral TCNP molecules that are associated with diamagnetic behaviour.

Fig. 7.9 shows the magnetic susceptibility of (7)(TCNP) in the temperature range from 1.9 K to 300 K. The compound has positive molar susceptibilities over the measured temperature range, however, a broad spreading is observed. The order of magnitude of the molar susceptibilities are in the range of $10^{-5} \text{ cm}^3 \text{ mol}^{-1}$. As expected, (7)(TCNP) is predominantly diamagnetic.

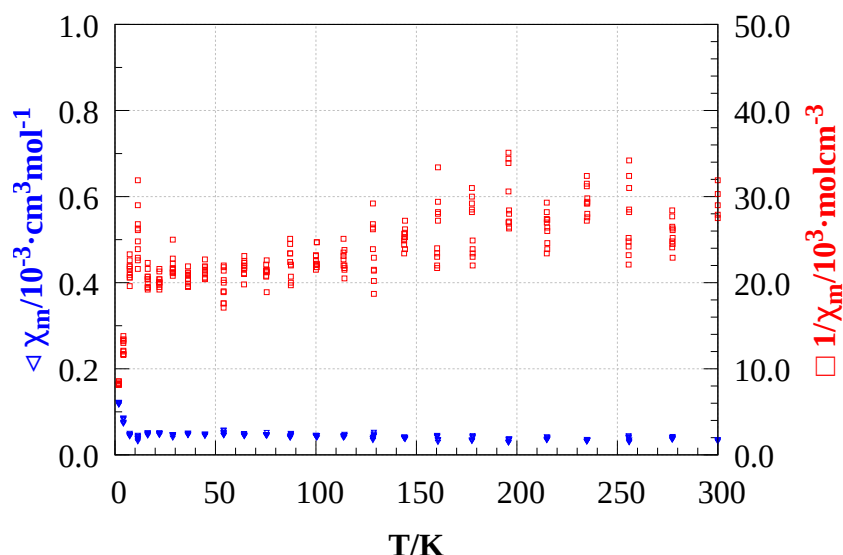


Figure 7.9: Magnetic behaviour of (7)(TCNP). The plots of the functions $\chi_{mol} = f(T)$ (blue open triangles) and $\chi_{mol}^{-1} = f(T)$ (red open squares) are presented.

7.3 Conductivity

Measurement of the electrical conductivity of (7)(TCNP) was performed from 320 K up to 420 K. (7)(TCNP) shows typical semiconducting properties. With increasing temperature the electrical resistance decreases (Fig. 7.10).

The specific electrical conductivities are quite small with $1.4 \times 10^{-11} \text{ Scm}^{-1}$ at 320 K and $8.7 \times 10^{-9} \text{ Scm}^{-1}$ at 420 K. The Arrhenius plot of the function $-\ln(R^{-1}) = f(T^{-1})$ allows the estimation of the activation energy for the thermally activated electron transfer from valence into the conduction band. The activation energy amounts to 1.5 eV. However, the light green colour of the compound does not fit to the band gap. For the light green colour absorption at circa 450 nm in ultra violet is expected. The appropriate absorption energy amounts to 2.8 eV. Hence, the determined band gap should have to absorb at about 825 nm and should have a black colour.

Nonetheless, measurements of the magnetic susceptibility and the electrical conductivity are in agreement with the structural features and the estimated degree of charge transfer in (7)(TCNP). Therefore (7)(TCNP) is a diamagnetic, high-ohmic semiconductor.

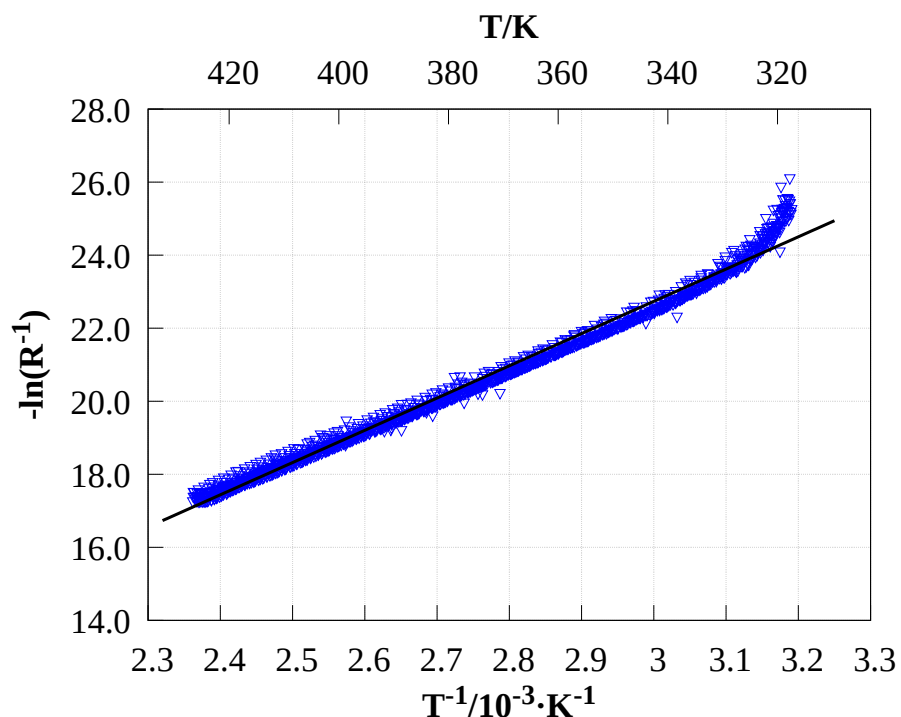


Figure 7.10: The Arrhenius plot $-\ln(R^{-1}) = f(T^{-1})$ for the electrical resistivities of (7)(TCNP). The blue circles are the measured resistance and the black line represents the best linear fit. The band gap amounts to 1.5 eV.

CHAPTER 8

Charge Transfer Salt with DTeF

2,4,5,7-tetrinitro-9-dicyanomethylenefluorene (DTeF) belongs to a class of fluorene based electron acceptors that are prone to form charge transfer compounds.

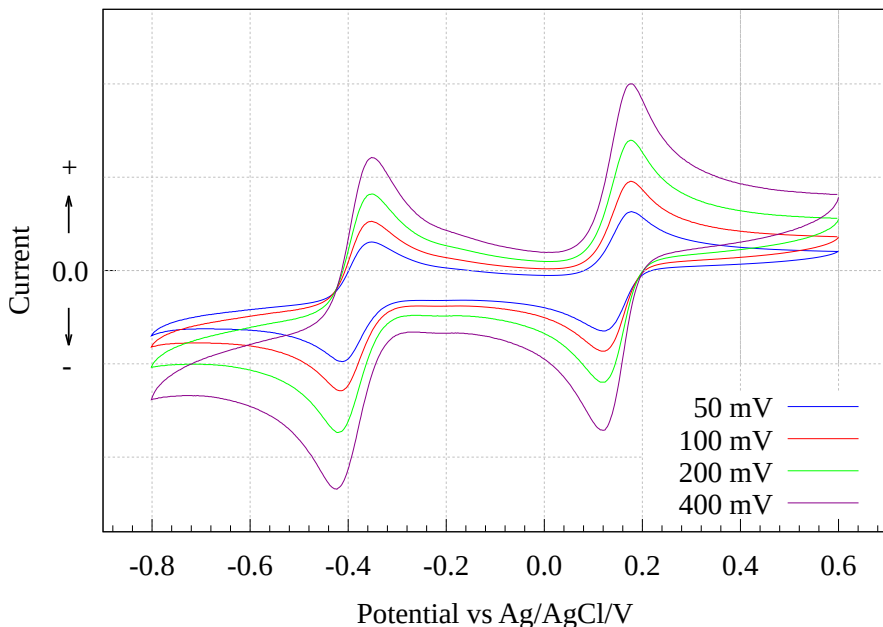


Figure 8.1: Cyclic voltammogram of 2,4,5,7-tetrinitro-9-dicyanomethylenefluorene (DTeF) shows two reversible one-electron reduction processes at $E_1 = +0.15$ V to radical anion stage, $\text{DTeF}^{\cdot-}$, and $E_2 = -0.38$ V to dianionic species, DTeF^{2-} vs. Ag/AgCl. In literature, the semi potentials are at $E_1 = +0.23$ V and $E_2 = -0.31$ V vs. Ag/AgCl. An additional third reduction process is observed in a wider potential spectrum at $E_3 = -1.13$ V to the radical trianion $\text{DTeF}^{\cdot3-}$ [148].

In this work, cyclic voltammetric measurement of DTeF shows two reversible one-electron reduction processes at $E_1 = +0.15$ V and $E_2 = -0.38$ V vs. Ag/AgCl that are in agreement with literature ($E_1 = +0.23$ V and $E_2 = -0.31$ V vs. Ag/AgCl). Investigations in a wider potential spectrum showing a third reversible one-electron reduction process at $E_3 = -1.13$ V vs. Ag/AgCl have been reported[148].

Hence, DTeF can be reduced to the radical anion $\text{DTeF}^{\cdot-}$, the dianion DTeF^{2-} ending up to the radical trianion $\text{DTeF}^{\cdot3-}$. Since the introduction of electron withdrawing groups increases the electron

affinity by 0.2 to 0.3 eV each, DTeF represents one of the strongest fluorene electron acceptors by an electron affinity of 2.77 eV. The shape of the fluorene is highly influenced by steric hindrance and electrostatic repulsion of the nitro (NO_2) groups in position 4 and 5. Resultingly, the boat-like conformation of neutral DTeF remains in the radical anion DTeF^- .

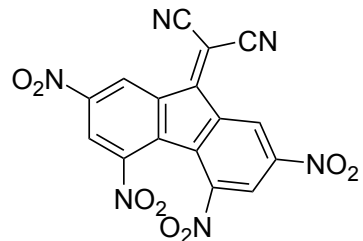


Figure 8.2: The molecular structure of 2,4,5,7-tetranitro-9-dicyanomethylenefluorene (DTeF).

In the following, the CT salt (**1**)(DTeF) is presented. Crystal structure determination and results of the band structure, PDOS, electrical conductivity and Mulliken population analysis calculations are reported.

8.1 Crystal Structure of (1)(DTeF)

The reaction of **1** and DTeF in acetonitrile led to polymorphic crystal phases in shape of very thin needles and of rhomboid-shaped crystals. By first contact of the azine solution with the DTeF solution, the thin needles were formed, immediately. After complete removal of solvent, the rhomboid crystals were observed (Fig. 8.3).



Figure 8.3: Polymorphic phases by the reaction of **1** and DTeF. Crystals in form of rhomboids and in shape of thin needles could be observed.

multiple independent attempts, this problem persisted and could not be satisfactorily resolved. In this case, the determination of properties such as conductivity and magnetism, which were determined on bulk samples, cannot be readily transferred or interpreted by the single crystal structure. CHNS analysis underscores that all phases composed of a 1:1 ratio of donor to acceptor molecule.

Separation of the rhomboids was possible by different solubilities since the thin needle-shaped phase was dissolved in dimethylformamide. Hence, the crystal mixture was washed with dimethylformamide. X-ray single crystal structure determinations for several rhomboid-shaped crystals were performed and yielded in the 1:1 CT salt (1)(DTeF).

The analyses of the samples by X-ray powder diffraction showed the multi-phase nature of the product of **1** and DTeF. A particular problem in this case is that the diffractograms of samples even consisting of manually sorted crystals of the rhomboid phase did not agree with the diffractograms calculated from single crystal structure determination data (Fig. 8.5). Despite

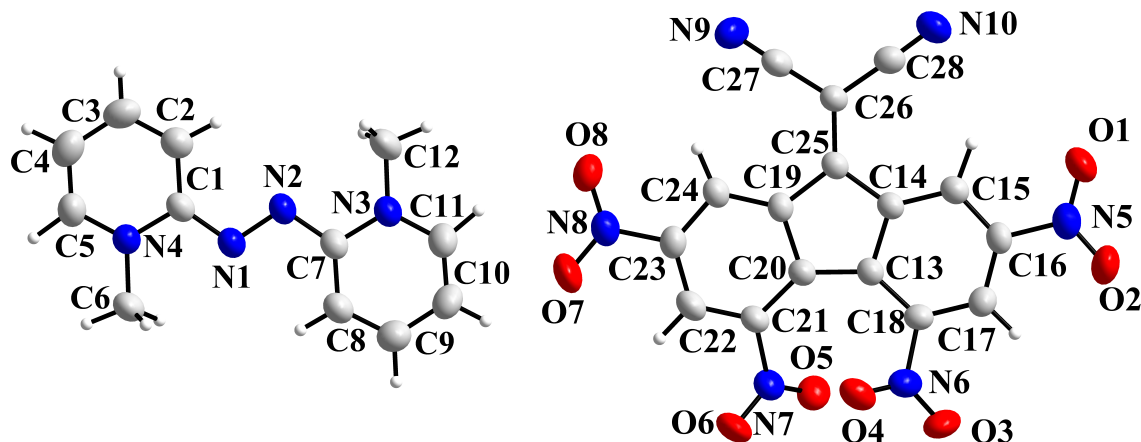


Figure 8.4: The two building units of (1)(DTeF), the slightly bent molecules of **1** and DTeF. Bond lengths/Å: C1–N1 1.358(3), N1–N2 1.333(3), N2–C7 1.360(3).

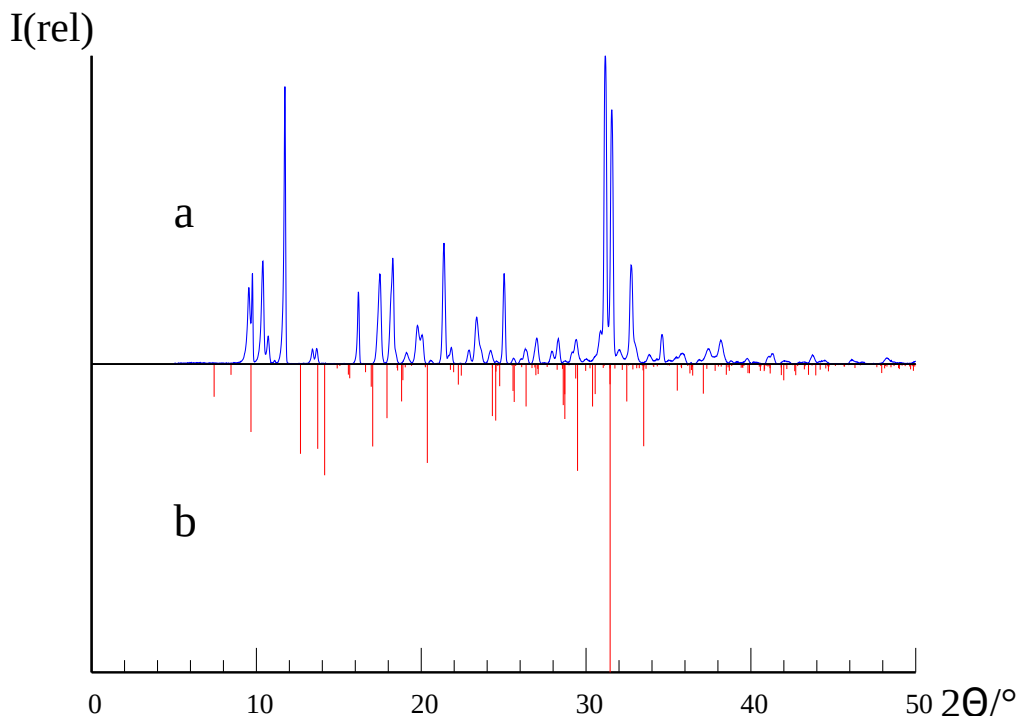


Figure 8.5: Powder diffractogram of the rhomboid-shaped crystals obtained in the reaction of **1** with DTeF (blue) and simulated powder diffractogram from single crystal data of **(1)(DTeF)** (red). No coincidence between experimental and calculated diffractogram is present. Used radiation: Co-K α_1 , a = measured diffractogram, b = simulated diffractogram on basis of single crystal data of **(1)(DTeF)**.

(1)(DTeF) crystallises in the space group $P\bar{1}$ (No. 2) and consists of molecules of **1** and DTeF (Fig 8.4). All atoms are located at general positions.

The molecules of **1** are slightly bent. The angle between the planes made up by the two 2'-(py)-*N* units amounts to 12.5°. The bond order in the central CNNC moiety is in accordance to the radical cation species **1** $^{+}$ due to length delocalisation with 1.36 Å for C1–N1, 1.33 Å for N1–N2 and 1.36 Å for N2–C7.

The fluorene fragment of the acceptor molecule DTeF is planar. The electrostatic repulsion of the NO₂ groups on position 4 and 5, connected to C18 and C21, leads to a boat-like conformation. By charge balance, the acceptor is present as the radical anion DTeF $^{+-}$.

In the crystals, donor or respectively acceptor molecules form segregated stacks. These stacks run along the crystallographic *a* axis. The **1** $^{+}$ molecules form dimeric aggregates, $(\mathbf{1})_2^{2+}$, that are stacked in a zig-zag pattern. In the $(\mathbf{1})_2^{2+}$ dimers, the center-of-gravity distance amounts to 4.19 Å with an offset of 2.00 Å and an averaged intermolecular plane distance of 3.68 Å. The electrostatic attraction emphasises the predominant Peierls distortion. Between the $(\mathbf{1})_2^{2+}$ dimers, the center-of-gravity distance is significantly longer by 6.19 Å with a highly large shift of 5.32 Å. The large offset leads to a significantly shorter intermolecular plane distance of 3.16 Å, however, interactions between the dimeric aggregates are not assured.

As the donor stacks, the acceptor molecules form dimeric aggregates in the stacks, $(\text{DTeF})_2^{2-}$. Hence, Peierls distortion is the common structural feature in both stack types. In the $(\text{DTeF})_2^{2-}$ dimers, the center-of-gravity distance amounts to 3.56 Å with an offset of 1.81 Å and an average plane distance of 3.08 Å. Between the $(\text{DTeF})_2^{2-}$ dimers, the center-of-gravity distance is significantly larger by 6.44 Å

with a highly enlarged slippage of 5.34 Å. The average intermolecular plane-to-plane distance amounts to 3.61 Å. Concluding, the $(DTeF)_2^{2-}$ dimers form stacks in a step-like manner (Fig. 8.6).

Additionally, X-ray single crystal determination from 103 K to 303 K (in 20 K steps) were performed. An anisotropic lattice parameter contraction is observed. In Tab. 8.1 the lattice parameters for all temperatures and their relative contractions (RT data to data at 103 K) are collected. The a axis, which is the stacking direction, shrinks by cooling about 1.75 % from 7.639 Å at 303 K to 7.775 Å at 103 K. The β angle changes from 85.34° to 86.11° and is therefore enlarged by 0.90 %. The other parameters are less effected with changes of 0.05 % for b (13.049 Å to 13.056 Å), -0.77 % for c (14.340 Å to 14.229 Å), -0.26 % for α (73.94° to 73.76°) and -0.46 % for γ (74.37° to 74.03°). Except for the lattice parameter b , the shrinking or, respectively, enlarging proceeds progressively.

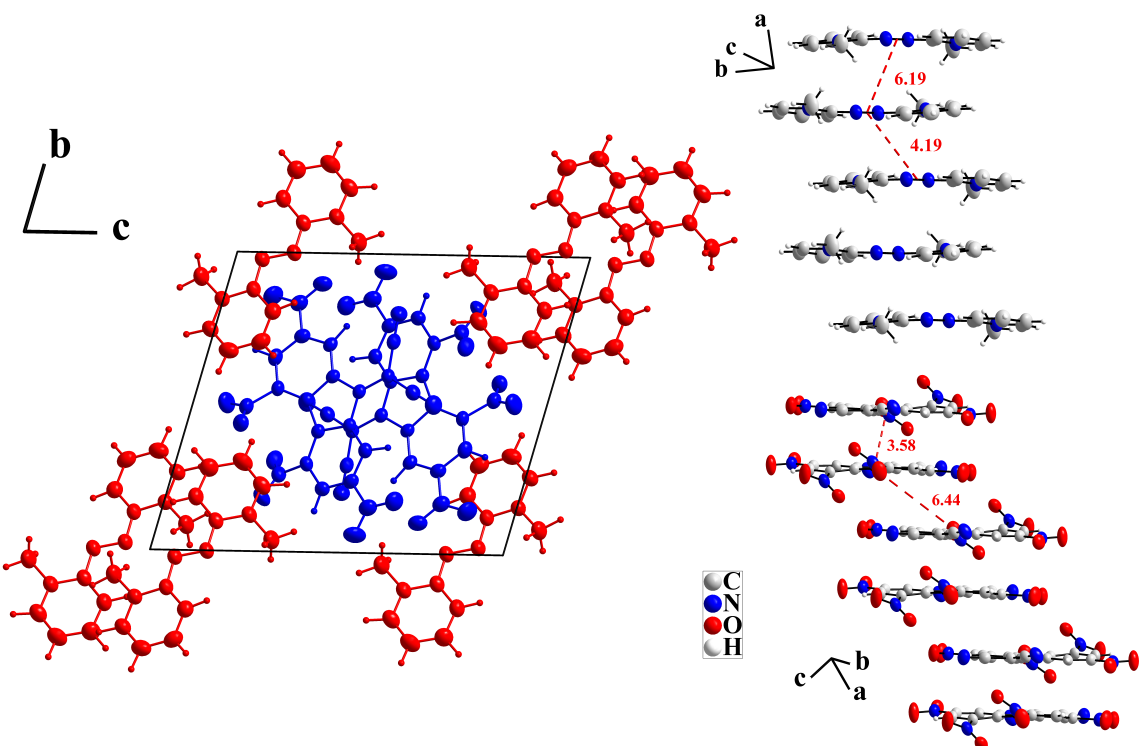


Figure 8.6: The unit cell of (1)(DTeF) depicted along the crystallographic a axis (left). The segregated stacks in the structure of (1)(DTeF) (right). Both molecules form stacks consisting of dimeric aggregates, $(1)_2^{2+}$ or $(DTeF)_2^{2-}$, that run along the crystallographic a axis. The center-of-gravity distances are given in Å.

On cooling, the general structure motif of segregated stacks made up of donor or acceptor dimers remains, but, there are significant changes.

The 1^{+} molecules are more strongly inclined by an angle of 14.39° between the 2'-(py)- N units. In the donor stacks, the center-of-gravity distance in the $(1)_2^{2+}$ unit decreases by about 4.53 % from 4.19 Å to 4.00 Å and the offset of the molecules decreases by 3.84 % from 2.75 Å to 2.65 Å. Consequently, the mean intermolecular plane-to-plane distance is shortened by -5.06 % to 3.00 Å compared to 3.16 Å at 303 K. Between the $(1)_2^{2+}$ units, the center-of-gravity distance lasts constantly at about 6.19 Å while the horizontal slippage raises slightly from 4.98 Å to 5.02 Å (+0.73 %). The mean intermolecular plane-to-plane distance is reduced to 3.61 Å (-1.37 % compared to 3.66 Å at 303 K).

In the acceptor stacks, the center-of-gravity distance in the $(DTeF)_2^{2-}$ units is swagged by 1.10 % from 3.56 Å to 3.59 Å with a reduced offset from 1.94 Å to 1.91 Å (-1.42 %). By cooling, the mean

intermolecular plane-to-plane distance contracts to 3.04 Å (-0.98% from 3.08 Å at 303 K). Between the $(\text{DTeF})_2^{2-}$ dimers, the center-of-gravity distance is shortened from 6.44 Å to 6.34 Å (-1.55%) and the offset by 1.00 % from 5.34 Å to 5.28 Å. Resultingly, the mean intermolecular plane-to-plane distance is reduced to 3.51 Å (-2.77% compared to 3.61 Å).

By theoretical calculations of band structure, PDOS, Mulliken population analysis and conductivity, a prediction of the electronic properties of **(1)**(DTeF) was performed. The detailed structure analysis enables deeper insights into the electronic structure.

Table 8.1: Lattice parameters of **(1)**(DTeF) crystallising in the triclinic space group $P\bar{1}$ (No. 2) determined at the temperatures from 103 K to 303 K (in 20 K steps). The relative contraction refers to RT data related to data recorded at 103 K and is expressed in percent.

T/K	a/Å	b/Å	c/Å	$\alpha /^\circ$	$\beta /^\circ$	$\gamma /^\circ$
303	7.7751(4)	13.0491(6)	14.3396(6)	73.9440(3)	85.3430(3)	74.3710(3)
293	7.7780(3)	13.0623(7)	14.3556(9)	73.9590(3)	85.3970(3)	74.3460(3)
283	7.7592(4)	13.0446(5)	14.3275(6)	73.9250(3)	85.4500(3)	74.3280(2)
263	7.7440(4)	13.0427(5)	14.3155(6)	73.8990(3)	85.5430(3)	74.2770(2)
243	7.7290(3)	13.0413(5)	14.3039(6)	73.8750(3)	85.6370(3)	74.2460(2)
223	7.7146(3)	13.0415(5)	14.2930(5)	73.8610(2)	85.7310(2)	74.2130(2)
203	7.6998(3)	13.0415(5)	14.2803(5)	73.8530(2)	85.8230(2)	74.1750(2)
183	7.6848(3)	13.0430(5)	14.2669(5)	73.8180(2)	85.9010(2)	74.1390(2)
163	7.6715(3)	13.0437(5)	14.2547(5)	73.7890(2)	85.9710(2)	74.1050(2)
143	7.6587(3)	13.0470(5)	14.2438(5)	73.7660(2)	86.0200(2)	74.0720(2)
123	7.6477(3)	13.0503(4)	14.2351(4)	73.7500(2)	86.0680(2)	74.0370(2)
103	7.6390(2)	13.0556(4)	14.2289(2)	73.7550(2)	86.1120(2)	74.0290(2)
Rel. Contr./%	-1.75	0.05	-0.77	-0.26	0.90	-0.46

8.2 Theoretical calculations on (1)(DTeF)

8.2.1 Band Structure and PDOS

For description of the electronic properties of (1)(DTeF), band structure and projected density of states (PDOS) calculations for all crystal data, recorded from 103 K to 303 K, were performed. The PDOS were calculated for individual atoms as well as the donor and acceptor molecules. As for the TCNQ-containing CT salts (see Chapter 6.3), hybrid density functional theory with dispersion correction and triple-zeta basis sets (PW1PW+D3/pob-TZVP-rev2[114–119]) is employed as level of theory. All computational details are described in Chapter 2.8.

For the donor **1** and the acceptor DTeF four different spin states were investigated. Non-magnetic, NM, refers to closed shell state with paired electrons. The ferromagnetic, FM, state relates to parallel unpaired electrons of all atoms in the majority channel. The antiferromagnetic order was investigated in two different states. In the AFM1 state, both the donor and the acceptor molecule exhibit a net magnetic moment of zero with anti-parallel spins on neighboring atoms. For AFM2 the donor and acceptor molecules are FM individually but anti-parallel with respect to the other molecule. Fig. 8.7 shows a schematic representation of the spin ordering.

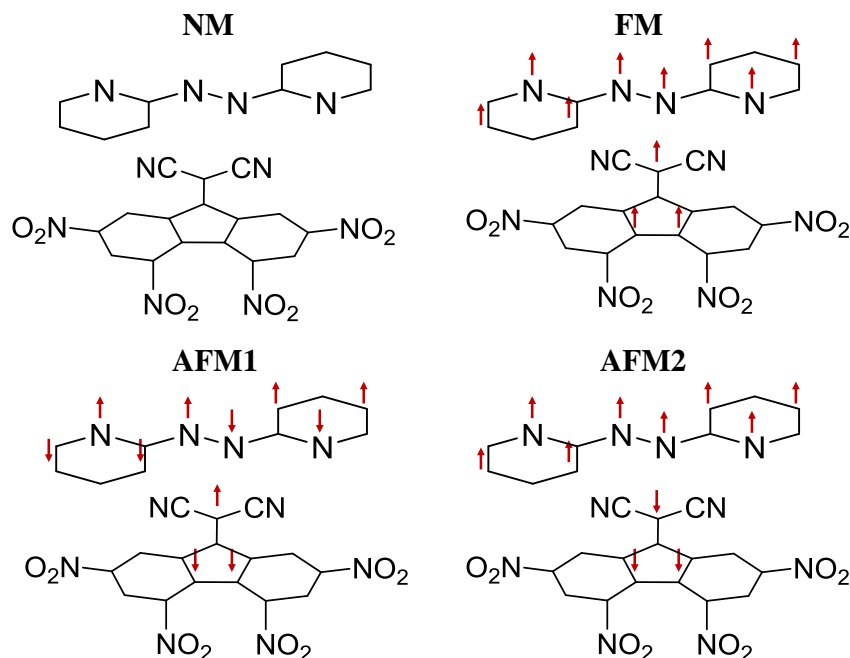


Figure 8.7: Investigated spin states for the CT salt (1)(DTeF): non-magnetic (NM), ferromagnetic (FM), antiferromagnetic (AFM1 and AFM2), with schematic molecules.

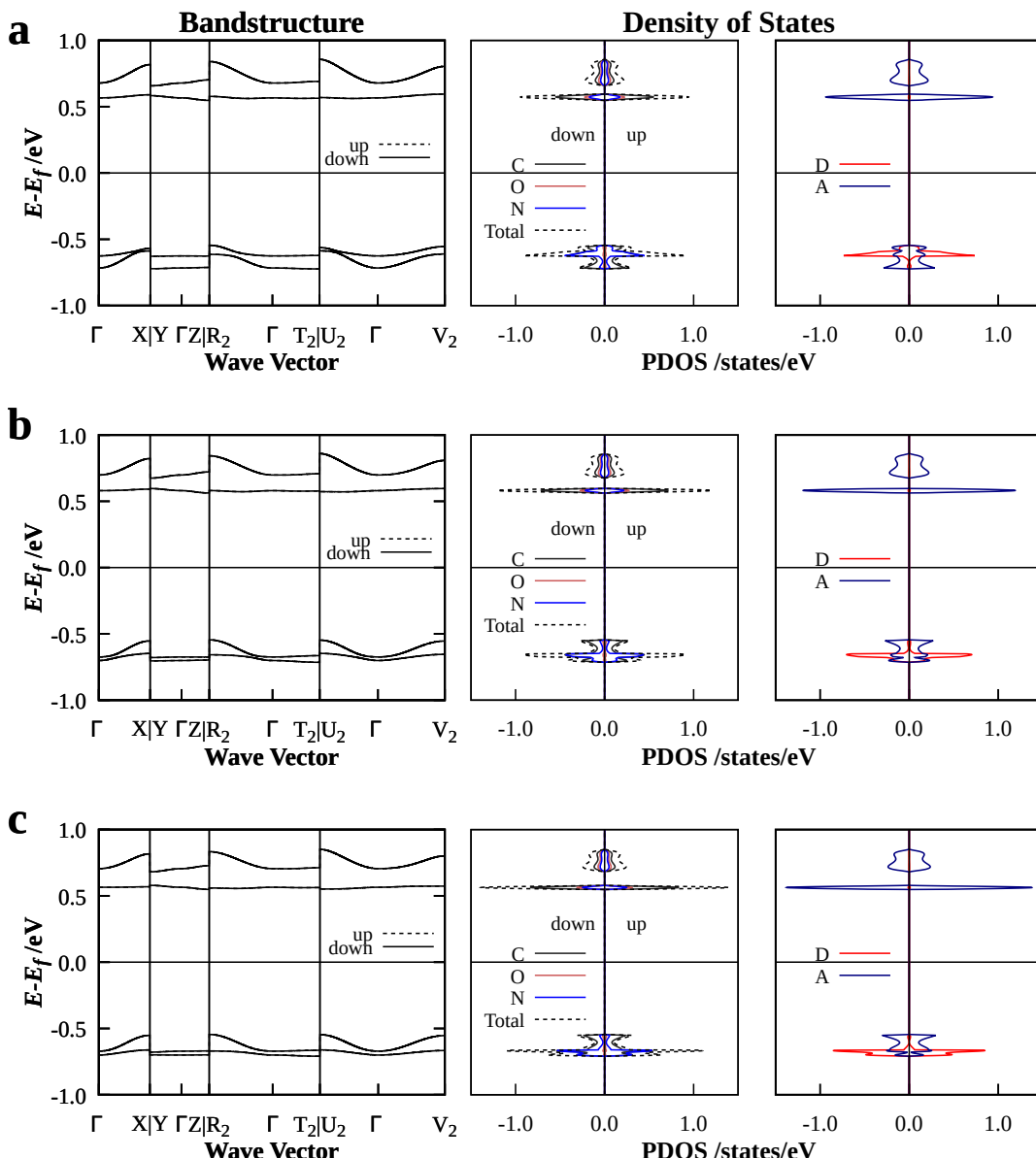


Figure 8.8: Band structures, PDOS for atom orbitals and PDOS for orbitals belonging to donor or acceptor of (1)(DTeF) at 103 K **a**, 203 K **b** and 303 K **c** calculated with CRYSTAL17, PW1PW+D3/pob-TZVP-rev2.

The energetically favoured state of (1)(DTeF) is AFM1. Fig. 8.8 shows the calculated band structures and PDOS for structures measured at 103 K, 203 K and 303 K, exemplary. Band structures for all temperatures between 103 K and 303 K are attached in the appendix A.6. The three crystallographic axes run from Γ to X (a axis), from Γ to Z (b axis) and B to Γ (c axis).

Over the whole temperature range, no band crossing in the proximity of the Fermi level occurs. Thus, (1)(DTeF) is expected to show typical semiconducting behaviour with an invariable band gap of about 1.1 eV and a charge transfer of about 0.9 e⁻/molecule determined by Mulliken population analysis. The PDOS shows that the VBM is dominated by the orbitals of 1 and the CBM mainly by the orbitals of DTeF.

Although the crystal structure of (**1**)(DTeF) is made up by segregated stacks, the strong Peierls distortion indicates semiconductivity. Band structure and PDOS calculations are in agreement with the electronic behaviour that can be expected from the details of the crystal structure. In accordance to the Mulliken population analyses, the structure parameters of **1** refer to the radical cation **1**⁺.

8.2.2 Conductivity

(**1**)(DTeF) consists of segregated stacks built up by (**1**)₂²⁺ or, respectively, (DTeF)₂²⁻ dimers that run in *a* direction. Concluding, electron migration along the stacking direction is expected to lead to semiconducting or insulating properties due to the formation of Coulomb sinks.

Based on crystal data, the transport properties of (**1**)(DTeF) were calculated from 103 K to 303 K by application of the Boltzmann transport equation implemented in CRYSTAL17.

Over the whole temperature range, for (**1**)(DTeF) small specific electrical conductivities are obtained by calculation. These are listed in Tab. 8.2.

Table 8.2: Calculated anisotropic electrical conductivities σ_a , σ_b and σ_c in Scm^{-1} , activation energies of the electron excitement from valence into conduction band (E_a) in eV and charge transfer by Mulliken for (**1**)(DTeF) with CRYSTAL17, PW1PW+D3/pob-TZVP-rev2.

T/K	σ_a	σ_b	σ_c	E_a/eV	Mulliken
103	-	-	-	1.09	0.88
123	-	-	-	1.10	0.88
143	-	-	-	1.10	0.88
163	9.82×10^{-17}	2.78×10^{-16}	3.79×10^{-16}	1.10	0.88
183	-	-	-	1.10	0.88
203	3.53×10^{-12}	4.36×10^{-13}	3.46×10^{-13}	1.11	0.88
223	8.06×10^{-11}	1.44×10^{-11}	1.74×10^{-11}	1.09	0.88
243	1.01×10^{-9}	1.77×10^{-10}	2.02×10^{-10}	1.09	0.89
263	8.38×10^{-9}	1.66×10^{-9}	2.01×10^{-9}	1.09	0.89
283	8.49×10^{-8}	1.61×10^{-8}	1.70×10^{-8}	1.09	0.89
303	2.07×10^{-7}	2.99×10^{-8}	2.79×10^{-8}	1.10	0.89

Especially, at low temperature the Boltzmann transport calculations yield zero. This can be interpreted as the limit of the applied method. Essentially, it is observed that with increasing temperature the conductivity increases. Resultingly, the substance is predicted to show semiconducting behaviour. As expected from crystal structure, the electrical conduction is suggested to be primarily dominated by the contribution along the stacking direction. The specific conductivities in *a* direction, σ_a , are 10 up to 100 times larger compared to the other directions, σ_b and σ_c .

In summary, the calculated electronic properties of (**1**)(DTeF) by hybrid density functional theory with dispersion correction and triple-zeta basis sets are in line with the structural features in the crystals. However, it must be mentioned, that experimental confirmation is not possible due to the missing phase assignment between bulk samples and single crystal data.

CHAPTER 9

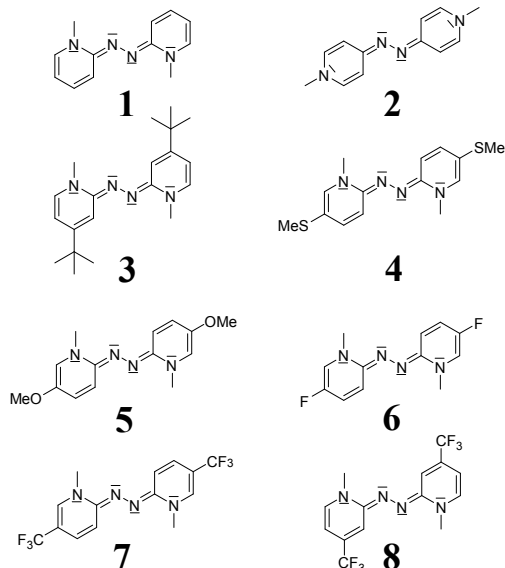
Conclusion

Bis(pyridone)azines represent two stage redox systems. In the 60 years since their discovery, they found only little attraction, however, their structural and electronic properties make them highly interesting in the area of materials design. The ability to form stable radical cations makes the pyridone azines a promising class of organic building blocks for molecular conductors and charge transfer compounds.

The redox abilities of representatives based on the parent scaffold bis(*N*-methylpyridone)azine (MPA, **1**) were investigated. The two oxidation steps are reversible and well-separated. Symmetric substitution in meta- or para-position to the pyridinium N atoms shows the impact on the reducing power. Hence, the +M effect of the methoxy group enhances the reducing strength, whereas the introduction of the -I substituent CF₃ decreases the reducing power significantly bringing the potentials in the same region as the oxidation of the well-known TTF to its stable radical cation TTF⁺. Potentials of the derivatives containing SMe, ^tBu or F groups are not influenced by substitution. Differentiation of the oxidation states 0, +1 and +2 of the azines is possible by the bond lengths in the central CNNC azine moiety. The bond lengths in the neutral state follow the order -C=N-N=C-. Equality of the bond lengths indicates the electron delocalisation over the whole molecules in the radical cation. Inverted bond order -C-N=N-C- with diaryl azo function is present in the +2 state.

Copper(II) halides, CuCl₂ and CuBr₂, turned out as suitable oxidants to convert the pyridone azines via one-electron transfer to the persistent radical cation and also two-electron transfer to the dication. In these reactions, a series of new organic-inorganic hybrids in form of radical cation salts and dicationic salts with halogenido cuprates(I)/(II) as counter ions were obtained successfully.

In the radical cation salts (**1**)[CuCl₂], (**1**)[CuBr₂] and (**8**)[CuBr₂], the planarity of the corresponding radical cations and their delocalised π systems facilitate the formation of stacks in equidistant arrangement. Cu²⁺ is reduced to Cu⁺ and converted to cuprate anions in form of the molecular linear [CuCl₂]⁻ or chains of edge-sharing [CuBr_{4/2}]_n tetrahedra. The CF₃ groups of **8** bring in a steric



hindrance on the stacking formation yielding a loose stacking. Low temperature data demonstrate lattice parameter contractions that are anisotropic in the radical cation salts of **1** and rather isotropic in the radical cation salt of **8**.

Magnetic properties of the radical ion containing halogenido cuprates provide a clear differentiation. The temperature dependence of the susceptibility of **(1)[CuCl₂]** and **(1)[CuBr₂]** is nearly identical. Largely suppressed spin momenta indicate substantial coupling between the cations. An almost temperature independent paramagnetism with susceptibilities in the order of $10^{-4} \text{ cm}^3 \text{ mol}^{-1}$ is observed above 50 K. Below 50 K, small paramagnetic moments with magnitudes corresponding to a content of 9.6 % Cu²⁺ for **(1)[CuCl₂]** and 13.7 % for **(1)[CuBr₂]** are present.

(8)[CuBr₂] with its almost isolated **8⁺** radical cation is mainly paramagnetic with a magnetic moment of one unpaired electron per formula unit. A weak antiferromagnetic coupling is present up to a Neél temperature T_N of 6 K and a coupling constant J of -2.1 cm^{-1} .

For all three radical cation halogenido cuprates, electrical conductivities measured on compacted powder samples are relatively low in the region of 10^{-10} and 10^{-9} Scm^{-1} . The energies for the thermal activated electron excitation are between 0.95 eV and 1.34 eV, giving the cuprates the character of small band gap semiconductors.

There is no clear relation of the conductivities with the structural parameters. For **(1)[CuCl₂]** with isolated [CuCl₂]⁻ anions, the conductivity path is expected to arise from the radical cation stacks, solely. The polymeric [CuBr_{4/2}]_n in **(1)[CuBr₂]** and **(8)[CuBr₂]** might contribute to the conduction.

In reactions with copper(II) bromide the second oxidation state of the pyridone azines **1**, **2** and **8** is accessible forming the corresponding bis(*N*-methyl-2,2'-pyridinium) dication or azo-bis(*N*-methyl-4,4'-pyridinium) dication. The reactions yielded six new pyridone azine dication salts: **(1)[Cu₂Br₄]**, α -(**2)[Cu₂Br₄]**), β -(**2)[Cu₂Br₄]**)·CH₃CN, **(2)[CuBr₃]**, **(2)[CuBr₄]** and **(8)[CuBr₄]**. The bromido cuprate anions form molecular units such as trigonal planar [CuBr₃]⁻ or tetrahedral [CuBr₄]²⁻ with oxidation state +1 or +2 on copper. As for the bromido cuprate radical salts, the cuprate(I) anions form one-dimensional chains of edge-sharing tetrahedra. Their common structural feature is the stacking formation made up by the corresponding azine dications.

The magnetic state of the compounds is mainly dominated by the specific bromido cuprate(I/II) counter anions. The magnetic susceptibilities of the dication salts **(1)[Cu₂Br₄]** and α -(**2)[Cu₂Br₄]**) are consistent with the magnetic behaviour of the radical cation salts **(1)[CuCl₂]** and **(1)[CuBr₂]**. At low temperature, small magnetic momenta are observed running into nearly temperature independent paramagnetism. The magnetic momenta are connected to 2.2 % or 4.5 % amount of Cu²⁺ in **(1)[Cu₂Br₄]** or α -(**2)[Cu₂Br₄]**). Since the singlet state of the dications, **1²⁺** or **2²⁺**, does not influence the magnetic phenomena, the spin momenta of the radical cations **1⁺** are largely suppressed.

(2)[CuBr₄] and **(8)[CuBr₄]** exhibit paramagnetic phenomena. At T < 10 K, **(2)[CuBr₄]** shows ideal Curie behaviour with $1.38 \mu_B$ corresponding to $\frac{3}{4}$ electrons and turns into Curie-Weiss behaviour with $2.02 \mu_B$ and a large Weiss constant θ of -22.84 K that might reduce the overall magnetic moment. **(8)[CuBr₄]** has a magnetic momentum of $1.87 \mu_B$ close to that of a pure Cu(II) paramagnet. Magnetic susceptibility confirms the presence of *d*⁹-configured Cu(II) in both compounds.

At room temperature, **(1)[Cu₂Br₄]** and α -(**2)[Cu₂Br₄]**) are small band gap semiconductors. The specific electrical conductivities of the two salts range in the order of 10^{-9} Scm^{-1} and are found to be in the same region as in the group of the radical-containing compounds **(1)[CuCl₂]**, **(1)[CuBr₂]** and **(8)[CuBr₂]**. The electronic singlet state of the dications **1²⁺** and **2²⁺** supports the assumption that the [CuBr_{4/2}]_n chains are mainly responsible for conduction whereas the cation-cation interactions are negligible. The activation energy of **(1)[Cu₂Br₄]** is around 1 eV. For α -(**2)[Cu₂Br₄]**), structural changes during the heating process could be observed. Conductivity measurement, X-ray powder diffraction and DSC measurement indicate an irreversible or monotropic phase transition. Within the

scope of this work, crystal structure determination using single crystals of the second phase was not experimentally accessible.

(**2**) $[\text{CuBr}_4]$ and (**8**) $[\text{CuBr}_4]$ have insulating properties at room temperature. For both compounds, activation energies are determined above 380 K amounting to 2.05 eV for (**2**) $[\text{CuBr}_4]$ and 2.06 eV for (**8**) $[\text{CuBr}_4]$.

The radical cation as well as the dication salts indicate interesting structure-property relations.

The observed magnetic phenomena are induced by the *d* electrons of cuprate anions. Cuprate(I) containing organic-inorganic hybrids show nearly similar magnetic properties as small magnetic momenta at low temperatures that turns into nearly temperature independent paramagnetism. Hybrids with integrated Cu^{2+} exhibit paramagnetic phenomena.

Conduction is usually provided by organic stacks in which adjacent π electron systems can interact. In (**1**) $[\text{CuCl}_2]$ with a molecular $[\text{CuCl}_2]^-$ anion, the conductivity arises from the cation-cation interaction along the stacks. Interestingly, the conductivities of the radical cation salts as the dication salts containing the polymeric $[\text{CuBr}_{4/2}]_n^-$ chains are found to be in the same region. The different electronic states of the specific cations (doublet or singlet) emphasise that conduction is caused predominantly from the polymeric anion.

New charge transfer salts were obtained in reactions with the organic acceptor molecules TCNQ, TCNP and DTeF.

In reactions of the pyridone azines **1–8** with TCNQ, the four ionic CT salts $\alpha\text{-}(\mathbf{1})^+(\text{TCNQ})^-$, $\beta\text{-}(\mathbf{2})^+(\text{TCNQ})^-$ and $(\mathbf{3})^+(\text{TCNQ})^-$, the three mixed valent CT salts $\alpha\text{-}(\mathbf{2})^{+0.54}(\text{TCNQ})^{-0.54}$, $(\mathbf{2})^{+0.82}(\text{TCNQ})^{-0.82}$, $(\mathbf{7})^{+0.30}(\text{TCNQ})^{-0.30}$ and $(\mathbf{8})^{+0.41}(\text{TCNQ})^{-0.41}$ and the neutral CT salt $(\mathbf{7})(\text{TCNQ})_2$ were obtained. The specific charge transfer was determined according to the Kistenmacher relationship.

$\alpha\text{-}(\mathbf{2})(\text{TCNQ})$ and $(\mathbf{8})(\text{TCNQ})$ crystallise in segregated stacks with equidistantly arranged donor molecules and alternatingly arranged TCNQ molecules. In the crystals of $\beta\text{-}(\mathbf{2})(\text{TCNQ})$, $(\mathbf{3})(\text{TCNQ})$, $(\mathbf{4})(\text{TCNQ})$, $(\mathbf{7})(\text{TCNQ})$ and $(\mathbf{7})(\text{TCNQ})_2$ stacks, made up of donor and acceptor alternatingly, are present.

Their magnetic properties vary strongly indicating no straightforward relations. For $\alpha\text{-}(\mathbf{1})(\text{TCNQ})$, antiferromagnetism with a Néel temperature T_N of 50 K is observed. Almost similar magnetic behaviour is examined for $\alpha\text{-}(\mathbf{2})(\text{TCNQ})$, $\beta\text{-}(\mathbf{2})(\text{TCNQ})$, $(\mathbf{4})(\text{TCNQ})$ and $(\mathbf{7})(\text{TCNQ})_2$. At low temperatures, small magnetic moments of $0.24 \mu_B$ for $\alpha\text{-}(\mathbf{2})(\text{TCNQ})$, $0.26 \mu_B$ for $\beta\text{-}(\mathbf{2})(\text{TCNQ})$, $0.74 \mu_B$ for $(\mathbf{4})(\text{TCNQ})$ and $0.23 \mu_B$ for $(\mathbf{7})(\text{TCNQ})_2$ are determined. At higher temperatures, a nearly temperature independent paramagnetism is detected ranging from 10^{-5} to $10^{-3} \text{ cm}^3 \text{ mol}^{-1}$. Diamagnetic behaviour is detected for $(\mathbf{3})(\text{TCNQ})$. Substantial coupling of the electron in the stacking framework might lead to largely suppressed spin momenta. $(\mathbf{8})(\text{TCNQ})$ shows paramagnetism with a magnetic moment that corresponds to nearly a half free electron in agreement to the empirically estimated charge transfer.

Benchmark studies by hybrid density functional theory with dispersion correction and triple-zeta basis sets calculations on (TTF)(TCNQ) yield overall consistency with literature. Therefore, band structure calculations on this level of theory of the CT salts containing a pyridone azine and TCNQ correlate to the corresponding crystal structures. Calculated band structures of the compounds consisting of segregated stacks indicate anisotropic metallic conductivity. While calculated band structures of the CT salts with mixed stacks show no band crossing and semiconductivity at best. PDOS suggests a direct relation to the amount of charge transfer concerning the contributions of the donor and acceptor orbitals to the VBM, or respectively the CBM. Calculated PDOS, Mulliken population analysis and empirically estimated charge transfer by the Kistenmacher relationship are in well agreement.

The experimental conductivities of the CT salts measured on compact powder samples range from

10^{-10} to 10^0 Scm $^{-1}$ at room temperature. α -(1)(TCNQ), α -(2)(TCNQ), β -(2)(TCNQ), (4)(TCNQ), (7)(TCNQ) $_2$ and (8)(TCNQ) show typical semiconducting behaviour. (3)(TCNQ) exhibits insulating behaviour at room temperature. The energies for the thermal activated electron excitation range between 0.14 eV to 0.98 eV. Therefore, the CT salts represent small band gap semiconductors, except for (3)(TCNQ) that show typical insulating behaviour with a band gap of 2.9 eV determined for temperatures over 330 K.

Calculated specific conductivities by the above mentioned method predict anisotropic character of conduction. In stacking direction the contribution to electron migration is the largest. This holds for all CT salts except (7)(TCNQ) $_2$ where a four times larger conductivity along another direction is calculated. In general, calculated electronic properties confirm the expectations derived from the crystallographic point of view. Experimental findings are in agreement with calculations, except for (8)(TCNQ) where calculations predict conducting behaviour. In the crystal, the electron mobility may be influenced by additional intra- or intermolecular interactions. For the compounds crystallising in mixed stacks, semiconductivity is observed by experiment and predicted by calculation. β -(2)(TCNQ), (4)(TCNQ), (7)(TCNQ) and (7)(TCNQ) $_2$ can be classified as small band gap semiconductors. For (3)(TCNQ) insulating behaviour is detected by experiment and anticipated by calculation.

Concluding, for most cases the properties of CT salts obtained by experiment are in line with calculations. Therefore, description of the electronic properties of CT compounds by hybrid density functional theory with dispersion correction and triple-zeta basis sets represents a suitable method yielding reasonable results.

In reaction with the acceptor TCNP, the new azine-containing CT salts (5)(OTCNP) $_2$ and (7)(TCNP) were obtained. Under ambient conditions, TCNP undergoes hydrolysis in the reaction with 5, yielding the OTCNP $^-$ mono-anion and the 5 $^{2+}$ dication. The structure can be derived from the tungsten structure type with partially occupation of the pseudo-tetrahedral holes. Structural parameters of (7)(TCNP) indicate low degree of charge transfer. Measurements of the electronic properties show that this neutral CT salt consisting of mixed stacks is a diamagnetic, high-ohmic semiconductor.

The reaction of the fluorene based acceptor DTeF with the parent scaffold 1 affords (1)(DTeF). The basic structural features are segregated stacks that are built up by the dimeric aggregates (1) $^{2+}_2$ and (DTeF) $^{2-}_2$. Calculations of the electronic properties suggest semiconducting behaviour with low absolute specific conductivities. X-ray powder diffraction underscores the multi-phase nature of the reaction between 1 and DTeF which could not be satisfactorily resolved so far.

This work shows the great potential of the class of pyridone azines. The bis(*N*-methylpyridone)azine hardly gained attention since S. Hünig studies. However, itself and its derivatives are highly prone to function as organic building blocks in organic-inorganic hybrids and charge transfer compounds. The huge variety of air-stable compounds obtained in this work underscore the opportunities concerning material design. Furthermore, a suitable method for the prediction of electronic properties has been identified by calculations with hybrid density functional theory with dispersion correction and triple-zeta basis sets.

APPENDIX A

Useful Information

A.1 Used Computer Programs

In course of this work, several computer programs were used. These are listed in Tab. A.1.

The computer programs used in the course of this work as well as the number of the corresponding version, the respective application, the respective programmer and the year of publication of the version used.

program	version	application	programmer	year
ChemDraw[149]	15.1.0.144	Chemical formula editor	PerkinElmer informatics	2017
Inkscape[150]	1.1	Visualisation program	Inkscape development team	2021
Paint[151]	6.1	Visualisation program	Microsoft Corporation	2009
Diamond[106]	4.6.8	Visualisation of crystal structures	Crystal Impact	2022
MATCH[108]	2.4.7	Evaluation of X-ray powder diffractograms	Crystal Impact	2017
WinGX[152]	2013.3	Program interface to manage structure analysis tools	L. J. Farrugia	2012
Platon[153]	10	Tool for crystallographic questions	A. L. Spek, Utrecht	2014
SHELX[105]	97	Calculation and refinement of crystal structures	G. M. Sheldrick	1998
WinXPow[107]	1.05	Recording and evaluation of X-ray powder diffractograms	STOE & Cie GmbH	1999
MAGMUN[154]	4.1	Magnetic data fitting	Z. Xu, K. He	2002
molden[120]	5.9.2	Pre- and post processing program of molecular and electronic structure	G. Schaftenaar	2000
gnuplot[155]	4.4	Interactive plotting program	T. Williams, C. Kelley <i>et al.</i>	2010

A.2 Radical Cation Salts with Halogenocuprates

(1)[CuCl₂]

Crystallographic data and structure refinement of (1)[CuCl₂] at room temperature.

Compound	(1)[CuCl ₂]
Empirical Formula	C ₁₂ H ₁₄ Cl ₂ CuN ₄
Formula weight / g mol ⁻¹	348.71
Temperature / K	293(2)
Crystal system; space group	Monoclinic, C2/c
Lattice constants / Å °	$a = 11.131(2)$ $b = 16.636(4)$ $\beta = 95.652(12)$ $c = 7.9036(12)$
Volume / Å ³	1456.4(5)
Z; F(000); calc. density / g cm ⁻³	4; 708; 1.590
Wavelength	Mo-K _α (0.71073 Å)
Theta range for data collection / °	3.264 ≤ θ ≤ 27.471
Limiting indices	-12 ≤ h ≤ 14, -21 ≤ k ≤ 21, -9 ≤ l ≤ 10
Reflections collected / unique	6916 / 1652
R _{int}	0.0947
Completeness to theta = 25.242	99.80 %
Absorption coefficient / mm ⁻¹	1.857
Refinement method	Full-matrix least-squares on F^2
Data / restraints / parameters	1652 / 0 / 115
R indices [I > 4σ(I)] R ₁ ; wR ₂	0.0455; 0.0940
R indices (all data) R ₁ ; wR ₂	0.1386; 0.1192
Goodness-of-fit for F^2	0.930
Largest diff. Peak and hole / e ⁻ Å ⁻³	0.236 / -0.303

Table A.3: Fractional coordinates in Å and equivalent isotropic displacement parameter U_{eq} /Å² for the independent atoms in the structure of (1)[CuCl₂] at room temperature.

Atom	Wyck.	Site	x/a	y/b	z/c	U_{eq}
Cu(1)	4e	1	0.5000	0.2820(1)	0.2500	0.073(1)
Cl(1)	8f	1	0.4675(1)	0.2862(1)	0.5042(1)	0.085(1)
N(1)	8f	1	0.2070(3)	0.5524(2)	0.7152(4)	0.058(1)
N(2)	8f	1	0.0337(3)	0.5284(2)	0.5416(4)	0.061(1)
C(1)	8f	1	0.1306(3)	0.4968(2)	0.6342(5)	0.055(1)
C(2)	8f	1	0.1605(4)	0.4156(3)	0.6572(6)	0.066(1)
C(3)	8f	1	0.2638(4)	0.3929(3)	0.7517(6)	0.074(1)
C(4)	8f	1	0.3404(4)	0.4507(3)	0.8298(6)	0.072(1)
C(5)	8f	1	0.3092(4)	0.5284(3)	0.8118(5)	0.068(1)
C(6)	8f	1	0.1781(5)	0.6378(3)	0.7026(1)	0.081(2)
H(2)	8f	1	0.1110(4)	0.3820(2)	0.6110(5)	0.069(14)
H(3)	8f	1	0.2860(3)	0.3370(3)	0.7680(4)	0.075(13)
H(4)	8f	1	0.4160(3)	0.4390(2)	0.9080(4)	0.064(11)
H(5)	8f	1	0.3560(3)	0.5710(2)	0.8600(4)	0.047(1)
H(6A)	8f	1	0.0990(5)	0.6540(3)	0.7530(6)	0.125(18)

Table A.3 – continued from previous page

Atom	Wyck.	Site	x/a	y/b	z/c	U_{eq}
H(6B)	$8f$	1	0.2310(7)	0.6680(5)	0.7570(8)	0.170(3)
H(6C)	$8f$	1	0.1670(5)	0.6550(3)	0.5980(6)	0.100(2)

Table A.4: Anisotropic displacement parameters $U_{ij}/\text{\AA}^2$ for the independent atoms in the structure of **(1)**[CuCl₂] at room temperature.

Atom	U_{11}	U_{22}	U_{33}	U_{23}	U_{13}	U_{12}
Cu(1)	0.073(1)	0.059(1)	0.085(1)	0.000	0.003(1)	0.000
Cl(1)	0.103(1)	0.070(1)	0.082(1)	0.002(1)	0.007(1)	0.003(1)
N(1)	0.051(2)	0.050(2)	0.074(2)	-0.007(2)	0.005(2)	0.001(2)
N(2)	0.057(2)	0.055(2)	0.073(2)	-0.007(2)	0.005(2)	-0.004(2)
C(1)	0.054(2)	0.052(3)	0.059(2)	-0.007(2)	0.014(2)	-0.006(2)
C(2)	0.065(3)	0.059(3)	0.074(3)	-0.005(2)	0.005(2)	-0.003(3)
C(3)	0.081(4)	0.059(3)	0.083(3)	0.004(3)	0.013(3)	0.008(3)
C(4)	0.070(3)	0.069(4)	0.078(3)	0.002(2)	0.003(2)	0.011(3)
C(5)	0.055(3)	0.076(4)	0.071(3)	-0.010(2)	0.003(2)	-0.007(3)
C(6)	0.073(3)	0.054(3)	0.113(5)	-0.008(3)	-0.003(3)	0.001(3)

Table A.5: Crystallographic data and structure refinement of **(1)**[CuCl₂] at 123 K.

Compound	(1) [CuCl ₂]
Empirical Formula	C ₁₂ H ₁₄ Cl ₂ CuN ₄
Formula weight/ g mol ⁻¹	348.71
Temperature / K	123(2)
Crystal system; space group	Monoclinic, C2/c
Lattice constants / Å°	$a = 11.0979(4)$ $b = 16.5755(6)$ $\beta = 96.022(3)$ $c = 7.7405(2)$
Volume / Å ³	1416.03(8)
Z; F(000); calc. density / g cm ⁻³	4; 708; 1.636
Wavelength	Mo-K α (0.71073 Å)
Theta range for data collection / °	3.301 $\leq \theta \leq$ 27.492
Limiting indices	-14 $\leq h \leq$ 13, -21 $\leq k \leq$ 21, -9 $\leq l \leq$ 10
Reflections collected / unique	9475 / 1610
R _{int}	0.1024
Completeness to theta = 25.242	99.10 %
Absorption coefficient / mm ⁻¹	1.910
Refinement method	Full-matrix least-squares on F^2
Data / restraints / parameters	1610 / 0 / 115
R indices [I > 4σ(I)] R ₁ ; wR ₂	0.0330; 0.0858
R indices (all data) R ₁ ; wR ₂	0.0419; 0.0916
Goodness-of-fit for F^2	1.033
Largest diff. Peak and hole / e ⁻ Å ⁻³	0.342 / -0.602

Table A.6: Fractional coordinates in Å and equivalent isotropic displacement parameter $U_{eq}/\text{\AA}^2$ for the independent atoms in the structure of (1)[CuCl₂] at 123 K.

Atom	Wyck.	Site	x/a	y/b	z/c	U_{eq}
Cu(1)	4e	1	0.5000	0.7192(1)	0.7500	0.026(1)
Cl(1)	8f	1	0.5347(1)	0.7152(1)	0.4900(1)	0.031(1)
C(1)	8f	1	0.8684(2)	0.5033(1)	0.3618(2)	0.023(1)
C(2)	8f	1	0.8383(2)	0.5857(1)	0.3399(3)	0.026(1)
C(3)	8f	1	0.7336(2)	0.6085(1)	0.2429(3)	0.029(1)
C(4)	8f	1	0.6564(2)	0.5496(1)	0.1624(3)	0.028(1)
C(5)	8f	1	0.6876(2)	0.4702(1)	0.1806(3)	0.027(1)
C(6)	8f	1	0.8221(2)	0.3612(1)	0.2928(3)	0.030(1)
N(1)	8f	1	0.7911(2)	0.4474(1)	0.2785(2)	0.024(1)
N(2)	8f	1	0.9659(2)	0.4715(1)	0.4577(2)	0.025(1)
H(2)	8f	1	0.8890(2)	0.6217(15)	0.3930(3)	0.027(6)
H(3)	8f	1	0.7110(2)	0.6650(14)	0.2310(3)	0.023(6)
H(4)	8f	1	0.5860(2)	0.5641(15)	0.0920(3)	0.031(6)
H(5)	8f	1	0.6420(2)	0.4257(14)	0.1260(3)	0.023(5)
H(6A)	8f	1	0.8360(3)	0.3447(16)	0.4070(4)	0.046(8)
H(6B)	8f	1	0.8940(3)	0.3504(16)	0.2400(4)	0.041(7)
H(6C)	8f	1	0.7610(3)	0.3292(18)	0.2350(4)	0.045(7)

 Table A.7: Anisotropic displacement parameters $U_{ij}/\text{\AA}^2$ for the independent atoms in the structure of (1)[CuCl₂] at 123 K.

Atom	U_{11}	U_{22}	U_{33}	U_{23}	U_{13}	U_{12}
Cu(1)	0.029(1)	0.023(1)	0.026(1)	0.000	0.000(1)	0.000
Cl(1)	0.039(1)	0.027(1)	0.026(1)	0.001(1)	0.002(1)	0.001(1)
C(1)	0.024(1)	0.023(1)	0.022(1)	-0.002(1)	0.002(1)	-0.001(1)
C(2)	0.028(1)	0.024(1)	0.026(1)	-0.002(1)	0.000(1)	-0.002(1)
C(3)	0.031(1)	0.027(1)	0.027(1)	0.001(1)	0.003(1)	0.005(1)
C(4)	0.026(1)	0.032(1)	0.027(1)	0.000(1)	0.000(1)	0.005(1)
C(5)	0.023(1)	0.030(1)	0.026(1)	-0.002(1)	-0.001(1)	0.000(1)
C(6)	0.029(1)	0.021(1)	0.039(1)	-0.005(1)	-0.005(1)	0.001(1)
N(1)	0.024(1)	0.022(1)	0.026(1)	-0.003(1)	0.000(1)	0.001(1)
N(2)	0.024(1)	0.024(1)	0.025(1)	-0.004(1)	0.000(1)	-0.003(1)

(1)[CuBr₂]

 Table A.8: Crystallographic data and structure refinement of (1)[CuBr₂] at room temperature.

Compound	(1)[CuBr ₂]
Empirical Formula	C ₁₂ H ₁₄ Br ₂ CuN ₄
Formula weight/ g mol ⁻¹	437.63

Table A.8 – continued from previous page

Compound	(1)[CuBr ₂]
Temperature / K	293(2)
Crystal system; space group	Tetragonal, $P4_2/mcm$
Lattice constants / Å	$a = b = 10.504(2)$ $c = 6.4591(15)$
Volume / Å ³	712.7(3)
Z; F(000); calc. density / g cm ⁻³	2; 426; 2.039
Wavelength	Mo-K _α (0.71073 Å)
Theta range for data collection / °	3.880 $\leq \theta \leq$ 27.301
Limiting indices	-13 $\leq h \leq$ 13, -9 $\leq k \leq$ 9, -7 $\leq l \leq$ 8
Reflections collected / unique	1383 / 475
R _{int}	0.0729
Completeness to theta = 25.242	99.50 %
Absorption coefficient / mm ⁻¹	7.130
Refinement method	Full-matrix least-squares on F^2
Data / restraints / parameters	475 / 0 / 54
R indices [I > 4σ(I)] R ₁ ; wR ₂	0.0359; 0.0622
R indices (all data) R ₁ ; wR ₂	0.1087; 0.0779
Goodness-of-fit for F^2	0.933
Largest diff. Peak and hole / e ⁻ Å ⁻³	0.325 / -0.252

Table A.9: Fractional coordinates in Å and equivalent isotropic displacement parameter U_{eq} /Å² for the independent atoms in the structure of (1)[CuBr₂] at room temperature.

Atom	Wyck.	Site	x/a	y/b	z/c	U_{eq}
Br(1)	2b	1	0.1288(1)	0.8712(1)	0.5000	0.076(1)
Cu(1)	4i	1	0.0000	1.0000	0.7500	0.086(1)
N(1)	8n	0.5	0.5589(14)	0.5222(11)	0.5000	0.056(5)
N(2)	4j	1	0.6916(5)	0.6916(5)	0.5000	0.084(2)
C(1)	8n	0.5	0.5579(1)	0.6489(13)	0.5000	0.057(3)
C(2)	8n	0.5	0.4565(1)	0.7343(12)	0.5000	0.063(3)
C(3)	8n	0.5	0.4699(11)	0.8600(12)	0.5000	0.080(4)
C(4)	8n	0.5	0.5929(12)	0.9106(12)	0.5000	0.073(4)
C(5)	8n	0.5	0.6921(19)	0.8374(18)	0.5000	0.068(5)
C(6)	8n	0.5	0.6340(2)	0.7920(15)	0.5000	0.101(7)
H(2)	8n	0.5	0.3744	0.7013	0.5000	0.076
H(3)	8n	0.5	0.3991	0.9131	0.5000	0.096
H(4)	8n	0.5	0.6037	0.9985	0.5000	0.088
H(5)	8n	0.5	0.7712	0.8772	0.5000	0.082
H(6A)	16p	0.5	0.6814	0.8547	0.5755	0.152
H(6B)	16p	0.5	0.5522	0.7802	0.5645	0.152
H(6C)	16p	0.5	0.6219	0.8203	0.3600	0.152

Appendix A Useful Information

Table A.10: Anisotropic displacement parameters $U_{ij}/\text{\AA}^2$ for the independent atoms in the structure of **(1)**[CuBr₂] at room temperature.

Atom	U_{11}	U_{22}	U_{33}	U_{23}	U_{13}	U_{12}
Br(1)	0.069(1)	0.069(1)	0.090(1)	0.000	0.000	0.009(1)
Cu(1)	0.080(1)	0.080(1)	0.099(1)	0.000	0.000	0.000
N(1)	0.040(7)	0.059(1)	0.067(5)	0.000	0.000	0.002(9)
N(2)	0.091(4)	0.091(4)	0.070(5)	0.000	0.000	-0.031(6)
C(1)	0.038(7)	0.083(1)	0.050(7)	0.000	0.000	-0.010(7)
C(2)	0.047(7)	0.064(8)	0.079(8)	0.000	0.000	0.004(6)
C(3)	0.057(8)	0.071(9)	0.111(1)	0.000	0.000	0.009(6)
C(4)	0.061(8)	0.059(7)	0.100(11)	0.000	0.000	-0.018(7)
C(5)	0.093(14)	0.050(11)	0.062(1)	0.000	0.000	-0.021(9)
C(6)	0.116(17)	0.028(1)	0.160(17)	0.000	0.000	-0.013(1)

Table A.11: Crystallographic data and structure refinement of **(1)**[CuBr₂] at 123 K.

Compound	(1)[CuBr ₂]
Empirical Formula	C ₁₂ H ₁₄ Br ₂ CuN ₄
Formula weight/ $gmol^{-1}$	437.63
Temperature / K	123(2)
Crystal system; space group	Tetragonal, $P4_2/mcm$
Lattice constants / \AA	$a = b = 10.485(2)$ $c = 6.3404(15)$
Volume / \AA^3	697.1(3)
Z; F(000); calc. density / gcm^{-3}	2; 426; 2.085
Wavelength	Mo-K α (0.71073 \AA)
Theta range for data collection / $^\circ$	3.887 $\leq \theta \leq$ 34.954
Limiting indices	$-16 \leq h \leq 16, -16 \leq k \leq 16, -10 \leq l \leq 9$
Reflections collected / unique	12231 / 870
R _{int}	0.1173
Completeness to theta = 25.242	99.20 %
Absorption coefficient / mm^{-1}	7.289
Refinement method	Full-matrix least-squares on F^2
Data / restraints / parameters	870 / 0 / 55
R indices [I > 4σ(I)] R ₁ ; wR ₂	0.0300; 0.0686
R indices (all data) R ₁ ; wR ₂	0.0403; 0.0735
Goodness-of-fit for F^2	1.041
Extinction coefficient	0.011(3)
Largest diff. Peak and hole / $e^- \text{\AA}^{-3}$	0.721 / -0.777

Table A.12: Fractional coordinates in \AA and equivalent isotropic displacement parameter $U_{eq}/\text{\AA}^2$ for the independent atoms in the structure of **(1)**[CuBr₂] at 123 K.

Atom	Wyck.	Site	x/a	y/b	z/c	U_{eq}
Br(1)	2b	1	0.1302(1)	0.8699(1)	0.5000	0.024(1)

Table A.12 – continued from previous page

Atom	Wyck.	Site	<i>x/a</i>	<i>y/b</i>	<i>z/c</i>	<i>U_{eq}</i>
Cu(1)	<i>4i</i>	1	0.0000	1.0000	0.7500	0.026(1)
N(1)	<i>8n</i>	0.5	0.5599(3)	0.5230(3)	0.5000	0.020(1)
N(2)	<i>4j</i>	1	0.6939(2)	0.6939(2)	0.5000	0.040(1)
C(1)	<i>8n</i>	0.5	0.5607(4)	0.6521(4)	0.5000	0.020(1)
C(2)	<i>8n</i>	0.5	0.4539(5)	0.7335(5)	0.5000	0.026(1)
C(3)	<i>8n</i>	0.5	0.4703(5)	0.8642(5)	0.5000	0.033(1)
C(4)	<i>8n</i>	0.5	0.5930(5)	0.9168(5)	0.5000	0.030(1)
C(5)	<i>8n</i>	0.5	0.6949(5)	0.8366(5)	0.5000	0.025(1)
C(6)	<i>8n</i>	0.5	0.6301(7)	0.7953(6)	0.5000	0.054(2)
H(2)	<i>8n</i>	0.5	0.3704	0.6984	0.5000	0.031
H(3)	<i>8n</i>	0.5	0.3979	0.9186	0.5000	0.040
H(4)	<i>8n</i>	0.5	0.6048	1.0066	0.5000	0.035
H(5)	<i>8n</i>	0.5	0.7766	0.8759	0.5000	0.030
H(6A)	<i>16p</i>	0.5	0.6044	0.8159	0.3554	0.081
H(6B)	<i>16p</i>	0.5	0.6821	0.8648	0.5570	0.081
H(6C)	<i>16p</i>	0.5	0.5539	0.7841	0.5877	0.081

Table A.13: Anisotropic displacement parameters $U_{ij}/\text{\AA}^2$ for the independent atoms in the structure of (1)[CuBr₂] at 123 K.

Atom	<i>U₁₁</i>	<i>U₂₂</i>	<i>U₃₃</i>	<i>U₂₃</i>	<i>U₁₃</i>	<i>U₁₂</i>
Br(1)	0.024(1)	0.024(1)	0.023(1)	0.000	0.000	0.005(1)
Cu(1)	0.025(1)	0.025(1)	0.026(1)	0.000	0.000	0.000
N(1)	0.020(2)	0.023(2)	0.018(1)	0.000	0.000	0.001(2)
N(2)	0.050(2)	0.050(2)	0.020(1)	0.000	0.000	-0.032(2)
C(1)	0.017(2)	0.028(2)	0.016(2)	0.000	0.000	-0.003(2)
C(2)	0.021(2)	0.027(2)	0.030(2)	0.000	0.000	-0.002(2)
C(3)	0.021(2)	0.026(2)	0.053(3)	0.000	0.000	0.003(2)
C(4)	0.027(2)	0.026(2)	0.036(2)	0.000	0.000	-0.004(2)
C(5)	0.025(2)	0.029(2)	0.020(2)	0.000	0.000	-0.006(2)
C(6)	0.036(3)	0.014(2)	0.111(7)	0.000	0.000	0.002(2)

(8)[CuBr₂]Table A.14: Crystallographic data and structure refinement of (8)[CuBr₂] at room temperature.

Compound	(8)[CuBr ₂]
Empirical Formula	C ₁₄ H ₁₂ Br ₂ CuF ₆ N ₄
Formula weight/ <i>gmol⁻¹</i>	573.64
Temperature / <i>K</i>	298(2)
Crystal system; space group	Tetragonal, <i>P4₂/n</i>
Lattice constants / <i>\text{\AA}</i>	<i>a</i> = <i>b</i> = 17.6214(4) <i>c</i> = 6.03570(1)
Volume / <i>\text{\AA}^3</i>	1874.17(9)

Table A.14 – continued from previous page

Compound	(8)[CuBr ₂]
Z; F(000); calc. density / gcm ⁻³	4; 1108; 2.033
Wavelength	Mo-K _α (0.71073 Å)
Theta range for data collection / °	3.270 ≤ θ ≤ 27.483
Limiting indices	-22 ≤ h ≤ 22, -22 ≤ k ≤ 22, -7 ≤ l ≤ 7
Reflections collected / unique	19404 / 2146
R _{int}	0.1555
Completeness to theta = 25.242	99.90 %
Absorption coefficient / mm ⁻¹	5.493
Refinement method	Full-matrix least-squares on F ²
Data / restraints / parameters	2146 / 0 / 178
R indices [I > 4σ(I)] R ₁ ; wR ₂	0.0386; 0.0949
R indices (all data) R ₁ ; wR ₂	0.0592; 0.1045
Goodness-of-fit for F ²	1.012
Extinction coefficient	0.0061(9)
Largest diff. Peak and hole / e ⁻ Å ⁻³	0.462 / -0.802

Table A.15: Fractional coordinates in Å and equivalent isotropic displacement parameter U_{eq}/Å² for the independent atoms in the structure of (8)[CuBr₂] at room temperature.

Atom	Wyck.	Site	x/a	y/b	z/c	U _{eq}
Cu(1)	4e	1	0.7500	0.2500	0.1582(1)	0.055(1)
Br(1)	8g	1	0.8165(1)	0.3409(1)	0.4049(1)	0.047(1)
F(1)	8g	0.33	0.7125(16)	0.5721(14)	0.3160(5)	0.118(12)
F(2)	8g	0.33	0.6830(2)	0.6330(2)	0.6310(5)	0.161(16)
F(3)	8g	0.33	0.7790(2)	0.6699(19)	0.4090(7)	0.082(8)
F(4)	8g	0.33	0.7299(16)	0.5840(12)	0.2730(3)	0.069(6)
F(5)	8g	0.33	0.7640(2)	0.6720(3)	0.4780(8)	0.096(13)
F(6)	8g	0.33	0.6764(15)	0.6090(2)	0.5730(5)	0.088(9)
F(7)	8g	0.33	0.6711(14)	0.6011(14)	0.5130(5)	0.088(9)
F(8)	8g	0.33	0.7525(17)	0.6149(16)	0.2680(4)	0.125(12)
F(9)	8g	0.33	0.7620(2)	0.6779(14)	0.5520(8)	0.166(19)
N(1)	8g	1	0.8863(2)	0.4517(2)	0.8110(4)	0.044(1)
N(2)	8g	1	0.9881(2)	0.4796(2)	0.5857(4)	0.047(1)
C(5)	8g	1	0.9151(2)	0.4932(2)	0.6380(5)	0.042(1)
C(4)	8g	1	0.8658(2)	0.5452(2)	0.5343(6)	0.048(1)
C(3)	8g	1	0.7931(2)	0.5531(2)	0.6035(5)	0.047(1)
C(2)	8g	1	0.7656(2)	0.5089(2)	0.7781(6)	0.054(1)
C(1)	8g	1	0.8137(2)	0.4587(2)	0.8764(5)	0.053(1)
C(6)	8g	1	0.9343(2)	0.3940(3)	0.9177(6)	0.064(1)
C(7)	8g	1	0.7421(3)	0.6075(3)	0.4846(9)	0.065(1)
H(3)	8g	1	0.8835	0.5745	0.4169	0.057
H(2)	8g	1	0.7157	0.5137	0.8260	0.065
H(10)	8g	1	0.7959	0.4285	0.9916	0.063
H(6A)	8g	1	0.9843	0.3956	0.8547	0.096
H(6B)	8g	1	0.9373	0.4041	1.0738	0.096
H(6C)	8g	1	0.9126	0.3447	0.8944	0.096

Table A.16: Anisotropic displacement parameters $U_{ij}/\text{\AA}^2$ for the independent atoms in the structure of (8)[CuBr₂] at room temperature.

Atom	U_{11}	U_{22}	U_{33}	U_{23}	U_{13}	U_{12}
Br(1)	0.061(1)	0.047(1)	0.034(1)	-0.003(1)	0.004(1)	-0.010(1)
Cu(1)	0.062(1)	0.055(1)	0.047(1)	0.000	0.000	-0.002(1)
F(1)	0.133(16)	0.116(14)	0.105(18)	0.044(1)	-0.069(16)	-0.039(1)
F(2)	0.190(3)	0.180(3)	0.116(19)	0.026(15)	0.086(18)	0.150(2)
F(3)	0.059(1)	0.046(1)	0.140(2)	0.031(11)	0.011(12)	-0.014(7)
F(4)	0.116(16)	0.044(9)	0.047(7)	0.009(8)	0.004(8)	0.030(1)
F(5)	0.068(18)	0.086(18)	0.130(3)	0.049(15)	-0.002(14)	-0.000(12)
F(6)	0.065(12)	0.137(18)	0.063(12)	-0.012(1)	0.021(8)	0.065(11)
F(7)	0.053(9)	0.100(12)	0.110(2)	0.048(13)	-0.006(1)	-0.007(8)
F(8)	0.150(2)	0.130(2)	0.099(12)	0.070(16)	0.024(12)	0.064(17)
F(9)	0.240(3)	0.029(8)	0.220(4)	-0.029(14)	-0.110(3)	0.030(11)
N(1)	0.048(2)	0.046(2)	0.039(1)	0.002(1)	0.005(1)	-0.010(1)
N(2)	0.046(2)	0.050(2)	0.046(2)	0.005(1)	0.009(1)	-0.008(1)
C(5)	0.047(2)	0.044(2)	0.035(2)	-0.001(1)	0.005(1)	-0.011(2)
C(4)	0.053(2)	0.041(2)	0.048(2)	0.000(2)	0.006(2)	-0.006(2)
C(3)	0.052(2)	0.040(2)	0.050(2)	-0.005(2)	0.005(2)	-0.004(2)
C(2)	0.047(2)	0.061(2)	0.054(2)	-0.007(2)	0.015(2)	-0.002(2)
C(1)	0.054(2)	0.064(2)	0.041(2)	-0.001(2)	0.015(2)	-0.013(2)
C(6)	0.059(3)	0.075(3)	0.059(2)	0.026(2)	0.010(2)	-0.001(2)
C(7)	0.059(3)	0.052(3)	0.084(4)	0.004(3)	0.011(3)	0.006(2)

Table A.17: Crystallographic data and structure refinement of (8)[CuBr₂] at 123 K.

Compound	<i>p</i> -CF ₃ (1)[CuBr ₂]
Empirical Formula	C ₁₄ H ₁₂ Br ₂ CuF ₆ N ₄
Formula weight / g mol ⁻¹	573.64
Temperature / K	123(2)
Crystal system; space group	Tetragonal, P4 ₂ /n
Lattice constants / Å	$a = b = 17.4417(4)$ $c = 5.98740(1)$
Volume / Å ³	1821.44(9)
Z; F(000); calc. density / g cm ⁻³	4; 1108; 2.092
Wavelength	Mo-K _α (0.71073 Å)
Theta range for data collection / °	3.304 ≤ θ ≤ 27.496
Limiting indices	-22 ≤ h ≤ 22, -22 ≤ k ≤ 22, -7 ≤ l ≤ 7
Reflections collected / unique	15540 / 2087
R _{int}	0.1265
Completeness to theta = 25.242	99.80 %
Absorption coefficient / mm ⁻¹	5.652
Refinement method	Full-matrix least-squares on F^2
Data / restraints / parameters	2087 / 0 / 147
R indices [I > 4σ(I)] R ₁ ; wR ₂	0.0381; 0.0910
R indices (all data) R ₁ ; wR ₂	0.0536; 0.0989
Goodness-of-fit for F^2	1.023
Largest diff. Peak and hole / e ⁻ Å ⁻³	0.941 / -0.629

Table A.18: Fractional coordinates in Å and equivalent isotropic displacement parameter $U_{eq}/\text{\AA}^2$ for the independent atoms in the structure of (8)[CuBr₂] at 123 K.

Atom	Wyck.	Site	x/a	y/b	z/c	U_{eq}
Cu(1)	4e	1	0.2500	0.7500	0.8342(1)	0.024(1)
Br(1)	8g	1	0.3418(1)	0.8169(1)	0.5866(1)	0.021(1)
F(1)	8g	1	0.6754(2)	0.7693(2)	0.5336(9)	0.091(1)
F(2)	8g	1	0.5848(2)	0.7264(2)	0.7234(6)	0.081(1)
F(3)	8g	1	0.6133(2)	0.6704(2)	0.4266(6)	0.069(1)
N(1)	8g	1	0.4520(2)	0.8859(2)	0.1826(5)	0.023(1)
N(2)	8g	1	0.4793(2)	0.9885(2)	0.4124(5)	0.023(1)
C(1)	8g	1	0.4933(2)	0.9141(2)	0.3595(6)	0.022(1)
C(2)	8g	1	0.5455(2)	0.8648(2)	0.4656(6)	0.022(1)
C(3)	8g	1	0.5534(2)	0.7906(2)	0.3936(6)	0.024(1)
C(4)	8g	1	0.5093(2)	0.7630(2)	0.2150(7)	0.026(1)
C(5)	8g	1	0.4589(2)	0.8127(2)	0.1153(6)	0.026(1)
C(6)	8g	1	0.3933(3)	0.9347(3)	0.0781(8)	0.031(1)
C(7)	8g	1	0.6085(2)	0.7394(2)	0.5147(8)	0.031(1)
H(2)	8g	1	0.5710(3)	0.8830(3)	0.5760(8)	0.039(14)
H(4)	8g	1	0.5140(2)	0.7120(2)	0.1680(7)	0.020(1)
H(5)	8g	1	0.4310(2)	0.7970(2)	0.0000(7)	0.019(1)
H(6A)	8g	1	0.3710(3)	0.9060(3)	-0.0380(1)	0.051(15)
H(6B)	8g	1	0.3530(3)	0.9440(3)	0.1880(9)	0.042(14)
H(6C)	8g	1	0.4130(3)	0.9780(3)	0.0440(7)	0.029(12)

 Table A.19: Anisotropic displacement parameters $U_{ij}/\text{\AA}^2$ for the independent atoms in the structure of (8)[CuBr₂] at 123 K.

Atom	U_{11}	U_{22}	U_{33}	U_{23}	U_{13}	U_{12}
Cu(1)	0.023(1)	0.025(1)	0.023(1)	0.000	0.000	-0.004(1)
Br(1)	0.021(1)	0.026(1)	0.016(1)	-0.002(1)	0.001(1)	-0.001(1)
F(1)	0.035(2)	0.057(2)	0.180(4)	0.025(3)	-0.043(2)	-0.008(1)
F(2)	0.088(3)	0.107(3)	0.047(2)	0.018(2)	0.003(2)	0.050(2)
F(3)	0.087(3)	0.047(2)	0.073(2)	-0.025(2)	-0.032(2)	0.030(2)
N(1)	0.023(2)	0.026(2)	0.018(2)	-0.004(1)	0.001(1)	-0.006(1)
N(2)	0.025(2)	0.024(2)	0.020(2)	-0.003(1)	-0.001(1)	-0.007(1)
C(1)	0.022(2)	0.026(2)	0.018(2)	-0.003(1)	0.003(1)	-0.008(2)
C(2)	0.019(2)	0.027(2)	0.021(2)	-0.002(2)	0.000(1)	-0.006(1)
C(3)	0.022(2)	0.027(2)	0.025(2)	-0.001(2)	0.004(2)	-0.003(2)
C(4)	0.029(2)	0.026(2)	0.024(2)	-0.008(2)	0.004(2)	-0.002(2)
C(5)	0.027(2)	0.029(2)	0.020(2)	-0.008(2)	0.002(2)	-0.009(2)
C(6)	0.037(2)	0.026(2)	0.029(2)	-0.003(2)	-0.011(2)	-0.002(2)
C(7)	0.031(2)	0.028(2)	0.036(2)	-0.006(2)	-0.001(2)	0.001(2)

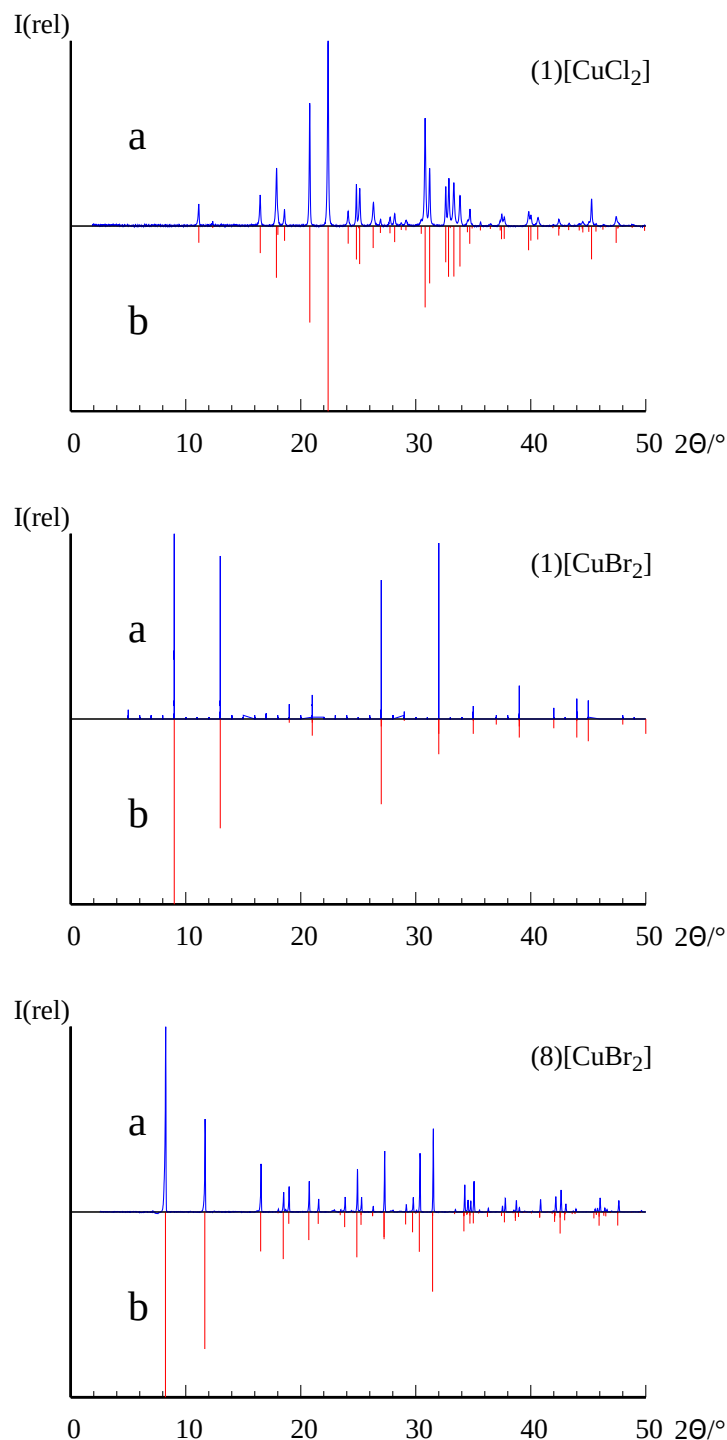


Figure A.1: X-ray powder diffraction pattern of the radical cation bearing compounds **(1)[CuCl₂]**, **(1)[CuBr₂]** and **(8)[CuBr₂]**. Used radiation: Co-K_{α1}, a = measured diffractogram, b = simulated diffractogram on basis of single crystal data.

A.3 Dication Salts with Halogenocuprates

(1)[Cu₂Br₄]

Table A.20: Crystallographic data and structure refinement of (1)[Cu₂Br₄] at room temperature.

Compound	(1)[Cu ₂ Br ₄]
Empirical Formula	C ₁₂ H ₁₄ Br ₄ Cu ₂ N ₄
Formula weight / g mol ⁻¹	660.99
Crystal size / mm ³	0.1744×0.050×0.018
Temperature / K	293(2)
Crystal system; space group	Triclinic, P [̄] 1
Lattice constants / Å°	$a = 6.38370(1)$ $\alpha = 67.6530(1)$ $b = 7.8675(2)$ $\beta = 85.4980(1)$ $c = 9.7762(2)$ $\gamma = 80.5630(1)$
Volume / Å ³	448.159(17)
Z; F(000); calc. density / g cm ⁻³	1; 312; 2.449
Wavelength	Mo-K _α (0.71073 Å)
Theta range for data collection / °	3.234 ≤ θ ≤ 27.641
Limiting indices	-8 ≤ h ≤ 8, -10 ≤ k ≤ 10, -12 ≤ l ≤ 12
Reflections collected / unique	13973 / 2055
R _{int}	0.0679
Completeness to theta = 25.242	99.80 %
Absorption coefficient / mm ⁻¹	11.287
Refinement method	Full-matrix least-squares on F^2
Data / restraints / parameters	2055 / 0 / 129
R indices [I > 4σ(I)] R ₁ ; wR ₂	0.0351; 0.0866
R indices (all data) R ₁ ; wR ₂	0.0545; 0.0968
Goodness-of-fit for F^2	0.916
Extinction coefficient	0.019(2)
Largest diff. Peak and hole / e ⁻ Å ⁻³	0.603 / -0.970

Table A.21: Fractional coordinates in Å and equivalent isotropic displacement parameter U_{eq} /Å² for the independent atoms in the structure of (1)[Cu₂Br₄] at room temperature.

Atom	Wyck.	Site	x/a	y/b	z/c	U_{eq}
Cu(1)	2i	1	0.2485(1)	0.5024(1)	0.4998(1)	0.059(1)
Br(1)	2i	1	0.4527(1)	0.6913(1)	0.5801(1)	0.041(1)
Br(2)	2i	1	-0.0134(1)	0.6877(1)	0.3012(1)	0.047(1)
N(1)	2i	1	0.7425(5)	0.8200(5)	0.8060(4)	0.038(1)
N(2)	2i	1	0.9909(5)	0.5777(5)	0.9471(4)	0.040(1)
C(1)	2i	1	0.7835(6)	0.6753(5)	0.9372(4)	0.035(1)
C(2)	2i	1	0.6334(7)	0.6407(6)	1.0492(5)	0.045(1)
C(3)	2i	1	0.4377(8)	0.7510(7)	1.0281(6)	0.049(1)
C(4)	2i	1	0.3975(8)	0.8959(7)	0.8936(5)	0.049(1)
C(5)	2i	1	0.5514(7)	0.9281(6)	0.7851(5)	0.044(1)
C(6)	2i	1	0.8994(8)	0.8543(7)	0.6817(5)	0.047(1)
H(2)	2i	1	0.6730(7)	0.5430(7)	1.1490(5)	0.051(13)
H(3)	2i	1	0.3360(8)	0.7260(7)	1.0980(5)	0.048(13)

Table A.21 – continued from previous page

Atom	Wyck.	Site	x/a	y/b	z/c	U_{eq}
H(4)	2 <i>i</i>	1	0.2680(9)	0.9720(9)	0.9000(7)	0.090(2)
H(5)	2 <i>i</i>	1	0.5300(1)	1.0150(9)	0.6950(7)	0.083(19)
H(6A)	2 <i>i</i>	1	0.9260(8)	0.7470(9)	0.6530(6)	0.062(15)
H(6B)	2 <i>i</i>	1	0.8450(14)	0.9540(13)	0.6130(8)	0.120(3)
H(6C)	2 <i>i</i>	1	1.0470(9)	0.8640(7)	0.7160(6)	0.068(16)

Table A.22: Anisotropic displacement parameters $U_{ij}/\text{\AA}^2$ for the independent atoms in the structure of **(1)[Cu₂Br₄]** at room temperature.

Atom	U_{11}	U_{22}	U_{33}	U_{23}	U_{13}	U_{12}
Cu(1)	0.052(1)	0.063(1)	0.060(1)	-0.022(1)	-0.002(1)	-0.007(1)
Br(1)	0.041(1)	0.041(1)	0.039(1)	-0.012(1)	0.002(1)	-0.007(1)
Br(2)	0.039(1)	0.052(1)	0.041(1)	-0.006(1)	-0.002(1)	-0.006(1)
N(1)	0.041(2)	0.035(2)	0.033(2)	-0.009(1)	-0.004(2)	-0.005(1)
N(2)	0.041(2)	0.036(2)	0.037(2)	-0.008(1)	-0.006(2)	-0.002(2)
C(1)	0.036(2)	0.032(2)	0.034(2)	-0.007(2)	-0.004(2)	-0.006(2)
C(2)	0.044(2)	0.047(2)	0.035(2)	-0.007(2)	0.001(2)	-0.007(2)
C(3)	0.042(2)	0.056(3)	0.048(3)	-0.021(2)	0.004(2)	-0.007(2)
C(4)	0.044(2)	0.051(3)	0.051(3)	-0.019(2)	-0.007(2)	0.002(2)
C(5)	0.044(2)	0.038(2)	0.041(2)	-0.007(2)	-0.012(2)	0.003(2)
C(6)	0.048(3)	0.045(3)	0.036(2)	-0.004(2)	0.005(2)	-0.008(2)

 α -(2)[Cu₂Br₄]Table A.23: Crystallographic data and structure refinement of α -(2)[Cu₂Br₄] at room temperature.

Compound	α -(2)[Cu ₂ Br ₄]
Empirical Formula	C ₁₂ H ₁₄ Br ₄ Cu ₂ N ₄
Formula weight / g mol ⁻¹	660.99
Crystal size / mm ³	0.600×0.015×0.012
Temperature / K	293(2)
Crystal system; space group	Tetragonal, P4 ₂ /mbc
Lattice constants / Å°	$a = b = 18.1974(6)$ $c = 6.0786(2)$
Volume / Å ³	2012.90(15)
Z; F(000); calc. density / g cm ⁻³	6; 1872; 3.272
Wavelength	Mo-K _α (0.71073 Å)
Theta range for data collection / °	3.166 ≤ θ ≤ 27.470
Limiting indices	-21 ≤ h ≤ 23, -23 ≤ k ≤ 20, -7 ≤ l ≤ 7
Reflections collected / unique	17887 / 1264
R _{int}	0.0945
Completeness to theta = 25.242	99.70 %
Absorption coefficient / mm ⁻¹	15.078

Table A.23 – continued from previous page

Compound	$\alpha\text{-}(\mathbf{2})[\text{Cu}_2\text{Br}_4]$
Refinement method	Full-matrix least-squares on F^2
Data / restraints / parameters	1264 / 0 / 68
R indices [$I > 4\sigma(I)$] R_1 ; wR_2	0.0454; 0.1563
R indices (all data) R_1 ; wR_2	0.0850; 0.1824
Goodness-of-fit for F^2	1.029
Largest diff. Peak and hole / $e^{-\text{\AA}^{-3}}$	1.118 / -0.512

Table A.24: Fractional coordinates in Å and equivalent isotropic displacement parameter $U_{eq}/\text{\AA}^2$ for the independent atoms in the structure of $\alpha\text{-}(\mathbf{2})[\text{Cu}_2\text{Br}_4]$ at room temperature.

Atom	Wyck.	Site	x/a	y/b	z/c	U_{eq}
Cu(1)	8g	1	0.7076(1)	0.2076(1)	0.7500	0.089(1)
Br(1)	8h	1	0.7223(1)	0.3179(1)	1.0000	0.072(1)
Br(2)	8h	1	0.5996(1)	0.2032(1)	0.5000	0.079(1)
N(1)	8h	1	0.7416(5)	0.4571(5)	0.5000	0.079(2)
N(2)	8h	1	0.5132(5)	0.4692(4)	0.5000	0.069(2)
C(1)	8h	1	0.7021(7)	0.3984(6)	0.5000	0.076(3)
C(2)	8h	1	0.6275(7)	0.4025(6)	0.5000	0.077(3)
C(3)	8h	1	0.5926(6)	0.4693(5)	0.5000	0.071(3)
C(4)	8h	1	0.6369(6)	0.5320(6)	0.5000	0.070(3)
C(5)	8h	1	0.7091(7)	0.5259(6)	0.5000	0.077(3)
C(6)	8h	1	0.8207(8)	0.4478(8)	0.5000	0.112(5)
H(10)	8h	1	0.7249	0.3526	0.5000	0.091
H(2)	8h	1	0.5998	0.3595	0.5000	0.092
H(4)	8h	1	0.6154	0.5783	0.5000	0.084
H(5)	8h	1	0.7383	0.5678	0.5000	0.093
H(6A)	16i	1	0.8330	0.4019	0.5686	0.169
H(6B)	16i	1	0.8431	0.4874	0.5801	0.169
H(6C)	16i	1	0.8384	0.4479	0.3512	0.169

Table A.25: Anisotropic displacement parameters $U_{ij}/\text{\AA}^2$ for the independent atoms in the structure of $\alpha\text{-}(\mathbf{2})[\text{Cu}_2\text{Br}_4]$ at room temperature.

Atom	U_{11}	U_{22}	U_{33}	U_{23}	U_{13}	U_{12}
Cu(1)	0.083(1)	0.083(1)	0.100(1)	0.000(1)	0.000(1)	-0.001(1)
Br(1)	0.069(1)	0.066(1)	0.081(1)	0.000	0.000	0.006(1)
Br(2)	0.070(1)	0.081(1)	0.088(1)	0.000	0.000	-0.008(1)
N(1)	0.080(6)	0.078(7)	0.080(6)	0.000	0.000	0.001(5)
N(2)	0.087(7)	0.061(5)	0.059(4)	0.000	0.000	-0.002(4)
C(1)	0.093(8)	0.068(7)	0.068(6)	0.000	0.000	0.020(6)
C(2)	0.107(9)	0.061(6)	0.062(5)	0.000	0.000	-0.002(6)
C(3)	0.106(9)	0.058(6)	0.048(5)	0.000	0.000	-0.003(6)
C(4)	0.086(8)	0.054(6)	0.069(6)	0.000	0.000	0.005(5)
C(5)	0.081(8)	0.069(7)	0.081(7)	0.000	0.000	0.005(5)
C(6)	0.101(11)	0.100(1)	0.137(12)	0.000	0.000	0.014(8)

β -(2)[Cu₂Br₄]Table A.26: Crystallographic data and structure refinement of β -(2)[Cu₂Br₄]·CH₃CN at room temperature.

Compound	β -(2)[Cu ₂ Br ₄]·CH ₃ CN
Empirical Formula	C ₅₂ H ₆₂ Br ₁₆ Cu ₈ N ₄
Formula weight/ g mol ⁻¹	2726.07
Crystal size/ mm ³	0.270×0.046×0.032
Temperature / K	293(2)
Crystal system; space group	Monoclinic, P2 ₁ /n
Lattice constants / Å°	$a = 17.9707(3)$ $b = 12.4835(2) \beta = 93.165(1)$ $c = 17.9662(3)$
Volume / Å ³	4024.34(11)
Z; F(000); calc. density / g cm ⁻³	2; 2584; 2.250
Wavelength	Mo-K α (0.71073 Å)
Theta range for data collection	2.970 $\leq \theta \leq$ 27.575
Limiting indices	-23 $\leq h \leq$ 23, -16 $\leq k \leq$ 14, -22 $\leq l \leq$ 23
Reflections collected / unique	59485 / 9254
R _{int}	0.1087
Completeness to theta = 25.242	99.80 %
Absorption coefficient / mm ⁻¹	10.060
Refinement method	Full-matrix least-squares on F^2
Data / restraints / parameters	9254 / 0 / 430
R indices [I > 4σ(I)] R ₁ ; wR ₂	0.0614; 0.1890
R indices (all data) R ₁ ; wR ₂	0.0988; 0.2087
Goodness-of-fit for F^2	1.021
Largest diff. Peak and hole / e ⁻ Å ⁻³	1.473 / -0.844

Table A.27: Fractional coordinates in Å and equivalent isotropic displacement parameter U_{eq} /Å² for the independent atoms in the structure of β -(2)[Cu₂Br₄]·CH₃CN at room temperature.

Atom	Wyck.	Site	x/a	y/b	z/c	U_{eq}
Cu(1)	4e	1	0.2620(1)	0.5643(1)	0.2514(1)	0.072(1)
Cu(2)	4e	1	0.2574(1)	0.3265(1)	0.2548(1)	0.069(1)
Br(1)	4e	1	0.3575(1)	0.7057(1)	0.2360(1)	0.059(1)
Br(2)	4e	1	0.2649(1)	0.4492(1)	0.3630(1)	0.070(1)
Br(3)	4e	1	0.2596(1)	0.4426(1)	0.1414(1)	0.057(1)
Br(4)	4e	1	0.3532(1)	0.1865(1)	0.2409(1)	0.054(1)
Cu(3)	4e	1	0.7588(1)	0.1634(1)	0.2504(1)	0.070(1)
Cu(4)	4e	1	0.7686(1)	-0.0743(1)	0.2547(1)	0.074(1)
Br(5)	4e	1	0.6434(1)	0.2676(1)	0.2168(1)	0.057(1)
Br(6)	4e	1	0.8032(1)	0.0421(1)	0.1518(1)	0.064(1)
Br(7)	4e	1	0.7622(1)	0.0483(1)	0.3641(1)	0.057(1)
Br(8)	4e	1	0.6515(1)	-0.1803(1)	0.2194(1)	0.053(1)
N(1)	4e	1	0.2527(4)	0.1824(5)	0.4989(4)	0.051(2)

Table A.27 – continued from previous page

Atom	Wyck.	Site	x/a	y/b	z/c	U_{eq}
N(2)	4e	1	0.4776(4)	0.2551(6)	0.5279(4)	0.051(2)
N(3)	4e	1	0.5122(4)	0.2656(6)	0.4718(4)	0.057(2)
N(4)	4e	1	0.7424(4)	0.2931(5)	0.5021(4)	0.051(2)
C(1)	4e	1	0.2843(5)	0.1961(7)	0.5648(5)	0.054(2)
C(2)	4e	1	0.3583(5)	0.2202(7)	0.5764(5)	0.054(2)
C(3)	4e	1	0.3996(5)	0.2316(6)	0.5138(4)	0.048(2)
C(4)	4e	1	0.3654(5)	0.2179(7)	0.4427(5)	0.054(2)
C(5)	4e	1	0.2936(5)	0.1916(7)	0.4371(5)	0.053(2)
C(6)	4e	1	0.1735(6)	0.1475(1)	0.4883(6)	0.075(3)
C(7)	4e	1	0.7002(5)	0.2940(6)	0.5633(5)	0.052(2)
C(8)	4e	1	0.6265(5)	0.2869(7)	0.5575(5)	0.054(2)
C(9)	4e	1	0.5915(5)	0.2799(6)	0.4864(5)	0.051(2)
C(10)	4e	1	0.6330(5)	0.2860(7)	0.4243(5)	0.057(2)
C(11)	4e	1	0.7088(5)	0.2926(6)	0.4343(5)	0.054(2)
C(12)	4e	1	0.8237(6)	0.2901(1)	0.5137(7)	0.085(3)
N(5)	4e	1	0.4829(5)	-0.0160(6)	0.2523(5)	0.063(2)
N(6)	4e	1	0.5253(5)	0.0148(6)	0.4818(5)	0.065(2)
C(13)	4e	1	0.4317(6)	-0.0440(8)	0.2965(6)	0.071(3)
C(14)	4e	1	0.4388(5)	-0.0363(7)	0.3721(6)	0.059(2)
C(15)	4e	1	0.5066(5)	0.0018(7)	0.4014(6)	0.062(2)
C(16)	4e	1	0.5623(6)	0.0318(7)	0.3581(6)	0.064(2)
C(17)	4e	1	0.5484(6)	0.0239(7)	0.2801(7)	0.068(3)
C(18)	4e	1	0.4691(8)	-0.0314(1)	0.1710(7)	0.088(4)
N(7)	4e	1	-0.0060(4)	0.0049(7)	0.7479(6)	0.070(2)
N(8)	4e	1	0.0191(5)	-0.0272(7)	0.5187(7)	0.083(3)
C(19)	4e	1	-0.0371(7)	0.0782(11)	0.7009(1)	0.099(5)
C(20)	4e	1	-0.0302(8)	0.0713(11)	0.6262(1)	0.103(5)
C(21)	4e	1	0.0092(6)	-0.0080(8)	0.5985(7)	0.073(3)
C(22)	4e	1	0.0403(6)	-0.0854(9)	0.6469(7)	0.078(3)
C(23)	4e	1	0.0317(6)	-0.0780(9)	0.7205(7)	0.078(3)
C(24)	4e	1	-0.0141(7)	0.0156(12)	0.8254(8)	0.099(4)
N(9)	4e	1	1.0003(7)	0.3385(12)	0.5048(8)	0.130(5)
C(25)	4e	1	1.1259(9)	0.4208(12)	0.5428(9)	0.112(5)
C(26)	4e	1	1.0543(8)	0.3738(12)	0.5205(8)	0.095(4)
H(10)	4e	1	0.2554	0.1893	0.6059	0.064
H(2)	4e	1	0.3800	0.2286	0.6242	0.064
H(4)	4e	1	0.3923	0.2268	0.4003	0.065
H(5)	4e	1	0.2706	0.1793	0.3902	0.063
H(6A)	4e	1	0.1482	0.1616	0.5329	0.112
H(6B)	4e	1	0.1717	0.0722	0.4776	0.112
H(6C)	4e	1	0.1496	0.1863	0.4475	0.112
H(7)	4e	1	0.7240	0.2997	0.6105	0.062
H(8)	4e	1	0.5989	0.2866	0.5997	0.065
H(10)	4e	1	0.6100	0.2855	0.3766	0.068
H(11)	4e	1	0.7375	0.2969	0.3928	0.065
H(12A)	4e	1	0.8399	0.3472	0.5466	0.127
H(12B)	4e	1	0.8460	0.2986	0.4667	0.127
H(12C)	4e	1	0.8386	0.2226	0.5354	0.127
H(13)	4e	1	0.3872	-0.0710	0.2752	0.085
H(14)	4e	1	0.4005	-0.0555	0.4022	0.071
H(16)	4e	1	0.6077	0.0564	0.3788	0.077
H(17)	4e	1	0.5843	0.0462	0.2481	0.082
H(18A)	4e	1	0.4387	-0.0938	0.1621	0.133
H(18B)	4e	1	0.5157	-0.0408	0.1482	0.133
H(18C)	4e	1	0.4439	0.0303	0.1500	0.133

Table A.27 – continued from previous page

Atom	Wyck.	Site	<i>x/a</i>	<i>y/b</i>	<i>z/c</i>	<i>U_{eq}</i>
H(19)	4e	1	-0.0638	0.1346	0.7201	0.119
H(2)	4e	1	-0.0530	0.1219	0.5945	0.123
H(22)	4e	1	0.0670	-0.1422	0.6281	0.093
H(23)	4e	1	0.0517	-0.1304	0.7525	0.093
H(24A)	4e	1	0.0326	0.0009	0.8518	0.148
H(24B)	4e	1	-0.0510	-0.0341	0.8408	0.148
H(24C)	4e	1	-0.0296	0.0873	0.8361	0.148
H(25A)	4e	1	1.1482	0.4495	0.4997	0.168
H(25B)	4e	1	1.1579	0.3668	0.5653	0.168
H(25C)	4e	1	1.1189	0.4772	0.5780	0.168

Table A.28: Anisotropic displacement parameters $U_{ij}/\text{\AA}^2$ for the independent atoms in the structure of β -(2)[Cu₂Br₄]·CH₃CN at room temperature.

Atom	<i>U₁₁</i>	<i>U₂₂</i>	<i>U₃₃</i>	<i>U₂₃</i>	<i>U₁₃</i>	<i>U₁₂</i>
Cu(1)	0.089(1)	0.065(1)	0.064(1)	0.000(1)	0.007(1)	0.000(1)
Cu(2)	0.077(1)	0.065(1)	0.066(1)	0.003(1)	0.009(1)	0.009(1)
Br(1)	0.054(1)	0.061(1)	0.061(1)	-0.003(1)	0.008(1)	0.003(1)
Br(2)	0.105(1)	0.053(1)	0.053(1)	0.000(1)	0.006(1)	0.005(1)
Br(3)	0.071(1)	0.049(1)	0.053(1)	0.001(1)	0.012(1)	0.006(1)
Br(4)	0.055(1)	0.047(1)	0.061(1)	0.003(1)	0.011(1)	0.001(1)
Cu(3)	0.085(1)	0.063(1)	0.064(1)	0.002(1)	0.013(1)	0.002(1)
Cu(4)	0.098(1)	0.063(1)	0.063(1)	0.000(1)	0.016(1)	-0.010(1)
Br(5)	0.057(1)	0.061(1)	0.055(1)	-0.001(1)	0.008(1)	-0.001(1)
Br(6)	0.088(1)	0.050(1)	0.056(1)	0.000(1)	0.021(1)	-0.003(1)
Br(7)	0.069(1)	0.049(1)	0.053(1)	-0.001(1)	0.010(1)	-0.006(1)
Br(8)	0.054(1)	0.048(1)	0.057(1)	-0.004(1)	0.008(1)	0.000(1)
N(1)	0.063(5)	0.038(3)	0.051(4)	0.004(3)	0.007(3)	-0.002(3)
N(2)	0.062(4)	0.052(4)	0.042(4)	0.002(3)	0.014(3)	-0.001(3)
N(3)	0.060(5)	0.066(5)	0.046(4)	0.002(3)	0.009(3)	-0.006(4)
N(4)	0.059(4)	0.037(3)	0.058(4)	0.006(3)	0.011(3)	0.002(3)
C(1)	0.065(6)	0.048(5)	0.049(5)	-0.006(4)	0.015(4)	0.002(4)
C(2)	0.060(6)	0.058(5)	0.043(4)	-0.006(4)	0.012(4)	0.002(4)
C(3)	0.058(5)	0.044(4)	0.043(4)	-0.002(3)	0.010(4)	0.004(4)
C(4)	0.062(6)	0.063(5)	0.038(4)	-0.005(4)	0.005(4)	-0.004(4)
C(5)	0.063(6)	0.049(5)	0.047(5)	0.006(4)	0.006(4)	-0.006(4)
C(6)	0.055(6)	0.094(8)	0.076(7)	-0.009(6)	0.013(5)	-0.009(5)
C(7)	0.063(6)	0.049(5)	0.044(4)	-0.002(3)	0.003(4)	-0.004(4)
C(8)	0.069(6)	0.051(5)	0.043(5)	-0.003(3)	0.010(4)	-0.001(4)
C(9)	0.065(6)	0.042(4)	0.045(4)	-0.003(3)	0.010(4)	0.003(4)
C(10)	0.064(6)	0.061(5)	0.046(5)	0.001(4)	0.010(4)	0.000(4)
C(11)	0.072(6)	0.039(4)	0.054(5)	0.006(3)	0.018(4)	-0.003(4)
C(12)	0.063(7)	0.099(9)	0.094(9)	0.029(7)	0.023(6)	0.001(6)
N(5)	0.060(5)	0.050(4)	0.078(6)	0.002(4)	0.009(4)	0.009(4)
N(6)	0.057(5)	0.049(4)	0.090(6)	-0.001(4)	0.009(4)	0.000(4)
C(13)	0.064(7)	0.068(6)	0.081(7)	0.012(5)	0.008(6)	-0.012(5)
C(14)	0.054(5)	0.060(5)	0.064(6)	0.013(4)	0.004(4)	-0.010(4)
C(15)	0.061(6)	0.041(5)	0.083(7)	-0.007(4)	-0.004(5)	0.001(4)
C(16)	0.063(6)	0.050(5)	0.080(7)	-0.007(4)	0.009(5)	-0.013(4)
C(17)	0.057(6)	0.053(5)	0.096(8)	-0.008(5)	0.026(5)	0.000(4)
C(18)	0.117(11)	0.082(8)	0.067(7)	-0.005(6)	0.007(7)	0.019(7)

Table A.28 – continued from previous page

Atom	Wyck.	Site	<i>x/a</i>	<i>y/b</i>	<i>z/c</i>	<i>U_{eq}</i>
N(7)	0.047(5)	0.061(5)	0.104(7)	-0.008(5)	0.002(4)	-0.002(4)
N(8)	0.061(6)	0.073(6)	0.115(9)	0.020(5)	0.006(5)	0.015(4)
C(19)	0.063(7)	0.078(8)	0.154(15)	-0.020(9)	-0.013(8)	0.022(6)
C(20)	0.098(1)	0.074(8)	0.134(13)	0.025(8)	-0.013(9)	0.024(7)
C(21)	0.055(6)	0.057(6)	0.105(9)	0.005(6)	-0.002(6)	0.000(5)
C(22)	0.068(7)	0.073(7)	0.093(8)	0.012(6)	0.015(6)	0.017(5)
C(23)	0.067(7)	0.068(6)	0.098(9)	0.005(6)	0.006(6)	0.017(5)
C(24)	0.071(8)	0.114(1)	0.112(11)	-0.040(9)	0.010(7)	0.002(7)
N(9)	0.072(8)	0.174(14)	0.144(12)	-0.029(1)	0.009(8)	0.007(9)
C(25)	0.109(12)	0.091(1)	0.137(14)	-0.001(9)	0.017(1)	-0.001(9)
C(26)	0.075(9)	0.107(1)	0.105(1)	0.026(8)	0.021(8)	0.022(8)

(2)[CuBr₃]Table A.29: Crystallographic data and structure refinement of (2)[CuBr₃] at room temperature.

Compound	(2)[CuBr ₃]
Empirical Formula	C ₁₂ H ₁₄ Br ₃ CuN ₄
Formula weight / g mol ⁻¹	517.54
Crystal size / mm ³	0.100×0.080×0.078
Temperature / K	293(2)
Crystal system; space group	Monoclinic, P2 ₁ /n
Lattice constants / Å°	<i>a</i> = 7.5848(2) <i>b</i> = 17.9230(3) β = 94.492(1) <i>c</i> = 12.6185(3)
Volume / Å ³	1710.12(7)
Z; F(000); calc. density / g cm ⁻³	4; 992; 2.010
Wavelength	Mo-K _α (0.71073 Å)
Theta range for data collection / °	3.239 ≤ θ ≤ 27.490
Limiting indices	-9 ≤ <i>h</i> ≤ 9, -23 ≤ <i>k</i> ≤ 22, -16 ≤ <i>l</i> ≤ 16
Reflections collected / unique	24059 / 3925
R _{int}	0.0858
Completeness to theta = 25.242	99.70 %
Absorption coefficient / mm ⁻¹	8.281
Refinement method	Full-matrix least-squares on <i>F</i> ²
Data / restraints / parameters	3925 / 0 / 215
R indices [I > 4σ(I)] R ₁ ; wR ₂	0.0384; 0.0941
R indices (all data) R ₁ ; wR ₂	0.0727; 0.1062
Goodness-of-fit for <i>F</i> ²	1.003
Largest diff. Peak and hole / e ⁻ Å ⁻³	0.956 / -0.770

Table A.30: Fractional coordinates in Å and equivalent isotropic displacement parameter $U_{eq}/\text{\AA}^2$ for the independent atoms in the structure of (2)[CuBr₃] at room temperature.

Atom	Wyck.	Site	x/a	y/b	z/c	U_{eq}
Cu(1)	4e	1	0.8851(1)	0.1867(1)	0.5232(1)	0.058(1)
Br(1)	4e	1	0.6944(1)	0.0995(1)	0.4287(1)	0.061(1)
Br(2)	4e	1	0.9265(1)	0.1903(1)	0.7098(1)	0.065(1)
Br(3)	4e	1	1.0416(1)	0.2737(1)	0.4257(1)	0.066(1)
N(1)	4e	1	0.5251(6)	0.0266(2)	0.0247(4)	0.070(1)
N(2)	4e	1	0.2730(4)	0.0563(2)	0.3053(3)	0.047(1)
C(1)	4e	1	0.4303(6)	0.0332(2)	0.1221(3)	0.054(1)
C(2)	4e	1	0.3720(7)	-0.0276(3)	0.1782(4)	0.059(1)
C(3)	4e	1	0.2945(6)	-0.0142(2)	0.2703(4)	0.056(1)
C(4)	4e	1	0.3314(6)	0.1148(2)	0.2501(4)	0.050(1)
C(5)	4e	1	0.4099(6)	0.1042(2)	0.1592(4)	0.054(1)
C(6)	4e	1	0.1930(7)	0.0685(3)	0.4059(4)	0.070(1)
N(3)	4e	1	-0.0372(5)	0.0073(2)	0.0391(3)	0.064(1)
N(4)	4e	1	-0.0738(5)	0.2335(2)	0.1123(3)	0.054(1)
C(7)	4e	1	-0.0458(6)	0.0873(3)	0.0602(4)	0.057(1)
C(8)	4e	1	-0.1189(6)	0.1071(3)	0.1535(4)	0.060(1)
C(9)	4e	1	-0.1298(6)	0.1809(3)	0.1781(4)	0.060(1)
C(10)	4e	1	-0.0060(6)	0.2146(3)	0.0218(4)	0.061(1)
C(11)	4e	1	0.0097(7)	0.1408(3)	-0.0073(4)	0.062(1)
C(12)	4e	1	-0.0912(7)	0.3123(3)	0.1413(4)	0.068(1)
H(6A)	4e	1	0.1669	0.1205	0.4135	0.105
H(6B)	4e	1	0.2739	0.0528	0.4640	0.105
H(6C)	4e	1	0.0857	0.0401	0.4063	0.105
H(12A)	4e	1	-0.0520	0.3432	0.0856	0.102
H(12B)	4e	1	-0.0203	0.3221	0.2062	0.102
H(12C)	4e	1	-0.2128	0.3232	0.1511	0.102
H(2)	4e	1	0.4000(7)	-0.0680(3)	0.1520(4)	0.073(16)
H(3)	4e	1	0.2500(5)	-0.0500(2)	0.3110(3)	0.046(11)
H(4)	4e	1	0.3120(5)	0.1600(2)	0.2870(3)	0.042(1)
H(5)	4e	1	0.4620(7)	0.1440(3)	0.1300(4)	0.076(16)
H(8)	4e	1	-0.1700(5)	0.0680(2)	0.2060(3)	0.043(1)
H(9)	4e	1	-0.1730(7)	0.1940(2)	0.2420(4)	0.065(14)
H(10)	4e	1	0.0410(6)	0.2510(2)	-0.0270(4)	0.057(12)
H(11)	4e	1	0.0590(6)	0.1260(2)	-0.0670(4)	0.059(13)

Table A.31: Anisotropic displacement parameters $U_{ij}/\text{\AA}^2$ for the independent atoms in the structure of (2)[CuBr₃] at room temperature.

Atom	U_{11}	U_{22}	U_{33}	U_{23}	U_{13}	U_{12}
Cu(1)	0.058(1)	0.059(1)	0.060(1)	0.001(1)	0.010(1)	0.003(1)
Br(1)	0.058(1)	0.068(1)	0.058(1)	-0.002(1)	0.004(1)	-0.008(1)
Br(2)	0.086(1)	0.057(1)	0.052(1)	0.001(1)	0.011(1)	-0.010(1)
Br(3)	0.087(1)	0.058(1)	0.052(1)	0.005(1)	0.004(1)	-0.018(1)
N(1)	0.070(3)	0.054(2)	0.083(3)	-0.003(2)	-0.005(2)	-0.006(2)
N(2)	0.047(2)	0.045(2)	0.051(2)	0.001(2)	0.005(2)	0.003(2)
C(1)	0.050(3)	0.066(3)	0.046(3)	0.002(2)	0.004(2)	0.006(2)
C(2)	0.070(3)	0.046(2)	0.060(3)	-0.010(2)	-0.002(2)	0.009(2)
C(3)	0.063(3)	0.043(2)	0.062(3)	0.005(2)	0.005(2)	-0.002(2)
C(4)	0.051(2)	0.041(2)	0.056(3)	0.001(2)	-0.002(2)	-0.001(2)

Table A.31 – continued from previous page

Atom	Wyck.	Site	x/a	y/b	z/c	U_{eq}
C(5)	0.054(3)	0.052(2)	0.057(3)	0.005(2)	0.002(2)	-0.002(2)
C(6)	0.075(3)	0.066(3)	0.071(3)	0.001(2)	0.020(3)	0.008(2)
N(3)	0.069(3)	0.072(2)	0.050(2)	0.004(2)	0.005(2)	-0.008(2)
N(4)	0.046(2)	0.071(2)	0.043(2)	0.004(2)	-0.003(2)	-0.009(2)
C(7)	0.047(2)	0.068(3)	0.052(3)	0.003(2)	-0.009(2)	-0.007(2)
C(8)	0.054(3)	0.079(3)	0.049(3)	0.004(2)	0.007(2)	-0.014(2)
C(9)	0.057(3)	0.080(3)	0.042(3)	-0.001(2)	0.003(2)	-0.017(2)
C(10)	0.056(3)	0.075(3)	0.052(3)	0.010(3)	0.001(2)	-0.007(2)
C(11)	0.063(3)	0.082(3)	0.043(3)	-0.001(2)	0.007(2)	0.000(2)
C(12)	0.070(3)	0.072(3)	0.063(3)	0.006(2)	0.008(3)	-0.001(2)

(2)[CuBr₄]Table A.32: Crystallographic data and structure refinement of (2)[CuBr₄] at room temperature.

Compound	(2)[CuBr ₄]
Empirical Formula	C ₁₂ H ₁₄ Br ₄ CuN ₄
Formula weight / g mol ⁻¹	597.45
Crystal size / mm ³	0.180×0.030×0.018
Temperature / K	293(2)
Crystal system; space group	Monoclinic, P2 ₁ /n
Lattice constants / Å°	$a = 7.3844(4)$ $b = 19.5433(18) \beta = 97.696(5)$ $c = 12.4243(11)$
Volume / Å ³	1776.9(2)
Z; F(000); calc. density / g cm ⁻³	4; 1132; 2.233
Wavelength	Mo-K _α (0.71073 Å)
Theta range for data collection	2.972 ≤ θ ≤ 27.616
Limiting indices	-8 ≤ h ≤ 8, -25 ≤ k ≤ 19, -16 ≤ l ≤ 16
Reflections collected / unique	6256 / 3693
R _{int}	0.0767
Completeness to theta = 25.242	94.70 %
Absorption coefficient / mm ⁻¹	10.221
Refinement method	Full-matrix least-squares on F ²
Data / restraints / parameters	3693 / 0 / 193
R indices [I > 4σ(I)] R ₁ ; wR ₂	0.0520; 0.1017
R indices (all data) R ₁ ; wR ₂	0.1619; 0.1313
Goodness-of-fit for F ²	0.918
Largest diff. Peak and hole / e ⁻ Å ⁻³	0.870 / -0.846

Table A.33: Fractional coordinates in Å and equivalent isotropic displacement parameter $U_{eq}/\text{\AA}^2$ for the independent atoms in the structure of (2)[CuBr₄] at room temperature.

Atom	Wyck.	Site	x/a	y/b	z/c	U_{eq}
Cu(1)	4e	1	0.5033(2)	0.1739(1)	0.4087(1)	0.044(1)
Br(1)	4e	1	0.7369(1)	0.1231(1)	0.5376(1)	0.051(1)
Br(2)	4e	1	0.4185(2)	0.2617(1)	0.5241(1)	0.079(1)
Br(3)	4e	1	0.5059(2)	0.2389(1)	0.2485(1)	0.070(1)
Br(4)	4e	1	0.3695(2)	0.0742(1)	0.3188(1)	0.059(1)
N(1)	4e	1	0.0038(9)	0.2882(4)	0.3650(6)	0.041(2)
N(2)	4e	1	0.0412(12)	0.4929(5)	0.4637(6)	0.060(2)
C(1)	4e	1	0.0669(12)	0.3374(5)	0.3044(8)	0.047(2)
C(2)	4e	1	0.0759(12)	0.4027(5)	0.3357(9)	0.047(3)
C(3)	4e	1	0.0198(12)	0.4205(5)	0.4328(8)	0.047(3)
C(4)	4e	1	-0.0465(13)	0.3703(6)	0.4936(8)	0.054(3)
C(5)	4e	1	-0.0530(13)	0.3040(5)	0.4592(8)	0.050(3)
C(6)	4e	1	0.0038(14)	0.2163(5)	0.3268(9)	0.058(3)
N(3)	4e	1	0.3316(1)	0.5368(4)	0.8242(6)	0.049(2)
N(4)	4e	1	0.4828(13)	0.4768(4)	0.5202(1)	0.077(3)
C(7)	4e	1	0.3895(13)	0.5869(6)	0.7645(9)	0.059(3)
C(8)	4e	1	0.4473(12)	0.5731(7)	0.6658(9)	0.066(3)
C(9)	4e	1	0.4359(14)	0.5046(7)	0.6309(9)	0.065(3)
C(10)	4e	1	0.3790(15)	0.4543(7)	0.6944(9)	0.066(3)
C(11)	4e	1	0.3231(14)	0.4724(6)	0.7905(9)	0.060(3)
C(12)	4e	1	0.2666(15)	0.5560(6)	0.9283(8)	0.066(3)
H(10)	4e	1	0.1055	0.3256	0.2387	0.057
H(2)	4e	1	0.1198	0.4358	0.2922	0.056
H(4)	4e	1	-0.0876	0.3815	0.5590	0.065
H(5)	4e	1	-0.0968	0.2700	0.5013	0.060
H(6A)	4e	1	-0.1034	0.2082	0.2756	0.086
H(6B)	4e	1	0.0039	0.1860	0.3876	0.086
H(6C)	4e	1	0.1108	0.2082	0.2925	0.086
H(7)	4e	1	0.3909	0.6317	0.7898	0.071
H(8)	4e	1	0.4916	0.6074	0.6244	0.079
H(10)	4e	1	0.3784	0.4088	0.6726	0.079
H(11)	4e	1	0.2783	0.4390	0.8333	0.072
H(12A)	4e	1	0.2195	0.5162	0.9603	0.099
H(12B)	4e	1	0.1718	0.5897	0.9147	0.099
H(12C)	4e	1	0.3666	0.5744	0.9770	0.099

Table A.34: Anisotropic displacement parameters $U_{ij}/\text{\AA}^2$ for the independent atoms in the structure of (2)[CuBr₄] at room temperature.

Atom	U_{11}	U_{22}	U_{33}	U_{23}	U_{13}	U_{12}
Cu(1)	0.050(1)	0.041(1)	0.040(1)	0.000(1)	0.005(1)	0.002(1)
Br(1)	0.058(1)	0.054(1)	0.042(1)	-0.001(1)	0.002(1)	0.008(1)
Br(2)	0.092(1)	0.080(1)	0.059(1)	-0.025(1)	-0.006(1)	0.037(1)
Br(3)	0.091(1)	0.065(1)	0.054(1)	0.019(1)	0.007(1)	-0.010(1)
Br(4)	0.071(1)	0.047(1)	0.057(1)	-0.008(1)	0.004(1)	-0.006(1)
N(1)	0.044(5)	0.042(5)	0.038(5)	0.004(4)	0.007(4)	-0.001(4)
N(2)	0.075(7)	0.062(6)	0.044(6)	0.006(5)	0.015(4)	0.002(5)
C(1)	0.049(6)	0.051(7)	0.042(6)	0.006(5)	0.004(5)	0.001(5)
C(2)	0.040(5)	0.040(6)	0.060(7)	0.015(5)	0.001(5)	-0.007(4)

Table A.34 – continued from previous page

Atom	Wyck.	Site	x/a	y/b	z/c	U_{eq}
C(3)	0.044(6)	0.041(6)	0.054(7)	0.002(5)	0.000(5)	0.004(5)
C(4)	0.063(7)	0.059(8)	0.045(6)	0.001(6)	0.018(5)	0.001(6)
C(5)	0.060(6)	0.049(7)	0.044(7)	0.001(5)	0.020(5)	-0.004(5)
C(6)	0.068(7)	0.045(7)	0.061(7)	-0.013(6)	0.013(6)	-0.005(5)
N(3)	0.055(5)	0.054(6)	0.039(5)	0.008(5)	0.011(4)	-0.006(4)
N(4)	0.070(6)	0.049(8)	0.112(9)	0.025(6)	0.015(6)	0.014(6)
C(7)	0.053(7)	0.053(7)	0.066(8)	-0.004(6)	-0.008(6)	0.004(5)
C(8)	0.034(6)	0.116(11)	0.044(7)	0.022(7)	-0.003(5)	-0.009(6)
C(9)	0.048(6)	0.103(11)	0.043(7)	-0.013(7)	0.005(5)	0.024(7)
C(10)	0.078(8)	0.082(9)	0.039(7)	-0.005(7)	0.008(6)	0.009(7)
C(11)	0.082(8)	0.045(7)	0.055(7)	-0.008(6)	0.014(6)	-0.008(5)
C(12)	0.089(8)	0.061(8)	0.050(7)	-0.002(6)	0.021(6)	-0.007(6)

(8)[CuBr₄]Table A.35: Crystallographic data and structure refinement of (8)[CuBr₄] at room temperature.

Compound	(8)[CuBr ₄]
Empirical Formula	C ₁₄ H ₁₂ Br ₄ CuF ₆ N ₄
Formula weight / g mol ⁻¹	733.43
Crystal size / mm ³	0.210×0.022×0.014
Temperature / K	293(2)
Crystal system; space group	Monoclinic, C2/c
Lattice constants / Å°	$a = 16.2095(7)$ $b = 9.3273(4)$ $\beta = 101.100(2)$ $c = 14.4273(6)$
Volume / Å ³	2140.47(16)
Z; F(000); calc. density / g cm ⁻³	4; 1388; 2.276
Wavelength	Mo-K α (0.71073 Å)
Theta range for data collection / °	3.031 ≤ θ ≤ 27.541
Limiting indices	-20 ≤ h ≤ 21, -12 ≤ k ≤ 12, -18 ≤ l ≤ 18
Reflections collected / unique	4398 / 2442
R _{int}	0.0616
Completeness to theta = 25.242	99.70 %
Absorption coefficient / mm ⁻¹	8.547
Refinement method	Full-matrix least-squares on F^2
Data / restraints / parameters	2442 / 0 / 156
R indices [I > 4σ(I)] R ₁ ; wR ₂	0.0425; 0.0868
R indices (all data) R ₁ ; wR ₂	0.1193; 0.1064
Goodness-of-fit for F^2	0.891
Largest diff. Peak and hole / e ⁻ Å ⁻³	0.793 / -0.622

Table A.36: Fractional coordinates in Å and equivalent isotropic displacement parameter $U_{eq}/\text{\AA}^2$ for the independent atoms in the structure of (8)[CuBr₄] at room temperature.

Atom	Wyck.	Site	x/a	y/b	z/c	U_{eq}
Cu(1)	2 <i>i</i>	1	0.5000	0.6403(1)	0.7500	0.047(1)
Br(1)	2 <i>i</i>	1	0.6138(1)	0.4775(1)	0.8011(1)	0.054(1)
Br(2)	2 <i>i</i>	1	0.4275(1)	0.7989(1)	0.8362(1)	0.063(1)
F(1)	2 <i>i</i>	1	0.8738(3)	0.4435(7)	0.5646(5)	0.136(2)
F(2)	2 <i>i</i>	1	0.8423(4)	0.5838(7)	0.6611(4)	0.134(2)
F(3)	2 <i>i</i>	1	0.7998(3)	0.6143(8)	0.5181(5)	0.167(3)
N(1)	2 <i>i</i>	1	0.5968(3)	0.2720(5)	0.5975(3)	0.040(1)
N(2)	2 <i>i</i>	1	0.5029(3)	0.4389(4)	0.5197(3)	0.035(1)
C(1)	2 <i>i</i>	1	0.5869(3)	0.4026(6)	0.5551(3)	0.035(1)
C(2)	2 <i>i</i>	1	0.6567(3)	0.4859(7)	0.5497(4)	0.040(1)
C(3)	2 <i>i</i>	1	0.7355(4)	0.4352(7)	0.5877(4)	0.046(2)
C(4)	2 <i>i</i>	1	0.7451(4)	0.3024(7)	0.6314(5)	0.056(2)
C(5)	2 <i>i</i>	1	0.6738(4)	0.2230(7)	0.6345(5)	0.053(2)
C(6)	2 <i>i</i>	1	0.5214(5)	0.1855(8)	0.6058(6)	0.052(2)
C(7)	2 <i>i</i>	1	0.8116(4)	0.5226(8)	0.5830(5)	0.062(2)
H(2)	2 <i>i</i>	1	0.6430(3)	0.5770(6)	0.5220(4)	0.043(16)
H(4)	2 <i>i</i>	1	0.8050(4)	0.2560(8)	0.6660(5)	0.080(2)
H(5)	2 <i>i</i>	1	0.6790(4)	0.1360(7)	0.6570(4)	0.060(2)
H(6A)	2 <i>i</i>	1	0.4850(4)	0.2520(7)	0.6420(4)	0.062(18)
H(6B)	2 <i>i</i>	1	0.4940(4)	0.1590(7)	0.5460(5)	0.060(2)
H(6C)	2 <i>i</i>	1	0.5430(4)	0.1030(8)	0.6370(4)	0.060(2)

Table A.37: Anisotropic displacement parameters $U_{ij}/\text{\AA}^2$ for the independent atoms in the structure of (8)[CuBr₄] at room temperature.

Atom	U_{11}	U_{22}	U_{33}	U_{23}	U_{13}	U_{12}
Cu(1)	0.060(1)	0.037(1)	0.044(1)	0.000	0.007(1)	0.000
Br(1)	0.068(1)	0.046(1)	0.048(1)	0.004(1)	0.009(1)	0.009(1)
Br(2)	0.082(1)	0.048(1)	0.059(1)	-0.012(1)	0.014(1)	0.005(1)
F(1)	0.055(3)	0.144(5)	0.221(7)	-0.054(4)	0.055(3)	-0.013(3)
F(2)	0.133(4)	0.170(6)	0.105(4)	-0.056(4)	0.041(3)	-0.101(4)
F(3)	0.061(3)	0.228(7)	0.198(6)	0.144(6)	-0.011(3)	-0.048(4)
N(1)	0.043(3)	0.038(3)	0.036(3)	-0.001(2)	0.004(2)	0.005(2)
N(2)	0.036(2)	0.031(2)	0.037(3)	0.001(2)	0.005(2)	0.002(2)
C(1)	0.043(3)	0.033(3)	0.029(3)	0.001(2)	0.007(2)	0.001(3)
C(2)	0.039(3)	0.047(4)	0.034(3)	0.002(3)	0.005(3)	0.010(3)
C(3)	0.044(4)	0.056(4)	0.038(3)	0.003(3)	0.004(3)	0.004(3)
C(4)	0.048(4)	0.059(4)	0.055(4)	-0.001(3)	-0.004(3)	0.012(4)
C(5)	0.061(5)	0.043(4)	0.049(4)	0.001(3)	-0.001(3)	0.015(4)
C(6)	0.056(4)	0.036(4)	0.061(5)	0.006(4)	0.004(4)	-0.004(3)
C(7)	0.043(4)	0.083(5)	0.058(5)	0.011(4)	-0.002(3)	0.005(4)

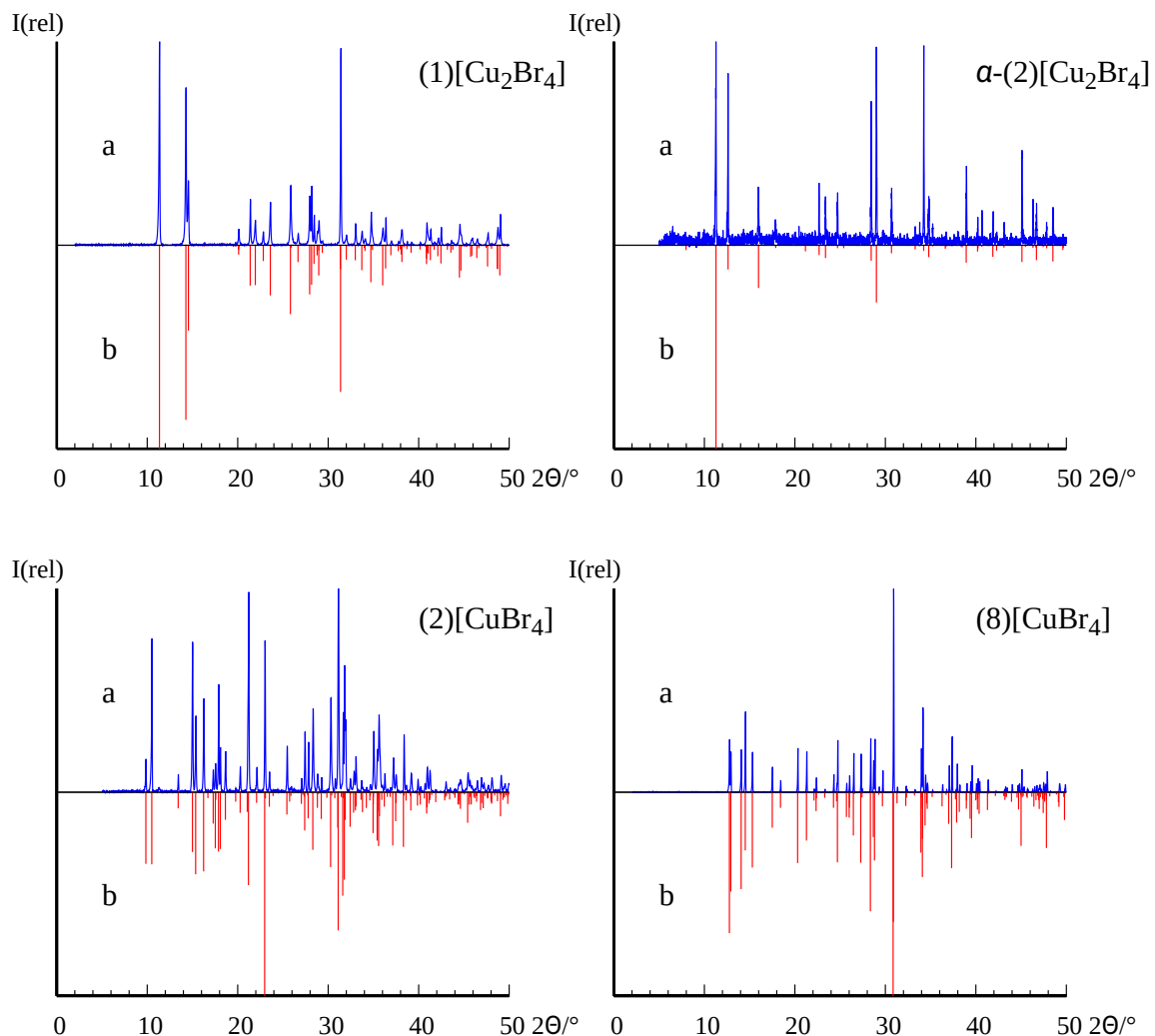


Figure A.2: X-ray powder diffraction pattern of the dication bearing compounds **(1)**[Cu₂Br₄], α -**(2)**[Cu₂Br₄], **(2)**[CuBr₄] and **(8)**[CuBr₄]. Used radiation: Co-K α_1 , a = measured diffractogram, b = simulated diffractogram on basis of single crystal data.

A.4 Charge Transfer Salts with TCNQ

α -(1)(TCNQ)

Table A.38: Crystallographic data and structure refinement of α -(1)(TCNQ) at 123 K.

Compound	α -(1)(TCNQ)
Empirical Formula	C ₁₂ H ₉ N ₄
Formula weight / g mol ⁻¹	209.23
Temperature / K	123(2)
Crystal size / mm ³	0.336×0.040×0.018
Crystal system; space group	Triclinic, $P\bar{1}$
Lattice constants / Å°	$a = 7.6012(3)$ $\alpha = 71.195(2)$ $b = 7.8192(3)$ $\beta = 76.359(2)$ $c = 9.8542(4)$ $\gamma = 72.085(2)$
Volume / Å ³	521.43(4)
Z; F(000); calc. density / g cm ⁻³	2; 218; 1.333
Wavelength	Mo-K α (0.71073 Å)
Theta range for data collection / °	3.094 ≤ θ ≤ 27.542
Limiting indices	-9 ≤ h ≤ 9, -10 ≤ k ≤ 10, -12 ≤ l ≤ 12
Reflections collected / unique	14491 / 2393
R _{int}	0.0937
Completeness to theta = 25.242	99.80 %
Absorption coefficient / mm ⁻¹	0.085
Refinement method	Full-matrix least-squares on F^2
Data / restraints / parameters	2393 / 0 / 181
R indices [I > 4σ(I)] R ₁ ; wR ₂	0.0477; 0.0936
R indices (all data) R ₁ ; wR ₂	0.0934; 0.1100
Goodness-of-fit for F^2	1.042
Largest diff. Peak and hole / e ⁻ Å ⁻³	0.201 / -0.219

Table A.39: Fractional coordinates in Å and equivalent isotropic displacement parameter U_{eq} /Å² for the independent atoms in the structure of α -(1)(TCNQ) at 123 K.

Atom	Wyck.	Site	x/a	y/b	z/c	U_{eq}
N(1)	2i	1	0.8683(2)	0.2974(2)	0.2574(2)	0.027(1)
N(2)	2i	1	0.9774(2)	0.0899(2)	0.4634(2)	0.024(1)
C(1)	2i	1	0.9197(2)	0.1136(2)	0.3368(2)	0.022(1)
C(2)	2i	1	0.9081(2)	0.9748(3)	0.2807(2)	0.025(1)
C(3)	2i	1	0.8422(3)	0.0218(3)	0.1518(2)	0.030(1)
C(4)	2i	1	0.7874(3)	0.2096(3)	0.0760(2)	0.033(1)
C(5)	2i	1	0.8013(3)	0.3433(3)	0.1302(2)	0.032(1)
C(6)	2i	1	0.8855(3)	0.4460(3)	0.3106(2)	0.036(1)
N(3)	2i	1	0.3768(2)	0.6074(2)	0.2762(2)	0.037(1)
N(4)	2i	1	0.2910(2)	0.2014(2)	0.0452(2)	0.032(1)
C(7)	2i	1	0.4380(2)	0.1509(2)	0.3849(2)	0.021(1)
C(8)	2i	1	0.4894(2)	0.1812(2)	0.4971(2)	0.021(1)
C(9)	2i	1	0.4473(2)	0.9675(2)	0.3833(2)	0.020(1)
C(10)	2i	1	0.3950(2)	0.9346(2)	0.2667(2)	0.022(1)

Table A.39 – continued from previous page

Atom	Wyck.	Site	x/a	y/b	z/c	U_{eq}
C(11)	$2i$	1	0.3863(2)	0.7543(3)	0.2712(2)	0.025(1)
C(12)	$2i$	1	0.3380(2)	0.0807(2)	0.1448(2)	0.023(1)
H(2)	$2i$	1	0.9460(3)	0.8400(3)	0.3370(2)	0.033(5)
H(3)	$2i$	1	0.8340(2)	-0.0790(3)	0.1130(2)	0.031(5)
H(4)	$2i$	1	0.7370(3)	0.2510(3)	-0.0150(2)	0.035(5)
H(5)	$2i$	1	0.7620(3)	0.4810(3)	0.0820(2)	0.033(5)
H(6A)	$2i$	1	0.8310(3)	0.5660(3)	0.2470(2)	0.045(6)
H(6B)	$2i$	1	0.8120(3)	0.4390(3)	0.4120(3)	0.055(6)
H(6C)	$2i$	1	1.0210(3)	0.4290(3)	0.3150(2)	0.043(6)
H(7)	$2i$	1	0.3950(2)	0.2560(2)	0.3019(19)	0.020(4)
H(8)	$2i$	1	0.4800(2)	0.3110(3)	0.4962(19)	0.025(5)

Table A.40: Anisotropic displacement parameters $U_{ij}/\text{\AA}^2$ for the independent atoms in the structure of α -(1)(TCNQ) at 123 K.

Atom	U_{11}	U_{22}	U_{33}	U_{23}	U_{13}	U_{12}
N(1)	0.027(1)	0.024(1)	0.024(1)	-0.003(1)	-0.004(1)	-0.004(1)
N(2)	0.024(1)	0.023(1)	0.021(1)	-0.003(1)	-0.004(1)	-0.005(1)
C(1)	0.019(1)	0.023(1)	0.021(1)	-0.003(1)	-0.003(1)	-0.003(1)
C(2)	0.023(1)	0.028(1)	0.024(1)	-0.008(1)	-0.003(1)	-0.005(1)
C(3)	0.026(1)	0.039(1)	0.026(1)	-0.013(1)	-0.003(1)	-0.007(1)
C(4)	0.031(1)	0.041(1)	0.022(1)	-0.004(1)	-0.008(1)	-0.006(1)
C(5)	0.029(1)	0.034(1)	0.023(1)	0.001(1)	-0.005(1)	-0.003(1)
C(6)	0.043(1)	0.024(1)	0.039(1)	-0.005(1)	-0.012(1)	-0.007(1)
N(3)	0.057(1)	0.025(1)	0.031(1)	-0.004(1)	-0.017(1)	-0.010(1)
N(4)	0.040(1)	0.027(1)	0.028(1)	-0.004(1)	-0.010(1)	-0.009(1)
C(7)	0.022(1)	0.017(1)	0.021(1)	-0.002(1)	-0.003(1)	-0.004(1)
C(8)	0.022(1)	0.018(1)	0.023(1)	-0.005(1)	-0.003(1)	-0.005(1)
C(9)	0.018(1)	0.020(1)	0.020(1)	-0.004(1)	-0.002(1)	-0.004(1)
C(10)	0.025(1)	0.018(1)	0.021(1)	-0.003(1)	-0.005(1)	-0.004(1)
C(11)	0.032(1)	0.025(1)	0.018(1)	-0.002(1)	-0.009(1)	-0.006(1)
C(12)	0.026(1)	0.023(1)	0.022(1)	-0.005(1)	-0.004(1)	-0.008(1)

 α -(2)(TCNQ)Table A.41: Crystallographic data and structure refinement of α -(2)(TCNQ) at room temperature.

Compound	α -(2)(TCNQ)
Empirical Formula	$C_{24}H_{18}N_4$
Formula weight / $gmol^{-1}$	418.46
Temperature / K	293(2)
Crystal size / mm^3	0.192×0.016×0.0140
Crystal system; space group	Monoclinic, $P2_1/n$
Lattice constants / \AA°	$a = 13.952(3)$ $b = 22.913(7)$ $\beta = 102.094(13)$

Table A.41 – continued from previous page

Compound	α -(2)(TCNQ)
Volume / \AA^3	$c = 6.7204(16)$
Z; F(000); calc. density / gcm^{-3}	2100.7(9)
Wavelength	4; 872; 1.323
Theta range for data collection / $^\circ$	Mo-K α (0.71073 \AA) 2.986 $\leq \theta \leq$ 23.532
Limiting indices	-14 $\leq h \leq$ 14, -23 $\leq k \leq$ 22, -7 $\leq l \leq$ 7
Reflections collected / unique	4498 / 2550
R_{int}	0.3191
Completeness to theta = 25.242	81.6 %
Absorption coefficient / mm^{-1}	0.085
Refinement method	Full-matrix least-squares on F^2
Data / restraints / parameters	2550 / 0 / 291
R indices [I > 4 σ (I)] R_1 ; wR_2	0.0778; 0.0905
R indices (all data) R_1 ; wR_2	0.4208; 0.1598
Goodness-of-fit for F^2	0.829
Largest diff. Peak and hole / $e^- \text{\AA}^{-3}$	0.190 / -0.180

Table A.42: Fractional coordinates in \AA and equivalent isotropic displacement parameter $U_{eq}/\text{\AA}^2$ for the independent atoms in the structure of α -(2)(TCNQ) at room temperature.

Atom	Wyck.	Site	x/a	y/b	z/c	U_{eq}
N(1)	4e	1	0.6834(1)	0.1897(6)	0.7070(2)	0.095(5)
N(2)	4e	1	0.7152(11)	0.1535(6)	0.5830(3)	0.112(6)
N(3)	4e	1	0.5634(1)	0.0929(7)	1.1410(2)	0.071(5)
N(4)	4e	1	0.8630(1)	0.2544(7)	0.2030(2)	0.071(5)
C(1)	4e	1	0.6436(15)	0.1526(11)	0.8430(3)	0.095(8)
C(2)	4e	1	0.5918(14)	0.1812(7)	0.9780(3)	0.090(7)
C(3)	4e	1	0.5556(11)	0.1502(9)	1.1180(2)	0.077(6)
C(4)	4e	1	0.6150(11)	0.0625(7)	1.0220(3)	0.083(6)
C(5)	4e	1	0.6504(12)	0.0928(11)	0.8700(3)	0.091(8)
C(6)	4e	1	0.5192(1)	0.0667(6)	1.3001(18)	0.085(7)
C(7)	4e	1	0.7688(13)	0.1927(1)	0.4690(3)	0.076(7)
C(8)	4e	1	0.8107(13)	0.1641(8)	0.3170(3)	0.088(7)
C(9)	4e	1	0.8515(12)	0.1939(11)	0.1930(2)	0.088(8)
C(10)	4e	1	0.8238(13)	0.2816(7)	0.3480(3)	0.094(7)
C(11)	4e	1	0.7765(11)	0.2543(9)	0.4790(2)	0.081(6)
C(12)	4e	1	0.9078(9)	0.2823(6)	0.0445(19)	0.098(7)
N(5)	4e	1	0.6400(12)	0.3108(5)	0.8240(2)	0.087(6)
N(6)	4e	1	0.8554(11)	0.4394(8)	1.0930(3)	0.089(6)
N(7)	4e	1	0.4576(12)	0.7060(6)	0.7250(3)	0.090(6)
N(8)	4e	1	0.2258(1)	0.5787(9)	0.4950(3)	0.085(6)
C(13)	4e	1	0.6144(15)	0.4622(9)	0.8560(3)	0.072(6)
C(14)	4e	1	0.6386(12)	0.5233(8)	0.8700(2)	0.064(6)
C(15)	4e	1	0.5727(13)	0.5661(6)	0.8100(2)	0.049(5)
C(16)	4e	1	0.4706(15)	0.5543(8)	0.7280(2)	0.054(5)
C(17)	4e	1	0.4495(11)	0.4936(9)	0.7140(2)	0.059(5)
C(18)	4e	1	0.5160(15)	0.4508(7)	0.7780(2)	0.057(6)
C(19)	4e	1	0.6799(13)	0.4178(9)	0.9220(3)	0.064(6)
C(20)	4e	1	0.6562(14)	0.3573(7)	0.8700(3)	0.065(6)

Table A.42 – continued from previous page

Atom	Wyck.	Site	x/a	y/b	z/c	U_{eq}
C(21)	4e	1	0.7798(15)	0.4280(8)	1.0150(3)	0.068(6)
C(22)	4e	1	0.4021(14)	0.6005(9)	0.6700(3)	0.069(6)
C(23)	4e	1	0.4334(14)	0.6612(8)	0.7020(3)	0.077(7)
C(24)	4e	1	0.3033(15)	0.5864(1)	0.5700(3)	0.066(7)
H(2)	4e	1	0.5830	0.2214	0.9702	0.108
H(3)	4e	1	0.5230	0.1706	1.2034	0.093
H(4)	4e	1	0.6263	0.0227	1.0418	0.099
H(5)	4e	1	0.6802	0.0713	0.7824	0.110
H(6A)	4e	1	0.5497	0.0828	1.4300	0.127
H(6B)	4e	1	0.5289	0.0252	1.3020	0.127
H(6C)	4e	1	0.4503	0.0751	1.2726	0.127
H(8)	4e	1	0.8087	0.1236	0.3078	0.105
H(9)	4e	1	0.8742	0.1739	0.0916	0.106
H(10)	4e	1	0.8299	0.3220	0.3581	0.113
H(11)	4e	1	0.7498	0.2754	0.5721	0.097
H(12A)	4e	1	0.8571	0.2936	-0.0687	0.148
H(12B)	4e	1	0.9510	0.2551	-0.0006	0.148
H(12C)	4e	1	0.9442	0.3161	0.1006	0.148
H(14)	4e	1	0.7032	0.5339	0.9242	0.076
H(15)	4e	1	0.5938	0.6047	0.8215	0.059
H(17)	4e	1	0.3855	0.4824	0.6576	0.071
H(18)	4e	1	0.4948	0.4122	0.7686	0.069

Table A.43: Anisotropic displacement parameters $U_{ij}/\text{\AA}^2$ for the independent atoms in the structure of α -(2)(TCNQ) at room temperature.

Atom	U_{11}	U_{22}	U_{33}	U_{23}	U_{13}	U_{12}
N(1)	0.087(13)	0.120(14)	0.077(12)	-0.022(12)	0.017(1)	0.005(12)
N(2)	0.092(14)	0.104(13)	0.143(16)	-0.024(12)	0.031(12)	0.027(11)
N(3)	0.070(12)	0.065(11)	0.081(12)	-0.011(11)	0.020(9)	-0.019(11)
N(4)	0.062(11)	0.071(11)	0.077(13)	0.016(1)	0.008(9)	0.016(1)
C(1)	0.064(17)	0.110(2)	0.090(2)	0.024(17)	-0.029(14)	-0.037(17)
C(2)	0.111(19)	0.040(12)	0.118(19)	0.010(13)	0.019(15)	0.019(13)
C(3)	0.075(15)	0.079(17)	0.083(16)	-0.005(13)	0.027(13)	-0.020(14)
C(4)	0.055(15)	0.059(13)	0.126(18)	-0.029(15)	-0.002(13)	0.020(12)
C(5)	0.079(15)	0.150(2)	0.059(14)	-0.034(16)	0.038(13)	-0.017(17)
C(6)	0.115(17)	0.095(14)	0.055(12)	0.011(11)	0.040(13)	-0.007(12)
C(7)	0.041(13)	0.087(18)	0.084(19)	0.041(16)	-0.026(12)	-0.002(14)
C(8)	0.088(17)	0.107(17)	0.060(14)	-0.002(15)	-0.005(12)	0.026(15)
C(9)	0.061(14)	0.150(2)	0.062(15)	0.043(16)	0.028(12)	0.039(16)
C(10)	0.110(17)	0.085(14)	0.091(15)	-0.038(13)	0.032(13)	0.029(13)
C(11)	0.055(13)	0.123(19)	0.075(15)	0.007(15)	0.037(11)	0.017(14)
C(12)	0.111(16)	0.109(14)	0.093(15)	0.023(12)	0.061(14)	-0.007(13)
N(5)	0.141(15)	0.055(1)	0.074(12)	0.009(1)	0.041(11)	-0.006(12)
N(6)	0.089(15)	0.108(15)	0.077(14)	-0.034(1)	0.032(12)	-0.029(13)
N(7)	0.096(14)	0.067(11)	0.114(14)	0.009(12)	0.039(11)	-0.028(11)
N(8)	0.071(13)	0.100(13)	0.087(15)	-0.007(11)	0.023(12)	0.007(14)
C(13)	0.049(17)	0.100(2)	0.072(15)	0.002(14)	0.024(13)	-0.019(14)
C(14)	0.074(16)	0.058(13)	0.068(13)	-0.012(12)	0.036(13)	-0.030(13)
C(15)	0.048(14)	0.051(13)	0.047(12)	0.003(11)	0.006(1)	-0.011(12)
C(16)	0.075(18)	0.053(15)	0.042(12)	-0.017(11)	0.029(13)	-0.021(13)

Table A.43 – continued from previous page

Atom	Wyck.	Site	x/a	y/b	z/c	U_{eq}
C(17)	0.041(13)	0.085(14)	0.056(12)	-0.024(13)	0.023(1)	-0.040(13)
C(18)	0.082(18)	0.053(13)	0.045(13)	-0.007(11)	0.033(13)	0.011(14)
C(19)	0.041(15)	0.102(18)	0.047(12)	0.014(14)	0.003(11)	0.010(16)
C(20)	0.078(16)	0.058(14)	0.066(15)	0.018(14)	0.028(12)	-0.017(14)
C(21)	0.076(18)	0.052(13)	0.079(18)	-0.001(13)	0.025(16)	0.004(17)
C(22)	0.080(17)	0.075(15)	0.060(15)	-0.001(13)	0.036(13)	-0.012(16)
C(23)	0.086(17)	0.084(17)	0.068(15)	0.013(16)	0.032(13)	-0.023(16)
C(24)	0.101(19)	0.066(15)	0.038(15)	0.001(13)	0.034(16)	0.020(2)

 β -(2)(TCNQ)Table A.44: Crystallographic data and structure refinement of β -(2)(TCNQ) at room temperature.

Compound	β -(2)(TCNQ)
Empirical Formula	$C_{24}H_{18}N_8$
Formula weight / $gmol^{-1}$	418.46
Temperature	293(2)
Crystal size / mm^3	0.390×0.130×0.076
Crystal system; space group	Orthorhombic, $Ccca$
Lattice constants / \AA	$a = 13.0289(3)$ $b = 13.3983(4)$ $c = 24.4860(5)$
Volume / \AA^3	4274.40(18)
Z; F(000); calc. density / gcm^{-3}	8; 1744; 1.301
Wavelength	Mo-K α (0.71073 \AA)
Theta range for data collection / $^\circ$	1.663 $\leq \theta \leq$ 27.578
Limiting indices	-16 $\leq h \leq$ 17, -17 $\leq k \leq$ 17, -31 $\leq l \leq$ 31
Reflections collected / unique	4686 / 2478
R_{int}	0.0254
Completeness to theta = 25.242	99.80 %
Absorption coefficient / mm^{-1}	0.083
Refinement method	Full-matrix least-squares on F^2
Data / restraints / parameters	2478 / 36 / 193
R indices [I > 4 σ (I)] R_1 ; wR_2	0.0388; 0.1151
R indices (all data) R_1 ; wR_2	0.0741; 0.1419
Goodness-of-fit for F^2	1.070
Largest diff. Peak and hole / $e^{-\text{\AA}^{-3}}$	0.144 / -0.182

Table A.45: Fractional coordinates in Å and equivalent isotropic displacement parameter $U_{eq}/\text{\AA}^2$ for the independent atoms in the structure of β -(2)(TCNQ) at room temperature.

Atom	Wyck.	Site	x/a	y/b	z/c	U_{eq}
N(1)	$16i$	1	0.3816(1)	0.8556(1)	0.4230(1)	0.048(1)
N(2)	$16i$	1	0.3656(1)	0.7197(1)	0.2713(1)	0.043(1)
C(1)	$16i$	1	0.3703(1)	0.7700(1)	0.3199(1)	0.041(1)
C(2)	$16i$	1	0.3837(1)	0.8733(1)	0.3268(1)	0.048(1)
C(3)	$16i$	1	0.3888(1)	0.9134(1)	0.3776(1)	0.051(1)
C(4)	$16i$	1	0.3706(1)	0.7561(1)	0.4178(1)	0.046(1)
C(5)	$16i$	1	0.3645(1)	0.7121(1)	0.3680(1)	0.043(1)
C(6)	$16i$	1	0.3872(2)	0.9014(2)	0.4777(1)	0.066(1)
N(3)	$16i$	1	0.1113(1)	0.5258(2)	0.3987(1)	0.076(1)
N(4)	$16i$	1	0.1281(1)	0.8390(1)	0.4377(1)	0.060(1)
C(7)	$16i$	1	0.1347(1)	0.7276(1)	0.3067(1)	0.043(1)
C(8)	$16i$	1	0.1376(1)	0.6509(1)	0.2664(1)	0.047(1)
C(9)	$16i$	1	0.1363(1)	0.6732(1)	0.2123(1)	0.047(1)
C(10)	$16i$	1	0.1288(1)	0.7043(1)	0.3632(1)	0.044(1)
C(11)	$16i$	1	0.1201(1)	0.6058(2)	0.3824(1)	0.051(1)
C(12)	$16i$	1	0.1278(1)	0.7795(1)	0.4040(1)	0.045(1)
H(2)	$16i$	1	0.3883(11)	0.9163(14)	0.2958(7)	0.048(4)
H(3)	$16i$	1	0.3972(12)	0.9839(16)	0.3848(7)	0.062(5)
H(4)	$16i$	1	0.3630(11)	0.7191(14)	0.4533(7)	0.051(5)
H(5)	$16i$	1	0.3551(11)	0.6398(14)	0.3650(7)	0.049(5)
H(6A)	$16i$	0.5	0.4490(15)	0.8730(18)	0.4963(1)	0.025(6)
H(6B)	$16i$	0.5	0.3900(2)	0.9754(13)	0.4728(11)	0.034(8)
H(6C)	$16i$	0.5	0.3205(15)	0.8810(2)	0.4973(11)	0.042(8)
H(6D)	$16i$	0.5	0.3830(2)	0.8490(3)	0.5071(15)	0.107(19)
H(6E)	$16i$	0.5	0.4510(16)	0.9369(19)	0.4790(15)	0.094(15)
H(6F)	$16i$	0.5	0.3268(18)	0.9460(2)	0.4830(16)	0.097(15)
H(8)	$16i$	1	0.1393(11)	0.5813(17)	0.2782(7)	0.058(5)
H(9)	$16i$	1	0.1395(11)	0.6210(16)	0.1850(8)	0.060(5)

Table A.46: Anisotropic displacement parameters $U_{ij}/\text{\AA}^2$ for the independent atoms in the structure of β -(2)(TCNQ) at room temperature.

Atom	U_{11}	U_{22}	U_{33}	U_{23}	U_{13}	U_{12}
N(1)	0.053(1)	0.046(1)	0.044(1)	-0.002(1)	-0.009(1)	-0.003(1)
N(2)	0.043(1)	0.043(1)	0.044(1)	-0.001(1)	0.000(1)	0.001(1)
C(1)	0.035(1)	0.042(1)	0.045(1)	-0.001(1)	-0.004(1)	-0.001(1)
C(2)	0.059(1)	0.040(1)	0.046(1)	0.005(1)	-0.006(1)	-0.005(1)
C(3)	0.065(1)	0.037(1)	0.051(1)	-0.002(1)	-0.011(1)	-0.006(1)
C(4)	0.045(1)	0.045(1)	0.047(1)	0.005(1)	-0.006(1)	-0.001(1)
C(5)	0.042(1)	0.038(1)	0.048(1)	0.002(1)	-0.004(1)	0.000(1)
C(6)	0.088(2)	0.061(1)	0.048(1)	-0.009(1)	-0.016(1)	-0.005(1)
N(3)	0.104(1)	0.053(1)	0.071(1)	-0.011(1)	0.015(1)	-0.012(1)
N(4)	0.075(1)	0.056(1)	0.049(1)	-0.013(1)	-0.001(1)	0.005(1)
C(7)	0.034(1)	0.052(1)	0.042(1)	-0.010(1)	0.000(1)	-0.002(1)
C(8)	0.049(1)	0.048(1)	0.044(1)	-0.011(1)	0.002(1)	-0.006(1)
C(9)	0.048(1)	0.050(1)	0.044(1)	-0.015(1)	0.002(1)	-0.005(1)
C(10)	0.042(1)	0.047(1)	0.043(1)	-0.009(1)	0.003(1)	-0.003(1)
C(11)	0.057(1)	0.051(1)	0.046(1)	-0.013(1)	0.006(1)	-0.007(1)
C(12)	0.045(1)	0.048(1)	0.041(1)	-0.004(1)	0.001(1)	0.001(1)

Table A.47: Crystallographic data and structure refinement of β -(2)(TCNQ) at 123 K.

Compound	β -(2)(TCNQ)
Empirical Formula	C ₂₄ H ₁₈ N ₈
Formula weight / g mol ⁻¹	418.46
Temperature	123(2)
Crystal size / mm ³	0.390×0.130×0.076
Crystal system; space group	Orthorhombic, Ccc _a
Lattice constants / Å	$a = 12.7838(4)$ $b = 13.3622(5)$ $c = 24.3011(6)$
Volume / Å ³	4151.1(2)
Z; F(000); calc. density / g cm ⁻³	8; 1744; 1.339
Wavelength	Mo-K α (0.71073 Å)
Theta range for data collection / °	1.676 ≤ θ ≤ 30.088
Limiting indices	-17 ≤ h ≤ 18, -18 ≤ k ≤ 18, -34 ≤ l ≤ 34
Reflections collected / unique	5621 / 3026
R _{int}	0.0357
Completeness to theta = 25.242	99.30 %
Absorption coefficient / mm ⁻¹	0.086
Refinement method	Full-matrix least-squares on F^2
Data / restraints / parameters	3026 / 0 / 182
R indices [I > 4σ(I)] R ₁ ; wR ₂	0.0443; 0.1177
R indices (all data) R ₁ ; wR ₂	0.0756; 0.1406
Goodness-of-fit for F^2	1.061
Largest diff. Peak and hole / e ⁻ Å ⁻³	0.299 / -0.240

Table A.48: Fractional coordinates in Å and equivalent isotropic displacement parameter U_{eq} /Å² for the independent atoms in the structure of β -(2)(TCNQ) at 123 K.

Atom	Wyck.	Site	x/a	y/b	z/c	U_{eq}
N(1)	16 <i>i</i>	1	0.3813(1)	0.1421(1)	0.5762(1)	0.023(1)
N(2)	16 <i>i</i>	1	0.3662(1)	0.2799(1)	0.7285(1)	0.022(1)
C(1)	16 <i>i</i>	1	0.3709(1)	0.2290(1)	0.6797(1)	0.021(1)
C(2)	16 <i>i</i>	1	0.3843(1)	0.1246(1)	0.6732(1)	0.024(1)
C(3)	16 <i>i</i>	1	0.3886(1)	0.0843(1)	0.6219(1)	0.024(1)
C(4)	16 <i>i</i>	1	0.3708(1)	0.2425(1)	0.5810(1)	0.023(1)
C(5)	16 <i>i</i>	1	0.3649(1)	0.2872(1)	0.6313(1)	0.022(1)
C(6)	16 <i>i</i>	1	0.3864(1)	0.0963(1)	0.5211(1)	0.031(1)
N(3)	16 <i>i</i>	1	0.1268(1)	0.1618(1)	0.5607(1)	0.028(1)
N(4)	16 <i>i</i>	1	0.1110(1)	0.4768(1)	0.6008(1)	0.035(1)
C(7)	16 <i>i</i>	1	0.1349(1)	0.2731(1)	0.6929(1)	0.022(1)
C(8)	16 <i>i</i>	1	0.1367(1)	0.1728(1)	0.7116(1)	0.024(1)
C(9)	16 <i>i</i>	1	0.1384(1)	0.1504(1)	0.7663(1)	0.024(1)
C(10)	16 <i>i</i>	1	0.1287(1)	0.2967(1)	0.6361(1)	0.022(1)
C(11)	16 <i>i</i>	1	0.1270(1)	0.2218(1)	0.5949(1)	0.023(1)
C(12)	16 <i>i</i>	1	0.1197(1)	0.3964(1)	0.6172(1)	0.025(1)

Table A.48 – continued from previous page

Atom	Wyck.	Site	x/a	y/b	z/c	U_{eq}
H(2)	16 <i>i</i>	1	0.3890(1)	0.0793(12)	0.7065(7)	0.022(4)
H(3)	16 <i>i</i>	1	0.3964(11)	0.0133(14)	0.6155(7)	0.031(4)
H(4)	16 <i>i</i>	1	0.3643(11)	0.2789(13)	0.5456(7)	0.030(4)
H(5)	16 <i>i</i>	1	0.3559(12)	0.3606(14)	0.6342(7)	0.030(4)
H(6B)	16 <i>i</i>	1	0.4454(13)	0.1246(13)	0.5020(7)	0.039(4)
H(6A)	16 <i>i</i>	1	0.3187(15)	0.1177(14)	0.5002(8)	0.050(5)
H(6C)	16 <i>i</i>	1	0.3885(15)	0.0275(17)	0.5247(8)	0.053(6)
H(8)	16 <i>i</i>	1	0.1388(1)	0.1221(13)	0.6827(7)	0.026(4)
H(9)	16 <i>i</i>	1	0.1404(1)	0.0793(14)	0.7786(6)	0.026(4)

Table A.49: Anisotropic displacement parameters $U_{ij}/\text{\AA}^2$ for the independent atoms in the structure of β -(2)(TCNQ) at 123 K.

Atom	U_{11}	U_{22}	U_{33}	U_{23}	U_{13}	U_{12}
N(1)	0.025(1)	0.021(1)	0.022(1)	-0.001(1)	0.003(1)	0.000(1)
N(2)	0.022(1)	0.021(1)	0.023(1)	-0.001(1)	0.001(1)	-0.001(1)
C(1)	0.018(1)	0.022(1)	0.024(1)	0.000(1)	0.002(1)	-0.001(1)
C(2)	0.026(1)	0.022(1)	0.024(1)	0.001(1)	0.003(1)	0.002(1)
C(3)	0.029(1)	0.019(1)	0.026(1)	0.000(1)	0.005(1)	0.002(1)
C(4)	0.022(1)	0.021(1)	0.026(1)	0.003(1)	0.002(1)	0.000(1)
C(5)	0.020(1)	0.020(1)	0.025(1)	0.001(1)	0.001(1)	0.000(1)
C(6)	0.041(1)	0.028(1)	0.023(1)	-0.003(1)	0.005(1)	0.002(1)
N(3)	0.033(1)	0.026(1)	0.025(1)	-0.004(1)	0.001(1)	-0.002(1)
N(4)	0.045(1)	0.026(1)	0.034(1)	-0.006(1)	-0.005(1)	0.003(1)
C(7)	0.019(1)	0.026(1)	0.022(1)	-0.004(1)	0.000(1)	0.001(1)
C(8)	0.024(1)	0.025(1)	0.023(1)	-0.006(1)	0.001(1)	-0.002(1)
C(9)	0.024(1)	0.024(1)	0.024(1)	-0.004(1)	0.001(1)	-0.002(1)
C(10)	0.022(1)	0.024(1)	0.022(1)	-0.004(1)	0.000(1)	0.002(1)
C(11)	0.022(1)	0.024(1)	0.022(1)	-0.001(1)	0.000(1)	0.000(1)
C(12)	0.026(1)	0.026(1)	0.023(1)	-0.006(1)	-0.001(1)	0.002(1)

(3)(TCNQ)

Table A.50: Crystallographic data and structure refinement of (3)(TCNQ) at room temperature.

Compound	(3)(TCNQ)
Empirical Formula	$\text{C}_{32}\text{H}_{34}\text{N}_8$
Formula weight / $gmol^{-1}$	530.67
Temperature / K	293(2)
Crystal size / mm^3	0.256×0.130×0.046
Crystal system; space group	Monoclinic, $P2_1/c$
Lattice constants / \AA or $^\circ$	$a = 22.1408(8)$ $b = 7.0610(2)$ $\beta = 109.2240(1)$ $c = 20.5201(8)$

Table A.50 – continued from previous page

Compound	(3)(TCNQ)
Volume / \AA^3	3029.15(18)
Z; F(000); calc. density / gcm^{-3}	4; 1128; 1.164
Wavelength	Mo-K α (0.71073 \AA)
Theta range for data collection / $^\circ$	2.923 $\leq \theta \leq$ 25.723
Limiting indices	-27 $\leq h \leq$ 26, -8 $\leq k \leq$ 8, -25 $\leq l \leq$ 25
Reflections collected / unique	25029 / 5760
R _{int}	0.0975
Completeness to theta = 25.242	99.90 %
Absorption coefficient / mm^{-1}	0.072
Refinement method	Full-matrix least-squares on F^2
Data / restraints / parameters	5760 / 0 / 498
R indices [I > 4 σ (I)] R ₁ ; wR ₂	0.0489; 0.1199
R indices (all data) R ₁ ; wR ₂	0.1188; 0.1406
Goodness-of-fit for F^2	0.943
Largest diff. Peak and hole / $e^- \text{\AA}^{-3}$	0.204 / -0.167

Table A.51: Fractional coordinates in \AA and equivalent isotropic displacement parameter $U_{eq}/\text{\AA}^2$ for the independent atoms in the structure of (3)(TCNQ) at room temperature.

Atom	Wyck.	Site	x/a	y/b	z/c	U_{eq}
N(1)	4e	1	0.1016(1)	0.6634(2)	0.5150(1)	0.048(1)
N(2)	4e	1	0.2057(1)	0.5711(2)	0.5366(1)	0.048(1)
N(3)	4e	1	0.2590(1)	0.5115(2)	0.5849(1)	0.048(1)
N(4)	4e	1	0.3611(1)	0.4009(2)	0.6046(1)	0.045(1)
C(1)	4e	1	0.1578(1)	0.6030(2)	0.5628(1)	0.044(1)
C(2)	4e	1	0.1592(1)	0.5786(3)	0.6308(1)	0.049(1)
C(3)	4e	1	0.1076(1)	0.6125(3)	0.6516(1)	0.052(1)
C(4)	4e	1	0.0515(1)	0.6743(3)	0.6004(1)	0.058(1)
C(5)	4e	1	0.0497(1)	0.6959(3)	0.5346(1)	0.055(1)
C(6)	4e	1	0.0967(1)	0.6859(4)	0.4421(1)	0.059(1)
C(7)	4e	1	0.1092(1)	0.5938(4)	0.7260(1)	0.070(1)
C(8)	4e	1	0.1687(2)	0.4916(8)	0.7701(2)	0.118(1)
C(9)	4e	1	0.0494(2)	0.4913(7)	0.7288(2)	0.107(1)
C(10)	4e	1	0.1092(2)	0.7991(6)	0.7542(2)	0.117(1)
C(11)	4e	1	0.3051(1)	0.4632(2)	0.5574(1)	0.044(1)
C(12)	4e	1	0.3002(1)	0.4662(3)	0.4878(1)	0.051(1)
C(13)	4e	1	0.3491(1)	0.4077(3)	0.4653(1)	0.055(1)
C(14)	4e	1	0.4058(1)	0.3443(3)	0.5162(1)	0.056(1)
C(15)	4e	1	0.4101(1)	0.3426(3)	0.5831(1)	0.052(1)
C(16)	4e	1	0.3673(1)	0.3858(4)	0.6778(1)	0.058(1)
C(17)	4e	1	0.3444(1)	0.4073(4)	0.3899(1)	0.083(1)
C(18)	4e	1	0.3526(2)	0.1999(7)	0.3690(2)	0.123(1)
C(19)	4e	1	0.3981(2)	0.5291(8)	0.3815(2)	0.123(1)
C(20)	4e	1	0.2791(2)	0.4786(8)	0.3433(2)	0.121(2)
N(5)	4e	1	0.0807(1)	1.1351(3)	0.6077(1)	0.087(1)
N(6)	4e	1	0.1039(1)	1.2056(3)	0.4084(1)	0.091(1)
N(7)	4e	1	0.4679(1)	0.7773(3)	0.7627(1)	0.097(1)
N(8)	4e	1	0.4731(1)	0.8084(4)	0.5508(2)	0.111(1)
C(21)	4e	1	0.2162(1)	1.0243(2)	0.5590(1)	0.051(1)

Table A.51 – continued from previous page

Atom	Wyck.	Site	<i>x/a</i>	<i>y/b</i>	<i>z/c</i>	<i>U_{eq}</i>
C(22)	4e	1	0.2453(1)	0.9749(3)	0.6285(1)	0.054(1)
C(23)	4e	1	0.3069(1)	0.9106(3)	0.6528(1)	0.054(1)
C(24)	4e	1	0.3445(1)	0.8940(2)	0.6091(1)	0.051(1)
C(25)	4e	1	0.3145(1)	0.9372(3)	0.5391(1)	0.057(1)
C(26)	4e	1	0.2526(1)	0.9995(3)	0.5147(1)	0.058(1)
C(27)	4e	1	0.1531(1)	1.0991(3)	0.5340(1)	0.058(1)
C(28)	4e	1	0.1144(1)	1.1196(3)	0.5757(1)	0.064(1)
C(29)	4e	1	0.1260(1)	1.1583(3)	0.4650(2)	0.067(1)
C(30)	4e	1	0.4098(1)	0.8415(3)	0.6343(1)	0.058(1)
C(31)	4e	1	0.4423(1)	0.8078(3)	0.7048(2)	0.069(1)
C(32)	4e	1	0.4455(1)	0.8241(3)	0.5889(2)	0.073(1)
H(2)	4e	1	0.1982(1)	0.5390(2)	0.6616(11)	0.053(5)
H(4)	4e	1	0.0138(11)	0.7040(3)	0.6106(11)	0.073(7)
H(5)	4e	1	0.0122(1)	0.7400(3)	0.4954(11)	0.062(6)
H(6A)	4e	1	0.1017(12)	0.5620(4)	0.4221(14)	0.107(9)
H(6B)	4e	1	0.1337(11)	0.7630(3)	0.4366(11)	0.074(6)
H(6C)	4e	1	0.0558(12)	0.7480(3)	0.4195(11)	0.074(6)
H(8A)	4e	1	0.2128(17)	0.5710(4)	0.7722(17)	0.139(12)
H(8B)	4e	1	0.1671(16)	0.4910(4)	0.8150(2)	0.130(12)
H(8C)	4e	1	0.1674(15)	0.3560(4)	0.7481(17)	0.120(12)
H(9A)	4e	1	0.0583(17)	0.3510(5)	0.7167(19)	0.147(15)
H(9B)	4e	1	0.0085(19)	0.5570(5)	0.7010(2)	0.159(14)
H(9C)	4e	1	0.0530(14)	0.4840(4)	0.7796(17)	0.115(1)
H(10A)	4e	1	0.0720(2)	0.8610(5)	0.7240(2)	0.168(18)
H(10B)	4e	1	0.1530(3)	0.8590(7)	0.7530(3)	0.240(2)
H(10C)	4e	1	0.1087(19)	0.7770(5)	0.8050(2)	0.174(15)
H(12)	4e	1	0.2595(1)	0.5100(2)	0.4569(11)	0.059(6)
H(14)	4e	1	0.4436(11)	0.2990(3)	0.5034(11)	0.068(6)
H(15)	4e	1	0.4477(11)	0.3050(3)	0.6219(11)	0.062(6)
H(16A)	4e	1	0.3370(13)	0.3030(4)	0.6851(13)	0.099(9)
H(16B)	4e	1	0.4120(15)	0.3420(4)	0.7017(14)	0.106(9)
H(16C)	4e	1	0.3581(11)	0.5090(3)	0.6967(13)	0.086(7)
H(18A)	4e	1	0.3520(2)	0.2110(5)	0.3150(2)	0.180(16)
H(18B)	4e	1	0.3990(2)	0.1530(6)	0.3970(2)	0.189(18)
H(18C)	4e	1	0.3110(2)	0.1240(6)	0.3740(2)	0.191(18)
H(19A)	4e	1	0.3989(19)	0.4860(6)	0.3330(2)	0.178(17)
H(19B)	4e	1	0.4394(18)	0.4870(4)	0.4081(18)	0.126(12)
H(19C)	4e	1	0.3905(18)	0.6850(6)	0.3950(2)	0.171(17)
H(20A)	4e	1	0.2396(19)	0.4000(5)	0.3482(19)	0.157(14)
H(20B)	4e	1	0.2770(15)	0.4760(4)	0.2900(2)	0.140(12)
H(20C)	4e	1	0.2865(15)	0.6380(5)	0.3529(17)	0.129(13)
H(22)	4e	1	0.2214(9)	0.9890(2)	0.6614(11)	0.057(6)
H(23)	4e	1	0.3256(9)	0.8790(3)	0.7024(11)	0.060(6)
H(25)	4e	1	0.3351(1)	0.9250(3)	0.5051(11)	0.064(6)
H(26)	4e	1	0.2359(1)	1.0300(3)	0.4656(13)	0.066(6)

Table A.52: Anisotropic displacement parameters $U_{ij}/\text{\AA}^2$ for the independent atoms in the structure of (3)(TCNQ) at room temperature.

Atom	U_{11}	U_{22}	U_{33}	U_{23}	U_{13}	U_{12}
N(1)	0.037(1)	0.054(1)	0.050(1)	0.000(1)	0.009(1)	0.002(1)
N(2)	0.037(1)	0.053(1)	0.050(1)	-0.002(1)	0.011(1)	0.002(1)
N(3)	0.036(1)	0.053(1)	0.054(1)	-0.002(1)	0.014(1)	0.002(1)
N(4)	0.038(1)	0.051(1)	0.045(1)	-0.002(1)	0.011(1)	0.002(1)
C(1)	0.033(1)	0.048(1)	0.050(1)	-0.001(1)	0.010(1)	0.000(1)
C(2)	0.035(1)	0.058(1)	0.051(2)	0.001(1)	0.010(1)	0.000(1)
C(3)	0.038(1)	0.062(1)	0.057(2)	-0.004(1)	0.015(1)	-0.003(1)
C(4)	0.036(1)	0.071(1)	0.068(2)	-0.002(1)	0.019(1)	0.003(1)
C(5)	0.036(1)	0.061(1)	0.064(2)	0.000(1)	0.009(1)	0.004(1)
C(6)	0.051(1)	0.070(2)	0.049(2)	0.002(1)	0.007(1)	0.006(1)
C(7)	0.052(1)	0.108(2)	0.055(2)	-0.003(1)	0.024(1)	0.002(1)
C(8)	0.091(3)	0.206(5)	0.061(2)	0.036(3)	0.030(2)	0.036(3)
C(9)	0.081(2)	0.168(4)	0.082(3)	0.023(2)	0.041(2)	-0.017(2)
C(10)	0.122(3)	0.149(3)	0.082(3)	-0.035(2)	0.036(3)	-0.006(3)
C(11)	0.035(1)	0.048(1)	0.046(1)	-0.001(1)	0.011(1)	0.001(1)
C(12)	0.038(1)	0.064(1)	0.049(1)	0.001(1)	0.011(1)	0.005(1)
C(13)	0.045(1)	0.070(1)	0.051(1)	-0.002(1)	0.017(1)	0.002(1)
C(14)	0.040(1)	0.073(1)	0.058(2)	-0.005(1)	0.019(1)	0.006(1)
C(15)	0.037(1)	0.059(1)	0.057(2)	-0.003(1)	0.012(1)	0.005(1)
C(16)	0.050(1)	0.071(2)	0.049(2)	0.001(1)	0.012(1)	0.003(1)
C(17)	0.060(2)	0.137(2)	0.054(2)	0.004(2)	0.023(1)	0.014(1)
C(18)	0.108(3)	0.180(4)	0.084(3)	-0.047(2)	0.036(2)	0.013(3)
C(19)	0.089(3)	0.198(5)	0.094(3)	0.045(3)	0.046(2)	0.005(3)
C(20)	0.082(2)	0.229(5)	0.050(2)	0.025(2)	0.017(2)	0.030(3)
N(5)	0.070(1)	0.084(1)	0.108(2)	-0.007(1)	0.032(1)	0.016(1)
N(6)	0.084(2)	0.087(2)	0.088(2)	0.002(1)	0.009(1)	0.027(1)
N(7)	0.058(1)	0.127(2)	0.087(2)	-0.011(1)	-0.001(1)	0.003(1)
N(8)	0.076(2)	0.142(2)	0.131(2)	0.005(2)	0.056(2)	0.019(1)
C(21)	0.044(1)	0.043(1)	0.065(2)	-0.002(1)	0.013(1)	0.001(1)
C(22)	0.045(1)	0.052(1)	0.063(2)	-0.008(1)	0.016(1)	-0.001(1)
C(23)	0.046(1)	0.055(1)	0.056(2)	-0.007(1)	0.011(1)	0.000(1)
C(24)	0.039(1)	0.047(1)	0.065(2)	-0.008(1)	0.014(1)	-0.003(1)
C(25)	0.050(1)	0.057(1)	0.067(2)	-0.001(1)	0.023(1)	-0.003(1)
C(26)	0.052(1)	0.056(1)	0.061(2)	0.002(1)	0.015(1)	-0.001(1)
C(27)	0.045(1)	0.049(1)	0.075(2)	-0.005(1)	0.013(1)	0.004(1)
C(28)	0.047(1)	0.055(1)	0.083(2)	-0.008(1)	0.010(1)	0.008(1)
C(29)	0.055(1)	0.058(1)	0.078(2)	-0.003(1)	0.008(1)	0.013(1)
C(30)	0.040(1)	0.060(1)	0.072(2)	-0.007(1)	0.015(1)	-0.002(1)
C(31)	0.039(1)	0.074(2)	0.085(2)	-0.014(1)	0.008(1)	-0.003(1)
C(32)	0.046(1)	0.080(2)	0.096(2)	-0.003(1)	0.025(2)	0.004(1)

Table A.53: Crystallographic data and structure refinement of (3)(TCNQ) at 123 K.

Compound	(3)(TCNQ)
Empirical Formula	$\text{C}_{32}\text{H}_{34}\text{N}_8$
Formula weight / gmol^{-1}	530.67
Temperature	123(2)
Crystal size / mm^3	0.210×0.072×0.050

Table A.53 – continued from previous page

Compound	(3)(TCNQ)
Crystal system; space group	Monoclinic, $P2_1/c$
Lattice constants / Å°	$a = 22.0481(6)$ $b = 6.9330(2) \beta = 109.3010(1)$ $c = 20.4318(6)$
Volume / Å³	2947.65(15)
Z; F(000); calc. density / gcm⁻³	4; 1128; 1.196
Wavelength	Mo-K α (0.71073 Å)
Theta range for data collection / °	2.937 ≤ θ ≤ 26.446
Limiting indices	-27 ≤ h ≤ 27, -8 ≤ k ≤ 8, -25 ≤ l ≤ 25
Reflections collected / unique	36664 / 6031
R_{int}	0.0854
Completeness to theta = 25.242	99.80 %
Absorption coefficient / mm⁻¹	0.074
Refinement method	Full-matrix least-squares on F^2
Data / restraints / parameters	6031 / 0 / 498
R indices [I > 4σ(I)] R_1 ; wR_2	0.0435; 0.0967
R indices (all data) R_1 ; wR_2	0.0811; 0.1124
Goodness-of-fit for F^2	1.019
Extinction coefficient	0.0067(8)
Largest diff. Peak and hole / e⁻Å⁻³	0.219 / -0.173

Table A.54: Fractional coordinates in Å and equivalent isotropic displacement parameter $U_{eq}/\text{Å}^2$ for the independent atoms in the structure of (3)(TCNQ) at 123 K.

Atom	Wyck.	Site	x/a	y/b	z/c	U_{eq}
N(1)	4e	1	0.8996(1)	0.6650(2)	0.4852(1)	0.024(1)
N(2)	4e	1	0.7948(1)	0.5721(2)	0.4638(1)	0.024(1)
N(3)	4e	1	0.7412(1)	0.5103(2)	0.4156(1)	0.024(1)
N(4)	4e	1	0.6386(1)	0.3979(2)	0.3957(1)	0.024(1)
C(1)	4e	1	0.8430(1)	0.6019(2)	0.4375(1)	0.023(1)
C(2)	4e	1	0.8413(1)	0.5726(2)	0.3685(1)	0.025(1)
C(3)	4e	1	0.8935(1)	0.6056(2)	0.3479(1)	0.026(1)
C(4)	4e	1	0.9503(1)	0.6701(2)	0.3992(1)	0.029(1)
C(5)	4e	1	0.9521(1)	0.6958(2)	0.4654(1)	0.026(1)
C(6)	4e	1	0.9044(1)	0.6914(3)	0.5583(1)	0.029(1)
C(7)	4e	1	0.8916(1)	0.5847(3)	0.2729(1)	0.034(1)
C(8)	4e	1	0.8899(1)	0.7901(3)	0.2435(1)	0.048(1)
C(9)	4e	1	0.9521(1)	0.4809(3)	0.2699(1)	0.044(1)
C(10)	4e	1	0.8325(1)	0.4733(4)	0.2293(1)	0.050(1)
C(11)	4e	1	0.6949(1)	0.4618(2)	0.4433(1)	0.023(1)
C(12)	4e	1	0.6999(1)	0.4645(2)	0.5136(1)	0.025(1)
C(13)	4e	1	0.6507(1)	0.4046(2)	0.5355(1)	0.028(1)
C(14)	4e	1	0.5935(1)	0.3395(2)	0.4845(1)	0.028(1)
C(15)	4e	1	0.5892(1)	0.3374(2)	0.4169(1)	0.026(1)
C(16)	4e	1	0.6332(1)	0.3825(3)	0.3220(1)	0.028(1)
C(17)	4e	1	0.6550(1)	0.4033(3)	0.6118(1)	0.039(1)
C(18)	4e	1	0.6467(1)	0.1948(3)	0.6328(1)	0.052(1)
C(19)	4e	1	0.6012(1)	0.5309(4)	0.6202(1)	0.052(1)
C(20)	4e	1	0.7199(1)	0.4812(4)	0.6586(1)	0.051(1)

Table A.54 – continued from previous page

Atom	Wyck.	Site	x/a	y/b	z/c	U_{eq}
N(5)	4e	1	0.9208(1)	1.1288(2)	0.3890(1)	0.038(1)
N(6)	4e	1	0.8969(1)	1.2087(2)	0.5906(1)	0.039(1)
N(7)	4e	1	0.5307(1)	0.7633(2)	0.2358(1)	0.043(1)
N(8)	4e	1	0.5266(1)	0.8045(2)	0.4498(1)	0.049(1)
C(21)	4e	1	0.7846(1)	1.0212(2)	0.4391(1)	0.026(1)
C(22)	4e	1	0.7479(1)	0.9980(2)	0.4843(1)	0.028(1)
C(23)	4e	1	0.6860(1)	0.9352(2)	0.4605(1)	0.027(1)
C(24)	4e	1	0.6555(1)	0.8881(2)	0.3896(1)	0.026(1)
C(25)	4e	1	0.6933(1)	0.9020(2)	0.3453(1)	0.027(1)
C(26)	4e	1	0.7552(1)	0.9685(2)	0.3690(1)	0.026(1)
C(27)	4e	1	0.8480(1)	1.0969(2)	0.4639(1)	0.028(1)
C(28)	4e	1	0.8871(1)	1.1158(2)	0.4217(1)	0.029(1)
C(29)	4e	1	0.8752(1)	1.1602(2)	0.5335(1)	0.031(1)
C(30)	4e	1	0.5899(1)	0.8342(2)	0.3648(1)	0.029(1)
C(31)	4e	1	0.5567(1)	0.7964(2)	0.2937(1)	0.032(1)
C(32)	4e	1	0.5539(1)	0.8187(2)	0.4109(1)	0.034(1)
H(2)	4e	1	0.8014(8)	0.5300(2)	0.3374(8)	0.027(4)
H(4)	4e	1	0.9885(8)	0.6970(2)	0.3868(8)	0.029(4)
H(5)	4e	1	0.9886(8)	0.7400(2)	0.5014(8)	0.028(4)
H(6A)	4e	1	0.9018(9)	0.5670(3)	0.5789(1)	0.052(6)
H(6B)	4e	1	0.9445(8)	0.7570(2)	0.5806(8)	0.028(4)
H(6C)	4e	1	0.8687(8)	0.7750(3)	0.5627(8)	0.036(5)
H(8A)	4e	1	0.9297(1)	0.8640(3)	0.2727(1)	0.057(6)
H(8B)	4e	1	0.8483(1)	0.8600(3)	0.2432(1)	0.059(6)
H(8C)	4e	1	0.8911(11)	0.7790(3)	0.1946(12)	0.074(7)
H(9A)	4e	1	0.9554(1)	0.3450(3)	0.2940(11)	0.061(6)
H(9B)	4e	1	0.9479(9)	0.4630(3)	0.2197(11)	0.049(5)
H(9C)	4e	1	0.9945(1)	0.5560(3)	0.2956(1)	0.052(5)
H(10A)	4e	1	0.8348(1)	0.4590(3)	0.1823(12)	0.060(6)
H(10B)	4e	1	0.8350(1)	0.3380(3)	0.2481(11)	0.059(7)
H(10C)	4e	1	0.7908(1)	0.5380(3)	0.2253(1)	0.052(6)
H(12)	4e	1	0.7408(8)	0.5130(2)	0.5451(8)	0.026(4)
H(14)	4e	1	0.5556(8)	0.2960(2)	0.4972(8)	0.026(4)
H(15)	4e	1	0.5512(8)	0.2990(2)	0.3792(9)	0.031(4)
H(16A)	4e	1	0.6654(8)	0.2820(3)	0.3174(9)	0.039(5)
H(16B)	4e	1	0.6439(8)	0.5160(3)	0.3048(9)	0.041(5)
H(16C)	4e	1	0.5880(1)	0.3430(3)	0.2975(9)	0.048(5)
H(18A)	4e	1	0.6028(1)	0.1380(3)	0.6028(1)	0.059(6)
H(18B)	4e	1	0.6525(11)	0.1920(3)	0.6853(13)	0.075(7)
H(18C)	4e	1	0.6853(12)	0.1140(3)	0.6288(11)	0.072(7)
H(19A)	4e	1	0.5586(1)	0.4860(3)	0.5932(1)	0.049(5)
H(19B)	4e	1	0.6062(1)	0.6690(3)	0.6073(11)	0.063(7)
H(19C)	4e	1	0.6009(1)	0.5270(3)	0.6699(12)	0.068(7)
H(20A)	4e	1	0.7575(1)	0.4020(3)	0.6566(1)	0.059(6)
H(20B)	4e	1	0.7216(1)	0.4760(3)	0.7091(12)	0.065(6)
H(20C)	4e	1	0.7258(9)	0.6290(3)	0.6478(1)	0.055(6)
H(22)	4e	1	0.7675(8)	1.0300(2)	0.5340(9)	0.035(5)
H(23)	4e	1	0.6611(8)	0.9220(2)	0.4937(9)	0.033(4)
H(25)	4e	1	0.6743(8)	0.8710(2)	0.2968(9)	0.034(5)
H(26)	4e	1	0.7808(7)	0.9810(2)	0.3363(8)	0.029(4)

Appendix A Useful Information

Table A.55: Anisotropic displacement parameters $U_{ij}/\text{\AA}^2$ for the independent atoms in the structure of (3)(TCNQ) at 123 K.

Atom	U_{11}	U_{22}	U_{33}	U_{23}	U_{13}	U_{12}
N(1)	0.022(1)	0.025(1)	0.024(1)	0.000(1)	0.005(1)	0.000(1)
N(2)	0.021(1)	0.023(1)	0.028(1)	0.001(1)	0.006(1)	0.000(1)
N(3)	0.021(1)	0.024(1)	0.027(1)	0.001(1)	0.005(1)	-0.001(1)
N(4)	0.023(1)	0.024(1)	0.023(1)	0.001(1)	0.006(1)	-0.001(1)
C(1)	0.021(1)	0.020(1)	0.026(1)	0.002(1)	0.006(1)	0.000(1)
C(2)	0.022(1)	0.026(1)	0.026(1)	-0.001(1)	0.006(1)	0.000(1)
C(3)	0.024(1)	0.027(1)	0.027(1)	0.002(1)	0.007(1)	0.003(1)
C(4)	0.022(1)	0.030(1)	0.035(1)	0.001(1)	0.011(1)	-0.001(1)
C(5)	0.019(1)	0.026(1)	0.032(1)	0.000(1)	0.005(1)	-0.001(1)
C(6)	0.027(1)	0.031(1)	0.024(1)	-0.003(1)	0.004(1)	-0.003(1)
C(7)	0.028(1)	0.047(1)	0.028(1)	-0.001(1)	0.011(1)	-0.001(1)
C(8)	0.048(1)	0.063(1)	0.035(1)	0.013(1)	0.016(1)	0.005(1)
C(9)	0.038(1)	0.060(1)	0.036(1)	-0.006(1)	0.017(1)	0.005(1)
C(10)	0.039(1)	0.081(2)	0.031(1)	-0.016(1)	0.013(1)	-0.013(1)
C(11)	0.020(1)	0.021(1)	0.026(1)	0.000(1)	0.006(1)	0.000(1)
C(12)	0.023(1)	0.026(1)	0.025(1)	-0.001(1)	0.005(1)	-0.001(1)
C(13)	0.025(1)	0.031(1)	0.027(1)	0.001(1)	0.009(1)	0.001(1)
C(14)	0.023(1)	0.032(1)	0.030(1)	0.002(1)	0.009(1)	0.000(1)
C(15)	0.021(1)	0.025(1)	0.030(1)	0.001(1)	0.006(1)	-0.001(1)
C(16)	0.026(1)	0.033(1)	0.024(1)	-0.002(1)	0.006(1)	-0.002(1)
C(17)	0.029(1)	0.060(1)	0.028(1)	-0.002(1)	0.010(1)	-0.004(1)
C(18)	0.044(1)	0.075(2)	0.037(1)	0.017(1)	0.013(1)	-0.004(1)
C(19)	0.039(1)	0.081(2)	0.040(1)	-0.019(1)	0.018(1)	-0.003(1)
C(20)	0.038(1)	0.088(2)	0.028(1)	-0.009(1)	0.009(1)	-0.010(1)
N(5)	0.034(1)	0.036(1)	0.044(1)	0.002(1)	0.012(1)	-0.006(1)
N(6)	0.036(1)	0.036(1)	0.040(1)	-0.001(1)	0.007(1)	-0.009(1)
N(7)	0.030(1)	0.051(1)	0.041(1)	0.004(1)	0.003(1)	-0.001(1)
N(8)	0.035(1)	0.061(1)	0.054(1)	-0.001(1)	0.020(1)	-0.007(1)
C(21)	0.024(1)	0.019(1)	0.033(1)	0.002(1)	0.007(1)	0.001(1)
C(22)	0.027(1)	0.024(1)	0.030(1)	0.000(1)	0.007(1)	0.001(1)
C(23)	0.028(1)	0.024(1)	0.031(1)	0.001(1)	0.012(1)	0.002(1)
C(24)	0.024(1)	0.021(1)	0.032(1)	0.004(1)	0.006(1)	0.003(1)
C(25)	0.025(1)	0.025(1)	0.029(1)	0.003(1)	0.006(1)	0.002(1)
C(26)	0.025(1)	0.023(1)	0.030(1)	0.004(1)	0.009(1)	0.002(1)
C(27)	0.024(1)	0.023(1)	0.034(1)	0.002(1)	0.005(1)	-0.001(1)
C(28)	0.023(1)	0.024(1)	0.035(1)	0.002(1)	0.003(1)	-0.003(1)
C(29)	0.025(1)	0.025(1)	0.038(1)	0.003(1)	0.006(1)	-0.004(1)
C(30)	0.023(1)	0.027(1)	0.035(1)	0.003(1)	0.008(1)	0.001(1)
C(31)	0.020(1)	0.032(1)	0.043(1)	0.007(1)	0.007(1)	0.002(1)
C(32)	0.022(1)	0.034(1)	0.042(1)	0.002(1)	0.008(1)	-0.002(1)

(4)(TCNQ)

Table A.56: Crystallographic data and structure refinement of (4)(TCNQ) at room temperature.

Compound	(4)(TCNQ)
Empirical Formula	$\text{C}_{26}\text{H}_{22}\text{N}_8\text{S}_2$
Formula weight / g mol^{-1}	510.63

Table A.56 – continued from previous page

Compound	(4)(TCNQ)
Temperature	293(2)
Crystal size / mm ³	0.210×0.072×0.050
Crystal system; space group	Monoclinic, P2 ₁ /c
Lattice constants / Å°	$a = 10.7276(17)$ $b = 7.3347(13) \beta = 91.787(9)$ $c = 15.907(3)$
Volume / Å ³	1251.0(4)
Z; F(000); calc. density / gcm ⁻³	2; 532; 1.356
Wavelength	Mo-K α (0.71073 Å)
Theta range for data collection / °	1.899 ≤ θ ≤ 25.190
Limiting indices	-12 ≤ h ≤ 12, -8 ≤ k ≤ 8, -18 ≤ l ≤ 18
Reflections collected / unique	3221 / 1855
R _{int}	0.2027
Completeness to theta = 25.242	82.40 %
Absorption coefficient / mm ⁻¹	0.245
Refinement method	Full-matrix least-squares on F^2
Data / restraints / parameters	1855 / 0 / 165
R indices [I > 4σ(I)] R ₁ ; wR ₂	0.0655; 0.1074
R indices (all data) R ₁ ; wR ₂	0.2826; 0.1611
Goodness-of-fit for F^2	0.833
Largest diff. Peak and hole / e ⁻ Å ⁻³	0.239 / -0.200

Table A.57: Fractional coordinates in Å and equivalent isotropic displacement parameter U_{eq} /Å² for the independent atoms in the structure of (4)(TCNQ) at room temperature.

Atom	Wyck.	Site	x/a	y/b	z/c	U_{eq}
S(1)	4e	1	0.9255(2)	0.6622(4)	0.7258(2)	0.077(1)
N(1)	4e	1	0.7495(6)	0.8589(9)	0.5170(4)	0.050(2)
N(2)	4e	1	0.5561(4)	0.9773(9)	0.4840(4)	0.053(2)
C(1)	4e	1	0.8388(7)	0.7884(1)	0.5707(5)	0.052(2)
C(2)	4e	1	0.8195(7)	0.7595(1)	0.6526(6)	0.053(2)
C(3)	4e	1	0.7008(8)	0.8091(11)	0.6819(5)	0.060(2)
C(4)	4e	1	0.6120(7)	0.8828(1)	0.6287(6)	0.057(3)
C(5)	4e	1	0.6324(7)	0.9094(1)	0.5445(5)	0.051(3)
C(6)	4e	1	0.7803(6)	0.8852(11)	0.4283(5)	0.068(3)
C(7)	4e	1	1.0616(6)	0.6328(12)	0.6672(5)	0.086(3)
N(3)	4e	1	0.3473(7)	0.6873(15)	0.2336(6)	0.106(3)
N(4)	4e	1	0.1017(6)	0.7449(11)	0.4464(5)	0.085(3)
C(8)	4e	1	0.1951(8)	0.7019(11)	0.4195(6)	0.060(3)
C(9)	4e	1	0.3323(8)	0.6699(16)	0.3030(7)	0.068(3)
C(10)	4e	1	0.3138(7)	0.6506(12)	0.3903(6)	0.058(3)
C(11)	4e	1	0.4066(8)	0.5775(1)	0.4446(6)	0.052(2)
C(12)	4e	1	0.3874(7)	0.5596(11)	0.5327(6)	0.056(2)
C(13)	4e	1	0.4797(8)	0.4860(11)	0.5847(5)	0.058(2)
H(10)	4e	1	0.9162	0.7592	0.5497	0.062
H(3)	4e	1	0.6830	0.7913	0.7381	0.073
H(4)	4e	1	0.5355	0.9161	0.6499	0.069
H(6A)	4e	1	0.8668	0.8576	0.4211	0.102
H(6B)	4e	1	0.7644	1.0095	0.4124	0.102

Table A.57 – continued from previous page

Atom	Wyck.	Site	x/a	y/b	z/c	U_{eq}
H(6C)	$4e$	1	0.7298	0.8057	0.3935	0.102
H(7A)	$4e$	1	1.0416	0.5636	0.6173	0.128
H(7B)	$4e$	1	1.1234	0.5689	0.7007	0.128
H(7C)	$4e$	1	1.0936	0.7499	0.6517	0.128
H(12)	$4e$	1	0.3127	0.5976	0.5551	0.067
H(13)	$4e$	1	0.4656	0.4782	0.6420	0.069

Table A.58: Anisotropic displacement parameters $U_{ij}/\text{\AA}^2$ for the independent atoms in the structure of (4)(TCNQ) at room temperature.

Atom	U_{11}	U_{22}	U_{33}	U_{23}	U_{13}	U_{12}
S(1)	0.069(2)	0.106(2)	0.056(2)	0.012(2)	-0.004(1)	0.010(2)
N(1)	0.047(5)	0.059(5)	0.045(5)	0.010(4)	0.006(4)	-0.003(4)
N(2)	0.039(4)	0.059(4)	0.061(5)	0.004(4)	-0.002(4)	0.013(4)
C(1)	0.041(5)	0.069(7)	0.045(6)	-0.012(5)	0.002(5)	0.008(5)
C(2)	0.048(6)	0.058(6)	0.052(7)	-0.002(5)	-0.006(5)	-0.004(5)
C(3)	0.073(7)	0.057(6)	0.052(6)	0.010(5)	0.019(5)	-0.001(5)
C(4)	0.054(6)	0.054(7)	0.065(7)	0.003(5)	0.024(5)	0.005(5)
C(5)	0.038(6)	0.062(7)	0.054(7)	0.000(5)	0.011(5)	-0.009(5)
C(6)	0.057(5)	0.087(7)	0.062(7)	0.011(6)	0.014(5)	0.016(5)
C(7)	0.039(5)	0.107(8)	0.111(8)	0.018(7)	0.003(5)	0.001(5)
N(3)	0.086(6)	0.142(8)	0.091(7)	0.003(8)	0.009(6)	0.018(6)
N(4)	0.052(5)	0.113(7)	0.089(7)	0.000(5)	0.001(5)	0.014(5)
C(8)	0.054(6)	0.053(7)	0.072(7)	-0.001(6)	-0.019(6)	0.002(5)
C(9)	0.045(6)	0.083(7)	0.075(8)	0.002(9)	-0.003(6)	0.016(5)
C(10)	0.042(6)	0.063(6)	0.070(7)	-0.015(7)	-0.005(5)	0.004(5)
C(11)	0.045(6)	0.049(6)	0.063(8)	-0.006(6)	0.013(5)	-0.005(5)
C(12)	0.048(6)	0.061(6)	0.059(7)	-0.001(5)	0.009(5)	0.001(4)
C(13)	0.057(5)	0.068(6)	0.048(6)	0.000(5)	0.001(6)	-0.004(5)

(7)(TCNQ)

Table A.59: Crystallographic data and structure refinement of (7)(TCNQ) at room temperature.

Compound	(7)(TCNQ)
Empirical Formula	$\text{C}_{26}\text{H}_{16}\text{F}_6\text{N}_8$
Formula weight / $gmol^{-1}$	554.47
Temperature / K	298(2)
Crystal size / mm^3	0.400×0.160×0.086
Crystal system; space group	Triclinic, $P\bar{1}$
Lattice constants / \AA°	$a = 7.2533(13)$ $\alpha = 93.098(9)$ $b = 8.4348(9)$ $\beta = 92.001(5)$ $c = 10.7661(19)$ $\gamma = 91.593(10)$
Volume / \AA^3	657.02(18)

Table A.59 – continued from previous page

Compound	(7)(TCNQ)
Z; F(000); calc. density / $g\text{cm}^{-3}$	1; 282; 1.401
Wavelength	Mo-K α (0.71073 Å)
Theta range for data collection / °	2.991 ≤ θ ≤ 27.358
Limiting indices	-7 ≤ h ≤ 8, -8 ≤ k ≤ 10, -12 ≤ l ≤ 13
Reflections collected / unique	2922 / 1895
R _{int}	0.0932
Completeness to theta = 25.242	77.10 %
Absorption coefficient / mm^{-1}	0.118
Refinement method	Full-matrix least-squares on F^2
Data / restraints / parameters	1895 / 0 / 214
R indices [I > 4σ(I)] R ₁ ; wR ₂	0.0800; 0.1713
R indices (all data) R ₁ ; wR ₂	0.2776; 0.2518
Goodness-of-fit for F^2	0.900
Largest diff. Peak and hole / $e^{-\text{\AA}^{-3}}$	0.212 / -0.245

Table A.60: Fractional coordinates in Å and equivalent isotropic displacement parameter $U_{eq}/\text{\AA}^2$ for the independent atoms in the structure of (7)(TCNQ) at room temperature.

Atom	Wyck.	Site	x/a	y/b	z/c	U_{eq}
F(1)	2 <i>i</i>	1	0.3198(15)	0.8009(7)	0.4884(7)	0.202(4)
F(2)	2 <i>i</i>	1	0.4344(13)	0.9516(11)	0.6221(7)	0.210(5)
F(3)	2 <i>i</i>	1	0.1771(13)	0.9835(1)	0.5694(8)	0.214(5)
N(1)	2 <i>i</i>	1	0.1396(9)	0.5133(7)	0.7537(6)	0.065(2)
N(2)	2 <i>i</i>	1	0.0253(8)	0.4647(7)	0.9430(5)	0.060(2)
C(1)	2 <i>i</i>	1	0.0897(1)	0.5711(9)	0.8692(7)	0.055(2)
C(2)	2 <i>i</i>	1	0.1170(12)	0.7397(1)	0.8944(9)	0.068(3)
C(3)	2 <i>i</i>	1	0.1780(11)	0.8323(11)	0.8089(9)	0.068(3)
C(4)	2 <i>i</i>	1	0.2237(1)	0.7717(1)	0.6893(8)	0.069(2)
C(5)	2 <i>i</i>	1	0.1998(12)	0.6126(12)	0.6658(8)	0.066(3)
C(6)	2 <i>i</i>	1	0.1150(2)	0.3423(12)	0.7206(11)	0.090(4)
C(7)	2 <i>i</i>	1	0.2810(2)	0.8691(13)	0.5897(12)	0.113(4)
N(3)	2 <i>i</i>	1	0.6983(12)	0.9981(9)	0.8737(7)	0.109(3)
N(4)	2 <i>i</i>	1	0.7467(12)	0.5867(9)	0.6130(8)	0.103(3)
C(8)	2 <i>i</i>	1	0.5759(1)	0.5964(1)	0.9128(7)	0.060(2)
C(9)	2 <i>i</i>	1	0.5565(11)	0.4308(11)	0.8857(9)	0.067(3)
C(10)	2 <i>i</i>	1	0.4834(13)	0.3370(11)	0.9695(9)	0.070(3)
C(11)	2 <i>i</i>	1	0.6469(11)	0.6968(1)	0.8276(8)	0.072(3)
C(12)	2 <i>i</i>	1	0.6718(12)	0.8657(12)	0.8493(8)	0.078(3)
C(13)	2 <i>i</i>	1	0.7028(12)	0.6392(9)	0.7053(9)	0.073(3)
H(2)	2 <i>i</i>	1	0.0970(7)	0.7640(6)	0.9720(5)	0.030(18)
H(3)	2 <i>i</i>	1	0.1990(8)	0.9390(7)	0.8380(6)	0.060(2)
H(5)	2 <i>i</i>	1	0.2300(9)	0.5690(6)	0.5930(6)	0.050(2)
H(6A)	2 <i>i</i>	1	0.1800(11)	0.2780(8)	0.8000(8)	0.110(3)
H(6B)	2 <i>i</i>	1	-0.0130(9)	0.3070(7)	0.7130(6)	0.050(2)
H(6C)	2 <i>i</i>	1	0.1250(8)	0.3210(6)	0.6530(6)	0.030(2)
H(9)	2 <i>i</i>	1	0.5840(8)	0.3720(6)	0.8070(6)	0.042(18)
H(10)	2 <i>i</i>	1	0.4670(7)	0.2310(6)	0.9580(5)	0.025(17)

Appendix A Useful Information

Table A.61: Anisotropic displacement parameters $U_{ij}/\text{\AA}^2$ for the independent atoms in the structure of (7)(TCNQ) at room temperature.

Atom	U_{11}	U_{22}	U_{33}	U_{23}	U_{13}	U_{12}
F(1)	0.384(12)	0.135(5)	0.088(5)	0.004(4)	0.106(6)	-0.068(6)
F(2)	0.209(1)	0.271(9)	0.149(8)	0.121(7)	-0.039(6)	-0.135(9)
F(3)	0.246(11)	0.181(7)	0.240(1)	0.143(7)	0.081(8)	0.077(7)
N(1)	0.080(5)	0.067(5)	0.048(5)	-0.006(4)	0.013(4)	0.001(4)
N(2)	0.062(5)	0.070(4)	0.047(4)	-0.008(3)	0.012(4)	-0.006(3)
C(1)	0.046(6)	0.070(6)	0.046(6)	-0.010(5)	-0.003(4)	-0.001(4)
C(2)	0.083(7)	0.069(7)	0.051(6)	-0.014(5)	0.022(5)	-0.010(5)
C(3)	0.059(6)	0.067(6)	0.075(7)	-0.018(6)	0.005(5)	0.000(5)
C(4)	0.054(6)	0.075(6)	0.076(7)	0.005(5)	0.004(5)	-0.002(5)
C(5)	0.057(6)	0.100(8)	0.040(6)	0.002(6)	0.001(5)	0.006(5)
C(6)	0.123(11)	0.094(8)	0.050(8)	-0.030(6)	0.028(7)	-0.024(8)
C(7)	0.159(13)	0.085(8)	0.100(1)	0.031(7)	0.051(9)	-0.021(8)
N(3)	0.125(8)	0.089(6)	0.108(7)	-0.025(5)	0.013(6)	0.000(5)
N(4)	0.109(7)	0.130(6)	0.070(6)	-0.014(5)	0.023(5)	0.014(5)
C(8)	0.054(6)	0.080(6)	0.044(6)	-0.009(5)	-0.003(4)	0.019(5)
C(9)	0.056(6)	0.075(7)	0.068(7)	-0.015(6)	0.005(5)	0.022(5)
C(10)	0.085(7)	0.058(6)	0.064(7)	-0.019(6)	0.002(5)	0.007(5)
C(11)	0.057(7)	0.094(7)	0.064(7)	-0.014(6)	0.004(5)	0.012(5)
C(12)	0.070(7)	0.086(7)	0.076(7)	-0.023(5)	0.006(5)	-0.004(6)
C(13)	0.063(7)	0.082(6)	0.075(7)	-0.005(5)	0.011(5)	0.008(5)

(7)(TCNQ)₂

Table A.62: Crystallographic data and structure refinement of (7)(TCNQ)₂ at room temperature.

Compound	(7)(TCNQ) ₂
Empirical Formula	C ₃₈ H ₂₀ F ₆ N ₁₂
Formula weight/ g mol ⁻¹	758.66
Temperature / K	293(2)
Crystal size / mm ³	0.400×0.160×0.086
Crystal system; space group	Triclinic, P $\bar{1}$
Lattice constants / Å °	$a = 8.1062(3)$ $\alpha = 73.720(2)$ $b = 10.3183(4)$ $\beta = 80.931(2)$ $c = 11.2985(4)$ $\gamma = 86.566(2)$
Volume / Å ³	895.68(6)
Z; F(000); calc. density / g cm ⁻³	1; 386; 1.407
Wavelength	Mo-K α (0.71073 Å)
Theta range for data collection / °	1.898 ≤ θ ≤ 27.759
Limiting indices	-9 ≤ h ≤ 10, -13 ≤ k ≤ 13, -14 ≤ l ≤ 14
Reflections collected / unique	9379 / 4101
R _{int}	0.0615
Completeness to theta = 25.242	98.60 %
Absorption coefficient / mm ⁻¹	0.111
Refinement method	Full-matrix least-squares on F^2
Data / restraints / parameters	4101 / 0 / 294
R indices [I > 4σ(I)] R ₁ ; wR ₂	0.0709; 0.2059

Table A.62 – continued from previous page

Compound	(7)(TCNQ) ₂
R indices (all data) R_1 ; wR_2	0.1039; 0.2370
Goodness-of-fit for F^2	1.091
Largest diff. Peak and hole / $e^{-\text{\AA}^{-3}}$	0.691 / -0.417

Table A.63: Fractional coordinates in Å and equivalent isotropic displacement parameter $U_{eq}/\text{\AA}^2$ for the independent atoms in the structure of (7)(TCNQ)₂ at room temperature.

Atom	Wyck.	Site	x/a	y/b	z/c	U_{eq}
F(1)	$2i$	1	0.7194(4)	-0.1370(2)	0.7575(4)	0.168(2)
F(2)	$2i$	1	0.8854(6)	-0.0276(3)	0.8107(4)	0.195(2)
F(3)	$2i$	1	0.9276(5)	-0.0648(4)	0.6464(4)	0.200(2)
N(1)	$2i$	1	0.4817(2)	0.2086(2)	0.5908(2)	0.048(1)
N(2)	$2i$	1	0.4606(3)	0.4384(2)	0.5116(2)	0.049(1)
C(1)	$2i$	1	0.5529(3)	0.3363(2)	0.5628(2)	0.044(1)
C(2)	$2i$	1	0.7183(3)	0.3374(2)	0.5940(2)	0.050(1)
C(3)	$2i$	1	0.8000(3)	0.2226(3)	0.6437(3)	0.056(1)
C(4)	$2i$	1	0.7225(3)	0.0959(2)	0.6679(2)	0.055(1)
C(5)	$2i$	1	0.5653(3)	0.0939(2)	0.6410(2)	0.053(1)
C(6)	$2i$	1	0.3135(4)	0.2009(3)	0.5625(4)	0.065(1)
C(7)	$2i$	1	0.8081(4)	-0.0307(3)	0.7226(3)	0.076(1)
N(3)	$2i$	1	0.9534(3)	0.5476(3)	0.2931(3)	0.078(1)
N(4)	$2i$	1	0.6679(3)	0.1881(2)	0.3226(2)	0.070(1)
N(5)	$2i$	1	-0.0444(3)	0.6637(2)	-0.0468(2)	0.069(1)
N(6)	$2i$	1	0.2453(4)	1.0263(3)	-0.1010(3)	0.090(1)
C(8)	$2i$	1	0.5756(3)	0.5272(2)	0.1875(2)	0.046(1)
C(9)	$2i$	1	0.4269(3)	0.4692(2)	0.1679(2)	0.049(1)
C(10)	$2i$	1	0.3105(3)	0.5467(2)	0.1084(2)	0.049(1)
C(11)	$2i$	1	0.3294(3)	0.6916(2)	0.0604(2)	0.047(1)
C(12)	$2i$	1	0.4766(3)	0.7497(2)	0.0809(2)	0.053(1)
C(13)	$2i$	1	0.5925(3)	0.6715(2)	0.1416(2)	0.051(1)
C(14)	$2i$	1	0.6949(3)	0.4468(2)	0.2480(2)	0.050(1)
C(15)	$2i$	1	0.8394(3)	0.5018(3)	0.2730(2)	0.057(1)
C(16)	$2i$	1	0.6806(3)	0.3030(3)	0.2907(2)	0.054(1)
C(17)	$2i$	1	0.2125(3)	0.7701(2)	-0.0044(2)	0.051(1)
C(18)	$2i$	1	0.0688(3)	0.7124(2)	-0.0278(2)	0.053(1)
C(19)	$2i$	1	0.2303(4)	0.9128(3)	-0.0568(3)	0.063(1)
H(2)	$2i$	1	0.7700(3)	0.4200(3)	0.5730(2)	0.056(7)
H(3)	$2i$	1	0.9160(4)	0.2210(3)	0.6720(3)	0.063(8)
H(5)	$2i$	1	0.5000(3)	0.0100(3)	0.6590(2)	0.059(7)
H(6A)	$2i$	1	0.2830(5)	0.1120(4)	0.5820(3)	0.097(11)
H(6B)	$2i$	1	0.2360(5)	0.2530(4)	0.6080(4)	0.109(13)
H(6C)	$2i$	1	0.3120(5)	0.2380(4)	0.4730(4)	0.106(13)
H(9)	$2i$	1	0.4130(3)	0.3710(3)	0.1980(2)	0.048(6)
H(10)	$2i$	1	0.2110(4)	0.5080(3)	0.0960(3)	0.061(7)
H(12)	$2i$	1	0.4940(4)	0.8500(3)	0.0530(3)	0.068(8)
H(13)	$2i$	1	0.6870(4)	0.7080(3)	0.1520(3)	0.069(8)

Appendix A Useful Information

Table A.64: Anisotropic displacement parameters $U_{ij}/\text{\AA}^2$ for the independent atoms in the structure of (7)(TCNQ)₂ at room temperature.

Atom	U_{11}	U_{22}	U_{33}	U_{23}	U_{13}	U_{12}
F(1)	0.139(2)	0.050(1)	0.295(4)	0.025(2)	-0.106(3)	-0.008(1)
F(2)	0.313(5)	0.084(2)	0.235(4)	-0.037(2)	-0.219(4)	0.054(2)
F(3)	0.186(4)	0.151(3)	0.207(4)	-0.003(3)	0.007(3)	0.108(3)
N(1)	0.045(1)	0.039(1)	0.058(1)	-0.011(1)	-0.010(1)	-0.008(1)
N(2)	0.049(1)	0.039(1)	0.059(1)	-0.014(1)	-0.008(1)	-0.007(1)
C(1)	0.045(1)	0.040(1)	0.047(1)	-0.013(1)	-0.005(1)	-0.008(1)
C(2)	0.047(1)	0.045(1)	0.058(1)	-0.012(1)	-0.010(1)	-0.010(1)
C(3)	0.049(2)	0.052(1)	0.067(2)	-0.013(1)	-0.015(1)	-0.005(1)
C(4)	0.056(2)	0.045(1)	0.063(2)	-0.011(1)	-0.016(1)	-0.002(1)
C(5)	0.059(2)	0.040(1)	0.059(1)	-0.009(1)	-0.011(1)	-0.007(1)
C(6)	0.051(2)	0.053(2)	0.095(2)	-0.019(2)	-0.021(2)	-0.011(1)
C(7)	0.078(2)	0.054(2)	0.097(2)	-0.014(2)	-0.036(2)	0.006(2)
N(3)	0.060(2)	0.089(2)	0.095(2)	-0.036(2)	-0.016(1)	-0.017(1)
N(4)	0.074(2)	0.056(1)	0.082(2)	-0.018(1)	-0.013(1)	-0.007(1)
N(5)	0.061(2)	0.052(1)	0.094(2)	-0.010(1)	-0.025(1)	-0.010(1)
N(6)	0.107(2)	0.051(2)	0.109(2)	-0.006(1)	-0.035(2)	-0.024(1)
C(8)	0.045(1)	0.047(1)	0.048(1)	-0.018(1)	0.001(1)	-0.012(1)
C(9)	0.052(1)	0.043(1)	0.054(1)	-0.016(1)	-0.002(1)	-0.016(1)
C(10)	0.046(1)	0.043(1)	0.057(1)	-0.015(1)	-0.003(1)	-0.014(1)
C(11)	0.046(1)	0.045(1)	0.052(1)	-0.016(1)	-0.001(1)	-0.013(1)
C(12)	0.054(2)	0.044(1)	0.061(1)	-0.014(1)	-0.006(1)	-0.017(1)
C(13)	0.048(1)	0.047(1)	0.060(1)	-0.019(1)	-0.003(1)	-0.016(1)
C(14)	0.050(1)	0.049(1)	0.051(1)	-0.017(1)	-0.001(1)	-0.012(1)
C(15)	0.053(2)	0.060(2)	0.059(1)	-0.018(1)	-0.005(1)	-0.011(1)
C(16)	0.054(2)	0.055(2)	0.057(1)	-0.020(1)	-0.006(1)	-0.006(1)
C(17)	0.056(2)	0.044(1)	0.055(1)	-0.013(1)	-0.005(1)	-0.013(1)
C(18)	0.055(2)	0.042(1)	0.061(1)	-0.009(1)	-0.011(1)	-0.007(1)
C(19)	0.065(2)	0.050(2)	0.075(2)	-0.014(1)	-0.017(1)	-0.013(1)

Table A.65: Crystallographic data and structure refinement of (7)(TCNQ)₂ at 123 K.

Compound	(7)(TCNQ) ₂
Empirical Formula	C ₃₈ H ₂₀ F ₆ N ₁₂
Formula weight / $gmol^{-1}$	758.66
Temperature / K	123(2)
Crystal size / mm ³	0.400×0.160×0.086
Crystal system; space group	Triclinic, $P\bar{1}$
Lattice constants / Å °	$a = 8.0837(3)$ $\alpha = 74.165(2)$ $b = 10.2331(3)$ $\beta = 80.570(2)$ $c = 11.0147(3)$ $\gamma = 86.335(2)$
Volume / Å ³	864.55(5)
Z; F(000); calc. density / gcm ⁻³	1; 386; 1.457
Wavelength	Mo-K α (0.71073 Å)
Theta range for data collection / °	2.069 ≤ θ ≤ 27.499
Limiting indices	-10 ≤ h ≤ 10, -13 ≤ k ≤ 13, -14 ≤ l ≤ 14
Reflections collected / unique	8724 / 3583
R _{int}	0.0664

Table A.65 – continued from previous page

Compound	(7)(TCNQ) ₂
Completeness to theta = 25.242	92.30 %
Absorption coefficient / mm ⁻¹	0.115
Refinement method	Full-matrix least-squares on F^2
Data / restraints / parameters	3583 / 0 / 293
R indices [I > 4σ(I)] R_1 ; wR_2	0.0524; 0.1415
R indices (all data) R_1 ; wR_2	0.0621; 0.1507
Goodness-of-fit for F^2	1.033
Largest diff. Peak and hole / e ⁻ Å ⁻³	0.557 / -0.593

Table A.66: Fractional coordinates in Å and equivalent isotropic displacement parameter U_{eq} /Å² for the independent atoms in the structure of (7)(TCNQ)₂ at 123 K.

Atom	Wyck.	Site	x/a	y/b	z/c	U_{eq}
F(1)	2i	1	0.1017(2)	1.0277(1)	0.1890(2)	0.074(1)
F(2)	2i	1	0.0740(2)	1.0746(2)	0.3644(2)	0.082(1)
F(3)	2i	1	0.2872(2)	1.1408(1)	0.2314(2)	0.067(1)
N(1)	2i	1	0.5176(2)	0.7929(1)	0.4091(1)	0.020(1)
N(2)	2i	1	0.5394(2)	0.5621(1)	0.4883(1)	0.020(1)
C(1)	2i	1	0.4461(2)	0.6651(2)	0.4369(1)	0.018(1)
C(2)	2i	1	0.2792(2)	0.6632(2)	0.4068(2)	0.020(1)
C(3)	2i	1	0.1970(2)	0.7798(2)	0.3569(2)	0.023(1)
C(4)	2i	1	0.2760(2)	0.9075(2)	0.3322(2)	0.022(1)
C(5)	2i	1	0.4335(2)	0.9088(2)	0.3589(2)	0.021(1)
C(6)	2i	1	0.6870(2)	0.8001(2)	0.4378(2)	0.026(1)
C(7)	2i	1	0.1866(2)	1.0362(2)	0.2787(2)	0.030(1)
N(3)	2i	1	0.0415(2)	0.4523(2)	0.7053(2)	0.030(1)
N(4)	2i	1	0.3264(2)	0.8163(2)	0.6781(2)	0.028(1)
N(5)	2i	1	1.0448(2)	0.3375(2)	1.0457(2)	0.028(1)
N(6)	2i	1	0.7548(2)	-0.0287(2)	1.1006(2)	0.038(1)
C(8)	2i	1	0.4208(2)	0.4744(2)	0.8122(2)	0.020(1)
C(9)	2i	1	0.5698(2)	0.5329(2)	0.8306(2)	0.021(1)
C(10)	2i	1	0.6883(2)	0.4543(2)	0.8898(2)	0.021(1)
C(11)	2i	1	0.6694(2)	0.3090(2)	0.9380(2)	0.020(1)
C(12)	2i	1	0.5215(2)	0.2504(2)	0.9182(2)	0.022(1)
C(13)	2i	1	0.4033(2)	0.3292(2)	0.8582(2)	0.021(1)
C(14)	2i	1	0.2995(2)	0.5553(2)	0.7518(2)	0.021(1)
C(15)	2i	1	0.1557(2)	0.4995(2)	0.7262(2)	0.023(1)
C(16)	2i	1	0.3143(2)	0.7000(2)	0.7092(2)	0.022(1)
C(17)	2i	1	0.7882(2)	0.2296(2)	1.0028(2)	0.022(1)
C(18)	2i	1	0.9321(2)	0.2878(2)	1.0262(2)	0.022(1)
C(19)	2i	1	0.7704(2)	0.0861(2)	1.0562(2)	0.027(1)
H(2)	2i	1	0.2260(3)	0.5770(2)	0.4240(2)	0.033(6)
H(3)	2i	1	0.0890(3)	0.7770(2)	0.3370(2)	0.028(5)
H(5)	2i	1	0.4980(2)	0.9900(2)	0.3432(17)	0.018(4)
H(6A)	2i	1	0.7690(3)	0.7460(2)	0.3920(2)	0.031(5)
H(6B)	2i	1	0.6840(3)	0.7650(2)	0.5280(2)	0.039(6)
H(6C)	2i	1	0.7230(3)	0.8940(2)	0.4090(2)	0.034(6)
H(9)	2i	1	0.5840(3)	0.6290(2)	0.8010(2)	0.027(5)
H(10)	2i	1	0.7830(3)	0.4910(2)	0.9013(19)	0.024(5)
H(12)	2i	1	0.5040(3)	0.1560(2)	0.9440(19)	0.025(5)
H(13)	2i	1	0.3040(3)	0.2900(2)	0.8460(2)	0.032(5)

Table A.67: Anisotropic displacement parameters $U_{ij}/\text{\AA}^2$ for the independent atoms in the structure of $(7)(\text{TCNQ})_2$ at 123 K.

Atom	U_{11}	U_{22}	U_{33}	U_{23}	U_{13}	U_{12}
F(1)	0.115(1)	0.033(1)	0.091(1)	-0.011(1)	-0.083(1)	0.016(1)
F(2)	0.082(1)	0.066(1)	0.075(1)	-0.001(1)	0.005(1)	0.050(1)
F(3)	0.051(1)	0.022(1)	0.118(1)	0.016(1)	-0.036(1)	-0.006(1)
N(1)	0.019(1)	0.017(1)	0.023(1)	-0.004(1)	-0.003(1)	-0.003(1)
N(2)	0.022(1)	0.016(1)	0.022(1)	-0.005(1)	-0.003(1)	-0.002(1)
C(1)	0.020(1)	0.017(1)	0.018(1)	-0.005(1)	-0.001(1)	-0.004(1)
C(2)	0.019(1)	0.020(1)	0.022(1)	-0.004(1)	-0.002(1)	-0.004(1)
C(3)	0.020(1)	0.023(1)	0.025(1)	-0.005(1)	-0.005(1)	-0.002(1)
C(4)	0.024(1)	0.020(1)	0.023(1)	-0.003(1)	-0.006(1)	-0.001(1)
C(5)	0.025(1)	0.017(1)	0.022(1)	-0.003(1)	-0.003(1)	-0.003(1)
C(6)	0.020(1)	0.021(1)	0.039(1)	-0.007(1)	-0.009(1)	-0.004(1)
C(7)	0.031(1)	0.023(1)	0.038(1)	-0.004(1)	-0.014(1)	0.001(1)
N(3)	0.025(1)	0.034(1)	0.035(1)	-0.011(1)	-0.006(1)	-0.004(1)
N(4)	0.029(1)	0.024(1)	0.031(1)	-0.006(1)	-0.005(1)	-0.003(1)
N(5)	0.026(1)	0.022(1)	0.036(1)	-0.004(1)	-0.010(1)	-0.002(1)
N(6)	0.041(1)	0.023(1)	0.050(1)	-0.002(1)	-0.015(1)	-0.009(1)
C(8)	0.020(1)	0.022(1)	0.018(1)	-0.007(1)	0.001(1)	-0.004(1)
C(9)	0.020(1)	0.020(1)	0.022(1)	-0.007(1)	0.000(1)	-0.006(1)
C(10)	0.019(1)	0.022(1)	0.021(1)	-0.007(1)	-0.001(1)	-0.007(1)
C(11)	0.020(1)	0.021(1)	0.020(1)	-0.007(1)	0.000(1)	-0.004(1)
C(12)	0.024(1)	0.019(1)	0.023(1)	-0.006(1)	-0.002(1)	-0.007(1)
C(13)	0.021(1)	0.021(1)	0.022(1)	-0.007(1)	0.000(1)	-0.006(1)
C(14)	0.020(1)	0.021(1)	0.021(1)	-0.006(1)	0.000(1)	-0.005(1)
C(15)	0.023(1)	0.023(1)	0.022(1)	-0.005(1)	-0.003(1)	-0.001(1)
C(16)	0.022(1)	0.024(1)	0.020(1)	-0.007(1)	-0.003(1)	-0.002(1)
C(17)	0.023(1)	0.020(1)	0.023(1)	-0.006(1)	-0.002(1)	-0.005(1)
C(18)	0.023(1)	0.017(1)	0.024(1)	-0.003(1)	-0.005(1)	0.000(1)
C(19)	0.026(1)	0.025(1)	0.032(1)	-0.008(1)	-0.009(1)	-0.004(1)

(8)(TCNQ)

Table A.68: Crystallographic data and structure refinement of $(8)(\text{TCNQ})$ at room temperature.

Compound	(8)(TCNQ)
Empirical Formula	$\text{C}_{26}\text{H}_{16}\text{F}_6\text{N}_8$
Formula weight / $gmol^{-1}$	554.47
Temperature / K	298(2)
Crystal size / mm^3	0.375×0.130×0.029
Crystal system; space group	Triclinic, $P\bar{1}$
Lattice constants / \AA°	$a = 8.3256(12) \alpha = 93.026(7)$ $b = 9.2850(8) \beta = 95.146(4)$ $c = 16.144(2) \gamma = 100.673(8)$
Volume / \AA^3	1218.4(3)
Z; F(000); calc. density / gcm^{-3}	2; 564; 1.511

Table A.68 – continued from previous page

Compound	(8)(TCNQ)
Wavelength	Mo-K α (0.71073 Å)
Theta range for data collection /°	2.919 ≤ θ ≤ 26.010
Limiting indices	-10 ≤ h ≤ 9, -11 ≤ k ≤ 11, -19 ≤ l ≤ 17
Reflections collected / unique	11360 / 4638
R _{int}	0.1427
Completeness to theta = 25.242	98.50 %
Absorption coefficient / mm ⁻¹	0.127
Refinement method	Full-matrix least-squares on F ²
Data / restraints / parameters	4630 / 0 / 361
R indices [I > 4σ(I)] R ₁ ; wR ₂	0.1064; 0.2325
R indices (all data) R ₁ ; wR ₂	0.2563; 0.3040
Goodness-of-fit for F ²	0.922
Largest diff. Peak and hole / e ⁻ Å ⁻³	0.799 / -0.358

Table A.69: Fractional coordinates in Å and equivalent isotropic displacement parameter $U_{eq}/\text{Å}^2$ for the independent atoms in the structure of (8)(TCNQ) at room temperature.

Atom	Wyck.	Site	x/a	y/b	z/c	U_{eq}
F(1)	2i	1	0.3560(6)	0.9838(4)	0.4166(3)	0.086(1)
F(2)	2i	1	0.1065(7)	1.0042(4)	0.4144(3)	0.097(2)
F(3)	2i	1	0.2163(6)	0.9937(4)	0.2996(3)	0.098(2)
F(4)	2i	1	0.2627(6)	-0.0177(4)	0.6031(2)	0.087(2)
F(5)	2i	1	0.1803(6)	0.0388(4)	0.7197(3)	0.086(1)
F(6)	2i	1	0.4192(6)	-0.0067(4)	0.7167(3)	0.090(2)
N(1)	2i	1	0.0423(6)	0.4775(5)	0.3620(3)	0.050(1)
N(2)	2i	1	0.2029(6)	0.4495(5)	0.4807(3)	0.047(1)
N(3)	2i	1	0.3200(6)	0.5265(5)	0.5413(3)	0.048(1)
N(4)	2i	1	0.4902(6)	0.5122(4)	0.6584(3)	0.050(1)
C(1)	2i	1	0.1563(8)	0.5404(6)	0.4273(4)	0.047(2)
C(2)	2i	1	0.2114(8)	0.6958(6)	0.4281(4)	0.051(2)
C(3)	2i	1	0.1572(8)	0.7745(6)	0.3681(4)	0.048(2)
C(4)	2i	1	0.0452(8)	0.7056(6)	0.3006(4)	0.059(2)
C(5)	2i	1	-0.0090(8)	0.5583(6)	0.3002(4)	0.056(2)
C(6)	2i	1	-0.0264(8)	0.3197(5)	0.3594(4)	0.058(2)
C(7)	2i	1	0.2096(11)	0.9373(7)	0.3736(5)	0.070(2)
C(8)	2i	1	0.3707(8)	0.4411(6)	0.5972(4)	0.047(2)
C(9)	2i	1	0.3159(8)	0.2865(6)	0.6024(4)	0.049(2)
C(10)	2i	1	0.3769(8)	0.2174(6)	0.6672(4)	0.051(2)
C(11)	2i	1	0.4922(8)	0.2952(6)	0.7283(4)	0.055(2)
C(12)	2i	1	0.5466(8)	0.4400(6)	0.7227(4)	0.057(2)
C(13)	2i	1	0.5523(8)	0.6711(6)	0.6546(4)	0.059(2)
C(14)	2i	1	0.3102(1)	0.0574(7)	0.6762(5)	0.064(2)
N(5)	2i	1	0.3803(8)	0.5833(6)	1.0754(4)	0.078(2)
N(6)	2i	1	0.3403(8)	0.6759(6)	0.8125(4)	0.074(2)
N(7)	2i	1	1.1310(8)	1.3110(6)	1.1761(4)	0.079(2)
N(8)	2i	1	1.0934(8)	1.3980(6)	0.9091(4)	0.085(2)
C(15)	2i	1	0.8619(8)	1.1221(6)	1.0108(4)	0.048(2)
C(16)	2i	1	0.7833(8)	1.0792(6)	0.9278(4)	0.053(2)
C(17)	2i	1	0.6649(8)	0.9603(6)	0.9116(4)	0.054(2)
C(18)	2i	1	0.6077(8)	0.8685(6)	0.9764(4)	0.047(2)

Table A.69 – continued from previous page

Atom	Wyck.	Site	x/a	y/b	z/c	U_{eq}
C(19)	2 <i>i</i>	1	0.6898(8)	0.9108(6)	1.0587(4)	0.051(2)
C(20)	2 <i>i</i>	1	0.8073(7)	1.0310(6)	1.0751(4)	0.049(2)
C(21)	2 <i>i</i>	1	0.9879(8)	1.2444(6)	1.0279(4)	0.053(2)
C(22)	2 <i>i</i>	1	1.0472(9)	1.3306(6)	0.9627(4)	0.059(2)
C(23)	2 <i>i</i>	1	1.0698(9)	1.2824(6)	1.1099(4)	0.057(2)
C(24)	2 <i>i</i>	1	0.4839(8)	0.7454(6)	0.9599(4)	0.050(2)
C(25)	2 <i>i</i>	1	0.4266(8)	0.6541(6)	1.0237(4)	0.053(2)
C(26)	2 <i>i</i>	1	0.4037(9)	0.7055(6)	0.8782(4)	0.056(2)
H(2)	2 <i>i</i>	1	0.2869	0.7435	0.4714	0.061
H(4)	2 <i>i</i>	1	0.0098	0.7591	0.2578	0.070
H(5)	2 <i>i</i>	1	-0.0836	0.5110	0.2565	0.067
H(6A)	2 <i>i</i>	1	0.0214	0.2783	0.4067	0.087
H(6B)	2 <i>i</i>	1	-0.1433	0.3054	0.3607	0.087
H(6C)	2 <i>i</i>	1	-0.0021	0.2721	0.3090	0.087
H(9)	2 <i>i</i>	1	0.2386	0.2333	0.5616	0.058
H(11)	2 <i>i</i>	1	0.5318	0.2479	0.7729	0.066
H(12)	2 <i>i</i>	1	0.6245	0.4918	0.7637	0.068
H(13A)	2 <i>i</i>	1	0.5006	0.7049	0.6058	0.089
H(13B)	2 <i>i</i>	1	0.5276	0.7232	0.7034	0.089
H(13C)	2 <i>i</i>	1	0.6691	0.6886	0.6523	0.089
H(16)	2 <i>i</i>	1	0.8160	1.1358	0.8843	0.063
H(17)	2 <i>i</i>	1	0.6179	0.9359	0.8571	0.065
H(19)	2 <i>i</i>	1	0.6601	0.8526	1.1021	0.062
H(2)	2 <i>i</i>	1	0.8544	1.0557	1.1296	0.059

Table A.70: Anisotropic displacement parameters $U_{ij}/\text{\AA}^2$ for the independent atoms in the structure of (8)(TCNQ) at room temperature.

Atom	U_{11}	U_{22}	U_{33}	U_{23}	U_{13}	U_{12}
F(1)	0.101(4)	0.052(2)	0.090(3)	0.010(2)	-0.015(3)	-0.010(2)
F(2)	0.136(5)	0.050(2)	0.107(4)	-0.002(2)	0.010(3)	0.025(3)
F(3)	0.155(5)	0.060(2)	0.066(3)	0.031(2)	-0.007(3)	-0.007(2)
F(4)	0.145(4)	0.046(2)	0.057(3)	-0.002(2)	-0.003(3)	-0.008(2)
F(5)	0.099(4)	0.069(3)	0.092(3)	0.027(2)	0.032(3)	0.006(2)
F(6)	0.120(4)	0.056(2)	0.092(3)	0.026(2)	-0.017(3)	0.021(2)
N(1)	0.067(4)	0.034(3)	0.041(3)	0.001(2)	-0.007(3)	-0.002(2)
N(2)	0.059(4)	0.042(3)	0.035(3)	0.001(2)	-0.005(3)	0.003(2)
N(3)	0.062(4)	0.041(3)	0.040(3)	0.005(2)	0.001(3)	0.008(2)
N(4)	0.072(4)	0.032(3)	0.040(3)	0.001(2)	-0.003(3)	0.000(2)
C(1)	0.066(5)	0.039(3)	0.033(3)	0.004(3)	0.000(3)	0.004(3)
C(2)	0.070(5)	0.036(3)	0.043(4)	0.000(3)	0.003(3)	0.003(3)
C(3)	0.061(5)	0.038(3)	0.047(4)	0.008(3)	0.006(3)	0.010(3)
C(4)	0.075(5)	0.046(4)	0.051(4)	0.013(3)	-0.010(4)	0.005(3)
C(5)	0.068(5)	0.054(4)	0.042(4)	-0.007(3)	-0.007(3)	0.013(3)
C(6)	0.079(5)	0.034(3)	0.054(4)	0.000(3)	-0.006(4)	0.000(3)
C(7)	0.091(7)	0.052(4)	0.060(5)	0.008(4)	-0.009(5)	0.005(4)
C(8)	0.060(5)	0.039(3)	0.039(4)	0.002(3)	0.000(3)	0.005(3)
C(9)	0.064(5)	0.044(3)	0.036(4)	0.000(3)	0.003(3)	0.009(3)
C(10)	0.073(5)	0.034(3)	0.041(4)	0.005(3)	-0.005(3)	0.004(3)
C(11)	0.077(5)	0.045(4)	0.041(4)	0.008(3)	-0.008(4)	0.013(3)
C(12)	0.077(5)	0.048(4)	0.041(4)	0.000(3)	-0.009(3)	0.011(3)

Table A.70 – continued from previous page

Atom	Wyck.	Site	x/a	y/b	z/c	U_{eq}
C(13)	0.083(6)	0.038(3)	0.048(4)	-0.003(3)	-0.002(4)	-0.004(3)
C(14)	0.078(6)	0.055(4)	0.055(5)	0.004(4)	-0.003(4)	0.004(4)
N(5)	0.118(6)	0.061(4)	0.047(4)	0.012(3)	0.002(4)	-0.006(3)
N(6)	0.097(5)	0.071(4)	0.042(4)	-0.003(3)	-0.007(3)	-0.004(3)
N(7)	0.093(5)	0.080(4)	0.047(4)	-0.007(3)	-0.012(4)	-0.013(3)
N(8)	0.103(6)	0.079(4)	0.061(4)	0.021(3)	-0.003(4)	-0.009(4)
C(15)	0.062(5)	0.045(3)	0.034(3)	0.004(3)	0.002(3)	0.004(3)
C(16)	0.069(5)	0.049(4)	0.036(4)	0.007(3)	-0.001(3)	0.005(3)
C(17)	0.073(5)	0.051(4)	0.032(3)	0.001(3)	-0.004(3)	0.002(3)
C(18)	0.063(5)	0.041(3)	0.035(4)	0.001(3)	0.002(3)	0.007(3)
C(19)	0.077(5)	0.046(4)	0.030(4)	0.004(3)	0.004(3)	0.007(3)
C(20)	0.063(5)	0.045(4)	0.034(3)	0.006(3)	-0.003(3)	0.002(3)
C(21)	0.071(5)	0.046(4)	0.037(4)	0.000(3)	0.000(3)	-0.001(3)
C(22)	0.078(5)	0.047(4)	0.042(4)	0.007(3)	-0.006(4)	-0.006(3)
C(23)	0.069(5)	0.045(4)	0.052(5)	0.000(3)	0.008(4)	-0.001(3)
C(24)	0.066(5)	0.042(3)	0.038(4)	0.001(3)	0.003(3)	0.000(3)
C(25)	0.074(5)	0.042(4)	0.038(4)	-0.002(3)	-0.003(3)	0.004(3)
C(26)	0.077(5)	0.045(4)	0.040(4)	0.004(3)	0.000(4)	-0.004(3)

Table A.71: Crystallographic data and structure refinement of (8)(TCNQ) at 253 K.

Compound	(8)(TCNQ)
Empirical Formula	$C_{26}H_{16}F_6N_8$
Formula weight / $gmol^{-1}$	554.47
Temperature / K	253(2)
Crystal size / mm^3	0.235×0.090×0.024
Crystal system; space group	Triclinic, $P\bar{1}$
Lattice constants / \AA or $^\circ$	$a = 8.2505(5)$ $\alpha = 92.984(3)$ $b = 9.2619(5)$ $\beta = 95.040(3)$ $c = 16.1416(6)$ $\gamma = 100.399(2)$
Volume / \AA^3	1205.61(11)
Z; F(000); calc. density / gcm^{-3}	2; 564; 1.527
Wavelength	Mo-K α (0.71073 \AA)
Theta range for data collection / $^\circ$	$2.934 \leq \theta \leq 27.548$
Limiting indices	$-10 \leq h \leq 10, -12 \leq k \leq 12, -20 \leq l \leq 20$
Reflections collected / unique	12901 / 5017
R_{int}	0.0703
Completeness to theta = 27.548	92.50 %
Absorption coefficient / mm^{-1}	0.129
Refinement method	Full-matrix least-squares on F^2
Data / restraints / parameters	5017 / 0 / 426
R indices [I > 4 σ (I)] R_1 ; wR_2	0.0501; 0.1088
R indices (all data) R_1 ; wR_2	0.1076; 0.1318
Goodness-of-fit for F^2	0.941
Extinction coefficient	0.0127(19)
Largest diff. Peak and hole / $e^{-\text{\AA}^{-3}}$	0.248 / -0.260

Table A.72: Fractional coordinates in Å and equivalent isotropic displacement parameter $U_{eq}/\text{\AA}^2$ for the independent atoms in the structure of (8)(TCNQ) at 253 K.

Atom	Wyck.	Site	x/a	y/b	z/c	U_{eq}
F(1)	$2i$	1	0.2128(2)	0.9960(1)	0.3005(1)	0.073(1)
F(2)	$2i$	1	0.1031(2)	1.0042(1)	0.4152(1)	0.073(1)
F(3)	$2i$	1	0.3568(2)	0.9845(1)	0.4164(1)	0.065(1)
F(4)	$2i$	1	0.4229(2)	-0.0093(1)	0.7169(1)	0.067(1)
F(5)	$2i$	1	0.1799(2)	0.0365(1)	0.7194(1)	0.065(1)
F(6)	$2i$	1	0.2662(2)	-0.0206(1)	0.6030(1)	0.065(1)
N(1)	$2i$	1	0.0406(2)	0.4781(2)	0.3608(1)	0.035(1)
N(2)	$2i$	1	0.2016(2)	0.4500(2)	0.4813(1)	0.036(1)
N(3)	$2i$	1	0.3180(2)	0.5250(2)	0.5411(1)	0.037(1)
N(4)	$2i$	1	0.4895(2)	0.5102(2)	0.6584(1)	0.035(1)
C(1)	$2i$	1	0.1551(3)	0.5411(2)	0.4263(1)	0.033(1)
C(2)	$2i$	1	0.2116(3)	0.6960(2)	0.4281(1)	0.036(1)
C(3)	$2i$	1	0.1554(3)	0.7753(2)	0.3675(1)	0.036(1)
C(4)	$2i$	1	0.0444(3)	0.7065(2)	0.3002(1)	0.040(1)
C(5)	$2i$	1	-0.0102(3)	0.5590(2)	0.2990(1)	0.041(1)
C(6)	$2i$	1	-0.0290(4)	0.3197(2)	0.3582(2)	0.043(1)
C(7)	$2i$	1	0.2079(3)	0.9391(2)	0.3745(2)	0.048(1)
C(8)	$2i$	1	0.3704(3)	0.4391(2)	0.5972(1)	0.033(1)
C(9)	$2i$	1	0.3159(3)	0.2852(2)	0.6020(1)	0.036(1)
C(10)	$2i$	1	0.3764(3)	0.2161(2)	0.6671(1)	0.036(1)
C(11)	$2i$	1	0.4928(3)	0.2935(2)	0.7295(1)	0.042(1)
C(12)	$2i$	1	0.5462(3)	0.4396(2)	0.7230(1)	0.040(1)
C(13)	$2i$	1	0.5521(4)	0.6690(2)	0.6548(2)	0.042(1)
C(14)	$2i$	1	0.3118(3)	0.0562(2)	0.6753(1)	0.046(1)
N(5)	$2i$	1	0.3801(3)	0.5824(2)	1.0758(1)	0.058(1)
N(6)	$2i$	1	0.3392(3)	0.6747(2)	0.8126(1)	0.055(1)
N(7)	$2i$	1	1.1313(3)	1.3115(2)	1.1763(1)	0.059(1)
N(8)	$2i$	1	1.0954(3)	1.3993(2)	0.9087(1)	0.066(1)
C(15)	$2i$	1	0.8625(3)	1.1224(2)	1.0108(1)	0.035(1)
C(16)	$2i$	1	0.7850(3)	1.0802(2)	0.9286(1)	0.038(1)
C(17)	$2i$	1	0.6656(3)	0.9598(2)	0.9122(1)	0.038(1)
C(18)	$2i$	1	0.6095(3)	0.8685(2)	0.9769(1)	0.036(1)
C(19)	$2i$	1	0.6884(3)	0.9109(2)	1.0595(1)	0.037(1)
C(20)	$2i$	1	0.8081(3)	1.0316(2)	1.0756(1)	0.038(1)
C(21)	$2i$	1	0.9893(3)	1.2453(2)	1.0276(1)	0.038(1)
C(22)	$2i$	1	1.0492(3)	1.3332(2)	0.9626(2)	0.045(1)
C(23)	$2i$	1	1.0692(3)	1.2850(2)	1.1097(2)	0.041(1)
C(24)	$2i$	1	0.4841(3)	0.7458(2)	0.9603(1)	0.037(1)
C(25)	$2i$	1	0.4264(3)	0.6542(2)	1.0239(1)	0.041(1)
C(26)	$2i$	1	0.4044(3)	0.7046(2)	0.8785(1)	0.040(1)
H(10)	$2i$	1	0.2850(3)	0.7370(2)	0.4723(13)	0.036(6)
H(2)	$2i$	1	0.0010(3)	0.7640(2)	0.2571(14)	0.056(7)
H(4)	$2i$	1	-0.0810(3)	0.5070(2)	0.2554(14)	0.044(6)
H(6A)	$2i$	1	-0.0710(4)	0.2940(3)	0.4120(18)	0.077(9)
H(6B)	$2i$	1	0.0580(4)	0.2670(3)	0.3561(16)	0.072(9)
H(6C)	$2i$	1	-0.1060(4)	0.2970(3)	0.3105(17)	0.062(8)
H(9)	$2i$	1	0.2340(3)	0.2330(2)	0.5620(13)	0.040(6)
H(11)	$2i$	1	0.5450(3)	0.2440(2)	0.7758(13)	0.039(6)
H(12)	$2i$	1	0.6240(3)	0.4970(3)	0.7624(14)	0.054(7)
H(13A)	$2i$	1	0.4640(3)	0.7160(2)	0.6562(13)	0.045(7)
H(13B)	$2i$	1	0.5920(3)	0.6830(2)	0.5990(16)	0.057(7)
H(13C)	$2i$	1	0.6340(4)	0.6960(3)	0.7016(17)	0.065(8)
H(16)	$2i$	1	0.8140(3)	1.1340(2)	0.8850(13)	0.038(6)

Table A.72 – continued from previous page

Atom	Wyck.	Site	x/a	y/b	z/c	U_{eq}
H(17)	$2i$	1	0.6150(3)	0.9350(2)	0.8572(13)	0.036(6)
H(19)	$2i$	1	0.6550(3)	0.8490(2)	1.1011(14)	0.049(6)
H(20)	$2i$	1	0.8610(3)	1.0590(2)	1.1316(15)	0.052(7)

Table A.73: Anisotropic displacement parameters $U_{ij}/\text{\AA}^2$ for the independent atoms in the structure of (8)(TCNQ) at 253 K.

Atom	U_{11}	U_{22}	U_{33}	U_{23}	U_{13}	U_{12}
F(1)	0.102(1)	0.049(1)	0.061(1)	0.026(1)	-0.006(1)	-0.005(1)
F(2)	0.086(1)	0.041(1)	0.093(1)	-0.004(1)	0.009(1)	0.022(1)
F(3)	0.066(1)	0.041(1)	0.079(1)	0.011(1)	-0.012(1)	-0.007(1)
F(4)	0.080(1)	0.042(1)	0.082(1)	0.020(1)	-0.010(1)	0.018(1)
F(5)	0.071(1)	0.052(1)	0.073(1)	0.020(1)	0.025(1)	0.004(1)
F(6)	0.102(1)	0.036(1)	0.049(1)	-0.001(1)	0.000(1)	-0.004(1)
N(1)	0.040(1)	0.030(1)	0.034(1)	0.002(1)	0.000(1)	0.004(1)
N(2)	0.042(1)	0.032(1)	0.032(1)	0.003(1)	-0.001(1)	0.006(1)
N(3)	0.043(1)	0.032(1)	0.034(1)	0.004(1)	-0.001(1)	0.007(1)
N(4)	0.040(1)	0.030(1)	0.033(1)	0.001(1)	0.002(1)	0.004(1)
C(1)	0.037(1)	0.033(1)	0.029(1)	0.003(1)	0.004(1)	0.005(1)
C(2)	0.041(1)	0.034(1)	0.031(1)	-0.001(1)	0.001(1)	0.004(1)
C(3)	0.042(1)	0.032(1)	0.036(1)	0.006(1)	0.004(1)	0.006(1)
C(4)	0.048(2)	0.038(1)	0.036(1)	0.007(1)	-0.001(1)	0.011(1)
C(5)	0.048(2)	0.040(1)	0.034(1)	0.000(1)	-0.005(1)	0.010(1)
C(6)	0.049(2)	0.031(1)	0.045(2)	0.001(1)	-0.004(1)	0.000(1)
C(7)	0.057(2)	0.037(1)	0.049(2)	0.009(1)	0.000(1)	0.005(1)
C(8)	0.037(1)	0.033(1)	0.028(1)	0.000(1)	0.003(1)	0.006(1)
C(9)	0.041(1)	0.032(1)	0.035(1)	0.003(1)	0.001(1)	0.004(1)
C(10)	0.044(2)	0.031(1)	0.034(1)	0.003(1)	0.006(1)	0.006(1)
C(11)	0.051(2)	0.039(1)	0.034(1)	0.006(1)	-0.002(1)	0.011(1)
C(12)	0.046(2)	0.040(1)	0.034(1)	-0.002(1)	-0.004(1)	0.008(1)
C(13)	0.049(2)	0.031(1)	0.044(2)	0.001(1)	0.001(1)	0.000(1)
C(14)	0.055(2)	0.039(1)	0.045(1)	0.009(1)	0.003(1)	0.007(1)
N(5)	0.069(2)	0.051(1)	0.046(1)	0.009(1)	0.003(1)	-0.009(1)
N(6)	0.061(2)	0.054(1)	0.043(1)	-0.001(1)	-0.002(1)	-0.007(1)
N(7)	0.060(2)	0.059(1)	0.048(1)	0.001(1)	-0.006(1)	-0.006(1)
N(8)	0.070(2)	0.065(1)	0.057(1)	0.020(1)	0.004(1)	-0.010(1)
C(15)	0.039(1)	0.033(1)	0.032(1)	0.003(1)	0.002(1)	0.007(1)
C(16)	0.049(2)	0.036(1)	0.029(1)	0.007(1)	0.002(1)	0.003(1)
C(17)	0.047(2)	0.039(1)	0.025(1)	0.001(1)	0.001(1)	0.004(1)
C(18)	0.042(1)	0.031(1)	0.034(1)	0.001(1)	0.004(1)	0.006(1)
C(19)	0.045(2)	0.035(1)	0.031(1)	0.005(1)	0.004(1)	0.005(1)
C(20)	0.045(2)	0.038(1)	0.028(1)	0.001(1)	0.000(1)	0.004(1)
C(21)	0.042(1)	0.034(1)	0.036(1)	0.002(1)	0.000(1)	0.002(1)
C(22)	0.047(2)	0.039(1)	0.044(1)	0.002(1)	0.000(1)	0.000(1)
C(23)	0.042(2)	0.036(1)	0.043(1)	0.001(1)	0.003(1)	-0.001(1)
C(24)	0.047(2)	0.032(1)	0.031(1)	0.000(1)	0.000(1)	0.005(1)
C(25)	0.048(2)	0.033(1)	0.038(1)	0.000(1)	0.001(1)	0.002(1)
C(26)	0.041(2)	0.032(1)	0.042(1)	0.001(1)	0.003(1)	-0.002(1)

Table A.74: Crystallographic data and structure refinement of (8)(TCNQ) at 203 K.

Compound	(8)(TCNQ)
Empirical Formula	C ₂₆ H ₁₆ F ₆ N ₈
Formula weight / g mol ⁻¹	554.47
Temperature / K	203(2)
Crystal size / mm ³	0.235×0.090×0.024
Crystal system; space group	Triclinic, P <bar{1}< td=""></bar{1}<>
Lattice constants / Å °	$a = 8.1771(4)$ $\alpha = 92.914(3)$ $b = 9.2431(5)$ $\beta = 94.948(4)$ $c = 16.1273(7)$ $\gamma = 100.062(2)$
Volume / Å ³	1193.01(1)
Z; F(000); calc. density / g cm ⁻³	2; 564; 1.544
Wavelength	Mo-K α (0.71073 Å)
Theta range for data collection / °	3.073 $\leq \theta \leq$ 27.543
Limiting indices	-10 $\leq h \leq$ 10, -12 $\leq k \leq$ 11, -20 $\leq l \leq$ 20
Reflections collected / unique	10801 / 4770
R _{int}	0.0799
Completeness to theta = 27.543	89.50 %
Absorption coefficient / mm ⁻¹	0.130
Refinement method	Full-matrix least-squares on F^2
Data / restraints / parameters	4770 / 0 / 426
R indices [I > 4σ(I)] R ₁ ; wR ₂	0.0478; 0.1078
R indices (all data) R ₁ ; wR ₂	0.0941; 0.1273
Goodness-of-fit for F^2	0.957
Extinction coefficient	0.015(2)
Largest diff. Peak and hole / e ⁻ Å ⁻³	0.225 / -0.243

Table A.75: Fractional coordinates in Å and equivalent isotropic displacement parameter U_{eq} /Å² for the independent atoms in the structure of (8)(TCNQ) at 203 K.

Atom	Wyck.	Site	x/a	y/b	z/c	U_{eq}
F(1)	2 <i>i</i>	1	0.2104(2)	0.9984(1)	0.3002(1)	0.057(1)
F(2)	2 <i>i</i>	1	0.0998(2)	1.0049(1)	0.4157(1)	0.056(1)
F(3)	2 <i>i</i>	1	0.3561(2)	0.9847(1)	0.4159(1)	0.051(1)
F(4)	2 <i>i</i>	1	0.4252(2)	-0.0113(1)	0.7171(1)	0.052(1)
F(5)	2 <i>i</i>	1	0.1787(2)	0.0342(1)	0.7189(1)	0.050(1)
F(6)	2 <i>i</i>	1	0.2682(2)	-0.0229(1)	0.6025(1)	0.050(1)
N(1)	2 <i>i</i>	1	0.0400(2)	0.4783(2)	0.3596(1)	0.028(1)
N(2)	2 <i>i</i>	1	0.2004(2)	0.4493(2)	0.4806(1)	0.029(1)
N(3)	2 <i>i</i>	1	0.3171(2)	0.5240(2)	0.5410(1)	0.030(1)
N(4)	2 <i>i</i>	1	0.4890(2)	0.5093(2)	0.6587(1)	0.029(1)
C(1)	2 <i>i</i>	1	0.1538(2)	0.5408(2)	0.4256(1)	0.027(1)
C(2)	2 <i>i</i>	1	0.2100(3)	0.6962(2)	0.4275(1)	0.029(1)
C(3)	2 <i>i</i>	1	0.1543(3)	0.7763(2)	0.3669(1)	0.030(1)
C(4)	2 <i>i</i>	1	0.0434(3)	0.7072(2)	0.2994(1)	0.034(1)
C(5)	2 <i>i</i>	1	-0.0104(3)	0.5597(2)	0.2978(1)	0.033(1)
C(6)	2 <i>i</i>	1	-0.0291(3)	0.3195(2)	0.3571(2)	0.036(1)
C(7)	2 <i>i</i>	1	0.2062(3)	0.9398(2)	0.3742(2)	0.039(1)
C(8)	2 <i>i</i>	1	0.3691(2)	0.4380(2)	0.5968(1)	0.027(1)

Table A.75 – continued from previous page

Atom	Wyck.	Site	x/a	y/b	z/c	U_{eq}
C(9)	2 <i>i</i>	1	0.3162(3)	0.2831(2)	0.6018(1)	0.029(1)
C(10)	2 <i>i</i>	1	0.3766(3)	0.2143(2)	0.6671(1)	0.029(1)
C(11)	2 <i>i</i>	1	0.4926(3)	0.2919(2)	0.7300(1)	0.034(1)
C(12)	2 <i>i</i>	1	0.5452(3)	0.4384(2)	0.7233(1)	0.033(1)
C(13)	2 <i>i</i>	1	0.5493(3)	0.6680(2)	0.6542(2)	0.034(1)
C(14)	2 <i>i</i>	1	0.3127(3)	0.0539(2)	0.6753(2)	0.037(1)
N(5)	2 <i>i</i>	1	0.3805(3)	0.5820(2)	1.0766(1)	0.046(1)
N(6)	2 <i>i</i>	1	0.3409(3)	0.6750(2)	0.8127(1)	0.045(1)
N(7)	2 <i>i</i>	1	1.1321(3)	1.3127(2)	1.1771(1)	0.047(1)
N(8)	2 <i>i</i>	1	1.0971(3)	1.4013(2)	0.9090(1)	0.052(1)
C(15)	2 <i>i</i>	1	0.8645(3)	1.1233(2)	1.0117(1)	0.030(1)
C(16)	2 <i>i</i>	1	0.7871(3)	1.0813(2)	0.9290(1)	0.031(1)
C(17)	2 <i>i</i>	1	0.6669(3)	0.9601(2)	0.9126(1)	0.031(1)
C(18)	2 <i>i</i>	1	0.6111(3)	0.8689(2)	0.9775(1)	0.029(1)
C(19)	2 <i>i</i>	1	0.6895(3)	0.9110(2)	1.0601(1)	0.030(1)
C(20)	2 <i>i</i>	1	0.8091(3)	1.0325(2)	1.0762(1)	0.031(1)
C(21)	2 <i>i</i>	1	0.9907(3)	1.2472(2)	1.0281(1)	0.031(1)
C(22)	2 <i>i</i>	1	1.0503(3)	1.3345(2)	0.9631(1)	0.036(1)
C(23)	2 <i>i</i>	1	1.0695(3)	1.2861(2)	1.1105(1)	0.033(1)
C(24)	2 <i>i</i>	1	0.4856(3)	0.7457(2)	0.9608(1)	0.030(1)
C(25)	2 <i>i</i>	1	0.4275(3)	0.6540(2)	1.0246(1)	0.032(1)
C(26)	2 <i>i</i>	1	0.4055(3)	0.7046(2)	0.8787(1)	0.032(1)
H(2)	2 <i>i</i>	1	0.2860(3)	0.7380(2)	0.4695(14)	0.030(6)
H(4)	2 <i>i</i>	1	0.0090(3)	0.7620(2)	0.2568(14)	0.037(6)
H(5)	2 <i>i</i>	1	-0.0900(3)	0.5090(2)	0.2542(13)	0.029(5)
H(6A)	2 <i>i</i>	1	0.0630(3)	0.2690(3)	0.3537(16)	0.058(8)
H(6B)	2 <i>i</i>	1	-0.0770(3)	0.2980(3)	0.4074(16)	0.046(7)
H(6C)	2 <i>i</i>	1	-0.1120(3)	0.2920(3)	0.3091(16)	0.048(7)
H(9)	2 <i>i</i>	1	0.2340(3)	0.2310(2)	0.5621(14)	0.038(6)
H(11)	2 <i>i</i>	1	0.5460(3)	0.2440(2)	0.7768(14)	0.037(6)
H(12)	2 <i>i</i>	1	0.6230(3)	0.4980(3)	0.7621(15)	0.051(7)
H(13A)	2 <i>i</i>	1	0.6270(3)	0.6990(2)	0.7004(15)	0.039(6)
H(13B)	2 <i>i</i>	1	0.6000(3)	0.6830(3)	0.6012(16)	0.048(7)
H(13C)	2 <i>i</i>	1	0.4590(3)	0.7150(3)	0.6577(15)	0.046(7)
H(16)	2 <i>i</i>	1	0.8190(3)	1.1360(2)	0.8860(15)	0.036(6)
H(17)	2 <i>i</i>	1	0.6170(3)	0.9370(2)	0.8574(14)	0.030(6)
H(19)	2 <i>i</i>	1	0.6570(3)	0.8560(2)	1.1006(15)	0.034(6)
H(20)	2 <i>i</i>	1	0.8600(3)	1.0580(2)	1.1302(15)	0.036(6)

Table A.76: Anisotropic displacement parameters $U_{ij}/\text{\AA}^2$ for the independent atoms in the structure of (8)(TCNQ) at 203 K.

Atom	U_{11}	U_{22}	U_{33}	U_{23}	U_{13}	U_{12}
F(1)	0.077(1)	0.038(1)	0.050(1)	0.021(1)	-0.001(1)	-0.004(1)
F(2)	0.066(1)	0.035(1)	0.071(1)	-0.004(1)	0.007(1)	0.017(1)
F(3)	0.050(1)	0.033(1)	0.062(1)	0.009(1)	-0.008(1)	-0.006(1)
F(4)	0.059(1)	0.035(1)	0.063(1)	0.015(1)	-0.006(1)	0.014(1)
F(5)	0.053(1)	0.041(1)	0.058(1)	0.015(1)	0.018(1)	0.001(1)
F(6)	0.075(1)	0.030(1)	0.040(1)	-0.002(1)	0.001(1)	-0.003(1)
N(1)	0.031(1)	0.024(1)	0.029(1)	0.002(1)	0.002(1)	0.002(1)
N(2)	0.032(1)	0.029(1)	0.026(1)	0.002(1)	0.001(1)	0.004(1)

Table A.76 – continued from previous page

Atom	Wyck.	Site	x/a	y/b	z/c	U_{eq}
N(3)	0.034(1)	0.027(1)	0.029(1)	0.002(1)	0.000(1)	0.005(1)
N(4)	0.033(1)	0.024(1)	0.028(1)	0.000(1)	0.002(1)	0.002(1)
C(1)	0.030(1)	0.028(1)	0.024(1)	0.003(1)	0.006(1)	0.005(1)
C(2)	0.032(1)	0.027(1)	0.027(1)	-0.001(1)	0.003(1)	0.003(1)
C(3)	0.033(1)	0.026(1)	0.031(1)	0.006(1)	0.007(1)	0.005(1)
C(4)	0.042(1)	0.030(1)	0.030(1)	0.006(1)	-0.001(1)	0.009(1)
C(5)	0.036(1)	0.034(1)	0.028(1)	0.000(1)	-0.002(1)	0.007(1)
C(6)	0.039(1)	0.025(1)	0.039(2)	0.000(1)	0.000(1)	-0.002(1)
C(7)	0.043(1)	0.032(1)	0.040(1)	0.006(1)	0.000(1)	0.004(1)
C(8)	0.029(1)	0.027(1)	0.027(1)	0.001(1)	0.004(1)	0.005(1)
C(9)	0.032(1)	0.026(1)	0.027(1)	0.001(1)	0.002(1)	0.003(1)
C(10)	0.033(1)	0.025(1)	0.030(1)	0.003(1)	0.006(1)	0.004(1)
C(11)	0.038(1)	0.031(1)	0.032(1)	0.003(1)	-0.002(1)	0.007(1)
C(12)	0.036(1)	0.033(1)	0.027(1)	-0.002(1)	-0.002(1)	0.006(1)
C(13)	0.039(1)	0.026(1)	0.035(2)	-0.003(1)	0.002(1)	-0.001(1)
C(14)	0.041(1)	0.031(1)	0.039(1)	0.007(1)	0.001(1)	0.005(1)
N(5)	0.055(1)	0.041(1)	0.038(1)	0.008(1)	0.001(1)	-0.007(1)
N(6)	0.050(1)	0.044(1)	0.035(1)	0.000(1)	0.000(1)	-0.005(1)
N(7)	0.050(1)	0.047(1)	0.039(1)	0.001(1)	-0.001(1)	-0.004(1)
N(8)	0.056(1)	0.050(1)	0.046(1)	0.014(1)	0.004(1)	-0.007(1)
C(15)	0.033(1)	0.026(1)	0.031(1)	0.002(1)	0.004(1)	0.004(1)
C(16)	0.036(1)	0.029(1)	0.026(1)	0.003(1)	0.005(1)	0.002(1)
C(17)	0.038(1)	0.032(1)	0.022(1)	0.002(1)	0.001(1)	0.003(1)
C(18)	0.033(1)	0.027(1)	0.027(1)	0.000(1)	0.004(1)	0.005(1)
C(19)	0.036(1)	0.029(1)	0.026(1)	0.004(1)	0.004(1)	0.004(1)
C(20)	0.036(1)	0.032(1)	0.023(1)	0.002(1)	0.000(1)	0.003(1)
C(21)	0.036(1)	0.028(1)	0.030(1)	0.002(1)	0.004(1)	0.003(1)
C(22)	0.038(1)	0.031(1)	0.034(1)	0.001(1)	-0.003(1)	-0.001(1)
C(23)	0.036(1)	0.029(1)	0.032(1)	0.004(1)	0.006(1)	0.000(1)
C(24)	0.035(1)	0.029(1)	0.026(1)	0.001(1)	0.002(1)	0.004(1)
C(25)	0.037(1)	0.028(1)	0.029(1)	-0.002(1)	-0.001(1)	0.001(1)
C(26)	0.036(1)	0.027(1)	0.031(1)	0.002(1)	0.006(1)	0.000(1)

Table A.77: Crystallographic data and structure refinement of **(8)(TCNQ)** at 153 K.

Compound	(8)(TCNQ)
Empirical Formula	$C_{26}H_{16}F_6N_8$
Formula weight / $gmol^{-1}$	554.47
Temperature / K	153(2)
Crystal size / mm^3	0.235×0.090×0.024
Crystal system; space group	Triclinic, $P\bar{1}$
Lattice constants / \AA°	$a = 8.1147(4) \alpha = 92.935(3)$ $b = 9.2265(5) \beta = 94.818(3)$ $c = 16.1205(7) \gamma = 99.753(2)$
Volume / \AA^3	1182.67(1)
Z; F(000); calc. density / gcm^{-3}	2; 564; 1.557
Wavelength	Mo-K α (0.71073 \AA)
Theta range for data collection / $^\circ$	$2.962 \leq \theta \leq 27.516$
Limiting indices	$-10 \leq h \leq 10, -11 \leq k \leq 11, -20 \leq l \leq 20$

Table A.77 – continued from previous page

Compound	(8)(TCNQ)
Reflections collected / unique	15348 / 5139
R_{int}	0.0717
Completeness to theta = 25.242	96.60 %
Absorption coefficient / mm^{-1}	0.131
Refinement method	Full-matrix least-squares on F^2
Data / restraints / parameters	5139 / 0 / 425
R indices [$I > 4\sigma(I)$] R_1 ; wR_2	0.0480; 0.1071
R indices (all data) R_1 ; wR_2	0.0873; 0.1232
Goodness-of-fit for F^2	0.979
Largest diff. Peak and hole / $e^{-\text{\AA}^{-3}}$	0.224 / -0.359

Table A.78: Fractional coordinates in Å and equivalent isotropic displacement parameter $U_{eq}/\text{\AA}^2$ for the independent atoms in the structure of (8)(TCNQ) at 153 K.

Atom	Wyck.	Site	x/a	y/b	z/c	U_{eq}
F(1)	2i	1	0.2084(2)	1.0003(1)	0.3001(1)	0.045(1)
F(2)	2i	1	0.0970(2)	1.0055(1)	0.4163(1)	0.045(1)
F(3)	2i	1	0.3562(2)	0.9854(1)	0.4158(1)	0.042(1)
F(4)	2i	1	0.4276(2)	-0.0131(1)	0.7171(1)	0.041(1)
F(5)	2i	1	0.1775(2)	0.0317(1)	0.7183(1)	0.040(1)
F(6)	2i	1	0.2701(2)	-0.0246(1)	0.6020(1)	0.040(1)
N(1)	2i	1	0.0390(2)	0.4790(2)	0.3588(1)	0.025(1)
N(2)	2i	1	0.1991(2)	0.4490(2)	0.4801(1)	0.026(1)
N(3)	2i	1	0.3158(2)	0.5230(2)	0.5407(1)	0.026(1)
N(4)	2i	1	0.4877(2)	0.5083(1)	0.6586(1)	0.025(1)
C(1)	2i	1	0.1526(2)	0.5407(2)	0.4247(1)	0.024(1)
C(2)	2i	1	0.2084(2)	0.6964(2)	0.4273(1)	0.025(1)
C(3)	2i	1	0.1533(2)	0.7768(2)	0.3664(1)	0.026(1)
C(4)	2i	1	0.0428(3)	0.7090(2)	0.2980(1)	0.029(1)
C(5)	2i	1	-0.0114(3)	0.5601(2)	0.2966(1)	0.028(1)
C(6)	2i	1	-0.0291(3)	0.3200(2)	0.3564(1)	0.029(1)
C(7)	2i	1	0.2047(3)	0.9407(2)	0.3745(1)	0.033(1)
C(8)	2i	1	0.3686(2)	0.4369(2)	0.5968(1)	0.024(1)
C(9)	2i	1	0.3159(2)	0.2818(2)	0.6014(1)	0.026(1)
C(10)	2i	1	0.3766(2)	0.2128(2)	0.6669(1)	0.026(1)
C(11)	2i	1	0.4928(3)	0.2907(2)	0.7302(1)	0.028(1)
C(12)	2i	1	0.5448(3)	0.4378(2)	0.7236(1)	0.028(1)
C(13)	2i	1	0.5475(3)	0.6676(2)	0.6543(1)	0.029(1)
C(14)	2i	1	0.3143(3)	0.0520(2)	0.6749(1)	0.031(1)
N(5)	2i	1	0.3804(2)	0.5814(2)	1.0772(1)	0.040(1)
N(6)	2i	1	0.3422(2)	0.6749(2)	0.8131(1)	0.037(1)
N(7)	2i	1	1.1335(2)	1.3139(2)	1.1779(1)	0.039(1)
N(8)	2i	1	1.0988(2)	1.4029(2)	0.9094(1)	0.043(1)
C(15)	2i	1	0.8649(2)	1.1243(2)	1.0118(1)	0.025(1)
C(16)	2i	1	0.7882(3)	1.0821(2)	0.9295(1)	0.028(1)
C(17)	2i	1	0.6677(3)	0.9605(2)	0.9126(1)	0.028(1)
C(18)	2i	1	0.6119(2)	0.8693(2)	0.9782(1)	0.026(1)
C(19)	2i	1	0.6902(3)	0.9114(2)	1.0605(1)	0.027(1)
C(20)	2i	1	0.8098(3)	1.0331(2)	1.0772(1)	0.027(1)
C(21)	2i	1	0.9917(2)	1.2479(2)	1.0288(1)	0.026(1)

Table A.78 – continued from previous page

Atom	Wyck.	Site	x/a	y/b	z/c	U_{eq}
C(22)	2 <i>i</i>	1	1.0517(2)	1.3361(2)	0.9636(1)	0.030(1)
C(23)	2 <i>i</i>	1	1.0705(3)	1.2873(2)	1.1111(1)	0.029(1)
C(24)	2 <i>i</i>	1	0.4861(2)	0.7456(2)	0.9610(1)	0.026(1)
C(25)	2 <i>i</i>	1	0.4281(2)	0.6537(2)	1.0253(1)	0.029(1)
C(26)	2 <i>i</i>	1	0.4070(2)	0.7044(2)	0.8791(1)	0.028(1)
H(2)	2 <i>i</i>	1	0.2820(3)	0.7374(19)	0.4715(12)	0.025(5)
H(4)	2 <i>i</i>	1	0.0040(3)	0.7660(2)	0.2539(12)	0.031(5)
H(5)	2 <i>i</i>	1	-0.0850(2)	0.5059(19)	0.2533(12)	0.021(5)
H(6A)	2 <i>i</i>	1	-0.0850(3)	0.2960(2)	0.4052(13)	0.036(6)
H(6B)	2 <i>i</i>	1	0.0600(3)	0.2653(19)	0.3508(11)	0.025(5)
H(6C)	2 <i>i</i>	1	-0.1110(3)	0.2980(2)	0.3087(14)	0.037(6)
H(9)	2 <i>i</i>	1	0.2380(3)	0.2280(2)	0.5595(13)	0.032(5)
H(11)	2 <i>i</i>	1	0.5440(3)	0.2430(2)	0.7769(13)	0.033(5)
H(12)	2 <i>i</i>	1	0.6230(2)	0.4991(19)	0.7643(12)	0.028(5)
H(13A)	2 <i>i</i>	1	0.6260(3)	0.6942(19)	0.6996(13)	0.024(5)
H(13B)	2 <i>i</i>	1	0.4550(3)	0.7167(19)	0.6581(11)	0.025(5)
H(13C)	2 <i>i</i>	1	0.6000(2)	0.6831(19)	0.6049(13)	0.027(5)
H(16)	2 <i>i</i>	1	0.8210(3)	1.1360(2)	0.8852(12)	0.030(5)
H(17)	2 <i>i</i>	1	0.6160(2)	0.9326(18)	0.8565(12)	0.020(5)
H(19)	2 <i>i</i>	1	0.6560(3)	0.8560(2)	1.1013(13)	0.032(5)
H(2)	2 <i>i</i>	1	0.8640(2)	1.0626(18)	1.1325(12)	0.023(5)

Table A.79: Anisotropic displacement parameters $U_{ij}/\text{\AA}^2$ for the independent atoms in the structure of (8)(TCNQ) at 153 K.

Atom	U_{11}	U_{22}	U_{33}	U_{23}	U_{13}	U_{12}
F(1)	0.061(1)	0.031(1)	0.042(1)	0.016(1)	0.001(1)	-0.004(1)
F(2)	0.054(1)	0.026(1)	0.054(1)	-0.003(1)	0.006(1)	0.011(1)
F(3)	0.042(1)	0.027(1)	0.051(1)	0.007(1)	-0.004(1)	-0.005(1)
F(4)	0.048(1)	0.027(1)	0.049(1)	0.011(1)	-0.004(1)	0.008(1)
F(5)	0.045(1)	0.032(1)	0.045(1)	0.011(1)	0.013(1)	0.000(1)
F(6)	0.059(1)	0.022(1)	0.035(1)	-0.001(1)	0.001(1)	-0.003(1)
N(1)	0.030(1)	0.020(1)	0.025(1)	0.002(1)	0.002(1)	0.000(1)
N(2)	0.030(1)	0.023(1)	0.024(1)	0.001(1)	0.001(1)	0.002(1)
N(3)	0.031(1)	0.022(1)	0.023(1)	0.001(1)	0.002(1)	0.002(1)
N(4)	0.030(1)	0.019(1)	0.025(1)	0.001(1)	0.003(1)	-0.001(1)
C(1)	0.025(1)	0.023(1)	0.022(1)	0.002(1)	0.005(1)	0.003(1)
C(2)	0.028(1)	0.022(1)	0.024(1)	0.000(1)	0.004(1)	0.001(1)
C(3)	0.032(1)	0.020(1)	0.027(1)	0.004(1)	0.007(1)	0.003(1)
C(4)	0.034(1)	0.026(1)	0.026(1)	0.004(1)	0.003(1)	0.006(1)
C(5)	0.032(1)	0.026(1)	0.025(1)	0.001(1)	-0.002(1)	0.005(1)
C(6)	0.034(1)	0.021(1)	0.031(1)	0.001(1)	-0.001(1)	0.000(1)
C(7)	0.039(1)	0.026(1)	0.032(1)	0.005(1)	0.001(1)	0.002(1)
C(8)	0.027(1)	0.022(1)	0.023(1)	0.001(1)	0.005(1)	0.003(1)
C(9)	0.030(1)	0.022(1)	0.026(1)	0.000(1)	0.003(1)	0.002(1)
C(10)	0.030(1)	0.020(1)	0.026(1)	0.002(1)	0.006(1)	0.002(1)
C(11)	0.035(1)	0.026(1)	0.024(1)	0.004(1)	0.002(1)	0.005(1)
C(12)	0.032(1)	0.026(1)	0.023(1)	-0.002(1)	-0.001(1)	0.003(1)
C(13)	0.034(1)	0.022(1)	0.029(1)	-0.001(1)	0.003(1)	-0.001(1)
C(14)	0.037(1)	0.026(1)	0.031(1)	0.004(1)	0.004(1)	0.003(1)
N(5)	0.050(1)	0.031(1)	0.034(1)	0.005(1)	0.003(1)	-0.006(1)

Table A.79 – continued from previous page

Atom	Wyck.	Site	x/a	y/b	z/c	U_{eq}
N(6)	0.043(1)	0.033(1)	0.030(1)	0.000(1)	0.001(1)	-0.005(1)
N(7)	0.044(1)	0.036(1)	0.033(1)	0.001(1)	0.000(1)	-0.004(1)
N(8)	0.048(1)	0.038(1)	0.038(1)	0.009(1)	0.002(1)	-0.007(1)
C(15)	0.029(1)	0.021(1)	0.026(1)	0.002(1)	0.003(1)	0.004(1)
C(16)	0.035(1)	0.024(1)	0.024(1)	0.004(1)	0.007(1)	0.001(1)
C(17)	0.035(1)	0.025(1)	0.021(1)	0.000(1)	0.002(1)	0.003(1)
C(18)	0.032(1)	0.022(1)	0.025(1)	0.001(1)	0.005(1)	0.004(1)
C(19)	0.033(1)	0.023(1)	0.023(1)	0.003(1)	0.005(1)	0.002(1)
C(20)	0.034(1)	0.025(1)	0.022(1)	0.001(1)	0.001(1)	0.002(1)
C(21)	0.029(1)	0.023(1)	0.026(1)	0.001(1)	0.003(1)	0.001(1)
C(22)	0.032(1)	0.025(1)	0.030(1)	-0.002(1)	-0.002(1)	-0.001(1)
C(23)	0.032(1)	0.021(1)	0.034(1)	0.003(1)	0.007(1)	0.000(1)
C(24)	0.032(1)	0.023(1)	0.022(1)	0.000(1)	0.004(1)	0.003(1)
C(25)	0.033(1)	0.023(1)	0.028(1)	-0.002(1)	0.000(1)	0.000(1)
C(26)	0.031(1)	0.020(1)	0.031(1)	0.002(1)	0.006(1)	-0.001(1)

Table A.80: Crystallographic data and structure refinement of (8)(TCNQ) at 123 K.

Compound	(8)(TCNQ)
Empirical Formula	$C_{26}H_{16}F_6N_8$
Formula weight / $gmol^{-1}$	554.47
Temperature / K	123(2)
Crystal size / mm^3	$0.235 \times 0.090 \times 0.024$
Crystal system; space group	Triclinic, $P\bar{1}$
Lattice constants / \AA°	$a = 8.0798(4)$ $\alpha = 92.905(3)$ $b = 9.2136(4)$ $\beta = 94.822(2)$ $c = 16.1189(9)$ $\gamma = 99.563(3)$
Volume / \AA^3	1176.54(1)
Z; F(000); calc. density / gcm^{-3}	2; 564; 1.565
Wavelength	Mo-K α (0.71073 \AA)
Theta range for data collection / $^\circ$	$2.970 \leq \theta \leq 27.631$
Limiting indices	$-10 \leq h \leq 10, -11 \leq k \leq 11, -20 \leq l \leq 20$
Reflections collected / unique	12617 / 4885
R_{int}	0.0666
Completeness to theta = 25.242	93.20 %
Absorption coefficient / mm^{-1}	0.132
Refinement method	Full-matrix least-squares on F^2
Data / restraints / parameters	4865 / 0 / 425
R indices [I > 4 σ (I)] R_1 ; wR_2	0.0456; 0.1075
R indices (all data) R_1 ; wR_2	0.0791; 0.1223
Goodness-of-fit for F^2	0.973
Largest diff. Peak and hole / $e^- \text{\AA}^{-3}$	0.227 / -0.324

Table A.81: Fractional coordinates in Å and equivalent isotropic displacement parameter $U_{eq}/\text{\AA}^2$ for the independent atoms in the structure of (8)(TCNQ) at 123 K.

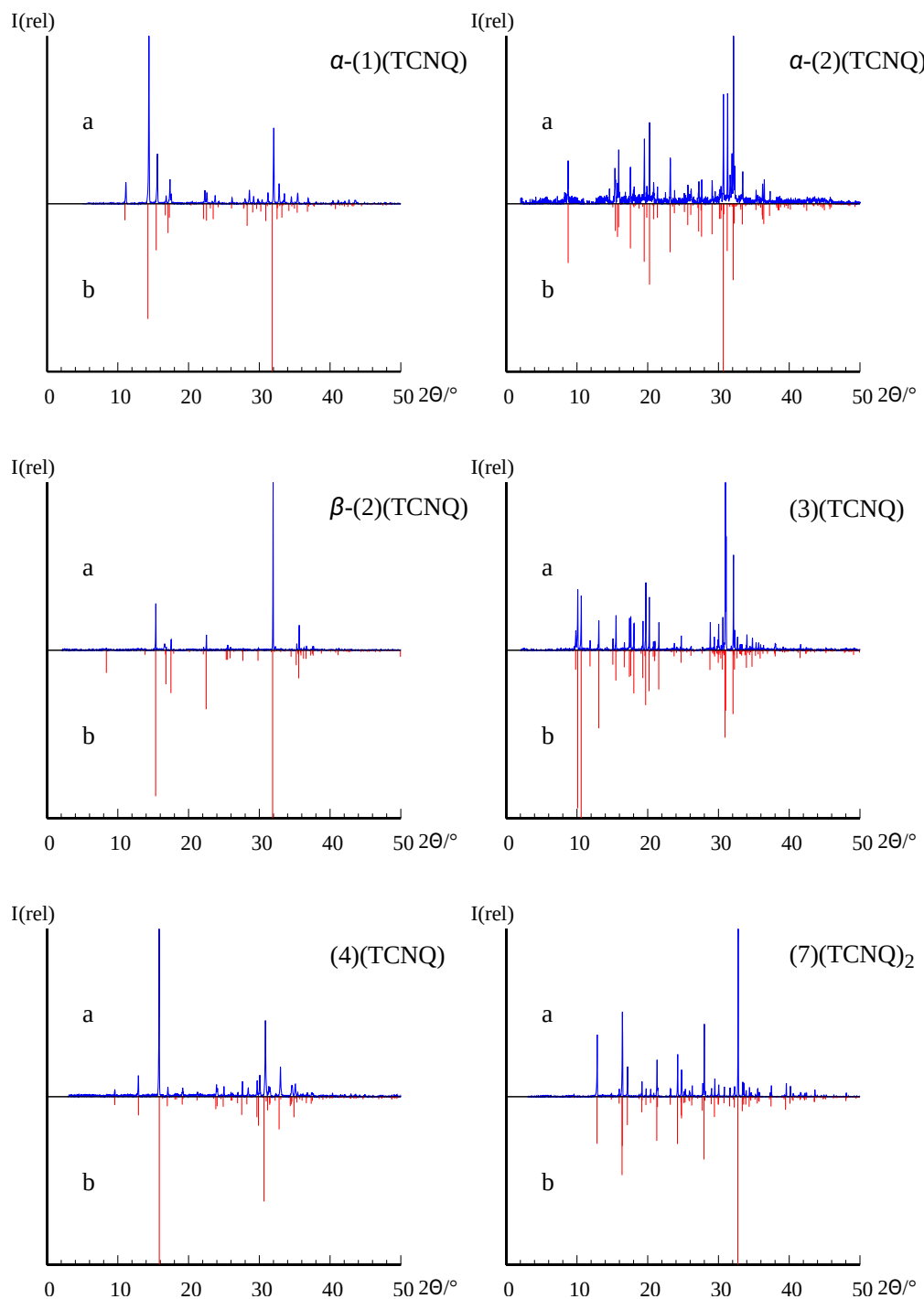
Atom	Wyck.	Site	x/a	y/b	z/c	U_{eq}
F(1)	$2i$	1	0.0953(2)	1.0057(1)	0.4166(1)	0.035(1)
F(2)	$2i$	1	0.3559(1)	0.9856(1)	0.4158(1)	0.034(1)
F(3)	$2i$	1	0.2070(2)	1.0014(1)	0.3002(1)	0.036(1)
F(4)	$2i$	1	0.2714(2)	-0.0254(1)	0.6018(1)	0.032(1)
F(5)	$2i$	1	0.1771(1)	0.0303(1)	0.7181(1)	0.033(1)
F(6)	$2i$	1	0.4293(2)	-0.0137(1)	0.7172(1)	0.033(1)
N(1)	$2i$	1	0.0386(2)	0.4788(2)	0.3584(1)	0.020(1)
N(2)	$2i$	1	0.1984(2)	0.4487(2)	0.4797(1)	0.021(1)
N(3)	$2i$	1	0.3149(2)	0.5228(2)	0.5403(1)	0.021(1)
N(4)	$2i$	1	0.4876(2)	0.5079(2)	0.6586(1)	0.021(1)
C(1)	$2i$	1	0.1521(2)	0.5403(2)	0.4246(1)	0.020(1)
C(2)	$2i$	1	0.2082(2)	0.6964(2)	0.4270(1)	0.021(1)
C(3)	$2i$	1	0.1527(2)	0.7774(2)	0.3661(1)	0.022(1)
C(4)	$2i$	1	0.0425(2)	0.7096(2)	0.2977(1)	0.023(1)
C(5)	$2i$	1	-0.0115(2)	0.5605(2)	0.2960(1)	0.023(1)
C(6)	$2i$	1	-0.0294(3)	0.3199(2)	0.3558(1)	0.024(1)
C(7)	$2i$	1	0.2032(2)	0.9411(2)	0.3742(1)	0.026(1)
C(8)	$2i$	1	0.3677(2)	0.4364(2)	0.5965(1)	0.019(1)
C(9)	$2i$	1	0.3161(2)	0.2813(2)	0.6012(1)	0.021(1)
C(10)	$2i$	1	0.3769(2)	0.2118(2)	0.6668(1)	0.021(1)
C(11)	$2i$	1	0.4922(2)	0.2898(2)	0.7303(1)	0.024(1)
C(12)	$2i$	1	0.5445(2)	0.4370(2)	0.7236(1)	0.023(1)
C(13)	$2i$	1	0.5468(3)	0.6672(2)	0.6544(1)	0.024(1)
C(14)	$2i$	1	0.3149(2)	0.0516(2)	0.6746(1)	0.025(1)
N(5)	$2i$	1	0.3807(2)	0.5815(2)	1.0774(1)	0.032(1)
N(6)	$2i$	1	0.3424(2)	0.6751(2)	0.8133(1)	0.030(1)
N(7)	$2i$	1	1.1338(2)	1.3143(2)	1.1781(1)	0.031(1)
N(8)	$2i$	1	1.0991(2)	1.4035(2)	0.9096(1)	0.035(1)
C(15)	$2i$	1	0.8654(2)	1.1246(2)	1.0121(1)	0.021(1)
C(16)	$2i$	1	0.7887(2)	1.0827(2)	0.9294(1)	0.022(1)
C(17)	$2i$	1	0.6686(2)	0.9610(2)	0.9128(1)	0.022(1)
C(18)	$2i$	1	0.6129(2)	0.8695(2)	0.9780(1)	0.021(1)
C(19)	$2i$	1	0.6905(2)	0.9113(2)	1.0609(1)	0.022(1)
C(20)	$2i$	1	0.8101(2)	1.0332(2)	1.0772(1)	0.022(1)
C(21)	$2i$	1	0.9922(2)	1.2489(2)	1.0289(1)	0.022(1)
C(22)	$2i$	1	1.0520(2)	1.3366(2)	0.9637(1)	0.024(1)
C(23)	$2i$	1	1.0713(2)	1.2878(2)	1.1107(1)	0.023(1)
C(24)	$2i$	1	0.4868(2)	0.7450(2)	0.9613(1)	0.022(1)
C(25)	$2i$	1	0.4287(2)	0.6540(2)	1.0254(1)	0.023(1)
C(26)	$2i$	1	0.4077(2)	0.7044(2)	0.8795(1)	0.022(1)
H(2)	$2i$	1	0.2810(3)	0.7340(2)	0.4704(13)	0.025(5)
H(4)	$2i$	1	0.0020(3)	0.7670(2)	0.2531(14)	0.038(6)
H(5)	$2i$	1	-0.0890(2)	0.5060(2)	0.2529(12)	0.020(5)
H(6A)	$2i$	1	-0.1090(3)	0.2990(2)	0.3050(14)	0.030(6)
H(6B)	$2i$	1	0.0610(3)	0.2610(2)	0.3513(14)	0.039(6)
H(6C)	$2i$	1	-0.0820(3)	0.2950(2)	0.4064(14)	0.036(6)
H(9)	$2i$	1	0.2330(2)	0.2320(2)	0.5614(12)	0.019(5)
H(11)	$2i$	1	0.5420(2)	0.2400(2)	0.7764(13)	0.024(5)
H(12)	$2i$	1	0.6210(2)	0.4950(2)	0.7627(13)	0.024(5)
H(13A)	$2i$	1	0.5960(3)	0.6860(2)	0.6008(15)	0.037(6)
H(13B)	$2i$	1	0.4530(3)	0.7190(2)	0.6542(12)	0.022(5)
H(13C)	$2i$	1	0.6300(3)	0.6960(2)	0.7024(14)	0.030(6)
H(16)	$2i$	1	0.8240(3)	1.1410(2)	0.8847(14)	0.031(6)

Table A.81 – continued from previous page

Atom	Wyck.	Site	x/a	y/b	z/c	U_{eq}
H(17)	$2i$	1	0.6190(2)	0.9320(2)	0.8568(14)	0.026(5)
H(19)	$2i$	1	0.6570(2)	0.8520(2)	1.1024(13)	0.022(5)
H(20)	$2i$	1	0.8660(2)	1.0630(2)	1.1317(13)	0.022(5)

Table A.82: Anisotropic displacement parameters $U_{ij}/\text{\AA}^2$ for the independent atoms in the structure of (8)(TCNQ) at 123 K.

Atom	U_{11}	U_{22}	U_{33}	U_{23}	U_{13}	U_{12}
F(1)	0.042(1)	0.025(1)	0.041(1)	-0.003(1)	0.003(1)	0.010(1)
F(2)	0.032(1)	0.027(1)	0.038(1)	0.006(1)	-0.005(1)	-0.004(1)
F(3)	0.046(1)	0.027(1)	0.034(1)	0.014(1)	-0.001(1)	-0.001(1)
F(4)	0.044(1)	0.022(1)	0.026(1)	-0.002(1)	0.001(1)	-0.001(1)
F(5)	0.034(1)	0.029(1)	0.035(1)	0.008(1)	0.011(1)	0.000(1)
F(6)	0.038(1)	0.024(1)	0.037(1)	0.008(1)	-0.005(1)	0.008(1)
N(1)	0.022(1)	0.017(1)	0.021(1)	0.000(1)	0.002(1)	0.001(1)
N(2)	0.022(1)	0.021(1)	0.019(1)	0.001(1)	0.000(1)	0.003(1)
N(3)	0.023(1)	0.021(1)	0.019(1)	0.000(1)	-0.001(1)	0.003(1)
N(4)	0.023(1)	0.018(1)	0.021(1)	0.001(1)	0.001(1)	0.002(1)
C(1)	0.023(1)	0.021(1)	0.018(1)	0.002(1)	0.003(1)	0.003(1)
C(2)	0.021(1)	0.021(1)	0.019(1)	-0.001(1)	0.002(1)	0.002(1)
C(3)	0.025(1)	0.019(1)	0.024(1)	0.003(1)	0.006(1)	0.004(1)
C(4)	0.027(1)	0.024(1)	0.020(1)	0.004(1)	0.002(1)	0.007(1)
C(5)	0.023(1)	0.024(1)	0.020(1)	0.000(1)	-0.002(1)	0.005(1)
C(6)	0.028(1)	0.019(1)	0.025(1)	0.001(1)	0.000(1)	0.000(1)
C(7)	0.028(1)	0.025(1)	0.024(1)	0.004(1)	-0.001(1)	0.003(1)
C(8)	0.019(1)	0.021(1)	0.018(1)	-0.001(1)	0.002(1)	0.003(1)
C(9)	0.022(1)	0.022(1)	0.019(1)	0.001(1)	0.001(1)	0.002(1)
C(10)	0.022(1)	0.020(1)	0.021(1)	0.000(1)	0.004(1)	0.004(1)
C(11)	0.028(1)	0.024(1)	0.021(1)	0.003(1)	0.000(1)	0.006(1)
C(12)	0.024(1)	0.022(1)	0.020(1)	-0.004(1)	-0.002(1)	0.003(1)
C(13)	0.026(1)	0.019(1)	0.026(1)	0.000(1)	0.001(1)	0.000(1)
C(14)	0.028(1)	0.024(1)	0.023(1)	0.004(1)	0.001(1)	0.005(1)
N(5)	0.038(1)	0.029(1)	0.026(1)	0.004(1)	0.002(1)	-0.001(1)
N(6)	0.033(1)	0.029(1)	0.026(1)	0.001(1)	0.001(1)	-0.003(1)
N(7)	0.033(1)	0.030(1)	0.027(1)	0.000(1)	0.001(1)	-0.003(1)
N(8)	0.036(1)	0.035(1)	0.031(1)	0.008(1)	0.001(1)	-0.003(1)
C(15)	0.022(1)	0.021(1)	0.021(1)	0.001(1)	0.003(1)	0.005(1)
C(16)	0.026(1)	0.022(1)	0.017(1)	0.004(1)	0.003(1)	0.002(1)
C(17)	0.027(1)	0.023(1)	0.016(1)	0.000(1)	0.002(1)	0.005(1)
C(18)	0.022(1)	0.019(1)	0.021(1)	0.000(1)	0.002(1)	0.004(1)
C(19)	0.028(1)	0.020(1)	0.018(1)	0.004(1)	0.003(1)	0.004(1)
C(20)	0.024(1)	0.024(1)	0.019(1)	0.001(1)	0.000(1)	0.004(1)
C(21)	0.022(1)	0.023(1)	0.021(1)	0.002(1)	0.001(1)	0.004(1)
C(22)	0.024(1)	0.021(1)	0.024(1)	-0.001(1)	-0.002(1)	-0.001(1)
C(23)	0.023(1)	0.020(1)	0.025(1)	0.002(1)	0.005(1)	0.000(1)
C(24)	0.024(1)	0.022(1)	0.019(1)	0.000(1)	0.001(1)	0.003(1)
C(25)	0.024(1)	0.021(1)	0.021(1)	-0.003(1)	-0.001(1)	0.001(1)
C(26)	0.023(1)	0.018(1)	0.024(1)	0.002(1)	0.003(1)	0.001(1)



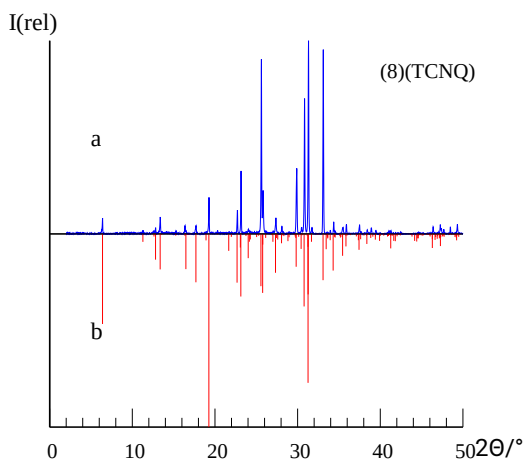


Figure A.3: X-ray powder diffraction pattern of α -(1)(TCNQ), α -(2)(TCNQ), β -(2)(TCNQ), (3)(TCNQ), (4)(TCNQ), (7)(TCNQ)₂ and (8)(TCNQ). Used radiation: Co-K $_{\alpha 1}$, a = measured diffractogram, b = simulated diffractogram on basis of single crystal data.

Table A.83: Space groups, lattice parameters in Å and Monkhorst-Pack grids for pyridone azine-containing CT salts with TCNQ for room temperature data.

compound	space group	lattice parameter <i>a</i> /Å	<i>b</i> /Å	<i>c</i> /Å	Monkhorst-Pack	
(TTF)(TCNQ)	<i>P</i> 2 ₁ / <i>c</i>	12.298(6)	3.819(2)	18.468(8)	2	6
α -(2)(TCNQ)	<i>P</i> 2 ₁ / <i>n</i>	13.952(3)	22.913(7)	6.7204(16)	4	2
β -(2)(TCNQ)	<i>C</i> cc <i>a</i>	13.0289(3)	13.3983(4)	24.4860(5)	4	4
(3)(TCNQ)	<i>P</i> 2 ₁ / <i>c</i>	22.1408(8)	7.0610(2)	20.5201(8)	2	4
(4)(TCNQ)	<i>P</i> 2 ₁ / <i>c</i>	10.7276(17)	7.3347(13)	15.907(3)	4	4
(7)(TCNQ)	<i>P</i> 1̄	7.2533(12)	8.4348(8)	10.7661(18)	4	4
(7)(TCNQ) ₂	<i>P</i> 1̄	8.1062(3)	10.3183(4)	11.2985(4)	4	4
(8)(TCNQ)	<i>P</i> 1̄	8.3256(12)	9.2850(8)	16.144(2)	4	4

Table A.84: Space groups and all special points in the band structure calculations with the κ -path according to the recommendations by Hinuma *et al.*[121] for the pyridone azine-containing CT salts with TCNQ.

compound	space group	κ -path
(TTF)(TCNQ)	<i>P</i> 2 ₁ / <i>c</i>	Γ —Z—D—B— Γ —A—E—Z—C ₂ —Y ₂ — Γ
α -(2)(TCNQ)	<i>P</i> 2 ₁ / <i>n</i>	Γ —Z—D—B— Γ —A—E—Z—C ₂ —Y ₂ — Γ
β -(2)(TCNQ)	<i>C</i> cc <i>a</i>	Γ —Y— Γ —Z—T—Y Γ S—R—Z— Γ
(3)(TCNQ)	<i>P</i> 2 ₁ / <i>c</i>	Γ —Z—D—B— Γ —A—E—Z—C ₂ —Y ₂ — Γ
(4)(TCNQ)	<i>P</i> 2 ₁ / <i>c</i>	Γ —Z—D—B— Γ —A—E—Z—C ₂ —Y ₂ — Γ
(7)(TCNQ)	<i>P</i> 1̄	Γ —X Y— Γ —Z R ₂ — Γ —T ₂ U ₂ — Γ —V
(7)(TCNQ) ₂	<i>P</i> 1̄	Γ —X Y— Γ —Z R— Γ —T U— Γ —V
(8)(TCNQ)	<i>P</i> 1̄	Γ —X Y— Γ —Z R ₂ — Γ —T ₂ U ₂ — Γ —V

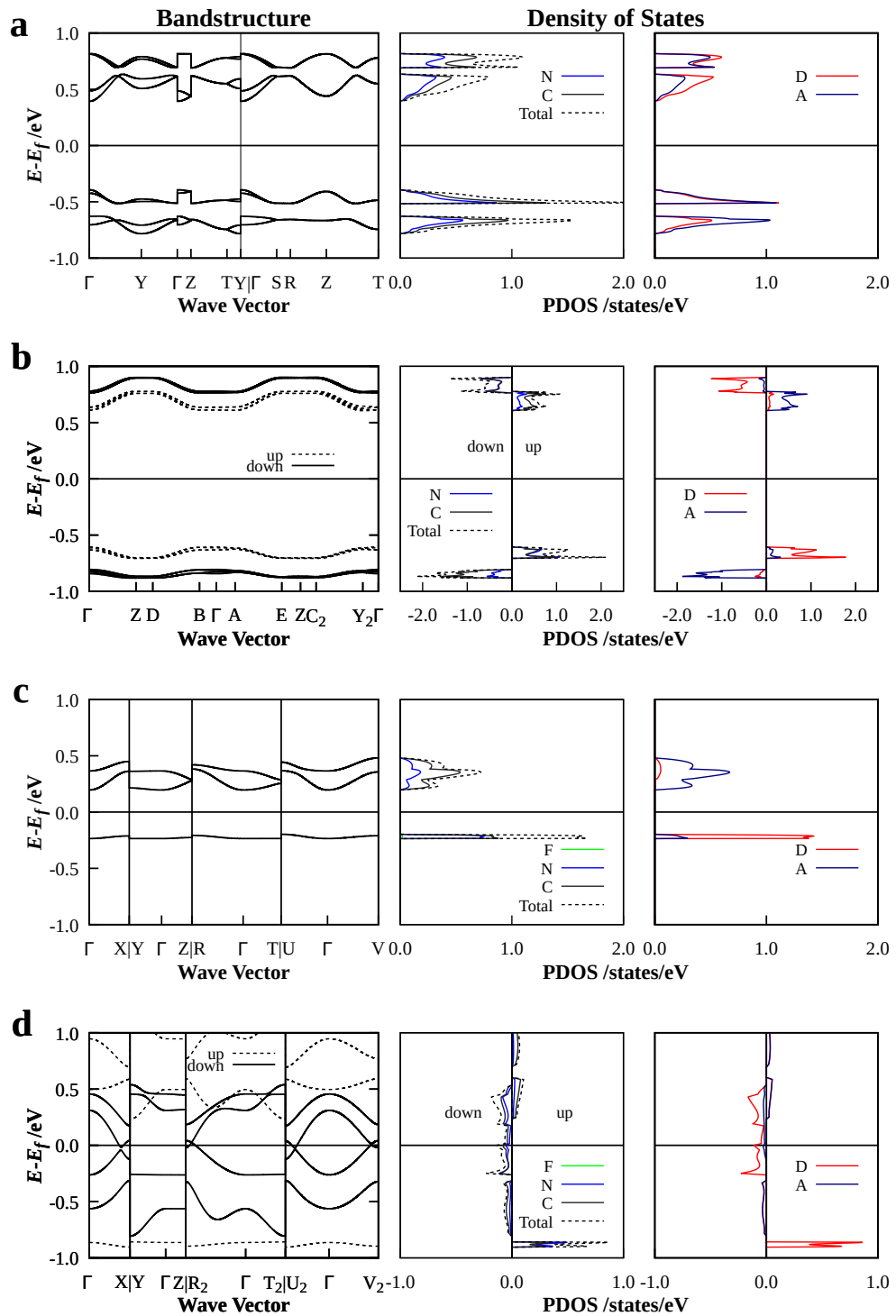


Figure A.4: Band structures, PDOS for atom orbitals and PDOS for orbitals belonging to donor or acceptor molecule for structures at 123 K of β -**(2)(TCNQ)** **a**, **(3)(TCNQ)** **b**, **(7)(TCNQ)₂** **c** and **(8)(TCNQ)** **d** calculated with CRYSTAL17, PW1PW+D3/pob-TZVP-rev2.

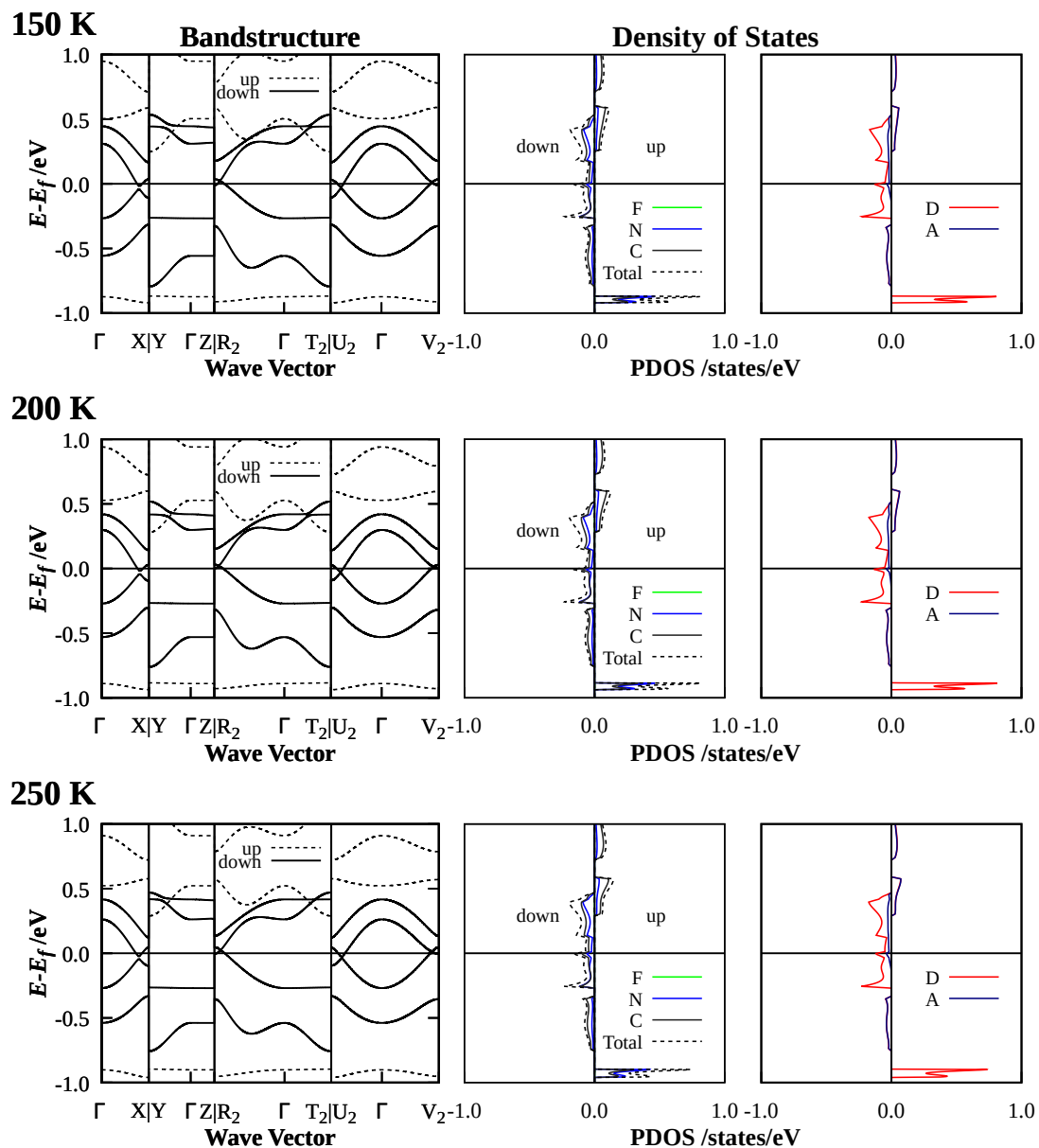


Figure A.5: Band structures, PDOS for atom orbitals and PDOS for orbitals belonging to donor or acceptor of (8)(TCNQ) for structures at 150 K, 200 K and 250 K calculated with CRYSTAL17, PW1PW+D3/pob-TZVP-rev2.

A.5 Charge Transfer Salts with TCNP

(5)(OTCNP)₂

Table A.85: Crystallographic data and structure refinement of (5)(OTCNP)₂ at room temperature.

Compound	(5)(OTCNP) ₂
Empirical Formula	C ₂₈ H ₁₈ N ₁₄ O ₄
Formula weight / g mol ⁻¹	614.56
Temperature / K	293(2)
Crystal size / mm ³	0.290×0.052×0.036
Crystal system; space group	Monoclinic, P2 ₁ /n
Lattice constants / Å°	$a = 9.3423(5)$ $b = 14.4980(1)$ $\beta = 110.978(4)$ $c = 11.3773(9)$
Volume / Å ³	1438.85(17)
Z; F(000); calc. density / g cm ⁻³	2: 632; 1.418
Wavelength	Mo-K α (0.71073 Å)
Theta range for data collection / °	3.402 $\leq \theta \leq$ 25.337
Limiting indices	-11 \leq h \leq 11, -17 \leq k \leq 16, -13 \leq l \leq 13
Reflections collected / unique	4846 / 2576
R _{int}	0.0889
Completeness to theta = 25.242	98.20 %
Absorption coefficient / mm ⁻¹	0.103
Refinement method	Full-matrix least-squares on F^2
Data / restraints / parameters	2576 / 0 / 245
R indices [I > 4σ(I)] R ₁ ; wR ₂	0.0486; 0.0957
R indices (all data) R ₁ ; wR ₂	0.1872; 0.1286
Goodness-of-fit for F^2	0.875
Largest diff. Peak and hole / e ⁻ Å ⁻³	0.168 / -0.177

Table A.86: Fractional coordinates in Å and equivalent isotropic displacement parameter U_{eq} /Å² for the independent atoms in the structure of (5)(OTCNP)₂ at room temperature.

Atom	Wyck.	Site	x/a	y/b	z/c	U_{eq}
O(1)	4e	1	0.7199(3)	0.2862(2)	0.9609(3)	0.074(1)
N(1)	4e	1	0.5970(3)	0.4890(2)	0.7677(3)	0.050(1)
N(2)	4e	1	0.5115(3)	0.5179(2)	0.5532(2)	0.054(1)
C(1)	4e	1	0.5649(3)	0.4536(3)	0.6508(3)	0.050(1)
C(2)	4e	1	0.5845(4)	0.3598(3)	0.6391(4)	0.058(1)
C(3)	4e	1	0.6352(4)	0.3037(3)	0.7427(4)	0.061(1)
C(4)	4e	1	0.6682(4)	0.3429(3)	0.8602(4)	0.057(1)
C(5)	4e	1	0.6473(4)	0.4367(3)	0.8716(4)	0.052(1)
C(6)	4e	1	0.5697(6)	0.5883(3)	0.7840(4)	0.065(1)
C(7)	4e	1	0.7603(6)	0.3257(4)	1.0861(4)	0.081(1)
O(2)	4e	1	0.3247(3)	0.4563(2)	0.8775(2)	0.077(1)
N(3)	4e	1	0.2325(3)	0.4408(2)	0.6634(3)	0.058(1)
N(4)	4e	1	-0.0212(3)	0.3450(2)	0.6863(3)	0.058(1)
N(5)	4e	1	0.0652(4)	0.3605(3)	1.0019(4)	0.101(1)

Table A.86 – continued from previous page

Atom	Wyck.	Site	x/a	y/b	z/c	U_{eq}
N(6)	4e	1	-0.2136(4)	0.2944(3)	0.3751(4)	0.104(1)
N(7)	4e	1	0.1333(4)	0.4324(2)	0.3442(3)	0.079(1)
C(8)	4e	1	0.2231(4)	0.4287(2)	0.7802(4)	0.056(1)
C(9)	4e	1	0.0881(4)	0.3802(2)	0.7837(3)	0.053(1)
C(10)	4e	1	-0.0054(4)	0.3580(2)	0.5743(3)	0.052(1)
C(11)	4e	1	0.1193(4)	0.4056(2)	0.5655(3)	0.051(1)
C(12)	4e	1	0.0742(4)	0.3682(3)	0.9051(4)	0.068(1)
C(13)	4e	1	-0.1211(5)	0.3220(3)	0.4650(4)	0.068(1)
C(14)	4e	1	0.1283(4)	0.4207(3)	0.4424(4)	0.061(1)
H(2)	4e	1	0.5620(3)	0.3400(19)	0.5560(3)	0.052(1)
H(3)	4e	1	0.6500(4)	0.2360(2)	0.7370(3)	0.082(12)
H(5)	4e	1	0.6660(3)	0.4740(2)	0.9610(3)	0.075(11)
H(6A)	4e	1	0.6180(4)	0.5980(2)	0.8870(3)	0.084(11)
H(6B)	4e	1	0.4670(4)	0.6030(2)	0.7370(3)	0.082(13)
H(6C)	4e	1	0.6220(4)	0.6240(2)	0.7390(4)	0.099(15)
H(7A)	4e	1	0.6840(4)	0.3540(2)	1.1100(4)	0.097(15)
H(7B)	4e	1	0.8380(5)	0.3820(3)	1.0980(4)	0.138(18)
H(7C)	4e	1	0.7790(5)	0.2690(3)	1.1450(4)	0.129(18)

Table A.87: Anisotropic displacement parameters $U_{ij}/\text{\AA}^2$ for the independent atoms in the structure of **(5)(OTCNP)₂** at room temperature.

Atom	U_{11}	U_{22}	U_{33}	U_{23}	U_{13}	U_{12}
O(1)	0.091(2)	0.071(2)	0.056(2)	0.007(2)	0.022(2)	0.001(2)
N(1)	0.045(2)	0.055(2)	0.052(2)	-0.002(2)	0.018(2)	-0.001(1)
N(2)	0.052(2)	0.067(2)	0.042(2)	-0.001(2)	0.015(2)	-0.002(2)
C(1)	0.045(2)	0.062(3)	0.042(2)	-0.004(2)	0.016(2)	-0.001(2)
C(2)	0.065(3)	0.067(3)	0.045(3)	-0.003(2)	0.024(2)	0.002(2)
C(3)	0.070(3)	0.062(3)	0.055(3)	-0.005(3)	0.026(2)	0.000(2)
C(4)	0.052(2)	0.067(3)	0.050(3)	0.007(2)	0.016(2)	0.003(2)
C(5)	0.047(2)	0.063(3)	0.049(3)	0.001(2)	0.018(2)	0.002(2)
C(6)	0.077(3)	0.061(3)	0.054(3)	-0.004(2)	0.019(3)	0.002(2)
C(7)	0.103(4)	0.087(4)	0.055(3)	0.000(3)	0.032(3)	0.002(3)
O(2)	0.066(2)	0.106(2)	0.056(2)	-0.024(2)	0.019(2)	-0.025(2)
N(3)	0.055(2)	0.067(2)	0.057(2)	-0.008(2)	0.026(2)	-0.012(2)
N(4)	0.054(2)	0.066(2)	0.054(2)	0.005(2)	0.020(2)	-0.001(2)
N(5)	0.093(3)	0.150(4)	0.071(3)	0.009(3)	0.043(2)	-0.008(2)
N(6)	0.100(3)	0.125(3)	0.074(3)	-0.002(3)	0.014(3)	-0.042(3)
N(7)	0.092(3)	0.080(2)	0.074(3)	-0.006(2)	0.042(2)	-0.006(2)
C(8)	0.051(2)	0.062(3)	0.057(3)	-0.003(2)	0.023(2)	-0.005(2)
C(9)	0.050(2)	0.066(3)	0.042(2)	0.003(2)	0.015(2)	0.003(2)
C(10)	0.048(2)	0.060(2)	0.046(2)	-0.003(2)	0.014(2)	-0.007(2)
C(11)	0.054(2)	0.049(2)	0.054(3)	-0.004(2)	0.023(2)	0.000(2)
C(12)	0.052(2)	0.089(3)	0.062(3)	-0.001(2)	0.019(2)	-0.006(2)
C(13)	0.064(3)	0.075(3)	0.062(3)	0.000(2)	0.021(3)	-0.015(2)
C(14)	0.063(2)	0.067(3)	0.058(3)	-0.007(2)	0.029(2)	-0.006(2)

(7)(TCNP)

Compound	(7)(TCNP)
Empirical Formula	C ₂₂ H ₁₂ F ₆ N ₁₀
Formula weight / g mol ⁻¹	530.42
Temperature / K	293(2)
Crystal size / mm ³	0.530×0.072×0.012
Crystal system; space group	Monoclinic, P2 ₁ /c
Lattice constants / Å°	$a = 11.3842(9)$ $b = 15.2916(12)$ $\beta = 107.517(5)$ $c = 7.0062(5)$
Volume / Å ³	1163.10(16)
Z; F(000); calc. density / g cm ⁻³	2: 536; 1.515
Wavelength	Mo-K _α (0.71073 Å)
Theta range for data collection / °	3.259 ≤ θ ≤ 27.437
Limiting indices	-14 ≤ h ≤ 14, -19 ≤ k ≤ 17, -8 ≤ l ≤ 9
Reflections collected / unique	4468 / 2533
R _{int}	0.0822
Completeness to theta = 25.242	99.60 %
Absorption coefficient / mm ⁻¹	0.132
Refinement method	Full-matrix least-squares on F ²
Data / restraints / parameters	2533 / 0 / 173
R indices [I > 4σ(I)] R ₁ ; wR ₂	0.0536; 0.1193
R indices (all data) R ₁ ; wR ₂	0.2343; 0.1708
Goodness-of-fit for F ²	0.867
Largest diff. Peak and hole / e ⁻ Å ⁻³	0.243 / -0.239

Table A.89: Fractional coordinates in Å and equivalent isotropic displacement parameter U_{eq}/Å² for the independent atoms in the structure of (7)(TCNP) at room temperature.

Atom	Wyck.	Site	x/a	y/b	z/c	U _{eq}
F(1)	4e	1	0.6037(3)	0.5709(2)	0.8063(6)	0.151(1)
F(2)	4e	1	0.5488(3)	0.6493(2)	0.5537(5)	0.136(1)
F(3)	4e	1	0.5309(3)	0.6940(2)	0.8212(5)	0.143(1)
N(1)	4e	1	0.0511(3)	0.4730(2)	0.5464(4)	0.056(1)
N(2)	4e	1	0.2615(3)	0.4656(2)	0.6605(4)	0.053(1)
C(1)	4e	1	0.1556(4)	0.5148(2)	0.5742(5)	0.050(1)
C(2)	4e	1	0.1735(4)	0.6029(2)	0.5230(5)	0.053(1)
C(3)	4e	1	0.2873(4)	0.6375(2)	0.5639(5)	0.059(1)
C(4)	4e	1	0.3918(3)	0.5864(2)	0.6587(5)	0.055(1)
C(5)	4e	1	0.3748(4)	0.5020(2)	0.7006(5)	0.057(1)
C(6)	4e	1	0.5156(4)	0.6240(3)	0.7119(7)	0.074(1)
C(7)	4e	1	0.2492(3)	0.3731(2)	0.7040(6)	0.068(1)
N(3)	4e	1	0.6880(4)	0.3762(2)	0.9207(5)	0.088(1)
N(4)	4e	1	0.9918(4)	0.7309(2)	0.7550(5)	0.084(1)
N(5)	4e	1	0.8879(3)	0.5375(2)	0.8878(4)	0.059(1)
C(8)	4e	1	0.8935(4)	0.4589(3)	0.9728(5)	0.058(1)
C(10)	4e	1	0.9953(4)	0.5785(2)	0.9173(5)	0.055(1)
C(11)	4e	1	0.7777(4)	0.4134(3)	0.9424(6)	0.068(1)

Table A.89 – continued from previous page

Atom	Wyck.	Site	x/a	y/b	z/c	U_{eq}
C(12)	4e	1	0.9930(4)	0.6640(3)	0.8259(6)	0.066(1)
H(2)	4e	1	0.1053	0.6371	0.4602	0.063
H(3)	4e	1	0.2970	0.6953	0.5296	0.071
H(5)	4e	1	0.4435	0.4675	0.7593	0.069
H(7A)	4e	1	0.3294	0.3482	0.7622	0.101
H(7B)	4e	1	0.2080	0.3428	0.5823	0.101
H(7C)	4e	1	0.2020	0.3676	0.7962	0.101

Table A.90: Anisotropic displacement parameters $U_{ij}/\text{\AA}^2$ for the independent atoms in the structure of (7)(TCNP) at room temperature.

Atom	U_{11}	U_{22}	U_{33}	U_{23}	U_{13}	U_{12}
F(1)	0.058(2)	0.118(2)	0.246(4)	0.052(2)	0.001(2)	-0.010(2)
F(2)	0.105(2)	0.189(3)	0.122(2)	0.003(2)	0.049(2)	-0.057(2)
F(3)	0.095(2)	0.131(2)	0.204(3)	-0.090(2)	0.046(2)	-0.045(2)
N(1)	0.048(2)	0.056(2)	0.059(2)	0.003(1)	0.010(2)	0.007(2)
N(2)	0.045(2)	0.049(2)	0.061(2)	0.000(1)	0.010(2)	0.002(2)
C(1)	0.047(2)	0.052(2)	0.050(2)	-0.006(2)	0.013(2)	0.005(2)
C(2)	0.050(3)	0.053(2)	0.054(2)	0.001(2)	0.014(2)	0.006(2)
C(3)	0.067(3)	0.055(2)	0.057(2)	0.002(2)	0.023(2)	0.002(2)
C(4)	0.045(2)	0.056(2)	0.059(2)	-0.004(2)	0.010(2)	-0.002(2)
C(5)	0.047(2)	0.064(3)	0.057(2)	-0.005(2)	0.011(2)	0.006(2)
C(6)	0.062(3)	0.065(3)	0.093(3)	0.004(3)	0.019(3)	-0.001(3)
C(7)	0.058(3)	0.054(3)	0.083(3)	0.008(2)	0.009(2)	0.007(2)
N(3)	0.079(3)	0.102(3)	0.089(3)	-0.003(2)	0.033(2)	-0.018(2)
N(4)	0.108(3)	0.066(2)	0.073(2)	-0.008(2)	0.020(2)	-0.002(2)
N(5)	0.053(2)	0.072(2)	0.052(2)	-0.007(2)	0.016(2)	0.002(2)
C(8)	0.065(3)	0.061(3)	0.050(2)	-0.008(2)	0.021(2)	-0.003(2)
C(10)	0.062(3)	0.061(2)	0.042(2)	-0.002(2)	0.014(2)	0.004(2)
C(11)	0.072(3)	0.073(3)	0.060(3)	0.000(2)	0.024(2)	-0.001(3)
C(12)	0.068(3)	0.068(3)	0.060(3)	-0.014(2)	0.016(2)	0.007(2)

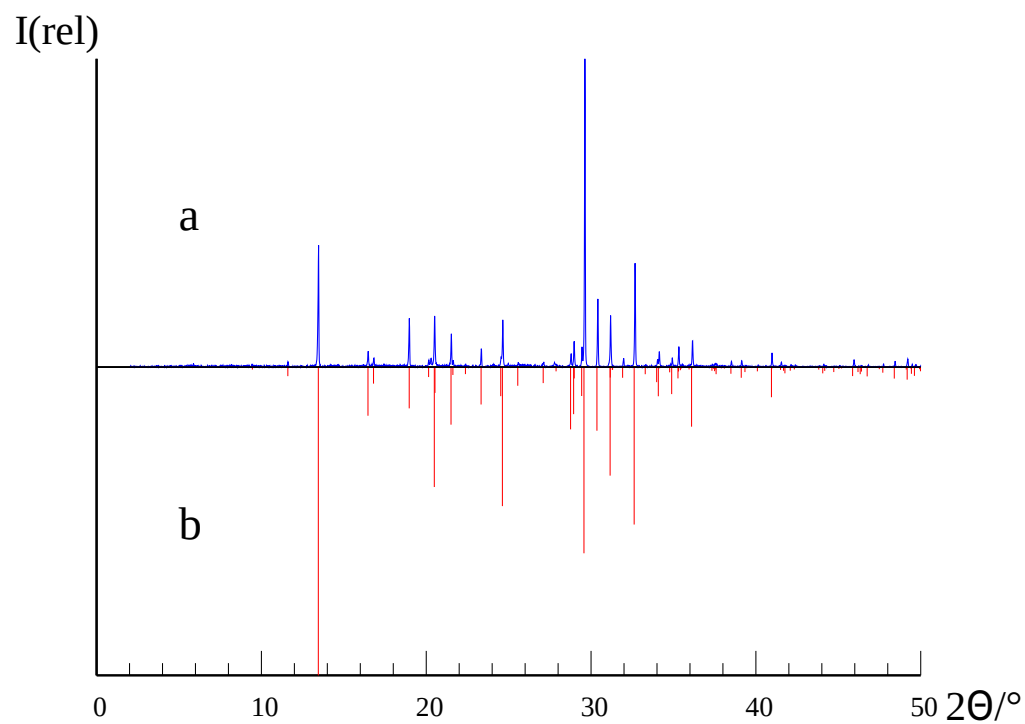


Figure A.6: X-ray powder diffraction pattern of (7)(TCNP). Used radiation: Co-K α_1 , a = measured diffractogram, b = simulated diffractogram on basis of single crystal data.

A.6 Charge Transfer Salt with DTeF

Table A.91: Crystallographic data and structure refinement of (1)(DTeF) at room temperature.

Compound	(1)(DTeF)
Empirical Formula	C ₂₈ H ₁₈ N ₁₀ O ₈
Formula weight / g mol ⁻¹	622.52
Temperature / K	293(2)
Crystal system; space group	Triclinic, P $\bar{1}$
Lattice constants / Å °	$a = 7.7780(3)$ $\alpha = 73.959(3)$ $b = 13.0623(7)$ $\beta = 85.397(3)$ $c = 14.3556(9)$ $\gamma = 74.346(3)$
Volume / Å ³	1349.70(13)
Z; F(000); calc. density / g cm ⁻³	2: 640; 1.532
Wavelength	Mo-K α (0.71073 Å)
Theta range for data collection / °	2.945 $\leq \theta \leq$ 27.463
Limiting indices	-10 $\leq h \leq$ 9, -16 $\leq k \leq$ 16, -16 $\leq l \leq$ 18
Reflections collected / unique	9323 / 6048
R _{int}	0.0555
Completeness to theta = 25.242	98.80 %
Absorption coefficient / mm ⁻¹	0.117
Refinement method	Full-matrix least-squares on F^2
Data / restraints / parameters	6048 / 0 / 487
R indices [I > 4σ(I)] R ₁ ; wR ₂	0.0511; 0.0977
R indices (all data) R ₁ ; wR ₂	0.1691; 0.1299
Goodness-of-fit for F^2	0.875
Largest diff. Peak and hole / e ⁻ Å ⁻³	0.181 / -0.241

Table A.92: Fractional coordinates in Å and equivalent isotropic displacement parameter U_{eq} /Å² for the independent atoms in the structure of (1)(DTeF) at room temperature.

Atom	Wyck.	Site	x/a	y/b	z/c	U_{eq}
C(1)	2i	1	-0.1638(3)	1.1248(2)	0.9235(2)	0.045(1)
C(2)	2i	1	-0.0894(4)	1.1974(3)	0.8510(2)	0.054(1)
C(3)	2i	1	-0.0914(4)	1.2989(3)	0.8597(3)	0.062(1)
C(4)	2i	1	-0.1671(4)	1.3303(3)	0.9429(3)	0.064(1)
C(5)	2i	1	-0.2366(4)	1.2600(2)	1.0125(3)	0.056(1)
C(6)	2i	1	-0.3145(5)	1.0850(3)	1.0813(3)	0.062(1)
C(7)	2i	1	-0.1452(3)	0.9006(2)	0.8378(2)	0.044(1)
C(8)	2i	1	-0.1954(4)	0.8207(3)	0.9144(2)	0.054(1)
C(9)	2i	1	-0.2035(4)	0.7232(3)	0.9012(3)	0.064(1)
C(10)	2i	1	-0.1644(4)	0.7022(3)	0.8108(3)	0.062(1)
C(11)	2i	1	-0.1198(3)	0.7803(3)	0.7376(3)	0.054(1)
C(12)	2i	1	-0.0639(7)	0.9610(3)	0.6657(3)	0.075(1)
C(13)	2i	1	0.5658(3)	0.5956(2)	0.6240(2)	0.036(1)
C(14)	2i	1	0.6709(3)	0.5747(2)	0.5400(2)	0.036(1)
C(15)	2i	1	0.7333(3)	0.6573(2)	0.4751(2)	0.038(1)
C(16)	2i	1	0.6878(3)	0.7612(2)	0.4893(2)	0.041(1)
C(17)	2i	1	0.5768(3)	0.7880(2)	0.5645(2)	0.043(1)

Table A.92 – continued from previous page

Atom	Wyck.	Site	x/a	y/b	z/c	U_{eq}
C(18)	$2i$	1	0.5171(3)	0.7053(2)	0.6298(2)	0.039(1)
C(19)	$2i$	1	0.6068(3)	0.4117(2)	0.6274(2)	0.036(1)
C(20)	$2i$	1	0.5358(3)	0.4925(2)	0.6811(2)	0.037(1)
C(21)	$2i$	1	0.4632(3)	0.4545(2)	0.7729(2)	0.040(1)
C(22)	$2i$	1	0.4371(3)	0.3506(2)	0.8055(2)	0.047(1)
C(23)	$2i$	1	0.4964(3)	0.2784(2)	0.7473(2)	0.043(1)
C(24)	$2i$	1	0.5866(3)	0.3053(2)	0.6610(2)	0.039(1)
C(25)	$2i$	1	0.6944(3)	0.4610(2)	0.5408(2)	0.036(1)
C(26)	$2i$	1	0.7895(3)	0.4073(2)	0.4725(2)	0.038(1)
C(27)	$2i$	1	0.8235(3)	0.2920(2)	0.4850(2)	0.044(1)
C(28)	$2i$	1	0.8738(3)	0.4610(2)	0.3885(2)	0.044(1)
N(1)	$2i$	1	-0.1775(3)	1.0232(2)	0.9240(2)	0.049(1)
N(2)	$2i$	1	-0.1266(3)	1.0007(2)	0.8394(2)	0.048(1)
N(3)	$2i$	1	-0.1108(3)	0.8781(2)	0.7490(2)	0.048(1)
N(4)	$2i$	1	-0.2344(3)	1.1589(2)	1.0040(2)	0.047(1)
N(5)	$2i$	1	0.7530(3)	0.8484(2)	0.4202(2)	0.055(1)
N(6)	$2i$	1	0.3842(3)	0.7421(2)	0.6991(2)	0.053(1)
N(7)	$2i$	1	0.4307(3)	0.5166(2)	0.8467(2)	0.052(1)
N(8)	$2i$	1	0.4689(3)	0.1684(2)	0.7831(2)	0.053(1)
N(9)	$2i$	1	0.8528(3)	0.1989(2)	0.4932(2)	0.062(1)
N(10)	$2i$	1	0.9457(3)	0.5014(2)	0.3204(2)	0.062(1)
O(1)	$2i$	1	0.8441(3)	0.8257(2)	0.3515(2)	0.068(1)
O(2)	$2i$	1	0.7125(3)	0.9402(2)	0.4352(2)	0.078(1)
O(3)	$2i$	1	0.3954(3)	0.8195(2)	0.7279(2)	0.076(1)
O(4)	$2i$	1	0.2636(2)	0.6946(2)	0.7228(2)	0.059(1)
O(5)	$2i$	1	0.5332(3)	0.5724(2)	0.8484(2)	0.058(1)
O(6)	$2i$	1	0.3092(3)	0.5052(2)	0.9053(2)	0.078(1)
O(7)	$2i$	1	0.3966(3)	0.1446(2)	0.8629(2)	0.082(1)
O(8)	$2i$	1	0.5186(2)	0.1029(2)	0.7332(2)	0.062(1)
H(2)	$2i$	1	-0.0360(3)	1.1680(2)	0.7970(2)	0.061(8)
H(3)	$2i$	1	-0.0410(4)	1.3450(3)	0.8130(3)	0.082(11)
H(4)	$2i$	1	-0.1660(3)	1.4020(2)	0.9540(2)	0.068(9)
H(5)	$2i$	1	-0.2950(3)	1.2790(2)	1.0750(2)	0.075(9)
H(6A)	$2i$	1	-0.4110(5)	1.0610(3)	1.0520(3)	0.119(14)
H(6B)	$2i$	1	-0.3710(3)	1.1230(2)	1.1330(2)	0.068(8)
H(6C)	$2i$	1	-0.2330(4)	1.0170(3)	1.1080(3)	0.102(14)
H(8)	$2i$	1	-0.2270(3)	0.8400(2)	0.9740(2)	0.054(8)
H(9)	$2i$	1	-0.2400(4)	0.6670(3)	0.9570(3)	0.095(12)
H(10)	$2i$	1	-0.1690(3)	0.6350(2)	0.8020(2)	0.057(8)
H(11)	$2i$	1	-0.0900(3)	0.7750(2)	0.6680(2)	0.070(9)
H(12A)	$2i$	1	-0.1520(5)	1.0270(3)	0.6510(3)	0.119(15)
H(12B)	$2i$	1	-0.0350(4)	0.9330(3)	0.6090(3)	0.107(13)
H(12C)	$2i$	1	0.0470(5)	0.9780(3)	0.6800(3)	0.141(19)
H(15)	$2i$	1	0.8090(3)	0.6468(18)	0.4135(19)	0.042(7)
H(17)	$2i$	1	0.5400(3)	0.8630(2)	0.5690(19)	0.052(7)
H(22)	$2i$	1	0.3830(3)	0.3270(2)	0.8680(2)	0.053(8)
H(24)	$2i$	1	0.6370(3)	0.2432(19)	0.6300(18)	0.042(7)

Table A.93: Anisotropic displacement parameters $U_{ij}/\text{\AA}^2$ for the independent atoms in the structure of **(1)**(DTeF) at room temperature.

Atom	U_{11}	U_{22}	U_{33}	U_{23}	U_{13}	U_{12}
C(1)	0.046(2)	0.049(2)	0.039(2)	-0.014(2)	0.004(1)	-0.009(1)
C(2)	0.057(2)	0.053(2)	0.048(2)	-0.012(2)	0.003(2)	-0.012(1)
C(3)	0.070(2)	0.052(2)	0.058(3)	-0.001(2)	-0.002(2)	-0.023(2)
C(4)	0.072(2)	0.047(2)	0.072(3)	-0.017(2)	-0.009(2)	-0.014(2)
C(5)	0.068(2)	0.049(2)	0.053(2)	-0.021(2)	0.003(2)	-0.013(2)
C(6)	0.081(2)	0.064(2)	0.048(2)	-0.021(2)	0.021(2)	-0.029(2)
C(7)	0.041(1)	0.050(2)	0.043(2)	-0.018(2)	0.005(1)	-0.011(1)
C(8)	0.060(2)	0.057(2)	0.045(2)	-0.018(2)	0.009(2)	-0.016(2)
C(9)	0.072(2)	0.061(2)	0.063(3)	-0.016(2)	0.009(2)	-0.028(2)
C(10)	0.062(2)	0.058(2)	0.078(3)	-0.031(2)	0.011(2)	-0.027(2)
C(11)	0.049(2)	0.060(2)	0.062(2)	-0.029(2)	0.006(2)	-0.018(1)
C(12)	0.114(3)	0.064(3)	0.049(3)	-0.021(2)	0.028(2)	-0.027(2)
C(13)	0.037(1)	0.038(2)	0.033(2)	-0.008(1)	0.001(1)	-0.012(1)
C(14)	0.038(1)	0.038(2)	0.031(2)	-0.008(1)	0.001(1)	-0.012(1)
C(15)	0.039(1)	0.043(2)	0.034(2)	-0.010(1)	0.001(1)	-0.013(1)
C(16)	0.044(1)	0.040(2)	0.038(2)	-0.005(1)	0.000(1)	-0.018(1)
C(17)	0.052(2)	0.039(2)	0.041(2)	-0.011(2)	-0.002(1)	-0.015(1)
C(18)	0.042(1)	0.042(2)	0.034(2)	-0.014(1)	0.002(1)	-0.011(1)
C(19)	0.039(1)	0.035(2)	0.032(2)	-0.004(1)	-0.003(1)	-0.011(1)
C(20)	0.040(1)	0.039(2)	0.033(2)	-0.010(1)	0.002(1)	-0.012(1)
C(21)	0.045(1)	0.044(2)	0.030(2)	-0.009(1)	0.003(1)	-0.013(1)
C(22)	0.049(2)	0.054(2)	0.036(2)	-0.008(2)	0.008(1)	-0.019(1)
C(23)	0.047(2)	0.038(2)	0.044(2)	-0.005(2)	-0.002(1)	-0.015(1)
C(24)	0.040(1)	0.038(2)	0.033(2)	-0.003(1)	-0.002(1)	-0.010(1)
C(25)	0.037(1)	0.039(2)	0.031(2)	-0.006(1)	0.000(1)	-0.011(1)
C(26)	0.042(1)	0.038(2)	0.032(2)	-0.008(1)	0.003(1)	-0.009(1)
C(27)	0.046(2)	0.047(2)	0.033(2)	-0.008(2)	0.004(1)	-0.007(1)
C(28)	0.044(2)	0.045(2)	0.042(2)	-0.015(2)	0.003(1)	-0.009(1)
N(1)	0.058(1)	0.047(2)	0.042(2)	-0.016(1)	0.006(1)	-0.012(1)
N(2)	0.056(1)	0.049(2)	0.043(2)	-0.019(1)	0.005(1)	-0.012(1)
N(3)	0.051(1)	0.049(2)	0.046(2)	-0.019(1)	0.007(1)	-0.012(1)
N(4)	0.055(1)	0.045(1)	0.043(2)	-0.015(1)	0.003(1)	-0.013(1)
N(5)	0.061(1)	0.049(2)	0.056(2)	-0.008(1)	0.002(1)	-0.025(1)
N(6)	0.064(2)	0.047(2)	0.040(2)	-0.012(1)	0.004(1)	-0.005(1)
N(7)	0.068(2)	0.050(2)	0.036(2)	-0.009(1)	0.004(1)	-0.017(1)
N(8)	0.060(1)	0.047(2)	0.050(2)	-0.005(1)	0.001(1)	-0.021(1)
N(9)	0.082(2)	0.044(2)	0.051(2)	-0.012(1)	0.003(1)	-0.005(1)
N(10)	0.066(2)	0.068(2)	0.055(2)	-0.019(2)	0.018(1)	-0.022(1)
O(1)	0.083(1)	0.068(2)	0.056(2)	-0.013(1)	0.024(1)	-0.035(1)
O(2)	0.100(2)	0.046(1)	0.091(2)	-0.016(1)	0.026(1)	-0.034(1)
O(3)	0.119(2)	0.056(1)	0.062(2)	-0.034(1)	0.020(1)	-0.022(1)
O(4)	0.054(1)	0.067(1)	0.048(1)	-0.011(1)	0.011(1)	-0.010(1)
O(5)	0.078(1)	0.056(1)	0.045(1)	-0.013(1)	-0.006(1)	-0.023(1)
O(6)	0.105(2)	0.081(2)	0.057(2)	-0.029(1)	0.044(1)	-0.042(1)
O(7)	0.117(2)	0.066(2)	0.063(2)	-0.005(1)	0.031(2)	-0.045(1)
O(8)	0.078(1)	0.043(1)	0.065(2)	-0.010(1)	0.000(1)	-0.022(1)

Table A.94: Crystallographic data and structure refinement of **(1)**(DTeF) at 103 K.

Compound	(1) (DTeF)
Empirical Formula	C ₂₈ H ₁₈ N ₁₀ O ₈
Formula weight / g mol ⁻¹	622.52
Crystal size / mm ³	0.190×0.180×0.030
Temperature / K	103(2)
Crystal system; space group	Triclinic, P $\bar{1}$
Lattice constants / Å °	$a = 7.6390(2)$ $\alpha = 73.761(2)$ $b = 13.0560(4)$ $\beta = 86.115(2)$ $c = 14.2292(4)$ $\gamma = 74.028(2)$
Volume / Å ³	1309.86(7)
Z; F(000); calc. density / g cm ⁻³	2: 640; 1.578
Wavelength	Mo-K α (0.71073 Å)
Theta range for data collection / °	2.982 ≤ θ ≤ 27.463
Limiting indices	-11 ≤ h ≤ 11, -20 ≤ k ≤ 19, -21 ≤ l ≤ 21
Reflections collected / unique	15322 / 9207
R _{int}	0.0420
Completeness to theta = 25.242	96.50 %
Absorption coefficient / mm ⁻¹	0.121
Refinement method	Full-matrix least-squares on F^2
Data / restraints / parameters	9207 / 0 / 487
R indices [I > 4σ(I)] R ₁ ; wR ₂	0.0503; 0.1223
R indices (all data) R ₁ ; wR ₂	0.0858; 0.1400
Goodness-of-fit for F^2	0.977
Largest diff. Peak and hole / e ⁻ Å ⁻³	0.331 / -0.340

Table A.95: Fractional coordinates in Å and equivalent isotropic displacement parameter U_{eq} /Å² for the independent atoms in the structure of **(1)**(DTeF) at 103 K.

Atom	Wyck.	Site	x/a	y/b	z/c	U_{eq}
C(1)	2i	1	-0.1583(2)	1.1233(1)	0.9266(1)	0.017(1)
C(2)	2i	1	-0.0830(2)	1.1965(1)	0.8531(1)	0.020(1)
C(3)	2i	1	-0.0875(2)	1.2988(1)	0.8623(1)	0.022(1)
C(4)	2i	1	-0.1666(2)	1.3312(1)	0.9448(1)	0.022(1)
C(5)	2i	1	-0.2392(2)	1.2598(1)	1.0147(1)	0.021(1)
C(6)	2i	1	-0.3203(2)	1.0844(1)	1.0814(1)	0.022(1)
C(7)	2i	1	-0.1416(2)	0.9003(1)	0.8391(1)	0.017(1)
C(8)	2i	1	-0.1927(2)	0.8201(1)	0.9159(1)	0.020(1)
C(9)	2i	1	-0.2058(2)	0.7228(1)	0.9016(1)	0.023(1)
C(10)	2i	1	-0.1696(2)	0.7035(1)	0.8093(1)	0.023(1)
C(11)	2i	1	-0.1226(2)	0.7831(1)	0.7356(1)	0.020(1)
C(12)	2i	1	-0.0615(2)	0.9628(1)	0.6659(1)	0.027(1)
C(13)	2i	1	0.5660(2)	0.5953(1)	0.6234(1)	0.015(1)
C(14)	2i	1	0.6723(2)	0.5741(1)	0.5399(1)	0.014(1)
C(15)	2i	1	0.7341(2)	0.6572(1)	0.4738(1)	0.016(1)
C(16)	2i	1	0.6856(2)	0.7620(1)	0.4878(1)	0.017(1)
C(17)	2i	1	0.5731(2)	0.7891(1)	0.5635(1)	0.018(1)
C(18)	2i	1	0.5155(2)	0.7052(1)	0.6293(1)	0.016(1)
C(19)	2i	1	0.6108(2)	0.4107(1)	0.6282(1)	0.015(1)

Table A.95 – continued from previous page

Atom	Wyck.	Site	x/a	y/b	z/c	U_{eq}
C(20)	$2i$	1	0.5379(2)	0.4918(1)	0.6817(1)	0.014(1)
C(21)	$2i$	1	0.4651(2)	0.4537(1)	0.7743(1)	0.016(1)
C(22)	$2i$	1	0.4390(2)	0.3493(1)	0.8072(1)	0.018(1)
C(23)	$2i$	1	0.5001(2)	0.2768(1)	0.7490(1)	0.016(1)
C(24)	$2i$	1	0.5910(2)	0.3035(1)	0.6624(1)	0.016(1)
C(25)	$2i$	1	0.6974(2)	0.4604(1)	0.5403(1)	0.014(1)
C(26)	$2i$	1	0.7931(2)	0.4072(1)	0.4716(1)	0.016(1)
C(27)	$2i$	1	0.8301(2)	0.2910(1)	0.4850(1)	0.018(1)
C(28)	$2i$	1	0.8760(2)	0.4614(1)	0.3868(1)	0.018(1)
N(1)	$2i$	1	-0.1719(2)	1.0217(1)	0.9267(1)	0.019(1)
N(2)	$2i$	1	-0.1191(2)	0.9989(1)	0.8420(1)	0.019(1)
N(3)	$2i$	1	-0.1095(2)	0.8791(1)	0.7491(1)	0.018(1)
N(4)	$2i$	1	-0.2355(2)	1.1581(1)	1.0062(1)	0.018(1)
N(5)	$2i$	1	0.7484(2)	0.8502(1)	0.4179(1)	0.020(1)
N(6)	$2i$	1	0.3793(2)	0.7414(1)	0.6988(1)	0.019(1)
N(7)	$2i$	1	0.4326(2)	0.5158(1)	0.8481(1)	0.019(1)
N(8)	$2i$	1	0.4737(2)	0.1658(1)	0.7848(1)	0.019(1)
N(9)	$2i$	1	0.8610(2)	0.1973(1)	0.4935(1)	0.023(1)
N(10)	$2i$	1	0.9463(2)	0.5022(1)	0.3180(1)	0.024(1)
O(1)	$2i$	1	0.8402(1)	0.8272(1)	0.3487(1)	0.025(1)
O(2)	$2i$	1	0.7062(2)	0.9423(1)	0.4324(1)	0.029(1)
O(3)	$2i$	1	0.3873(2)	0.8205(1)	0.7271(1)	0.028(1)
O(4)	$2i$	1	0.2597(1)	0.6924(1)	0.7228(1)	0.022(1)
O(5)	$2i$	1	0.5371(1)	0.5723(1)	0.8497(1)	0.022(1)
O(6)	$2i$	1	0.3104(2)	0.5042(1)	0.9071(1)	0.029(1)
O(7)	$2i$	1	0.4004(2)	0.1429(1)	0.8648(1)	0.030(1)
O(8)	$2i$	1	0.5248(1)	0.1012(1)	0.7340(1)	0.023(1)
H(2)	$2i$	1	-0.0310(2)	1.1709(14)	0.7997(13)	0.024(4)
H(3)	$2i$	1	-0.0330(3)	1.3460(16)	0.8120(14)	0.035(5)
H(4)	$2i$	1	-0.1700(3)	1.4031(16)	0.9532(14)	0.035(5)
H(5)	$2i$	1	-0.2970(2)	1.2776(13)	1.0762(12)	0.019(4)
H(6A)	$2i$	1	-0.4140(2)	1.0690(15)	1.0464(13)	0.031(5)
H(6B)	$2i$	1	-0.3710(3)	1.1246(16)	1.1297(14)	0.036(5)
H(6C)	$2i$	1	-0.2290(3)	1.0183(17)	1.1141(14)	0.039(5)
H(8)	$2i$	1	-0.2140(3)	0.8357(17)	0.9775(15)	0.042(6)
H(9)	$2i$	1	-0.2380(2)	0.6664(15)	0.9596(13)	0.027(5)
H(10)	$2i$	1	-0.1790(3)	0.6371(16)	0.7967(14)	0.037(5)
H(11)	$2i$	1	-0.0970(2)	0.7761(14)	0.6724(12)	0.019(4)
H(12A)	$2i$	1	-0.1580(3)	1.0292(17)	0.6523(14)	0.036(5)
H(12B)	$2i$	1	-0.0450(3)	0.9323(18)	0.6127(16)	0.048(6)
H(12C)	$2i$	1	0.0540(3)	0.9776(17)	0.6803(15)	0.045(6)
H(15)	$2i$	1	0.8010(2)	0.6490(14)	0.4177(13)	0.025(4)
H(17)	$2i$	1	0.5330(2)	0.8623(15)	0.5693(13)	0.026(4)
H(22)	$2i$	1	0.3870(2)	0.3250(14)	0.8715(13)	0.024(4)
H(24)	$2i$	1	0.6360(2)	0.2468(14)	0.6283(12)	0.020(4)

Table A.96: Anisotropic displacement parameters $U_{ij}/\text{\AA}^2$ for the independent atoms in the structure of (1)(DTeF) at 103 K.

Atom	U_{11}	U_{22}	U_{33}	U_{23}	U_{13}	U_{12}
C(1)	0.017(1)	0.018(1)	0.016(1)	-0.006(1)	0.000(1)	-0.003(1)

Table A.96 – continued from previous page

Atom	Wyck.	Site	x/a	y/b	z/c	U_{eq}
C(2)	0.020(1)	0.022(1)	0.018(1)	-0.006(1)	0.002(1)	-0.005(1)
C(3)	0.024(1)	0.020(1)	0.021(1)	-0.002(1)	-0.002(1)	-0.007(1)
C(4)	0.025(1)	0.018(1)	0.024(1)	-0.006(1)	-0.003(1)	-0.004(1)
C(5)	0.022(1)	0.019(1)	0.021(1)	-0.007(1)	-0.002(1)	-0.002(1)
C(6)	0.025(1)	0.025(1)	0.019(1)	-0.008(1)	0.006(1)	-0.010(1)
C(7)	0.015(1)	0.018(1)	0.017(1)	-0.007(1)	0.001(1)	-0.002(1)
C(8)	0.021(1)	0.022(1)	0.018(1)	-0.007(1)	0.002(1)	-0.006(1)
C(9)	0.025(1)	0.022(1)	0.023(1)	-0.006(1)	0.002(1)	-0.008(1)
C(10)	0.022(1)	0.024(1)	0.028(1)	-0.012(1)	0.003(1)	-0.010(1)
C(11)	0.019(1)	0.024(1)	0.022(1)	-0.011(1)	0.001(1)	-0.006(1)
C(12)	0.039(1)	0.026(1)	0.019(1)	-0.009(1)	0.011(1)	-0.012(1)
C(13)	0.015(1)	0.017(1)	0.013(1)	-0.004(1)	-0.001(1)	-0.004(1)
C(14)	0.014(1)	0.016(1)	0.013(1)	-0.003(1)	0.000(1)	-0.004(1)
C(15)	0.015(1)	0.019(1)	0.014(1)	-0.004(1)	0.000(1)	-0.005(1)
C(16)	0.018(1)	0.016(1)	0.016(1)	-0.002(1)	-0.001(1)	-0.007(1)
C(17)	0.020(1)	0.016(1)	0.018(1)	-0.005(1)	0.000(1)	-0.006(1)
C(18)	0.017(1)	0.019(1)	0.013(1)	-0.005(1)	0.000(1)	-0.004(1)
C(19)	0.014(1)	0.017(1)	0.013(1)	-0.004(1)	-0.001(1)	-0.004(1)
C(20)	0.014(1)	0.016(1)	0.013(1)	-0.004(1)	0.000(1)	-0.004(1)
C(21)	0.017(1)	0.018(1)	0.014(1)	-0.005(1)	0.001(1)	-0.005(1)
C(22)	0.018(1)	0.020(1)	0.014(1)	-0.003(1)	0.001(1)	-0.007(1)
C(23)	0.018(1)	0.015(1)	0.016(1)	-0.001(1)	-0.001(1)	-0.006(1)
C(24)	0.016(1)	0.015(1)	0.015(1)	-0.002(1)	-0.001(1)	-0.004(1)
C(25)	0.014(1)	0.015(1)	0.013(1)	-0.004(1)	0.000(1)	-0.003(1)
C(26)	0.015(1)	0.017(1)	0.014(1)	-0.004(1)	0.001(1)	-0.003(1)
C(27)	0.017(1)	0.021(1)	0.014(1)	-0.005(1)	0.001(1)	-0.003(1)
C(28)	0.017(1)	0.018(1)	0.018(1)	-0.007(1)	0.000(1)	-0.003(1)
N(1)	0.020(1)	0.018(1)	0.018(1)	-0.007(1)	0.002(1)	-0.005(1)
N(2)	0.021(1)	0.020(1)	0.018(1)	-0.008(1)	0.002(1)	-0.005(1)
N(3)	0.018(1)	0.019(1)	0.017(1)	-0.007(1)	0.002(1)	-0.005(1)
N(4)	0.020(1)	0.018(1)	0.017(1)	-0.006(1)	0.002(1)	-0.005(1)
N(5)	0.020(1)	0.019(1)	0.020(1)	-0.003(1)	0.001(1)	-0.008(1)
N(6)	0.024(1)	0.017(1)	0.015(1)	-0.005(1)	0.001(1)	-0.002(1)
N(7)	0.024(1)	0.019(1)	0.013(1)	-0.004(1)	0.002(1)	-0.006(1)
N(8)	0.021(1)	0.018(1)	0.018(1)	-0.002(1)	0.000(1)	-0.007(1)
N(9)	0.028(1)	0.021(1)	0.018(1)	-0.005(1)	0.001(1)	-0.003(1)
N(10)	0.024(1)	0.026(1)	0.022(1)	-0.007(1)	0.005(1)	-0.009(1)
O(1)	0.028(1)	0.028(1)	0.020(1)	-0.005(1)	0.006(1)	-0.013(1)
O(2)	0.034(1)	0.017(1)	0.037(1)	-0.007(1)	0.009(1)	-0.011(1)
O(3)	0.044(1)	0.020(1)	0.022(1)	-0.012(1)	0.004(1)	-0.006(1)
O(4)	0.018(1)	0.027(1)	0.019(1)	-0.005(1)	0.002(1)	-0.004(1)
O(5)	0.027(1)	0.021(1)	0.019(1)	-0.006(1)	-0.003(1)	-0.009(1)
O(6)	0.037(1)	0.032(1)	0.021(1)	-0.011(1)	0.014(1)	-0.015(1)
O(7)	0.041(1)	0.026(1)	0.023(1)	-0.003(1)	0.011(1)	-0.017(1)
O(8)	0.028(1)	0.019(1)	0.026(1)	-0.008(1)	0.001(1)	-0.007(1)

Table A.97: Crystallographic data and structure refinement of **(1)(DTeF)** at 123 K.

Compound	(1)(DTeF)
Empirical Formula	$\text{C}_{28}\text{H}_{18}\text{N}_{10}\text{O}_8$
Formula weight / g mol^{-1}	622.52

Table A.97 – continued from previous page

Compound	(1)(DTeF)
Crystal size / mm^3	0.190×0.180×0.030
Temperature / K	123(2)
Crystal system; space group	Triclinic, $P\bar{1}$
Lattice constants / \AA°	$a = 7.6473(3) \alpha = 73.759(2)$ $b = 13.0498(4) \beta = 86.075(2)$ $c = 14.2353(4) \gamma = 74.028(2)$
Volume / \AA^3	1311.27(8)
Z; F(000); calc. density / $g\text{cm}^{-3}$	2: 640; 1.577
Wavelength	Mo-K α (0.71073 \AA)
Theta range for data collection / $^\circ$	2.981 $\leq \theta \leq$ 33.265
Limiting indices	-11 $\leq h \leq$ 11, -20 $\leq k \leq$ 19, -21 $\leq l \leq$ 21
Reflections collected / unique	15296 / 9174
R_{int}	0.0436
Completeness to theta = 25.242	95.50 %
Absorption coefficient / mm^{-1}	0.120
Refinement method	Full-matrix least-squares on F^2
Data / restraints / parameters	9174 / 0 / 487
R indices [I > 4 σ (I)] R_1 ; wR_2	0.0503; 0.1207
R indices (all data) R_1 ; wR_2	0.0920; 0.1407
Goodness-of-fit for F^2	0.977
Largest diff. Peak and hole / $e^{-\text{\AA}^{-3}}$	0.406 / -0.313

Table A.98: Fractional coordinates in \AA and equivalent isotropic displacement parameter $U_{eq}/\text{\AA}^2$ for the independent atoms in the structure of (1)(DTeF) at 123 K.

Atom	Wyck.	Site	x/a	y/b	z/c	U_{eq}
C(1)	2 <i>i</i>	1	-0.1587(2)	1.1234(1)	0.9265(1)	0.019(1)
C(2)	2 <i>i</i>	1	-0.0837(2)	1.1967(1)	0.8529(1)	0.022(1)
C(3)	2 <i>i</i>	1	-0.0878(2)	1.2990(1)	0.8622(1)	0.025(1)
C(4)	2 <i>i</i>	1	-0.1667(2)	1.3314(1)	0.9445(1)	0.025(1)
C(5)	2 <i>i</i>	1	-0.2392(2)	1.2600(1)	1.0146(1)	0.023(1)
C(6)	2 <i>i</i>	1	-0.3204(2)	1.0844(1)	1.0813(1)	0.024(1)
C(7)	2 <i>i</i>	1	-0.1423(2)	0.9006(1)	0.8389(1)	0.019(1)
C(8)	2 <i>i</i>	1	-0.1928(2)	0.8199(1)	0.9159(1)	0.023(1)
C(9)	2 <i>i</i>	1	-0.2056(2)	0.7227(1)	0.9017(1)	0.026(1)
C(10)	2 <i>i</i>	1	-0.1689(2)	0.7031(1)	0.8094(1)	0.026(1)
C(11)	2 <i>i</i>	1	-0.1223(2)	0.7829(1)	0.7358(1)	0.023(1)
C(12)	2 <i>i</i>	1	-0.0617(3)	0.9628(2)	0.6660(1)	0.030(1)
C(13)	2 <i>i</i>	1	0.5662(2)	0.5953(1)	0.6234(1)	0.017(1)
C(14)	2 <i>i</i>	1	0.6719(2)	0.5742(1)	0.5398(1)	0.016(1)
C(15)	2 <i>i</i>	1	0.7340(2)	0.6575(1)	0.4739(1)	0.018(1)
C(16)	2 <i>i</i>	1	0.6860(2)	0.7620(1)	0.4879(1)	0.018(1)
C(17)	2 <i>i</i>	1	0.5738(2)	0.7891(1)	0.5636(1)	0.019(1)
C(18)	2 <i>i</i>	1	0.5157(2)	0.7054(1)	0.6292(1)	0.018(1)
C(19)	2 <i>i</i>	1	0.6104(2)	0.4108(1)	0.6282(1)	0.016(1)
C(20)	2 <i>i</i>	1	0.5379(2)	0.4918(1)	0.6816(1)	0.016(1)
C(21)	2 <i>i</i>	1	0.4654(2)	0.4538(1)	0.7742(1)	0.018(1)
C(22)	2 <i>i</i>	1	0.4392(2)	0.3492(1)	0.8071(1)	0.019(1)

Table A.98 – continued from previous page

Atom	Wyck.	Site	x/a	y/b	z/c	U_{eq}
C(23)	$2i$	1	0.5001(2)	0.2768(1)	0.7489(1)	0.018(1)
C(24)	$2i$	1	0.5902(2)	0.3035(1)	0.6622(1)	0.018(1)
C(25)	$2i$	1	0.6973(2)	0.4605(1)	0.5402(1)	0.015(1)
C(26)	$2i$	1	0.7928(2)	0.4072(1)	0.4715(1)	0.017(1)
C(27)	$2i$	1	0.8290(2)	0.2912(1)	0.4849(1)	0.019(1)
C(28)	$2i$	1	0.8756(2)	0.4612(1)	0.3869(1)	0.019(1)
N(1)	$2i$	1	-0.1721(2)	1.0218(1)	0.9266(1)	0.020(1)
N(2)	$2i$	1	-0.1193(2)	0.9990(1)	0.8418(1)	0.021(1)
N(3)	$2i$	1	-0.1093(2)	0.8788(1)	0.7491(1)	0.020(1)
N(4)	$2i$	1	-0.2354(2)	1.1582(1)	1.0061(1)	0.020(1)
N(5)	$2i$	1	0.7489(2)	0.8501(1)	0.4181(1)	0.022(1)
N(6)	$2i$	1	0.3802(2)	0.7417(1)	0.6987(1)	0.021(1)
N(7)	$2i$	1	0.4328(2)	0.5157(1)	0.8479(1)	0.022(1)
N(8)	$2i$	1	0.4733(2)	0.1659(1)	0.7847(1)	0.021(1)
N(9)	$2i$	1	0.8603(2)	0.1973(1)	0.4934(1)	0.026(1)
N(10)	$2i$	1	0.9462(2)	0.5021(1)	0.3181(1)	0.026(1)
O(1)	$2i$	1	0.8408(2)	0.8272(1)	0.3488(1)	0.028(1)
O(2)	$2i$	1	0.7067(2)	0.9420(1)	0.4326(1)	0.034(1)
O(3)	$2i$	1	0.3884(2)	0.8204(1)	0.7272(1)	0.032(1)
O(4)	$2i$	1	0.2602(1)	0.6927(1)	0.7228(1)	0.025(1)
O(5)	$2i$	1	0.5370(2)	0.5722(1)	0.8496(1)	0.024(1)
O(6)	$2i$	1	0.3105(2)	0.5043(1)	0.9067(1)	0.033(1)
O(7)	$2i$	1	0.3999(2)	0.1431(1)	0.8645(1)	0.034(1)
O(8)	$2i$	1	0.5245(2)	0.1013(1)	0.7340(1)	0.026(1)
H(2)	$2i$	1	-0.0310(2)	1.1687(15)	0.7991(14)	0.032(5)
H(3)	$2i$	1	-0.0300(3)	1.3431(18)	0.8120(16)	0.045(6)
H(4)	$2i$	1	-0.1700(3)	1.4041(16)	0.9515(14)	0.032(5)
H(5)	$2i$	1	-0.2990(2)	1.2801(13)	1.0733(12)	0.019(4)
H(6A)	$2i$	1	-0.4180(3)	1.0695(15)	1.0472(14)	0.032(5)
H(6B)	$2i$	1	-0.3690(3)	1.1235(15)	1.1302(14)	0.033(5)
H(6C)	$2i$	1	-0.2250(3)	1.0184(17)	1.1130(15)	0.040(5)
H(8)	$2i$	1	-0.2150(3)	0.8369(16)	0.9765(14)	0.036(5)
H(9)	$2i$	1	-0.2380(3)	0.6668(16)	0.9581(14)	0.035(5)
H(10)	$2i$	1	-0.1780(3)	0.6356(16)	0.7947(14)	0.037(5)
H(11)	$2i$	1	-0.0960(2)	0.7778(14)	0.6713(13)	0.024(4)
H(12A)	$2i$	1	-0.1610(3)	1.0290(17)	0.6495(15)	0.041(6)
H(12B)	$2i$	1	-0.0390(3)	0.9316(16)	0.6114(16)	0.041(5)
H(12C)	$2i$	1	0.0520(3)	0.9796(17)	0.6804(15)	0.045(6)
H(15)	$2i$	1	0.7980(2)	0.6483(14)	0.4195(13)	0.028(5)
H(17)	$2i$	1	0.5360(2)	0.8610(16)	0.5690(13)	0.031(5)
H(22)	$2i$	1	0.3840(2)	0.3244(14)	0.8728(13)	0.026(4)
H(24)	$2i$	1	0.6400(2)	0.2464(14)	0.6297(13)	0.026(4)

Table A.99: Anisotropic displacement parameters $U_{ij}/\text{\AA}^2$ for the independent atoms in the structure of **(1)**(DTeF) at 123 K.

Atom	U_{11}	U_{22}	U_{33}	U_{23}	U_{13}	U_{12}
C(1)	0.020(1)	0.020(1)	0.018(1)	-0.007(1)	0.000(1)	-0.003(1)
C(2)	0.024(1)	0.023(1)	0.019(1)	-0.005(1)	0.002(1)	-0.006(1)
C(3)	0.026(1)	0.022(1)	0.023(1)	-0.002(1)	-0.002(1)	-0.007(1)
C(4)	0.029(1)	0.019(1)	0.027(1)	-0.007(1)	-0.004(1)	-0.004(1)

Table A.99 – continued from previous page

Atom	Wyck.	Site	x/a	y/b	z/c	U_{eq}
C(5)	0.025(1)	0.021(1)	0.024(1)	-0.010(1)	-0.002(1)	-0.003(1)
C(6)	0.028(1)	0.027(1)	0.020(1)	-0.008(1)	0.007(1)	-0.011(1)
C(7)	0.017(1)	0.020(1)	0.019(1)	-0.007(1)	0.001(1)	-0.003(1)
C(8)	0.024(1)	0.025(1)	0.020(1)	-0.007(1)	0.002(1)	-0.007(1)
C(9)	0.028(1)	0.025(1)	0.027(1)	-0.007(1)	0.003(1)	-0.011(1)
C(10)	0.024(1)	0.026(1)	0.032(1)	-0.014(1)	0.003(1)	-0.010(1)
C(11)	0.021(1)	0.027(1)	0.025(1)	-0.013(1)	0.002(1)	-0.007(1)
C(12)	0.045(1)	0.027(1)	0.021(1)	-0.008(1)	0.013(1)	-0.014(1)
C(13)	0.018(1)	0.018(1)	0.014(1)	-0.004(1)	0.000(1)	-0.005(1)
C(14)	0.015(1)	0.019(1)	0.014(1)	-0.005(1)	0.000(1)	-0.005(1)
C(15)	0.018(1)	0.021(1)	0.016(1)	-0.006(1)	0.002(1)	-0.007(1)
C(16)	0.020(1)	0.018(1)	0.017(1)	-0.002(1)	0.000(1)	-0.008(1)
C(17)	0.022(1)	0.017(1)	0.019(1)	-0.004(1)	-0.001(1)	-0.006(1)
C(18)	0.019(1)	0.021(1)	0.014(1)	-0.006(1)	0.001(1)	-0.005(1)
C(19)	0.017(1)	0.018(1)	0.014(1)	-0.004(1)	0.000(1)	-0.005(1)
C(20)	0.016(1)	0.019(1)	0.015(1)	-0.004(1)	0.000(1)	-0.005(1)
C(21)	0.019(1)	0.019(1)	0.015(1)	-0.005(1)	0.001(1)	-0.005(1)
C(22)	0.020(1)	0.022(1)	0.016(1)	-0.003(1)	0.001(1)	-0.007(1)
C(23)	0.019(1)	0.018(1)	0.018(1)	-0.003(1)	-0.001(1)	-0.007(1)
C(24)	0.018(1)	0.017(1)	0.016(1)	-0.003(1)	-0.001(1)	-0.005(1)
C(25)	0.015(1)	0.017(1)	0.013(1)	-0.003(1)	0.000(1)	-0.004(1)
C(26)	0.018(1)	0.018(1)	0.015(1)	-0.005(1)	0.002(1)	-0.004(1)
C(27)	0.020(1)	0.021(1)	0.014(1)	-0.005(1)	0.001(1)	-0.004(1)
C(28)	0.019(1)	0.020(1)	0.019(1)	-0.007(1)	0.001(1)	-0.004(1)
N(1)	0.023(1)	0.020(1)	0.019(1)	-0.008(1)	0.002(1)	-0.005(1)
N(2)	0.023(1)	0.021(1)	0.020(1)	-0.008(1)	0.002(1)	-0.005(1)
N(3)	0.022(1)	0.021(1)	0.019(1)	-0.007(1)	0.003(1)	-0.006(1)
N(4)	0.023(1)	0.021(1)	0.017(1)	-0.006(1)	0.001(1)	-0.005(1)
N(5)	0.024(1)	0.020(1)	0.023(1)	-0.003(1)	0.002(1)	-0.010(1)
N(6)	0.026(1)	0.020(1)	0.015(1)	-0.004(1)	0.001(1)	-0.002(1)
N(7)	0.027(1)	0.022(1)	0.015(1)	-0.005(1)	0.002(1)	-0.007(1)
N(8)	0.023(1)	0.020(1)	0.021(1)	-0.002(1)	0.000(1)	-0.008(1)
N(9)	0.032(1)	0.023(1)	0.021(1)	-0.007(1)	0.001(1)	-0.003(1)
N(10)	0.028(1)	0.029(1)	0.024(1)	-0.007(1)	0.006(1)	-0.010(1)
O(1)	0.032(1)	0.031(1)	0.023(1)	-0.006(1)	0.008(1)	-0.015(1)
O(2)	0.040(1)	0.019(1)	0.042(1)	-0.007(1)	0.012(1)	-0.012(1)
O(3)	0.049(1)	0.023(1)	0.026(1)	-0.014(1)	0.006(1)	-0.007(1)
O(4)	0.021(1)	0.030(1)	0.021(1)	-0.005(1)	0.003(1)	-0.004(1)
O(5)	0.030(1)	0.024(1)	0.020(1)	-0.006(1)	-0.003(1)	-0.009(1)
O(6)	0.042(1)	0.036(1)	0.024(1)	-0.013(1)	0.018(1)	-0.017(1)
O(7)	0.046(1)	0.029(1)	0.026(1)	-0.002(1)	0.012(1)	-0.019(1)
O(8)	0.032(1)	0.021(1)	0.029(1)	-0.008(1)	0.001(1)	-0.008(1)

Table A.100: Crystallographic data and structure refinement of **(1)(DTeF)** at 143 K.

Compound	(1)(DTeF)
Empirical Formula	$C_{28}H_{18}N_{10}O_8$
Formula weight / $g mol^{-1}$	622.52
Crystal size / mm^3	0.190×0.180×0.030
Temperature / K	143(2)

Table A.100 – continued from previous page

Compound	(1)(DTeF)
Crystal system; space group	Triclinic, $P\bar{1}$
Lattice constants / Å	$a = 7.6588(3)$ $\alpha = 73.772(2)$ $b = 13.0471(5)$ $\beta = 86.026(2)$ $c = 14.2451(5)$ $\gamma = 74.072(2)$
Volume / Å ³	1314.22(9)
Z; F(000); calc. density / gcm ⁻³	2: 640; 1.573
Wavelength	Mo-K α (0.71073 Å)
Theta range for data collection / °	2.979 ≤ θ ≤ 33.306
Limiting indices	-11 ≤ h ≤ 11, -20 ≤ k ≤ 19, -21 ≤ l ≤ 21
Reflections collected / unique	14717 / 9245
R _{int}	0.0451
Completeness to theta = 25.242	95.20 %
Absorption coefficient / mm ⁻¹	0.120
Refinement method	Full-matrix least-squares on F^2
Data / restraints / parameters	9245 / 0 / 487
R indices [I > 4σ(I)] R ₁ ; wR ₂	0.0518; 0.1216
R indices (all data) R ₁ ; wR ₂	0.1002; 0.1443
Goodness-of-fit for F^2	0.972
Largest diff. Peak and hole / e ⁻ Å ⁻³	0.347 / -0.312

Table A.101: Fractional coordinates in Å and equivalent isotropic displacement parameter $U_{eq}/\text{\AA}^2$ for the independent atoms in the structure of (1)(DTeF) at 143 K.

Atom	Wyck.	Site	x/a	y/b	z/c	U_{eq}
C(1)	2i	1	-0.1587(2)	1.1235(1)	0.9263(1)	0.021(1)
C(2)	2i	1	-0.0839(2)	1.1968(1)	0.8529(1)	0.025(1)
C(3)	2i	1	-0.0878(2)	1.2988(1)	0.8620(1)	0.028(1)
C(4)	2i	1	-0.1666(2)	1.3315(1)	0.9442(1)	0.029(1)
C(5)	2i	1	-0.2390(2)	1.2599(1)	1.0143(1)	0.026(1)
C(6)	2i	1	-0.3195(3)	1.0844(2)	1.0812(1)	0.028(1)
C(7)	2i	1	-0.1427(2)	0.9005(1)	0.8389(1)	0.021(1)
C(8)	2i	1	-0.1928(2)	0.8200(1)	0.9158(1)	0.025(1)
C(9)	2i	1	-0.2057(2)	0.7229(1)	0.9016(1)	0.029(1)
C(10)	2i	1	-0.1681(2)	0.7029(1)	0.8098(1)	0.029(1)
C(11)	2i	1	-0.1219(2)	0.7825(1)	0.7362(1)	0.025(1)
C(12)	2i	1	-0.0614(3)	0.9624(2)	0.6658(1)	0.035(1)
C(13)	2i	1	0.5661(2)	0.5954(1)	0.6232(1)	0.018(1)
C(14)	2i	1	0.6717(2)	0.5744(1)	0.5399(1)	0.018(1)
C(15)	2i	1	0.7337(2)	0.6576(1)	0.4739(1)	0.020(1)
C(16)	2i	1	0.6862(2)	0.7619(1)	0.4881(1)	0.021(1)
C(17)	2i	1	0.5743(2)	0.7888(1)	0.5637(1)	0.021(1)
C(18)	2i	1	0.5163(2)	0.7053(1)	0.6294(1)	0.020(1)
C(19)	2i	1	0.6103(2)	0.4109(1)	0.6281(1)	0.018(1)
C(20)	2i	1	0.5378(2)	0.4917(1)	0.6817(1)	0.018(1)
C(21)	2i	1	0.4654(2)	0.4537(1)	0.7741(1)	0.020(1)
C(22)	2i	1	0.4391(2)	0.3495(1)	0.8068(1)	0.021(1)
C(23)	2i	1	0.4999(2)	0.2768(1)	0.7487(1)	0.020(1)
C(24)	2i	1	0.5899(2)	0.3034(1)	0.6624(1)	0.019(1)
C(25)	2i	1	0.6971(2)	0.4604(1)	0.5403(1)	0.017(1)

Table A.101 – continued from previous page

Atom	Wyck.	Site	x/a	y/b	z/c	U_{eq}
C(26)	2 <i>i</i>	1	0.7922(2)	0.4072(1)	0.4717(1)	0.019(1)
C(27)	2 <i>i</i>	1	0.8284(2)	0.2912(1)	0.4850(1)	0.022(1)
C(28)	2 <i>i</i>	1	0.8753(2)	0.4613(1)	0.3871(1)	0.021(1)
N(1)	2 <i>i</i>	1	-0.1725(2)	1.0220(1)	0.9263(1)	0.023(1)
N(2)	2 <i>i</i>	1	-0.1200(2)	0.9994(1)	0.8415(1)	0.023(1)
N(3)	2 <i>i</i>	1	-0.1091(2)	0.8785(1)	0.7494(1)	0.023(1)
N(4)	2 <i>i</i>	1	-0.2354(2)	1.1586(1)	1.0057(1)	0.022(1)
N(5)	2 <i>i</i>	1	0.7494(2)	0.8500(1)	0.4182(1)	0.025(1)
N(6)	2 <i>i</i>	1	0.3812(2)	0.7416(1)	0.6987(1)	0.024(1)
N(7)	2 <i>i</i>	1	0.4329(2)	0.5157(1)	0.8478(1)	0.024(1)
N(8)	2 <i>i</i>	1	0.4730(2)	0.1660(1)	0.7846(1)	0.024(1)
N(9)	2 <i>i</i>	1	0.8594(2)	0.1972(1)	0.4934(1)	0.030(1)
N(10)	2 <i>i</i>	1	0.9460(2)	0.5019(1)	0.3185(1)	0.030(1)
O(1)	2 <i>i</i>	1	0.8409(2)	0.8272(1)	0.3492(1)	0.031(1)
O(2)	2 <i>i</i>	1	0.7075(2)	0.9418(1)	0.4329(1)	0.038(1)
O(3)	2 <i>i</i>	1	0.3892(2)	0.8203(1)	0.7274(1)	0.036(1)
O(4)	2 <i>i</i>	1	0.2609(2)	0.6930(1)	0.7228(1)	0.028(1)
O(5)	2 <i>i</i>	1	0.5368(2)	0.5722(1)	0.8494(1)	0.027(1)
O(6)	2 <i>i</i>	1	0.3108(2)	0.5043(1)	0.9065(1)	0.037(1)
O(7)	2 <i>i</i>	1	0.4000(2)	0.1432(1)	0.8644(1)	0.038(1)
O(8)	2 <i>i</i>	1	0.5241(2)	0.1013(1)	0.7340(1)	0.030(1)
H(2)	2 <i>i</i>	1	-0.0320(3)	1.1710(16)	0.7971(15)	0.036(5)
H(3)	2 <i>i</i>	1	-0.0400(3)	1.3449(18)	0.8124(16)	0.047(6)
H(4)	2 <i>i</i>	1	-0.1680(2)	1.4032(15)	0.9517(13)	0.030(5)
H(5)	2 <i>i</i>	1	-0.2990(2)	1.2782(14)	1.0752(13)	0.027(5)
H(6A)	2 <i>i</i>	1	-0.4180(3)	1.0690(14)	1.0502(13)	0.026(5)
H(6B)	2 <i>i</i>	1	-0.3680(3)	1.1237(16)	1.1300(15)	0.036(5)
H(6C)	2 <i>i</i>	1	-0.2210(3)	1.0158(19)	1.1121(16)	0.053(7)
H(8)	2 <i>i</i>	1	-0.2190(3)	0.8379(15)	0.9757(14)	0.030(5)
H(9)	2 <i>i</i>	1	-0.2350(3)	0.6678(18)	0.9557(16)	0.049(6)
H(10)	2 <i>i</i>	1	-0.1810(3)	0.6362(16)	0.7963(14)	0.038(5)
H(11)	2 <i>i</i>	1	-0.0920(2)	0.7741(13)	0.6708(12)	0.019(4)
H(12A)	2 <i>i</i>	1	-0.1560(3)	1.0310(19)	0.6557(16)	0.049(6)
H(12B)	2 <i>i</i>	1	-0.0450(3)	0.9312(18)	0.6115(17)	0.049(6)
H(12C)	2 <i>i</i>	1	0.0500(3)	0.9780(18)	0.6806(17)	0.055(7)
H(15)	2 <i>i</i>	1	0.8010(2)	0.6457(14)	0.4205(13)	0.025(5)
H(17)	2 <i>i</i>	1	0.5340(2)	0.8588(15)	0.5696(13)	0.026(5)
H(22)	2 <i>i</i>	1	0.3880(2)	0.3234(13)	0.8721(12)	0.019(4)
H(24)	2 <i>i</i>	1	0.6400(2)	0.2475(14)	0.6282(12)	0.023(4)

Table A.102: Anisotropic displacement parameters $U_{ij}/\text{\AA}^2$ for the independent atoms in the structure of **(1)**(DTeF) at 143 K.

Atom	U_{11}	U_{22}	U_{33}	U_{23}	U_{13}	U_{12}
C(1)	0.022(1)	0.021(1)	0.019(1)	-0.007(1)	-0.001(1)	-0.003(1)
C(2)	0.027(1)	0.025(1)	0.021(1)	-0.006(1)	0.002(1)	-0.007(1)
C(3)	0.031(1)	0.024(1)	0.027(1)	-0.002(1)	-0.004(1)	-0.008(1)
C(4)	0.034(1)	0.022(1)	0.031(1)	-0.007(1)	-0.005(1)	-0.006(1)
C(5)	0.029(1)	0.024(1)	0.027(1)	-0.011(1)	-0.002(1)	-0.005(1)
C(6)	0.032(1)	0.031(1)	0.024(1)	-0.010(1)	0.008(1)	-0.013(1)
C(7)	0.019(1)	0.023(1)	0.022(1)	-0.008(1)	0.001(1)	-0.004(1)

Table A.102 – continued from previous page

Atom	Wyck.	Site	x/a	y/b	z/c	U_{eq}
C(8)	0.026(1)	0.028(1)	0.023(1)	-0.007(1)	0.002(1)	-0.008(1)
C(9)	0.032(1)	0.029(1)	0.030(1)	-0.008(1)	0.005(1)	-0.013(1)
C(10)	0.027(1)	0.030(1)	0.036(1)	-0.014(1)	0.002(1)	-0.012(1)
C(11)	0.024(1)	0.029(1)	0.028(1)	-0.015(1)	0.003(1)	-0.009(1)
C(12)	0.052(1)	0.031(1)	0.024(1)	-0.010(1)	0.014(1)	-0.016(1)
C(13)	0.019(1)	0.020(1)	0.016(1)	-0.005(1)	0.000(1)	-0.006(1)
C(14)	0.018(1)	0.020(1)	0.016(1)	-0.006(1)	0.000(1)	-0.007(1)
C(15)	0.019(1)	0.022(1)	0.017(1)	-0.005(1)	0.001(1)	-0.007(1)
C(16)	0.022(1)	0.020(1)	0.020(1)	-0.002(1)	-0.001(1)	-0.008(1)
C(17)	0.025(1)	0.018(1)	0.021(1)	-0.005(1)	-0.001(1)	-0.006(1)
C(18)	0.021(1)	0.023(1)	0.017(1)	-0.007(1)	0.000(1)	-0.005(1)
C(19)	0.019(1)	0.020(1)	0.015(1)	-0.004(1)	-0.001(1)	-0.005(1)
C(20)	0.017(1)	0.020(1)	0.016(1)	-0.004(1)	-0.001(1)	-0.005(1)
C(21)	0.021(1)	0.021(1)	0.016(1)	-0.005(1)	0.001(1)	-0.005(1)
C(22)	0.022(1)	0.023(1)	0.017(1)	-0.002(1)	0.001(1)	-0.008(1)
C(23)	0.022(1)	0.019(1)	0.019(1)	-0.002(1)	-0.001(1)	-0.008(1)
C(24)	0.020(1)	0.019(1)	0.018(1)	-0.004(1)	-0.001(1)	-0.005(1)
C(25)	0.017(1)	0.019(1)	0.016(1)	-0.004(1)	0.000(1)	-0.006(1)
C(26)	0.019(1)	0.020(1)	0.018(1)	-0.005(1)	0.001(1)	-0.005(1)
C(27)	0.023(1)	0.024(1)	0.017(1)	-0.006(1)	0.001(1)	-0.005(1)
C(28)	0.020(1)	0.022(1)	0.022(1)	-0.008(1)	0.001(1)	-0.004(1)
N(1)	0.025(1)	0.023(1)	0.022(1)	-0.008(1)	0.002(1)	-0.005(1)
N(2)	0.026(1)	0.023(1)	0.022(1)	-0.009(1)	0.003(1)	-0.006(1)
N(3)	0.024(1)	0.025(1)	0.021(1)	-0.009(1)	0.004(1)	-0.008(1)
N(4)	0.025(1)	0.021(1)	0.022(1)	-0.008(1)	0.002(1)	-0.006(1)
N(5)	0.028(1)	0.023(1)	0.025(1)	-0.004(1)	0.003(1)	-0.011(1)
N(6)	0.030(1)	0.022(1)	0.017(1)	-0.006(1)	0.001(1)	-0.003(1)
N(7)	0.032(1)	0.024(1)	0.016(1)	-0.005(1)	0.003(1)	-0.008(1)
N(8)	0.027(1)	0.022(1)	0.024(1)	-0.002(1)	0.000(1)	-0.009(1)
N(9)	0.037(1)	0.026(1)	0.023(1)	-0.007(1)	0.002(1)	-0.003(1)
N(10)	0.031(1)	0.032(1)	0.026(1)	-0.008(1)	0.007(1)	-0.012(1)
O(1)	0.037(1)	0.033(1)	0.026(1)	-0.006(1)	0.009(1)	-0.017(1)
O(2)	0.046(1)	0.021(1)	0.048(1)	-0.009(1)	0.012(1)	-0.014(1)
O(3)	0.055(1)	0.026(1)	0.029(1)	-0.015(1)	0.007(1)	-0.007(1)
O(4)	0.024(1)	0.034(1)	0.023(1)	-0.006(1)	0.004(1)	-0.005(1)
O(5)	0.035(1)	0.026(1)	0.023(1)	-0.007(1)	-0.003(1)	-0.011(1)
O(6)	0.050(1)	0.040(1)	0.026(1)	-0.014(1)	0.020(1)	-0.019(1)
O(7)	0.053(1)	0.033(1)	0.030(1)	-0.003(1)	0.014(1)	-0.022(1)
O(8)	0.035(1)	0.023(1)	0.032(1)	-0.008(1)	0.001(1)	-0.010(1)

Table A.103: Crystallographic data and structure refinement of (**1**)(DTeF) at 163 K.

Compound	(1)(DTeF)
Empirical Formula	$C_{28}H_{18}N_{10}O_8$
Formula weight / $gmol^{-1}$	622.52
Crystal size / mm^3	0.190×0.180×0.030
Temperature / K	163(2)
Crystal system; space group	Triclinic, $P\bar{1}$
Lattice constants / Å °	$a = 7.6718(3) \alpha = 73.795(2)$ $b = 13.0441(5) \beta = 85.977(2)$

Table A.103 – continued from previous page

Compound	(1)(DTeF)
Volume / Å ³	$c = 14.2570(5) \gamma = 74.106(2)$
Z; F(000); calc. density / gcm ⁻³	1317.63(9)
Wavelength	2: 640; 1.569
Theta range for data collection / °	Mo-K α (0.71073 Å) 2.976 ≤ θ ≤ 33.189
Limiting indices	-11 ≤ h ≤ 11, -19 ≤ k ≤ 20, -21 ≤ l ≤ 21
Reflections collected / unique	14286 / 9092
R _{int}	0.0482
Completeness to theta = 25.242	94.60 %
Absorption coefficient / mm ⁻¹	0.120
Refinement method	Full-matrix least-squares on F^2
Data / restraints / parameters	9092 / 0 / 487
R indices [I > 4σ(I)] R ₁ ; wR ₂	0.0552; 0.1313
R indices (all data) R ₁ ; wR ₂	0.1089; 0.1563
Goodness-of-fit for F^2	0.963
Largest diff. Peak and hole / e ⁻ Å ⁻³	0.346 / -0.333

Table A.104: Fractional coordinates in Å and equivalent isotropic displacement parameter U_{eq} /Å² for the independent atoms in the structure of (1)(DTeF) at 163 K.

Atom	Wyck.	Site	x/a	y/b	z/c	U_{eq}
C(1)	2i	1	-0.1591(2)	1.1237(1)	0.9260(1)	0.024(1)
C(2)	2i	1	-0.0849(3)	1.1968(2)	0.8528(1)	0.028(1)
C(3)	2i	1	-0.0881(3)	1.2988(2)	0.8619(1)	0.031(1)
C(4)	2i	1	-0.1668(3)	1.3316(2)	0.9440(1)	0.032(1)
C(5)	2i	1	-0.2385(3)	1.2601(2)	1.0142(1)	0.029(1)
C(6)	2i	1	-0.3185(3)	1.0843(2)	1.0811(1)	0.031(1)
C(7)	2i	1	-0.1431(2)	0.9006(1)	0.8388(1)	0.023(1)
C(8)	2i	1	-0.1928(3)	0.8203(2)	0.9157(1)	0.028(1)
C(9)	2i	1	-0.2050(3)	0.7226(2)	0.9017(1)	0.033(1)
C(10)	2i	1	-0.1676(3)	0.7028(2)	0.8099(1)	0.032(1)
C(11)	2i	1	-0.1217(2)	0.7821(2)	0.7366(1)	0.028(1)
C(12)	2i	1	-0.0615(4)	0.9623(2)	0.6660(2)	0.039(1)
C(13)	2i	1	0.5665(2)	0.5954(1)	0.6233(1)	0.020(1)
C(14)	2i	1	0.6720(2)	0.5742(1)	0.5401(1)	0.019(1)
C(15)	2i	1	0.7339(2)	0.6576(1)	0.4742(1)	0.021(1)
C(16)	2i	1	0.6861(2)	0.7618(1)	0.4884(1)	0.023(1)
C(17)	2i	1	0.5747(2)	0.7890(1)	0.5636(1)	0.023(1)
C(18)	2i	1	0.5168(2)	0.7055(1)	0.6293(1)	0.022(1)
C(19)	2i	1	0.6101(2)	0.4107(1)	0.6281(1)	0.019(1)
C(20)	2i	1	0.5377(2)	0.4919(1)	0.6815(1)	0.019(1)
C(21)	2i	1	0.4651(2)	0.4537(1)	0.7739(1)	0.021(1)
C(22)	2i	1	0.4391(2)	0.3495(1)	0.8065(1)	0.024(1)
C(23)	2i	1	0.4993(2)	0.2771(1)	0.7485(1)	0.022(1)
C(24)	2i	1	0.5895(2)	0.3036(1)	0.6621(1)	0.021(1)
C(25)	2i	1	0.6972(2)	0.4601(1)	0.5405(1)	0.019(1)
C(26)	2i	1	0.7920(2)	0.4072(1)	0.4717(1)	0.021(1)
C(27)	2i	1	0.8274(2)	0.2910(1)	0.4851(1)	0.023(1)
C(28)	2i	1	0.8753(2)	0.4611(1)	0.3872(1)	0.023(1)

Table A.104 – continued from previous page

Atom	Wyck.	Site	x/a	y/b	z/c	U_{eq}
N(1)	$2i$	1	-0.1732(2)	1.0222(1)	0.9260(1)	0.026(1)
N(2)	$2i$	1	-0.1204(2)	0.9993(1)	0.8415(1)	0.026(1)
N(3)	$2i$	1	-0.1095(2)	0.8783(1)	0.7493(1)	0.025(1)
N(4)	$2i$	1	-0.2352(2)	1.1585(1)	1.0058(1)	0.025(1)
N(5)	$2i$	1	0.7497(2)	0.8499(1)	0.4185(1)	0.028(1)
N(6)	$2i$	1	0.3817(2)	0.7419(1)	0.6987(1)	0.027(1)
N(7)	$2i$	1	0.4326(2)	0.5158(1)	0.8476(1)	0.026(1)
N(8)	$2i$	1	0.4724(2)	0.1662(1)	0.7844(1)	0.027(1)
N(9)	$2i$	1	0.8580(2)	0.1976(1)	0.4933(1)	0.033(1)
N(10)	$2i$	1	0.9460(2)	0.5019(1)	0.3188(1)	0.033(1)
O(1)	$2i$	1	0.8413(2)	0.8270(1)	0.3495(1)	0.035(1)
O(2)	$2i$	1	0.7081(2)	0.9417(1)	0.4332(1)	0.042(1)
O(3)	$2i$	1	0.3907(2)	0.8204(1)	0.7273(1)	0.040(1)
O(4)	$2i$	1	0.2615(2)	0.6932(1)	0.7227(1)	0.031(1)
O(5)	$2i$	1	0.5366(2)	0.5722(1)	0.8493(1)	0.030(1)
O(6)	$2i$	1	0.3107(2)	0.5045(1)	0.9062(1)	0.041(1)
O(7)	$2i$	1	0.3995(2)	0.1435(1)	0.8640(1)	0.043(1)
O(8)	$2i$	1	0.5236(2)	0.1014(1)	0.7338(1)	0.033(1)
H(2)	$2i$	1	-0.0300(3)	1.1692(18)	0.7995(16)	0.040(6)
H(3)	$2i$	1	-0.0360(3)	1.3456(19)	0.8135(17)	0.044(6)
H(4)	$2i$	1	-0.1700(3)	1.4031(16)	0.9519(14)	0.027(5)
H(5)	$2i$	1	-0.2940(3)	1.2778(15)	1.0727(14)	0.024(5)
H(6A)	$2i$	1	-0.4130(3)	1.0676(18)	1.0487(17)	0.044(6)
H(6B)	$2i$	1	-0.3700(3)	1.1265(18)	1.1266(16)	0.042(6)
H(6C)	$2i$	1	-0.2190(4)	1.0140(2)	1.1104(18)	0.062(8)
H(8)	$2i$	1	-0.2180(3)	0.8384(18)	0.9749(17)	0.043(6)
H(9)	$2i$	1	-0.2370(3)	0.6670(2)	0.9580(19)	0.057(7)
H(10)	$2i$	1	-0.1760(3)	0.6364(17)	0.7975(15)	0.033(5)
H(11)	$2i$	1	-0.0940(3)	0.7776(17)	0.6724(15)	0.036(6)
H(12A)	$2i$	1	-0.1520(3)	1.0290(2)	0.6530(18)	0.052(7)
H(12B)	$2i$	1	-0.0420(3)	0.9308(19)	0.6149(18)	0.047(6)
H(12C)	$2i$	1	0.0520(4)	0.9800(2)	0.6808(18)	0.056(7)
H(15)	$2i$	1	0.8000(3)	0.6462(17)	0.4201(16)	0.038(6)
H(17)	$2i$	1	0.5360(3)	0.8594(16)	0.5712(14)	0.030(5)
H(22)	$2i$	1	0.3870(3)	0.3262(15)	0.8722(14)	0.026(5)
H(24)	$2i$	1	0.6390(3)	0.2455(16)	0.6294(14)	0.031(5)

Table A.105: Anisotropic displacement parameters $U_{ij}/\text{\AA}^2$ for the independent atoms in the structure of **(1)(DTeF)** at 163 K.

Atom	U_{11}	U_{22}	U_{33}	U_{23}	U_{13}	U_{12}
C(1)	0.026(1)	0.024(1)	0.021(1)	-0.007(1)	0.000(1)	-0.005(1)
C(2)	0.030(1)	0.028(1)	0.025(1)	-0.006(1)	0.003(1)	-0.007(1)
C(3)	0.034(1)	0.027(1)	0.030(1)	-0.001(1)	-0.002(1)	-0.010(1)
C(4)	0.038(1)	0.023(1)	0.035(1)	-0.009(1)	-0.004(1)	-0.006(1)
C(5)	0.031(1)	0.028(1)	0.030(1)	-0.012(1)	-0.001(1)	-0.004(1)
C(6)	0.035(1)	0.035(1)	0.026(1)	-0.012(1)	0.010(1)	-0.013(1)
C(7)	0.022(1)	0.025(1)	0.023(1)	-0.010(1)	0.002(1)	-0.005(1)
C(8)	0.031(1)	0.030(1)	0.025(1)	-0.008(1)	0.003(1)	-0.010(1)
C(9)	0.035(1)	0.032(1)	0.033(1)	-0.008(1)	0.004(1)	-0.014(1)
C(10)	0.031(1)	0.033(1)	0.039(1)	-0.016(1)	0.003(1)	-0.014(1)

Table A.105 – continued from previous page

Atom	Wyck.	Site	x/a	y/b	z/c	U_{eq}
C(11)	0.026(1)	0.033(1)	0.031(1)	-0.017(1)	0.003(1)	-0.009(1)
C(12)	0.059(2)	0.033(1)	0.026(1)	-0.012(1)	0.017(1)	-0.016(1)
C(13)	0.021(1)	0.022(1)	0.017(1)	-0.006(1)	0.000(1)	-0.006(1)
C(14)	0.019(1)	0.022(1)	0.017(1)	-0.006(1)	0.000(1)	-0.007(1)
C(15)	0.022(1)	0.024(1)	0.018(1)	-0.005(1)	0.002(1)	-0.008(1)
C(16)	0.025(1)	0.021(1)	0.022(1)	-0.003(1)	0.000(1)	-0.010(1)
C(17)	0.027(1)	0.021(1)	0.022(1)	-0.006(1)	-0.001(1)	-0.007(1)
C(18)	0.023(1)	0.025(1)	0.018(1)	-0.008(1)	0.001(1)	-0.006(1)
C(19)	0.020(1)	0.020(1)	0.017(1)	-0.005(1)	-0.001(1)	-0.004(1)
C(20)	0.019(1)	0.022(1)	0.018(1)	-0.005(1)	0.000(1)	-0.007(1)
C(21)	0.023(1)	0.023(1)	0.018(1)	-0.006(1)	0.001(1)	-0.006(1)
C(22)	0.025(1)	0.026(1)	0.019(1)	-0.003(1)	0.002(1)	-0.008(1)
C(23)	0.024(1)	0.021(1)	0.021(1)	-0.002(1)	-0.001(1)	-0.008(1)
C(24)	0.022(1)	0.021(1)	0.020(1)	-0.005(1)	-0.001(1)	-0.006(1)
C(25)	0.019(1)	0.019(1)	0.016(1)	-0.003(1)	0.000(1)	-0.005(1)
C(26)	0.021(1)	0.022(1)	0.018(1)	-0.005(1)	0.002(1)	-0.006(1)
C(27)	0.023(1)	0.026(1)	0.019(1)	-0.006(1)	0.002(1)	-0.004(1)
C(28)	0.022(1)	0.023(1)	0.023(1)	-0.008(1)	0.002(1)	-0.004(1)
N(1)	0.029(1)	0.025(1)	0.023(1)	-0.009(1)	0.003(1)	-0.006(1)
N(2)	0.030(1)	0.026(1)	0.024(1)	-0.010(1)	0.004(1)	-0.007(1)
N(3)	0.026(1)	0.026(1)	0.024(1)	-0.010(1)	0.005(1)	-0.007(1)
N(4)	0.028(1)	0.025(1)	0.023(1)	-0.009(1)	0.002(1)	-0.006(1)
N(5)	0.030(1)	0.025(1)	0.029(1)	-0.004(1)	0.003(1)	-0.012(1)
N(6)	0.033(1)	0.025(1)	0.020(1)	-0.006(1)	0.001(1)	-0.004(1)
N(7)	0.036(1)	0.027(1)	0.016(1)	-0.005(1)	0.004(1)	-0.009(1)
N(8)	0.029(1)	0.024(1)	0.025(1)	-0.002(1)	0.001(1)	-0.010(1)
N(9)	0.041(1)	0.027(1)	0.025(1)	-0.007(1)	0.002(1)	-0.002(1)
N(10)	0.035(1)	0.035(1)	0.028(1)	-0.009(1)	0.008(1)	-0.013(1)
O(1)	0.040(1)	0.037(1)	0.030(1)	-0.006(1)	0.010(1)	-0.019(1)
O(2)	0.052(1)	0.023(1)	0.053(1)	-0.010(1)	0.015(1)	-0.016(1)
O(3)	0.062(1)	0.029(1)	0.031(1)	-0.017(1)	0.008(1)	-0.008(1)
O(4)	0.026(1)	0.037(1)	0.026(1)	-0.007(1)	0.005(1)	-0.005(1)
O(5)	0.039(1)	0.029(1)	0.025(1)	-0.008(1)	-0.003(1)	-0.012(1)
O(6)	0.056(1)	0.045(1)	0.029(1)	-0.016(1)	0.023(1)	-0.023(1)
O(7)	0.062(1)	0.035(1)	0.033(1)	-0.003(1)	0.018(1)	-0.025(1)
O(8)	0.041(1)	0.025(1)	0.036(1)	-0.009(1)	0.002(1)	-0.011(1)

Table A.106: Crystallographic data and structure refinement of (**1**)(DTeF) at 183 K.

Compound	(1)(DTeF)
Empirical Formula	$C_{28}H_{18}N_{10}O_8$
Formula weight / $gmol^{-1}$	622.52
Crystal size / mm^3	0.190×0.180×0.030
Temperature/ K	183(2)
Crystal system; space group	Triclinic, $P\bar{1}$
Lattice constants / \AA°	$a = 7.6845(3)$ $\alpha = 73.821(2)$ $b = 13.0432(5)$ $\beta = 85.906(2)$ $c = 14.2688(5)$ $\gamma = 74.140(2)$
Volume / \AA^3	1321.22(9)
Z; F(000); calc. density / gcm^{-3}	2: 640; 1.565

Table A.106 – continued from previous page

Compound	(1)(DTeF)
Wavelength	Mo-K α (0.71073 Å)
Theta range for data collection / °	2.973 $\leq \theta \leq$ 33.220
Limiting indices	-11 $\leq h \leq$ 11, -19 $\leq k \leq$ 20, -21 $\leq l \leq$ 21
Reflections collected / unique	14114 / 9033
R _{int}	0.0475
Completeness to theta = 25.242	94.30 %
Absorption coefficient / mm ⁻¹	0.119
Refinement method	Full-matrix least-squares on F ²
Data / restraints / parameters	9033 / 0 / 487
R indices [I > 4σ(I)] R ₁ ; wR ₂	0.0541; 0.1238
R indices (all data) R ₁ ; wR ₂	0.1129; 0.1495
Goodness-of-fit for F ²	0.949
Largest diff. Peak and hole / e ⁻ Å ⁻³	0.275 / -0.349

Table A.107: Fractional coordinates in Å and equivalent isotropic displacement parameter U_{eq}/Å² for the independent atoms in the structure of (1)(DTeF) at 183 K.

Atom	Wyck.	Site	x/a	y/b	z/c	U _{eq}
C(1)	2i	1	-0.1600(2)	1.1239(1)	0.9256(1)	0.026(1)
C(2)	2i	1	-0.0854(3)	1.1972(2)	0.8523(1)	0.030(1)
C(3)	2i	1	-0.0888(3)	1.2988(2)	0.8615(1)	0.035(1)
C(4)	2i	1	-0.1665(3)	1.3317(2)	0.9437(1)	0.035(1)
C(5)	2i	1	-0.2379(3)	1.2600(1)	1.0139(1)	0.032(1)
C(6)	2i	1	-0.3190(3)	1.0848(2)	1.0809(1)	0.034(1)
C(7)	2i	1	-0.1431(2)	0.9005(1)	0.8387(1)	0.025(1)
C(8)	2i	1	-0.1934(2)	0.8202(2)	0.9156(1)	0.031(1)
C(9)	2i	1	-0.2045(3)	0.7227(2)	0.9016(2)	0.037(1)
C(10)	2i	1	-0.1669(3)	0.7024(2)	0.8103(1)	0.035(1)
C(11)	2i	1	-0.1210(2)	0.7817(2)	0.7369(1)	0.032(1)
C(12)	2i	1	-0.0618(4)	0.9618(2)	0.6659(2)	0.044(1)
C(13)	2i	1	0.5664(2)	0.5955(1)	0.6234(1)	0.022(1)
C(14)	2i	1	0.6717(2)	0.5743(1)	0.5400(1)	0.021(1)
C(15)	2i	1	0.7338(2)	0.6576(1)	0.4741(1)	0.023(1)
C(16)	2i	1	0.6866(2)	0.7618(1)	0.4884(1)	0.024(1)
C(17)	2i	1	0.5752(2)	0.7887(1)	0.5639(1)	0.025(1)
C(18)	2i	1	0.5169(2)	0.7054(1)	0.6293(1)	0.023(1)
C(19)	2i	1	0.6096(2)	0.4110(1)	0.6279(1)	0.021(1)
C(20)	2i	1	0.5370(2)	0.4920(1)	0.6815(1)	0.021(1)
C(21)	2i	1	0.4650(2)	0.4538(1)	0.7739(1)	0.023(1)
C(22)	2i	1	0.4389(2)	0.3498(1)	0.8063(1)	0.026(1)
C(23)	2i	1	0.4989(2)	0.2774(1)	0.7483(1)	0.025(1)
C(24)	2i	1	0.5891(2)	0.3039(1)	0.6619(1)	0.023(1)
C(25)	2i	1	0.6963(2)	0.4603(1)	0.5403(1)	0.020(1)
C(26)	2i	1	0.7917(2)	0.4071(1)	0.4718(1)	0.023(1)
C(27)	2i	1	0.8268(2)	0.2912(1)	0.4850(1)	0.025(1)
C(28)	2i	1	0.8753(2)	0.4610(1)	0.3875(1)	0.026(1)
N(1)	2i	1	-0.1736(2)	1.0224(1)	0.9258(1)	0.028(1)
N(2)	2i	1	-0.1215(2)	0.9993(1)	0.8411(1)	0.029(1)
N(3)	2i	1	-0.1096(2)	0.8782(1)	0.7493(1)	0.027(1)
N(4)	2i	1	-0.2353(2)	1.1587(1)	1.0055(1)	0.028(1)

Table A.107 – continued from previous page

Atom	Wyck.	Site	x/a	y/b	z/c	U_{eq}
N(5)	$2i$	1	0.7503(2)	0.8498(1)	0.4187(1)	0.031(1)
N(6)	$2i$	1	0.3823(2)	0.7417(1)	0.6987(1)	0.029(1)
N(7)	$2i$	1	0.4325(2)	0.5159(1)	0.8473(1)	0.029(1)
N(8)	$2i$	1	0.4719(2)	0.1665(1)	0.7842(1)	0.030(1)
N(9)	$2i$	1	0.8570(2)	0.1976(1)	0.4932(1)	0.036(1)
N(10)	$2i$	1	0.9460(2)	0.5016(1)	0.3191(1)	0.036(1)
O(1)	$2i$	1	0.8419(2)	0.8268(1)	0.3498(1)	0.039(1)
O(2)	$2i$	1	0.7092(2)	0.9413(1)	0.4335(1)	0.047(1)
O(3)	$2i$	1	0.3919(2)	0.8200(1)	0.7276(1)	0.045(1)
O(4)	$2i$	1	0.2621(2)	0.6936(1)	0.7227(1)	0.035(1)
O(5)	$2i$	1	0.5364(2)	0.5723(1)	0.8491(1)	0.033(1)
O(6)	$2i$	1	0.3108(2)	0.5047(1)	0.9058(1)	0.045(1)
O(7)	$2i$	1	0.3991(2)	0.1434(1)	0.8638(1)	0.048(1)
O(8)	$2i$	1	0.5228(2)	0.1017(1)	0.7338(1)	0.037(1)
H(2)	$2i$	1	-0.0340(3)	1.1696(17)	0.7966(15)	0.041(5)
H(3)	$2i$	1	-0.0390(3)	1.3467(18)	0.8123(16)	0.047(6)
H(4)	$2i$	1	-0.1680(3)	1.4037(16)	0.9509(14)	0.034(5)
H(5)	$2i$	1	-0.2940(3)	1.2779(15)	1.0771(14)	0.033(5)
H(6A)	$2i$	1	-0.4170(3)	1.0675(17)	1.0491(16)	0.050(6)
H(6B)	$2i$	1	-0.3730(3)	1.1270(17)	1.1278(16)	0.044(6)
H(6C)	$2i$	1	-0.2250(3)	1.0190(2)	1.1093(17)	0.054(7)
H(8)	$2i$	1	-0.2200(3)	0.8382(17)	0.9768(15)	0.043(6)
H(9)	$2i$	1	-0.2330(3)	0.6695(19)	0.9579(18)	0.061(7)
H(10)	$2i$	1	-0.1750(3)	0.6348(17)	0.7981(15)	0.042(6)
H(11)	$2i$	1	-0.0970(3)	0.7761(15)	0.6722(14)	0.034(5)
H(12A)	$2i$	1	-0.1500(3)	1.0270(2)	0.6529(17)	0.054(7)
H(12B)	$2i$	1	-0.0390(3)	0.9319(19)	0.6142(18)	0.057(7)
H(12C)	$2i$	1	0.0510(4)	0.9790(2)	0.6812(18)	0.069(8)
H(15)	$2i$	1	0.8040(3)	0.6458(16)	0.4198(15)	0.040(6)
H(17)	$2i$	1	0.5390(3)	0.8585(16)	0.5698(14)	0.035(5)
H(22)	$2i$	1	0.3820(2)	0.3249(14)	0.8692(13)	0.028(5)
H(24)	$2i$	1	0.6370(2)	0.2485(14)	0.6273(13)	0.025(5)

Table A.108: Anisotropic displacement parameters $U_{ij}/\text{\AA}^2$ for the independent atoms in the structure of **(1)**(DTeF) at 183 K.

Atom	U_{11}	U_{22}	U_{33}	U_{23}	U_{13}	U_{12}
C(1)	0.027(1)	0.026(1)	0.024(1)	-0.008(1)	0.001(1)	-0.004(1)
C(2)	0.033(1)	0.031(1)	0.026(1)	-0.008(1)	0.002(1)	-0.007(1)
C(3)	0.038(1)	0.031(1)	0.033(1)	-0.002(1)	-0.002(1)	-0.010(1)
C(4)	0.042(1)	0.027(1)	0.037(1)	-0.009(1)	-0.005(1)	-0.008(1)
C(5)	0.036(1)	0.030(1)	0.033(1)	-0.014(1)	-0.002(1)	-0.006(1)
C(6)	0.040(1)	0.038(1)	0.028(1)	-0.012(1)	0.010(1)	-0.014(1)
C(7)	0.022(1)	0.029(1)	0.027(1)	-0.012(1)	0.003(1)	-0.005(1)
C(8)	0.032(1)	0.033(1)	0.027(1)	-0.009(1)	0.004(1)	-0.009(1)
C(9)	0.039(1)	0.036(1)	0.038(1)	-0.010(1)	0.006(1)	-0.017(1)
C(10)	0.034(1)	0.037(1)	0.043(1)	-0.018(1)	0.006(1)	-0.016(1)
C(11)	0.029(1)	0.038(1)	0.035(1)	-0.019(1)	0.002(1)	-0.010(1)
C(12)	0.068(2)	0.037(1)	0.028(1)	-0.014(1)	0.018(1)	-0.018(1)
C(13)	0.023(1)	0.024(1)	0.018(1)	-0.007(1)	0.000(1)	-0.007(1)
C(14)	0.022(1)	0.023(1)	0.019(1)	-0.006(1)	0.000(1)	-0.008(1)

Table A.108 – continued from previous page

Atom	Wyck.	Site	x/a	y/b	z/c	U_{eq}
C(15)	0.023(1)	0.027(1)	0.020(1)	-0.006(1)	0.001(1)	-0.009(1)
C(16)	0.027(1)	0.024(1)	0.024(1)	-0.004(1)	0.000(1)	-0.011(1)
C(17)	0.030(1)	0.022(1)	0.025(1)	-0.006(1)	-0.001(1)	-0.007(1)
C(18)	0.024(1)	0.026(1)	0.020(1)	-0.009(1)	0.002(1)	-0.007(1)
C(19)	0.022(1)	0.023(1)	0.018(1)	-0.005(1)	0.000(1)	-0.005(1)
C(20)	0.021(1)	0.024(1)	0.019(1)	-0.005(1)	0.000(1)	-0.007(1)
C(21)	0.026(1)	0.026(1)	0.019(1)	-0.006(1)	0.001(1)	-0.007(1)
C(22)	0.027(1)	0.028(1)	0.021(1)	-0.003(1)	0.003(1)	-0.009(1)
C(23)	0.027(1)	0.023(1)	0.024(1)	-0.002(1)	-0.002(1)	-0.009(1)
C(24)	0.024(1)	0.022(1)	0.022(1)	-0.005(1)	0.000(1)	-0.006(1)
C(25)	0.020(1)	0.021(1)	0.019(1)	-0.005(1)	0.001(1)	-0.006(1)
C(26)	0.022(1)	0.025(1)	0.020(1)	-0.006(1)	0.002(1)	-0.006(1)
C(27)	0.025(1)	0.029(1)	0.020(1)	-0.007(1)	0.002(1)	-0.004(1)
C(28)	0.026(1)	0.026(1)	0.025(1)	-0.009(1)	0.002(1)	-0.005(1)
N(1)	0.032(1)	0.028(1)	0.025(1)	-0.010(1)	0.004(1)	-0.007(1)
N(2)	0.033(1)	0.029(1)	0.025(1)	-0.011(1)	0.005(1)	-0.008(1)
N(3)	0.028(1)	0.030(1)	0.027(1)	-0.012(1)	0.005(1)	-0.009(1)
N(4)	0.031(1)	0.027(1)	0.025(1)	-0.010(1)	0.003(1)	-0.007(1)
N(5)	0.033(1)	0.028(1)	0.032(1)	-0.004(1)	0.002(1)	-0.014(1)
N(6)	0.036(1)	0.026(1)	0.023(1)	-0.008(1)	0.002(1)	-0.003(1)
N(7)	0.038(1)	0.029(1)	0.019(1)	-0.006(1)	0.005(1)	-0.010(1)
N(8)	0.034(1)	0.026(1)	0.030(1)	-0.003(1)	0.000(1)	-0.011(1)
N(9)	0.046(1)	0.029(1)	0.027(1)	-0.008(1)	0.002(1)	-0.003(1)
N(10)	0.038(1)	0.039(1)	0.031(1)	-0.009(1)	0.010(1)	-0.013(1)
O(1)	0.046(1)	0.041(1)	0.032(1)	-0.008(1)	0.012(1)	-0.021(1)
O(2)	0.059(1)	0.027(1)	0.057(1)	-0.011(1)	0.016(1)	-0.019(1)
O(3)	0.071(1)	0.032(1)	0.035(1)	-0.020(1)	0.010(1)	-0.011(1)
O(4)	0.030(1)	0.041(1)	0.029(1)	-0.007(1)	0.006(1)	-0.006(1)
O(5)	0.043(1)	0.033(1)	0.027(1)	-0.009(1)	-0.003(1)	-0.014(1)
O(6)	0.062(1)	0.047(1)	0.033(1)	-0.018(1)	0.025(1)	-0.024(1)
O(7)	0.070(1)	0.039(1)	0.038(1)	-0.004(1)	0.020(1)	-0.030(1)
O(8)	0.046(1)	0.027(1)	0.039(1)	-0.009(1)	0.001(1)	-0.013(1)

Table A.109: Crystallographic data and structure refinement of (**1**)(DTeF) at 203 K.

Compound	(1)(DTeF)
Empirical Formula	$\text{C}_{28}\text{H}_{18}\text{N}_{10}\text{O}_8$
Formula weight / $gmol^{-1}$	622.52
Crystal size / mm^3	0.190×0.180×0.030
Temperature / K	203(2)
Crystal system; space group	Triclinic, $P\bar{1}$
Lattice constants / \AA°	$a = 7.6999(3) \alpha = 73.854(2)$ $b = 13.0418(5) \beta = 85.823(2)$ $c = 14.2827(5) \gamma = 74.176(2)$
Volume / \AA^3	1325.49(9)
Z; F(000); calc. density / gcm^{-3}	2: 640; 1.560
Wavelength	Mo-K α (0.71073 \AA)
Theta range for data collection / $^\circ$	$2.970 \leq \theta \leq 33.256$
Limiting indices	$-11 \leq h \leq 11, -20 \leq k \leq 19, -21 \leq l \leq 22$

Table A.109 – continued from previous page

Compound	(1)(DTeF)
Reflections collected / unique	14024 / 9014
R_{int}	0.0463
Completeness to theta = 25.242	93.70 %
Absorption coefficient / mm^{-1}	0.119
Refinement method	Full-matrix least-squares on F^2
Data / restraints / parameters	9014 / 0 / 487
R indices [I > 4σ(I)] R_1 ; wR_2	0.0548; 0.1239
R indices (all data) R_1 ; wR_2	0.1210; 0.1525
Goodness-of-fit for F^2	0.947
Largest diff. Peak and hole / $e^{-\text{\AA}^{-3}}$	0.297 / -0.287

Table A.110: Fractional coordinates in Å and equivalent isotropic displacement parameter $U_{eq}/\text{\AA}^2$ for the independent atoms in the structure of (1)(DTeF) at 203 K.

Atom	Wyck.	Site	x/a	y/b	z/c	U_{eq}
C(1)	2i	1	-0.1604(2)	1.1239(1)	0.9254(1)	0.029(1)
C(2)	2i	1	-0.0861(3)	1.1971(2)	0.8522(1)	0.033(1)
C(3)	2i	1	-0.0892(3)	1.2988(2)	0.8613(2)	0.039(1)
C(4)	2i	1	-0.1673(3)	1.3314(2)	0.9436(2)	0.040(1)
C(5)	2i	1	-0.2380(3)	1.2601(2)	1.0135(1)	0.036(1)
C(6)	2i	1	-0.3175(3)	1.0845(2)	1.0813(2)	0.038(1)
C(7)	2i	1	-0.1434(2)	0.9006(1)	0.8385(1)	0.028(1)
C(8)	2i	1	-0.1932(3)	0.8203(2)	0.9153(1)	0.035(1)
C(9)	2i	1	-0.2045(3)	0.7227(2)	0.9016(2)	0.040(1)
C(10)	2i	1	-0.1663(3)	0.7020(2)	0.8107(2)	0.039(1)
C(11)	2i	1	-0.1208(3)	0.7816(2)	0.7369(1)	0.035(1)
C(12)	2i	1	-0.0628(4)	0.9618(2)	0.6657(2)	0.047(1)
C(13)	2i	1	0.5666(2)	0.5955(1)	0.6233(1)	0.023(1)
C(14)	2i	1	0.6720(2)	0.5743(1)	0.5402(1)	0.023(1)
C(15)	2i	1	0.7337(2)	0.6576(1)	0.4743(1)	0.026(1)
C(16)	2i	1	0.6870(2)	0.7618(1)	0.4885(1)	0.026(1)
C(17)	2i	1	0.5757(2)	0.7888(1)	0.5640(1)	0.028(1)
C(18)	2i	1	0.5174(2)	0.7055(1)	0.6293(1)	0.026(1)
C(19)	2i	1	0.6093(2)	0.4109(1)	0.6277(1)	0.023(1)
C(20)	2i	1	0.5368(2)	0.4920(1)	0.6815(1)	0.023(1)
C(21)	2i	1	0.4645(2)	0.4540(1)	0.7736(1)	0.026(1)
C(22)	2i	1	0.4387(2)	0.3497(1)	0.8060(1)	0.028(1)
C(23)	2i	1	0.4986(2)	0.2775(1)	0.7482(1)	0.027(1)
C(24)	2i	1	0.5883(2)	0.3039(1)	0.6619(1)	0.025(1)
C(25)	2i	1	0.6961(2)	0.4604(1)	0.5404(1)	0.022(1)
C(26)	2i	1	0.7911(2)	0.4073(1)	0.4717(1)	0.024(1)
C(27)	2i	1	0.8264(2)	0.2913(1)	0.4850(1)	0.028(1)
C(28)	2i	1	0.8750(2)	0.4607(1)	0.3877(1)	0.028(1)
N(1)	2i	1	-0.1744(2)	1.0225(1)	0.9255(1)	0.031(1)
N(2)	2i	1	-0.1227(2)	0.9997(1)	0.8408(1)	0.031(1)
N(3)	2i	1	-0.1098(2)	0.8783(1)	0.7492(1)	0.031(1)
N(4)	2i	1	-0.2351(2)	1.1587(1)	1.0052(1)	0.031(1)
N(5)	2i	1	0.7509(2)	0.8496(1)	0.4191(1)	0.033(1)
N(6)	2i	1	0.3826(2)	0.7420(1)	0.6988(1)	0.032(1)
N(7)	2i	1	0.4326(2)	0.5160(1)	0.8473(1)	0.032(1)

Table A.110 – continued from previous page

Atom	Wyck.	Site	x/a	y/b	z/c	U_{eq}
N(8)	$2i$	1	0.4714(2)	0.1666(1)	0.7842(1)	0.033(1)
N(9)	$2i$	1	0.8562(2)	0.1979(1)	0.4933(1)	0.040(1)
N(10)	$2i$	1	0.9460(2)	0.5014(1)	0.3195(1)	0.039(1)
O(1)	$2i$	1	0.8421(2)	0.8267(1)	0.3502(1)	0.043(1)
O(2)	$2i$	1	0.7099(2)	0.9412(1)	0.4337(1)	0.051(1)
O(3)	$2i$	1	0.3926(2)	0.8201(1)	0.7275(1)	0.049(1)
O(4)	$2i$	1	0.2624(2)	0.6940(1)	0.7227(1)	0.038(1)
O(5)	$2i$	1	0.5360(2)	0.5724(1)	0.8490(1)	0.037(1)
O(6)	$2i$	1	0.3108(2)	0.5047(1)	0.9058(1)	0.051(1)
O(7)	$2i$	1	0.3988(2)	0.1438(1)	0.8636(1)	0.053(1)
O(8)	$2i$	1	0.5216(2)	0.1020(1)	0.7336(1)	0.041(1)
H(2)	$2i$	1	-0.0340(3)	1.1682(18)	0.7985(17)	0.050(6)
H(3)	$2i$	1	-0.0380(4)	1.3450(2)	0.8120(2)	0.072(8)
H(4)	$2i$	1	-0.1700(3)	1.4027(16)	0.9504(14)	0.037(5)
H(5)	$2i$	1	-0.2940(3)	1.2785(16)	1.0746(16)	0.043(6)
H(6A)	$2i$	1	-0.4130(3)	1.0696(18)	1.0470(17)	0.055(7)
H(6B)	$2i$	1	-0.3700(3)	1.1248(18)	1.1266(16)	0.047(6)
H(6C)	$2i$	1	-0.2230(4)	1.0160(2)	1.1105(19)	0.069(8)
H(8)	$2i$	1	-0.2150(3)	0.8367(17)	0.9758(16)	0.044(6)
H(9)	$2i$	1	-0.2330(4)	0.6660(2)	0.9590(2)	0.075(8)
H(10)	$2i$	1	-0.1790(3)	0.6350(17)	0.7988(14)	0.039(5)
H(11)	$2i$	1	-0.0960(3)	0.7751(16)	0.6742(15)	0.035(5)
H(12A)	$2i$	1	-0.1560(4)	1.0280(2)	0.6555(18)	0.067(8)
H(12B)	$2i$	1	-0.0430(4)	0.9310(2)	0.6130(2)	0.075(8)
H(12C)	$2i$	1	0.0480(4)	0.9790(2)	0.6810(2)	0.080(9)
H(15)	$2i$	1	0.8000(3)	0.6478(16)	0.4213(15)	0.041(6)
H(17)	$2i$	1	0.5340(3)	0.8632(17)	0.5691(14)	0.039(5)
H(22)	$2i$	1	0.3860(2)	0.3254(15)	0.8698(14)	0.031(5)
H(24)	$2i$	1	0.6360(2)	0.2481(15)	0.6289(13)	0.029(5)

Table A.111: Anisotropic displacement parameters $U_{ij}/\text{\AA}^2$ for the independent atoms in the structure of **(1)(DTeF)** at 203 K.

Atom	U_{11}	U_{22}	U_{33}	U_{23}	U_{13}	U_{12}
C(1)	0.029(1)	0.029(1)	0.027(1)	-0.009(1)	0.000(1)	-0.004(1)
C(2)	0.036(1)	0.034(1)	0.029(1)	-0.007(1)	0.002(1)	-0.008(1)
C(3)	0.042(1)	0.033(1)	0.039(1)	-0.003(1)	-0.004(1)	-0.011(1)
C(4)	0.045(1)	0.028(1)	0.045(1)	-0.011(1)	-0.007(1)	-0.006(1)
C(5)	0.040(1)	0.033(1)	0.036(1)	-0.015(1)	-0.002(1)	-0.006(1)
C(6)	0.045(1)	0.042(1)	0.031(1)	-0.015(1)	0.011(1)	-0.015(1)
C(7)	0.024(1)	0.031(1)	0.029(1)	-0.012(1)	0.002(1)	-0.005(1)
C(8)	0.038(1)	0.038(1)	0.030(1)	-0.011(1)	0.005(1)	-0.012(1)
C(9)	0.043(1)	0.038(1)	0.041(1)	-0.009(1)	0.004(1)	-0.017(1)
C(10)	0.039(1)	0.039(1)	0.048(1)	-0.020(1)	0.006(1)	-0.018(1)
C(11)	0.033(1)	0.041(1)	0.037(1)	-0.021(1)	0.004(1)	-0.011(1)
C(12)	0.072(2)	0.041(1)	0.031(1)	-0.014(1)	0.020(1)	-0.020(1)
C(13)	0.025(1)	0.026(1)	0.020(1)	-0.006(1)	-0.001(1)	-0.007(1)
C(14)	0.022(1)	0.025(1)	0.021(1)	-0.006(1)	-0.001(1)	-0.007(1)
C(15)	0.026(1)	0.030(1)	0.022(1)	-0.006(1)	0.001(1)	-0.009(1)
C(16)	0.029(1)	0.026(1)	0.026(1)	-0.003(1)	-0.001(1)	-0.012(1)
C(17)	0.033(1)	0.025(1)	0.026(1)	-0.006(1)	-0.002(1)	-0.009(1)

Table A.111 – continued from previous page

Atom	Wyck.	Site	x/a	y/b	z/c	U_{eq}
C(18)	0.028(1)	0.029(1)	0.021(1)	-0.009(1)	0.001(1)	-0.007(1)
C(19)	0.023(1)	0.026(1)	0.021(1)	-0.006(1)	0.000(1)	-0.006(1)
C(20)	0.023(1)	0.026(1)	0.021(1)	-0.005(1)	0.000(1)	-0.007(1)
C(21)	0.027(1)	0.028(1)	0.021(1)	-0.006(1)	0.002(1)	-0.006(1)
C(22)	0.030(1)	0.031(1)	0.023(1)	-0.003(1)	0.003(1)	-0.011(1)
C(23)	0.030(1)	0.026(1)	0.026(1)	-0.002(1)	-0.001(1)	-0.011(1)
C(24)	0.026(1)	0.026(1)	0.023(1)	-0.005(1)	0.000(1)	-0.007(1)
C(25)	0.023(1)	0.023(1)	0.020(1)	-0.005(1)	0.000(1)	-0.006(1)
C(26)	0.024(1)	0.026(1)	0.021(1)	-0.007(1)	0.002(1)	-0.005(1)
C(27)	0.029(1)	0.031(1)	0.022(1)	-0.007(1)	0.002(1)	-0.004(1)
C(28)	0.025(1)	0.029(1)	0.028(1)	-0.010(1)	0.002(1)	-0.004(1)
N(1)	0.036(1)	0.029(1)	0.028(1)	-0.011(1)	0.004(1)	-0.008(1)
N(2)	0.035(1)	0.032(1)	0.029(1)	-0.012(1)	0.005(1)	-0.008(1)
N(3)	0.031(1)	0.033(1)	0.030(1)	-0.012(1)	0.005(1)	-0.008(1)
N(4)	0.035(1)	0.030(1)	0.029(1)	-0.012(1)	0.004(1)	-0.009(1)
N(5)	0.038(1)	0.030(1)	0.033(1)	-0.005(1)	0.004(1)	-0.015(1)
N(6)	0.040(1)	0.028(1)	0.024(1)	-0.007(1)	0.001(1)	-0.003(1)
N(7)	0.043(1)	0.033(1)	0.020(1)	-0.005(1)	0.004(1)	-0.012(1)
N(8)	0.037(1)	0.029(1)	0.031(1)	-0.002(1)	0.001(1)	-0.013(1)
N(9)	0.052(1)	0.031(1)	0.032(1)	-0.009(1)	0.003(1)	-0.003(1)
N(10)	0.042(1)	0.044(1)	0.033(1)	-0.010(1)	0.010(1)	-0.014(1)
O(1)	0.051(1)	0.045(1)	0.035(1)	-0.008(1)	0.012(1)	-0.024(1)
O(2)	0.065(1)	0.029(1)	0.062(1)	-0.012(1)	0.019(1)	-0.021(1)
O(3)	0.077(1)	0.036(1)	0.039(1)	-0.022(1)	0.011(1)	-0.011(1)
O(4)	0.033(1)	0.044(1)	0.032(1)	-0.008(1)	0.007(1)	-0.006(1)
O(5)	0.047(1)	0.036(1)	0.030(1)	-0.011(1)	-0.003(1)	-0.015(1)
O(6)	0.069(1)	0.054(1)	0.036(1)	-0.021(1)	0.028(1)	-0.027(1)
O(7)	0.077(1)	0.043(1)	0.041(1)	-0.004(1)	0.021(1)	-0.032(1)
O(8)	0.051(1)	0.030(1)	0.043(1)	-0.010(1)	0.001(1)	-0.014(1)

Table A.112: Crystallographic data and structure refinement of (**1**)(DTeF) at 223 K.

Compound	(1)(DTeF)
Empirical Formula	$C_{28}H_{18}N_{10}O_8$
Formula weight / $gmol^{-1}$	622.52
Crystal size / mm^3	0.190×0.180×0.030
Temperature / K	223(2)
Crystal system; space group	Triclinic, $P\bar{1}$
Lattice constants / \AA°	$a = 7.7146(3) \alpha = 73.866(2)$ $b = 13.0419(5) \beta = 85.733(2)$ $c = 14.2947(5) \gamma = 74.210(2)$
Volume / \AA^3	1329.45(9)
Z; F(000); calc. density / gcm^{-3}	2: 640; 1.555
Wavelength	Mo-K α (0.71073 \AA)
Theta range for data collection / $^\circ$	$2.967 \leq \theta \leq 33.259$
Limiting indices	$-11 \leq h \leq 11, -20 \leq k \leq 19, -21 \leq l \leq 22$
Reflections collected / unique	13951 / 8848
R_{int}	0.0489
Completeness to theta = 25.242	92.60 %

Table A.112 – continued from previous page

Compound	(1)(DTeF)
Absorption coefficient / mm^{-1}	0.119
Refinement method	Full-matrix least-squares on F^2
Data / restraints / parameters	8848 / 0 / 487
R indices [I > 4σ(I)] R_1 ; wR_2	0.0553; 0.1284
R indices (all data) R_1 ; wR_2	0.1248; 0.1590
Goodness-of-fit for F^2	0.930
Largest diff. Peak and hole / $e^{-\text{\AA}^{-3}}$	0.272 / -0.379

Table A.113: Fractional coordinates in Å and equivalent isotropic displacement parameter $U_{eq}/\text{\AA}^2$ for the independent atoms in the structure of (1)(DTeF) at 223 K.

Atom	Wyck.	Site	x/a	y/b	z/c	U_{eq}
C(1)	2 <i>i</i>	1	-0.1611(2)	1.1243(2)	0.9247(1)	0.031(1)
C(2)	2 <i>i</i>	1	-0.0867(3)	1.1971(2)	0.8519(1)	0.037(1)
C(3)	2 <i>i</i>	1	-0.0898(3)	1.2991(2)	0.8609(2)	0.043(1)
C(4)	2 <i>i</i>	1	-0.1667(3)	1.3315(2)	0.9431(2)	0.043(1)
C(5)	2 <i>i</i>	1	-0.2377(3)	1.2603(2)	1.0133(2)	0.039(1)
C(6)	2 <i>i</i>	1	-0.3168(3)	1.0845(2)	1.0812(2)	0.042(1)
C(7)	2 <i>i</i>	1	-0.1443(2)	0.9008(2)	0.8383(1)	0.031(1)
C(8)	2 <i>i</i>	1	-0.1935(3)	0.8203(2)	0.9152(1)	0.037(1)
C(9)	2 <i>i</i>	1	-0.2042(3)	0.7229(2)	0.9016(2)	0.044(1)
C(10)	2 <i>i</i>	1	-0.1661(3)	0.7022(2)	0.8104(2)	0.043(1)
C(11)	2 <i>i</i>	1	-0.1203(3)	0.7813(2)	0.7370(2)	0.038(1)
C(12)	2 <i>i</i>	1	-0.0632(4)	0.9615(2)	0.6656(2)	0.052(1)
C(13)	2 <i>i</i>	1	0.5662(2)	0.5956(1)	0.6233(1)	0.025(1)
C(14)	2 <i>i</i>	1	0.6714(2)	0.5743(1)	0.5400(1)	0.024(1)
C(15)	2 <i>i</i>	1	0.7335(2)	0.6574(2)	0.4744(1)	0.028(1)
C(16)	2 <i>i</i>	1	0.6874(2)	0.7614(1)	0.4887(1)	0.029(1)
C(17)	2 <i>i</i>	1	0.5763(3)	0.7886(2)	0.5641(1)	0.031(1)
C(18)	2 <i>i</i>	1	0.5174(2)	0.7055(1)	0.6294(1)	0.027(1)
C(19)	2 <i>i</i>	1	0.6084(2)	0.4111(1)	0.6279(1)	0.025(1)
C(20)	2 <i>i</i>	1	0.5364(2)	0.4923(1)	0.6811(1)	0.025(1)
C(21)	2 <i>i</i>	1	0.4642(2)	0.4542(2)	0.7735(1)	0.028(1)
C(22)	2 <i>i</i>	1	0.4378(2)	0.3500(2)	0.8060(1)	0.031(1)
C(23)	2 <i>i</i>	1	0.4977(2)	0.2778(1)	0.7481(1)	0.029(1)
C(24)	2 <i>i</i>	1	0.5879(2)	0.3040(2)	0.6617(1)	0.028(1)
C(25)	2 <i>i</i>	1	0.6958(2)	0.4605(1)	0.5403(1)	0.024(1)
C(26)	2 <i>i</i>	1	0.7908(2)	0.4074(1)	0.4719(1)	0.027(1)
C(27)	2 <i>i</i>	1	0.8255(2)	0.2914(2)	0.4848(1)	0.031(1)
C(28)	2 <i>i</i>	1	0.8746(2)	0.4610(2)	0.3878(1)	0.030(1)
N(1)	2 <i>i</i>	1	-0.1752(2)	1.0228(1)	0.9248(1)	0.034(1)
N(2)	2 <i>i</i>	1	-0.1234(2)	1.0000(1)	0.8404(1)	0.035(1)
N(3)	2 <i>i</i>	1	-0.1100(2)	0.8779(1)	0.7491(1)	0.034(1)
N(4)	2 <i>i</i>	1	-0.2351(2)	1.1588(1)	1.0050(1)	0.034(1)
N(5)	2 <i>i</i>	1	0.7514(2)	0.8494(1)	0.4191(1)	0.037(1)
N(6)	2 <i>i</i>	1	0.3829(2)	0.7419(1)	0.6988(1)	0.035(1)
N(7)	2 <i>i</i>	1	0.4320(2)	0.5163(1)	0.8470(1)	0.035(1)
N(8)	2 <i>i</i>	1	0.4708(2)	0.1668(1)	0.7839(1)	0.036(1)
N(9)	2 <i>i</i>	1	0.8554(3)	0.1981(1)	0.4932(1)	0.043(1)
N(10)	2 <i>i</i>	1	0.9460(2)	0.5015(2)	0.3198(1)	0.043(1)

Table A.113 – continued from previous page

Atom	Wyck.	Site	x/a	y/b	z/c	U_{eq}
O(1)	$2i$	1	0.8427(2)	0.8265(1)	0.3505(1)	0.046(1)
O(2)	$2i$	1	0.7110(2)	0.9408(1)	0.4340(1)	0.056(1)
O(3)	$2i$	1	0.3932(2)	0.8200(1)	0.7276(1)	0.054(1)
O(4)	$2i$	1	0.2630(2)	0.6941(1)	0.7228(1)	0.041(1)
O(5)	$2i$	1	0.5355(2)	0.5724(1)	0.8488(1)	0.041(1)
O(6)	$2i$	1	0.3103(2)	0.5050(1)	0.9057(1)	0.056(1)
O(7)	$2i$	1	0.3984(2)	0.1440(1)	0.8633(1)	0.059(1)
O(8)	$2i$	1	0.5211(2)	0.1021(1)	0.7336(1)	0.045(1)
H(2)	$2i$	1	-0.0350(3)	1.1689(19)	0.7956(17)	0.054(6)
H(3)	$2i$	1	-0.0380(4)	1.3440(2)	0.8140(2)	0.072(8)
H(4)	$2i$	1	-0.1680(3)	1.4030(18)	0.9497(16)	0.046(6)
H(5)	$2i$	1	-0.2920(3)	1.2758(17)	1.0766(16)	0.041(6)
H(6A)	$2i$	1	-0.4160(3)	1.0669(19)	1.0498(18)	0.060(7)
H(6B)	$2i$	1	-0.3700(3)	1.1251(18)	1.1284(17)	0.049(6)
H(6C)	$2i$	1	-0.2250(4)	1.0180(3)	1.1110(2)	0.089(1)
H(8)	$2i$	1	-0.2190(3)	0.8407(19)	0.9725(18)	0.054(7)
H(9)	$2i$	1	-0.2350(4)	0.6670(2)	0.9561(19)	0.069(8)
H(10)	$2i$	1	-0.1790(3)	0.6381(18)	0.7957(15)	0.045(6)
H(11)	$2i$	1	-0.0970(3)	0.7762(17)	0.6726(16)	0.043(6)
H(12A)	$2i$	1	-0.1510(4)	1.0310(3)	0.6570(2)	0.085(1)
H(12B)	$2i$	1	-0.0400(4)	0.9310(2)	0.6160(2)	0.078(8)
H(12C)	$2i$	1	0.0470(4)	0.9810(2)	0.6800(2)	0.088(1)
H(15)	$2i$	1	0.8010(3)	0.6485(16)	0.4199(15)	0.040(6)
H(17)	$2i$	1	0.5390(3)	0.8590(16)	0.5708(13)	0.029(5)
H(22)	$2i$	1	0.3810(3)	0.3271(16)	0.8710(15)	0.037(5)
H(24)	$2i$	1	0.6380(2)	0.2470(15)	0.6260(14)	0.030(5)

Table A.114: Anisotropic displacement parameters $U_{ij}/\text{\AA}^2$ for the independent atoms in the structure of (1)(DTeF) at 223 K.

Atom	U_{11}	U_{22}	U_{33}	U_{23}	U_{13}	U_{12}
C(1)	0.031(1)	0.033(1)	0.029(1)	-0.011(1)	0.001(1)	-0.005(1)
C(2)	0.040(1)	0.036(1)	0.032(1)	-0.007(1)	0.003(1)	-0.009(1)
C(3)	0.046(1)	0.035(1)	0.041(1)	-0.001(1)	-0.003(1)	-0.011(1)
C(4)	0.052(1)	0.031(1)	0.046(1)	-0.012(1)	-0.006(1)	-0.009(1)
C(5)	0.044(1)	0.034(1)	0.040(1)	-0.016(1)	-0.002(1)	-0.004(1)
C(6)	0.050(1)	0.047(1)	0.034(1)	-0.016(1)	0.013(1)	-0.018(1)
C(7)	0.027(1)	0.035(1)	0.031(1)	-0.013(1)	0.003(1)	-0.006(1)
C(8)	0.041(1)	0.041(1)	0.032(1)	-0.012(1)	0.005(1)	-0.013(1)
C(9)	0.048(1)	0.042(1)	0.044(1)	-0.010(1)	0.006(1)	-0.019(1)
C(10)	0.042(1)	0.045(1)	0.054(1)	-0.024(1)	0.008(1)	-0.020(1)
C(11)	0.035(1)	0.045(1)	0.042(1)	-0.024(1)	0.005(1)	-0.013(1)
C(12)	0.081(2)	0.045(1)	0.035(1)	-0.016(1)	0.023(1)	-0.023(1)
C(13)	0.026(1)	0.028(1)	0.021(1)	-0.006(1)	0.000(1)	-0.007(1)
C(14)	0.024(1)	0.027(1)	0.022(1)	-0.006(1)	0.000(1)	-0.007(1)
C(15)	0.028(1)	0.033(1)	0.023(1)	-0.007(1)	0.002(1)	-0.012(1)
C(16)	0.032(1)	0.027(1)	0.028(1)	-0.004(1)	0.000(1)	-0.013(1)
C(17)	0.037(1)	0.027(1)	0.031(1)	-0.008(1)	-0.001(1)	-0.010(1)
C(18)	0.029(1)	0.029(1)	0.024(1)	-0.011(1)	0.000(1)	-0.006(1)
C(19)	0.027(1)	0.027(1)	0.021(1)	-0.005(1)	0.000(1)	-0.007(1)
C(20)	0.025(1)	0.028(1)	0.021(1)	-0.006(1)	0.000(1)	-0.007(1)

Table A.114 – continued from previous page

Atom	Wyck.	Site	x/a	y/b	z/c	U_{eq}
C(21)	0.031(1)	0.030(1)	0.022(1)	-0.007(1)	0.003(1)	-0.008(1)
C(22)	0.033(1)	0.035(1)	0.024(1)	-0.004(1)	0.003(1)	-0.011(1)
C(23)	0.031(1)	0.027(1)	0.028(1)	-0.002(1)	-0.001(1)	-0.010(1)
C(24)	0.029(1)	0.028(1)	0.026(1)	-0.006(1)	0.000(1)	-0.009(1)
C(25)	0.026(1)	0.026(1)	0.021(1)	-0.005(1)	0.000(1)	-0.007(1)
C(26)	0.026(1)	0.029(1)	0.025(1)	-0.008(1)	0.004(1)	-0.005(1)
C(27)	0.033(1)	0.033(1)	0.024(1)	-0.008(1)	0.003(1)	-0.005(1)
C(28)	0.030(1)	0.031(1)	0.030(1)	-0.011(1)	0.003(1)	-0.006(1)
N(1)	0.040(1)	0.034(1)	0.030(1)	-0.013(1)	0.006(1)	-0.009(1)
N(2)	0.040(1)	0.036(1)	0.030(1)	-0.013(1)	0.006(1)	-0.009(1)
N(3)	0.034(1)	0.035(1)	0.033(1)	-0.014(1)	0.006(1)	-0.009(1)
N(4)	0.037(1)	0.035(1)	0.030(1)	-0.013(1)	0.003(1)	-0.009(1)
N(5)	0.041(1)	0.035(1)	0.036(1)	-0.005(1)	0.002(1)	-0.017(1)
N(6)	0.043(1)	0.031(1)	0.026(1)	-0.008(1)	0.003(1)	-0.003(1)
N(7)	0.046(1)	0.034(1)	0.024(1)	-0.008(1)	0.006(1)	-0.012(1)
N(8)	0.040(1)	0.033(1)	0.034(1)	-0.003(1)	0.000(1)	-0.014(1)
N(9)	0.057(1)	0.033(1)	0.033(1)	-0.009(1)	0.003(1)	-0.003(1)
N(10)	0.046(1)	0.048(1)	0.037(1)	-0.012(1)	0.014(1)	-0.017(1)
O(1)	0.056(1)	0.049(1)	0.038(1)	-0.010(1)	0.015(1)	-0.027(1)
O(2)	0.072(1)	0.032(1)	0.068(1)	-0.015(1)	0.021(1)	-0.023(1)
O(3)	0.084(1)	0.038(1)	0.044(1)	-0.023(1)	0.012(1)	-0.012(1)
O(4)	0.035(1)	0.049(1)	0.033(1)	-0.008(1)	0.006(1)	-0.005(1)
O(5)	0.054(1)	0.040(1)	0.033(1)	-0.012(1)	-0.003(1)	-0.017(1)
O(6)	0.074(1)	0.060(1)	0.040(1)	-0.023(1)	0.031(1)	-0.029(1)
O(7)	0.087(1)	0.046(1)	0.046(1)	-0.005(1)	0.025(1)	-0.036(1)
O(8)	0.056(1)	0.033(1)	0.049(1)	-0.011(1)	0.001(1)	-0.015(1)

Table A.115: Crystallographic data and structure refinement of (**1**)(DTeF) at 243 K.

Compound	(1)(DTeF)
Empirical Formula	$\text{C}_{28}\text{H}_{18}\text{N}_{10}\text{O}_8$
Formula weight / $gmol^{-1}$	622.52
Crystal size / mm^3	0.190×0.180×0.030
Temperature / K	243(2)
Crystal system; space group	Triclinic, $P\bar{1}$
Lattice constants / \AA°	$a = 7.7286(3)$ $\alpha = 73.888(3)$ $b = 13.0408(5)$ $\beta = 85.646(3)$ $c = 14.3038(6)$ $\gamma = 74.248(2)$
Volume / \AA^3	1333.00(9)
Z; F(000); calc. density / gcm^{-3}	2: 640; 1.551
Wavelength	Mo-K α (0.71073 \AA)
Theta range for data collection / $^\circ$	$2.963 \leq \theta \leq 27.527$
Limiting indices	$-10 \leq h \leq 10, -16 \leq k \leq 16, -18 \leq l \leq 18$
Reflections collected / unique	8426 / 5434
R_{int}	0.0412
Completeness to theta = 25.242	90.30 %
Absorption coefficient / mm^{-1}	0.118
Refinement method	Full-matrix least-squares on F^2
Data / restraints / parameters	5434 / 0 / 487

Table A.115 – continued from previous page

Compound	(1)(DTeF)
R indices [$I > 4\sigma(I)$] R_1 ; wR_2	0.0478; 0.1176
R indices (all data) R_1 ; wR_2	0.0875; 0.1388
Goodness-of-fit for F^2	0.975
Largest diff. Peak and hole / $e^{-\text{\AA}^{-3}}$	0.208 / -0.238

Table A.116: Fractional coordinates in Å and equivalent isotropic displacement parameter $U_{eq}/\text{\AA}^2$ for the independent atoms in the structure of (1)(DTeF) at 243 K.

Atom	Wyck.	Site	x/a	y/b	z/c	U_{eq}
C(1)	2 <i>i</i>	1	-0.1613(3)	1.1243(2)	0.9247(2)	0.033(1)
C(2)	2 <i>i</i>	1	-0.0876(3)	1.1976(2)	0.8518(2)	0.042(1)
C(3)	2 <i>i</i>	1	-0.0911(4)	1.2987(2)	0.8610(2)	0.046(1)
C(4)	2 <i>i</i>	1	-0.1671(4)	1.3311(2)	0.9429(2)	0.048(1)
C(5)	2 <i>i</i>	1	-0.2367(3)	1.2604(2)	1.0130(2)	0.042(1)
C(6)	2 <i>i</i>	1	-0.3161(4)	1.0843(2)	1.0809(2)	0.047(1)
C(7)	2 <i>i</i>	1	-0.1449(3)	0.9009(2)	0.8382(2)	0.033(1)
C(8)	2 <i>i</i>	1	-0.1939(3)	0.8208(2)	0.9145(2)	0.041(1)
C(9)	2 <i>i</i>	1	-0.2040(4)	0.7230(2)	0.9013(2)	0.049(1)
C(10)	2 <i>i</i>	1	-0.1649(3)	0.7022(2)	0.8107(2)	0.048(1)
C(11)	2 <i>i</i>	1	-0.1202(3)	0.7806(2)	0.7376(2)	0.041(1)
C(12)	2 <i>i</i>	1	-0.0631(5)	0.9614(3)	0.6655(2)	0.058(1)
C(13)	2 <i>i</i>	1	0.5661(3)	0.5957(2)	0.6234(1)	0.026(1)
C(14)	2 <i>i</i>	1	0.6715(3)	0.5743(2)	0.5404(1)	0.026(1)
C(15)	2 <i>i</i>	1	0.7335(3)	0.6571(2)	0.4746(2)	0.029(1)
C(16)	2 <i>i</i>	1	0.6880(3)	0.7615(2)	0.4890(2)	0.031(1)
C(17)	2 <i>i</i>	1	0.5768(3)	0.7886(2)	0.5641(2)	0.034(1)
C(18)	2 <i>i</i>	1	0.5171(3)	0.7055(2)	0.6296(1)	0.030(1)
C(19)	2 <i>i</i>	1	0.6083(3)	0.4114(2)	0.6277(1)	0.027(1)
C(20)	2 <i>i</i>	1	0.5364(3)	0.4921(2)	0.6812(1)	0.027(1)
C(21)	2 <i>i</i>	1	0.4643(3)	0.4541(2)	0.7733(1)	0.031(1)
C(22)	2 <i>i</i>	1	0.4381(3)	0.3501(2)	0.8056(2)	0.034(1)
C(23)	2 <i>i</i>	1	0.4972(3)	0.2782(2)	0.7479(2)	0.032(1)
C(24)	2 <i>i</i>	1	0.5876(3)	0.3041(2)	0.6616(2)	0.029(1)
C(25)	2 <i>i</i>	1	0.6952(3)	0.4607(2)	0.5404(1)	0.026(1)
C(26)	2 <i>i</i>	1	0.7909(3)	0.4074(2)	0.4720(1)	0.029(1)
C(27)	2 <i>i</i>	1	0.8248(3)	0.2914(2)	0.4849(1)	0.033(1)
C(28)	2 <i>i</i>	1	0.8752(3)	0.4609(2)	0.3879(2)	0.033(1)
N(1)	2 <i>i</i>	1	-0.1758(2)	1.0230(1)	0.9248(1)	0.036(1)
N(2)	2 <i>i</i>	1	-0.1241(3)	1.0000(2)	0.8402(1)	0.037(1)
N(3)	2 <i>i</i>	1	-0.1102(2)	0.8780(1)	0.7493(1)	0.036(1)
N(4)	2 <i>i</i>	1	-0.2346(2)	1.1589(2)	1.0046(1)	0.036(1)
N(5)	2 <i>i</i>	1	0.7521(3)	0.8490(2)	0.4195(1)	0.041(1)
N(6)	2 <i>i</i>	1	0.3832(3)	0.7420(2)	0.6989(1)	0.038(1)
N(7)	2 <i>i</i>	1	0.4323(3)	0.5163(2)	0.8467(1)	0.038(1)
N(8)	2 <i>i</i>	1	0.4700(3)	0.1673(2)	0.7835(1)	0.040(1)
N(9)	2 <i>i</i>	1	0.8540(3)	0.1984(2)	0.4933(1)	0.047(1)
N(10)	2 <i>i</i>	1	0.9458(3)	0.5013(2)	0.3200(2)	0.047(1)
O(1)	2 <i>i</i>	1	0.8434(2)	0.8264(1)	0.3508(1)	0.051(1)
O(2)	2 <i>i</i>	1	0.7110(3)	0.9409(1)	0.4342(2)	0.062(1)
O(3)	2 <i>i</i>	1	0.3939(3)	0.8198(1)	0.7276(1)	0.059(1)

Table A.116 – continued from previous page

Atom	Wyck.	Site	x/a	y/b	z/c	U_{eq}
O(4)	$2i$	1	0.2636(2)	0.6943(1)	0.7230(1)	0.046(1)
O(5)	$2i$	1	0.5352(2)	0.5726(1)	0.8486(1)	0.044(1)
O(6)	$2i$	1	0.3106(3)	0.5051(2)	0.9052(1)	0.060(1)
O(7)	$2i$	1	0.3982(3)	0.1442(2)	0.8633(1)	0.065(1)
O(8)	$2i$	1	0.5201(2)	0.1026(1)	0.7332(1)	0.048(1)
H(2)	$2i$	1	-0.0420(3)	1.1700(2)	0.8020(2)	0.055(8)
H(3)	$2i$	1	-0.0410(4)	1.3430(2)	0.8160(2)	0.063(9)
H(4)	$2i$	1	-0.1700(3)	1.4020(2)	0.9498(17)	0.043(7)
H(5)	$2i$	1	-0.2930(3)	1.2762(19)	1.0784(19)	0.051(7)
H(6A)	$2i$	1	-0.4220(4)	1.0720(2)	1.0480(2)	0.060(8)
H(6B)	$2i$	1	-0.3620(4)	1.1220(2)	1.1290(2)	0.057(8)
H(6C)	$2i$	1	-0.2220(5)	1.0210(3)	1.1100(3)	0.102(13)
H(8)	$2i$	1	-0.2100(3)	0.8340(2)	0.9735(19)	0.046(7)
H(9)	$2i$	1	-0.2380(4)	0.6720(2)	0.9530(2)	0.068(9)
H(10)	$2i$	1	-0.1730(3)	0.6380(2)	0.8011(18)	0.054(7)
H(11)	$2i$	1	-0.0930(3)	0.7733(19)	0.6750(18)	0.041(6)
H(12A)	$2i$	1	-0.1570(5)	1.0260(3)	0.6550(2)	0.089(11)
H(12B)	$2i$	1	-0.0360(4)	0.9250(3)	0.6170(3)	0.086(1)
H(12C)	$2i$	1	0.0440(6)	0.9810(3)	0.6810(3)	0.114(15)
H(15)	$2i$	1	0.8080(3)	0.6460(18)	0.4207(18)	0.043(6)
H(17)	$2i$	1	0.5400(3)	0.8573(19)	0.5705(16)	0.039(6)
H(22)	$2i$	1	0.3830(3)	0.3271(17)	0.8665(17)	0.033(6)
H(24)	$2i$	1	0.6350(3)	0.2467(18)	0.6280(16)	0.037(6)

Table A.117: Anisotropic displacement parameters $U_{ij}/\text{\AA}^2$ for the independent atoms in the structure of **(1)(DTeF)** at 243 K.

Atom	U_{11}	U_{22}	U_{33}	U_{23}	U_{13}	U_{12}
C(1)	0.034(1)	0.034(1)	0.031(1)	-0.011(1)	0.000(1)	-0.006(1)
C(2)	0.046(1)	0.042(1)	0.035(1)	-0.009(1)	0.004(1)	-0.010(1)
C(3)	0.050(2)	0.040(1)	0.045(2)	-0.001(1)	-0.004(1)	-0.015(1)
C(4)	0.057(2)	0.034(1)	0.052(2)	-0.013(1)	-0.008(1)	-0.007(1)
C(5)	0.046(1)	0.038(1)	0.042(1)	-0.016(1)	-0.001(1)	-0.007(1)
C(6)	0.056(2)	0.054(2)	0.038(1)	-0.019(1)	0.016(1)	-0.022(1)
C(7)	0.027(1)	0.038(1)	0.034(1)	-0.015(1)	0.003(1)	-0.007(1)
C(8)	0.045(1)	0.046(1)	0.035(1)	-0.015(1)	0.005(1)	-0.014(1)
C(9)	0.051(2)	0.048(2)	0.050(2)	-0.010(1)	0.007(1)	-0.023(1)
C(10)	0.046(2)	0.047(1)	0.062(2)	-0.027(1)	0.010(1)	-0.022(1)
C(11)	0.038(1)	0.049(1)	0.045(1)	-0.026(1)	0.006(1)	-0.014(1)
C(12)	0.089(2)	0.049(2)	0.038(1)	-0.017(1)	0.025(2)	-0.023(2)
C(13)	0.026(1)	0.029(1)	0.023(1)	-0.006(1)	-0.003(1)	-0.008(1)
C(14)	0.026(1)	0.028(1)	0.025(1)	-0.007(1)	-0.003(1)	-0.007(1)
C(15)	0.026(1)	0.036(1)	0.025(1)	-0.007(1)	0.001(1)	-0.011(1)
C(16)	0.031(1)	0.029(1)	0.032(1)	-0.004(1)	-0.001(1)	-0.012(1)
C(17)	0.040(1)	0.029(1)	0.033(1)	-0.010(1)	-0.003(1)	-0.009(1)
C(18)	0.032(1)	0.032(1)	0.028(1)	-0.011(1)	-0.001(1)	-0.007(1)
C(19)	0.026(1)	0.030(1)	0.023(1)	-0.006(1)	-0.001(1)	-0.007(1)
C(20)	0.027(1)	0.031(1)	0.023(1)	-0.007(1)	0.000(1)	-0.009(1)
C(21)	0.032(1)	0.034(1)	0.026(1)	-0.008(1)	0.001(1)	-0.009(1)
C(22)	0.035(1)	0.038(1)	0.026(1)	-0.004(1)	0.002(1)	-0.012(1)
C(23)	0.034(1)	0.030(1)	0.031(1)	-0.003(1)	-0.003(1)	-0.013(1)

Table A.117 – continued from previous page

Atom	Wyck.	Site	x/a	y/b	z/c	U_{eq}
C(24)	0.029(1)	0.030(1)	0.027(1)	-0.004(1)	-0.002(1)	-0.008(1)
C(25)	0.025(1)	0.029(1)	0.024(1)	-0.006(1)	-0.002(1)	-0.005(1)
C(26)	0.029(1)	0.032(1)	0.026(1)	-0.008(1)	0.002(1)	-0.007(1)
C(27)	0.033(1)	0.036(1)	0.025(1)	-0.008(1)	0.001(1)	-0.004(1)
C(28)	0.031(1)	0.035(1)	0.033(1)	-0.013(1)	0.002(1)	-0.006(1)
N(1)	0.039(1)	0.036(1)	0.034(1)	-0.014(1)	0.005(1)	-0.009(1)
N(2)	0.042(1)	0.038(1)	0.034(1)	-0.015(1)	0.006(1)	-0.010(1)
N(3)	0.036(1)	0.039(1)	0.035(1)	-0.015(1)	0.006(1)	-0.010(1)
N(4)	0.040(1)	0.037(1)	0.032(1)	-0.012(1)	0.002(1)	-0.010(1)
N(5)	0.045(1)	0.037(1)	0.042(1)	-0.005(1)	0.002(1)	-0.019(1)
N(6)	0.045(1)	0.035(1)	0.028(1)	-0.008(1)	0.002(1)	-0.004(1)
N(7)	0.051(1)	0.040(1)	0.024(1)	-0.008(1)	0.006(1)	-0.013(1)
N(8)	0.044(1)	0.036(1)	0.038(1)	-0.003(1)	0.001(1)	-0.016(1)
N(9)	0.061(1)	0.034(1)	0.038(1)	-0.010(1)	0.004(1)	-0.002(1)
N(10)	0.050(1)	0.053(1)	0.039(1)	-0.012(1)	0.014(1)	-0.018(1)
O(1)	0.061(1)	0.053(1)	0.042(1)	-0.011(1)	0.017(1)	-0.029(1)
O(2)	0.079(1)	0.035(1)	0.074(1)	-0.014(1)	0.022(1)	-0.026(1)
O(3)	0.091(2)	0.044(1)	0.046(1)	-0.025(1)	0.013(1)	-0.014(1)
O(4)	0.039(1)	0.054(1)	0.038(1)	-0.010(1)	0.008(1)	-0.006(1)
O(5)	0.058(1)	0.044(1)	0.035(1)	-0.012(1)	-0.005(1)	-0.017(1)
O(6)	0.083(1)	0.062(1)	0.044(1)	-0.024(1)	0.034(1)	-0.031(1)
O(7)	0.096(2)	0.051(1)	0.051(1)	-0.006(1)	0.028(1)	-0.040(1)
O(8)	0.061(1)	0.034(1)	0.052(1)	-0.011(1)	0.002(1)	-0.016(1)

Table A.118: Crystallographic data and structure refinement of **(1)**(DTeF) at 263 K.

Compound	(1) (DTeF)
Empirical Formula	C ₂₈ H ₁₈ N ₁₀ O ₈
Formula weight / g mol ⁻¹	622.52
Crystal size / mm ³	0.190×0.180×0.030
Temperature / K	263(2)
Crystal system; space group	Triclinic, P [̄] 1
Lattice constants / Å	$a = 7.7439(4)$ $\alpha = 73.909(3)$ $b = 13.0432(5)$ $\beta = 85.547(3)$ $c = 14.3169(6)$ $\gamma = 74.282(2)$
Volume / Å ³	1337.47(11)
Z; F(000); calc. density / g cm ⁻³	2; 640; 1.546
Wavelength	Mo-K _α (0.71073 Å)
Theta range for data collection / °	2.957 $\leq \theta \leq$ 27.409
Limiting indices	-10 \leq h \leq 10, -16 \leq k \leq 16, -18 \leq l \leq 18
Reflections collected / unique	8568 / 5440
R _{int}	0.0403
Completeness to theta = 25.242	91.40 %
Absorption coefficient / mm ⁻¹	0.118
Refinement method	Full-matrix least-squares on F^2
Data / restraints / parameters	5440 / 0 / 487
R indices [I > 4σ(I)] R ₁ ; wR ₂	0.0488; 0.1151
R indices (all data) R ₁ ; wR ₂	0.0897; 0.1354
Goodness-of-fit for F^2	0.965

Table A.118 – continued from previous page

Compound	(1)(DTeF)
Largest diff. Peak and hole / $e^{-\text{Å}^{-3}}$	0.204 / -0.257

Table A.119: Fractional coordinates in Å and equivalent isotropic displacement parameter $U_{eq}/\text{Å}^2$ for the independent atoms in the structure of (1)(DTeF) at 263 K.

Atom	Wyck.	Site	x/a	y/b	z/c	U_{eq}
C(1)	2 <i>i</i>	1	-0.1616(3)	1.1242(2)	0.9242(2)	0.037(1)
C(2)	2 <i>i</i>	1	-0.0887(3)	1.1975(2)	0.8514(2)	0.045(1)
C(3)	2 <i>i</i>	1	-0.0913(4)	1.2990(2)	0.8607(2)	0.051(1)
C(4)	2 <i>i</i>	1	-0.1671(4)	1.3312(2)	0.9425(2)	0.053(1)
C(5)	2 <i>i</i>	1	-0.2365(3)	1.2599(2)	1.0126(2)	0.046(1)
C(6)	2 <i>i</i>	1	-0.3158(4)	1.0847(3)	1.0806(2)	0.053(1)
C(7)	2 <i>i</i>	1	-0.1455(3)	0.9009(2)	0.8380(2)	0.035(1)
C(8)	2 <i>i</i>	1	-0.1939(3)	0.8209(2)	0.9144(2)	0.045(1)
C(9)	2 <i>i</i>	1	-0.2041(4)	0.7231(2)	0.9012(2)	0.054(1)
C(10)	2 <i>i</i>	1	-0.1645(3)	0.7019(2)	0.8108(2)	0.051(1)
C(11)	2 <i>i</i>	1	-0.1199(3)	0.7806(2)	0.7376(2)	0.045(1)
C(12)	2 <i>i</i>	1	-0.0651(6)	0.9617(3)	0.6650(2)	0.063(1)
C(13)	2 <i>i</i>	1	0.5656(3)	0.5955(2)	0.6233(1)	0.030(1)
C(14)	2 <i>i</i>	1	0.6714(3)	0.5746(2)	0.5402(1)	0.030(1)
C(15)	2 <i>i</i>	1	0.7331(3)	0.6576(2)	0.4747(1)	0.031(1)
C(16)	2 <i>i</i>	1	0.6880(3)	0.7614(2)	0.4891(1)	0.034(1)
C(17)	2 <i>i</i>	1	0.5768(3)	0.7883(2)	0.5641(2)	0.036(1)
C(18)	2 <i>i</i>	1	0.5174(3)	0.7053(2)	0.6297(1)	0.033(1)
C(19)	2 <i>i</i>	1	0.6075(3)	0.4113(2)	0.6277(1)	0.029(1)
C(20)	2 <i>i</i>	1	0.5358(3)	0.4920(2)	0.6813(1)	0.030(1)
C(21)	2 <i>i</i>	1	0.4636(3)	0.4545(2)	0.7731(1)	0.032(1)
C(22)	2 <i>i</i>	1	0.4376(3)	0.3501(2)	0.8054(2)	0.037(1)
C(23)	2 <i>i</i>	1	0.4965(3)	0.2779(2)	0.7477(2)	0.034(1)
C(24)	2 <i>i</i>	1	0.5870(3)	0.3043(2)	0.6615(1)	0.032(1)
C(25)	2 <i>i</i>	1	0.6951(3)	0.4606(2)	0.5403(1)	0.029(1)
C(26)	2 <i>i</i>	1	0.7900(3)	0.4076(2)	0.4719(1)	0.031(1)
C(27)	2 <i>i</i>	1	0.8244(3)	0.2914(2)	0.4851(1)	0.036(1)
C(28)	2 <i>i</i>	1	0.8748(3)	0.4609(2)	0.3879(2)	0.036(1)
N(1)	2 <i>i</i>	1	-0.1764(2)	1.0231(1)	0.9245(1)	0.040(1)
N(2)	2 <i>i</i>	1	-0.1256(3)	1.0002(2)	0.8398(1)	0.041(1)
N(3)	2 <i>i</i>	1	-0.1103(2)	0.8779(2)	0.7491(1)	0.040(1)
N(4)	2 <i>i</i>	1	-0.2349(2)	1.1588(1)	1.0042(1)	0.039(1)
N(5)	2 <i>i</i>	1	0.7523(3)	0.8487(2)	0.4198(1)	0.044(1)
N(6)	2 <i>i</i>	1	0.3835(3)	0.7421(2)	0.6991(1)	0.042(1)
N(7)	2 <i>i</i>	1	0.4319(3)	0.5165(2)	0.8466(1)	0.042(1)
N(8)	2 <i>i</i>	1	0.4698(3)	0.1672(2)	0.7836(1)	0.042(1)
N(9)	2 <i>i</i>	1	0.8538(3)	0.1985(2)	0.4934(1)	0.052(1)
N(10)	2 <i>i</i>	1	0.9464(3)	0.5008(2)	0.3204(2)	0.051(1)
O(1)	2 <i>i</i>	1	0.8433(2)	0.8264(1)	0.3513(1)	0.055(1)
O(2)	2 <i>i</i>	1	0.7118(3)	0.9403(1)	0.4348(2)	0.066(1)
O(3)	2 <i>i</i>	1	0.3940(3)	0.8198(1)	0.7277(1)	0.065(1)
O(4)	2 <i>i</i>	1	0.2636(2)	0.6943(1)	0.7228(1)	0.049(1)
O(5)	2 <i>i</i>	1	0.5350(2)	0.5724(1)	0.8484(1)	0.048(1)
O(6)	2 <i>i</i>	1	0.3103(3)	0.5051(1)	0.9053(1)	0.066(1)
O(7)	2 <i>i</i>	1	0.3978(3)	0.1446(2)	0.8629(1)	0.070(1)

Table A.119 – continued from previous page

Atom	Wyck.	Site	x/a	y/b	z/c	U_{eq}
O(8)	2 <i>i</i>	1	0.5194(2)	0.1029(1)	0.7331(1)	0.053(1)
H(2)	2 <i>i</i>	1	-0.0400(3)	1.1740(2)	0.7970(19)	0.057(7)
H(3)	2 <i>i</i>	1	-0.0380(4)	1.3440(2)	0.8140(2)	0.075(9)
H(4)	2 <i>i</i>	1	-0.1700(3)	1.4060(2)	0.9494(16)	0.050(7)
H(5)	2 <i>i</i>	1	-0.2940(3)	1.2777(19)	1.0744(18)	0.052(7)
H(6A)	2 <i>i</i>	1	-0.4240(4)	1.0710(2)	1.0450(2)	0.082(9)
H(6B)	2 <i>i</i>	1	-0.3640(4)	1.1190(2)	1.1290(2)	0.073(8)
H(6C)	2 <i>i</i>	1	-0.2240(5)	1.0230(3)	1.1110(3)	0.104(13)
H(8)	2 <i>i</i>	1	-0.2170(4)	0.8380(2)	0.9730(2)	0.064(8)
H(9)	2 <i>i</i>	1	-0.2330(4)	0.6680(2)	0.9570(2)	0.077(9)
H(10)	2 <i>i</i>	1	-0.1740(3)	0.6370(2)	0.7997(18)	0.057(7)
H(11)	2 <i>i</i>	1	-0.0970(3)	0.7771(19)	0.6716(18)	0.054(7)
H(12A)	2 <i>i</i>	1	-0.1590(5)	1.0290(3)	0.6560(3)	0.113(13)
H(12B)	2 <i>i</i>	1	-0.0400(4)	0.9290(2)	0.6150(2)	0.078(9)
H(12C)	2 <i>i</i>	1	0.0380(5)	0.9810(3)	0.6780(3)	0.108(14)
H(15)	2 <i>i</i>	1	0.8000(3)	0.6466(19)	0.4206(18)	0.053(7)
H(17)	2 <i>i</i>	1	0.5430(3)	0.8568(18)	0.5723(14)	0.033(6)
H(22)	2 <i>i</i>	1	0.3840(3)	0.3259(17)	0.8676(17)	0.041(6)
H(24)	2 <i>i</i>	1	0.6300(3)	0.2471(17)	0.6253(15)	0.040(6)

Table A.120: Anisotropic displacement parameters $U_{ij}/\text{\AA}^2$ for the independent atoms in the structure of (1)(DTeF) at 263 K.

Atom	U_{11}	U_{22}	U_{33}	U_{23}	U_{13}	U_{12}
C(1)	0.039(1)	0.037(1)	0.033(1)	-0.010(1)	0.002(1)	-0.007(1)
C(2)	0.047(1)	0.046(1)	0.039(1)	-0.010(1)	0.005(1)	-0.012(1)
C(3)	0.054(2)	0.045(1)	0.051(2)	-0.002(1)	-0.004(1)	-0.018(1)
C(4)	0.061(2)	0.040(1)	0.058(2)	-0.016(1)	-0.009(1)	-0.009(1)
C(5)	0.053(2)	0.041(1)	0.044(1)	-0.017(1)	0.000(1)	-0.006(1)
C(6)	0.064(2)	0.059(2)	0.039(1)	-0.020(1)	0.018(1)	-0.021(2)
C(7)	0.030(1)	0.040(1)	0.036(1)	-0.015(1)	0.002(1)	-0.007(1)
C(8)	0.049(1)	0.048(1)	0.039(1)	-0.015(1)	0.007(1)	-0.015(1)
C(9)	0.056(2)	0.052(2)	0.056(2)	-0.012(1)	0.009(1)	-0.023(1)
C(10)	0.050(2)	0.050(1)	0.065(2)	-0.028(1)	0.007(1)	-0.021(1)
C(11)	0.042(1)	0.052(1)	0.049(1)	-0.027(1)	0.006(1)	-0.015(1)
C(12)	0.095(3)	0.057(2)	0.042(2)	-0.020(1)	0.025(2)	-0.027(2)
C(13)	0.030(1)	0.034(1)	0.026(1)	-0.008(1)	-0.001(1)	-0.010(1)
C(14)	0.028(1)	0.034(1)	0.028(1)	-0.009(1)	-0.001(1)	-0.009(1)
C(15)	0.030(1)	0.038(1)	0.027(1)	-0.008(1)	0.001(1)	-0.012(1)
C(16)	0.036(1)	0.034(1)	0.034(1)	-0.006(1)	-0.001(1)	-0.014(1)
C(17)	0.045(1)	0.031(1)	0.035(1)	-0.010(1)	-0.002(1)	-0.013(1)
C(18)	0.035(1)	0.035(1)	0.030(1)	-0.013(1)	0.001(1)	-0.008(1)
C(19)	0.027(1)	0.033(1)	0.025(1)	-0.006(1)	-0.001(1)	-0.007(1)
C(20)	0.029(1)	0.033(1)	0.027(1)	-0.007(1)	0.000(1)	-0.009(1)
C(21)	0.034(1)	0.036(1)	0.026(1)	-0.009(1)	0.002(1)	-0.011(1)
C(22)	0.040(1)	0.042(1)	0.028(1)	-0.005(1)	0.003(1)	-0.014(1)
C(23)	0.035(1)	0.033(1)	0.033(1)	-0.003(1)	-0.003(1)	-0.013(1)
C(24)	0.033(1)	0.033(1)	0.029(1)	-0.005(1)	-0.002(1)	-0.008(1)
C(25)	0.028(1)	0.031(1)	0.026(1)	-0.006(1)	-0.002(1)	-0.007(1)
C(26)	0.031(1)	0.034(1)	0.028(1)	-0.008(1)	0.002(1)	-0.007(1)
C(27)	0.037(1)	0.037(1)	0.029(1)	-0.009(1)	0.003(1)	-0.004(1)

Table A.120 – continued from previous page

Atom	Wyck.	Site	x/a	y/b	z/c	U_{eq}
C(28)	0.035(1)	0.038(1)	0.035(1)	-0.013(1)	0.003(1)	-0.007(1)
N(1)	0.047(1)	0.040(1)	0.036(1)	-0.016(1)	0.005(1)	-0.011(1)
N(2)	0.045(1)	0.042(1)	0.037(1)	-0.016(1)	0.007(1)	-0.010(1)
N(3)	0.040(1)	0.044(1)	0.038(1)	-0.017(1)	0.007(1)	-0.011(1)
N(4)	0.043(1)	0.038(1)	0.036(1)	-0.014(1)	0.004(1)	-0.009(1)
N(5)	0.050(1)	0.040(1)	0.044(1)	-0.007(1)	0.004(1)	-0.021(1)
N(6)	0.053(1)	0.036(1)	0.032(1)	-0.010(1)	0.003(1)	-0.004(1)
N(7)	0.055(1)	0.043(1)	0.029(1)	-0.008(1)	0.008(1)	-0.015(1)
N(8)	0.047(1)	0.038(1)	0.041(1)	-0.002(1)	0.000(1)	-0.017(1)
N(9)	0.069(1)	0.039(1)	0.040(1)	-0.011(1)	0.005(1)	-0.003(1)
N(10)	0.053(1)	0.057(1)	0.044(1)	-0.014(1)	0.016(1)	-0.020(1)
O(1)	0.067(1)	0.057(1)	0.046(1)	-0.010(1)	0.017(1)	-0.031(1)
O(2)	0.085(1)	0.039(1)	0.079(1)	-0.016(1)	0.024(1)	-0.029(1)
O(3)	0.100(2)	0.047(1)	0.051(1)	-0.028(1)	0.015(1)	-0.017(1)
O(4)	0.042(1)	0.057(1)	0.041(1)	-0.011(1)	0.009(1)	-0.008(1)
O(5)	0.063(1)	0.047(1)	0.039(1)	-0.013(1)	-0.005(1)	-0.018(1)
O(6)	0.089(1)	0.069(1)	0.049(1)	-0.027(1)	0.037(1)	-0.034(1)
O(7)	0.104(2)	0.055(1)	0.055(1)	-0.006(1)	0.030(1)	-0.042(1)
O(8)	0.066(1)	0.039(1)	0.057(1)	-0.012(1)	0.000(1)	-0.019(1)

Table A.121: Crystallographic data and structure refinement of **(1)(DTeF)** at 283 K.

Compound	(1)(DTeF)
Empirical Formula	$\text{C}_{28}\text{H}_{18}\text{N}_{10}\text{O}_8$
Formula weight / $gmol^{-1}$	622.52
Crystal size / mm^3	0.190×0.180×0.030
Temperature / K	283(2)
Crystal system; space group	Triclinic, $P\bar{1}$
Lattice constants / \AA°	$a = 7.7583(4) \alpha = 73.933(3)$ $b = 13.0449(5) \beta = 85.460(3)$ $c = 14.3269(6) \gamma = 74.327(2)$
Volume / \AA^3	1341.51(11)
Z; $F(000)$; calc. density / gcm^{-3}	2; 640; 1.541
Wavelength	Mo-K α (0.71073 \AA)
Theta range for data collection / $^\circ$	$2.952 \leq \theta \leq 27.302$
Limiting indices	$-10 \leq h \leq 10, -16 \leq k \leq 16, -18 \leq l \leq 18$
Reflections collected / unique	8530 / 5385
R_{int}	0.0416
Completeness to theta = 25.242	91.50 %
Absorption coefficient / mm^{-1}	0.118
Refinement method	Full-matrix least-squares on F^2
Data / restraints / parameters	5385 / 0 / 487
R indices [$I > 4\sigma(I)$] R_1 ; wR_2	0.0498; 0.1162
R indices (all data) R_1 ; wR_2	0.0968; 0.1388
Goodness-of-fit for F^2	0.973
Largest diff. Peak and hole / $e^{-\text{\AA}^{-3}}$	0.191 / -0.221

Table A.122: Fractional coordinates in Å and equivalent isotropic displacement parameter $U_{eq}/\text{\AA}^2$ for the independent atoms in the structure of (1)(DTeF) at 283 K.

Atom	Wyck.	Site	x/a	y/b	z/c	U_{eq}
C(1)	$2i$	1	-0.1630(3)	1.1249(2)	0.9237(2)	0.039(1)
C(2)	$2i$	1	-0.0887(4)	1.1976(2)	0.8510(2)	0.048(1)
C(3)	$2i$	1	-0.0920(4)	1.2992(2)	0.8602(2)	0.056(1)
C(4)	$2i$	1	-0.1678(4)	1.3308(2)	0.9425(2)	0.057(1)
C(5)	$2i$	1	-0.2361(4)	1.2596(2)	1.0125(2)	0.051(1)
C(6)	$2i$	1	-0.3150(5)	1.0844(3)	1.0809(2)	0.056(1)
C(7)	$2i$	1	-0.1460(3)	0.9012(2)	0.8376(2)	0.039(1)
C(8)	$2i$	1	-0.1944(3)	0.8211(2)	0.9142(2)	0.048(1)
C(9)	$2i$	1	-0.2037(4)	0.7233(2)	0.9009(2)	0.057(1)
C(10)	$2i$	1	-0.1644(4)	0.7022(2)	0.8107(2)	0.055(1)
C(11)	$2i$	1	-0.1197(3)	0.7805(2)	0.7376(2)	0.048(1)
C(12)	$2i$	1	-0.0645(6)	0.9609(3)	0.6653(2)	0.068(1)
C(13)	$2i$	1	0.5658(3)	0.5959(2)	0.6231(1)	0.032(1)
C(14)	$2i$	1	0.6712(3)	0.5746(2)	0.5400(1)	0.031(1)
C(15)	$2i$	1	0.7326(3)	0.6576(2)	0.4750(2)	0.034(1)
C(16)	$2i$	1	0.6879(3)	0.7612(2)	0.4892(2)	0.036(1)
C(17)	$2i$	1	0.5772(3)	0.7881(2)	0.5645(2)	0.038(1)
C(18)	$2i$	1	0.5178(3)	0.7049(2)	0.6298(2)	0.035(1)
C(19)	$2i$	1	0.6070(3)	0.4113(2)	0.6278(1)	0.031(1)
C(20)	$2i$	1	0.5356(3)	0.4922(2)	0.6811(1)	0.032(1)
C(21)	$2i$	1	0.4628(3)	0.4542(2)	0.7731(2)	0.035(1)
C(22)	$2i$	1	0.4367(3)	0.3501(2)	0.8052(2)	0.039(1)
C(23)	$2i$	1	0.4965(3)	0.2784(2)	0.7475(2)	0.036(1)
C(24)	$2i$	1	0.5866(3)	0.3047(2)	0.6614(2)	0.034(1)
C(25)	$2i$	1	0.6948(3)	0.4607(2)	0.5402(1)	0.031(1)
C(26)	$2i$	1	0.7899(3)	0.4076(2)	0.4721(2)	0.034(1)
C(27)	$2i$	1	0.8236(3)	0.2918(2)	0.4849(2)	0.039(1)
C(28)	$2i$	1	0.8741(3)	0.4612(2)	0.3882(2)	0.038(1)
N(1)	$2i$	1	-0.1765(3)	1.0232(2)	0.9242(1)	0.044(1)
N(2)	$2i$	1	-0.1265(3)	1.0007(2)	0.8395(1)	0.044(1)
N(3)	$2i$	1	-0.1108(3)	0.8780(2)	0.7490(1)	0.043(1)
N(4)	$2i$	1	-0.2348(3)	1.1589(2)	1.0041(1)	0.043(1)
N(5)	$2i$	1	0.7525(3)	0.8488(2)	0.4202(2)	0.047(1)
N(6)	$2i$	1	0.3840(3)	0.7422(2)	0.6993(1)	0.045(1)
N(7)	$2i$	1	0.4314(3)	0.5166(2)	0.8466(1)	0.045(1)
N(8)	$2i$	1	0.4691(3)	0.1675(2)	0.7836(2)	0.046(1)
N(9)	$2i$	1	0.8532(3)	0.1987(2)	0.4931(2)	0.055(1)
N(10)	$2i$	1	0.9460(3)	0.5014(2)	0.3206(2)	0.055(1)
O(1)	$2i$	1	0.8438(3)	0.8260(2)	0.3516(1)	0.061(1)
O(2)	$2i$	1	0.7121(3)	0.9404(2)	0.4347(2)	0.072(1)
O(3)	$2i$	1	0.3947(3)	0.8197(2)	0.7279(1)	0.070(1)
O(4)	$2i$	1	0.2640(2)	0.6944(1)	0.7230(1)	0.052(1)
O(5)	$2i$	1	0.5341(2)	0.5725(1)	0.8482(1)	0.052(1)
O(6)	$2i$	1	0.3104(3)	0.5052(2)	0.9050(1)	0.072(1)
O(7)	$2i$	1	0.3968(3)	0.1450(2)	0.8625(2)	0.076(1)
O(8)	$2i$	1	0.5190(3)	0.1029(1)	0.7331(1)	0.058(1)
H(2)	$2i$	1	-0.0430(4)	1.1720(2)	0.7980(2)	0.069(8)
H(3)	$2i$	1	-0.0400(4)	1.3440(2)	0.8130(2)	0.069(9)
H(4)	$2i$	1	-0.1660(4)	1.4000(2)	0.9500(2)	0.069(8)
H(5)	$2i$	1	-0.2940(4)	1.2760(2)	1.0720(2)	0.062(8)
H(6A)	$2i$	1	-0.4280(5)	1.0680(3)	1.0420(2)	0.104(11)
H(6B)	$2i$	1	-0.3680(4)	1.1210(2)	1.1280(2)	0.068(8)
H(6C)	$2i$	1	-0.2340(5)	1.0210(3)	1.1060(3)	0.099(13)

Table A.122 – continued from previous page

Atom	Wyck.	Site	x/a	y/b	z/c	U_{eq}
H(8)	$2i$	1	-0.2150(3)	0.8380(2)	0.9741(19)	0.055(7)
H(9)	$2i$	1	-0.2310(4)	0.6700(3)	0.9570(2)	0.090(1)
H(10)	$2i$	1	-0.1670(4)	0.6380(2)	0.7990(2)	0.077(9)
H(11)	$2i$	1	-0.0940(3)	0.7750(2)	0.6749(19)	0.055(7)
H(12A)	$2i$	1	-0.1630(5)	1.0260(3)	0.6550(3)	0.117(15)
H(12B)	$2i$	1	-0.0430(5)	0.9320(3)	0.6140(3)	0.102(12)
H(12C)	$2i$	1	0.0370(5)	0.9790(3)	0.6800(3)	0.100(14)
H(15)	$2i$	1	0.7980(3)	0.6485(17)	0.4204(17)	0.041(6)
H(17)	$2i$	1	0.5460(3)	0.8558(19)	0.5733(16)	0.039(6)
H(22)	$2i$	1	0.3800(3)	0.3258(17)	0.8691(17)	0.039(6)
H(24)	$2i$	1	0.6330(3)	0.2478(19)	0.6224(17)	0.047(6)

Table A.123: Anisotropic displacement parameters $U_{ij}/\text{\AA}^2$ for the independent atoms in the structure of **(1)**(DTeF) at 283 K.

Atom	U_{11}	U_{22}	U_{33}	U_{23}	U_{13}	U_{12}
C(1)	0.040(1)	0.041(1)	0.035(1)	-0.011(1)	0.001(1)	-0.007(1)
C(2)	0.053(2)	0.049(2)	0.041(1)	-0.011(1)	0.005(1)	-0.012(1)
C(3)	0.062(2)	0.047(2)	0.054(2)	-0.001(1)	-0.003(1)	-0.018(1)
C(4)	0.066(2)	0.040(1)	0.064(2)	-0.016(1)	-0.007(1)	-0.010(1)
C(5)	0.059(2)	0.047(2)	0.049(2)	-0.020(1)	-0.001(1)	-0.009(1)
C(6)	0.070(2)	0.062(2)	0.042(2)	-0.021(1)	0.021(2)	-0.024(2)
C(7)	0.033(1)	0.045(1)	0.041(1)	-0.020(1)	0.004(1)	-0.008(1)
C(8)	0.055(2)	0.050(2)	0.041(1)	-0.014(1)	0.005(1)	-0.014(1)
C(9)	0.062(2)	0.054(2)	0.058(2)	-0.014(1)	0.010(1)	-0.023(1)
C(10)	0.052(2)	0.056(2)	0.069(2)	-0.030(2)	0.008(1)	-0.023(1)
C(11)	0.044(2)	0.058(2)	0.052(2)	-0.028(1)	0.006(1)	-0.016(1)
C(12)	0.102(3)	0.063(2)	0.043(2)	-0.020(2)	0.027(2)	-0.029(2)
C(13)	0.034(1)	0.035(1)	0.026(1)	-0.007(1)	-0.001(1)	-0.011(1)
C(14)	0.030(1)	0.034(1)	0.028(1)	-0.007(1)	-0.001(1)	-0.009(1)
C(15)	0.033(1)	0.041(1)	0.028(1)	-0.008(1)	0.002(1)	-0.013(1)
C(16)	0.039(1)	0.036(1)	0.035(1)	-0.005(1)	-0.002(1)	-0.017(1)
C(17)	0.046(1)	0.032(1)	0.039(1)	-0.012(1)	-0.001(1)	-0.013(1)
C(18)	0.038(1)	0.039(1)	0.032(1)	-0.013(1)	0.000(1)	-0.011(1)
C(19)	0.031(1)	0.035(1)	0.027(1)	-0.007(1)	-0.002(1)	-0.008(1)
C(20)	0.032(1)	0.037(1)	0.028(1)	-0.007(1)	0.000(1)	-0.010(1)
C(21)	0.039(1)	0.039(1)	0.028(1)	-0.007(1)	0.002(1)	-0.011(1)
C(22)	0.044(1)	0.044(1)	0.029(1)	-0.005(1)	0.004(1)	-0.016(1)
C(23)	0.040(1)	0.035(1)	0.034(1)	-0.003(1)	-0.001(1)	-0.016(1)
C(24)	0.036(1)	0.035(1)	0.030(1)	-0.006(1)	-0.002(1)	-0.009(1)
C(25)	0.030(1)	0.034(1)	0.028(1)	-0.006(1)	-0.001(1)	-0.009(1)
C(26)	0.035(1)	0.035(1)	0.032(1)	-0.010(1)	0.004(1)	-0.008(1)
C(27)	0.040(1)	0.042(1)	0.030(1)	-0.010(1)	0.002(1)	-0.004(1)
C(28)	0.038(1)	0.039(1)	0.037(1)	-0.013(1)	0.002(1)	-0.006(1)
N(1)	0.051(1)	0.044(1)	0.039(1)	-0.018(1)	0.007(1)	-0.013(1)
N(2)	0.050(1)	0.047(1)	0.039(1)	-0.018(1)	0.009(1)	-0.012(1)
N(3)	0.044(1)	0.047(1)	0.043(1)	-0.018(1)	0.007(1)	-0.014(1)
N(4)	0.049(1)	0.042(1)	0.037(1)	-0.015(1)	0.003(1)	-0.010(1)
N(5)	0.053(1)	0.045(1)	0.046(1)	-0.008(1)	0.004(1)	-0.023(1)
N(6)	0.057(1)	0.040(1)	0.033(1)	-0.010(1)	0.004(1)	-0.006(1)
N(7)	0.060(1)	0.046(1)	0.028(1)	-0.009(1)	0.007(1)	-0.015(1)

Table A.123 – continued from previous page

Atom	Wyck.	Site	x/a	y/b	z/c	U_{eq}
N(8)	0.050(1)	0.042(1)	0.045(1)	-0.004(1)	-0.001(1)	-0.017(1)
N(9)	0.073(2)	0.040(1)	0.046(1)	-0.013(1)	0.006(1)	-0.004(1)
N(10)	0.060(1)	0.060(1)	0.045(1)	-0.012(1)	0.019(1)	-0.023(1)
O(1)	0.074(1)	0.063(1)	0.051(1)	-0.012(1)	0.018(1)	-0.034(1)
O(2)	0.093(2)	0.043(1)	0.085(2)	-0.017(1)	0.024(1)	-0.031(1)
O(3)	0.110(2)	0.049(1)	0.055(1)	-0.030(1)	0.016(1)	-0.018(1)
O(4)	0.045(1)	0.061(1)	0.043(1)	-0.010(1)	0.009(1)	-0.006(1)
O(5)	0.069(1)	0.051(1)	0.041(1)	-0.015(1)	-0.005(1)	-0.021(1)
O(6)	0.097(2)	0.075(1)	0.052(1)	-0.028(1)	0.040(1)	-0.038(1)
O(7)	0.111(2)	0.060(1)	0.059(1)	-0.006(1)	0.032(1)	-0.045(1)
O(8)	0.072(1)	0.043(1)	0.060(1)	-0.013(1)	-0.001(1)	-0.020(1)

Table A.124: Crystallographic data and structure refinement of (**1**)(DTeF) at 303 K.

Compound	(1)(DTeF)
Empirical Formula	C ₂₈ H ₁₈ N ₁₀ O ₈
Formula weight / g mol ⁻¹	622.52
Crystal size / mm ³	0.190×0.180×0.030
Temperature / K	303(2)
Crystal system; space group	Triclinic, P $\bar{1}$
Lattice constants / Å °	$a = 7.7751(4)$ $\alpha = 73.956(3)$ $b = 13.0494(6)$ $\beta = 85.353(3)$ $c = 14.3407(6)$ $\gamma = 74.368(3)$
Volume / Å ³	1346.59(11)
Z; F(000); calc. density / g cm ⁻³	2: 640; 1.535
Wavelength	Mo-K α (0.71073 Å)
Theta range for data collection / °	2.946 ≤ θ ≤ 33.261
Limiting indices	-11 ≤ h ≤ 11, -18 ≤ k ≤ 20, -22 ≤ l ≤ 21
Reflections collected / unique	12430 / 8308
R _{int}	0.0525
Completeness to theta = 25.242	90.70 %
Absorption coefficient / mm ⁻¹	0.117
Refinement method	Full-matrix least-squares on F^2
Data / restraints / parameters	8308 / 0 / 487
R indices [I > 4σ(I)] R ₁ ; wR ₂	0.0596; 0.1370
R indices (all data) R ₁ ; wR ₂	0.1612; 0.1795
Goodness-of-fit for F^2	0.910
Largest diff. Peak and hole / e ⁻ Å ⁻³	0.267 / -0.306

Table A.125: Fractional coordinates in Å and equivalent isotropic displacement parameter $U_{eq}/\text{Å}^2$ for the independent atoms in the structure of (1)(DTeF) at 303 K.

Atom	Wyck.	Site	x/a	y/b	z/c	U_{eq}
C(1)	$2i$	1	-0.1624(3)	1.1250(2)	0.9234(2)	0.041(1)
C(2)	$2i$	1	-0.0903(4)	1.1978(2)	0.8510(2)	0.053(1)
C(3)	$2i$	1	-0.0922(4)	1.2988(2)	0.8603(2)	0.060(1)
C(4)	$2i$	1	-0.1679(4)	1.3311(2)	0.9421(2)	0.062(1)
C(5)	$2i$	1	-0.2361(4)	1.2600(2)	1.0124(2)	0.055(1)
C(6)	$2i$	1	-0.3130(5)	1.0842(3)	1.0815(2)	0.061(1)
C(7)	$2i$	1	-0.1460(3)	0.9014(2)	0.8376(2)	0.041(1)
C(8)	$2i$	1	-0.1944(4)	0.8215(2)	0.9137(2)	0.052(1)
C(9)	$2i$	1	-0.2034(4)	0.7235(3)	0.9008(2)	0.063(1)
C(10)	$2i$	1	-0.1633(4)	0.7015(3)	0.8112(2)	0.060(1)
C(11)	$2i$	1	-0.1199(3)	0.7806(2)	0.7377(2)	0.053(1)
C(12)	$2i$	1	-0.0653(6)	0.9613(3)	0.6652(2)	0.073(1)
C(13)	$2i$	1	0.5656(3)	0.5956(2)	0.6232(1)	0.033(1)
C(14)	$2i$	1	0.6707(3)	0.5747(2)	0.5402(1)	0.033(1)
C(15)	$2i$	1	0.7324(3)	0.6574(2)	0.4751(2)	0.037(1)
C(16)	$2i$	1	0.6877(3)	0.7612(2)	0.4894(2)	0.039(1)
C(17)	$2i$	1	0.5770(3)	0.7883(2)	0.5647(2)	0.041(1)
C(18)	$2i$	1	0.5179(3)	0.7052(2)	0.6297(2)	0.039(1)
C(19)	$2i$	1	0.6067(3)	0.4114(2)	0.6275(1)	0.034(1)
C(20)	$2i$	1	0.5354(3)	0.4921(2)	0.6810(1)	0.036(1)
C(21)	$2i$	1	0.4629(3)	0.4544(2)	0.7729(2)	0.038(1)
C(22)	$2i$	1	0.4364(3)	0.3507(2)	0.8053(2)	0.043(1)
C(23)	$2i$	1	0.4957(3)	0.2784(2)	0.7476(2)	0.039(1)
C(24)	$2i$	1	0.5860(3)	0.3049(2)	0.6618(2)	0.037(1)
C(25)	$2i$	1	0.6940(3)	0.4609(2)	0.5404(1)	0.033(1)
C(26)	$2i$	1	0.7897(3)	0.4075(2)	0.4719(2)	0.037(1)
C(27)	$2i$	1	0.8233(3)	0.2920(2)	0.4850(2)	0.042(1)
C(28)	$2i$	1	0.8742(3)	0.4612(2)	0.3885(2)	0.041(1)
N(1)	$2i$	1	-0.1776(3)	1.0234(2)	0.9238(1)	0.046(1)
N(2)	$2i$	1	-0.1268(3)	1.0006(2)	0.8394(1)	0.047(1)
N(3)	$2i$	1	-0.1105(3)	0.8781(2)	0.7489(1)	0.046(1)
N(4)	$2i$	1	-0.2346(3)	1.1586(2)	1.0040(1)	0.046(1)
N(5)	$2i$	1	0.7520(3)	0.8493(2)	0.4204(2)	0.050(1)
N(6)	$2i$	1	0.3841(3)	0.7421(2)	0.6991(1)	0.048(1)
N(7)	$2i$	1	0.4309(3)	0.5169(2)	0.8463(1)	0.049(1)
N(8)	$2i$	1	0.4682(3)	0.1681(2)	0.7834(2)	0.051(1)
N(9)	$2i$	1	0.8518(3)	0.1987(2)	0.4932(2)	0.059(1)
N(10)	$2i$	1	0.9458(3)	0.5011(2)	0.3208(2)	0.060(1)
O(1)	$2i$	1	0.8435(3)	0.8260(2)	0.3519(1)	0.065(1)
O(2)	$2i$	1	0.7128(3)	0.9398(2)	0.4353(2)	0.078(1)
O(3)	$2i$	1	0.3954(3)	0.8195(2)	0.7279(1)	0.076(1)
O(4)	$2i$	1	0.2643(2)	0.6944(2)	0.7230(1)	0.057(1)
O(5)	$2i$	1	0.5342(3)	0.5725(1)	0.8482(1)	0.056(1)
O(6)	$2i$	1	0.3100(3)	0.5056(2)	0.9051(1)	0.077(1)
O(7)	$2i$	1	0.3962(3)	0.1451(2)	0.8625(2)	0.083(1)
O(8)	$2i$	1	0.5181(3)	0.1034(1)	0.7329(1)	0.063(1)
H(2)	$2i$	1	-0.0460(4)	1.1710(2)	0.7990(2)	0.066(8)
H(3)	$2i$	1	-0.0440(4)	1.3420(2)	0.8140(2)	0.071(9)
H(4)	$2i$	1	-0.1650(4)	1.4010(2)	0.9500(2)	0.073(9)
H(5)	$2i$	1	-0.2870(3)	1.2760(2)	1.0730(2)	0.061(8)
H(6A)	$2i$	1	-0.4110(5)	1.0680(3)	1.0500(3)	0.113(13)
H(6B)	$2i$	1	-0.3710(4)	1.1210(2)	1.1290(2)	0.066(8)
H(6C)	$2i$	1	-0.2340(6)	1.0110(4)	1.1020(3)	0.144(17)

Table A.125 – continued from previous page

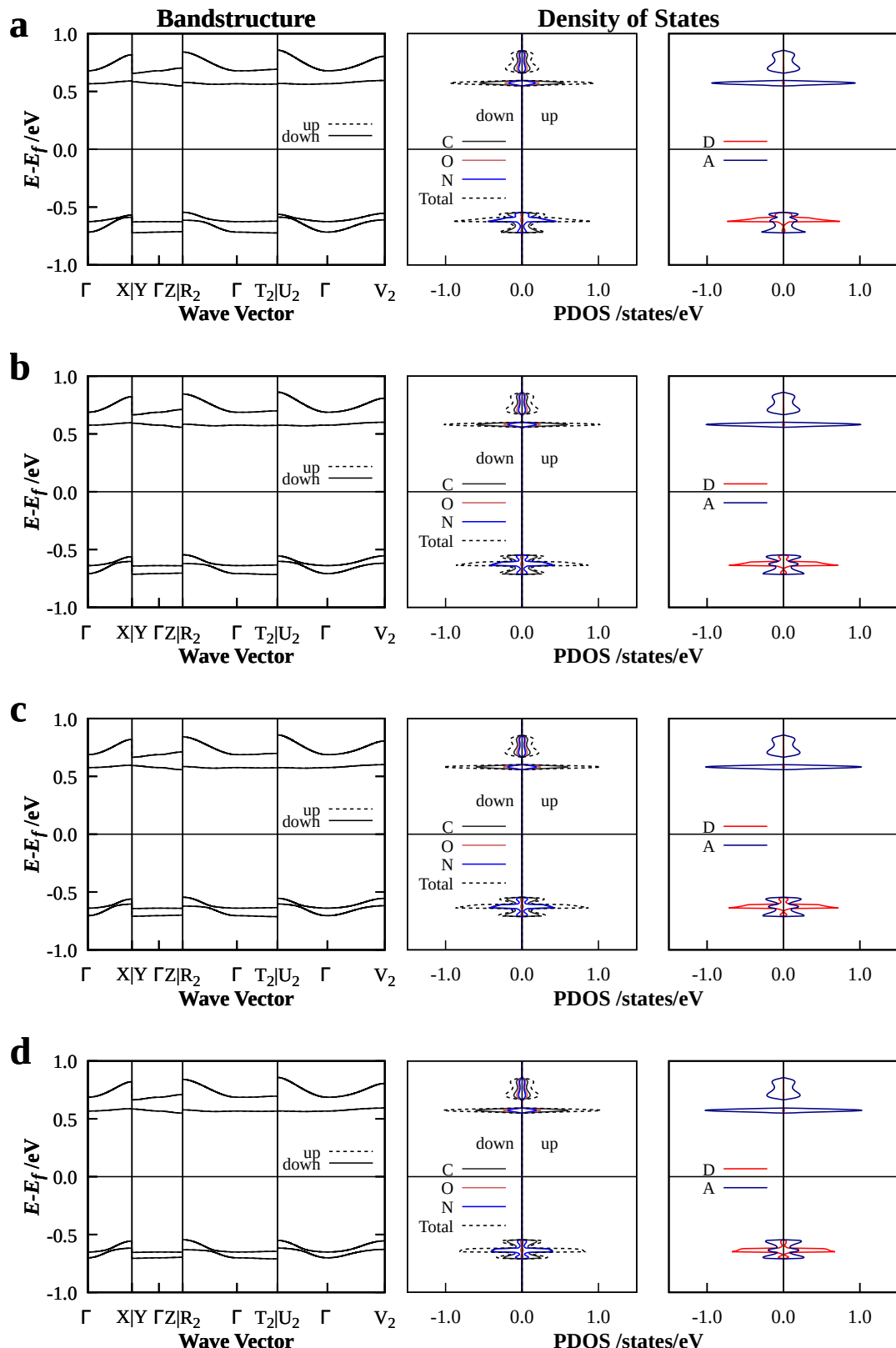
Atom	Wyck.	Site	x/a	y/b	z/c	U_{eq}
H(8)	2 <i>i</i>	1	-0.2170(4)	0.8380(2)	0.9730(2)	0.067(8)
H(9)	2 <i>i</i>	1	-0.2280(4)	0.6660(3)	0.9580(2)	0.096(11)
H(10)	2 <i>i</i>	1	-0.1670(3)	0.6380(2)	0.7995(18)	0.057(8)
H(11)	2 <i>i</i>	1	-0.0910(3)	0.7730(2)	0.6749(19)	0.054(7)
H(12A)	2 <i>i</i>	1	-0.1650(6)	1.0300(4)	0.6510(3)	0.127(15)
H(12B)	2 <i>i</i>	1	-0.0410(4)	0.9320(3)	0.6150(3)	0.086(1)
H(12C)	2 <i>i</i>	1	0.0430(6)	0.9780(3)	0.6820(3)	0.132(17)
H(15)	2 <i>i</i>	1	0.7980(3)	0.6492(19)	0.4205(18)	0.049(7)
H(17)	2 <i>i</i>	1	0.5380(3)	0.8620(2)	0.5680(17)	0.055(7)
H(22)	2 <i>i</i>	1	0.3820(3)	0.3280(17)	0.8692(17)	0.041(6)
H(24)	2 <i>i</i>	1	0.6360(3)	0.2503(18)	0.6304(16)	0.038(6)

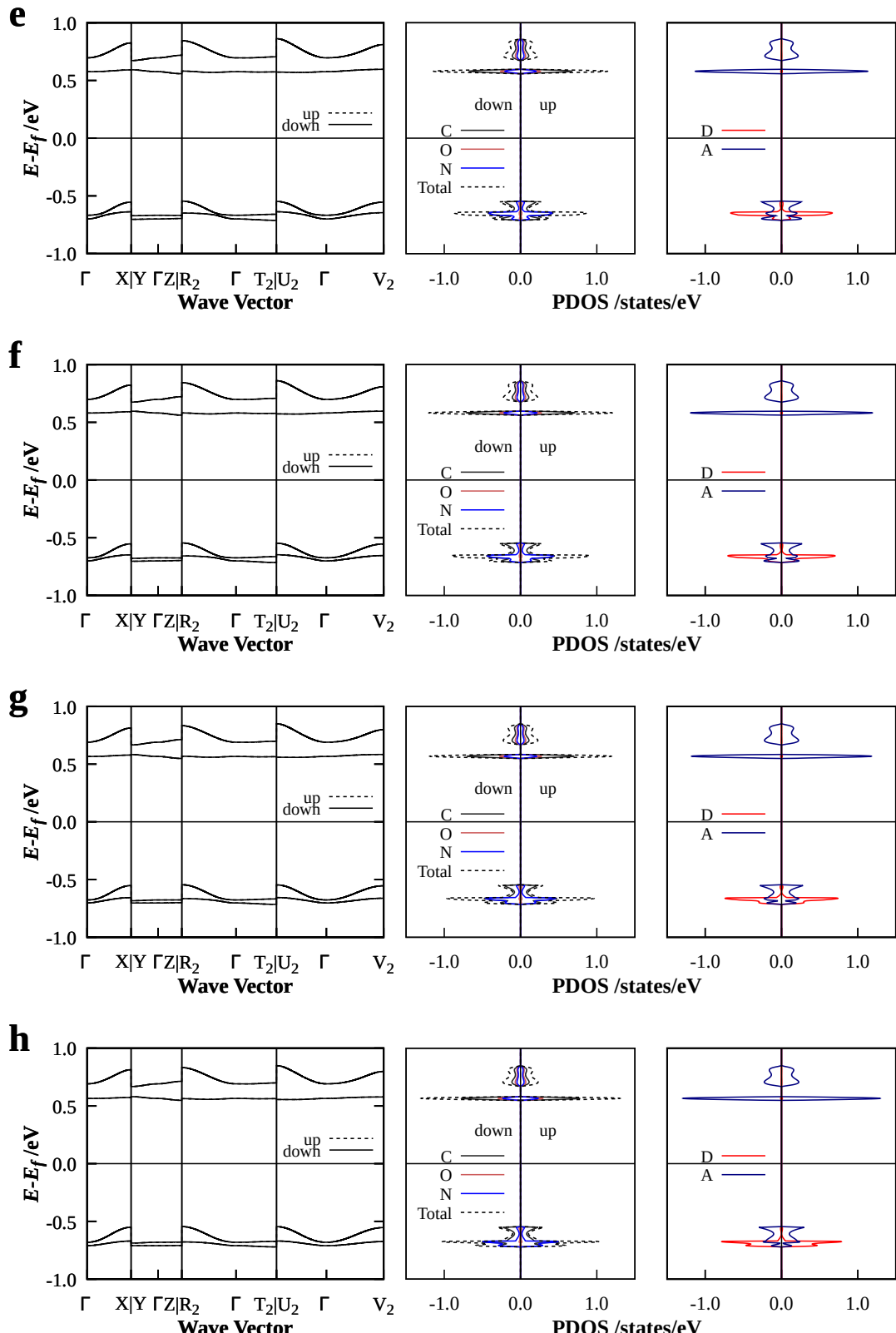
Table A.126: Anisotropic displacement parameters $U_{ij}/\text{\AA}^2$ for the independent atoms in the structure of **(1)(DTeF)** at 303 K.

Atom	U_{11}	U_{22}	U_{33}	U_{23}	U_{13}	U_{12}
C(1)	0.042(1)	0.043(1)	0.039(1)	-0.015(1)	0.002(1)	-0.007(1)
C(2)	0.061(2)	0.051(2)	0.044(1)	-0.010(1)	0.006(1)	-0.015(1)
C(3)	0.065(2)	0.052(2)	0.060(2)	-0.002(1)	-0.004(2)	-0.020(2)
C(4)	0.077(2)	0.044(2)	0.069(2)	-0.020(1)	-0.009(2)	-0.013(2)
C(5)	0.065(2)	0.050(2)	0.051(2)	-0.021(1)	-0.001(1)	-0.009(1)
C(6)	0.078(2)	0.066(2)	0.048(2)	-0.025(2)	0.027(2)	-0.031(2)
C(7)	0.034(1)	0.048(1)	0.042(1)	-0.018(1)	0.003(1)	-0.007(1)
C(8)	0.059(2)	0.055(2)	0.044(1)	-0.016(1)	0.008(1)	-0.019(1)
C(9)	0.072(2)	0.060(2)	0.062(2)	-0.015(2)	0.011(2)	-0.028(2)
C(10)	0.059(2)	0.059(2)	0.076(2)	-0.032(2)	0.010(2)	-0.028(2)
C(11)	0.049(2)	0.065(2)	0.056(2)	-0.033(1)	0.006(1)	-0.017(1)
C(12)	0.113(3)	0.063(2)	0.046(2)	-0.021(2)	0.031(2)	-0.029(2)
C(13)	0.036(1)	0.037(1)	0.029(1)	-0.009(1)	0.001(1)	-0.012(1)
C(14)	0.034(1)	0.037(1)	0.030(1)	-0.009(1)	0.002(1)	-0.011(1)
C(15)	0.039(1)	0.043(1)	0.032(1)	-0.010(1)	0.003(1)	-0.013(1)
C(16)	0.043(1)	0.039(1)	0.036(1)	-0.005(1)	0.000(1)	-0.019(1)
C(17)	0.051(1)	0.034(1)	0.040(1)	-0.011(1)	-0.002(1)	-0.012(1)
C(18)	0.046(1)	0.044(1)	0.032(1)	-0.014(1)	0.002(1)	-0.014(1)
C(19)	0.036(1)	0.037(1)	0.029(1)	-0.008(1)	-0.001(1)	-0.010(1)
C(20)	0.038(1)	0.039(1)	0.030(1)	-0.008(1)	0.000(1)	-0.011(1)
C(21)	0.040(1)	0.043(1)	0.032(1)	-0.010(1)	0.004(1)	-0.012(1)
C(22)	0.049(1)	0.045(1)	0.033(1)	-0.005(1)	0.006(1)	-0.016(1)
C(23)	0.044(1)	0.038(1)	0.036(1)	-0.003(1)	-0.003(1)	-0.016(1)
C(24)	0.038(1)	0.036(1)	0.035(1)	-0.007(1)	-0.003(1)	-0.008(1)
C(25)	0.032(1)	0.036(1)	0.030(1)	-0.007(1)	-0.001(1)	-0.009(1)
C(26)	0.036(1)	0.039(1)	0.034(1)	-0.010(1)	0.003(1)	-0.007(1)
C(27)	0.043(1)	0.046(1)	0.033(1)	-0.012(1)	0.005(1)	-0.005(1)
C(28)	0.040(1)	0.042(1)	0.040(1)	-0.014(1)	0.003(1)	-0.007(1)
N(1)	0.052(1)	0.048(1)	0.040(1)	-0.018(1)	0.007(1)	-0.012(1)
N(2)	0.053(1)	0.048(1)	0.043(1)	-0.019(1)	0.008(1)	-0.011(1)
N(3)	0.048(1)	0.048(1)	0.044(1)	-0.019(1)	0.009(1)	-0.013(1)
N(4)	0.052(1)	0.045(1)	0.043(1)	-0.018(1)	0.004(1)	-0.010(1)
N(5)	0.058(1)	0.046(1)	0.050(1)	-0.008(1)	0.007(1)	-0.025(1)
N(6)	0.058(1)	0.044(1)	0.037(1)	-0.013(1)	0.004(1)	-0.004(1)
N(7)	0.066(1)	0.049(1)	0.030(1)	-0.008(1)	0.008(1)	-0.017(1)

Table A.126 – continued from previous page

Atom	Wyck.	Site	x/a	y/b	z/c	U_{eq}
N(8)	0.057(1)	0.043(1)	0.051(1)	-0.004(1)	0.000(1)	-0.019(1)
N(9)	0.077(2)	0.042(1)	0.049(1)	-0.013(1)	0.003(1)	-0.002(1)
N(10)	0.066(2)	0.064(1)	0.051(1)	-0.016(1)	0.022(1)	-0.025(1)
O(1)	0.080(1)	0.066(1)	0.055(1)	-0.011(1)	0.020(1)	-0.037(1)
O(2)	0.099(2)	0.042(1)	0.095(2)	-0.018(1)	0.025(1)	-0.031(1)
O(3)	0.121(2)	0.057(1)	0.058(1)	-0.034(1)	0.020(1)	-0.021(1)
O(4)	0.048(1)	0.066(1)	0.048(1)	-0.013(1)	0.011(1)	-0.007(1)
O(5)	0.074(1)	0.055(1)	0.044(1)	-0.015(1)	-0.005(1)	-0.022(1)
O(6)	0.107(2)	0.079(1)	0.055(1)	-0.031(1)	0.044(1)	-0.041(1)
O(7)	0.124(2)	0.065(1)	0.063(1)	-0.007(1)	0.036(1)	-0.051(1)
O(8)	0.079(1)	0.045(1)	0.065(1)	-0.012(1)	0.000(1)	-0.021(1)





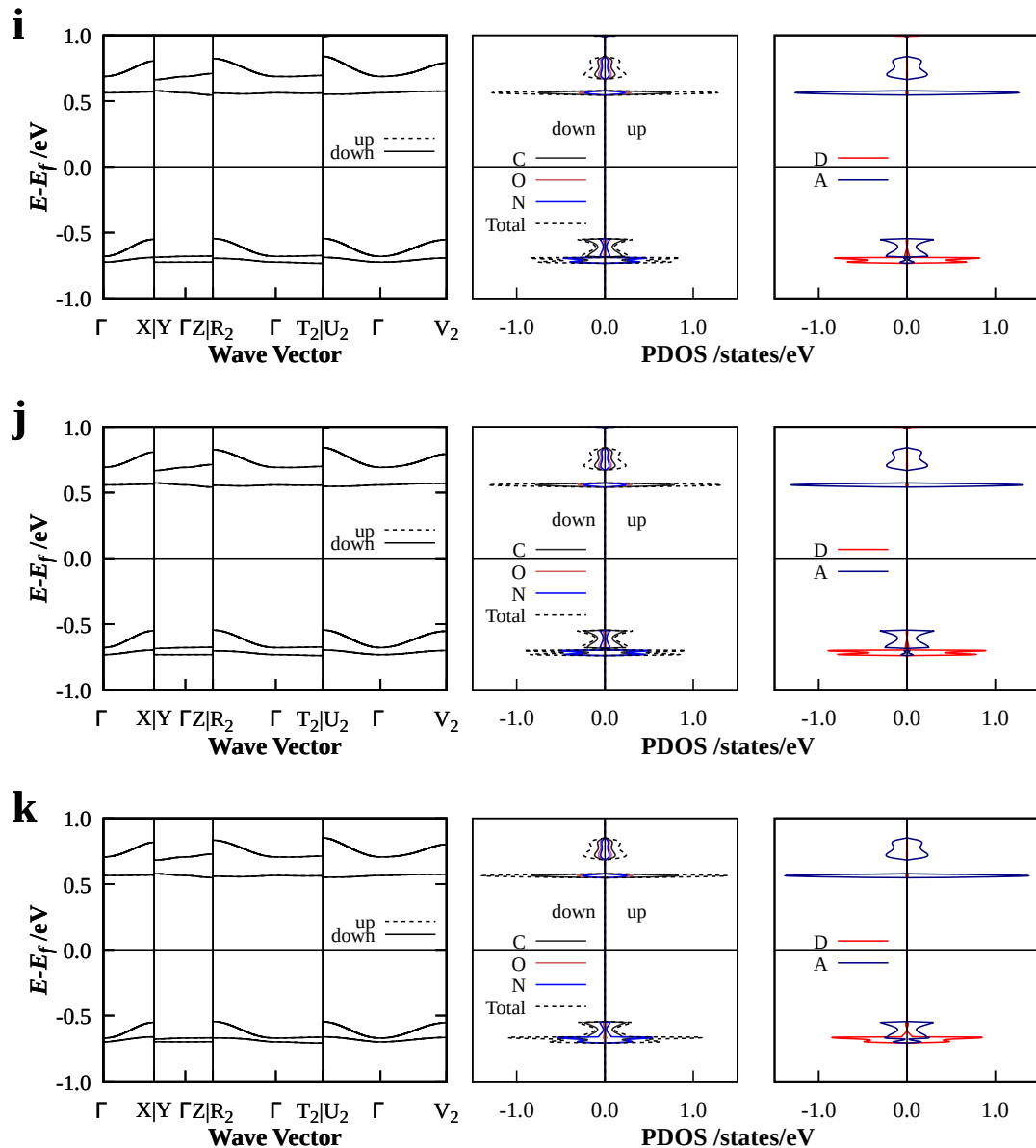


Figure A.7: Band structures, PDOS for atom orbitals and PDOS for orbitals belonging to donor or acceptor of (1)(DTeF) from 103 K to 303 K in 20 K steps calculated with CRYSTAL17, PW1PW+D3/pob-TZVP-rev2. **a:** 103 K, **b:** 123 K, **c:** 143 K, **d:** 163 K, **e:** 183 K, **f:** 203 K, **g:** 223 K, **h:** 243 K, **i:** 263 K, **j:** 283 K and **k:** 303 K.

Bibliography

- [1] H. Akamuta, H. Inokuchi and Y. Matsunaga, *Nature* **173** 168–169 1954, doi: [10.1038/173168a0](https://doi.org/10.1038/173168a0).
- [2] K. Kan and Y. Matsunaga, *Bull. Chem. Soc. Jpn.* **45** 2096–2100 1972, doi: [10.1246/bcsj.45.2096](https://doi.org/10.1246/bcsj.45.2096).
- [3] W. A. Little, *Phys. Rev.* **134** A1416–A1424 1964, doi: [10.1103/PhysRev.134.A1416](https://doi.org/10.1103/PhysRev.134.A1416).
- [4] J. D. Myers and J. Xue, *Polym. Rev.* **52** 1–37 2012, doi: [10.1080/15583724.2011.644368](https://doi.org/10.1080/15583724.2011.644368).
- [5] Y. Shirota, *J. Mater. Chem.* **10** 1–25 2000, doi: [10.1039/A908130E](https://doi.org/10.1039/A908130E).
- [6] D. R. MacFarlane, J. Huang and M. Forsyth, *Nature* **402** 792–794 1999, doi: [10.1038/45514](https://doi.org/10.1038/45514).
- [7] D. R. MacFarlane and M. Forsyth, *Adv. Mater.* **13** 957–966 2001, doi: [10.1002/1521-4095\(200107\)13:12/13<957::AID-ADMA957>3.0.CO;2-\\$\%\\$23](https://doi.org/10.1002/1521-4095(200107)13:12/13<957::AID-ADMA957>3.0.CO;2-$\%$23).
- [8] Y. Murata, T. Kobayashi, N. Uyeda and E. Suito, *J. Cryst. Growth* **26** 187–196 1974, doi: [10.1016/0022-0248\(74\)90244-9](https://doi.org/10.1016/0022-0248(74)90244-9).
- [9] B. J. Powell and R. H. McKenzie, *Phys. Rev. Lett.* **94** 047004 2005, doi: [10.1103/PhysRevLett.94.047004](https://doi.org/10.1103/PhysRevLett.94.047004).
- [10] K. Zantout, M. Altmeyer, S. Backes and R. Valentí, *Phys. Rev. B* **97** 014530 2018, doi: [10.1103/PhysRevB.97.014530](https://doi.org/10.1103/PhysRevB.97.014530).
- [11] F. Wöhler, *Liebigs Ann. Chem.* **51** 145–163 1844, doi: [10.1002/jlac.18440510202](https://doi.org/10.1002/jlac.18440510202).
- [12] M. Hanack, *NadC* **28** 632–636 1980, doi: [10.1002/nadc.19800280904](https://doi.org/10.1002/nadc.19800280904).
- [13] Y. Matsunaga, *J. Chem. Phys.* **41** 1609–1613 1964, doi: [10.1063/1.1726131](https://doi.org/10.1063/1.1726131).
- [14] Y. Matsunaga, *Nature* **205** 72–73 1965, doi: [10.1038/205072a0](https://doi.org/10.1038/205072a0).
- [15] Y. Matsunaga, *J. Chem. Phys.* **42** 1982–1986 1965, doi: [10.1063/1.1696234](https://doi.org/10.1063/1.1696234).
- [16] H. M. McConnell, B. M. Hoffman and R. M. Metzger, *Proc. Natl. Acad. Sci.* **53** 46–50 1965, doi: [10.1073/pnas.53.1.46](https://doi.org/10.1073/pnas.53.1.46).
- [17] T. Koopmans, *Physica* **1** 104–113 1934, doi: [10.1016/S0031-8914\(34\)90011-2](https://doi.org/10.1016/S0031-8914(34)90011-2).
- [18] J. B. Torrance and B. D. Silverman, *Phys. Rev. B* **15** 788–801 1977, doi: [10.1103/PhysRevB.15.788](https://doi.org/10.1103/PhysRevB.15.788).
- [19] H. Shiba, *Phys. Rev. B* **6** 930–938 1972, doi: [10.1103/PhysRevB.6.930](https://doi.org/10.1103/PhysRevB.6.930).
- [20] Z. G. Soos, S. Kuwajima and R. H. Harding, *J. Chem. Phys.* **85** 601–610 1986, doi: [10.1063/1.451585](https://doi.org/10.1063/1.451585).
- [21] Y. Matsunaga, *Bull. Chem. Soc. Jpn.* **42** 2490–2493 1969, doi: [10.1246/bcsj.42.2490](https://doi.org/10.1246/bcsj.42.2490).

- [22] Y. Matsunaga and G. Saito, *Bull. Chem. Soc. Jpn.* **44** 958–963 1971, doi: [10.1246/bcsj.44.958](https://doi.org/10.1246/bcsj.44.958).
- [23] G. Saito and Y. Yoshida, *Bull. Chem. Soc. Jpn.* **80** 1–137 2007, doi: [10.1246/bcsj.80.1](https://doi.org/10.1246/bcsj.80.1).
- [24] R. E. Peierls, *Quantum Theory of Solids*, Oxford University Press, 2001.
- [25] X. He, S. Ryu and S. Hirata, *J. Chem. Phys.* **140** 024702 2014, doi: [10.1063/1.4859257](https://doi.org/10.1063/1.4859257).
- [26] J. Ferraris, D. Cowan, V. Walatka and J. Perlstein, *J. Am. Chem. Soc.* **95** 948–949 1973, doi: [10.1021/ja00784a066](https://doi.org/10.1021/ja00784a066).
- [27] M. R. Bryce, *Chem. Soc. Rev.* **20** 355–390 1991, doi: [10.1039/CS9912000355](https://doi.org/10.1039/CS9912000355).
- [28] U. Geiser and J. A. Schlueter, *Chem. Rev.* **104** 5203–5242 2004, doi: [10.1021/cr0306844](https://doi.org/10.1021/cr0306844).
- [29] L. Bulaevskii, *Adv. Phys.* **37** 443–470 1988, doi: [10.1080/00018738800101409](https://doi.org/10.1080/00018738800101409).
- [30] D. Jérôme, *Chem. Rev.* **104** 5565–5592 2004, doi: [10.1021/cr030652g](https://doi.org/10.1021/cr030652g).
- [31] R. H. Blessing and P. Coppens, *Solid State Commun.* **15** 215–221 1974, doi: [10.1016/0038-1098\(74\)90744-3](https://doi.org/10.1016/0038-1098(74)90744-3).
- [32] S. Ishibashi and M. Kohyama, *Phys. Rev. B* **62** 7839–7844 2000, doi: [10.1103/PhysRevB.62.7839](https://doi.org/10.1103/PhysRevB.62.7839).
- [33] J. Fraxedas et al., *Phys. Rev. B* **68** 195115 2003, doi: [10.1103/PhysRevB.68.195115](https://doi.org/10.1103/PhysRevB.68.195115).
- [34] M. Sing et al., *Phys. Rev. B* **68** 125111 2003, doi: [10.1103/PhysRevB.68.125111](https://doi.org/10.1103/PhysRevB.68.125111).
- [35] M. A. Niyas, R. Ramakrishnan, V. Vijay and M. Hariharan, *Chem. Eur. J.* **24** 12318–12329 2018, doi: [10.1002/chem.201705537](https://doi.org/10.1002/chem.201705537).
- [36] S. Yasuzuka, K. Murata, T. Arimoto and R. Kato, *J. Phys. Soc. Japan* **76** 033701 2007, doi: [10.1143/JPSJ.76.033701](https://doi.org/10.1143/JPSJ.76.033701).
- [37] N. Wiberg, *Lehrbuch der Anorganischen Chemie*, De Gruyter, 2008 2148, doi: [10.1515/9783110206845](https://doi.org/10.1515/9783110206845).
- [38] S. Khanna, A. Garito, A. Heeger and R. Jaklevic, *Solid State Commun.* **16** 667–670 1975, doi: [10.1016/0038-1098\(75\)90448-2](https://doi.org/10.1016/0038-1098(75)90448-2).
- [39] F. Herman, D. R. Salahub and R. P. Messmer, *Phys. Rev. B* **16** 2453–2465 1977, doi: [10.1103/PhysRevB.16.2453](https://doi.org/10.1103/PhysRevB.16.2453).
- [40] S. Shitzkovsky, M. Weger and H. Gutfreund, *J. Phys. France* **39** 711–717 1978, doi: [10.1051/jphys:01978003906071100](https://doi.org/10.1051/jphys:01978003906071100).
- [41] P. Cea, S. Martin, A. Villares, D. Möbius and M. C. Lopez, *J. Phys. Chem. B* **110** 963–970 2006, doi: [10.1021/jp055673o](https://doi.org/10.1021/jp055673o).
- [42] Y. Morita et al., *J. Org. Chem.* **70** 2739–2744 2005, doi: [10.1021/jo047768c](https://doi.org/10.1021/jo047768c).
- [43] J. S. Miller, A. J. Epstein and W. M. Reiff, *Chem. Rev.* **88** 201–220 1988, doi: [10.1021/cr00083a010](https://doi.org/10.1021/cr00083a010).
- [44] G.-X. Liu, H. Xu, X.-M. Ren and W.-Y. Sun, *CrystEngComm* **10** 1574–1582 2008, doi: [10.1039/B808390H](https://doi.org/10.1039/B808390H).
- [45] R. Greene et al., *Solid State Commun.* **20** 943–946 1976, doi: [10.1016/0038-1098\(76\)90478-6](https://doi.org/10.1016/0038-1098(76)90478-6).
- [46] D. O. Cowan et al., *Mol. Cryst. Liq.* **32** 223–225 1976, doi: [10.1080/15421407608083658](https://doi.org/10.1080/15421407608083658).

- [47] A. N. Bloch et al., *Phys. Rev. Lett.* **34** 1561–1564 1975, doi: [10.1103/PhysRevLett.34.1561](https://doi.org/10.1103/PhysRevLett.34.1561).
- [48] T. E. Phillips, T. J. Kistenmacher, A. N. Bloch, J. P. Ferraris and O. D. Cowan, *Acta Cryst. B* **33** 422–428 1977, doi: [10.1107/S0567740877003793](https://doi.org/10.1107/S0567740877003793).
- [49] T. Mori and H. Inokuchi, *Bull. Chem. Soc. Jpn.* **60** 402–404 1987, doi: [10.1246/bcsj.60.402](https://doi.org/10.1246/bcsj.60.402).
- [50] T. Mori and H. Inokuchi, *Solid State Commun.* **59** 355–359 1986, doi: [10.1016/0038-1098\(86\)90562-4](https://doi.org/10.1016/0038-1098(86)90562-4).
- [51] H. Yamamoto, M. Hagiwara and R. Kato, *Synth. Met.* **133–134** 449–451 2003, doi: [10.1016/S0379-6779\(02\)00268-0](https://doi.org/10.1016/S0379-6779(02)00268-0).
- [52] H. Yamamoto, N. Tajima, M. Hagiwara, R. Kato and J.-I. Yamaura, *Synth. Met.* **135–136** 623–624 2003, doi: [10.1016/S0379-6779\(02\)00808-1](https://doi.org/10.1016/S0379-6779(02)00808-1).
- [53] M. A. Dobrowolski, G. Garbarino, M. Mezouar, A. Ciesielski and M. K. Cyrański, *CrystEngComm* **16** 415–429 2014, doi: [10.1039/C3CE41703D](https://doi.org/10.1039/C3CE41703D).
- [54] L. R. Melby et al., *J. Am. Chem. Soc.* **84** 3374–3387 1962, doi: [10.1021/ja00876a029](https://doi.org/10.1021/ja00876a029).
- [55] H. Jiang et al., *J. Mater. Chem. C* **6** 1884–1902 2018, doi: [10.1039/C7TC04982J](https://doi.org/10.1039/C7TC04982J).
- [56] P. Hu et al., *Cryst. Growth Des.* **14** 6376–6382 2014, doi: [10.1021/cg501206f](https://doi.org/10.1021/cg501206f).
- [57] D. Vermeulen et al., *J. Phys. Chem. C* **118** 24688–24696 2014, doi: [10.1021/jp508520x](https://doi.org/10.1021/jp508520x).
- [58] X. Chi et al., *Chem. Mater.* **16** 5751–5755 2004, doi: [10.1021/cm049187+](https://doi.org/10.1021/cm049187+).
- [59] F. Sanz and J. J. Daly, *J. Chem. Soc., Perkin Trans. 2* 1146–1150 1975, doi: [10.1039/P29750001146](https://doi.org/10.1039/P29750001146).
- [60] D. Kimball et al., *J. Chem. Cryst.* **45** 169–177 2015, doi: [10.1007/s10870-015-0575-1](https://doi.org/10.1007/s10870-015-0575-1).
- [61] J. Beck, J. Daniels, P. Krieger-Beck, G. Dittmann and A. B. d. Oliveira, *Acta Cryst. E* **70** o1090–o1091 2014, doi: [10.1107/S1600536814019795](https://doi.org/10.1107/S1600536814019795).
- [62] L. Kuz'mina, I. Perepichka, D. Perepichka, J. Howard and M. Bryce, *Kristallografiya* **47** 286–296 2002, doi: [10.1134/1.1466501](https://doi.org/10.1134/1.1466501).
- [63] S.-S. Pac and G. Saito, *J. Solid State Chem.* **168** 486–496 2002, doi: [10.1006/jssc.2002.9733](https://doi.org/10.1006/jssc.2002.9733).
- [64] S. Horiuchi, H. Yamochi, G. Saito, K.-i. Sakaguchi and M. Kusunoki, *J. Am. Chem. Soc.* **118** 8604–8622 1996, doi: [10.1021/ja960393v](https://doi.org/10.1021/ja960393v).
- [65] M. J. S. Palacio F., *Nature* **408** 421–422 2000, doi: [10.1038/35044179](https://doi.org/10.1038/35044179).
- [66] T. Sugawara, H. Komatsu and K. Suzuki, *Chem. Soc. Rev.* **40** 3105–3118 2011, doi: [10.1039/C0CS00157K](https://doi.org/10.1039/C0CS00157K).
- [67] S. Heutz, *Nat. Mater.* **14** 967–968 2015, doi: [10.1038/nmat4431](https://doi.org/10.1038/nmat4431).
- [68] T. Ishiguro, K. Yamaji and G. Saito, “Organic Conductors”, *Organic Superconductors*, Berlin, Heidelberg: Springer Berlin Heidelberg, 1998 15–43, doi: [10.1007/978-3-642-58262-2_2](https://doi.org/10.1007/978-3-642-58262-2_2).
- [69] L. Subramanian and R. Hoffmann, *Inorg. Chem.* **31** 1021–1029 1992, doi: [10.1021/ic00032a019](https://doi.org/10.1021/ic00032a019).

- [70] M. Asplund, S. Jagner and M. Nilsson, *Acta Chem. Scand. A* **37** 57–62 1983, doi: [10.3891/acta.chem.scand.37a-0057](https://doi.org/10.3891/acta.chem.scand.37a-0057).
- [71] S. Anderson and S. Jagner, *Acta Chem. Scand. A* **41** 230–236 1987, doi: [10.3891/acta.chem.scand.41a-0230](https://doi.org/10.3891/acta.chem.scand.41a-0230).
- [72] M. Asplund and S. Jagner, *Acta Chem. Scand. A* **38** 135–139 1984, doi: [10.3891/acta.chem.scand.38a-0135](https://doi.org/10.3891/acta.chem.scand.38a-0135).
- [73] S. Anderson and S. Jagner, *Acta Chem. Scand. A* **40** 177–181 1986, doi: [10.3891/acta.chem.scand.40a-0177](https://doi.org/10.3891/acta.chem.scand.40a-0177).
- [74] J. R. Boehm, A. L. Balch, K. F. Bizot and J. H. Enemark, *J. Am. Chem. Soc.* **97** 501–508 1975, doi: [10.1021/ja00836a006](https://doi.org/10.1021/ja00836a006).
- [75] M. Inoue, M. Inoue, C. Cruz-Vazquez, S. Roberts and Q. Fernando, *Synth. Met.* **19** 641–646 1987, doi: [10.1016/0379-6779\(87\)90429-2](https://doi.org/10.1016/0379-6779(87)90429-2).
- [76] M. Inoue and M. B. Inoue, *J. Chem. Soc., Chem. Commun.* 1043–1044 1985, doi: [10.1039/C39850001043](https://doi.org/10.1039/C39850001043).
- [77] M. Kurmoo et al., *Synth. Met.* **22** 415–418 1988, doi: [10.1016/0379-6779\(88\)90112-9](https://doi.org/10.1016/0379-6779(88)90112-9).
- [78] A. Kawamoto, J. Tanaka and M. Tanaka, *Acta Cryst. C* **43** 205–207 1987, doi: [10.1107/S0108270187096422](https://doi.org/10.1107/S0108270187096422).
- [79] I. R. Marsden et al., *Phys. Rev. B* **50** 2118–2127 1994, doi: [10.1103/PhysRevB.50.2118](https://doi.org/10.1103/PhysRevB.50.2118).
- [80] P. Day et al., *J. Am. Chem. Soc.* **114** 10722–10729 1992, doi: [10.1021/ja00053a007](https://doi.org/10.1021/ja00053a007).
- [81] T. Mori, F. Sakai, G. Saito and H. Inokuchi, *Chem. Lett.* **16** 927–930 1987, doi: [10.1246/cl.1987.927](https://doi.org/10.1246/cl.1987.927).
- [82] T. Enoki, J.-I. Yamaura, N. Sugiyasu, K. Suzuki and G. Saito, *Mol. Cryst. Liq. Cryst.* **233** 325–334 1993, doi: [10.1080/10587259308054974](https://doi.org/10.1080/10587259308054974).
- [83] N. Leblanc et al., *Chem. Commun.* **51** 12740–12743 2015, doi: [10.1039/C5CC04142B](https://doi.org/10.1039/C5CC04142B).
- [84] J. Bernstein, *J. Phys. D: Appl. Phys.* **26** B66–B76 1993, doi: [10.1088/0022-3727/26/8B/010](https://doi.org/10.1088/0022-3727/26/8B/010).
- [85] E. Mitscherlich, *Ann. Chim. Phys.* **19** 350–419 1822.
- [86] W. C. McCrone, “Polymorphism”, *Physics and Chemistry of the Organic Solid State Vol. 2*, New York: Wiley-Interscience, 1965 725–767.
- [87] T. J. Kistenmacher, T. J. Emge, A. N. Bloch and D. O. Cowan, *Acta. Cryst. B* **38** 1193–1199 1982, doi: [10.1107/S0567740882005275](https://doi.org/10.1107/S0567740882005275).
- [88] K. Bechgaard, T. J. Kistenmacher, A. N. Bloch and D. O. Cowan, *Acta. Cryst. B* **33** 417–422 1977, doi: [10.1107/S0567740877003781](https://doi.org/10.1107/S0567740877003781).
- [89] A. J. Moore et al., *J. Org. Chem.* **65** 8269–8276 2000, doi: [10.1021/jo000936q](https://doi.org/10.1021/jo000936q).
- [90] M. Bendikov, F. Wudl and D. F. Perepichka, *Chem. Rev.* **104** 4891–4946 2004, doi: [10.1021/cr030666m](https://doi.org/10.1021/cr030666m).
- [91] E. M. Engler and V. V. Patel, *J. Am. Chem. Soc.* **96** 7376–7378 1974, doi: [10.1021/ja00830a047](https://doi.org/10.1021/ja00830a047).
- [92] K. Bechgaard, D. O. Cowan and A. N. Bloch, *J. Chem. Soc., Chem. Commun.* 937–938 1974, doi: [10.1039/C39740000937](https://doi.org/10.1039/C39740000937).

- [93] R. D. McCullough, G. B. Kok, K. A. Lerstrup and D. O. Cowan, *J. Am. Chem. Soc.* **109** 4115–4116 1987, doi: [10.1021/ja00247a048](https://doi.org/10.1021/ja00247a048).
- [94] K. Lerstrup, D. Talham, A. Bloch, T. Poehler and D. Cowan, *J. Chem. Soc., Chem. Commun.* 336–337 1982, doi: [10.1039/C39820000336](https://doi.org/10.1039/C39820000336).
- [95] S. Hünig, *Liebigs Ann. Chem.* **676** 32–35 1964, doi: [10.1002/jlac.19646760105](https://doi.org/10.1002/jlac.19646760105).
- [96] S. Hünig, H. Balli, H. Conrad and A. Schott, *Liebigs Ann. Chem.* **676** 36–51 1964, doi: [10.1002/jlac.19646760106](https://doi.org/10.1002/jlac.19646760106).
- [97] S. Hünig, H. Balli, H. Conrad and A. Schott, *Liebigs Ann. Chem.* **676** 52–65 1964, doi: [10.1002/jlac.19646760107](https://doi.org/10.1002/jlac.19646760107).
- [98] R. Isenberg, P. Krieger-Beck and J. Beck, *Z. Anorg. Allg. Chem.* e202200020 2022, doi: [10.1002/zaac.202200020](https://doi.org/10.1002/zaac.202200020).
- [99] *EPR measurements of the radical cation I^{+} show the high delocalization of the electron over the whole entire molecule. The respective publication is in progress.*
- [100] G. Manecke and J. Kautz, *Die Makromolekulare Chemie* **172** 1–18 1973, doi: [10.1002/macp.1973.021720101](https://doi.org/10.1002/macp.1973.021720101).
- [101] J. Beck, *personal communication*, 2020.
- [102] Abdessabour Ben Hamed, *Neue Radikalionen-Salze mit dem Cluster-Komplex-Anion $[Mo_6Cl_{14}]^{2-}$* , PhD thesis: Rheinische Friedrich-Wilhelms-Universität Bonn, 2022.
- [103] J. Kaercher et al., *Acta Cryst. A* **58** C367 2002, doi: [10.1107/S0108767302099658](https://doi.org/10.1107/S0108767302099658).
- [104] Z. Otwinowski and W. Minor, *Macromolecular Crystallography Part A*, vol. 276, Academic Press, 1997 307–326, doi: [10.1016/S0076-6879\(97\)76066-X](https://doi.org/10.1016/S0076-6879(97)76066-X).
- [105] G. M. Sheldrick, *Acta Cryst. C* **71** 3–8 2015, doi: [10.1107/S2053229614024218](https://doi.org/10.1107/S2053229614024218).
- [106] K. Brandenburg, *DIAMOND 4.6.5*, Crystal Impact GbR 2021.
- [107] *STOE Win XPow 1.05*, STOE & Cie GmbH 1999.
- [108] H. Putz, *MATCH 2.0*, Crystal Impact 2016.
- [109] G. Gritzner and J. Kuta, *Pure Appl. Chem.* **56** 461–466 1984, doi: [10.1351/pac198456040461](https://doi.org/10.1351/pac198456040461).
- [110] C. H. Hamann and W. Vielstich, Wiesbaden: Wiley VCH, 2005 286–287.
- [111] G. A. Bain and J. F. Berry, *J. Chem. Educ.* **85** 532 2008, doi: [10.1021/ed085p532](https://doi.org/10.1021/ed085p532).
- [112] R. Dovesi et al., *WIREs Comput. Mol. Sci.* **8** e1360 2018, doi: [10.1002/wcms.1360](https://doi.org/10.1002/wcms.1360).
- [113] R. Dovesi et al., *CRYSTAL17 User's manual*, University of Torino, Torino, 2017.
- [114] C. Adamo and V. Barone, *J. Chem. Phys.* **108** 664–675 1998, doi: [10.1063/1.475428](https://doi.org/10.1063/1.475428).
- [115] T. Bredow and A. R. Gerson, *Phys. Rev. B* **61** 5194–5201 2000, doi: [10.1103/PhysRevB.61.5194](https://doi.org/10.1103/PhysRevB.61.5194).
- [116] S. Grimme, J. Antony, S. Ehrlich and H. Krieg, *J. Chem. Phys.* **132** 154104 2010, doi: [10.1063/1.3382344](https://doi.org/10.1063/1.3382344).
- [117] S. Grimme, S. Ehrlich and L. Goerigk, *J. Comput. Chem.* **32** 1456–1465 2011, doi: [10.1002/jcc.21759](https://doi.org/10.1002/jcc.21759).

- [118] D. Vilela Oliveira, J. Laun, M. F. Peintinger and T. Bredow, *J. Comput. Chem.* **40** 2364–2376 2019, doi: [10.1002/jcc.26013](https://doi.org/10.1002/jcc.26013).
- [119] J. Laun, D. Vilela Oliveira and T. Bredow, *J. Comput. Chem.* **39** 1285–1290 2018, doi: [10.1002/jcc.25195](https://doi.org/10.1002/jcc.25195).
- [120] G. Schaftenaar, *molden* 5.9.2, 2018.
- [121] Y. Hinuma, G. Pizzi, Y. Kumagai, F. Oba and I. Tanaka, *Comput. Mater. Sci.* **128** 140–184 2017, doi: [10.1016/j.commatsci.2016.10.015](https://doi.org/10.1016/j.commatsci.2016.10.015).
- [122] S. Vatsadze, Y. Loginova, G. dos Passos Gomes and I. Alabugin, *Chem. Eur. J* **23** 3225–3245 2017, doi: [10.1002/chem.201603491](https://doi.org/10.1002/chem.201603491).
- [123] B. Scott, R. Willett, A. Saccani, F. Sandrolini and B. Ramakrishna, *Inorg. Chim. Acta* **248** 73–80 1996, doi: [10.1016/0020-1693\(95\)04988-6](https://doi.org/10.1016/0020-1693(95)04988-6).
- [124] D. D. Swank, C. P. Landee and R. D. Willett, *Phys. Rev. B* **20** 2154–2162 1979, doi: [10.1103/PhysRevB.20.2154](https://doi.org/10.1103/PhysRevB.20.2154).
- [125] L. Dubicki, C. M. Harris, E. Kokot and R. L. Martin, *Inorg. Chem.* **5** 93–100 1966, doi: [10.1021/ic50035a023](https://doi.org/10.1021/ic50035a023).
- [126] R. D. Willett and B. Twamley, *Inorg. Chem.* **43** 954–957 2004, doi: [10.1021/ic030260s](https://doi.org/10.1021/ic030260s).
- [127] E. Redel, M. Fiederle and C. Janiak, *Z. allg. anorg. Chem.* **635** 1139–1147 2009, doi: [10.1002/zaac.200900091](https://doi.org/10.1002/zaac.200900091).
- [128] S. Maderlehner, M. J. Leitl, H. Yersin and A. Pfitzner, *Dalton Trans.* **44** 19305–19313 2015, doi: [10.1039/C5DT02709H](https://doi.org/10.1039/C5DT02709H).
- [129] B. Scott, R. Willett, L. Porter and J. Williams, *Inorg. Chem.* **31** 2483–2492 1992, doi: [10.1021/ic00038a034](https://doi.org/10.1021/ic00038a034).
- [130] A. Bencini and F. Mani, *Inorg. Chim. Acta* **87** L9–L13 1984, doi: [10.1016/S0020-1693\(00\)83606-3](https://doi.org/10.1016/S0020-1693(00)83606-3).
- [131] R. D. Willett and B. Twamley, *Acta Cryst. C* **57** 706–708 2001, doi: [10.1107/S0108270101005017](https://doi.org/10.1107/S0108270101005017).
- [132] G. A. Bowmaker, A. Camus, B. W. Skelton and A. H. White, *J. Chem. Soc., Dalton Trans.* 727–731 1990, doi: [10.1039/DT9900000727](https://doi.org/10.1039/DT9900000727).
- [133] H. A. Jahn, E. Teller and F. G. Donnan, *Proc. R. Soc. Lond. A* **161** 220–235 1937, doi: [10.1098/rspa.1937.0142](https://doi.org/10.1098/rspa.1937.0142).
- [134] J. Bernstein, *J. Phys. D: Appl. Phys.* **26** B66–B76 1993, doi: [10.1088/0022-3727/26/8B/010](https://doi.org/10.1088/0022-3727/26/8B/010).
- [135] P. Ehrenfest, *Proc. Akad. Wet. Amsterdam* **36** 153–157 1933.
- [136] “Polymorphie, Phasenumwandlungen”, *Anorganische Strukturchemie*, Wiesbaden: Vieweg+Teubner, 2008 51–63, doi: [10.1007/978-3-8348-9545-5_4](https://doi.org/10.1007/978-3-8348-9545-5_4).
- [137] D. S. Acker and W. R. Hertler, *J. Am. Chem. Soc.* **84** 3370–3374 1962, doi: [10.1021/ja00876a028](https://doi.org/10.1021/ja00876a028).
- [138] T. J. Kistenmacher, T. J. Emge, A. N. Bloch and D. O. Cowan, *Acta Cryst. B* **38** 1193–1199 1982, doi: [10.1107/S0567740882005275](https://doi.org/10.1107/S0567740882005275).

- [139] S. Flandrois and D. Chasseau, *Acta Cryst. B* **33** 2744–2750 1977, doi: [10.1107/S0567740877009406](https://doi.org/10.1107/S0567740877009406).
- [140] P. Coppens and T. N. G. Row, *Ann. N. Y. Acad. Sci.* **313** 244–255 1978, doi: [10.1111/j.1749-6632.1978.tb39420.x](https://doi.org/10.1111/j.1749-6632.1978.tb39420.x).
- [141] J. Farges, A. Brau and P. Dupuis, *Solid State Commun.* **54** 531–535 1985, doi: [10.1016/0038-1098\(85\)90662-3](https://doi.org/10.1016/0038-1098(85)90662-3).
- [142] A. Hoekstra, T. Spoelder and A. Vos, *Acta Cryst. B* **28** 14–25 1972, doi: [10.1107/S0567740872001803](https://doi.org/10.1107/S0567740872001803).
- [143] Y.-C. Chen, H.-B. Zhou, G.-X. Liu, X.-M. Ren and Y. Song, *Polyhedron* **28** 1888–1892 2009, doi: [10.1016/j.poly.2008.10.020](https://doi.org/10.1016/j.poly.2008.10.020).
- [144] G. A. Thomas et al., *Phys. Rev. B* **13** 5105–5110 1976, doi: [10.1103/PhysRevB.13.5105](https://doi.org/10.1103/PhysRevB.13.5105).
- [145] M. Moschersch, E. Waldhoer, H. Binder, W. Kaim and J. Fiedler, *Inorg. Chem.* **34** 4326–4335 1995, doi: [10.1021/ic00121a010](https://doi.org/10.1021/ic00121a010).
- [146] S. V. Rosokha, J. Lu, B. Han and J. K. Kochi, *New J. Chem.* **33** 545–553 2009, doi: [10.1039/B812829D](https://doi.org/10.1039/B812829D).
- [147] U. Müller, *Anorganische Strukturchemie*, Vieweg+Teubner Verlag, 2008 227–228, doi: [10.1007/9783834895455](https://doi.org/10.1007/9783834895455).
- [148] V. G. Pavelyev et al., *J. Phys. Chem. C* **118** 30291–30301 2014, doi: [10.1021/jp510543c](https://doi.org/10.1021/jp510543c).
- [149] *ChemDraw 15.1.0.144*, PerkinElmer Informatics 2017.
- [150] *Inkscape 1.1*, Inkscape Development Team 2021.
- [151] *Paint 6.1*, Microsoft Corporation 2009.
- [152] L. J. Farrugia, *J. Appl. Cryst.* **45** 849–854 2012, doi: [10.1107/S0021889812029111](https://doi.org/10.1107/S0021889812029111).
- [153] A. L. Spek, *Platon 10*, Utrecht University, 2014.
- [154] Z. Xu and K. He, *MAGMUN 4.1*, 2002.
- [155] T. Williams and C. Kelley, *gnuplot 4.4*, 2010.

Danksagung

An dieser Stelle möchte ich allen beteiligten Personen meinen großen Dank aussprechen, die mich bei der Anfertigung dieser Doktorarbeit unterstützt haben.

Ein besonderer Dank gilt meinem Doktorvater, Prof. Dr. Johannes Beck, der mich während der ganzen letzten Jahre unterstützt hat und mir die Möglichkeit gegeben hat diese Forschung weiterzuführen. Ich bedanke mich für die Betreuung all meiner Arbeiten, die Chance auf eine freie Themengestaltung und das entgegen gebrachte Vertrauen.

Bei Herr Prof. Dr. Thomas Bredow bedanke ich mich für die großartige und tatkräftige Unterstützung bei meinem Ausflug in die theoretische Chemie.

Bei Frau Dr. Petra Krieger-Beck und Frau Getrud Dittmann bedanke ich mich herzlich für die Synthese der Pyridonazine, die ohne jeden Zweifel die Basis für meine Arbeit waren. Darüber hinaus möchte ich mich für die vielen Male bedanken, in denen mir ihre Expertise, vor allem im Bereich der Synthese, weiter geholfen hat.

Bei Herrn Prof. Dr. Arne Lützen bedanke ich mich für die Gutachtertätigkeit. Außerdem möchte ich mich für die jährliche Zusammenkunft im Rahmen des BIGS Programms bedanken. Mein Dank geht an die gesamte Prüfungskommission.

Herrn Dr. Jörg Daniels danke ich für die Einkristallstrukturmessungen am Röntgendiffraktometer und die Unterstützung bei Strukturlösungen. Außerdem danke ich an der Stelle für zahlreiche Momente in denen ich vor lauter Bäumen nicht mehr den Wald gesehen habe.

Herrn Norbert Wagner danke ich für die zahlreichen magnetischen und Leitfähigkeitsmessungen. Auch danke ich ihm für die Vielzahl an Versuchen eine Erklärung für die ungewöhnlichen Messungen zu finden.

Herrn Dr. Ralf Weisbarth danke ich für die vielen DSC und EDX Messungen.

Herrn Volker Bendisch danke ich für die Fotos der Kristalle.

Katharina Bauerfeind danke ich für die tatkräftige Unterstützung in jeglichen Fragen der theoretischen Chemie, die diesen Teil meiner Arbeit maßgeblich beeinflusst haben. Zusätzlich danke ich ihr für das Korrekturlesen meiner Arbeit.

Außerdem möchte ich mich bei allen Mitgliedern des Arbeitskreises Beck für die freundliche Hilfsbereitschaft sowie die gute Arbeitsatmosphäre bedanken. Vor allem bedanke ich mich bei Dominik Offermanns, Elisa Müller, Jörg Daniels und Ralf Weißbarth für die ereignisreichen Stunden, die mich sowohl chemisch als auch persönlich bereichert haben.

Ich danke meiner Mutter und meinen kleinen Brüdern Lukas und Kosta, die mich in jeder Lebenslage unterstützt haben. Außerdem bedanke ich mich dafür, dass wir alle wichtigen Ereignisse und Erinnerungen in den letzten Jahren geteilt haben. Vor allem möchte ich meiner Mutter danken, die mir und meinen Brüdern alles ermöglicht hat. Außerdem möchte ich mich bei meiner Oma und meiner Tante Marika bedanken. Ich danke meinem Onkel Stefan, dass ich ihn auf seinem schweren Weg begleiten durfte, der trotz seines Schicksal immer an das Gute geglaubt hat. Ich vermisste Dich!

Dann möchte ich mich bei meinen Freunden Selina und Lars (Die Lockis), Svenja (Gotti), Alina, Laura, Hannah, Katha, Dominik, Sabrina und Jörn, David, Malin und dem TV Menden und damit

Danksagung

natürlich allen Menschen, die ich während meiner langen Volleyballzeit kennengelernt habe, bedanken.
Ihr habt alles um diese Arbeit herum schöner gemacht!

Abschließend möchte ich mich bei meinem Freund Arne und seiner Familie bedanken. Arne, du hast mich seit wir uns kennen in allen Dingen unterstützt und ermutigt. An Ralf, Claudia, Volker, Katharina, Marlena, Leonas und Feline Redlin: Danke, dass ihr mich so herzlich aufgenommen habt.

Großer Dank an Alle!